R-05-45

Statistical model of fractures and deformation zones

Preliminary site description, Laxemar subarea, version 1.2

Jan Hermanson, Ola Forssberg
Golder Associates AB

Aaron Fox, Paul La Pointe
Golder Associates Inc

October 2005

Svensk Kärnbränslehantering AB
Swedish Nuclear Fuel
and Waste Management Co
Box 5864
SE-102 40 Stockholm Sweden
Tel 08-459 84 00
+46 8 459 84 00
Fax 08-661 57 19
+46 8 661 57 19

ISSN 1402-3091
SKB Rapport R-05-45

Statistical model of fractures and deformation zones

Preliminary site description, Laxemar subarea, version 1.2

Jan Hermanson, Ola Forssberg
Golder Associates AB

Aaron Fox, Paul La Pointe
Golder Associates Inc

October 2005

A pdf version of this document can be downloaded from www.skb.se

Contents

1 Introduction and project objectives

1.1 Project objectives

The goal of this summary report is to document the data sources, software tools, experimental methods, assumptions, and model parameters in the discrete-fracture network (DFN) model for the local model volume in Laxemar, version 1.2.

The model parameters presented herein are intended for use by other project modeling teams. Individual modeling teams may elect to simplify or use only a portion of the DFN model, depending on their needs. This model is not intended to be a flow model or a mechanical model; as such, only the geometrical characterization is presented. The derivations of the hydraulic or mechanical properties of the fractures or their subsurface connectivities are not within the scope of this report. This model represents analyses carried out on particular data sets. If additional data are obtained, or values for existing data are changed or excluded, the conclusions reached in this report, and the parameter values calculated, may change as well.

1.2 Model domain description

1.2.1 Location

The Simpevarp area is located in the province of Småland, within the municipality of Oskarshamn and adjacent to the Oskarshamn nuclear power plant /SKB, 2004/. The model volume is divided into two subareas; one located on the Simpevarp peninsula adjacent to the power plant (Simpevarp), and one further to the west (Laxemar). Figure 1-1 illustrates the relative positions of the model subareas to prominent regional features and the larger-scale Simpevarp model region.

The DFN parameters described in this report were determined by analysis of data collected within the local model volume (dark red bordered box in Figure 1-1). As such, the final DFN model is only valid within this local model volume and the modeling subareas (Laxemar and Simpevarp) within.

1.2.2 Model subareas

The initial analysis of new outcrop mapping and borehole data from the Laxemar area suggested that the Laxemar subarea fracture networks exhibit different orientation patterns from those observed on the Simpevarp peninsula. Specifically, the strong east-northeast trending set of fractures seen in the Simpevarp outcrops (ASM000025, ASM000026, ASM000205, and ASM000206), was not seen in the Laxemar outcrops (ASM000208 and ASM000209). In addition, the two model domains are separated by the Äspö shear zone (see Figure 1-2), a major northeast-striking shear zone of considerable thickness and extent. Also, separate analyses of the deformation zones, /Wahlgren et al. 2005/, suggest that the area east of Äspö shear zone (NE005A) is in a shear dominated tectonic regime with predominantly NW trending deformation zones in contrast to the Laxemar area which have a wider spread in orientations of major deformation zones.

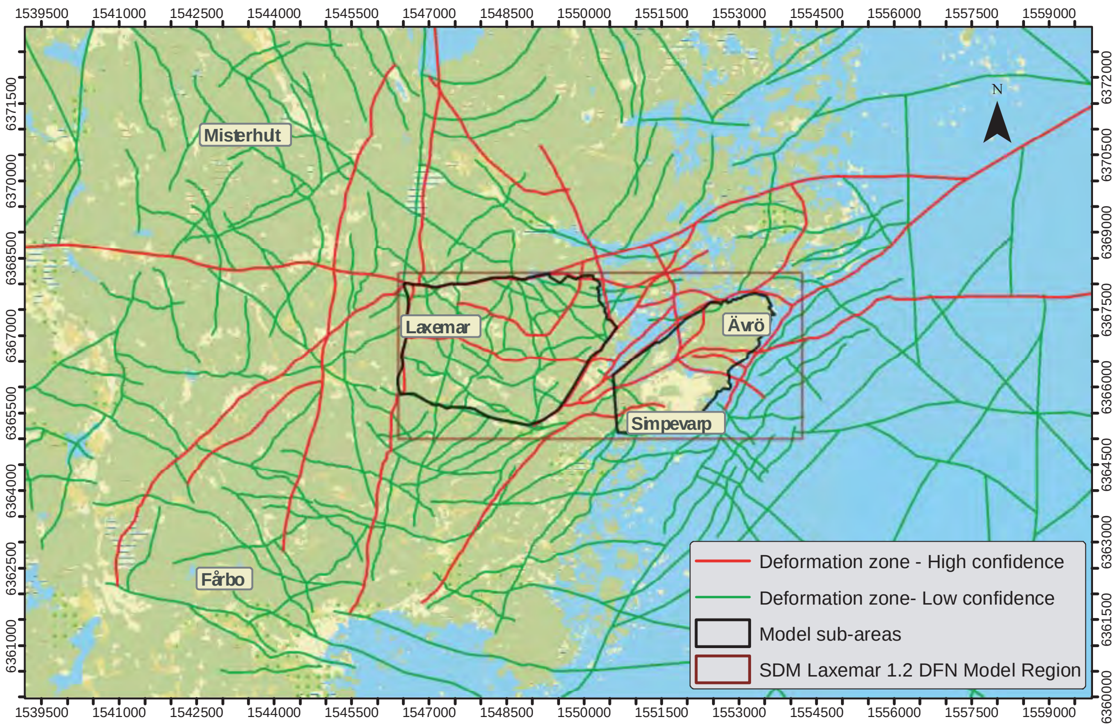

Figure 1-1. *Simpevarp and Laxemar subareas, Simpevarp study area (from /SKB, 2004/).*

Based on these two factors, the local model volume into two discrete subareas (Laxemar and Simpevarp) for the purposes of determining DFN properties.

1.2.3 Bedrock lithology and rock domains

The Simpevarp modeling region is underlain by a mixture of metamorphic, metasedimentary, and igneous rocks known colloquially as the Fenno-Scandian Shield. The oldest rocks in the region are deformed metasedimentary and metavolcanic rocks of Proterozoic age (younger than 2,500 Ma). The predominant lithologies in the Oskarshamn area are rocks from the Transscandinavian Igneous Belt (TIB, which is a mix of granites, syenitoids, dioritoids, and gabbroids emplaced approximately 1,800 Ma during the end stages of the Svecokarelian orogeny /SKB, 2004/. Younger rocks, including coarse- to fine-grained granitic plutons (1,450 Ma) and dolerite dikes (1,000–900 Ma) are also encountered within the modeling region.

In order to simplify the relatively complicated spatial relationships between units, bedrock lithologies have been grouped into 'domains' of similar properties (grain size, texture, quartz content) by a team of scientists from Golder, SKB, and the Geological Survey of Sweden (SGU). Both a two-dimensional and a three-dimensional bedrock domain model were produced by integrating cored borehole data with surface mapping /Wahlgren et al. 2005/. The rock domain model is then used as the base lithological modeling scale for DFN generation. Figure 1-2 (below) illustrates the used version (as of March 2005) of the Laxemar version 1.2 rock domain model, along with the SDM Laxemar 1.2 modeling sub-domains. Figure 1-3 illustrates the lithologic components of each rock domain.

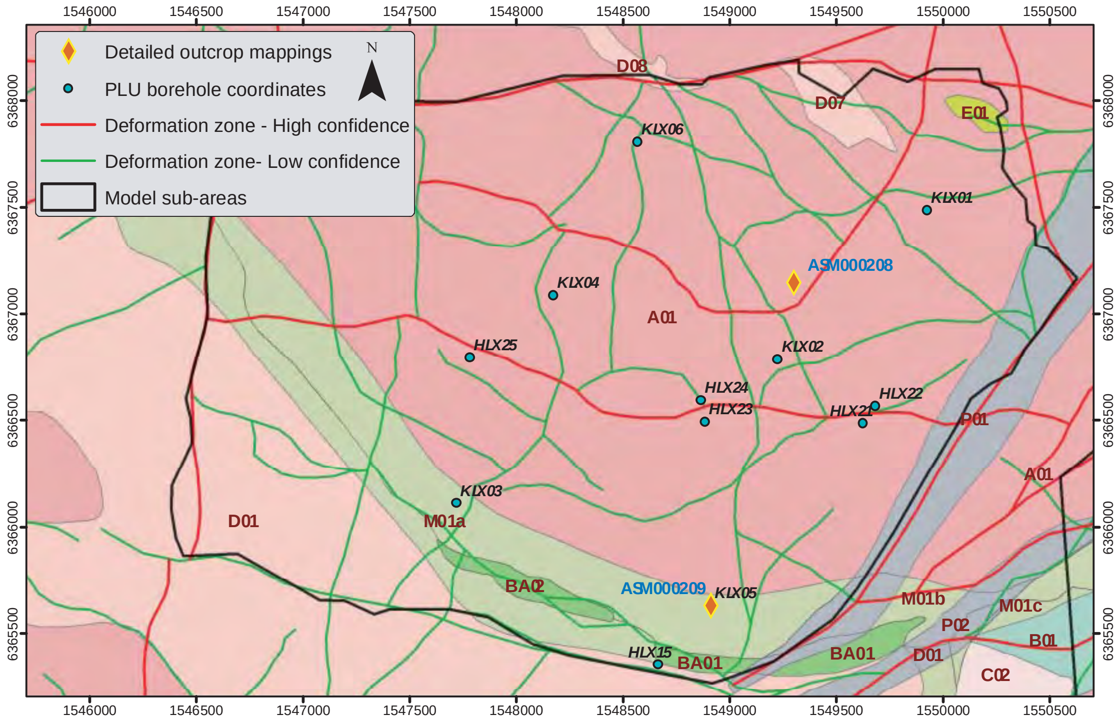

Figure 1-2. Laxemar 1.2 DFN modelling regions, including mapped rock domains and regional deformation zones. Red lines represent 'high confidence' deformation zones, while the green lines represent 'low confidence' deformation zones.

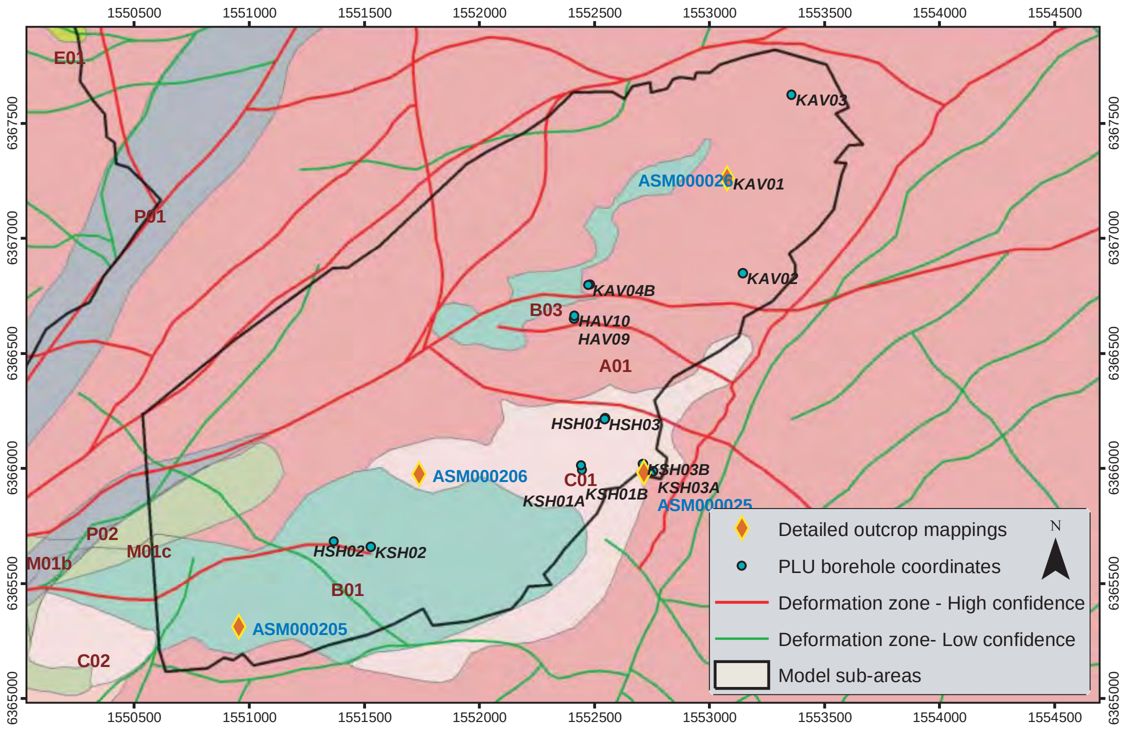

Figure 1-3. SDM Laxemar 1.2, Simpevarp subarea modeling region, including mapped rock domains and regional deformation zones. Red lines represent 'high confidence' deformation zones, while the green lines represent 'low confidence' deformation zones.

Table 1-1. Lithologic components of current SDM Laxemar 1.2 rock domain model.

Domain	Rock Types	Description
A	501044	Dominated by Ävrö Granite.
B	501030	Dominated by fine-grained dioritoid.
BA	501030, 501044	Mixture of Ävrö granite and fine-grained dioritoid.
C	501044, 501036	Mixture of Ävrö granite and quartz monzodiorite.
D	501036	Dominated by quartz monzodiorite.
E	501033	Dominated by diorite to gabbro.
F	511058	Dominated by fine- to medium-grained granite.
G	521058	Dominated by Götemar-type granite.
M	501033, 501036, 501044	High frequency of diorite to gabbro, with respect to proportion of Ävrö granite and quartz monzodiorite.
P	All above	Characterized by a high frequency of low-grade ductile deformation zones.

For further details regarding the geologic structure and tectonic development of the Oskarshamn region refer to the Simpevarp 1.1 preliminary site description report /SKB, 2004/ or the Laxemar 1.2 Rock Domain and Deformation zone models /Wahlgren et al. 2005/.

2 Description of data used

2.1 Data freeze date

Site characterization data for the site descriptive model (SDM) 1.2 Laxemar DFN is restricted to data produced up to the data freeze date (20041031). An exclusion from the data freeze was granted for cored borehole KLX03; this hole is located in the southern half of the Laxemar sub-region where data coverage is sparse. Only preliminary data from KLX03 was available. In addition, the deformation zone and rock domain models reflect input from preliminary lithology logs from cored boreholes KLX05 and KLX06; however, since no fracture-specific (BIPS or detailed core logs containing fracture orientation and material properties) data was available, these holes were not used to derive fracture properties for the SDM 1.2 Laxemar DFN model.

2.2 Detailed outcrop mapping

Fracture outcrop data, including fracture orientations, sizes, and lithological parameters, were taken from the detailed fracture maps (GIS) and SICADA property tables (Excel) of Outcrops ASM000025, ASM000026, ASM000205, ASM000206, ASM000208, and ASM000209. Detailed outcrop map data was primarily used to develop the orientation model for sub-vertical fractures, to assess the effect of bedrock lithology on fracture orientations, and to calculate size distributions for DFN model fracture sets.

Specific data sources include:

- ESRI shape files for Outcrops ASM000208 and ASM000209, /SDE, 2004a/.
  - SDEADM_GOL_LX_2349.shp: Contacts and foliations, ASM000208,
  - SDEADM_GOL_LX_2344.shp: Faults, ASM000208,
  - SDEADM_GOL_LX_2346.shp: Fracture traces, ASM000208,
  - SDEADM_GOL_LX_2350.shp: Lithology, ASM000208,
  - SDEADM_GOL_LX_2347.shp: Outcrop boundaries, ASM000208,
  - SDEADM_GOL_LX_2348.shp: Grid sample bounds, ASM000208,
  - SDEADM_GOL_LX_2345.shp: Scan line locations, ASM000208,
  - SDEADM_GOL_LX_2352.shp: Contacts and foliations, ASM000209,
  - SDEADM_GOL_LX_2353.shp: Faults, ASM000209,
  - SDEADM_GOL_LX_2355.shp: Fracture traces, ASM000209,
  - SDEADM_GOL_LX_2351.shp: Lithology, ASM000209,
  - SDEADM_GOL_LX_2356.shp: Outcrop boundaries, ASM000209,
  - SDEADM_GOL_LX_2357.shp: Grid sample bounds, ASM000209,
  - SDEADM_GOL_LX_2354.shp: Scan line locations, ASM000209.
- ESRI shape files for Outcrops ASM00026, ASM00025 and ASM000206 /SDE, 2004b/.
  - SDEADM_GOL_OH_GEO_1921.shp: Fracture traces, ASM000025,
  - SDEADM_GOL_OH_GEO_1922.shp: Outcrop boundaries, ASM000025,
  - SDEADM_GOL_OH_GEO_1923.shp: Grid sample bounds, ASM000025,
  - SDEADM_GOL_OH_GEO_1918.shp: Fracture traces, ASM000026,
  - SDEADM_GOL_OH_GEO_1919.shp: Outcrop boundaries, ASM000026,
  - SDEADM_GOL_OH_GEO_1920.shp: Grid sample bounds, ASM000026,
  - SDEADM_GOL_OH_GEO_1924.shp: Fracture traces, ASM000206,
  - SDEADM_GOL_OH_GEO_1925.shp: Outcrop boundaries, ASM000206,
  - SDEADM_GOL_OH_GEO_1926.shp: Grid sample bounds, ASM000206,

- ESRI shape files for Outcrop ASM000205, /SDE, 2004c/.
  - SDEADM_GOL_OH_GEO_1915.shp: Fracture traces, ASM000205,
  - SDEADM_GOL_OH_GEO_1916.shp: Outcrop boundaries, ASM000205,
  - SDEADM_GOL_OH_GEO_1917.shp: Grid sample bounds, ASM000205.
- Fracture properties recorded during detailed outcrop mapping efforts in Simpevarp and Laxemar /SICADA, 2004b/.
  - p_fract_area.xls,
  - p_fract_line.xls.
- AutoCAD (.DXF) drawings containing bedrock lithologies for Outcrops ASM000025, ASM000026, ASM000205, and ASM000206 /SDE, 2004d/.

In addition, detailed scan line survey data, consisting of fracture orientation and length mapping of every feature that crossed a set of intersecting survey lines, was also available. This data set was not used in the development of the SDM Laxemar 1.2 DFN model, for the following reasons:

- Scan line data can be strongly affected by sampling bias. Scan lines tend to preferentially intersect larger fractures over smaller fractures /Munier, 2004; La Pointe and Hudson, 1985/; however, these same larger fractures are already addressed in the outcrop-scale mapping (no "new" data). In addition, some of the outcrops (ASM000205 in particular) exhibit a strong directional anisotropy, which may result in misleading statistics for lines oriented parallel and perpendicular to the fracture fabric. It is possible to correct for the orientation bias; however, even after this correction, confidence levels of the frequency of a single joint set are relatively low for sets that are highly orthogonal to the scan line /La Pointe and Hudson, 1985/.
- The addition of "smaller" fractures (i.e. more fractures with a measured trace length below the outcrop truncation threshold of 0.5 m) does not produce a better DFN. It exacerbates the issue of the higher fracture intensities observed in outcrop (P_{21}) when compared to borehole data, and creates a more difficult environment to successfully match the power-law relation fracture set sizes and intensities (see Section 3.4.2 and Section 6.2.1.1).

2.3 Additional surface outcrop data

A limited amount of additional surface fracture data was available for the Laxemar and Simpevarp sub-regions. It consisted of 122 small (< 10 m^2) surface outcrops for which detailed cell mapping was completed. Of the outcrops, only 52 were inside the regional model domain; most of these were within the Simpevarp subarea. These maps were completed in 1987, and are described in PR-25-87-05 /Ericsson, 1987/. Raw data regarding the outcrops was obtained directly from SKB /SICADA, 2004a/.

- cell_map_d.xls,
- cell_map_f2.xls,
- 'table info cell_map_d.doc'.

In addition, 42 small outcrops within the model region were mapped using scan line techniques during 2003 and 2004. The scan lines typically consisted of 10 m long lines crossing at right angles; however, at some outcrops, the scan lines were split into smaller segments, or only one line of the pair was mapped /SICADA, 2004b/.

- Outcrop_frac_obs.xls.

2.4 Borehole data

2.4.1 Single hole interpretations

Single-hole interpretations were used to assign and correlate deterministic deformation zones to individual boreholes, for the purpose of a) excluding zones from DFN set intensity calculations and b) assessing the intensity of deformation zones (DZs) in the subsurface. The list of files used is presented below:

- KLX01, KLX02, KLX03, KSH01A, KSH01B, KSH02, KSH03A, KSH03B single-hole interpretation in borehole log format, delivered as PDF by SKB on 1/21/2005.
- Geological single-hole interpretation of KSH01A, KSH01B, HSH01, HSH02, and HSH03 /Mattsson et al. 2004a/.
  - P-04-32webb.pdf.
- Geological single-hole interpretation of KSH02 and KAV01 /Mattsson et al. 2004b/
  - SHI_KSH02_KAV01.pdf.
- SKB SICADA single-hole interpretation data tables for borehole KSH01A/SICADA, 2004a/.
  - bh_interpret_def_zon.xls,
  - bh_interpret_fzi.xls,
  - bh_interpret_rocktyp.xls,
  - 'Info geological single borehole interpretation.doc',
  - 'Info table bh_interpret_def_zon.doc',
  - 'Info table bh_interpret_fzi.doc',
  - 'Info table bh_interpret_rocktyp.doc'.
- SKB SICADA single-hole interpretation data table for boreholes HLX26, HLX27, and KLX03 /SICADA, 2005a/.
  - p_one_hole_interpret.xls.

2.4.2 Borehole fracture intensity

Fracture intensity data consists of SICADA data tables containing counts of all, open, and closed fractures within an observation window of a set size. Intervals are specified as a linear distance along a given borehole in lengths relative to the borehole collar (ADJUSTED_SECUP, ADJUSTED_SECLOW), and included data counted in 1 m-, 3 m-, 4 m-, 5 m-, 10 m-, and 30 m-long windows. In general, only the 1 m window data was used. Associated files are:

- Binned fracture frequency data, boreholes HLX25, HLX26, and HLX27. /SICADA, 2005a/.
  - p_freq_1m.xls,
  - p_freq_3m.xls,
  - p_freq_4m.xls,
  - p_freq_5m.xls,
  - p_freq_10m.xls,
  - p_freq_30m.xls.
- Binned fracture frequency data, borehole KLX03 /SICADA, 2004c/.
  - p_freq_1m.xls,
  - p_freq_3m.xls,
  - p_freq_4m.xls,
  - p_freq_5m.xls,
  - p_freq_10m.xls,
  - p_freq_30m.xls.

- Binned fracture frequency data, boreholes HLX15, HSH01, HSH02, HSH03, KAV01, KAV04A, KAV04B, KLX01, KLX02, KLX04, KSH01A, KSH01B, KSH02, KSH03A, and KSH03B /SICADA, 2004b/.
  - p_freq_1m.xls,
  - p_freq_3m.xls,
  - p_freq_4m.xls,
  - p_freq_5m.xls,
  - p_freq_10m.xls,
  - p_freq_30m.xls.

2.4.3 Crushed core zones and sealed fracture networks

SICADA data tables describing extents and orientations of zones of crushed rock core and dense networks of sealed fractures were included in the model development. This data was generally used as a quantitative check against stochastic deformation zone assignment and fracture-set intensity measurements. Associated files are:

- Location and extents of sealed fracture networks and crushed core zones in borehole KLX03 /SICADA, 2004c/.
  - p_fract_crush.xls,
  - p_fract_sealed_nw.xls.
- Location and extents sealed fracture networks and crushed core zones in boreholes HSH01, HSH03, KAV01, KAV04A, KAV04B, KLX01, KLX02, KLX04, KSH01A, KSH02, and KSH03A /SICADA, 2004b/.
  - p_fract_crush.xls,
  - p_fract_sealed_nw.xls.

2.4.4 Fracture orientations

Fracture orientation data from Oskarshamn site investigations (PLU) and Äspö boreholes were used to develop statistical orientation distributions for the sub-horizontal component of the Laxemar 1.2 DFN. The data was also used as a check on the sub-vertical set assignments computed using detailed outcrop mapping data. SICADA data tables were consolidated into two Excel files, one for each modeling subarea. Associated files are:

- Fracture orientation and property data from core and BIPS logs, borehole KLX03 /SICADA, 2004c/.
  - p_fract_core.xls.
- Fracture orientation and property data from core and BIPS logs, boreholes HAV09, HAV10, HLX15, HSH01, HSH02, HSH03, KAV01, KAV04A, KAV04B, KLX01, KLX02, KLX04, KSH01A, KSH01B, KSH02, KSH03A, and KSH03B /SICADA, 2004b/.
  - p_fract_core_001.xls,
  - p_fract_core_002.xls.

2.4.5 Other borehole data

Additional SICADA data tables were used to assess the influence of varying lithologies and degrees of alteration on fracture orientations and intensities in the PLU boreholes. SICADA tables were loaded into one of two Excel spreadsheets, one for each modeling sub-domain, and correlated to either fracture core logs (p_fract_core.xls) or to intensity intervals (p_freq_#m.xls) by using the feature elevations (in RT90-RHB70 coordinates), or, for boreholes where projected coordinates were not available within shipped data deliveries at the time of the SDM Laxemar 1.2 DFN data freeze (KLX03), the SECUP and SECLOW values for the feature. Associated files are:

- Core lithologies and degree of rock alteration data, boreholes HAV09, HAV10, HLX15, HSH01, HSH02, HSH03, KAV01, KAV04A, KAV04B, KLX01, KLX02, KLX04, KSH01A, KSH01B, KSH02, KSH03A, and KSH03B /SICADA, 2004b/.
  - p_rock_alter.xls,
  - p_rock_occur.xls,
  - bh_interpret_rocktyp.xls.

2.5 Deformation zones

Orientation analyses were performed on two dimensional cross-sections of the Simpevarp 1.2 deformation zone model at zero meters above mean sea level (MASL) /SKB, 2005/. In the previous DFN model report, linked lineaments were used assuming a relationship between lineaments and deformation zones.

This model version has made use of the high and low confidence deformation zone traces that was presented in the Simpevarp 1.2 model to better blend with the latest geological interpretations in the area. It was not possible to use the Laxemar 1.2 deformation zone model as it was developed simultaneously with this model.

The deformation zone model was based upon data extracted from the Simpevarp 1.2 model in RVS, and consisted of the following files:

- SM_V1.2.DZ-5_GreenZones_lin.shp: Trace map (2D) of lower-confidence deformation zones. Zone strikes and dips were exported as text files using Manifold GIS; the resulting data was used to assign fracture set memberships in FracMan/DOS 2.604.
- SM_V1.2.DZ-5_RedZones.lin.shp: Trace map (2D) of high-confidence deformation zones. Trace map (2D) of lower-confidence deformation zones. Zone strikes and dips were exported as text files using Manifold GIS; the resulting data was used to assign fracture set memberships in FracMan/DOS 2.604.

The deformation zone files were converted to DXF format and imported into FracWorks XP and subdivided into global sets (S_A, S_B, and S_C) using a mixture of Structure ID number matching and direct visual comparisions to set trace maps constructed in ArcGIS.

2.6 Rock domain model

Preliminary rock-domain models, dated 1/10/2005 and 2/21/2005 and constructed by Ola Forssberg (Golder) and Carl-Henric Wahlberg (Geological Survey of Sweden), were used for DFN fracture set property assignment. Though the DFN model contains global fracture set orientations and sizes, we assume that fracture intensity (P_{32}) varies as a function of rock domain.

The rock domain model is based on condensations of various surficial geologic mapping efforts with borehole lithology data. Boreholes KLX01 through KLX06, KSH01A, KSH02, KSH03A, KAV01, and KAV04A were used to provide depth and locations on subsurface extensions of surface-mapped domains /Wahlgren et al. 2005/.

2.7 Software used

Table 2-1 lists all of the software used to carry out the calculations in this report, including their name, version numbers, modules, address of vendor and what model parameters they were used for. Modules are listed in the case where there might be ambiguity as to which options were selected.

The Manifold GIS package (listed below) was used in addition to ESRI, Inc.'s ArcGIS software package due to the presence of some additional features not available in the standard ArcMap desktop install. Specifically, Manifold allowed for the manipulation of shapefile intrinsic fields such as polyline segment lengths and strike angles. This made extracting feature data from the deformation zone model files much easier. No data transformations or analyses were performed using Manifold GIS. This feature is available in an ArcEditor desktop install, which was not available during the modeling time frame.

Table 2-1. List of software used for this report.

Software name	Version	Company	Modules used	Calculation performed
Excel 2002	10.5815.4219	Microsoft Corp. www.microsoft.com	Analysis Tool-pack	Trace length scaling calculations; general data preparation for other programs, moving-average intensity tables.
Analyse-It	Version 1.71 Dec 11, 2003	Analyse-It Software, Ltd. PO Box 77, LeedsLS12 5XA, England, UK. www.analyse-it.com/ Tel: +44 (0)113 229 5599		Summary tables for fracture intensity as a function of alteration zones and rock types; variation of fracture intensity with depth.
DIPS	Version 5.103 June 9, 2004	Rocscience, Inc. 31 Balsam Avenue Toronto, Ontario M4E 3B5 Tel: (416) 698-8217 hwww.rocscience.com	None	Orientation and display of fracture orientations; calculation of modal poles to fracture sets, Terzaghi weighting of contoured pole plots.
GeoFractal	Version 1.2 Build 321, Dec. 27, 2001	Golder Associates Inc. 18300 NE Union Hill Rd. Redmond, WA 98052 +1 425 883-0777 fracman.golder.com	None	Calculation of fractal mass dimension and box dimension.
FracMan DOS	Version 2.604	Golder Associates Inc. 18300 NE Union Hill Rd. Redmond, WA 98052 +1 425 883-0777 fracman.golder.com	None	Analysis of fracture orientation statistics and size statistics for fracture sets.
FracWorks XP	Version 4.1, 4.2 and a preliminary build of 4.3	Golder Associates Inc. 18300 NE Union Hill Rd. Redmond, WA 98052 +1 425 883-0777 fracman.golder.com/	None	Visualization of simulated fracture orientations, conditional sampling of test DFN models.
SamEdit	Version 4.11	Golder Associates Inc. 18300 NE Union Hill Rd. Redmond, WA 98052 +1 425 883-0777 fracman.golder.com/	None	Creation and editing of sampling structure control files for FRED/ Fracworks XP/FracMan DOS.

Software name	Version	Company	Modules used	Calculation performed
ArcView	Version 8.3	ESRI Inc 380 New York St. Redlands, CA 92373 +1 909 793 2853 www.esri.com	ArcMap ArcCatalog	Display of fracture and deformation zone traces, creation of new GIS files and metadata to aid data analysis.
Manifold GIS	Version 6.0, Service Pack 2	Manifold.Net, Ltd. 1805 North Carson St. Suite 700 Carson City, NV 89701 +1 800 556 5919 /www.manifold.net	None	Extraction of feature data from lineament and deformation zone shapefiles.
SPSS	Version 13.0	SPSS, Inc. 233 S. Wacker Drive, 11th floor Chicago, Illinois 60606 +1 312 651 3000 www.spss.com	None	Contingency table analyses for relation between alteration, lithology and intensity.

3 Modeling methodology

3.1 Modeling workflow

Discrete fracture network parameters are calculated through a series of steps, each of which depend on the results of the previous steps. Set identification and definition is the first necessary step in constructing a DFN; each set may have a different spectrum of parameters that can be highly variable between sets. Fracture sets are defined for convenience in generating statistically significant fractures in terms of distribution of properties such as orientation, size, and hydraulic parameters. Sets need be neither homogenous nor stationary, provided there is a consistent reason, backed by geologic evidence, for grouping the fractures together. In addition, the formation of a set or a group of sets reflects the mechanics of fracture formation, including stress state, strain state, and rock strength of the lithologies surrounding the project site at a specific spatio-temporal location.

Once fracture sets have been specified, it is necessary to determine the geometrical description of each set. For a single fracture set, this description includes:

- Set orientation distributions, expressed as the trend and plunge of a mean pole calculated from all members of the set. Spatial variability in set orientations are quantified through the use of one of several probability models: Fisher, Bivariate Fisher, Bivariate Bingham, or Bivariate Normal.
- Fracture set sizes are expressed as a size-frequency radius distribution, following one or more of the following probability distribution functions: normal, lognormal, exponential, power law or uniform. Though not expressly part of the radius distributions, suggested maximum and minimum size truncations are also included. These truncation values have an impact on fracture intensity in any DFN model implementation.
- Fracture shapes. In this report, calculations and models assume either circular disc-shaped (DFN fractures) or rectangular (deterministically modeled deformation zones) fractures. However, terminations and intersections within a DFN can lead to other types of polygons.
- Fracture set intensity. These are generally specified as P_{32} values, which represent the amount of fracture surface area (m^2) per unit volume (m^3) of rock.
- Fracture set spatial model controls. The spatial model controls the spatial distribution of fractures within the model volume. Typical spatial models are Poissonian (randomly distributed), fractal, geostatistical, or a combination of multiple processes within specific geological domains. Different models will be tested in order to find a reasonable fit, starting with the simplest case (Poissonian). Our guiding philosophy is to select the simplest model that is adequate for the intended use (fracture spatial controls within a local-scale DFN).
- Fracture set terminations. This is expressed as a percentage of the fractures in a given set that terminate against other fractures.

Figure 3-1 summarizes the workflow process required to develop the Laxemar and Simpevarp DFN models. Additional parameter values may be included in the DFN model specifications, depending on the intended end-use. However, for the Laxemar 1.2 model phase, no additional parameters have been identified.

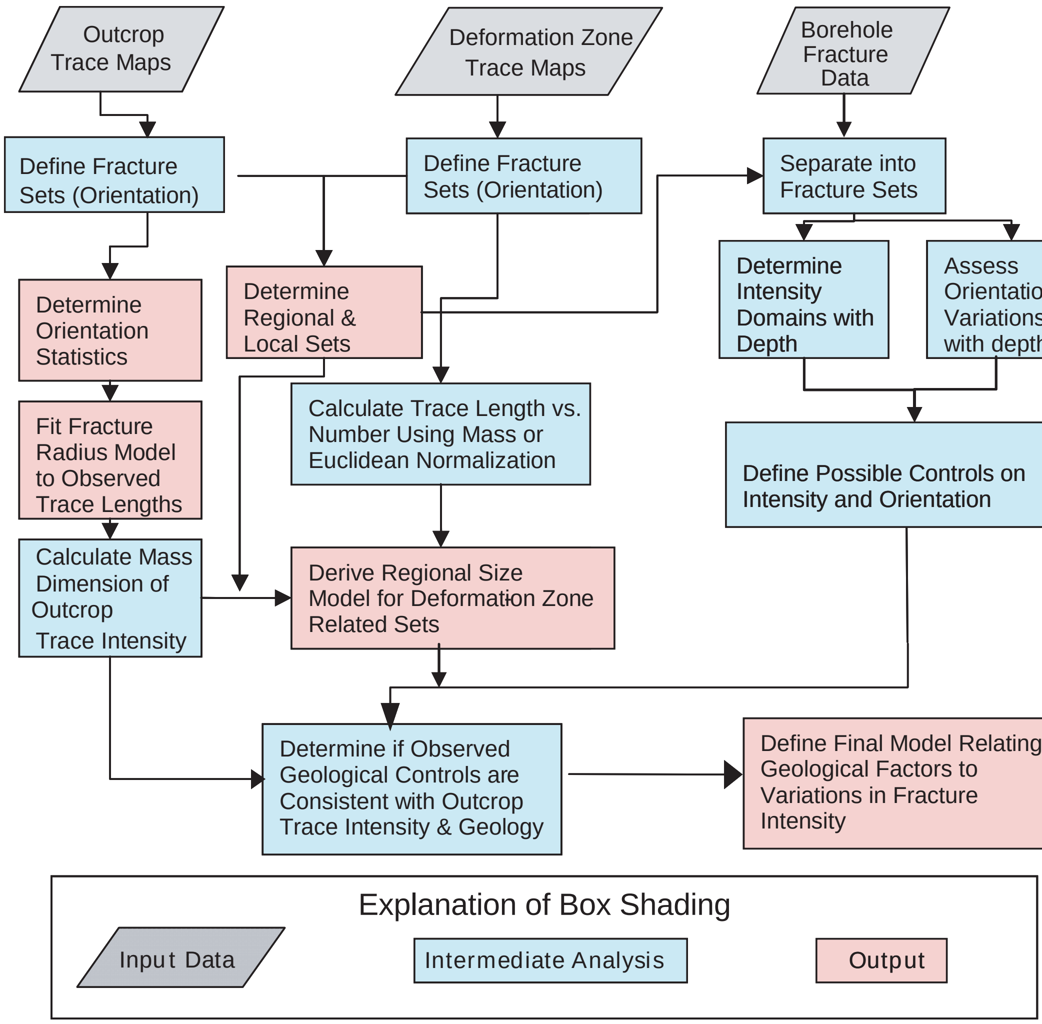

Figure 3-1. *DFN model development flowchart.*

3.2 Model assumptions and limitations

There are several assumptions that have been made in order to construct the DFN model for the Oskarshamn project sites (Laxemar and Simpevarp). Each assumption is described below, along with its impact on the model, a rationale for why the assumption is reasonable, and recommendations for future re-evaluation of the assumption.

Assumption 1: The length of a deformation zone trace or a fracture in outcrop is an accurate and appropriate measure of a single fracture's trace length for the purpose of deriving the radius distribution of geologic structures.

Discussion: This assumption contains two parts: that a deformation zone trace or a fracture in outcrop is a sufficiently accurate measure of a fracture's length; and that it is the appropriate one for computing size statistics. The purpose of using traces from the deformation zone model is to develop a DFN model that has fracture sizes and intensities that adequately reproduce flow and transport over large and small scales simultaneously.

Although the size model depends on the lengths of the deformation zone traces and the way underlying lineament segments are linked, the uncertainty can be bracketed and quantified. The potential uncertainties in trace lengths at the outcrop scale are manifested (along with other uncertainties) as the variance among area-normalized frequency values for the outcrops.

Assumption 2: If a fracture set in outcrop represents a size-censored portion of a population of fractures that include a deformation zone-related trace set, then the fracture set in outcrop should have the same orientation as the deformation zone set. Conversely, the similarity in orientation is evidence in support of (but not conclusive) combining the two separate groups of traces into a single set.

Discussion: If both the fractures in outcrop and the fractures defining the deformation zones are part of a single population formed, then they are formed by the same geological and mechanical processes. As such, they should have similar orientations. While similar orientations could occur even if the two fracture sets were not part of the same parent population, it is less probable. If there is evidence to suggest that the fractures in outcrop formed at a different time than the deformation zones, then this would be evidence that the two were not part of the same parent set. This assumption does not imply the existence or non-existence of fractures of intermediate size between outcrop and deformation zone scales.

Assumption 3: There is a 'tectonic continuum' between the outcrop-scale features (fractures) and the regional-scale structures (kilometer-scale deformation zones), and that some of the outcrop fracture patterns are a smaller-scale expression of regional features. The size calculation for deformation zone-related sets is based upon fitting a power law curve to the combined data set of deformation zone and outcrop fracture trace lengths.

Discussion: It is possible that most deformation zones are actually faults, while most outcrop fractures are mostly joints, which could be in different orientations and have different size characteristics. However, if the orientations are similar and the trace lengths appear to scale as a power law, then the simplest model to explain both these observations is that they are part of a tectonic continuum of fracturing extending from centimeter-scale fractures to kilometer scale fractures.

Assumption 4: Variations in fracture intensity as a function of rock type, alteration zone or other geological control can be extrapolated from sampled boreholes and outcrops to un-sampled rock units within the same rock domain.

Discussion: Thus far, information on geological controls for fracture intensity variation suggests that lithology and alteration degree may be important controls. In order to specify fracture intensity throughout the model region, it is necessary to infer geologic similarity of unsampled rock domains to sampled ones, or to adjust model parameters for unsampled rock domains based on the presence of similar geologic or tectonic controls. It would be useful to validate this extrapolation to unsampled rock types by acquiring data in one of these unsampled units and comparing predictions to observed conditions.

Assumption 5: For the Laxemar 1.2 DFN model, we assume that the fractures can be approximated as planar, circular discs possessing no thickness and whose orientations conform to the orientation statistics found through the methods described in Section 3.3. No statements are made regarding the aperture (width) or hydraulic properties of the DFN fractures.

Discussion: While the fractures in the rock are probably neither circular nor planar, there is not sufficient data to mathematically characterize deviations from these two idealizations. In outcrop, the deviations from planarity do not appear to be large. The major impact would be in the trace length computations, as the trace length will be equal to or longer than a straight line (or planar surface) connecting the fracture endpoint. The longer trace lengths will tend to promote greater fracture network connectivity and are thus conservative.

There are also mechanical reasons to suppose that the actual fracture shapes may tend towards being equant, as the mechanical layering present in sedimentary rocks which promotes non-equant fracture shape is far less well-developed in the crystalline rocks for Laxemar and Simpevarp.

Since existing outcrop data is insufficient for making detailed studies of fracture size throughout the regions of interest, it has been assumed that sizes may vary by subarea and rock domain, but that within each domain and subarea, sizes are homogeneous. It is not obvious whether this is a conservative assumption. Better resolution will require a much greater amount of outcrop and borehole data.

It is worth noting that there are no assumptions about the variation of orientations with spatial position. All data are first analyzed on all of the subdivisions available: individual outcrops, rock domains, individual boreholes and depth. If similarities or differences appear, then these are investigated further.

3.3 Fracture set orientations

3.3.1 Analysis of detailed outcrop mapping data (set assignment)

Fracture data generated from outcrop mapping is a principal component of DFN model generation. The orientations, sizes, spatial generation model, and geo-structural relationships of sub-vertical fractures are best assessed through detailed outcrop mapping.

Fracture data from the SICADA database (orientations, fracture properties, host lithologies) and the SKB GIS database (spatial locations of fracture endpoints) were incorporated into a single data set within ArcMap. The two datasets were linked together using attribute joins based on the IDCODE_GIS attribute, which is common to outcrop fracture data stored in both the SICADA and the SDE databases. The attribute join allows for the inclusion of the wealth of data stored for each outcrop fracture in SICADA in a GIS spatial analysis of fracture patterns without physically merging the two data sets or creating new data layers. ArcMap was used to perform basic visual analysis and classification of outcrop fractures into tentative orientation sets. The fracture data were classified, selected, and exported as text files from ArcGIS for further analysis using DIPS, Microsoft Excel, and FracSys/ISIS. DIPS was used to produce fracture pole plots, while Excel was used to generate and test basic descriptive statistics about both the combined data and the resulting identified orientation sets. The ISIS function within the FracSys module of the FracMan for DOS code (version 2.604) was used to calculate statistical parameters for spherical orientation distributions for the identified outcrop sets.

Outcrop fracture sets were identified visually using the following qualitative properties:

1. Pole clustering on contoured stereonet plots.
2. Similarity in orientation; i.e. representing a consistent groups of common strikes.
3. Fracture evolution (terminations, cross-cutting relationships, obvious steps or splays).
4. Relationships to bedrock structures (orientations of foliation, bedding planes, igneous dikes).
5. Characteristic lengths in outcrop (i.e. one grouping was consistently longer or shorter than another).

Fracture sets were preliminarily identified through hard-sector set assignment in DIPS. The resulting set memberships were then joined to the outcrop trace data and refined using the qualitative properties described above. The fundamental assumption in the set classification process was that feature orientation, rather than size or host lithology, was the single-most important factor in determining set membership.

This methodology for fracture set identification is slightly different from earlier SKB discrete-fracture network modeling efforts (Forsmark 1.2, Simpevarp 1.1/1.2). In the earlier models, orientation sets were identified through analysis and hard-sector assignment of trace map patterns. This has the potential to capture some smaller-scale sets that would be lost in the noise of a traditional stereoplot. However, this approach (in past reports) resulted in a large number of local outcrop sets (up to six subvertical sets with an additional subhorizontal set). However, for the scale of interest being studied (a regional scale DFN), set definition at this level of detail may not be required as the increased variability and uncertainty may be adequately compensated for by the uncertainties built into the larger set assignments (dispersion). However, the presence of these 'secondary' sets may be of importance for smaller-scale modeling efforts such as tunnel design, rock-mass stability, and canister failure analyses. Modeling teams using the SDM DFN developed in this report should consider the effect that the breakout of these additional sets might have upon their models.

Initially, local set definitions were defined for all six of the detailed fracture mapping outcrops. SICADA fracture data was then assigned a set number based on these local set definitions. The resulting classified fractures were then combined, by set, into a single 'regional' set. Orientation distribution parameters were then calculated for the regional sets using the ISIS algorithm. Two orientation models are presented; one using only univariate Fisher distributions to describe the variations in fracture orientations (Alternative Model 1), and a second using a bivariate Fisher, bivariate Bingham, and univariate Fisher distributions if these provided a more statistically significant fit to the data (Alternative Model 2). In general, the second model tends to produce more significant statistical fits, while the first model is a response to previous review comments regarding the ease of implementation of the Fisher distribution in earlier Simpevarp and Forsmark DFN models.

All fractures down to a minimum length of 0.5 m were included in the outcrop map. Several outcrops also contained additional detailed scan line surveys, which mapped fractures down to a minimum length of 0.3 m. The scan line fractures are not included in the orientation analysis, as they introduce a sampling bias (the probability of intersecting fractures perpendicular to the scan line orientation is high, while the probability of intersecting sub-parallel fractures is significantly lower) that is not present in the outcrop data. Although the bias can be partially corrected, the results are still not as robust as the outcrop data.

3.3.2 Relationship of identified outcrop sets to mapped regional deformation zones

Once the local assignments were completed, the sets were characterized as either regional or local in nature; this classification was based on the following criteria:

- Regional sets: Show consistent structural relationships to mapped deformation zones or to major geologic features (such as dikes, foliations, or bedding planes). Regional sets may also show a consistent orientation or age relationships between outcrops. Regional fracture sets are an important component of the final DFN, as they most likely represent the second major control on rock-mass stability and groundwater flow (the deformation zones being the principal control).

- Local sets: Show changing orientations, sizes, or intensities from outcrop to outcrop. May be related to rock parameters or stress conditions that are spatially varying. May affect rock mass stability and groundwater flow on a local scale, but are most likely less important on a regional scale. Local sets may be confined to a single outcrop.

The primary observations to decide whether any sets identified in individual outcrops form part of a regional set are whether the orientations are similar and the sets are in the same approximate chronological order; or if their orientations differ, do they still occupy about the same place in the chronological order and can the difference in orientation be explained by changes in the deformation zone pattern geometry? Figure 3-2 summarizes the decision tree necessary to identify 'regional' fracture sets. The rationale for this decision tree is that similarity in orientation may be insufficient given the large number of sets in each outcrop. The additional constraint of set timing helps to bolster confidence that the sets in each outcrop are actually part of a regional set. On the other hand, it may be that the stress pattern has rotated slightly, so that the fracturing that was developing at a particular time actually has different orientations in different outcrops. If this were the case, then it would be expected that the relative set chronology would be very similar, and that the orientations would reflect the difference in the orientations of the deformation zone pattern near the outcrop.

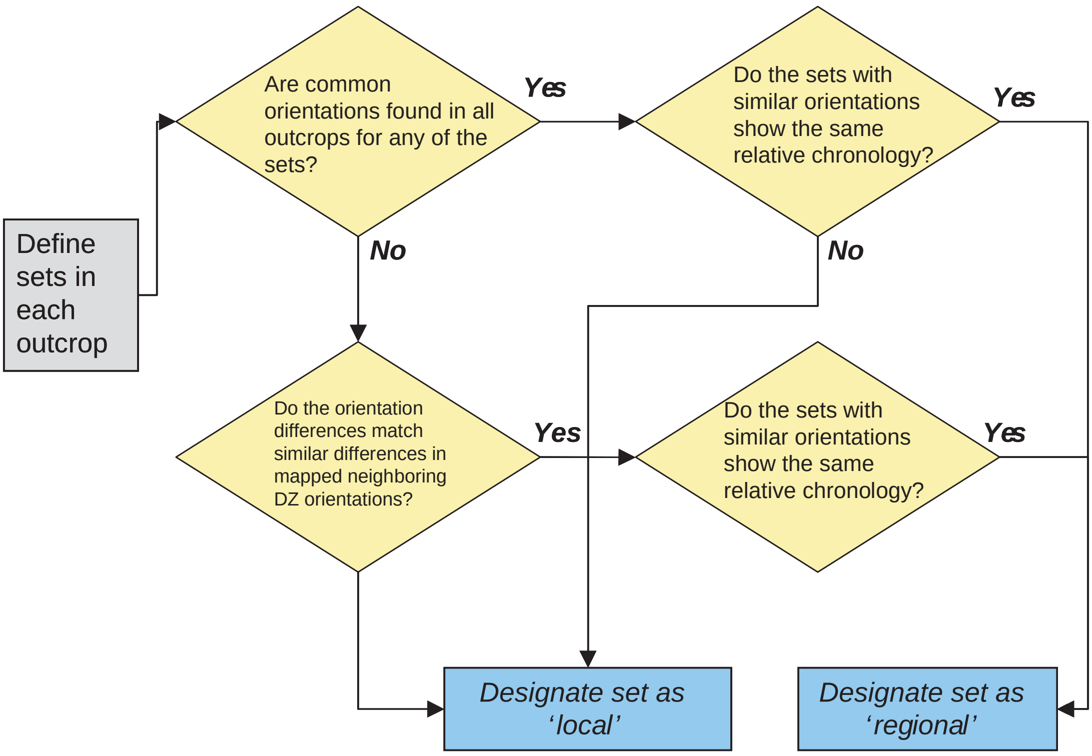

Figure 3-2. *Decision tree for designating local and regional fracture sets based on outcrop trace data.*

3.3.3 Qualitative analysis of additional scan line and cell mapping data

Additional cell mapping and the Swedish Geological Survey scan line data derived from regional bedrock efforts /SICADA, 2004a–b/ (see Section 2.3) from older projects within the Simpevarp region was utilized to determine the whether the models of fracture set orientations developed through detailed analysis of large-scale bedrock outcrops were visible on a regional scale. Rose diagrams and polar stereographs were constructed from fracture pole data, and the resulting graphics tied to spatial locations using ArcGIS 8.3. Plots were analyzed for the presence or absence of individual sets, as well as the general spatial relationships between identified sets, structural features, and rock domains. It should be noted that this was entirely a qualitative analysis based on the direct comparison of stereoplots and rose diagrams. Due to the nature of the data (scan lines for which detailed mapping procedures and quality assurance rules were not available) no rigorous statistical testing of significance was performed on the SGU scan-line dataset.

3.3.4 Deterministic deformation zones

The Simpevarp 1.2 deformation zone model contains deterministic deformation zones in the local and regional model domains. The local model volume, which is the intended scale for this DFN model, contains deformation zones longer than 1,000 m, cf Figure 3-3, whereas the regional model domain contains zones longer than 1,600 m, cf Figure 3-4 /SKB, 2004a/. Orientation analyses have been performed on all deformation zone traces in both regional and local model volumes.

3.3.5 Analysis of borehole fracture orientation data

Fracture orientations taken from drill core logs and borehole image logs (BIPS) were used as a check of the subvertical fracture set divisions developed from the detailed outcrop mapping analysis. Polar stereoplots and Fisher-contoured stereonets /Fisher, 1953/ derived from individual boreholes were compared directly to their counterparts in outcrop. For the SDM Laxemar 1.2 report, this is largely a qualitative comparison, as the subvertical set assignments from outcrop are the fundamental model component. The borehole data does, however, allow for a comparison of the 'goodness of fit' of the model, and provides insight into fracture intensity and orientation variations with depth.

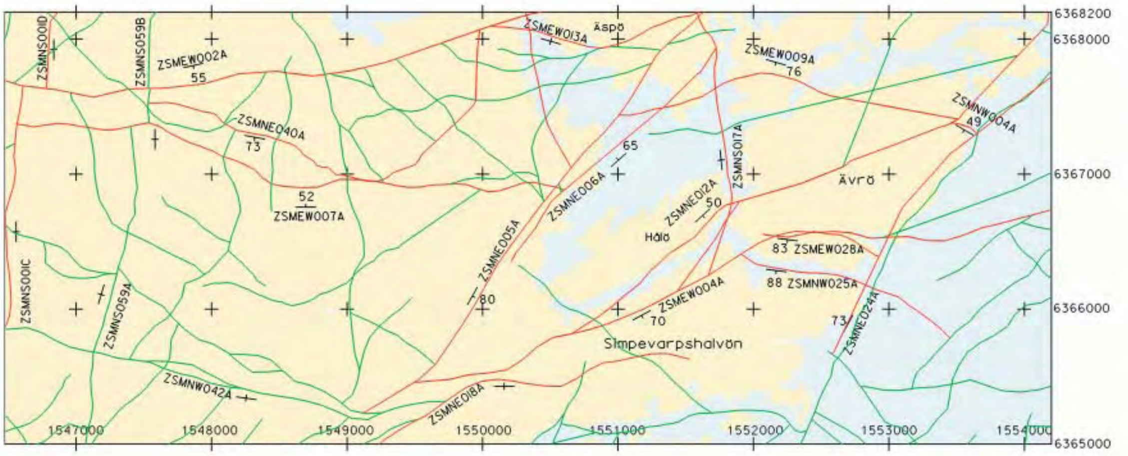

Figure 3-3. 2D map of deterministic deformation zones in the Simpevarp 1.2 model within the local model volume. Green color show zones with low confidence in existence, whereas red color show zones with high confidence in existence.

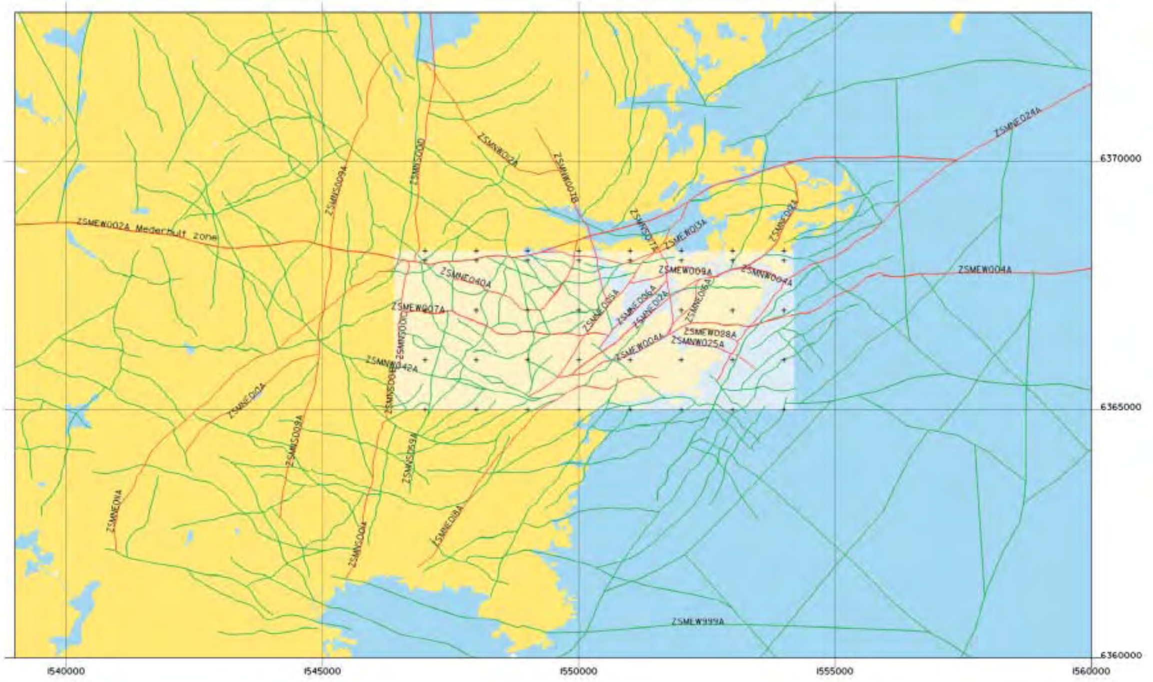

Figure 3-4. *2D map of deterministic deformation zones in the Simpevarp 1.2 model within the regional model domain. Green color show zones with low confidence in existence, whereas red color show zones with high confidence in existence.*

3.3.6 Regional orientation model development

Regional orientation models were developed through the analysis of detailed fracture mapping of four outcrops within the Simpevarp subarea and two outcrops within the Laxemar subarea. Fractures were pre-assigned into one of five global sets based on their membership in local outcrop sets of similar orientations. FracsSys/ISIS was then used, through a single-iteration hard-sector search, to derive distribution parameters for the aggregated outcrop sets. Set membership was not free to vary.

The regional orientation models are coupled to the outcrop-scale orientation analysis; the outcrop-scale sets are used, in conjunction with deformation zone orientations and bedrock structure, to produce a regional model that is valid at all scales. The goal of the regional outcrop model is to identify fracture sets that capture as much of the general variability in fracture orientations as possible with as few simple sets.

The SDM Laxemar 1.2 DFN model uses only Univariate Fisher spherical probability distributions for regional fracture set orientations (local set orientation Model 1) despite the fact that they are not always statistically significant or the most statistically significant; this is due to technical requirements of downstream model users. Alternative spherical probability distributions (Bivariate Bingham, Bivariate Fisher) were also considered (but not implemented); at the local scale (local set orientation Model 2), these distributions tended to show better statistical fits to observed data for some of the sets.

3.4 Size analysis

3.4.1 Local deterministic sets

Initial fracture size analyses were performed on each fracture set identified by the set assignment analysis. A non-linear optimization process was used to calculate the parameters (e.g. mean, standard deviation) for a probability distribution model (e.g. lognormal) that best reproduces the observed trace length statistics. This was accomplished using the FracSize algorithm in FracMan Version 2.606, which is used to fit a fracture radius model to each of these sets using the orientation model derived from the ISIS analysis /Dershowitz et al. 1998/.

In addition, this approach requires the specification of a sampling surface, referred to as the trace plane, upon which the fracture trace data was recorded. Trace planes were created using ArcView by calculating the surface normal to a hypothetical 'best-fit' planar surface visually aligned to major outcrop features. A rectangular polygon was then constructed with an orientation parallel to that of the outcrop, with a size just large enough to enclose the mapped outcrop perimeter. The corner coordinates were exported as a text file, and converted to a FracMan sampling structure (*.SAB) control file using SamEdit.

Next, a probability distribution type was selected for the fracture radius probability density function. A synthetic fracture set composed of discs with an initial "guess" of mean and standard deviation (or other appropriate parameters) was generated and intersected with a plane representing the outcrop surface. This intersection produced a set of trace lengths that can be compared with the measured trace lengths. All synthetic fracture sets were generated using the full outcrop trace plane area (which is slightly larger than the dimensions of the outcrop to prevent edge effects), and then removing all traces less than 0.5 m from the calculations. Note that the statistical fit to the distribution may suggest a minimum radius (x_{r0}) smaller than 0.5 m; however, all fits to the distribution are made only against fractures larger than the 0.5 m radius truncation.

Through a Simulated Annealing optimization routine /Press et al. 1992/, values of the mean and standard deviation were iterated until a statistically significant match was achieved. This process was repeated for several probability distribution functions, including lognormal, power law (Pareto), normal, exponential and uniform. The optimization process was performed so as to minimize the Kolmogorov-Smirnov (K-S) statistic, which is based on the single worst match in the cumulative probability distribution. Optimization through K-S minimization produces size distribution matches that minimize the maximum difference between the actual and theoretical cumulative probability distribution /Dershowitz et al. 1998/.

In the case where a statistically-significant (at the $\alpha = 0.1$ level) match between outcrop and simulated data was not reached, the 'closest match', based on the general shape of the cumulative density function (CDF) and both the K-S and Chi-squared test statistics, was chosen. Most of the local fracture sets identified within the Simpevarp sub-region outcrops fell into this category. The lack of a statistically-significant fit was most likely due to sampling a too-small slice of the parent distribution; local set fits could be improved by sampling larger outcrop areas to capture the upper end of the size curve, or by sampling fractures smaller than the 0.5 m size cut-off dictated by the outcrop mapping protocol. However, a better estimate of the lower tail of a positively skewed distribution is unlikely to provide much improvement; additional observations in the upper tail are far more important for reducing the uncertainty in the estimates of the mean and standard deviation /Aitchison and Brown, 1963/.

3.4.2 Regional deterministic sets

The second method, applied to deformation zone-related outcrop sets, was to calculate an area-normalized trace length frequency plot. This was done by combining trace lengths from outcrop and deformation zones for the same set, and fitting a scaling function to them. It should be noted that not all of the regional deterministic fracture sets are related to deformation zones; for those sets, size distributions were calculated by aggregating the outcrop data into single sets and performing a FracSize analysis, as described in Section 3.4.1.

In the trace length scaling analysis, the number of fractures greater than or equal to a particular trace length was plotted as a function of trace length. Since the number of fractures relates to the size of the map area, the number needs to be normalized for this effect in order to plot data gathered from different sized exposures.

A simple way to compensate for different map areas among the data sets is to divide each data set by the map area. This procedure assumes that doubling the area of the outcrop or map would lead to a doubling of the number of traces. This type of intensity scaling, in which the number of fractures is directly proportional to area, is Euclidean in nature and not fractal. The manner in which the fracture intensity scales with area can be quantified by the Mass Dimension of the fracture traces (Equation 3-1). When the Mass Dimension of the traces has a value of 2.0, the intensity (number of fractures per unit area) scales proportionately to area, and the spatial pattern of traces can be characterized by a Poissonian density function which inherently has no spatial correlation among the fractures.

It is possible that the intensity scaling of fractures is better described by a fractal model /La Pointe et al. 2002/. In this type of model, intensity varies according to:

$$N(r) = \rho * r^{D_m} \qquad \text{Equation 3-1}$$

where ρ is a constant, termed the prefactor,

r is the radius of a circle

D_m is the Mass Fractal dimension, and

N(r) is the number of fracture traces (partial or entire) contained within the circle of radius r.

The computation of the mass dimension can take several distinct forms, such as the scaling properties of fracture center points or random points selected along the fracture trace, of the number of traces (P_{20}) themselves, or of the P_{21} (fracture trace length per unit area) measure of fracture intensity. All are useful for certain purposes. For size-scaling analysis, the desired parameter is how the number of fractures (P_{20}) changes with scale.

The procedure for calculating the mass dimension is illustrated in Figure 3-5. The value for D_m in Equation 3-1 is equal to the slope of the line when the data are plotted on doubly logarithmic axes. The value of the prefactor is equal to the ordinate value corresponding to a circle with radius = 1.0, and can be read directly from the graph It is important to make this calculation on individual sets rather than all of the traces at once, as each set may have different scaling properties.

The methodology for analyzing the size of deformation zone-related fracture sets has been presented by /La Pointe, 2001/ and consists of a two-stage process. The first stage is to determine how fracture intensity for an individual fracture set scales with area. The second stage is to use this information to commensurate fracture trace data acquired over regions of different area.

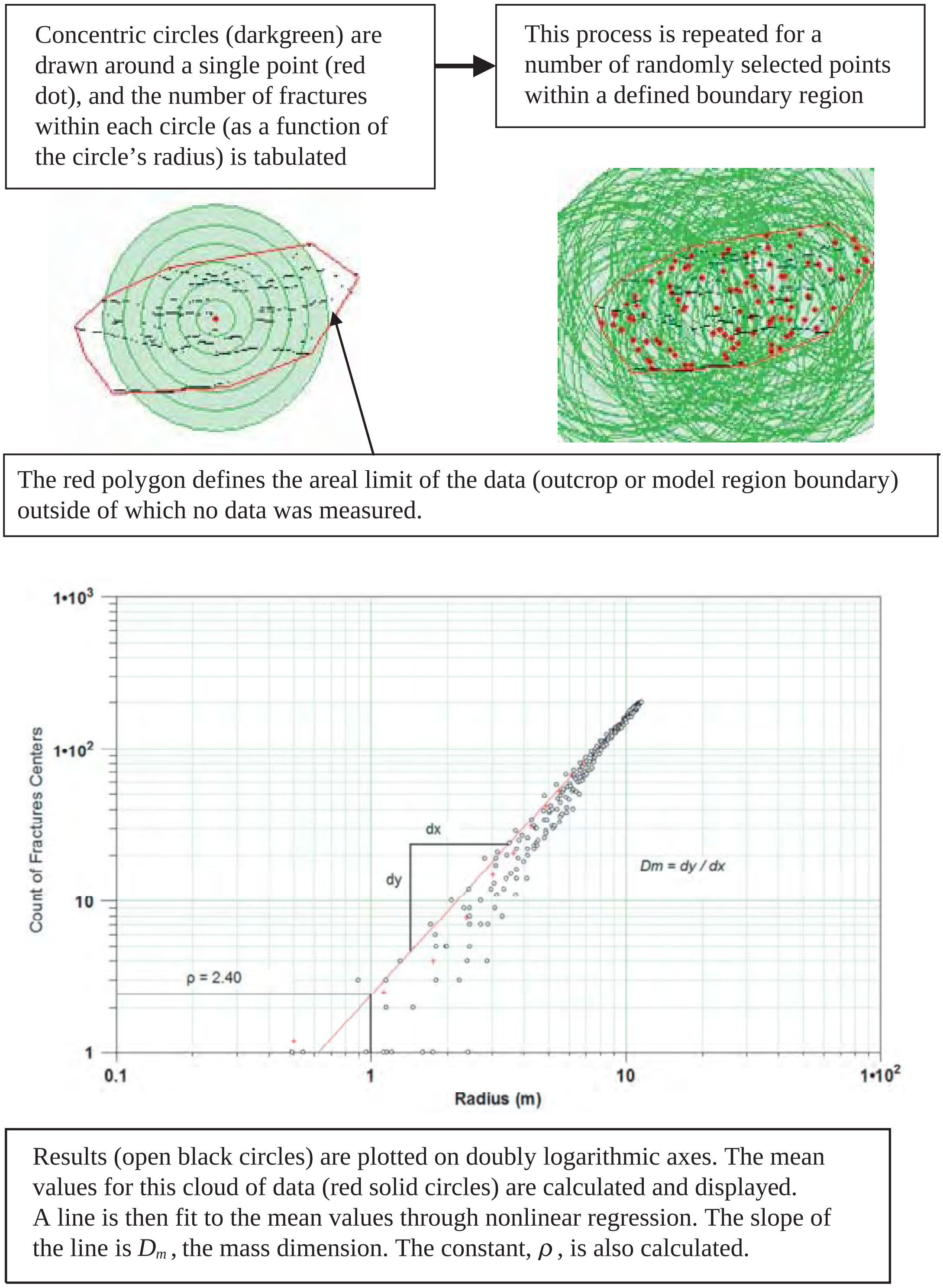

Figure 3-5. *Workflow for calculating the mass dimension from maps of fracture traces.*

The goal of this analysis is to relate the number of fractures of a given trace length measured over an area, A_i, to the number of fractures of the same size class measured over an area, A_j, of a different size. A simple way of resolving this issue is to assume that the number of fractures in a particular size class scales with area; if the area is doubled, the numbers of fractures are doubled. When the number scales linearly with area, as in this example, the scaling is termed Euclidean.

The calculation of the fractal mass dimension is used to determine whether Euclidean, Fractal or some other function best characterizes the scaling behavior of each individual deformation zone-related fracture set. The mass dimension exponent can vary from 2.0, which indicates Euclidean scaling, to lower values that imply that the traces scale in a fractal manner.

The procedure is to calculate and plot the cloud of mass dimension data points, as in Figure 3-5, and then compute a nonlinear least-squares fit of the Pareto equation to the locus of the mean, and then finally to test for statistical significance. If the regression is found significant for $\alpha = 0.05$, then the regression is deemed significant and the scaling is treated as fractal. The calculations are always performed on the data set with the least censoring on the small trace end of the distribution, as censoring produces an underestimation of the number of fractures per unit area. For this reason, the mass dimensions were always calculated on the outcrop trace data rather than the deformation zone data.

The second stage is to use these results to combine data obtained over regions of very different area. The process is as follows:

Let the "o" subscript denote outcrop fractures, and the "l" subscript denote deformation zones. Furthermore, let the variable "A" denote the area of the outcrop or deformation zone map, and "R" denote the radius of an imaginary circle that would have the same area as "A". Also, let "x" represent the trace length of a fracture. Then, from Equation 3-2, it is possible to calculate the number of fracture traces that would be expected in the deformation zone map area based on what was measured in the outcrop area, or:

$$A_l = \pi R_l^2$$

$$\text{So } R_l = \sqrt{\frac{A_l}{\pi}} \qquad \text{Equation 3-2}$$

$$\text{and } N(R_l) = \rho R_l^{D_m}$$

Equation 3-3 makes it possible to compensate for the difference in area by computing a normalization factor NF that is the ratio of the number of fracture traces measured in outcrop to the number estimated in Equation 3-2:

$$NF = N(R_o) / N(R_l) \qquad \text{Equation 3-3}$$

This equation also describes how many fractures would be expected in an area of any size, for example, a reference area of 1 square meter.

It is easiest when comparing multiple data sets to reference all of them to an easily converted reference scale like the number of fractures per square meter. In this case, Equation 3-3 becomes:

$$NF_i = N(R_i) / N\left(\sqrt{\frac{1}{\pi}}\right) \qquad \text{Equation 3-4}$$

where NF_i is the correction factor for converting the number of fractures actually measured in a domain, I, to the reference domain;

$N(R_i)$ is the number of fracture traces measured in domain i; and

$N(\sqrt{1/\pi})$ is the number of fractures estimated from Equation 3-2.

To construct the plot, the trace lengths actually measured in the domain are ordered from shortest to longest. Each trace is numbered according to its cumulative frequency. If there were 50 traces, then the shortest trace would be assigned the number 50, indicating that there are 50 traces greater than or equal to the length of this shortest trace. The second shortest trace would be assigned the number 49, and so on through the longest trace in the data set, which would have a complimentary cumulative frequency of 1. More generally, if k_i fracture traces were measured in domain I, then the shortest trace has the cumulative frequency value of k_i, and the next longest has the value of k_i –1, and so on such that the longest trace measured has the value of 1. Next, these cumulative frequency numbers are each divided by NF_i. The values are plotted with the normalized cumulative frequency value on the ordinate (Y-axis), and the trace length value on the abscissa (X-axis) as shown in Figure 3-6.

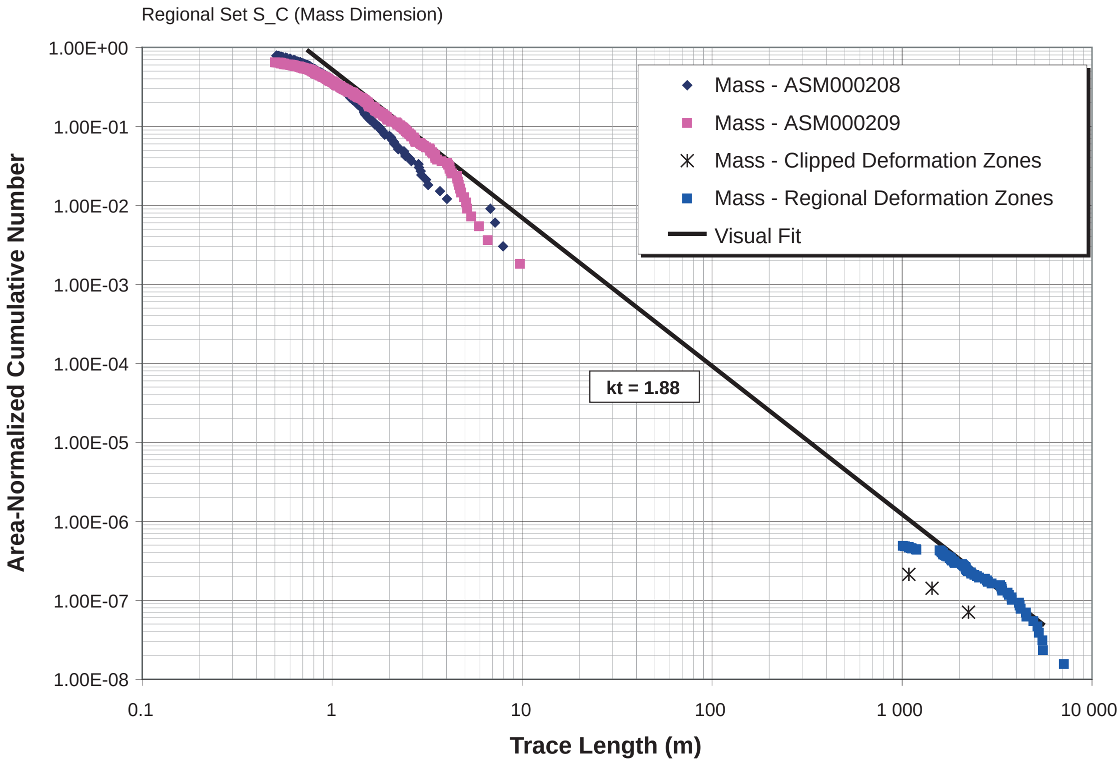

Figure 3-6. *Example trace length model estimation plot resulting from fractal mass dimension normalization of fracture intensity with area. Plot shown is for regional set S_C, Laxemar-sub region, and shows the results of the normalization outcrop sets and deformation zones within both the Simpevarp local model volume, and the Oskarshamn regional area.*

In order to distinguish between the parameters for the various power law distributions used in this report, the following nomenclature is adopted:

Table 3-1. Power-law distribution nomenclature.

Distribution name	Parameter 1	Parameter 2
Mass Dimension	ρ (prefactor)	D_m (mass dimension)
Cumulative number of trace lengths	t_{0n} (coefficient)	k_t (trace length exponent)
Trace length CCDF	x_{0t} (coefficient)	k_t (trace length exponent)
Radius CCDF	x_{0r} (coefficient)	k_r (radius exponent)

Note that Parameter 2 for both the cumulative number of trace lengths and the trace length CCDF are identical. The equation of the black line shown in Figure 3-6 conforms to a power law. The complementary cumulative number (CCN) plot shown in Figure 3-6 represents the number of traces, per unit area, greater than or equal to a specific trace length:

$$Number/area(x \geq t_{0n}) = \left(\frac{t_{0n}}{x} \right)^{k_t} \qquad \text{Equation 3-5}$$

The value of t_{0n} corresponds to a trace length of which it is expected that there is only one of them per unit area of this length or longer. Note that the relation depicted in Figure 3-6 does <u>not</u> describe a probability distribution, but rather a cumulative number distribution. The parameter k_t is the slope of the black line on Figure 3-6, and the parameter t_{0n} is the abscissa value that corresponds to the ordinate value of 1.0.

It is possible to calculate a probability distribution from the cumulative number distribution, but this requires fixing the value of x_{0t} or x_{0r}, as described in Section 3.5.3 This probability density (CCDF) function for trace lengths, which is quantified by this line, has the functional form:

$$\text{Prob}(X \geq x) = \left(\frac{x_t}{x} \right)^{k_t} \qquad \text{Equation 3-6}$$

where x_t is the minimum trace length;

x is any trace length greater than or equal to x_n;

k_t is the Trace Length Dimension.

The value of x_{0t} is not the same as t_{0n}. x_{0t} corresponds to a minimum trace length, and is not calculated from t_{0n}. x_{0r} and x_{0t} are related, however, as are k_r and k_t /La Pointe, 2002/, according to Equation 3-7:

$$k_r = k_t + 1.0$$
$$x_{0r} = x_{0t} * \frac{2}{\pi} \qquad \text{Equation 3-7}$$

This equation implies that the exponent describing the radius CCDF can be calculated from the slope of the cumulative number plot by simply adding 1.0 to the slope. The values of x_{0r} or x_{0t} are not calculated from the cumulative number plot, but are based either on the minimum fracture trace or radius required in the simulation. The methods for calculating P_{32} for a specific combination of minimum fracture size and power-law exponent, as well as a method for re-adjusting P_{32} values for different minimum sizes, are described in Section 3.5.3.

Note also that the exponent of the parent radius distribution is sometimes specified by a parameter, b, often termed the Pareto Exponent. This exponent is related to the trace dimension in Equation 3-8 as:

$$k_r = b - 1 \qquad \text{Equation 3-8}$$

Those using results from these analyses should be aware of which convention is being used in the specification of the radius distribution model parameters in their particular application. Also note that the parameter k_t is not the same as the mass fractal dimension, D_m! They are, in fact, independent parameters.

The value for the minimum radius value for each regional set can be derived by simultaneously fitting a size and intensity model that matches intensity values from boreholes, outcrops and the large-scale deformation zones. It is based upon the following considerations:

1. The outcrop trace data does not include fractures with traces shorter than 0.5 m.
2. The Deformation Zone trace data does not include traces shorter than 1 km.
3. The Deformation Zone fracture model has a vertical thickness of 1,100 m.
4. Fractures recorded in boreholes are generally those that are fully penetrating.
5. The size distribution for the fractures is approximated by a power law with two free parameters: k_r and x_{0r}.

The workflow is as follows:

1. Estimate P_{32} from Borehole P_{10} assuming zero-width boreholes (P_{32bh}).
2. Determine P_{32bh} percentiles ($\%P_{32bh}$) for each regional set, rock domain and subarea.
3. Determine P_{32} for regional fractures (lineaments) that belong to a set with a power-law relationship to mapped regional deformation zones (P_{32dz}).
4. Calculate minimum fracture radius corresponding to 1 km trace length (x_{0dz}).
5. Using the selected values of the borehole $\%P_{32bh}$ and fixed values of k_r and P_{32dz} for each regional set, rock domain and subarea, calculate values of x_{0r} pertaining to each $\%P_{32bh}$ percentile value.
6. For each triplet of $\{\%P_{32bh}, k_{ri}, x_{0ri}\}$, build a DFN model with 5 realizations and insert a relevant outcrop.
7. Calculate P_{21} for outcrop traces with lengths < 0.5 m removed (P_{21T}).
8. Determine which pair $\{\%P_{32bh}, x_{0ri}\}$ produces a P_{21T} that best matches the measured value in outcrop. This pair simulataneously matches the borehole, outcrop and deformation zone intensity and trace length scaling parameter values.
9. Evaluate the value of $\%P_{32bh}$ that produced the best match in terms of its percentile value. If this value is a very low or very high percentile, then geological explanations for this value should be in spatial proximity with known or inferred regions of higher or lower than average fracture intensity. If they are not, this result should be noted for possible further consideration.

3.5 Intensity analysis

Fracture intensity can be quantified by several measures, including the number of fractures per unit length (P_{10}), the number of fractures per unit area (P_{20}), the amount of trace length per unit area (P_{21}), and the amount of fracture surface area per unit volume of rock (P_{32}). The parameter P_{32} is often the most useful way to describe fracture intensity in a stochastic DFN model, as it is a volumetric property independent of sample orientation, and under certain common circumstances, scale-independent or nearly so. Scale independence occurs when the spatial pattern of the fractures are uncorrelated (Poissonian). In a fractal spatial pattern, intensity does depend upon scale, but the effect is often small unless the scale range spans several orders of magnitude. Intensity can be scaled using the Mass Dimension as illustrated in Section 6.4.

However, P_{32} is not measured in the field; usually only values of P_{10} from boreholes or P_{21} from outcrop maps are available. Fortunately, it is possible to estimate P_{32} from either P_{10} or P_{21} through simulation. Thus, the procedure to calculate fracture intensity involves first determining geological controls on P_{10} and/or P_{21}, and then converting these values to values of P_{32}.

3.5.1 Determination of geologic controls on fracture intensity

The determination of geological controls on fracture intensity relies upon comparing fracture intensity from boreholes with borehole geology, and subsequent evaluation of possible controls with intensity variations in outcrop. The boreholes form the primary source of data since:

1. They provide a record of fracturing from the surface or near-surface to beyond the depth of the proposed repository.
2. There are large volumes of fracture data from the boreholes, leading to better statistical power for hypothesis testing.
3. The boreholes encounter a wider variety of geological settings than do the outcrops.

Outcrop fracture data is much more limited. However, borehole data may be biased towards subhorizontal fracturing and hence be better suited for investigating controls on subhorizontal fracture intensity. Possible biases towards subhorizontal fracturing in boreholes were investigated by separating fractures into subhorizontal and subvertical sets, to assess if there were any significant differences. The determination of subvertical versus subhorizontal set membership was made, based on orientation set membership and by a visual assessment of the fracture pole data for each outcrop. As such, the cutoff angle varies slightly between outcrops, but is generally around 35–40° dip.

Three approaches were used to evaluate spatial trends in fracture intensity: by plotting the moving average (Figure 3-7) of the one-meter bin size fracture intensity data shipped from SKB (p_freq_1m) over a five-meter window, by calculating the number of fractures per unit length (P_{10}) for varying interval sizes, and through Cumulative Fracture Intensity (CFI) plots (Figure 3-8). For the first option, only the 1 m bin size data was analyzed. Initial plots of other bin sizes (3 m, 5 m) added little to the determination of zones of higher and lower fracture intensity while sacrificing a level of detail. The moving average calculation was centered on the zone of interest (i.e. symmetric) as opposed to a forward- or backwards-forecasting average. The second approach consisted of specifying a fixed interval length, and then dividing the number of fractures by the interval length. This method can be very sensitive to the interval length selected, and there are no simple procedures to ascertain what the most useful length might be.

The CFI plots do not have the interval-length limitations imposed by the first two analysis options, and they have a different purpose: to identify large-scale domains of homogenous fracture intensity rather than to detect smaller-scale zones of intense fracturing. These plots are constructed by sorting the fracture data by measured depth (MD) or true vertical depth (TVD or TVDSS), starting either at the top or the bottom of the borehole. The depth value is the ordinate in the CFI plot. Next, the fractures are numbered from 1 to n, where n is the total number of fractures that are to be plotted. These numbers are divided by n, such that the 1st fracture has the abscissa value of 1/n, the 2^{nd} fracture has the value 2/n, continuing to the last fracture, which has the value of n/n or 1. The CFI plots are chosen prior to non-cumulative plots or histograms as they represent better tools for the identification of intervals of more or less constant fracture intensity and of geological controls on intensity.

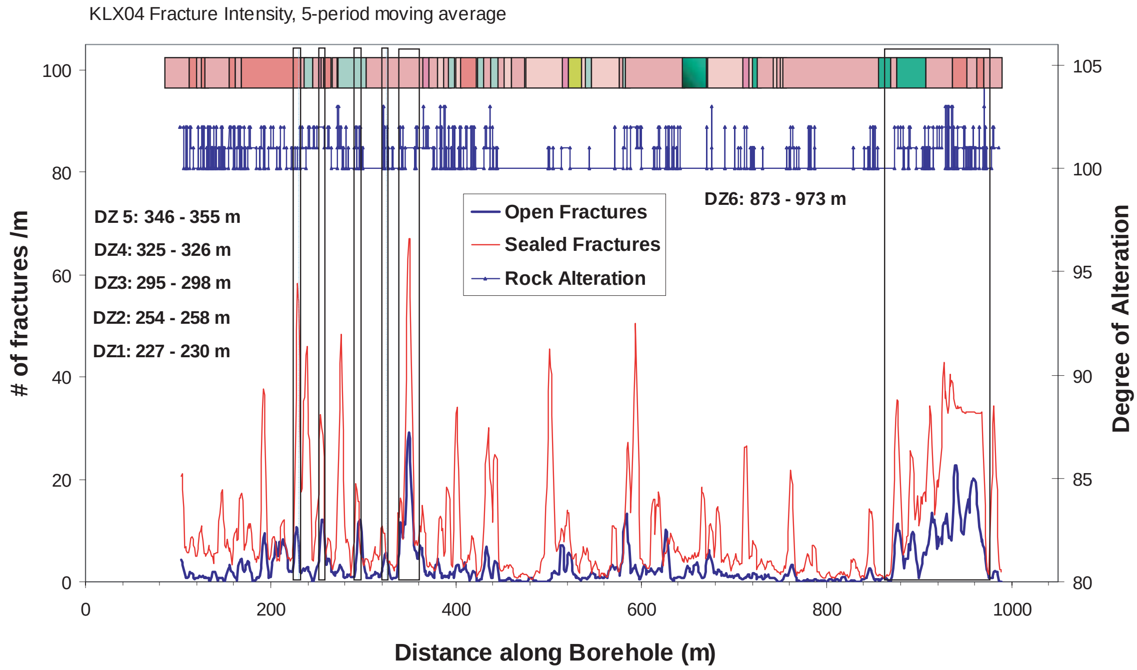

Figure 3-7. *Moving average plot for 1 m binned fracture intensity data for borehole KLX04, Laxemar subarea. Several geologic parameters (lithology, degree of alteration) are superimposed to offer insights as to potential intensity controls. Locations of deformation zones are taken from the single-hole interpretations.*

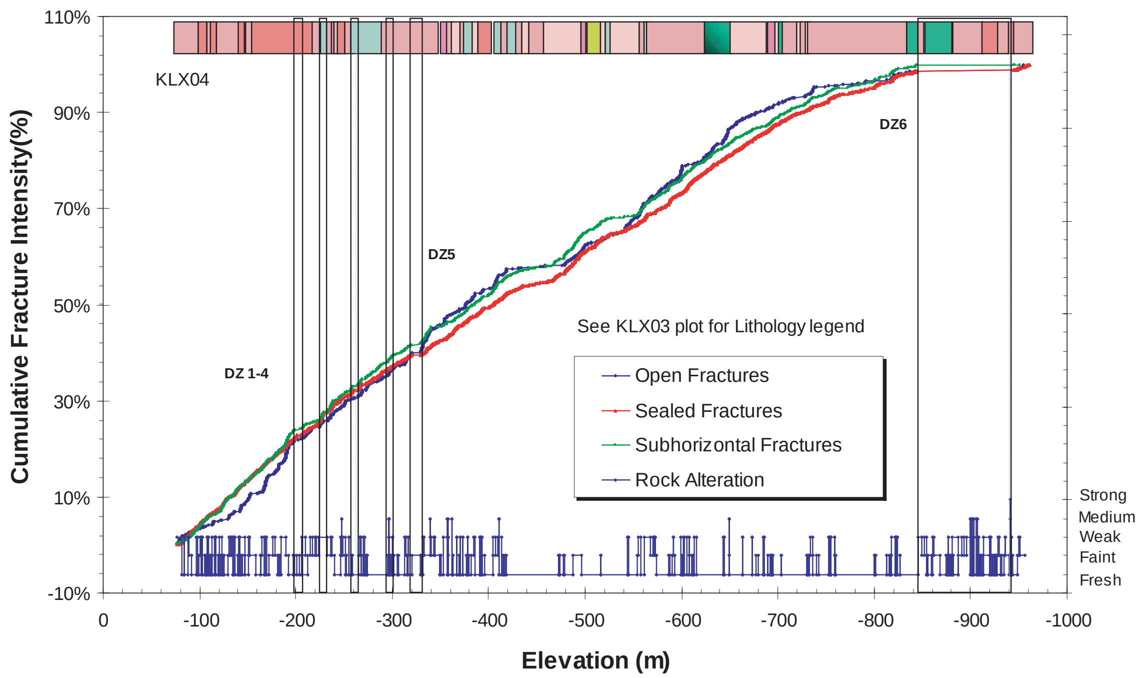

Figure 3-8. *Cumulative fracture intensity (CFI) plot for borehole KLX04, Laxemar subarea. Several geologic parameters (lithology, degree of alteration) are superimposed to offer insights as to potential intensity controls. Locations of deformation zones are taken from single-hole interpretations.*

Fracture frequency along a borehole is not only a property of the rock, but also, importantly, of the borehole orientation and diameter. There is no inherent difference in constructing a CFI plot using MD, TVD or TVDSS; they all give the same answer, because their purpose is to delineate spatially contiguous zones along the borehole of homogeneous fracture intensity. It does not matter if the boundaries of zones are identified by MD, TVD or TVDSS. CFI plots can be constructed using any of these axes, the choice depending upon other considerations.

In the process of building the DFN model, the P_{10} values for each domain are converted to a P_{32} value for the domain for comparison with geological factors such as lithology or alteration. It is far easier to convert the P_{10} from measured depth, rather than to try to convert the pseudo-P_{10} intensity representing the number of fractures per vertical distance from an inclined borehole, and so an MD ordinate is preferable. On the other hand, when intensity is being displayed with other data on a single plot, it may be preferable to present the CFI plot in terms of TVDSS, as in Figure 3-8.

In the CFI plot, portions of the line that have constant slope indicate where the fracture intensity has a constant value. Shallow slopes indicate lower intensity, while steeper slopes indicate higher intensity. The ranges of depth values over which the line maintains constant slope indicates domains of constant fracture intensity. Surface stress-relief effects leading to higher fracture intensities, for example, would manifest themselves as a domain extending down from the surface possibly a few tens of meters, with a slope much shallower than found below in rock of similar geological character.

The intensity domains can also be compared to mapped geological factors such as lithology, alteration, mineral infilling and other variables to see if zones of consistently higher or lower intensity correspond to specific geological characteristics.

The fracture frequency analysis was carried out in two steps: superimposition of the CFI plots on graphical displays of geological variables to formulate testable hypotheses regarding possible geological controls; and statistical testing and analysis to refute or buttress the hypotheses. The statistical tests employed standard parametric and non-parametric tests of confidence intervals about the mean and median, tests to examine the similarities of means and medians among groups, and linear regression.

The evaluation of whether alteration degree or lithological unit was associated with variations in fracture intensity was carried out using the non-parametric test Eta test /Garson, 2004/. Eta is a measure of association that ranges from 0 to 1, with 0 indicating no association between the row and column variables and values close to 1 indicating a high degree of association. Eta is appropriate for a dependent variable measured on an interval scale (for example, fracture intensity) and an independent variable with a limited number of categories (for example, lithology or alteration). Two Eta values are computed: one treats the row variable as the interval variable; the other treats the column variable as the interval variable. Eta is often interpreted to show what percentage of the variation is explained by the categorical variable.

Additional analyses involved the construction of depth vs orientation plots to see if orientation distributions and intensities remained constant within each domain or whether these are zones with distinct orientations, such as the absence of a set or the addition of a new set.

3.5.2 Estimation of P_{32} from P_{10} or P_{21}

The approach for calculating P_{32} from P_{10} or P_{21} requires simulation. The relation between P_{32} and the measurable fracture intensity quantities is given by:

$$P_{32} = C_1 P_{10} \text{ AND } P_{32} = C_2 P_{21} \qquad \text{Equation 3-9}$$

where the constants C_1 and C_2 depend only upon the orientation and diameter of the borehole and the orientation distribution of the fracture set. The goal of the simulations is to estimate C_1 if borehole data are being used and C_2 if outcrop data are used.

The first step is to create a DFN model with the same orientation statistics as the fracture set of interest. Next, a borehole or outcrop surface is inserted into the model with the same geometry as the borehole or outcrop for which actual data has been obtained (Figure 3-9).

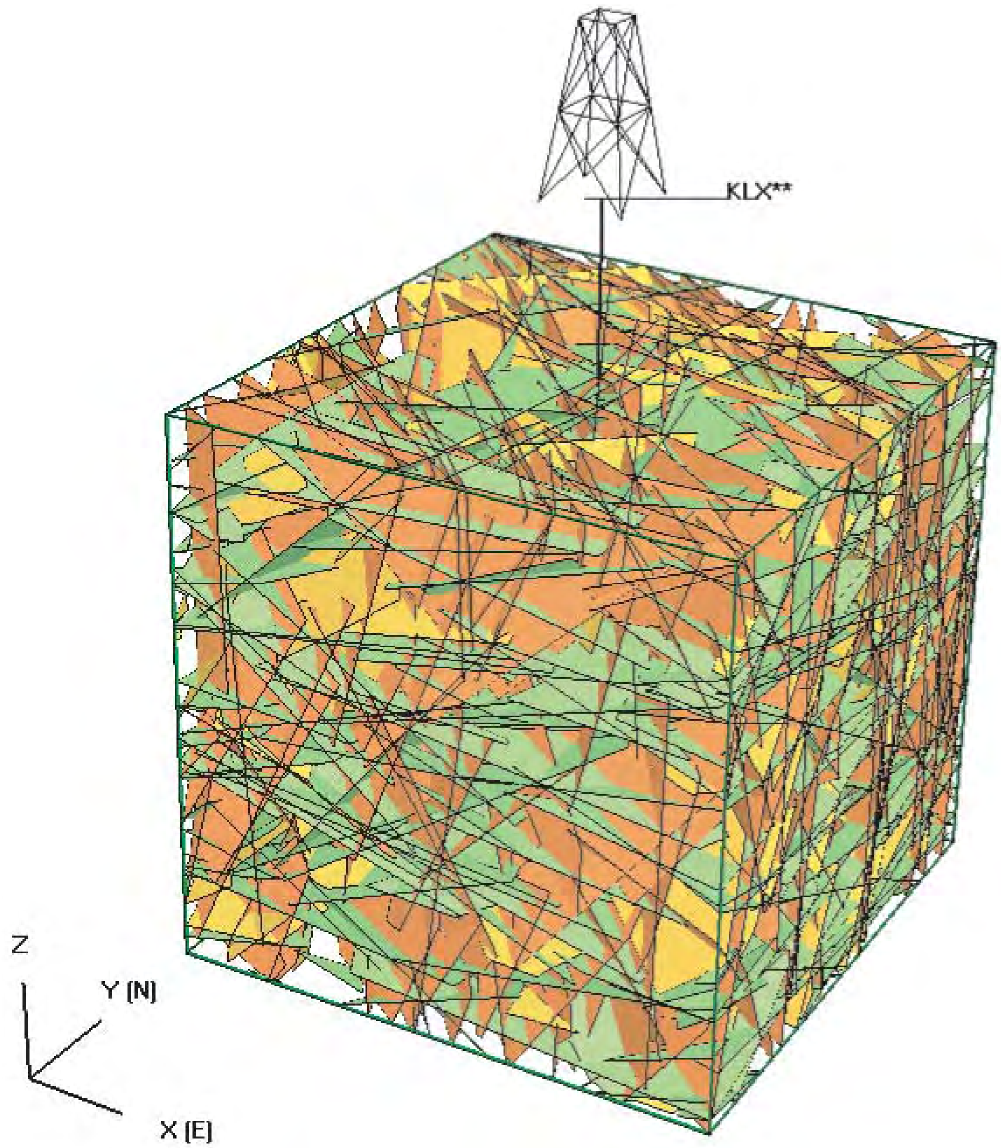

Figure 3-9. *Example DFN simulation used to estimate constant relating P_{10} to P_{32}.*

A guess for P_{32G} is made so that a statistically significant number of fractures in the simulation intersect the borehole. This results in a value of P_{10G} or P_{21G}. This computation for a specific P_{32G} is simulated as a Monte Carlo process for at least 25 realizations. The constant is estimated as:

$$E\left[C_1\right] = \frac{P_{32G}}{\langle P_{10G} \rangle} \qquad \text{Equation 3-10}$$

and similarly for C_2, where E[ ] denotes the expected value of the quantity in brackets, and ⟨ ⟩ represents the average value of the Monte Carlo realizations.

The value of the conversion factor between P_{21} and P_{32} when traces below a specified size have not been measured depends upon the specified minimum size and exponent for a power law CCDF. In other words, the form and parameter values of the size distribution model are important when the observed trace length distribution has been truncated. The amount of P_{21} that is removed by applying a threshold trace length size is sensitive to the distribution form (power law, lognormal, etc), and so the form of the distribution and its specific parameters become important. If there is no trace length sampling truncation applied, then the factor relating P_{32} to P_{21} does not depend upon either the form of the radius distribution or on its parameter values.

The workflow for calculating the conversion factor is as follows: For any specified value of kr, it is possible to find a combination of x_{0r} and P_{32} that will exactly match a value of P_{21} in which the measured and simulated traces have been excluded if they are shorter than L_t. In other words, the determination of P_{32} is not unique because there are two degrees of freedom, x_{0r} and P_{32}, and only one parameter to match, the truncated value of P_{21}.

However, it is possible to introduce a second constraint to make the solution unique. In this report, the second constraint is a value of P_{10} from boreholes in the same rock domain as the outcrop. A simultaneous match to the borehole P_{10} and the outcrop P_{21} does provide a unique set of values for x_{0r} and k_r.

The procedure for obtaining this unique match is not automated. First, a set of values for x_{0r} and P_{32} are selected as initial guesses. A series of realizations are run using these values. A trace plane or planes, representing the approximate size, shape and orientation of the outcrops are inserted into each DFN realization, and the resulting traces, truncated at L_t, are recorded. The mean value of the truncated P_{21} is compared to the target value of the measured P_{21}. This ratio is used to calculate the value for C_2 in Equation 3-9. The value of C_2 is then multiplied by the measured value of P_{21} from the outcrops to derive a new value of P_{32}. This process is repeated two or three times until a value of P_{32} is found that matches the truncated value of P_{32} for the specified combination of x_{0r} and k_r.

The second step is to then insert the target boreholes into the DFN realizations and calculate the value of P_{10} for the simulations. If the simulation P_{10} is too low, this implies that the value of x_{0r} is probably too large. If the simulation P_{10} is too high, then the value of x_{0r} is probably too small. The value of x_{0r} is re-adjusted based on the comparison between the simulation P_{10} and the measured P_{10}. Then the entire process starts over at Step 1, with a new P_{32} being determined and tested. In practice, it takes about four or five iterations in order to simultaneously match a truncated P_{21} and a borehole P_{10}.

This process does not guarantee that the values for x_{0r} for the various sets will be the same; in fact, it is likely that they will differ, reflecting differences in both size and intensity among the sets. The values reported in Section 6.2 are for a specific combination of k_r, x_{0r} and L_t.

3.5.3 Estimating P_{32} for different values of x_{0r}

If a different value for the minimum size is needed for a particular application, it is relatively straightforward to calculate the adjusted value of P_{32} that corresponds to this new value. If the new minimum radius size is denoted by x_1, a new maximum radius size by x_2, and the new adjusted value of intensity is denoted by P_{32ad}j, then:

$$t(x) = \left(\frac{k_r x_{0r}^{k_r}}{x^{k_r+1}}\right) * \pi x^2 \qquad \text{Equation 3-11}$$

$$T(x_{1r}, x_{2r}) = \int_{x_{1r}}^{x_{2r}} t(x)\partial x \qquad \text{Equation 3-12}$$

or

$$T(x_{1r}, x_{2r}) = \frac{\pi k_r x_{0r}^{k_r}}{2-k_r}\left[x^{2-k_r}\right]_{x_{1r}}^{x_{2r}} \qquad \text{Equation 3-13}$$

where t(x) is the fracture area density function for a fracture of radius x;

T(x) is the total area of all of the fractures;

x_{1r}, x_{2r} are, respectively, any minimum and maximum radius values.

All other parameters are as previously explained.

Now these equations hold for any minimum and maximum fracture radius. Therefore, the original P_{32} for fractures with radii from x_{0r} to ∞ is:

$$T(x_{0r}, \infty) = \frac{\pi k_r x_{0r}^{k_r}}{2-k_r}\left[x^{2-k_r}\right]_{x_{0r}}^{\infty} = -\frac{\pi k_r x_{0r}^{2-k_r}}{k_r-2} \qquad \text{Equation 3-14}$$

and

$$T(x_{1r}, x_{2r}) = \frac{\pi k_r x_{0r}^{k_r}}{2-k_r}\left[x^{2-k_r}\right]_{x_{1r}}^{x_{2r}} = \frac{\pi k_r \left[x_{2r}^{2-k_r} - x_{1r}^{2-k_r}\right]}{k_r-2} \qquad \text{Equation 3-15}$$

P_{32} relates to the radius distribution as:

$$P_{32} = \int_{x_{0r}}^{\infty} \bar{n} \frac{k_r\, x_{0r}^{k_r}}{x^{k_r+1}} \pi\, r^2 dr \qquad \text{Equation 3-16}$$

in which $\bar{n}$ is the average number of fractures per unit volume.

So the adjustment of P_{32} is the ratio of $T(x_{1r}, x_{2r})$ to $T(x_{0r},\infty)$ multiplied by the P_{32} corresponding to $T(x_{0r}, \infty)$:

$$P_{32}(x_{1r}, x_{2r}) = \frac{\dfrac{\pi k_r \left[x_{2r}^{2-k_r} - x_{1r}^{2-k_r}\right]}{k_r-2}}{\dfrac{-\pi k_r x_{0r}^{2-k_r}}{k_r-2}} * P_{32}(x_{0r}, \infty) = \frac{\left[x_{1r}^{2-k_r} - x_{2r}^{2-k_r}\right]}{x_{0r}^{2-k_r}} * P_{32}(x_{0r}, \infty) \qquad \text{Equation 3-17}$$

Note that $k_r > 2.0$ for Equations 3-14 to 3-16 to be valid. For values of $k_r \leq 2.0$, the correction must be done empirically through DFN simulation.

3.6 Spatial model

The location of the fractures is specified by a combination of the intensity and spatial models. For example, certain rock types have higher mean fracture intensities than others, but within each rock unit, the fractures are distributed according to the spatial model. Likewise, fractures related to deformation zones may have a zone of higher intensity around mapped deformation zones, but within this zone, they may be distributed according to a Poisson process. In this context, the spatial model describes how fractures vary within spatial domains of stationary intensity.

The spatial model is determined through the calculation of the mass dimension of the number of fractures per unit area (D_m) for outcrop trace data, and the number of fractures per unit length (P_{10}) for borehole data. The calculation of the mass dimension has previously been described in Section 3.4.2.

Outcrop trace data are used for calculating the spatial model for the subvertical fracture sets, as borehole data contain a bias that makes calculations for the subvertical sets in boreholes less reliable than the outcrop calculations. The borehole data is used to determine the spatial model in the vertical direction for all of the sets in the zones where intensity is stationary.

If the mass dimension has a value of 2.0 for trace data or 1.0 for borehole data, the fractures follow a Poisson distribution. Values less than 2.0 for trace data (less than 1.0 for borehole data) indicate a clustering process where there is some degree of spatial correlation among the locations of the fracturing. The failure of the data to approximate a straight line on the mass dimension plots indicates that the spatial model is something other than Poissonian or fractal. This would suggest that a further investigation of the spatial distribution of deformation zones and fracture sets is necessary, using a separate set of calculations and additional field data. The evaluation of additional spatial models (aside from Poissonian or fractal) is suggested as an additional task for further modeling efforts outside of the SDM Laxemar 1.2 DFN.

The workflow for the calculation of the spatial model passes in order to minimize unnecessary work and to produce the simplest model that adequately portrays the measured data.

The analysis starts with the calculation of the mass dimension from the fracture data in the cored boreholes according to Equation 3-1. Although Equation 3-1 is described in terms of circles on an outcrop, the circles in this case can be thought of as centred on the borehole, so that the circle diameter is mathematically equivalent to the interval length. Cored borehole fracture data from both the Simpevarp and the Laxemar modeling subareas was analyzed separately. In this calculation, the mean number of fractures for an interval of a specified length is calculated for interval lengths are varying from much less than the average fracture spacing, to sizes approaching half the borehole length. Very small intervals contain fewer fractures than large intervals. As the interval size decreases, the mean number of fractures per interval tends towards 1.0, and as the size continues to decrease, the mean number in an interval becomes independent of interval size. This flattening is essentially an artifact of the measurement resolution of fractures in the BIPS log or core. Very small interval sizes are purposely included in the calculation to identify where this artifact is obscuring the actual mass dimension of the data, as they are in the mass dimension of the outcrop traces. The onset of a constant, non-zero slope in the log-log plot of interval length vs mean number of fractures is the portion of the plot that best describes the scaling properties of the data. If this portion of the curve has a slope of approximately 1.0, then the data scales in a Euclidian manner. If there is a constant slope but it has a slope other (typically less than) 1.0, then it scales in a fractal manner. If it is not linear, then it may scale as a geostatistical model with second order stationarity, or even according to other scaling functions. If it scales either in a Euclidian or fractal manner, then the data is not tested for additional models, as these will fail.

4 Analysis of outcrop data

4.1 Outcrop ASM000209

Outcrop ASM000209 is located in the southwest corner of the Laxemar subarea, cf Figure 1-2 and spans approximately 446 square m in area. Lithologies exposed in the bedrock outcrop include diorite/gabbro (36%), granite to quartz monzonite, referred to as the 'Ävrö Granite' (61%), and dikes of fine- to medium-grained granite (3%), cf Figure 4-2. Minor quartz veining and mafic inclusions were also noted. The outcrop is oriented approximately north-south.

4.1.1 Outcrop data analysis

The SICADA database lists 1,044 fractures inside the mapping perimeter of ASM000209 above the minimum size threshold of 0.5 m; only 1,030 of these are present in the outcrop GIS files obtained from the SKB SDE database. Figure 4-1 (below) presents basic aggregated orientation data for all fractures within the outcrop, while Figure 4-2 illustrates the basic morphology and geology of Outcrop ASM000209.

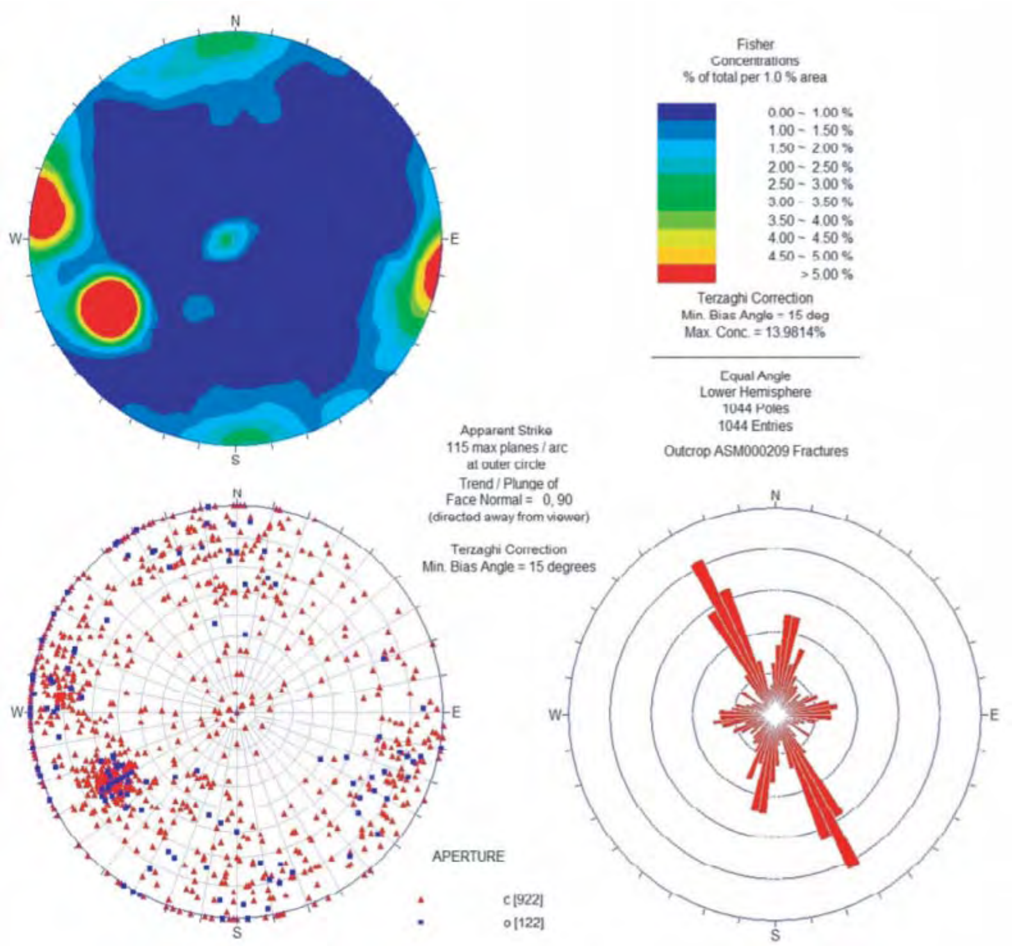

Figure 4-1. Fracture orientation data for outcrop ASM000209, Laxemar subarea. All data taken from SICADA database tables. Note that the Terzhagi correction assumes a horizontal planar outcrop. Symbolic pole plot represents fracture aperture; 'c' are sealed fractures, while 'o' are open fractures.

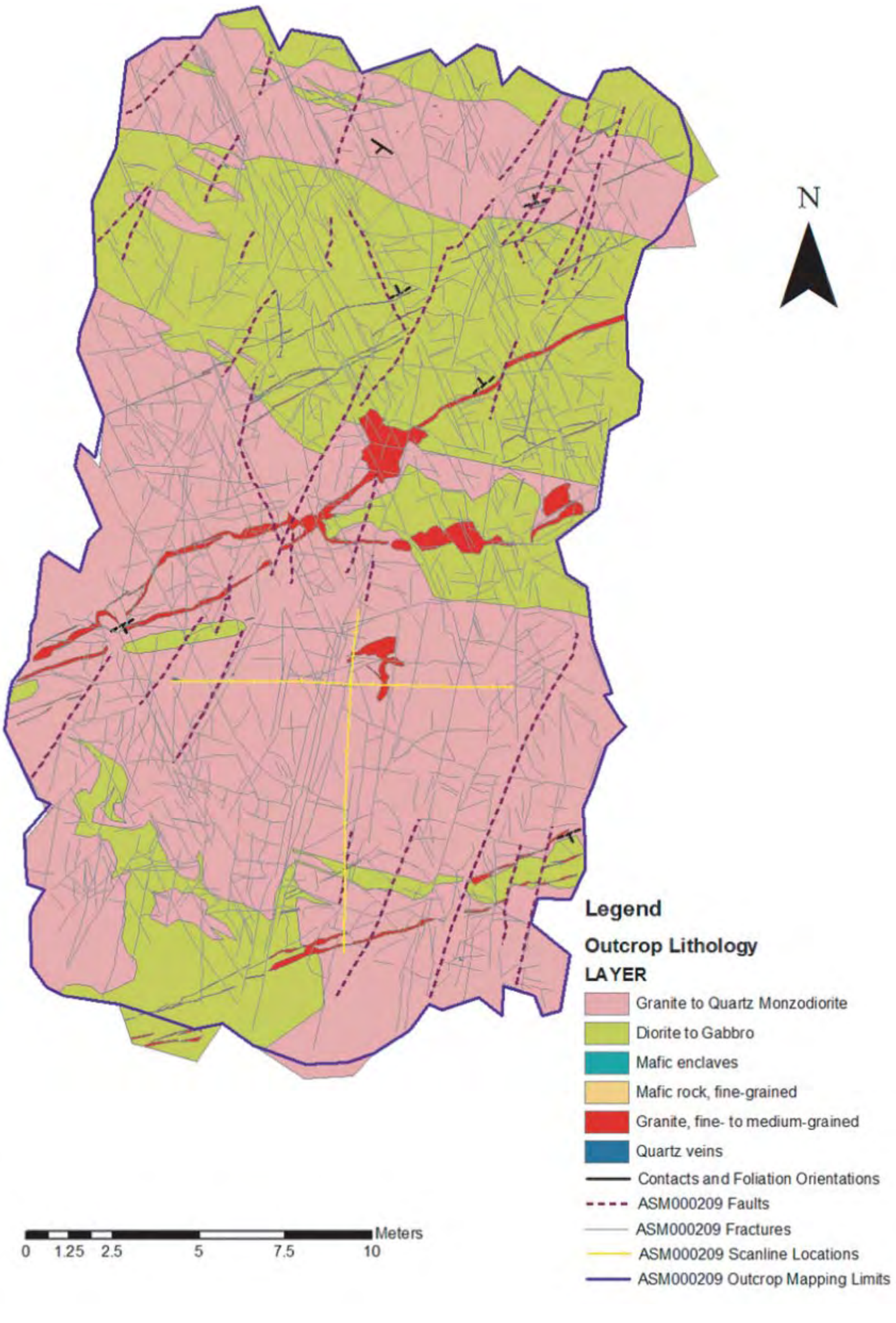

Figure 4-2. *Geologic map of outcrop ASM000209, Laxemar subarea. Black dashes represent structures mapped as faults in the SICADA database. The yellow cross represents the locations of scan-line surveys completed during the mapping program.*

Outcrop ASM000209 is largely dominated by two general fracture patterns (Figure 4-2); a north-northeast trending set of through-going fractures against which a second, presumably younger set of northwest-trending structures terminates. However, both the north-northeast and northwest trending fractures show evidence of termination against, truncation by, and of banding against, each other. This suggests that these features may either be coeval (conjugate faulting) or may have been re-activated at later dates. A third, roughly east-west trending set, is also visible in Figure 4-2; this set is decidedly more visible in the contour plot (Figure 4-1). Examination of stereoplots of fracture pole data, however, suggests an additional set of shallow-dipping (subhorizontal) fractures (Figure 4-1), and a potential fifth set striking northeast. In the interest of model simplification, however, this potential fifth set was lumped into the larger east-west set population.

4.1.2 Local fracture set orientations

Stereoplots of fracture poles and Fisher contoured intensities, created using the DIPS package were used to initially partition outcrop fractures into four tentative sets using a hard-sector algorithm, assuming a spherical Fisher distribution for pole orientations. A Terzaghi correction was applied to the contoured stereoplots within DIPS, assuming a gently dipping, planar sampling surface whose geometry calculated from the detailed outcrop mapping coordinate data. The ISIS algorithm /Dershowitz et al. 1998/ was then used to derive the distribution parameters (orientation of the mean pole, distribution dispersion) and to determine the statistical significance of the distribution fit. The results are presented below in Table 4-1, with set orientations expressed as a mean fracture pole trend and plunge, with an associated dispersion parameter. For bivariate distributions, such as the Bivariate Fisher and Bivariate Bingham, the major axis parameter, which describes the ellipticity of the distribution over the face of the sphere, is also presented; the parameter is not defined for univariate Fisher distributions. Fundamentally, the bivariate distributions are ellipsoids in three-dimensional space, projected on the surface of a hemisphere. The major axis is equivalent to that of the major axis (with an orthogonal minor axis) of an oblate spheroid. Trace plots of the resulting fracture sets are presented as Figure 4-3.

Due to the poor statistical matches using only univariate Fisher distributions, ISIS was also used to test whether alternative spherical probability distributions, such as the Bivariate Fisher or Bivariate Bingham, were better statistical fits to the identified sets. Results of this additional analysis are presented in Table 4-2.

Table 4-1. Local fracture set orientations for Alternative Model 1, outcrop ASM000209, Laxemar subarea.

Set id	Distribution	Mean pole (tr, pl.)	Major axis (tr, pl.)	Dispersion (k)	Number of fractures	K-S* Score, % significant
1	Univariate Fisher	352.6, 3.0	N/A[a]	11.95	293	0.058 (27.1%)
2	Univariate Fisher	284.6, 0.5	N/A[a]	21.43	328 (31.4%)	0.04 (65.8%)
3	Univariate Fisher	238.7, 18.2	N/A[a]	22.24	357 (34.2%)	0.242 (0.0%)
4	Univariate Fisher	233.8, 85.1	N/A[a]	11.44	68 (6.5%)	0.242 (0.0%)

* The Kolmogorov-Smirnov test was used to determine the statistical significance of the fit of the set orientation data to the chosen probability distribution.
[a] The major axis parameter is not relevant to univariate Fisher distributions.

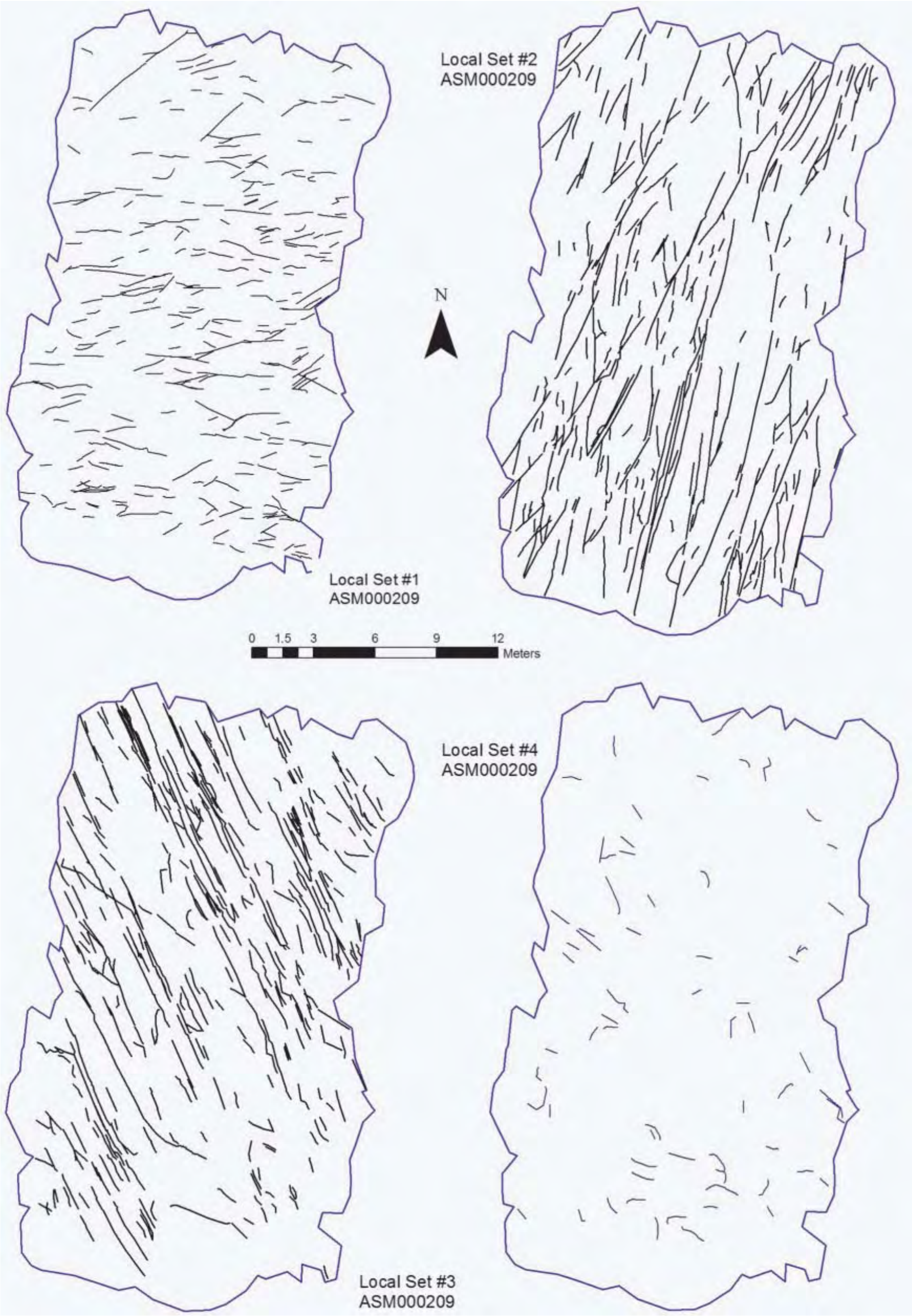

Figure 4-3. Outcrop ASM000209 local fracture sets, Laxemar subarea.

Table 4-2. Local fracture set orientations for Alternative Model 2, outcrop ASM000209, Laxemar subarea.

Set id	Distribution	Mean pole (tr, pl.)	Major axis (tr, pl.)	Dispersion (k/k1, k2)	Number of fractures	K-S* Score, % significant
1	Bivariate Bingham	353.1, 2.5	253.5, 75.1	–7.42, –5.24	314 (30%)	0.047 67.6%
2	Bivariate Bingham	280.8, 1.5	16.3, 74.6	–12.68, –7.14	365 (34.9%)	0.084 4.4%
3	Univariate Fisher	237.8, 20.5	N/A[a]	30.91	300 (28.7%)	0.223 0.0%
4	Univariate Fisher	238.6, 85.8	N/A[a]	11.45	66 (6.3%)	0.249 0.0%

* ISIS utilizes the Kolmogorov-Smirnov test to determine the statistical significance of the fit of the set orientation data to the chosen probability distribution.
[a] The major axis parameter is not relevant to univariate Fisher distribution.

None of the fitted orientation distributions were statistically significant at a reasonable (α = 0.1; > 90%) confidence level. This could be caused by the presence of additional fracture sets not broken out of the larger set populations, or to the fact that orientation variability simply does not conform to any of the models tested. Visual inspection of the outcrop traces suggest that the former explanation is the more likely, as a goal of the present model was to reduce the number of sets from the six vertical sets previously identified during SDM 1.2 Simpevarp

The chronology for the fitted outcrop ASM000209 fracture sets is:

1. Local Set #2 (Oldest): All other fracture sets show prominent terminations against this set or evidence of banding. This set also tends to host the longest continuous fractures. However, this outcrop may possess a second subset hidden within it (see Section 4.1.3.); cross-cutting relationships would suggest that this subset would be younger than the rest of Local Set #2.
2. Local Set #3: This set shows pronounced banding and termination against Local Set #2; however, both local sets #1 and #4 show terminations against this set.
3. Local Set #1 (Youngest): This set shows evidence of being formed within blocks created by the intersections of Local Sets #2 and #3, including orientation changes near longer features and fracture step-overs.
4. Local Set #4 (Age unknown): Due to the small size and lack of mapped fractures, the age of this subhorizontal set is not well constrained. Cross-cutting relationships are not clear.

4.1.3 Geologic controls on fracturing

An analysis of the raw outcrop fracture data for ASM000209 suggests little variation in fracture orientation distributions across the outcrop. Figure 4-4 suggests no significant variation in the distribution of open versus sealed fractures, of the degree of alteration, or orientation variations. Table 4-3 presents a brief analysis that also illustrates the general lack of geological controls on set orientations; note that all parameters are derived from the univariate Fisher-fitted sets.

Fracture aperture and degree of alteration appear to be independent of the host lithology or of the set assignment. There is, however, a slight decrease (approximately 9%) in the number of fractures of Local Sets 2 and 4 hosted within rocks mapped as diorite to gabbro, relative to that rock types' relative abundance in the outcrop (Table 4-3). The cause of this decrease is unknown.

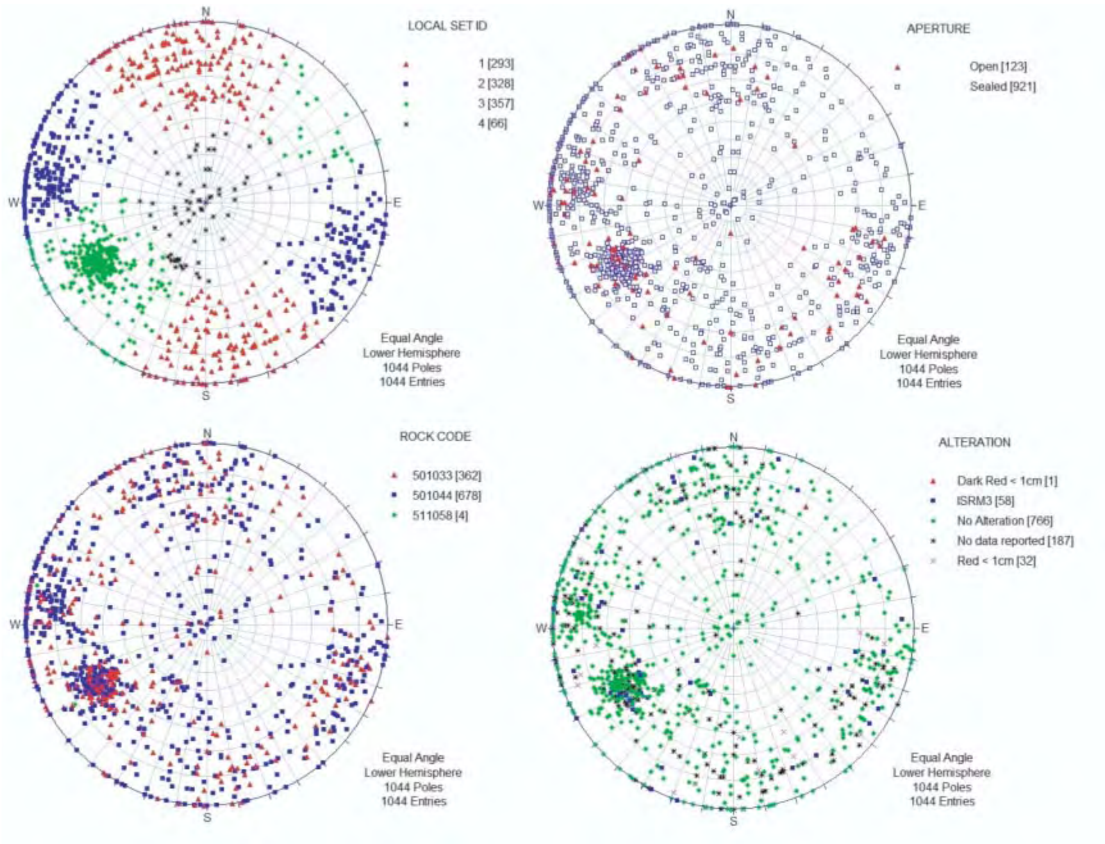

Figure 4-4. *Symbolic pole plots of ASM000209 fractures describing relevant geological parameters.*

Table 4-3. Descriptive statistics for Alternative Model 1, outcrop ASM000209, Laxemar subarea.

Parameter	Local set 1	Local set 2	Local set 3	Local set 4
Number/percentage of open fractures	36 (12.3%)	43 (13.1%)	41 (11.5%)	3 (4.5%)
Number/percentage of sealed fractures	257 (87.7%)	285 (86.9%)	316 (88.5%)	63 (95.5%)
Number/percentage of set in Ävrö Granite* (501044)	191 (65.2%)	237 (72.3%)	202 (56.6%)	48 (72.7%)
Number/percentage of set in Diorite/Gabbro* (501033)	101 (34.5%)	90 (27.4%)	153 (42.9%)	18 (27.3%)
Number/percentage of set in Granite Dikes	1 (0.3%)	1 (0.3%)	2 (0.5%)	0 (0.0%)
Mean/std deviation of trace length	1.14 ± 0.65	1.72 ± 1.58	1.48 ± 1.12	0.98 ± 0.4
P_{21}	0.754	1.277	1.197	0.148

* Note that, of the total outcrop area, 61% is underlain by Ävrö granite, and 36% by dioritic to gabbroic rocks.

Figure 4-5, however suggests that a further subdivision of Local Set #1 (E-W trending) is possible. There appears to be a subset of traces that trend sub-parallel to the younger granite dikes and quartz veins. The other half of Local Set #1 may trend subparallel to rock foliations and lithological boundaries (specifically, the contact between the granodiorite and the diorite-gabbro units). This could be due to re-activation of older zones of weakness during an episode of brittle deformation, or it might represent primary deformational features. It may also be possible to further subdivide Local Set #2 (Figure 4-3) into north-south and northeast-trending subsets, based on fracture lengths and set terminations.

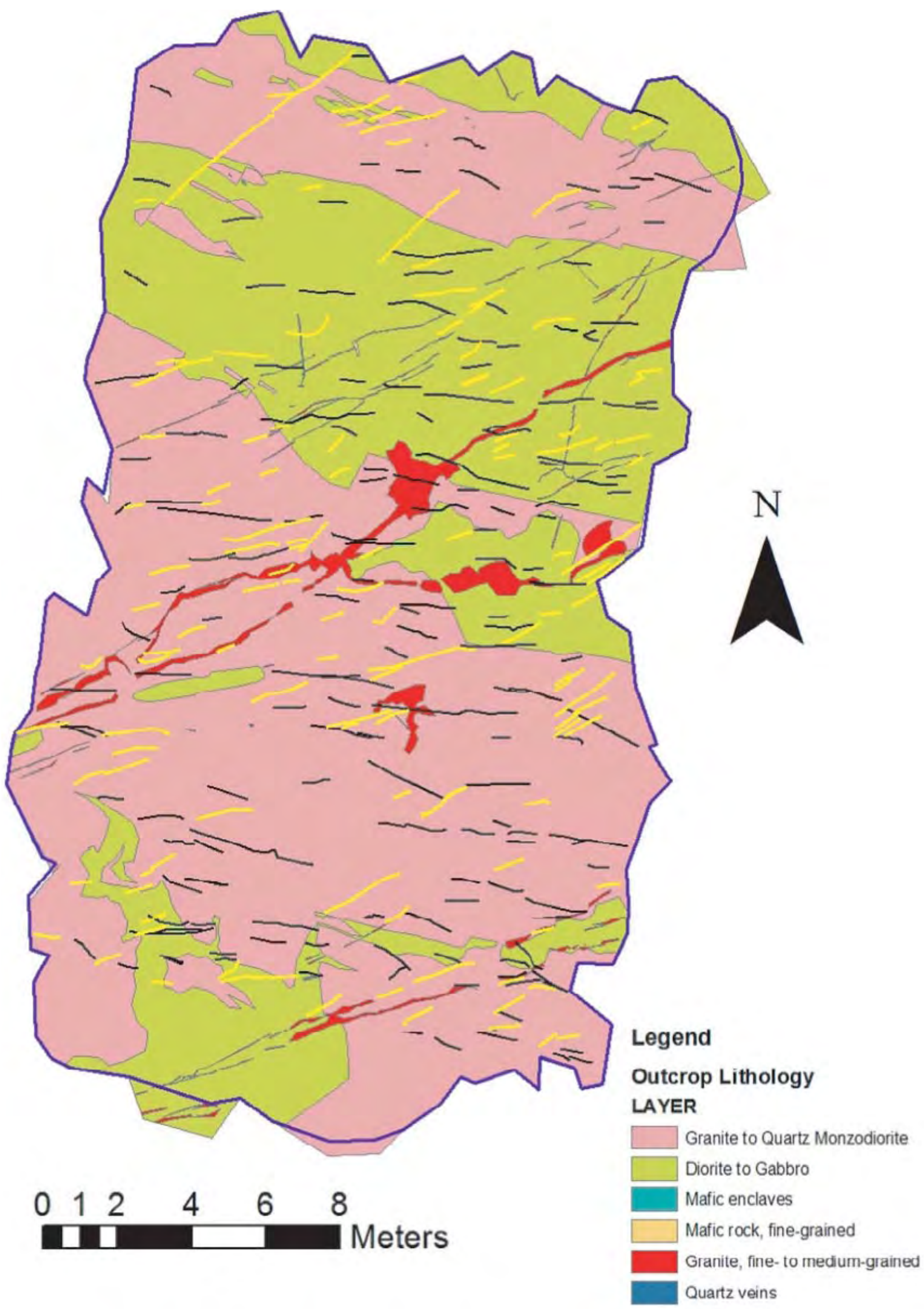

Figure 4-5. *Potential subdivision of Local Set #1 based on geologic controls, outcrop ASM000209, Laxemar subarea. Yellow fractures represent those potentially parallel to fine-grained granite dikes and quartz veining.*

4.1.4 Local fracture set sizes

Local fracture set sizes were analyzed with FracSize using the method discussed in Section 3.4.1. All distribution fits were optimized by minimizing the Kolmogorov-Smirnov statistic through a simulated annealing algorithm /Dershowitz et al. 1998/. Note that most of the size fits are not statistically significant at a reasonable ($\alpha = 0.1$; > 90%) confidence level. The preferred size model is highlighted in bold text, along with any additional size models that suggested reasonable correspondence to observed outcrop lengths.

Table 4-4. Fracture size parameters for ASM000209 local sets, Laxemar subarea. Best-fit model is presented in bolded and italicized text.

Local set	Size model	Radius distribution (arithmetic space) (mean, std dev or min rad, exp)	Radius distribution (Log10 space) (mean, std dev or min radius, exp.)	Fit Statistics (K-S,%)/ (Chi-sq, %)
1	Lognormal	0.32/0.254	–0.601, 0.303	0.0683, 50.2% 11.4, 78.7%
1	Power Law	0.334, 3.28	N/A*	0.0717, 43.9% 10.8, 21.1%
2	Lognormal	0.261, 0.384	–0.833, 0.466	0.064, 51.2% 18, 70.6%
2	Power Law	0.352, 3.01	N/A*	0.0579, 64.1% 18.1, 31.7%
3	Lognormal	0.529, 0.374	–0.364, 0.276	0.0588, 56.7% 21.6, 36.2%
3	Power Law	0.373, 3.13	N/A*	0.042, 91.1% 8.15, 83.4%
4	Lognormal	0.425, 0.235	–0.429, 0.224	0.091, 94.8% 13.1, 44.1%
4	Normal	0.5, 0.25	–0.349, 0.205	0.136, 57.1% 1.58, 66.3%
4	Power Law	0.322, 3.4	N/A*	0.121, 71.7% 7.28, 12.2%

* Not valid for power law distribution.

4.2 Outcrop ASM000208

Outcrop ASM000208 is located near the northern border of the Laxemar sub-region, and encompasses approximately 331 square m. Lithologies exposed in the bedrock outcrop include diorite/gabbro (11.7%), granite to quartz monzonite, often referred to as the 'Ävrö Granite' (75.5%), and dikes of fine- to medium-grained granite (11.9%). Minor quartz veining and mafic inclusions were also noted. The outcrop is oriented roughly north-south. Figure 4-6 illustrates the basic morphology and geology of outcrop ASM000208.

4.2.1 Outcrop data analysis

Both the SICADA and SDE databases lists 1,053 fractures inside the mapping perimeter of ASM000208 above the minimum size threshold of 0.5 m. Figure 4-6 (below) presents basic aggregated orientation data for all fractures within the outcrop, while Figure 4-7 illustrates the basic morphology and geology of Outcrop ASM000208.

4.2.2 Local fracture set orientations

The results of the local fracture set orientation analysis for ASM000208 are presented below in Table 4-5, with set orientations expressed as a mean fracture pole trend and plunge, with an associated dispersion parameter. Five sets were necessary to capture the complexity exhibited in outcrop. Figure 4-8 and Figure 4-9 illustrate the five sets in outcrop; a stereoplot of set poles is visible in Figure 4-10.

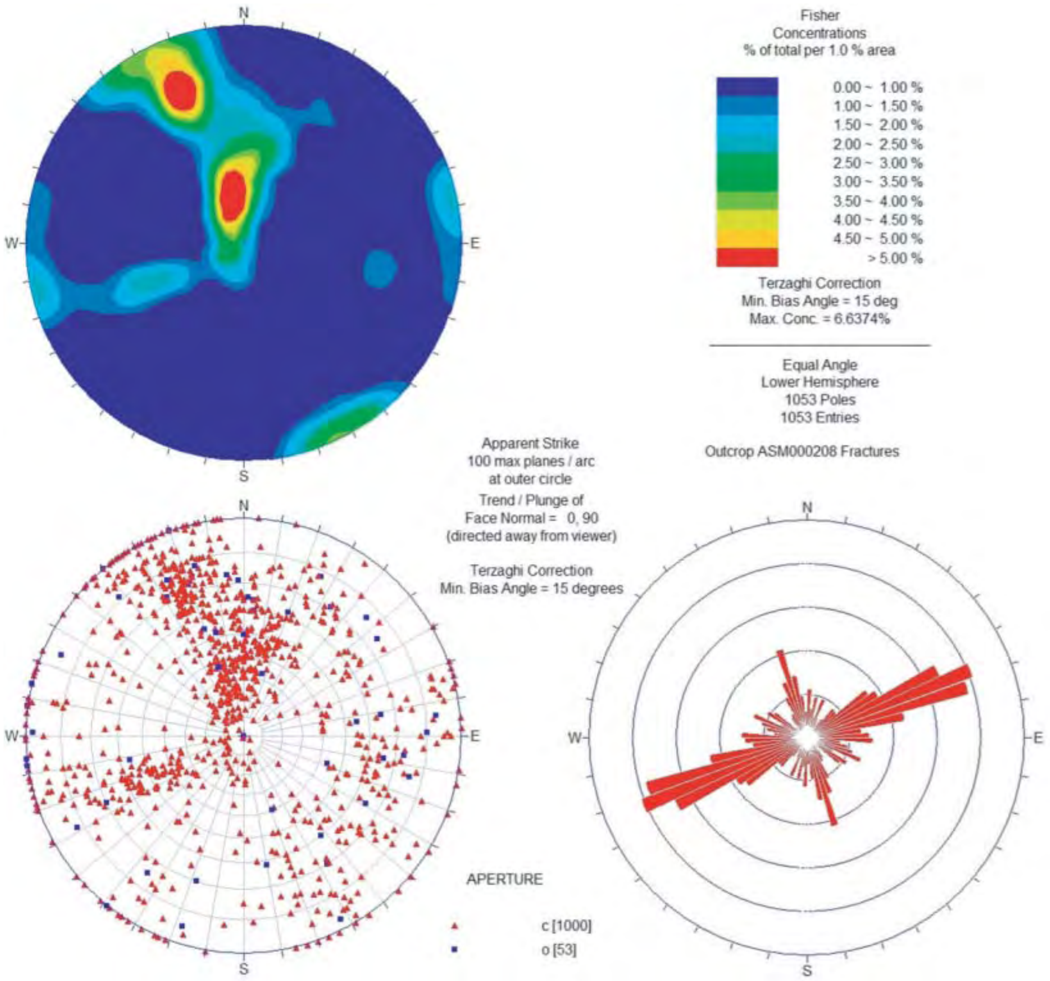

Figure 4-6. Fracture orientation data for outcrop ASM000208, Laxemar subarea. All data taken from SICADA database tables. Note that the Terzaghi correction assumes a horizontal planar outcrop. Symbolic pole plot represents fracture aperture; 'c' are sealed fractures, while 'o' are open fractures.

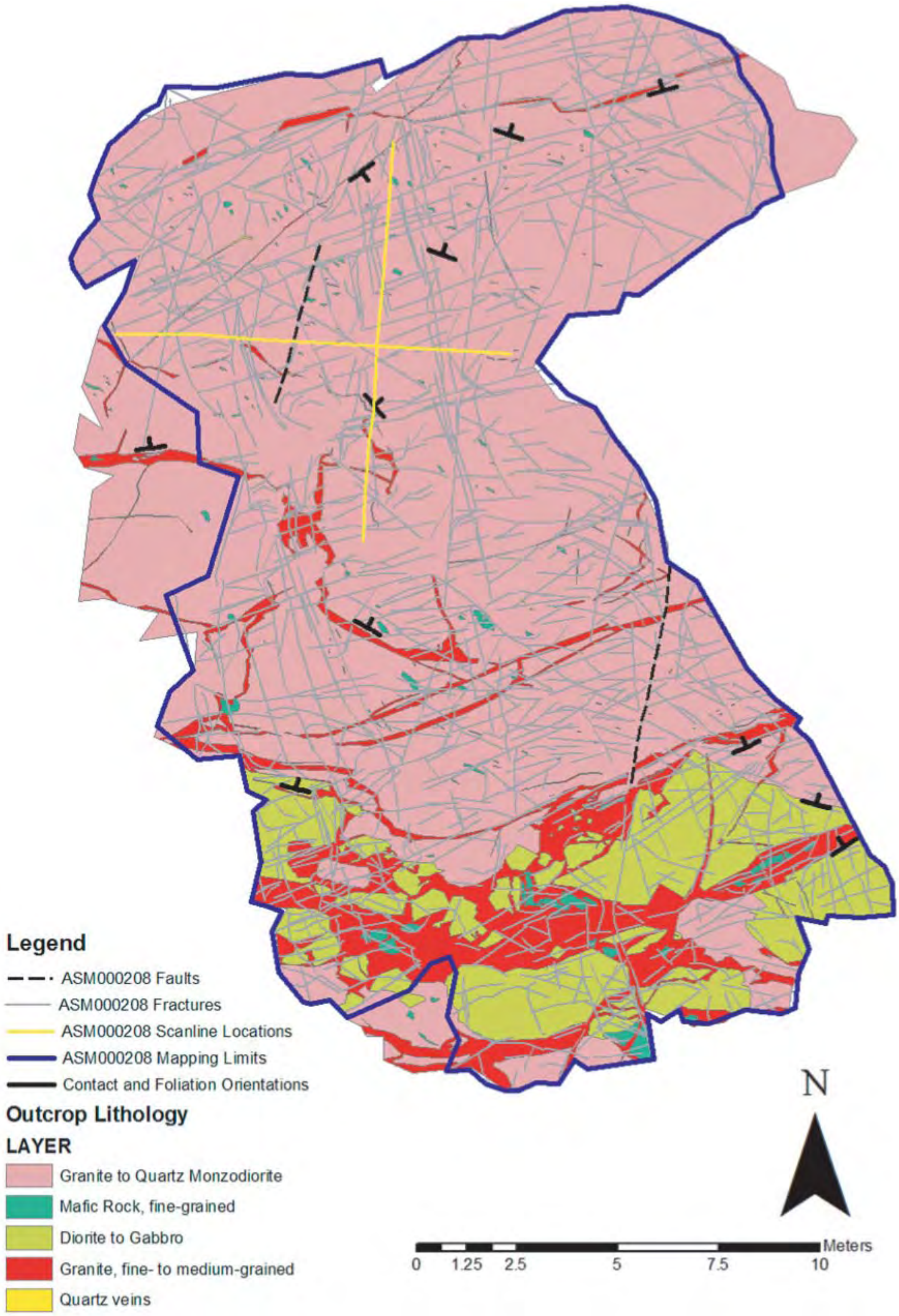

Figure 4-7. *Geologic Map of outcrop ASM000208, Laxemar subarea, illustrating mapping limits, the orientations of the scan-lines, and the general fracture patterning in the outcrop.*

Table 4-5. Local fracture set orientations for model Alternative 1, outcrop ASM000208, Laxemar subarea.

Set id	Orientation model	Mean pole (tr, pl)	Major axis (tr, pl)	Dispersion (k)	# of fractures	K-S*, significance
1	Univariate Fisher	332.0, 2.9	N/A[a]	16.55	300 (28.5%)	0.067 (13.4%)
2	Univariate Fisher	262.4, 0.8	N/A[a]	8.07	236 (22.4%)	0.090 (4.4%)
3	Univariate Fisher	239.6, 74.8	N/A[a]	11.31	120 (11.4%)	0.088 (12.8%)
4	Univariate Fisher	355.1, 63.9	N/A[a]	20.43	136 (12.9%)	0.134 (0.2%)
5	Univariate Fisher	5.0, 28.9	N/A[a]	9.30	261 (24.8%)	0.023 (99.9%)

* ISIS utilizes the Kolmogorov-Smirnov test to determine the statistical significance of the fit of the set orientation data to the chosen probability distribution.
[a] The major axis parameter is not relevant to univariate Fisher distributions.

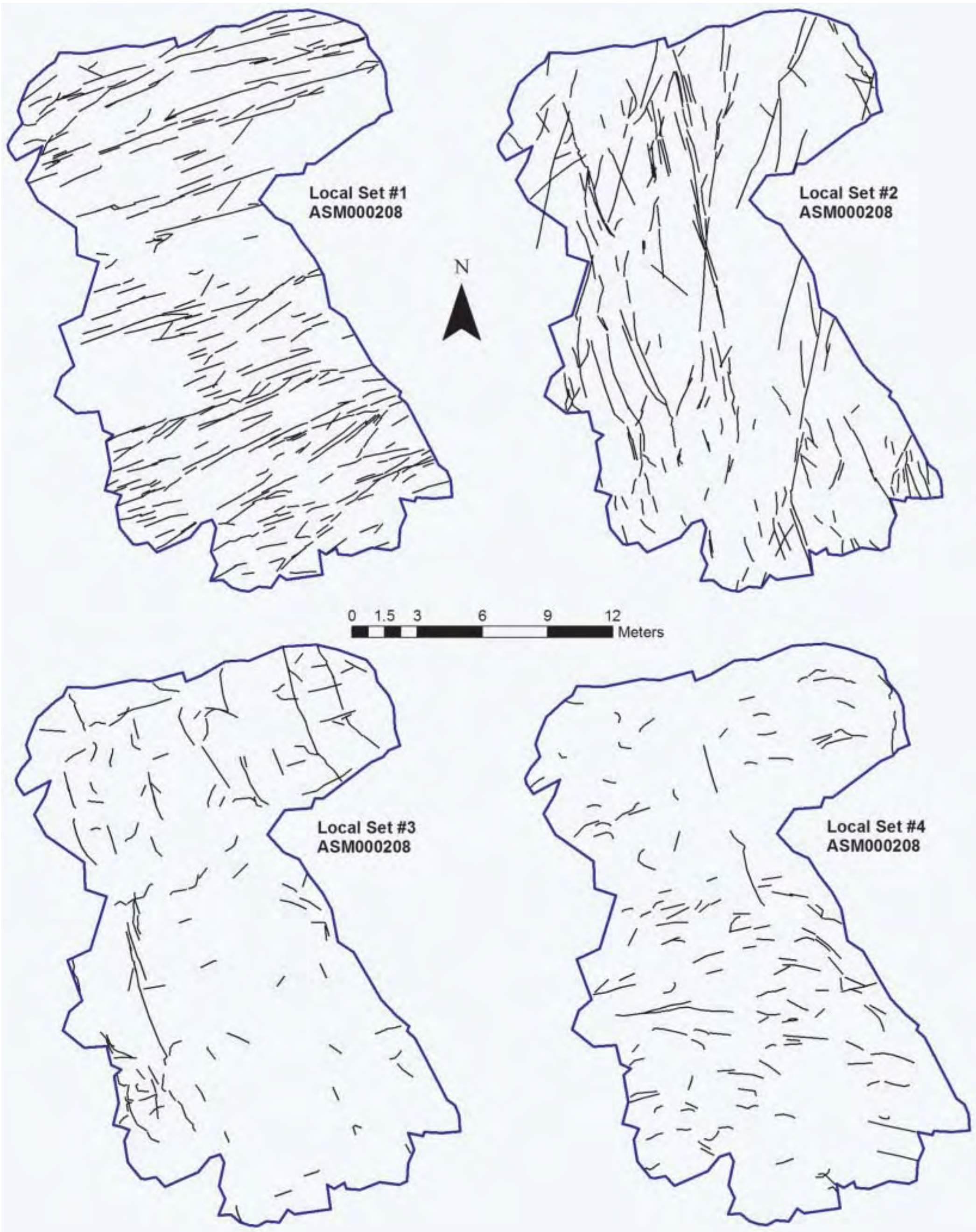

Figure 4-8. *Outcrop ASM000208 local fracture sets 1–4, model Alternative 1.*

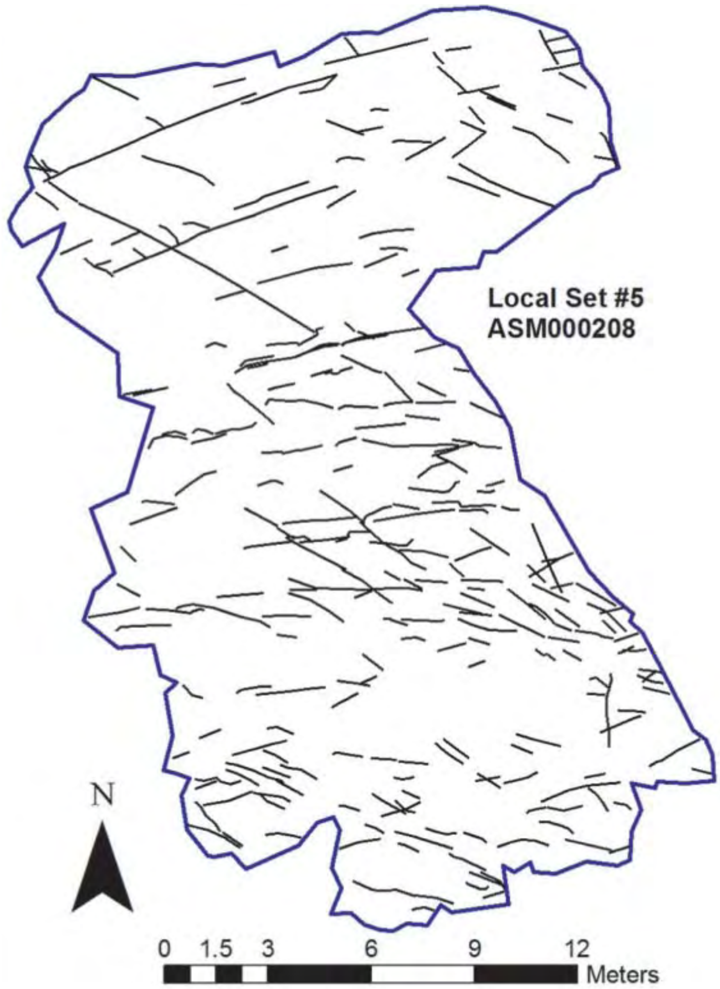

Figure 4-9. *Outcrop ASM000208 local fracture set 5, model alternative 1.*

Due to the poor statistical matches using only univariate Fisher distributions, ISIS was also used to test whether alternative spherical probability distributions, such as the Bivariate Fisher or Bivariate Bingham, were better statistical fits to the identified sets. Results of this additional analysis are presented in Table 4-6.

Table 4-6. Local fracture set orientations for model Alternative 2, outcrop ASM000208, Laxemar subarea.

Set id	Orientation model	Mean pole (tr, pl)	Major axis (tr, pl)	Dispersion (k/k1, k2)	# of fractures	K-S*, significance
1	Bivariate Bingham	335.7, 9.5	244.8, 5.3	–16.79,–9.37	287 (27.3%)	0.095 (3.6%)
2	Bivariate Fisher	249.9, 25.6	345.3, 11.1	6.66, 8.45	200 (19%)	0.074 (32.1%)
3	Bivariate Fisher	113.7, 19.0	302.9, 70.8	5.74, 6.70	174 (16.5%)	0.110 (5.6%)
4	Bivariate Bingham	342.5, 73.9	85.4, 3.7	–22.51,–7.50	154 (14.6%)	0.069 (25.6%)
5	Univariate Fisher	12.1, 31.9	N/A[a]	10.41	238 (22.6%)	0.034 (94.2%)

* ISIS utilizes the Kolmogorov-Smirnov test to determine the statistical significance of the fit of the set orientation data to the chosen probability distribution.
[a] The major axis parameter is not relevant to univariate Fisher distribution.

The set chronology for Outcrop ASM000208's local fracture sets is:

1. Local Set #1 (oldest): This set is spatially the most homogeneous, though it does show some evidence of banding against some of the larger fractures in Set #2. This set also tends to have the largest fractures.
2. Local Set #2: Some fractures in this set may be older than those in Set #1, but most fractures show distinct terminations or constrained growth against Set #1. There may be a northeast-trending subset of older fractures within Set #2 that is not broken out on stereoplots.
3. Local Set # 5: In general, constrained in growth directions by blocks formed by the intersection of Local Sets #1 and #2. This set shows terminations against Set #2, as well as growth from older fracture tips in both earlier sets. Note that, in the northern half of the outcrop, the distinction between Set #5 and Set #1 fractures becomes extremely vague.
4. Local Set # 3: Though determining age relationships in subhorizontally-dipping fractures is difficult, it appears that this set is older than Local Set #4. It shows pronounced constrained growth against all earlier sets, and is cross-cut by Local Set #5.
5. Local Set #4 (youngest): Nearly all the fractures in this set cut across Set #3 and Set #5, and show distinct banding against Sets #1 and #2. Statistically, this is also the shortest set.

4.2.3 Geologic controls on fracturing

An analysis of fracture parameters within ASM000208 indicates that, by in large, the fracture pattern is homogenous and relatively static. This suggests, but does not prove, that the fracturing is likely quite old. Figure 4-10 and Table 4-7 illustrate the lack of variance in fracture or

Table 4-7. Descriptive statistics for model alternative 1 fracture sets, outcrop ASM000208.

Parameter	Local set 1	Local set 2	Local set 3	Local set 4	Local set 5
Number/% of open fractures	12 (4%)	17 (7.2%)	4 (3.3%)	2 (1.5%)	18 (6.9%)
Number/% of sealed fractures	288 (96%)	219 (92.8%)	116 (96.7%)	134 (98.5%)	243 (93.1%)
Number/% in Ävrö Granite* (501044)	232 (77.3%)	193 (81.8%)	101 (84.2%)	118 (86.8%)	217 (83.1%)
Number/% in diorite/ gabbro* (501033)	32 (10.7%)	31 (13.1%)	12 (10.0%)	12 (8.8%)	30 (11.5%)
Number/% in fine-grained mafic rock (505102)	6 (2.0%)	1 (0.4%)	0	0	3 (1.2%)
Number/% in granite dikes (511058)	30 (10%)	11 (4.7%)	7 (5.8%)	6 (4.4%)	11 (4.2%)
Mean/std dev of trace length	1.30 ± 0.79	1.43 ± 1.00	1.18 ± 0.76	1.00 ± 0.51	1.20 ± 0.87
P_{21}	1.18	1.02	0.43	0.43	0.95

* Note that, of the total outcrop area, 75% is underlain by Ävrö granite, 12% by fine to medium-grained granitic dikes, and 12% by dioritic to gabbroic rock.

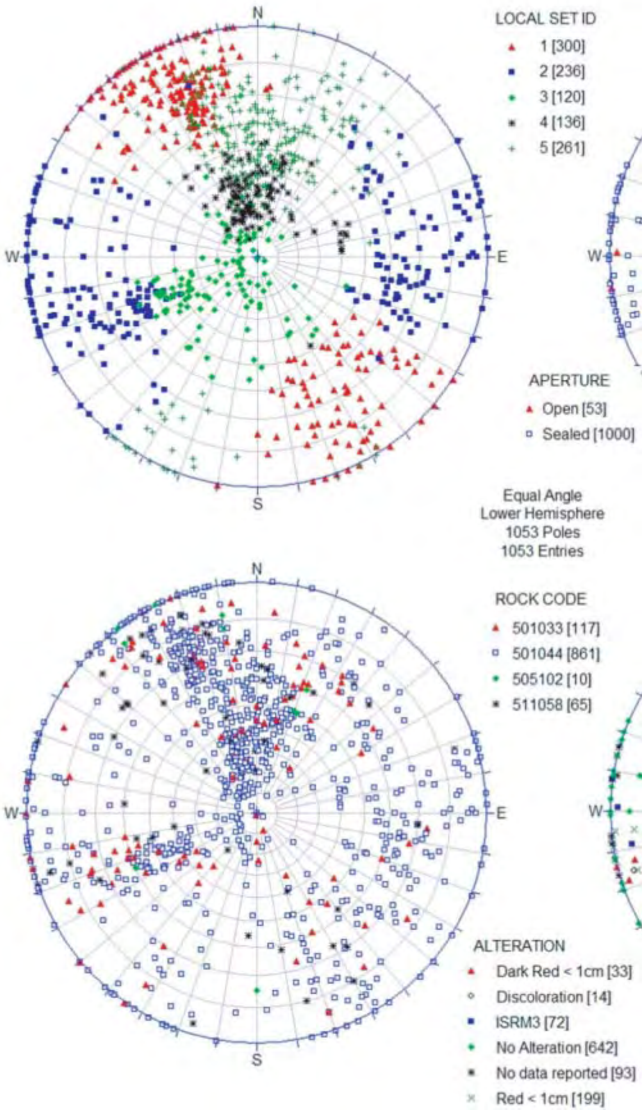

Figure 4-10. *Symbolic pole plots of ASM000208 fractures (Laxemar subarea, model Alternative 1) describing relevant geological parameters.*

4.2.4 Local fracture set sizes

Local fracture set sizes were analyzed using the FracSize method, discussed in detail in Section 3.4.1. All distribution fits were optimized by minimizing the Kolmogorov-Smirnov statistic through a simulated annealing algorithm /Dershowitz et al. 1998/. Note that most of the size fits are not statistically significant at a reasonable ($\alpha = 0.1$; > 90%) confidence level. The preferred size model is highlighted in bold text, along with any additional size models that suggested reasonable correspondence to observed outcrop lengths.

Table 4-8. Fracture size parameters for ASM000208 local sets (Laxemar subarea, model Alternative 1).

Local set	Size model	Radius distribution (arithmetic space) (mean, std dev or min radius, exponent)	Radius distribution (Log10 space) (mean, std dev or exp, min radius)	Fit statistics (K-S, %) (Chi-sq, %)
1	Lognormal	0.194, 0.281	–0.959, 0.463	0.073, 39.5% 19.5, 36.2%
2	Lognormal	0.413, 0.4	–0.527, 0.353	0.055, 86.6% 17.1, 51.9%
2	Power Law	0.358, 3.1	N/A*	0.055, 86.6% 6.44, 84.2%
3	Lognormal	0.596, 0.221	–0.252, 0.156	0.092, 69.4% 16.6, 34.2%
3	Power Law	0.323, 3.07	N/A*	0.092, 69.4% 11.7, 22.9%
4	Lognormal	0.437, 0.25	–0.421, 0.231	0.088, 66.5% 19.1, 21.1%
4	Power Law	0.246, 3.05	N/A*	0.132, 18.5% 4.56, 71.3%
5	Lognormal	0.474, 0.276	–0.388, 0.235	0.046, 94.5% 11.3, 83.9%

* Not valid for power law distribution.

4.3 Outcrop ASM000025

Outcrop ASM000025 is located in the southeastern corner of the Simpevarp model region, near the coastline of the Simpevarp peninsula. This rhombus-shaped outcrop is seated along the border between rock domains A01 and C01; lithologies exposed within the outcrop include granite to quartz monzodiorite (84.4%) and intermediate magmatic rock (13.5%). Minor (2.1%) dikes of fine-grained granite and pegmatite, along with quartz-filled veins, are also present. The outcrop spans approximately 422.5 square m in area.

4.3.1 Outcrop data analysis

Both the SICADA and the SDE databases contained 917 mapped fractures at outcrop ASM000025; however, this includes 55 fractures with reported trace lengths smaller than 0.5 m (as small as 0.29 m). These smaller fractures were included in the local set analysis; their presence may introduce a small bias when fitting a size model. Figure 4-12 illustrates the basic geology and structure of the outcrop, while Figure 4-11 presents a breakdown of fracture orientations within the outcrop.

It also appears that a dip window mask was utilized by the outcrop mapping team; most subvertical fractures are mapped to the nearest 5°, rather than to an absolute dip value. It is not known if this is a mapping-protocol decision or an error in the SICADA/SDE databases. The window mask produced a banded pole plot (Figure 4-11); however, a plot of pole contours reduces the noise and allows for easier identification of geologically relevant sets.

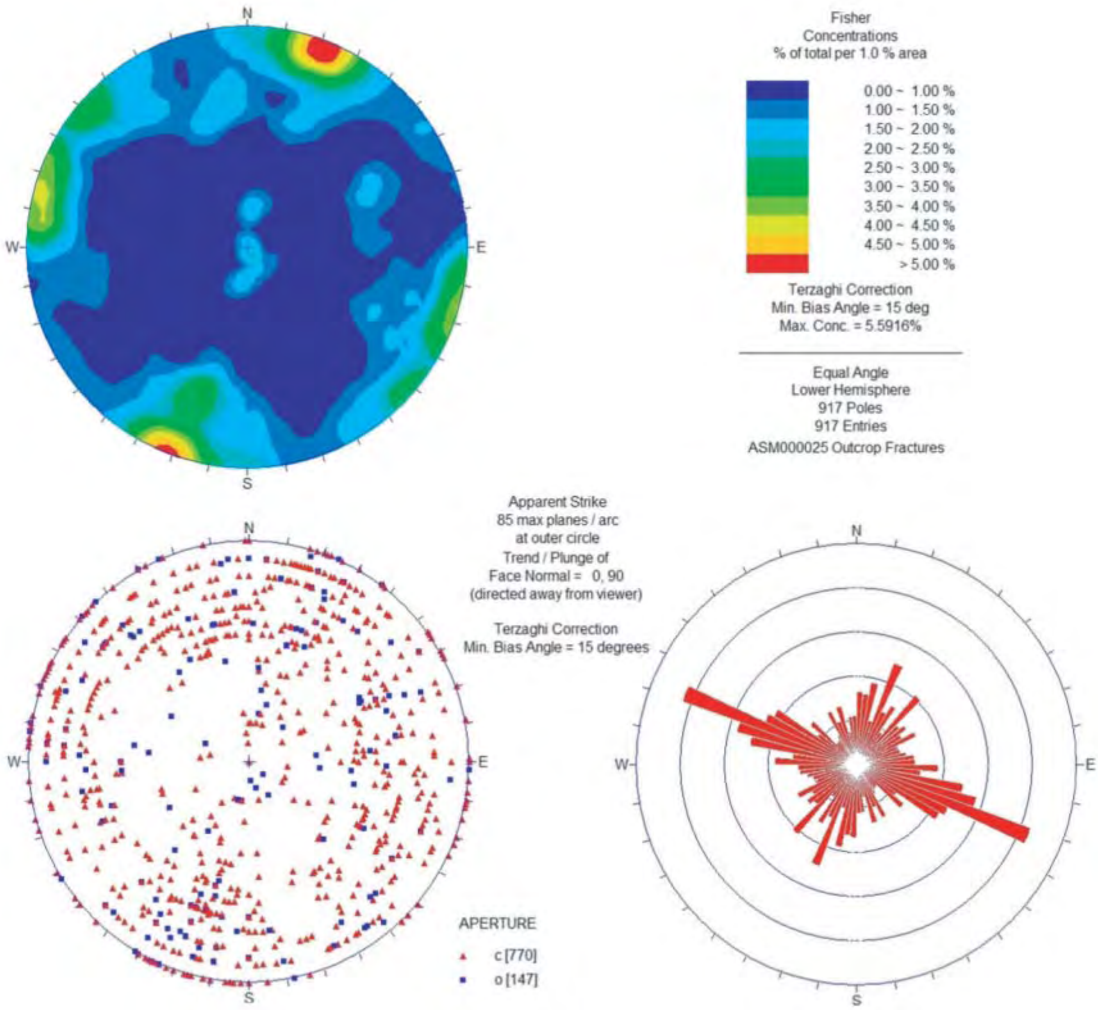

__Figure 4-11.__ Fracture orientation data for outcrop ASM000025, Simpevarp subarea. All data taken from SICADA database tables. Note that the Terzaghi correction assumes a horizontal planar outcrop. Symbolic pole plot represents fracture aperture; 'c' are sealed fractures, while 'o' are open fractures.

4.3.2 Local fracture set orientations

Fitted statistical distributions for local fracture sets are presented below in Table 4-9. Orientation distributions are expressed as a mean fracture pole trend and plunge, with an associated dispersion parameter. Due to the uncertainty in fracture pole orientations caused by the dip window mask, a second set of spherical probability distributions were not fitted to the outcrop data; all fits assume Univariate Fisher distributions

Five basic sets were necessary to capture the complexity exhibited in outcrop; it may be possible to further subdivide the fractures based on mineral fillings, orientations, or structural relationships. ASM000025 exhibits significant scatter in fracture orientations; though the same global sets observed in the Laxemar outcrops are also seen in ASM000025, fracture orientations appear to be less well constrained in ASM000025.

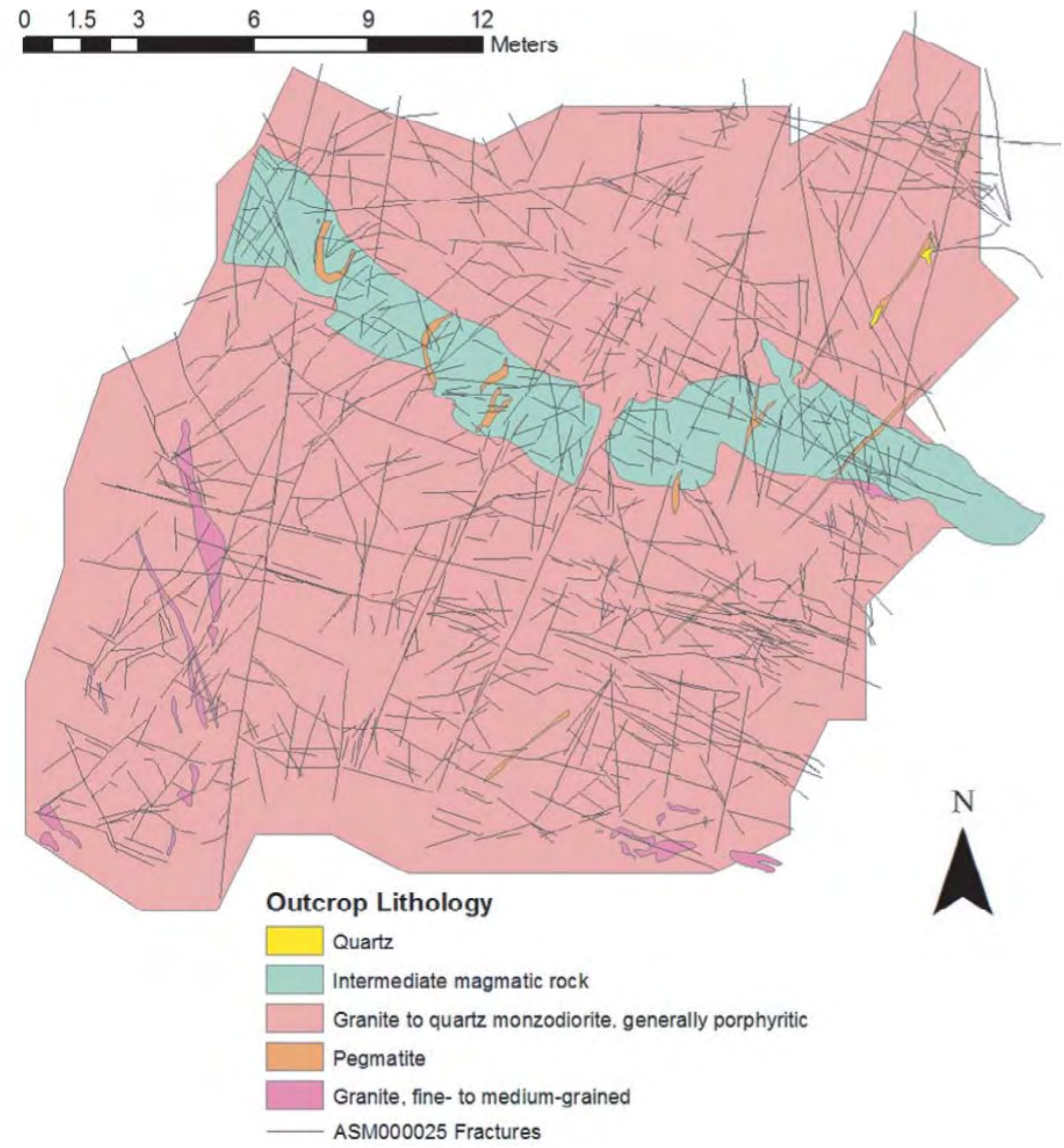

Figure 4-12. *Geologic map of outcrop ASM000025, Simpevarp subarea.*

Table 4-9. Local set orientations for model Alternative 1, outcrop ASM000025.

Set id	Orientation model	Mean pole (tr, pl)	Major axis (tr, pl)	Dispersion (k)	# of fractures	K-S*, significance
1	Univariate Fisher	199.7, 3.4	N/A[a]	14.51	333 (36.3%)	0.043 (57.9%)
2	Univariate Fisher	282.7, 0.8	N/A[a]	17.67	201 (21.9%)	0.090 (8.1%)
3	Univariate Fisher	327.9, 5.8	N/A[a]	13.12	206 (22.5%)	0.079 (15.0%)
4	Univariate Fisher	67.1, 18.9	N/A[a]	15.56	111 (12.1%)	0.121 (7.7%)
5	Univariate Fisher	85.3, 86.2	N/A[a]	10,.43	66 (7.2%)	0.152 (1.1%)

* The Kolmogorov-Smirnov test was used to determine the statistical significance of the fit of the set orientation data to the chosen probability distribution.

[a] The major axis parameter is not relevant to univariate Fisher distributions.

The fracture set chronology (based largely on size and structural relationships) for outcrop ASM000025 appears to be:

- Local Set #2 (oldest): This set generally possesses the longest traces and is the most spatially homogenous. All other sets show pronounced banding or terminations against this set. It might be possible to subdivide Local Set #2 further into longer NS-trending fractures and shorter NE-trending fractures.
- Local Set #1: This set shows evidence of banding and constrained growth against Set 2. However, the termination/penetration relationship between Set 2 and Set 1 is murky; the two sets may be contemporaneous. Two of the longer fractures (north half of the outcrop, Figure 4-13) in this set may be mismapped; the outcrop pattern suggests a different strike than the SICADA database indicates.
- Local Set #3: This set shows distinct terminations against Local Sets 1 and 2, and appears to start within blocks constrained by the intersection of the two older fracture sets.
- Local Set #4 (youngest): This set shows terminations against all older sets. Map patterns suggest it may be contemporaneous with Set 3.
- Local Set #5 (sub-horizontal): Due to the relatively low intensity and vague map patterns, the timing of this fracture set remains uncertain.

4.3.3 Geologic controls on fracturing

A qualitative analysis of fracture parameters recorded during the detailed outcrop mapping shows little evidence of variation among the five sets. Fracture aperture, alteration, and host rock lithology (Figure 4-14) do not appear to vary by set; however, the data coverage for fracture mineralogy and degree of alteration are very sparse.

The ratio of open to sealed fractures in outcrop appears relatively constant (Table 4-10); however, there is a slight (10%) increase in open fractures in Local Set #5. Local Sets #1 and #2 tend to have the longest fractures, while Set #3 has the shortest traces. The only visible controls (Figure 4-12) on orientation appear to occur with Set #3; fractures in this set trend subparallel to the small pegmatite dikes exposed in the outcrop.

Table 4-10. Descriptive statistics for model alternative 1 fracture sets at outcrop ASM000025, Simpevarp subarea.

Parameter	Local Set 1	Local Set 2	Local Set 3	Local Set 4	Local Set 5
Number/% of open fractures	58 (17.4%)	23 (11.4%)	33 (16.0%)	16 (14.4%)	17 (25.8%)
Number/% of sealed fractures	275 (82.6%)	178 (88.6%)	173 (84.0%)	95 (85.6%)	49 (74.2%)
Number/% in Ävrö Granite* (501044)	297 (89.2%)	173 (86.1%)	185 (89.8%)	96 (86.5%)	60 (90.9%)
Number/% in gabbro to diorite (501030)	36 (10.8%)	28 (13.9%)	21 (10.2%)	15 (13.5%)	6 (9.1%)
Mean/std deviation of trace length	1.31 ± 1.08	1.41 ± 1.14	1.00 ± 0.65	1.14 ± 0.92	1.27 ± 0.81
P_{21}	1.04	0.673	0.491	0.302	0.199

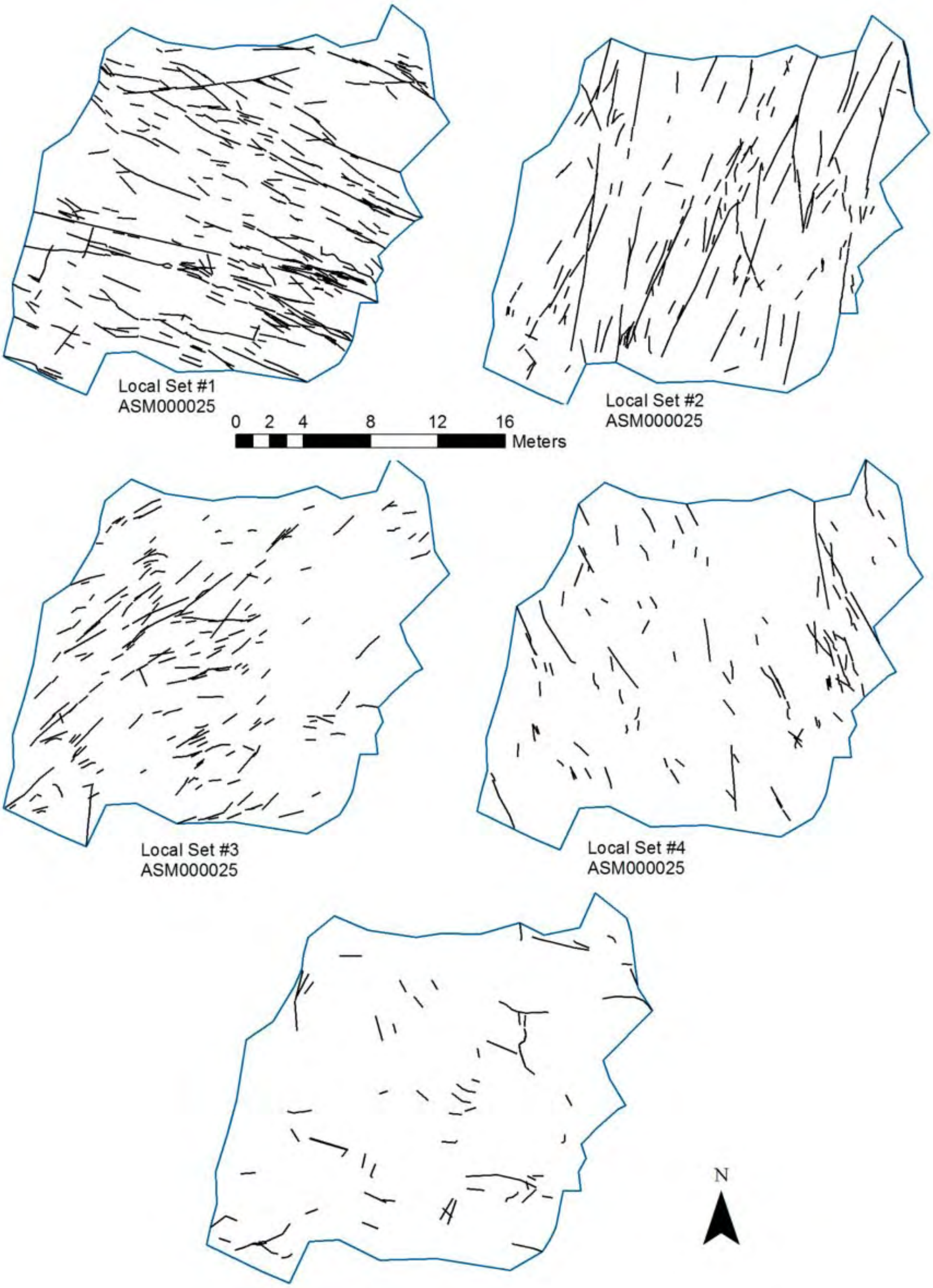

Figure 4-13. *Outcrop ASM000025 local fracture sets, model alternative 1, Simpevarp subarea.*

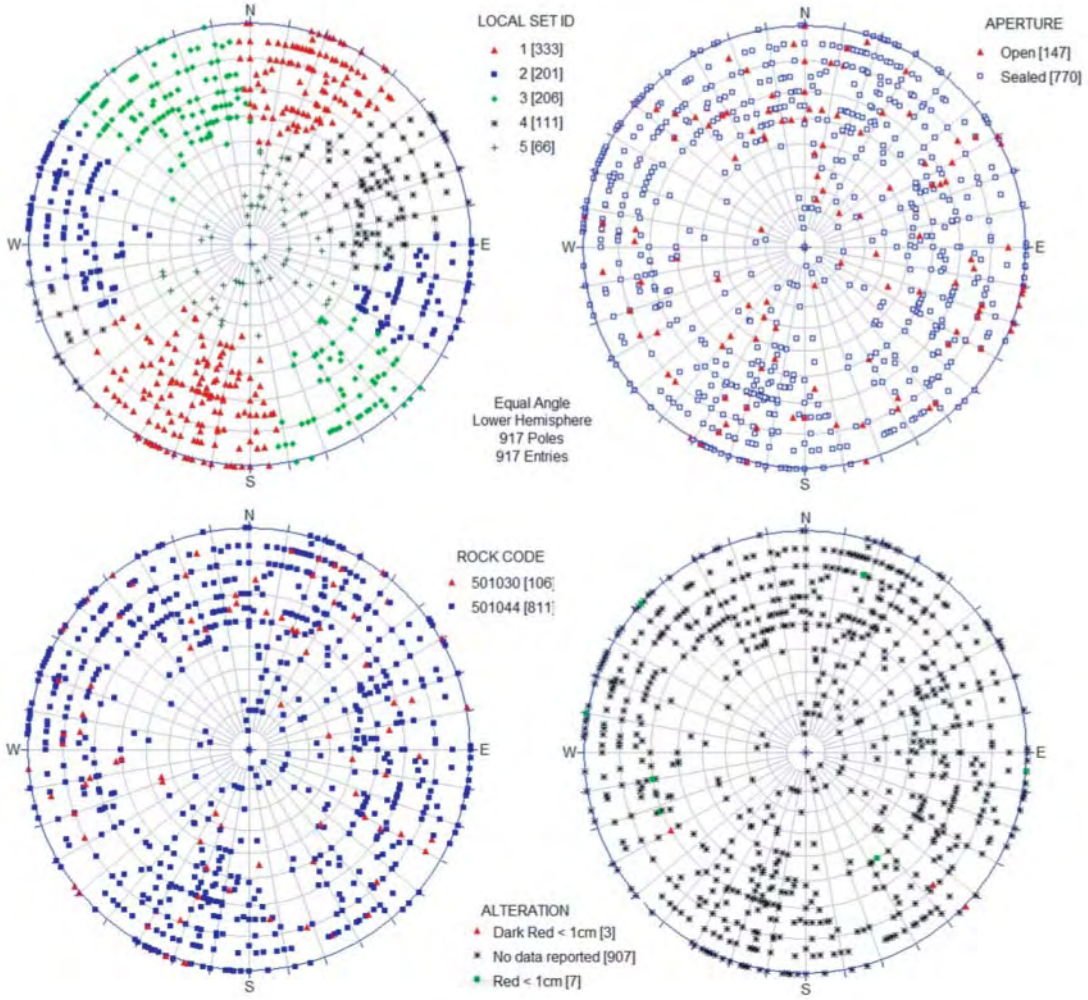

Figure 4-14. *Symbolic pole plots of ASM000025 fractures describing relevant geological parameters.*

4.3.4 Local fracture set sizes

Local fracture set sizes were analyzed using the FracSize method, discussed in detail in Section 3.4.1. All distribution fits were optimized by minimizing the Kolmogorov-Smirnov statistic through a simulated annealing algorithm /Dershowitz et al. 1998/. Note that most of the size fits are not statistically significant at a reasonable ($\alpha = 0.1$; > 90%) confidence level. The preferred size model is highlighted in bold text, along with any additional size models that suggested reasonable correspondence to observed outcrop lengths.

Table 4-11. Fracture size parameters for ASM000025 model alternative 1 sets, Simpevarp subarea.

Local set	Size model	Radius distribution (arithmetic space) (mean, std dev or min ra/, exp)	Radius distribution (Log10 space) (mean, std dev or min radius, exp)	Fit statistics (K-S,%)/(Chi-sq, %)
1	Lognormal	0.48, 0.34	-0.407, 0.277	0.0923, 2.83% 18.6, 61.1%
1	Power Law	0.29, 2.95	N/A*	0.048, 61.1% 23.8, 3.34%
2	Power Law	0.29, 2.9	N/A*	0.062, 64.2% 8.75, 79.2%
3	Lognormal	0.23, 0.21	-0.77, 0.338	0.117, 3.81% 19.6, 35.7%
4	Exponential	0.25, n/a	N/A*	0.106, 31.7% 17.8, 3.7%
4	Lognormal	0.5, 0.25	-0.349, 0.205	0.139, 8.77% 21.1, 33.1%
4	Power Law	0.2, 3.1	N/A*	0.0631, 90.4% 14.5, 10.7%
5	Lognormal	0.4, 0.3	-0.495, 0.29	0.0953, 44.6% 15, 44.8%
5	Exponential	0.31	N/A*	0.0929, 47.8% 9.84, 13.2%

* Not valid for power law or exponential distributions.

4.4 Outcrop ASM000026

Outcrop ASM000026 is located on the northeastern corner of the Simpevarp peninsula, in the eastern half of the Simpevarp model region. The outcrop is fully within Rock Domain A01 (dominated by Ävrö granite) and is part of the Simpevarp modeling sub-domain. Bedrock lithologies exposed within the outcrop is predominantly Ävrö granite (97%), with minor amounts of fine- to medium-grained granite and pegmatite. The outcrop is approximately 524 square m in area.

4.4.1 Outcrop data analysis

Both the SICADA and the SDE databases contained 875 mapped fractures at outcrop ASM000025; however, this includes 75 fractures with reported trace lengths smaller than 0.5 m (as small as 0.23 m). These smaller fractures were included in the local set analysis; their presence may introduce a small bias when fitting a size model.

4.4.2 Local fracture set orientations

Two fracture set orientation analysis realizations were performed; one assuming only univariate Fisher spherical probability distributions (Table 4-12), and a second using a mix of probability distributions (Table 4-13) that appeared to offer slightly better statistical fits. It should be noted that neither iteration produced sets that were statistically significant at an acceptable (α= 0.1) confidence level.

Four sets were necessary to adequately characterize the complexity observed in ASM000026; however, it is possible, using the outcrop trace map patterns (Figure 4-17) to further refine local set #3 into two distinct sets; one trending east-west, and one trending west-northwest. This division is not easily visible on plots of fracture poles or the contoured stereoplots (where sets were generally identified).

The chronology of fracture sets appears to be:

- Local Set #3 (oldest): This set appears to be the first formed, based on spatial extent and fracture length. However, this set does exhibit banding against a major structure (fault?) belonging to Local Set #2. This could suggest that the sets formed simultaneously; however, it seems more likely that the fault structure formed first, but that the rest of Local Set #2 is younger (re-activation). It is also possible to subdivide Local Set #3 into two ‘conjugate’ subsets; one trending east-west that appears older than the west-northwest trending set.
- Set #2: The north-trending fault structure cross-cutting the outcrop is decidedly older than Local Set #3; however the rest of the outcrop shows banding and termination against Set #3 fractures.

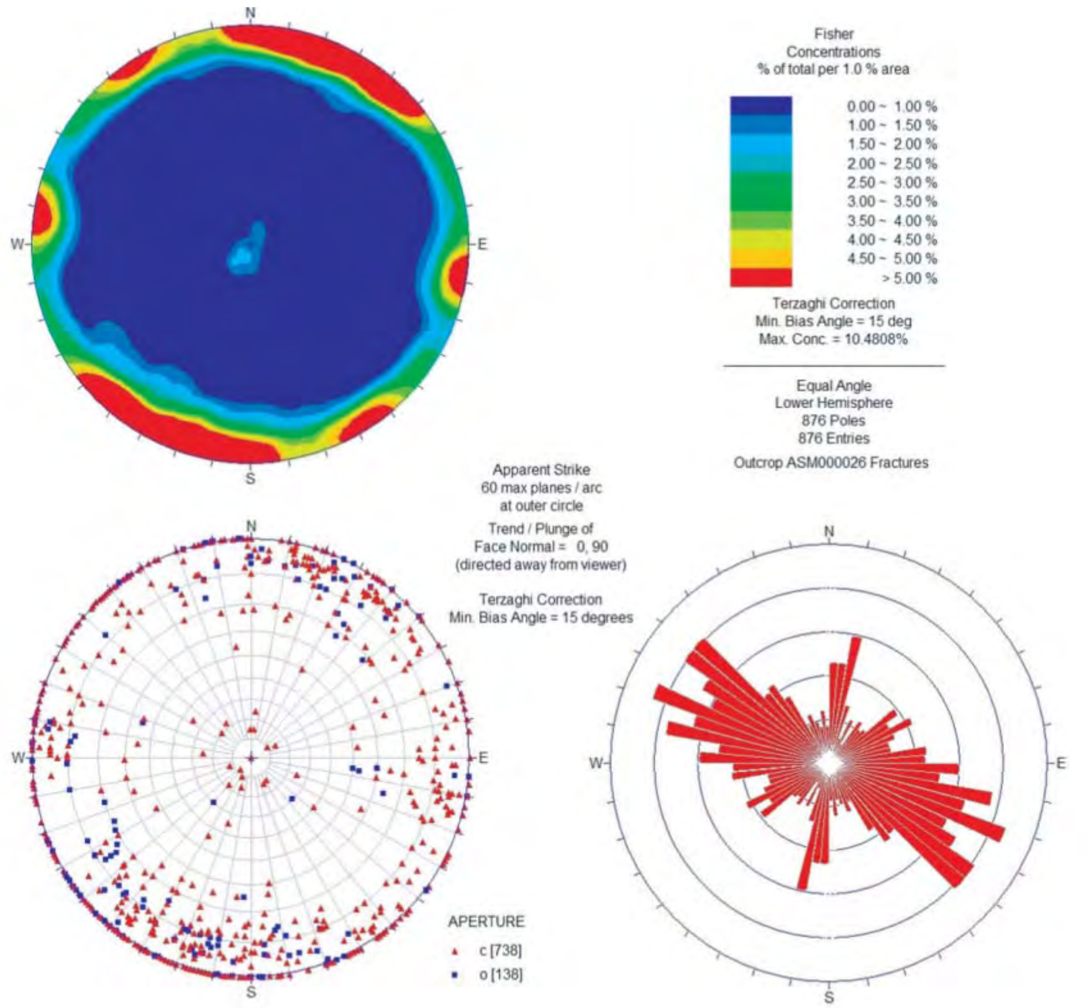

__Figure 4-15.__ Fracture orientation data for outcrop ASM000026. All data taken from SICADA database tables. Note that the Terzaghi correction assumes a horizontal planar outcrop. Symbolic pole plot represents fracture aperture; ‘c’ are sealed fractures, while ‘o’ are open fractures.

- Set #1 (youngest): This set shows pronounced terminations against both Local Set #2 and Local Set #3. It shows evidence of constrained growth within the fault zone defined by the long Local Set #2 fractures.
- Set #4 (age unknown): This set, composed of subhorizontally-dipping fractures, appears to span multiple ages. Some of the fractures that trend west-northwest may be contemporaneous with Local Set #3. Age relationships of the remaining fractures are difficult to determine.

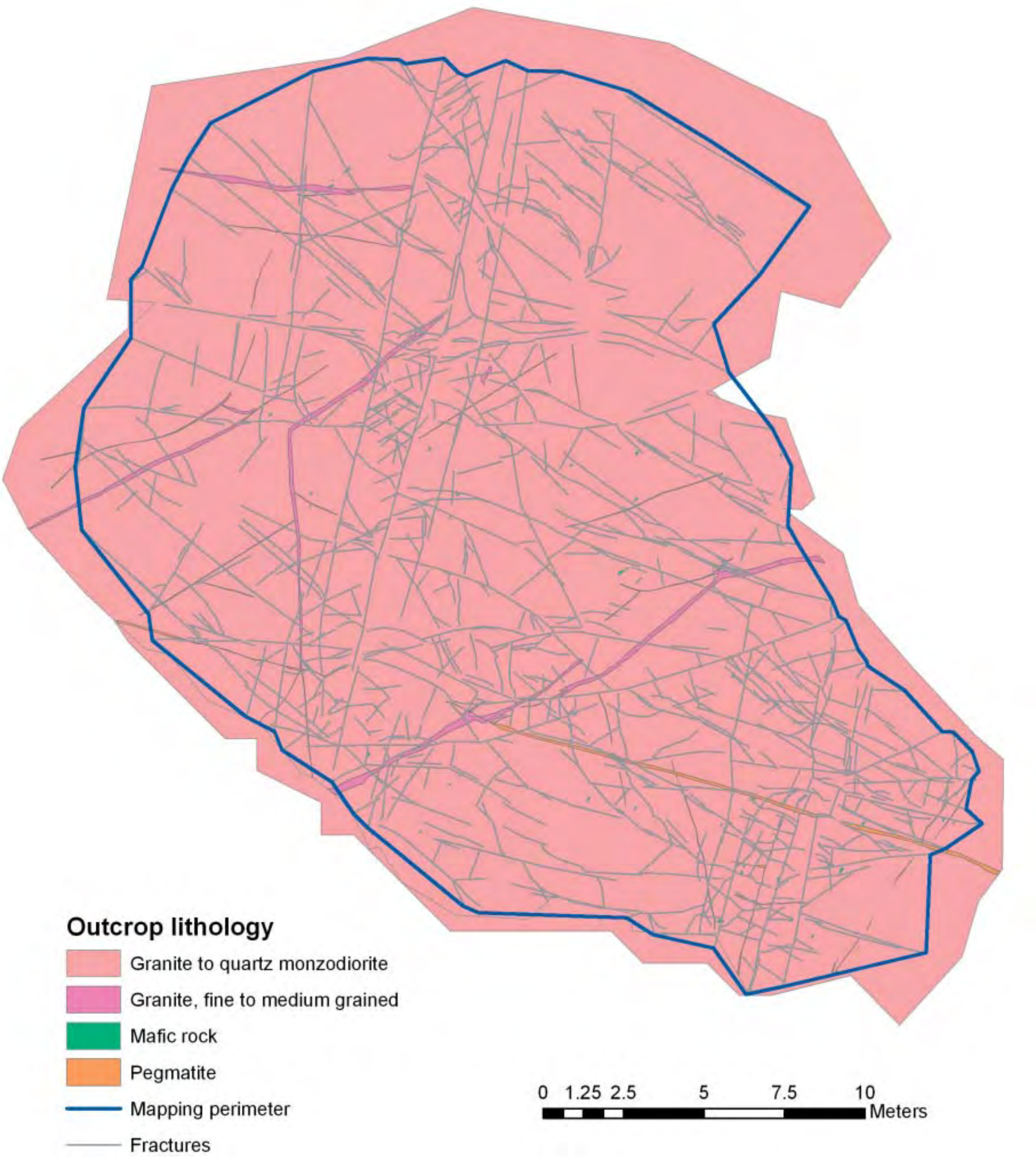

Figure 4-16. *Geologic map of outcrop ASM000026, Simpevarp subarea.*

Table 4-12. Local fracture set orientations for model Alternative 1, outcrop ASM000026, Simpevarp subarea.

Set id	Orientation model	Mean pole (tr, pl)	Major axis (tr, pl)	Dispersion (k)	# of fractures	K-S*, significance
1	Univariate Fisher	152.8, 0.2	N/A[a]	35.54	166 (18.9%)	0.097 (8.8%)
2	Univariate Fisher	99.7, 0.3	N/A[a]	21.14	183 (20.9%)	0.153 (0.04%)
3	Univariate Fisher	207.7, 1.2	N/A[a]	15.51	500 (57.1%)	0.046 (24.0%)
4	Univariate Fisher	203.0, 87.8	N/A[a]	14.29	27 (3.1%)	0.213 (1.8%)

* The Kolmogorov-Smirnov test was used to determine the statistical significance of the fit of the set orientation data to the chosen probability distribution.
[a] The major axis parameter is not relevant to univariate Fisher distributions.

Table 4-13. Local fracture set orientations for model Alternative 2, outcrop ASM000026.

Set id	Orientation model	Mean pole (tr, pl)	Major axis (tr, pl)	Dispersion (k)	# of fractures	K-S*, significance
1	Bivariate Bingham	89.4, 0.7	354.5, 82.0	–13.49,–7.88	195 (22.2%)	0.085 (19.1%)
2	Univariate Fisher	326.8, 0.1	N/A[a]	26.34	178 (20.3%)	0.122 (1.0%)
3	Bivariate Bingham	203.8, 1.2	325.2, 87.6	–23.81,–7.94	477 (54.4%)	0.056 (26.9%)
4	Univariate Fisher	207.5, 84.6	N/A[a]	10.9	27 (3.1%)	0.295 (0.03%)

* The Kolmogorov-Smirnov test was used to determine the statistical significance of the fit of the set orientation data to the chosen probability distribution.
[a] The major axis parameter is not relevant to univariate Fisher distributions.

4.4.3 Geologic controls on fracturing

A qualitative analysis of fracture property data recorded during the detailed outcrop mapping effort suggests several interesting relationships. First, fracture alteration appears to be confined largely to the younger (Local Sets #1 and #2) fracture sets in outcrop; relatively few of the older Local Set #3 fractures exhibit any recorded fracture alteration. This would suggest that most of the earliest fractures were sealed relatively quickly. Secondly, the highest proportion of open fractures occurs within Local Set #3, suggesting possible reactivation or re-opening at a later date.

In terms of geological controls, Local Set #1 appears oriented sub-parallel to the fine- to medium-grained granitic dikes present in the outcrop. Additionally, the growth of Local Set #3 is constrained by a large north-northeast trending structure (presumably a fault) cutting across the entire outcrop. Though the set is relatively homogenous on either side of this zone, the fracture pattern does exhibit significant variation inside the zone (short fractures, some evidence of banding).

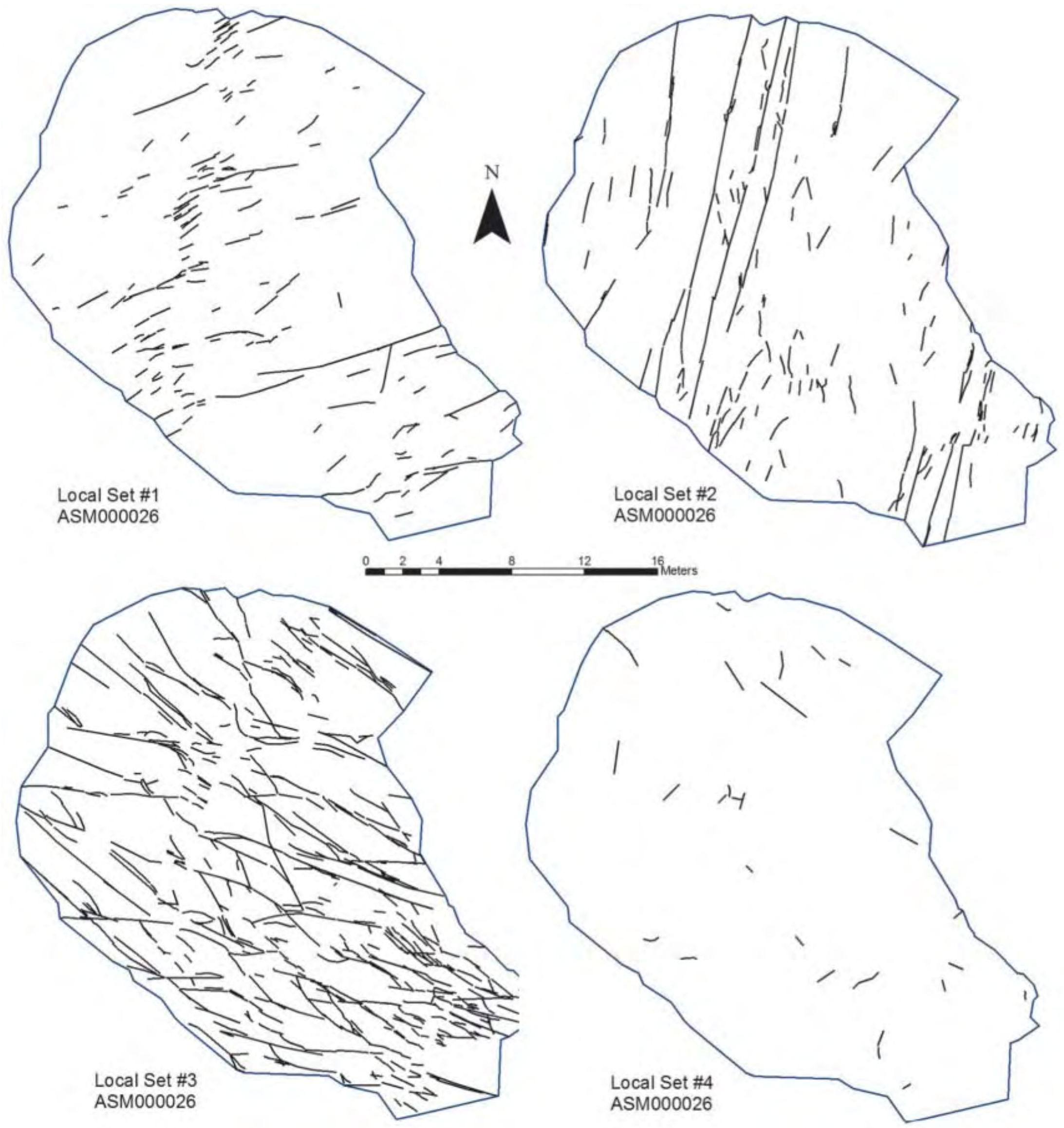

***Figure 4-17.** Outcrop ASM000026 local fracture sets, model Alternative 1, Simpevarp subarea.*

Table 4-14. Descriptive statistics for model Alternative 1 fracture sets, outcrop ASM000026, Simpevarp subarea.

Parameter	Local Set 1	Local Set 2	Local Set 3	Local Set 4
Number/% of open fractures	21 (12.7%)	23 (12.6%)	92 (18.4%)	2 (7.4%)
Number/% of sealed fractures	145 (87.3%)	160 (87.4%)	408 (81.6%)	25 (92.6%)
Number/% in Ävrö Granite* (501044)	164 (98.8%)	183 (100%)	499 (99.8%)	27 (100%)
Number/% in Pegmatite (501061)	1 (0.6%)	0	0	0
Number/% in granite dikes (511058)	1 (0.6%)	0	1 (0.2%)	0
Mean/std deviation of trace length	1.06 ± 0.85	1.34 ± 1.09	1.33 ± 1.04	1.00 ± 0.6
P_{21}	0.334	0.468	1.273	0.057

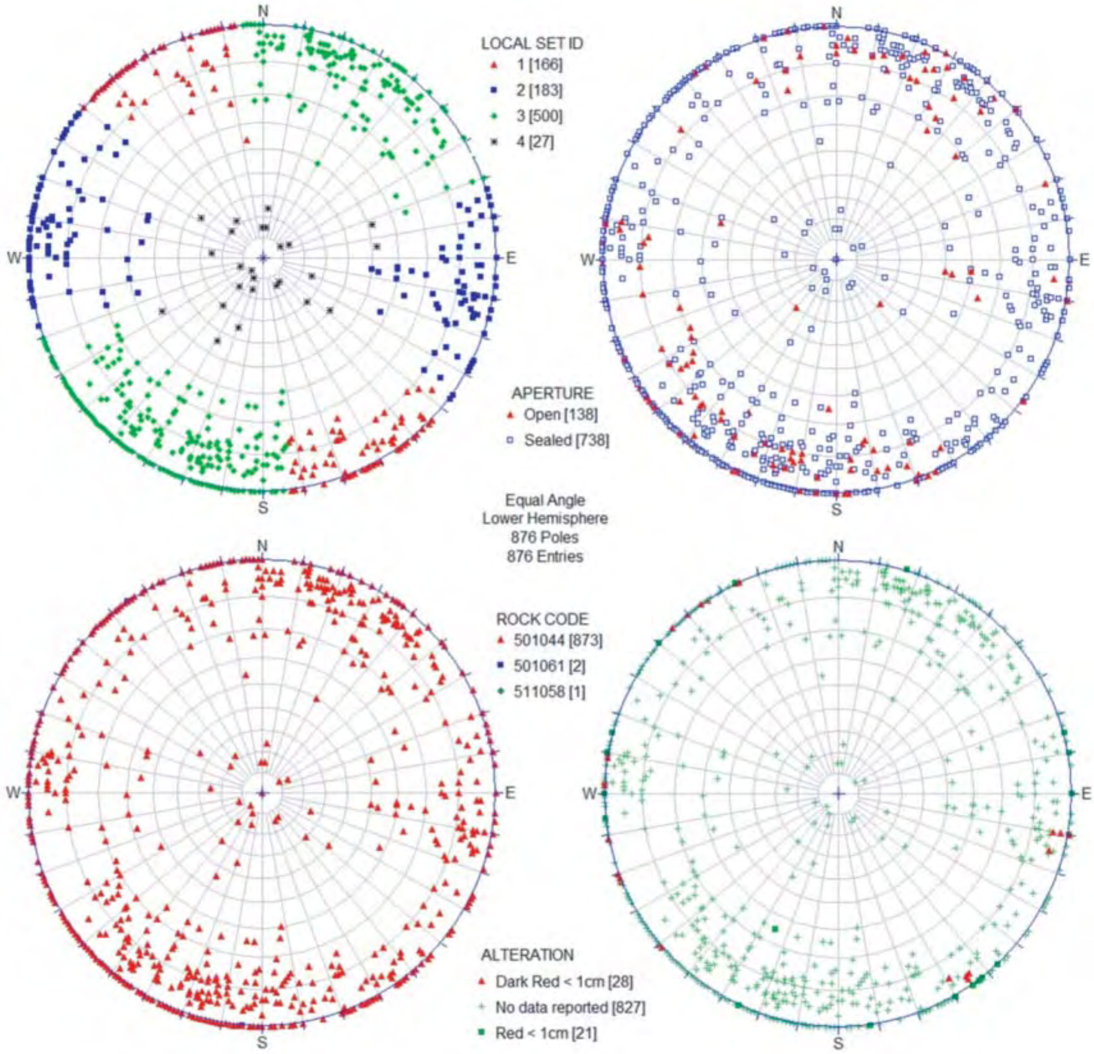

Figure 4-18. *Symbolic pole plots of ASM000026 fractures describing relevant geological parameters*

4.4.4 Local fracture set sizes

Local fracture set sizes were analyzed using the FracSize method, discussed in detail in Section 3.4.1. All distribution fits were optimized by minimizing the Kolmogorov-Smirnov statistic through a simulated annealing algorithm /Dershowitz et al. 1998/. Note that most of the size fits are not statistically significant at a reasonable ($\alpha = 0.1$; > 90%) confidence level. The preferred size model is highlighted in bold text, along with any additional size models that suggested reasonable correspondence to observed outcrop lengths.

Table 4-15. Fracture size parameters for ASM000026 local sets, model Alternative 1, Simpevarp subarea.

Local set	Size Model	Radius distribution (arithmetic space) (mean, std dev or min radius, exp)	Radius distribution (Log10 space) (mean, std dev or min radius, exp)	Fit statistics (K-S, %), (Chi-sq, %)
1	Lognormal	0.400, 0.290	–0.49, 0.282	0.152, 2.07% 35.1, 1.36%
1	Power Law	0.260, 3.10	N/A*	0.128, 7.84% 22.2, 1.39%
2	Lognormal	0.300, 0.350	–0.709, 0.403	0.0984, 25.8% 27.4, 15.9%
2	Power Law	0.310, 3.00	N/A*	0.0986, 25.6% 24.4, 1.81%
3	Lognormal	0.430, 0.350	–0.477, 0.31	0.084, 3.26% 48.2, 0.2%
4	Lognormal	0.500, 0.300	–0.368, 0.241	0.242, 12.2% 13.3, 65.2%
4	Power Law	0.240, 3.10	N/A*	0.114, 91.7% 6.93, 54.4%

* Not valid for power law distribution.

4.5 Outcrop ASM000205

Outcrop ASM000205 is located in the southwestern corner of the Simpevarp peninsula, near the southern edge of the SDM Laxemar 1.2 model limits. The outcrop is fully within Rock Domain B01 (dominated by fine-grained dioritic rocks) and is part of the Simpevarp modeling sub-domain. It is the only outcrop entirely inside the B domain. Bedrock lithologies exposed within the outcrop is predominantly fine-grained diorite (93.3%), with minor amounts of fine- to medium-grained granite (4.1%), fine-grained mafic rock (2.5%) and pegmatite dikes. The outcrop is approximately 215 square m in area.

4.5.1 Outcrop data analysis

The SICADA database file contained 1,175 mapped fractures at outcrop scale, while the SDE dataset contained traces for only 1,173 fractures. The source of this discrepancy was not known. The SICADA database was assumed authoritative for all analyses. The total number of fractures includes 102 fractures mapped that contain trace lengths shorter than the 0.5 m cut-off value. These smaller fractures were included in the local set analysis; however, they were excluded from the size analysis by truncating the fitted distribution at 0.5 m.

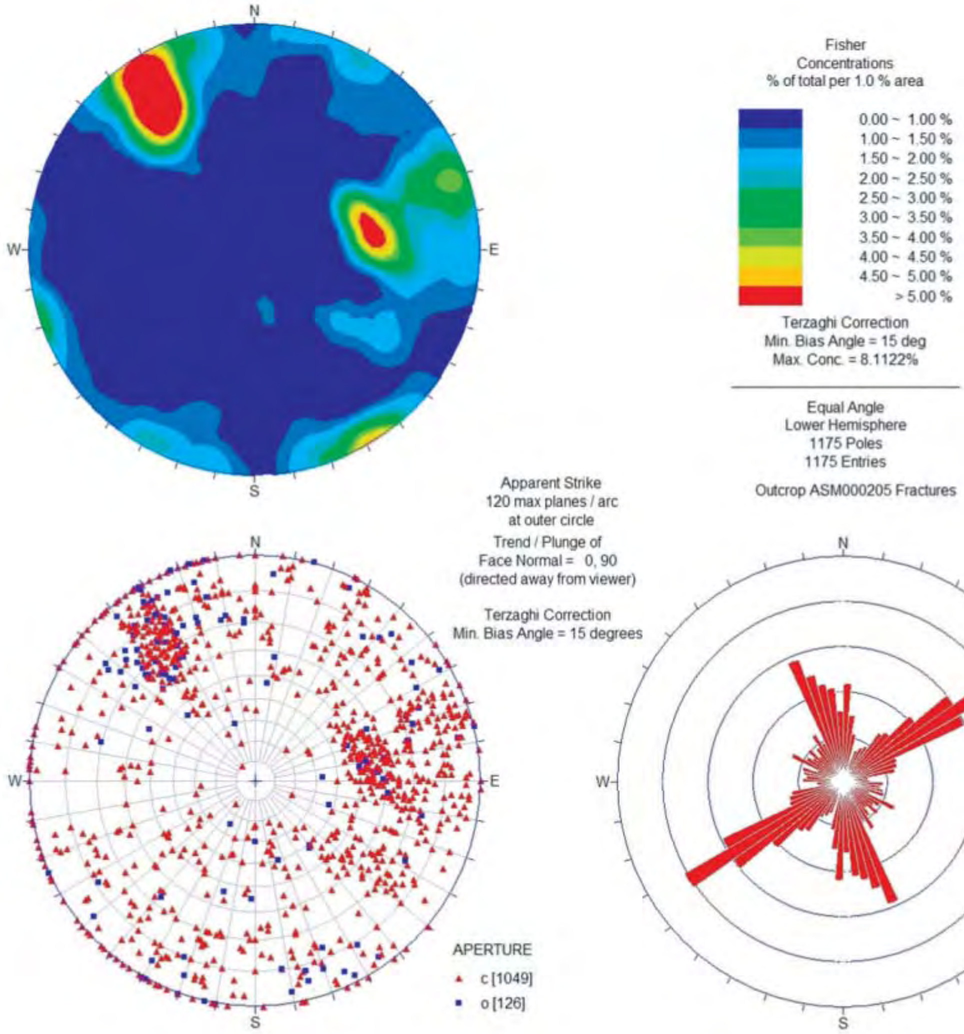

Figure 4-19. *Fracture orientation data for outcrop ASM000205. All data taken from SICADA database tables. Note that the Terzaghi correction assumes a horizontal planar outcrop. Symbolic pole plot represents fracture aperture; 'c' are sealed fractures, while 'o' are open fractures.*

4.5.2 Local fracture set orientations

Two fracture set orientation realizations were performed; one assuming only univariate Fisher spherical probability distributions (Table 4-16), and a second using a mix of probability distributions (Table 4-17) that appeared to offer slightly better statistical fits. It should be noted that neither iteration produced sets that were statistically significant at an acceptable ($\alpha = 0.1$) confidence level. Four sets were necessary to adequately characterize the polar stereoplots. However, further subdivision of Local Set #2 (and potentially Local Set #3) through more detailed tracemap analysis is possible. We elected to lump the sets together based on the desire to have a DFN model that is simpler to implement.

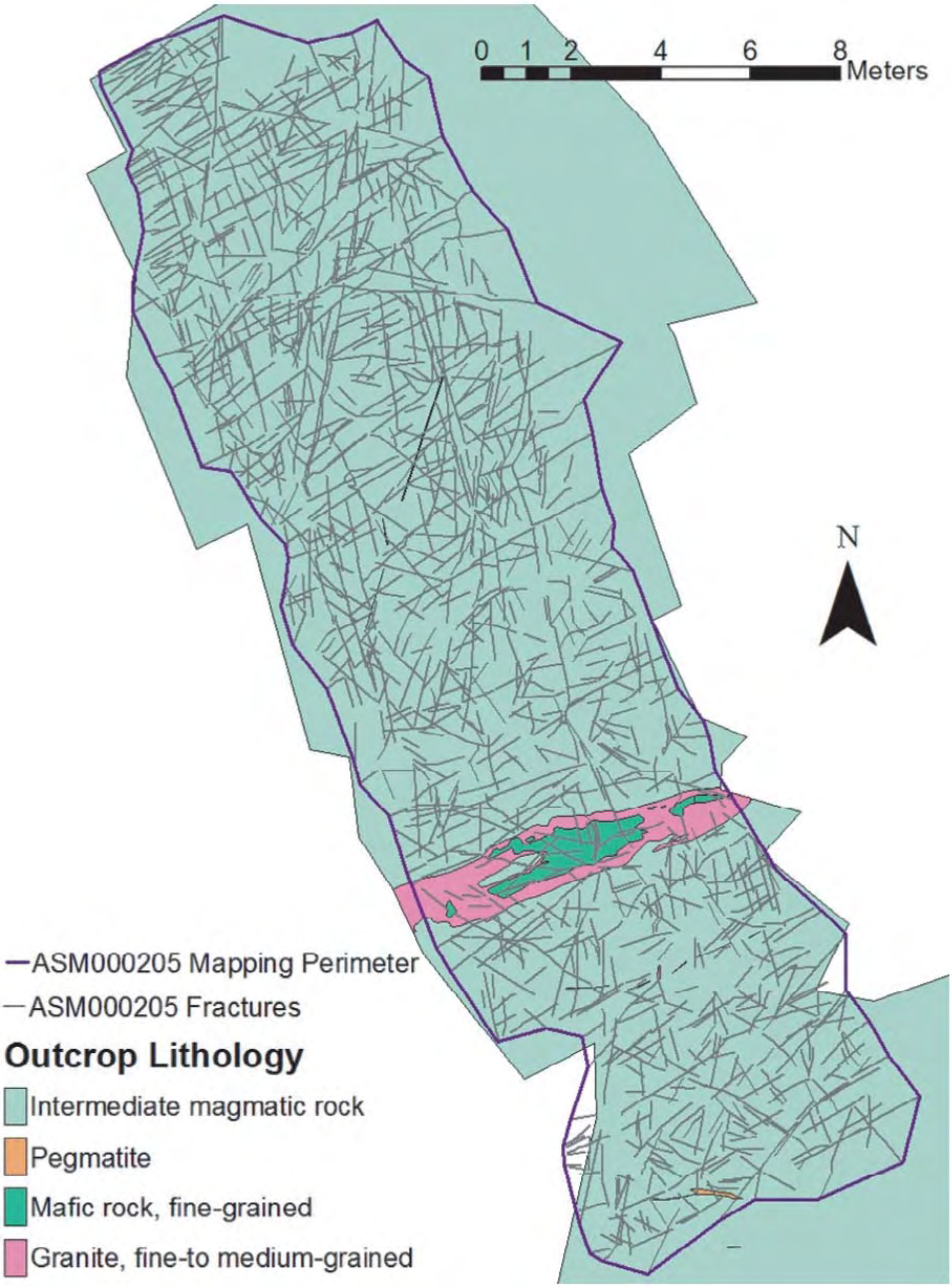

Figure 4-20. *Geologic map of outcrop ASM000205, Simpevarp subarea.*

Table 4-16. Local fracture set orientations for model Alternative 1, outcrop ASM000205, Simpevarp subarea.

Set id	Orientation model	Mean pole (tr, pl)	Major axis (tr, pl)	Dispersion (k)	Number of fractures	K-S* significance
1	Univariate Fisher	328.5, 14.3	N/A[a]	14.85	443 (37.7%)	0.120 (0.0%)
2	Univariate Fisher	76.9, 22.5	N/A[a]	17.13	359 (30.6%)	0.113 (0.02%)
3	Univariate Fisher	211.5, 10.0	N/A[a]	9.29	232 (19.7%)	0.059 (40.0%)
4	Univariate Fisher	126.7, 34.9	N/A[a]	10.10	141 (12%)	0.048 (88.0%)

* The Kolmogorov-Smirnov test was used to determine the statistical significance of the fit of the set orientation data to the chosen probability distribution.
[a] The major axis parameter is not relevant to univariate Fisher distributions.

Table 4-17. Local fracture set orientations for model Alternative 2, outcrop ASM000205, Simpevarp subarea.

Set id	Orientation model	Mean pole (tr, pl)	Major axis (tr, pl)	Dispersion (k)	# of fractures	K-S* significance
1	Bivariate Bingham	328.9, 13.3	72.6, 45	–10.44, –8.90	437	0.080 (4.2%)
2	Bivariate Bingham	78.4, 21.1	175.4, 17.5	–10.79, –7.20	399	0.122 (0.04%)
3	Univariate Fisher	210.5, 10.1	N/A[a]	9.77	219	0.060 (40.4%)
4	Univariate Fisher	133.5, 41.0	N/A[a]	10.12	154	0.076 (42.0%)

* The Kolmogorov-Smirnov test was used to determine the statistical significance of the fit of the set orientation data to the chosen probability distribution.
[a] The major axis parameter is not relevant to univariate Fisher distributions.

Outcrop fracture set chronology appears to be:

- Local Set #1 (oldest): This set is the most spatially homogenous and generally possesses the longest fractures. It does, however, show evidence of terminations against some of the longer fractures in Local Set #2. As in Outcrop ASM000026, this suggests that Local Sets #1 and #2 are contemporaneous or have experienced multiple episodes of deformation.
- Local Set #2: In general, this set shows pronounced terminations against Local Set #1 fractures. However, there are some older features within Local Set#2 that appear to cause banding or terminate Local Set #1 fractures. It may be possible to further subdivide this set (Figure 4-22) into two sub-sets, a north-northwest trending set of slightly longer fractures and a north-northeast trending set
- Local Set #3 shows pronounced banding and termination against both Local Set #1 and Local Set #2. Several of the fractures in this set also appear to have propagated from ends of Local Set #2 fractures.
- Local Set #4: This set is the youngest of all visible sets, and shows evidence of constrained growth within blocks defined by Local Set #1 and #2. This set also shows terminations against Local Set #3.

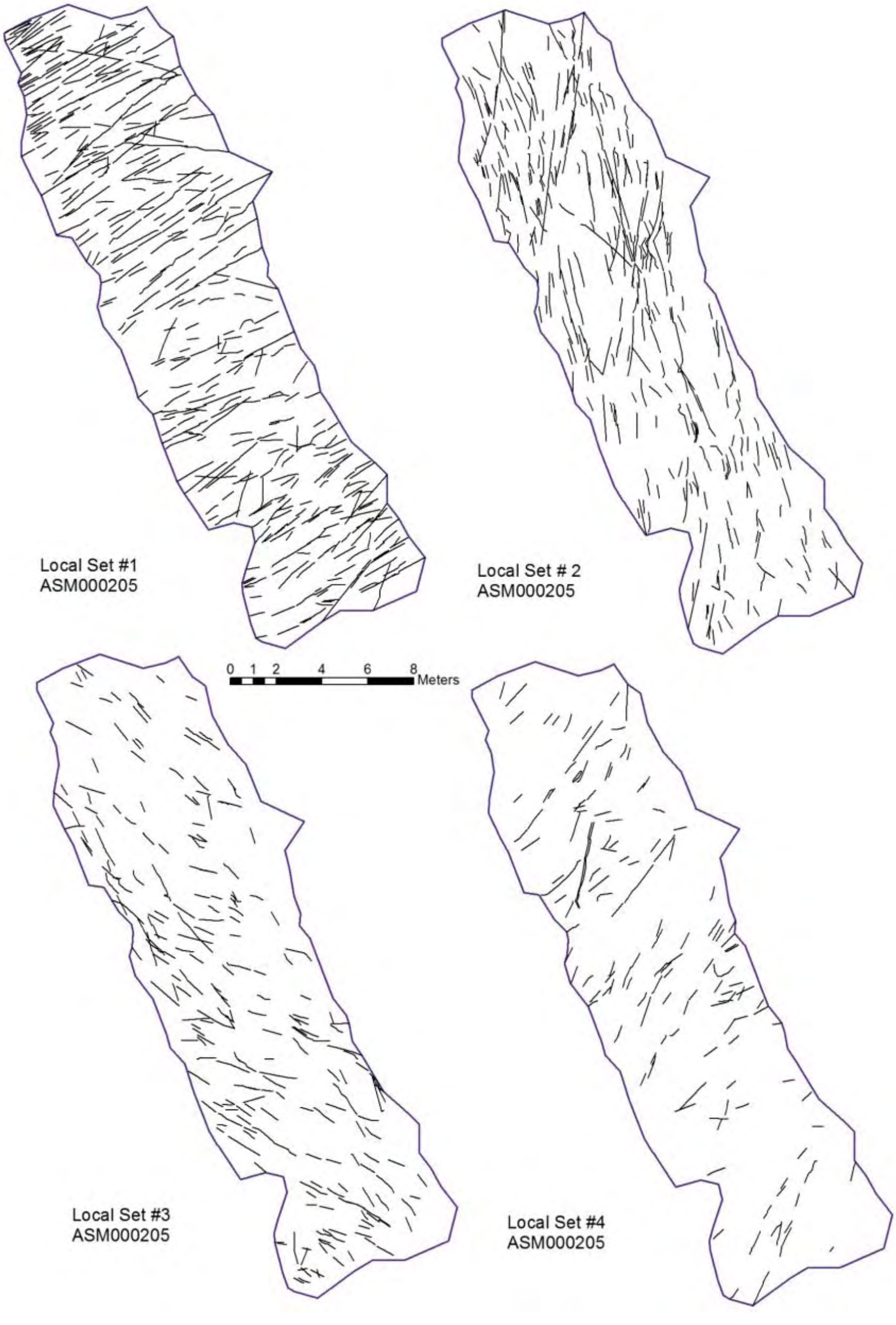

Figure 4-21. *Outcrop ASM000205 fracture sets, Simpevarp subarea.*

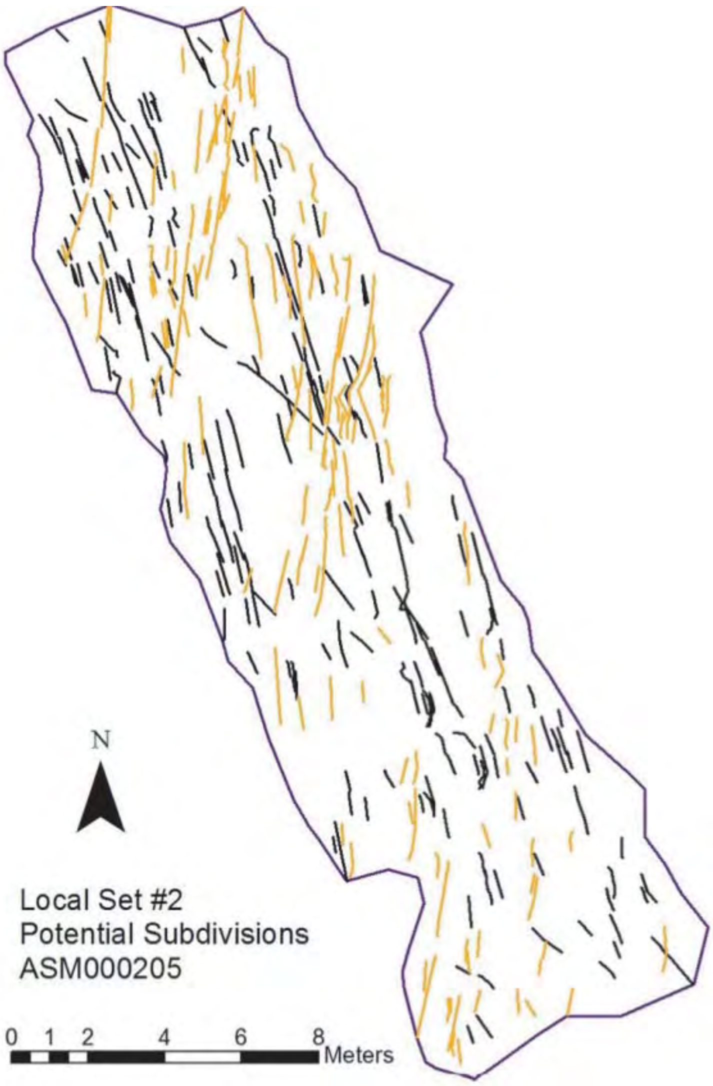

Figure 4-22. *Potential subdivision of Local Set 2 into NNW and NS/NNE trending sets.*

4.5.3 Geologic controls on fracturing

A qualitative analysis of fracture properties recorded during detailed outcrop mapping suggests that fracture orientations within ASM000205 are not controlled by host lithology ( ). However, the relative homogeneity of the outcrop (almost 94% of the outcrop area is underlain by dioritic rocks) makes this hypothesis difficult to test. Fractures exposed in this outcrop are primarily sealed fractures; however, significantly more (+10–13%) open fractures were recorded within Local Set #1. This is surprising, considering that Local Set #1 is interpreted to be the oldest fracture set. There does not appear to be a set bias with respect to fracture alteration.

Local Set #1 appears to trend subparallel to the few fine-grained granite, pegmatite, and fine-grained mafic rock intrusions present within the outcrop. This may represent a response to an older developed foliation, or contemporaneous intrusion and brittle deformation.

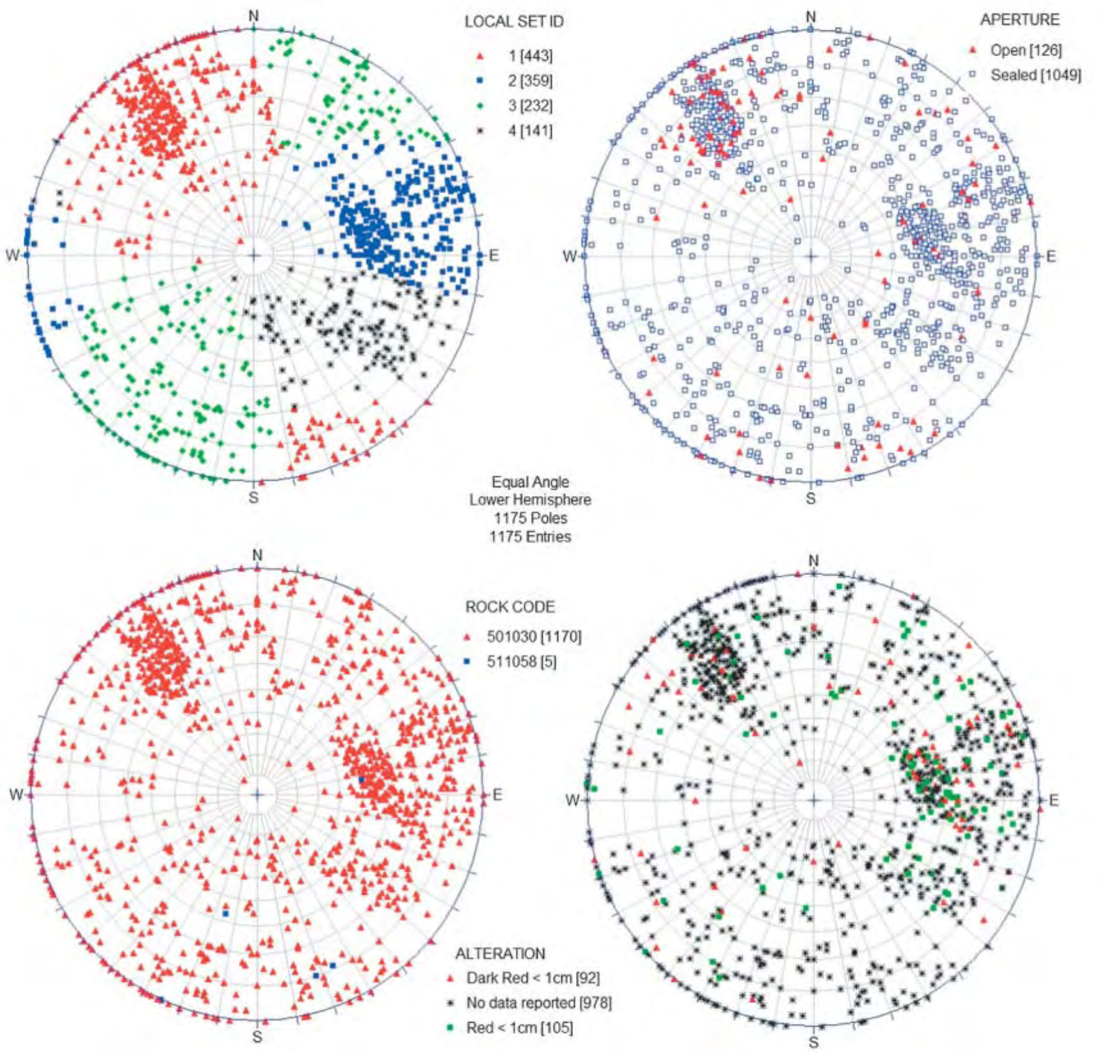

Figure 4-23. *Symbolic pole plots of ASM000205 fractures describing relevant geological parameters.*

Table 4-18. Descriptive statistics for model Alternative 1 fracture sets at outcrop ASM000205, Simpevarp subarea.

Parameter	Local Set 1	Local Set 2	Local Set 3	Local Set 4
Number/% of open fractures	78 (17.6%)	20 (5.6%)	21 (9.1%)	7 (5%)
Number/% of sealed fractures	365 (82.4%)	339 (94.4%)	211 (90.9%)	134 (95%)
Number/% in intermediate magmatic rock (501030)	441 (99.5%)	358 (99.7%)	230 (99.1%)	141 (100%)
Number/% in granite dikes (511058)	2 (0.5%)	1 (0.3%)	2 (0.9%)	0 (0%)
Mean/std deviation of trace length	0.98 ± 0.54	0.92 ± 0.55	0.82 ± 0.38	0.82 ± 0.52
P_{21}	2.017	1.535	0.88	0.547

4.5.4 Local fracture set sizes

Local fracture set sizes were analyzed using the FracSize method, discussed in detail in Section 3.4.1. All distribution fits were optimized by minimizing the Kolmogorov-Smirnov statistic through a simulated annealing algorithm /Dershowitz et al. 1998/. Note that none of the size fits are not statistically significant at a reasonable (α = 0.1; > 90%) confidence level. The preferred size model is highlighted in bold text, along with any additional size models that suggested reasonable correspondence to observed outcrop lengths. The lack of a statistically significant fit is likely due to the very limited size range (0.5 m – < 10 m) of fractures exposed in the outcrop. In addition, Outcrop ASM000205 has a significant north-south elongation; this may introduce a sampling bias, as the dominant fracture sets in the outcrop appear to trend east-west.

Table 4-19. Fracture size parameters for ASM000205 local sets, model Alternative 1, Simpevarp subarea.

Local set	Size model	Radius distribution (arithmetic space) (mean, std dev or min radius, exp)	Radius distribution (Log10 space) (mean, std dev or min radius, exp)	Fit Statistics (K-S, %)/ (Chi-sq, %)
1	Lognormal	0.285, 0.190	–0.625, 0.263	0.088, 6.46% 31.4, 1.2%
2	Power Law	0.235, 3.58	N/A*	0.114, 1.85% 47.2, 0.0%
3	Lognormal	0.143, 0.136	–0.985, 0.348	0.147, 1.37% 34, 0.34%
3	Power Law	0.103, 3.30	N/A*	0.138, 2.42% 50.2, 0.0%
4	Lognormal	0.235, 0.129	–0.685, 0.222	0.0922, 58.7% 21, 17.8%
4	Power Law	0.244, 3.85	N/A*	0.0922, 58.7% 13.3, 3.0%

* Not valid for power law distribution.

4.6 Outcrop ASM000206

Outcrop ASM000206 is located along the northern edge of the Simpevarp peninsula within the Simpevarp model subarea. The outcrop lies completely within Rock Domain C01 (a mixture of Ävrö granite and quartz monzodiorite); lithologies exposed in outcrop include quartz monzodiorite (69.5%), fine- to medium-grained granite (17.1%), pegmatite (13.3%), and fine-grained mafic rock (0.1%). Outcrop ASM000206 spans approximately 245.5 square m.

4.6.1 Outcrop data analysis

Both the SICADA and SDE databases record 940 fractures within the mapping perimeter of outcrop ASM000206. This includes 136 fractures with recorded trace lengths smaller than the 0.5 m cut-off indicated by the mapping protocol. These smaller fractures were included in the local set analysis; however, they were excluded from the size analysis by truncating the fitted distribution at 0.5 m.

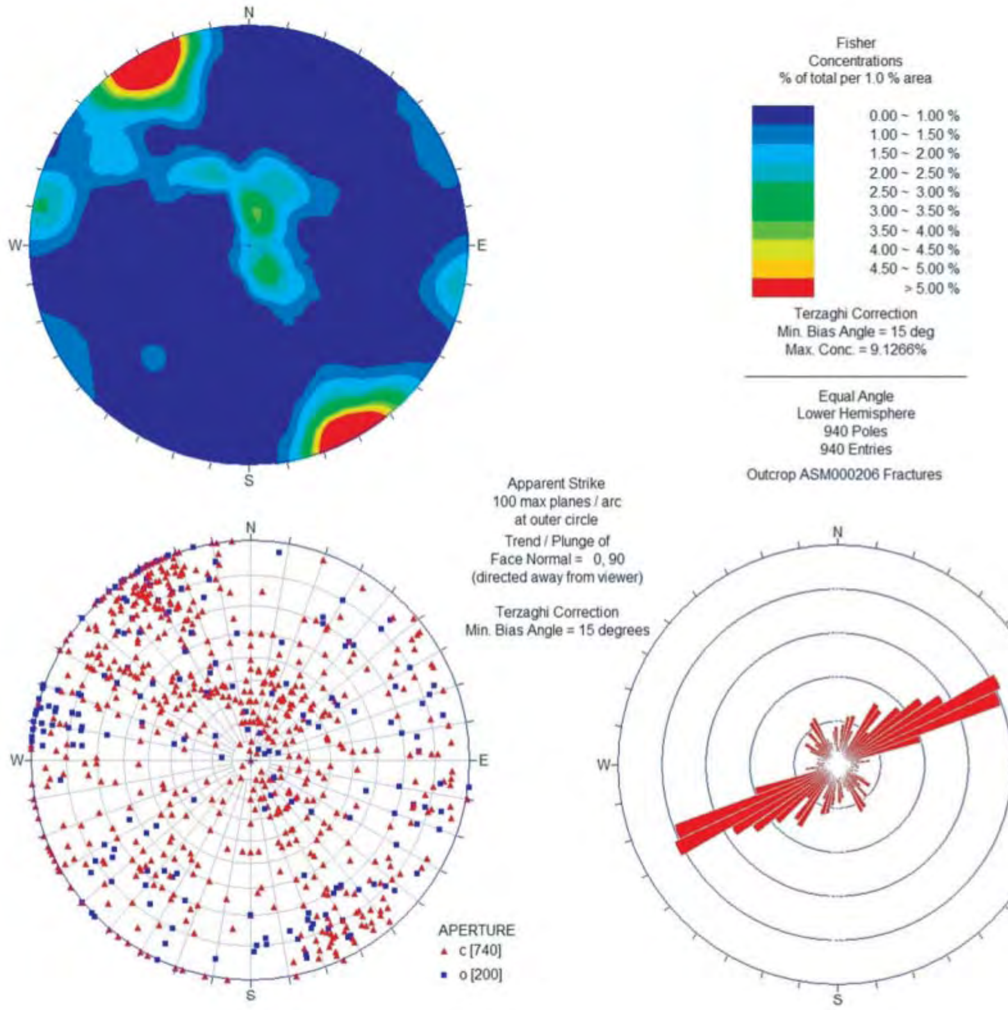

Figure 4-24. *Fracture orientation data for outcrop ASM000206. All data taken from SICADA database tables. Note that the Terzaghi correction assumes a horizontal planar outcrop. Symbolic pole plot represents fracture aperture; 'c' are sealed fractures, while 'o' are open fractures.*

4.6.2 Local fracture set orientations

Four sets (Table 4-20) were necessary to adequately characterize the polar stereoplots. However, it may be possible to further subdivide Local Set #3 based on trace map refinement; a longer north-northeast trending fracture set can potentially be broken out from the bulk of the shorter northeast trending fractures. It may also be possible to further subdivide the subhorizontal fracture set, or to partition some of its members into subvertical sets by assigning larger dispersions to the fitted orientation probability distributions. Set orientations were chosen to minimize model complexity.

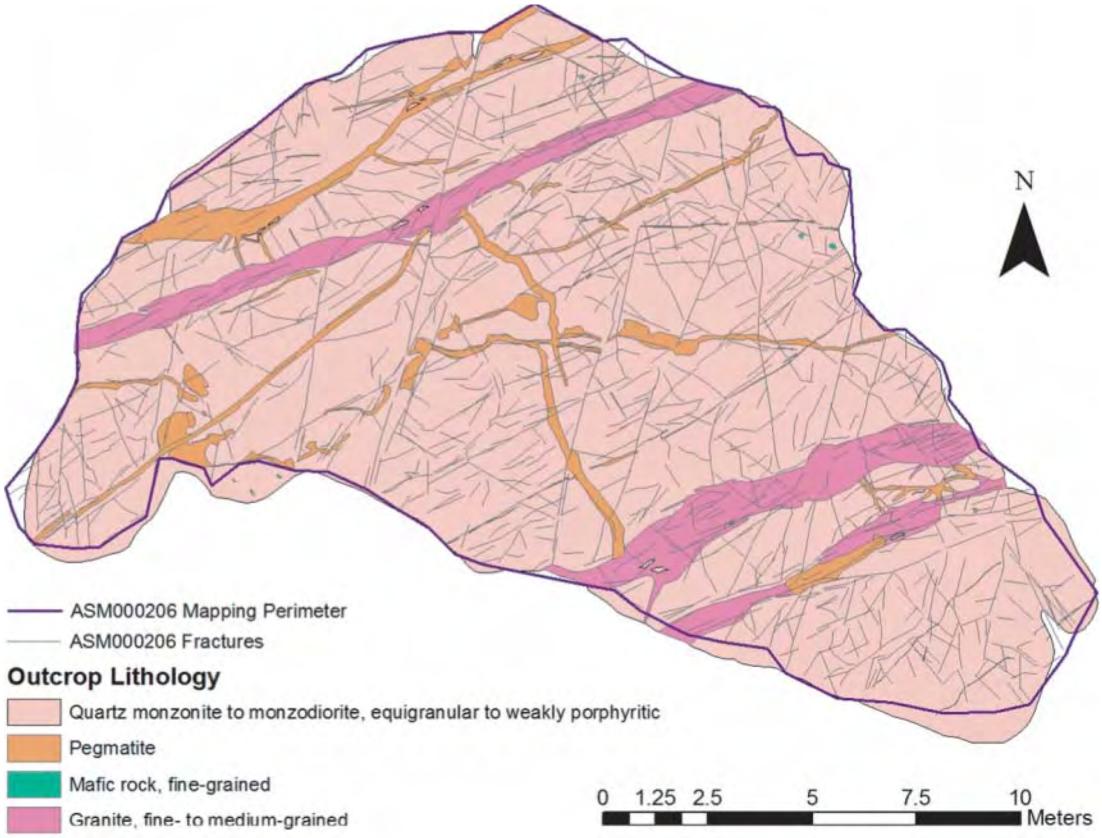

Figure 4-25. Geologic map of outcrop ASM000206, Simpevarp subarea.

Table 4-20. Local fracture set orientations for model Alternative 1, outcrop ASM000206, Simpevarp subarea.

Set id	Orientation model	Mean pole (tr, pl)	Major axis (tr, pl)	Dispersion (k)	Number of fractures	K-S* significance
1	Univariate Fisher	331.3, 3.3	N/A[a]	18.37	372 (39.6%)	0.161 (0.0%)
2	Univariate Fisher	46.3, 77.6	N/A[a]	7.95	232 (24.7%)	0.080 (2.9%)
3	Univariate Fisher	287.6, 6.3	N/A[a]	11.47	182 (19.4%)	0.048 (79.1%)
4	Univariate Fisher	227.3, 6.6	N/A[a]	10.03	154 (16.4%)	0.047 (69.0%)

* The Kolmogorov-Smirnov test was used to determine the statistical significance of the fit of the set orientation data to the chosen probability distribution.
[a] The major axis parameter is not relevant to univariate Fisher distributions.

The chronology of Outcrop ASM000206 fracturing appears to be:

- Local Set #3 (oldest): Though this set is neither the most spatially homogenous nor the most intense, it does possess the longest fractures. In addition, both Local Set #1 and #4 show evidence of banding against this set.

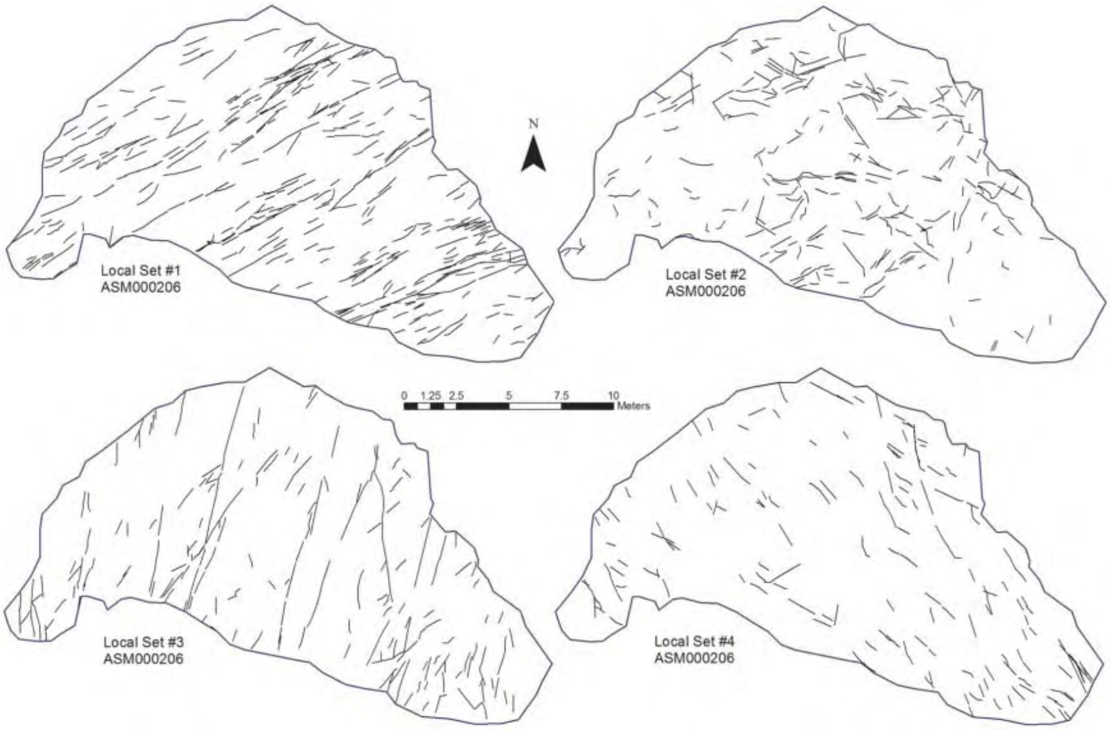

Figure 4-26. *Outcrop ASM000206 fracture sets, Simpevarp subarea.*

- Local Set #1: This set is the most spatially homogenous, and shows decided banding against Local Set #3. Offsets of earlier fracturing can be seen in several places. This set has surprisingly consistent fracture orientations in outcrop.
- Local Set #4 (youngest): This set has pronounced terminations against Local Set #3, and shows evidence of constrained growth within local blocks created by the intersections of fractures in Local Set #1 and Local Set #3.
- Local Set #2 (age unknown): This predominantly subhorizontal set appears to be younger than Local Set #1; it shows some degree of termination against both Local Set #1 and Local Set #2. However, it is difficult to determine relative ages of subhorizontal fractures from outcrop pattern alone.

4.6.3 Geologic controls on fracturing

A qualitative analysis of fracture properties recorded during detailed outcrop mapping suggests some significant geologic controls on outcrop fracture patterns. Local Set #1 trends subparallel to the orientations of fine-grained granite, pegmatite, and fine grained mafic rock dikes within the outcrop. In addition, a significantly larger (10%) of Local Set #1 fractures are hosted within the fine-grained granite veins and dikes (see Table 4-21). This pattern of intensity variation is not seen in other outcrops, even where a set subparallel to lithological contacts is noted.

Local Sets #3 and #4 host approximately 10% more open fractures than Local Sets #1 and #2; this may represent either later reactivation of existing structures. Fracture alteration appears to be limited largely to the subhorizontal fracture set (Figure 4-27).

Table 4-21. Descriptive statistics for model Alternative 1 fracture sets at outcrop ASM000206, Simpevarp subarea.

Parameter	Local Set 1	Local Set 2	Local Set 3	Local Set 4
Number/% of open fractures	72 (19.4%)	31 (13.4%)	53 (29.1%)	44 (28.6%)
Number/% of sealed fractures	300 (80.6%)	201 (86.6%)	129 (70.9%)	110 (71.4%)
Number/% in Äspö diorite (501036)	276 (74.2%)	215 (92.7%)	168 (92.3%)	142 (92.2%)
Number/% in pegmatite (501061)	13 (3.5%)	2 (0.9%)	4 (2.2%)	2 (1.3%)
Number/% in granite dikes (511058)	83 (22.3%)	15 (6.5%)	10 (5.5%)	10 (6.5%)
Mean/std deviation of trace length	0.83 ± 0.41	0.79 ± 0.38	1.0 ± 0.74	0.83 ± 0.42
P_{21}	1.259	0.759	0.74	0.516

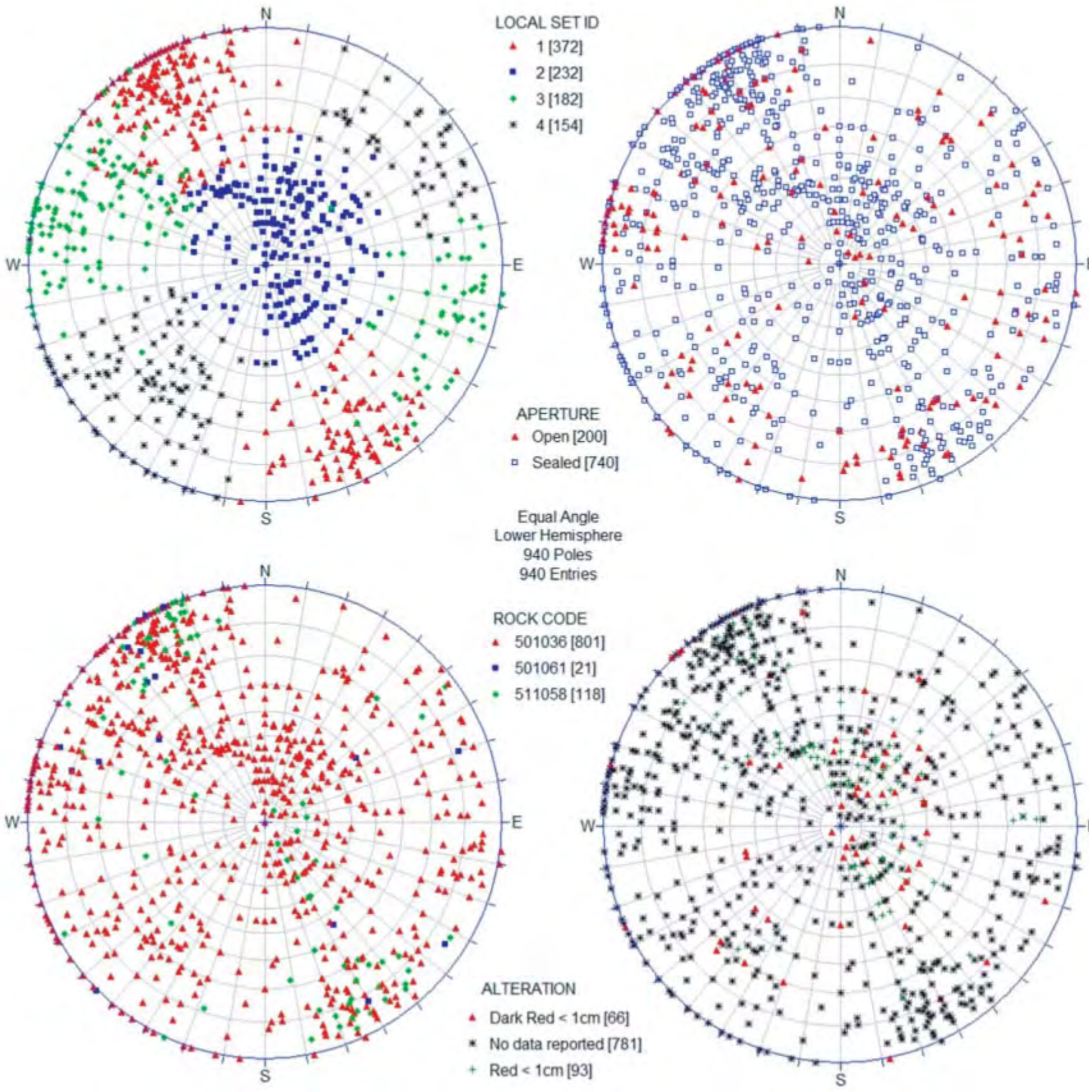

Figure 4-27. *Symbolic pole plots of ASM000206 fractures describing relevant geological parameters*

4.6.4 Local fracture set sizes

Local fracture set sizes were analyzed using the FracSize method, discussed in detail in Section 3.4.1. All distribution fits were optimized by minimizing the Kolomogorov-Smirnov statistic through a simulated annealing algorithm /Dershowitz et al. 1998/. Note that none of the size fits are not statistically significant at a reasonable (α = 0.1; > 90%) confidence level. The preferred size model is highlighted in bold text, along with any additional size models that suggested reasonable correspondence to observed outcrop lengths. The lack of a statistically significant fit is likely due to the very limited size range (0.5 m – < 10 m) of fractures exposed in the outcrop.

Table 4-22. Fracture size parameters for ASM000206 local sets, model Alternative 1, Simpevarp subarea.

Local set	Size model	Radius distribution (arithmetic space) (mean, std dev or min radius, exp)	Radius distribution (Log10 space) (mean, std dev or min radius, exp)	Fit statistics (K-S, %)/ (Chi-sq, %)
1	Lognormal	0.369, 0.143	–0.463, 0.162	0.132, 0.32% 44.6, 0.05%
2	Lognormal	0.100, 0.110	–1.17, 0.387	0.207, 0.01% 37.4, 0.1%
3	Lognormal	0.234, 0.168	–0.722, 0.281	0.17, 0.88% 41.5, 0.08%
3	Power Law	0.251, 3.32	N/A*	0.17, 0.88% 43.8, 0.0%
4	Lognormal	0.158, 0.133	–0.917, 0.318	0.131, 14.5% 25.1, 3.4%
4	Power Law	0.135, 3.37	N/A*	0.131, 14.5% 27, 0.01%

* Not valid for power law distribution.

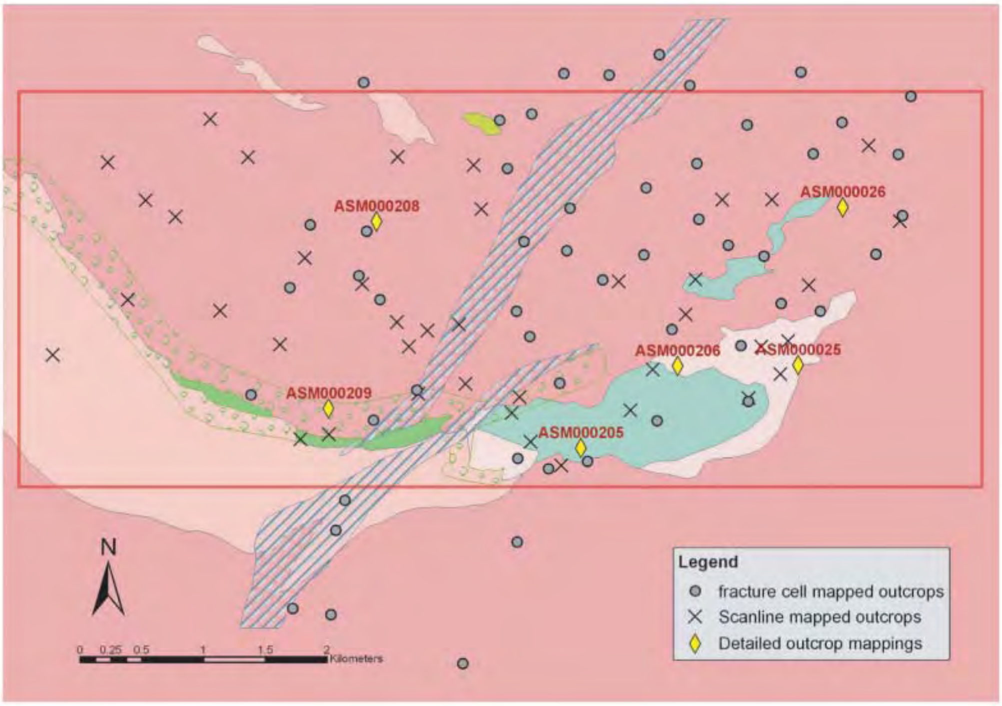

Figure 4-28. *Location of small-scale cell mapping and scanline outcrops within the Oskarshamn model region. Map units represent preliminary (January 2005) SDM Laxemar 1.2 rock-domain model.*

4.7 Qualitative analysis of additional outcrop data

Once local and tentative regional-scale fracture set assignments were made based on the detailed large-scale outcrop mapping, an additional qualitative analysis of fracturing along scanlines and smaller outcrops across the Oskarshamn region was performed. A total of 52 fracture cell-mapped outcrops and 31 scan line sets were used /SICADA, 2004a/. Note that the scanline data developed during detailed outcrop mapping (ASM000025–ASM000209) was not used in this qualitative analysis. The analysis was entirely qualitative, and the fracture pole data not used to develop global set orientations.

Fracture orientation data was combined in contoured pole stereoplots and linked to spatial domains via ArcGIS; this allowed for the identification of areas where certain fracture sets were either missing or more intense. No other parameters besides spatial distribution and fracture orientation were analyzed; the mapping coverage in this data set was too sparse for further work.

The analysis confirms that, in general, the three subvertical-dipping 'global' sets (WNW-trending, ENE- trending, and NS-trending) seen in outcrops ASM000025 through ASM000208 are seen elsewhere across the Simpevarp region. However, some variation in set intensity was noted across the region. The WNW and ENE sets predominate; the NS set is generally much weaker in intensity, and appears to be confined largely to the Simpevarp subarea. The only truly specific spatial effect was noted in the northwestern corner of the model region; both the WNW and NS sets were absent from outcrops in this area.

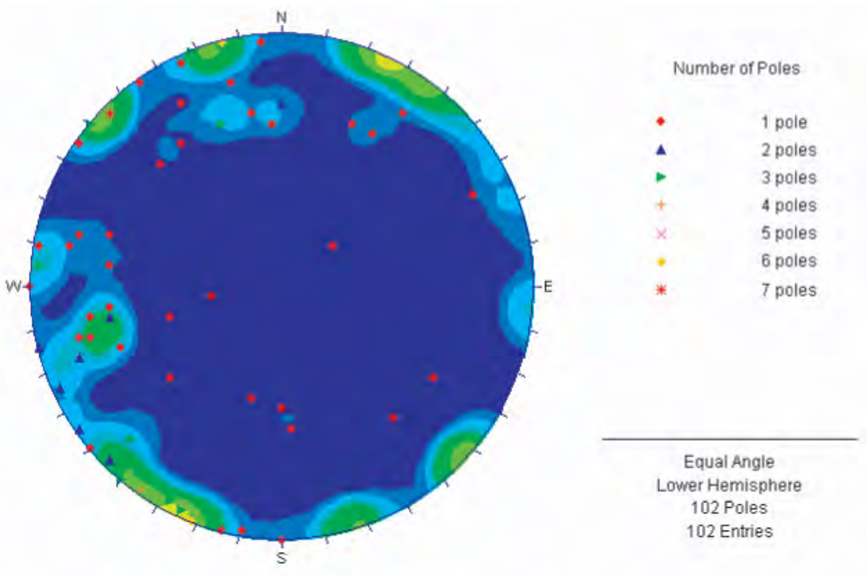

Figure 4-29. *Example combined polar/contoured stereoplot. This graphic illustrates outcrop PSM100045; note the presence of all three of the 'global' sets identified in the detailed outcrop mapping.*

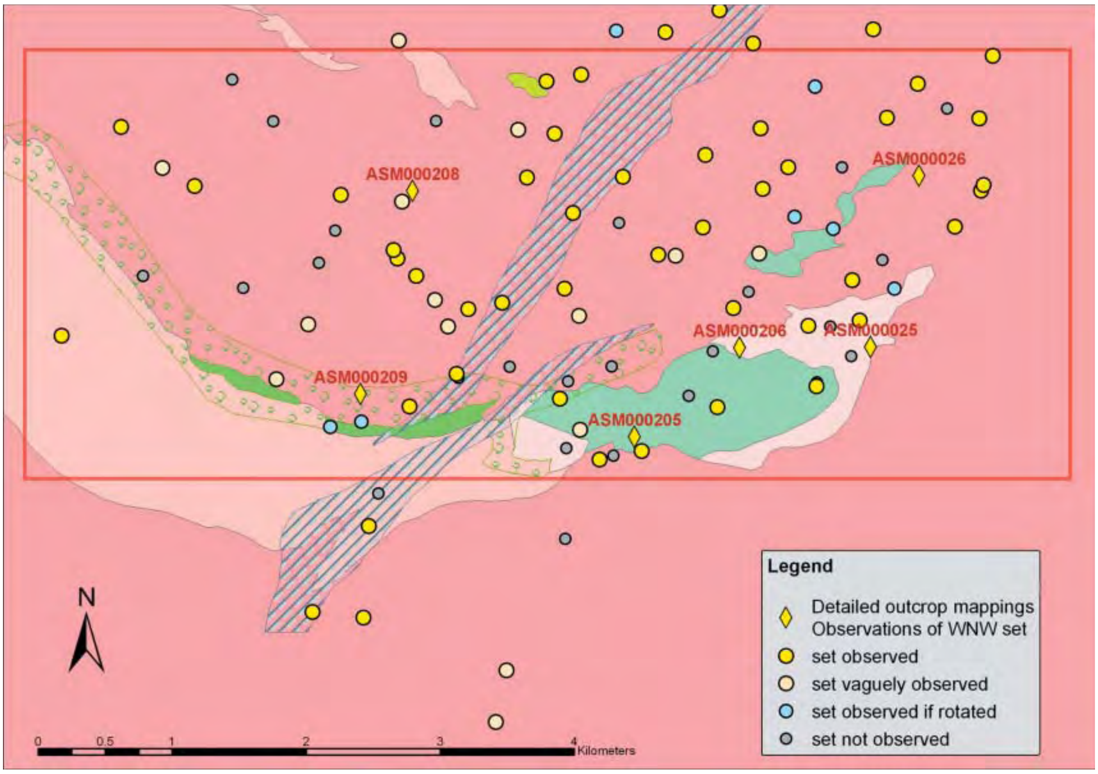

Figure 4-30. *Map of outcrops where the WNW-trending fracture set was observed. Note the teal-colored outcrops; these represent areas where, if the stereonet is rotated slightly, the WNW set appears in the correct location.*

The analysis also indicates a shallow to moderately-dipping set of NW-trending fractures; this set is seen only in the southern half of the map. These 'local' sets are labeled Set S_e and Set S_f in the Simpevarp and Laxemar modeling sub-regions, respectively. These sets are visible on many outcrops, but only as a weakly defined and diffuse set. Both sets are most visible near the intersection of a mapped mixing zone (the green stippled rock domain in Figure 4-31 and Figure 4-32) and the Äspö shear zone (blue hashed zone in Figure 4-31 and 4-32); they may be a side effect of deformation along these structures. Set S_f, however does, however, increase intensity in the areas surrounding the southernmost Laxemar detailed outcrop (ASM000209).

For some of the small-scale cell map or scanline outcrops, there was no correspondence between the mapped fracture pattern and the tentative regional set model. However, if a minor (10°–20°) counterclockwise rotation was introduced (Figure 4-33), the stereoplot began to look similar to those created from the detailed outcrop mapping (ASM000025–ASM000209). No spatial correlation of these 'rotated' outcrops was possible; there were slightly more of them in the eastern part of the Simpevarp model region than on the Simpevarp penninsula. In addition, no specific evidence for block rotations is visible in the detailed outcrop mapping.

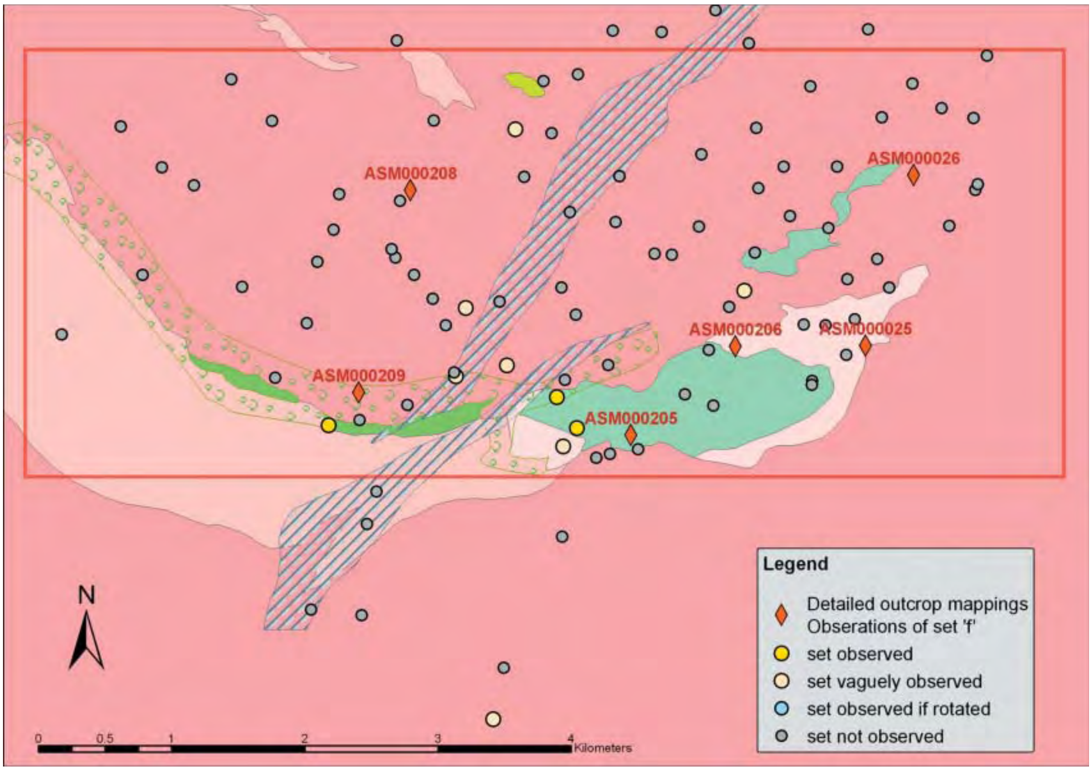

Figure 4-31. *Map showing outcrops containing 'local' fracture set S_f, identified in Laxemar outcrop ASM000209. Notice the set is also visible within the Simpevarp subarea.*

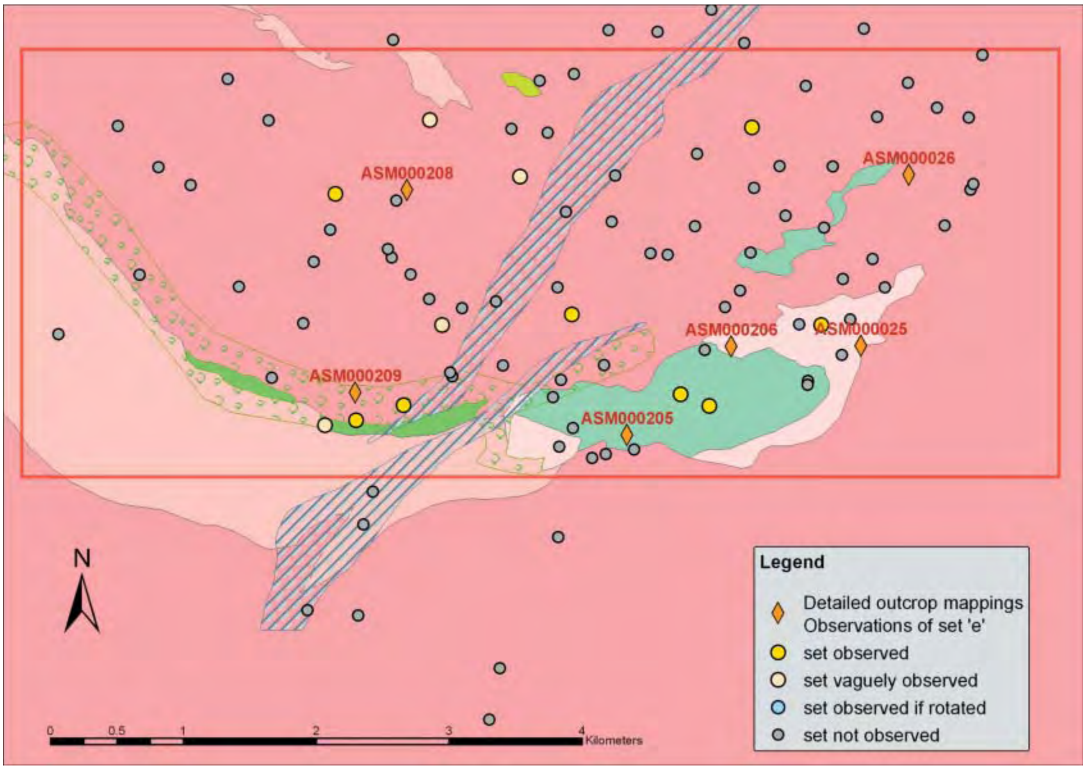

Figure 4-32. *Map showing outcrops containing 'local' fracture set S_e, identified in Simpevarp outcrops ASM000025 and (tentatively) in ASM000205.*

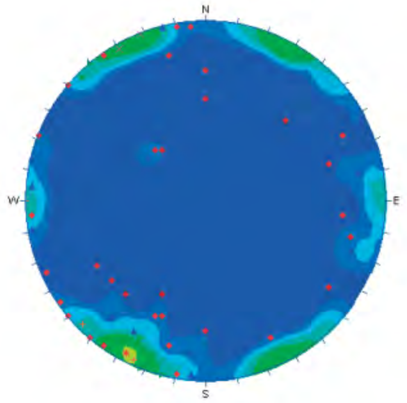

PSM 100017 Outcrop with typical distribution of sets. Resembling the DFN analyses.

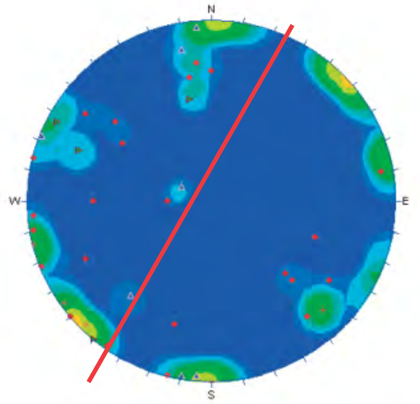

PSM 100006 Outcrop resembles the DFN distribution of set if applied to a 30 degrees twist to the left.

Figure 4-33. *Illustration of potential block rotations observed in small-scale outcrop cell mapping and scanline data.*

4.8 Summary of local outcrop analysis and derivation of global orientation model

In general, four to five distinct fracture sets were required to adequately characterize the fracturing observed in the six detailed outcrops. However, it is possible to create further set subdivisions based on analysis of cross-cutting relationships in fracture trace maps. Specifically, the sets designated NS* (North-South striking) can be broken into two roughly conjugate components; one striking slightly east of north, and one striking slightly west of north. Since a fundamental assumption of this iteration of the Oskarshamn region DFN was that the model should have as few fracture sets as possible, these potential subsets were not partitioned out. Table 4-23 presents a summary of local outcrop set orientations.

In general, local fracture sets were best fit using lognormal or power law probability distributions. However, except for a few cases, none of the fitted distributions was statistically significant at a reasonable ($\alpha = 0.1$) confidence level. This is most likely due to the combination of the lower-size mapping cutoff at 0.5 m with a lack of larger (> 5 m) fractures. This tends to produce an extremely narrow range of size data, which makes fitting any probability distribution difficult.

Table 4-23. Summary of local outcrop set orientations. The numbers corresponds to the local set number assigned during the outcrop evaluation (Section 4.1 through 4.6).

Outcrop	Local Set Number (general fracture strike)								
	ENE	NE	NNE	WNW	NNW	NW	EW	NS*	Sub-horizontal
ASM000025		3	2	1	4				5
ASM000026	1		2	3					4
ASM000205	1		4	3				2	
ASM000206		1	3			4			2
ASM000208	1				3			2	4
ASM000209			2		3		1		4

4.8.1 Generating global fracture sets

The next step after analyzing local-scale fracture set orientations observed in outcrop is to generate a domain-scale orientation model. The orientation model is 'simplified' by combining outcrop sets with similar strikes on stereonet plots to form larger (and more disperse) scale sets. Set membership was determined by a qualitative 'goodness of fit' judgement, which was guided by the outcrop stereonets, the orientations of the regional deformation zones, and by the knowledge of the tectonic history of the area. The resulting fracture sets emphasize reasonable stereonet and outcrop pattern results over statistical goodness-of-fit (Kolomgrov-Smirnov, Chi-Squared) test statistics.

The analysis of detailed outcrop maps, along with the qualitative assessment of scanlines and smaller-scale outcrops, suggests that there are three regional fracture set trends observed in both the Laxemar and Simpevarp subareas:

- Northeast – Southwest Trending.
- Northwest – Southeast Trending.
- East-West Trending.

Note that many of these trends are also visible in contoured steroeplots of deformation zone orientations; however, the scatter in the DZ orientations is quite large. These five basic sets should adequately characterize fracturing within Laxemar and Simpevarp at the global scale (kilometers); however, additional refinement is probably necessary for site-scale (10–100 m) and repository-scale (100 m–1,000 m) modeling.

The DFN model for both the Laxemar and the Simpevarp subareas share the following definitions:

1. All fracture sets identified as DFN model components are specified using the following syntax: 'S_set-letter'.
2. fracture sets that are 'regional' in scope (i.e. follow a power-law scaling relationship between outcrop-scale and deformation zone-scale, and are seen in both subareas) are labeled using a capitalized letter (S_A, B, C).
3. Fracture sets that are 'local' in scope (i.e. their distribution is confined to a single subarea) are labeled using a lower-case letter (d, e, f).
4. Both the Laxemar and Simpevarp subareas feature a fracture set consisting of primarily subhorizontally-dipping fractures. To avoid confusion, this set is defined as 'Set d' in both subareas, even though the actual set properties vary between modeling subareas.

Once all outcrop fractures were assigned to a global-scale set, the results were entered into FracSys/ISIS, where a single orientation analysis iteration, using the global set parameters and a hard-sector assignment, was completed to generate global distribution parameters and fit statistics. Two alternative orientation models were fitted to the global data. The first assumed only univariate Fisher spherical probability distributions, while the second assumed a mixture of probability distributions, with the intent to improve the goodness-of-fit statistics. Only the univariate Fisher fits are presented as a formal DFN model specification. Some overlap, especially in the Simpevarp outcrops, is noted between fracture sets. This is caused by the fact that global fracture sets are assigned a priori from the local fracture sets, and not 'fitted' using a clustering algorithm. Table 4-24 presents the local fracture set assignments at each outcrop to the global (model-scale) fracture sets. Figures 4-34 to 4-39 illustrates the set orientation alternatives for each subarea.

Table 4-24. Local fracture set assignment to global (model-scale) fracture sets. The numbers corresponds to the local set number assigned during the outcrop evaluation (Section 4.1 through 4.6).

Global set	Local outcrop sets					
	ASM000025	ASM000026	ASM000205	ASM000206	ASM000208	ASM000209
S_A	3	1	1	1	1	1
S_B	2	2	4	3	2	2
S_C	1	3	3	4	5	3
S_d	5	4	N/A	2	4	4
S_e/f	4	N/A	2	N/A	3	N/A

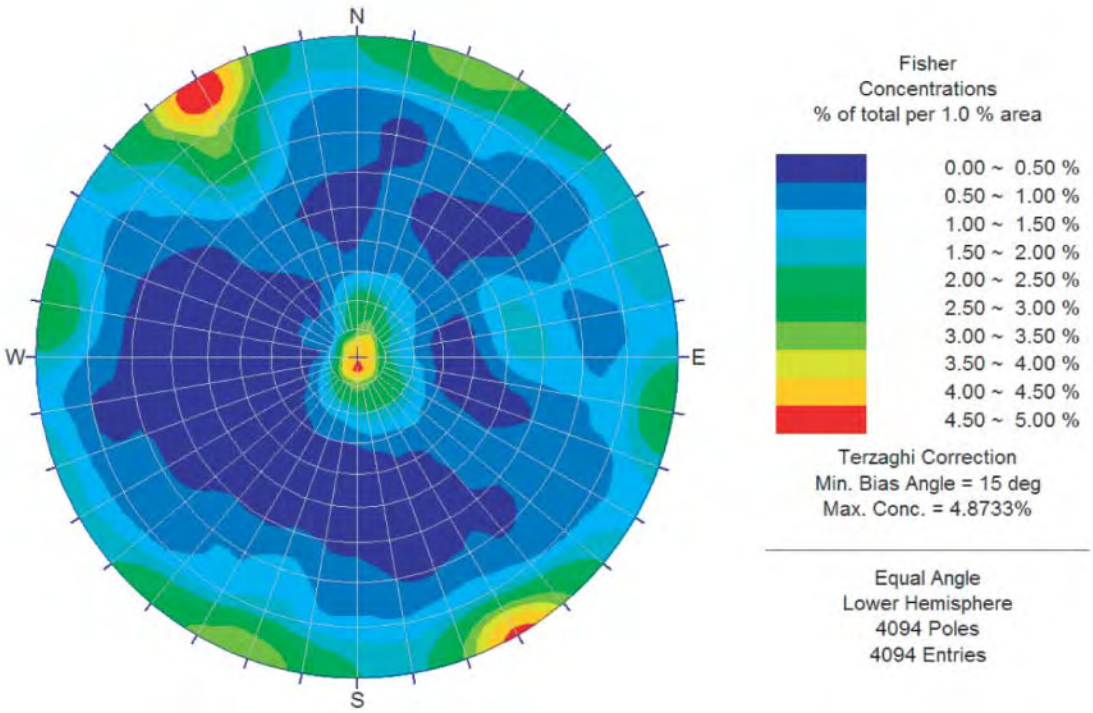

***Figure 4-34.** Fisher contoured polar stereoplot of all fractures recorded during detailed outcrop mapping within the Simpevarp subarea.*

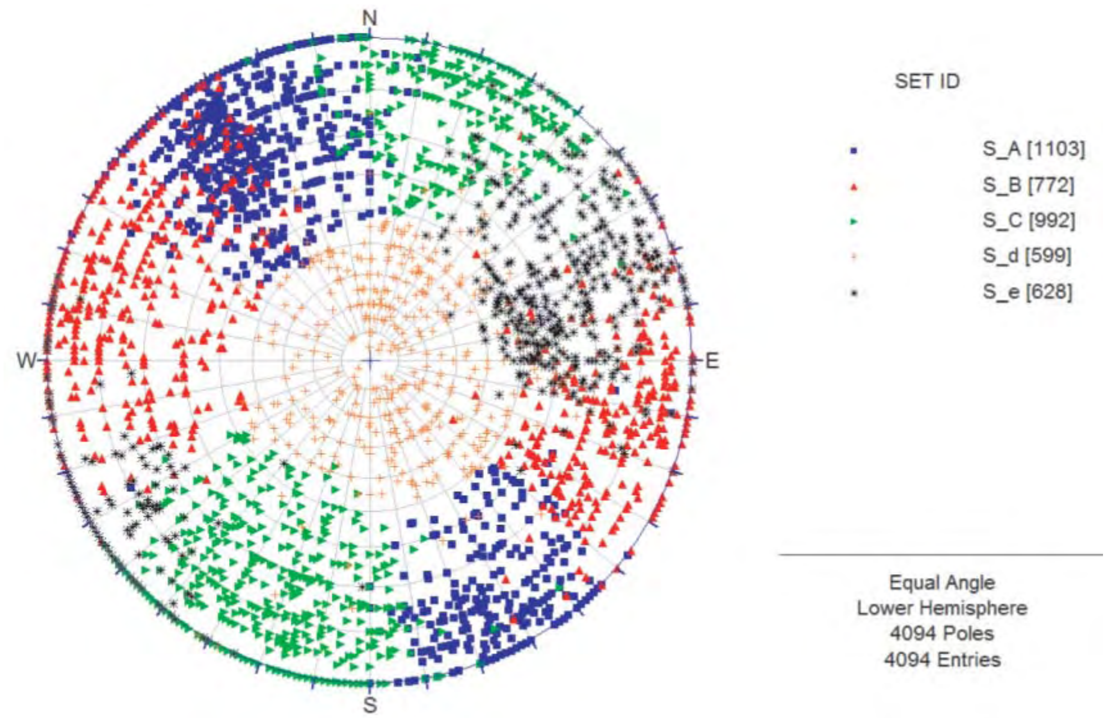

***Figure 4-35.** Simpevarp model sub-domain global fracture sets, Alternative 1.*

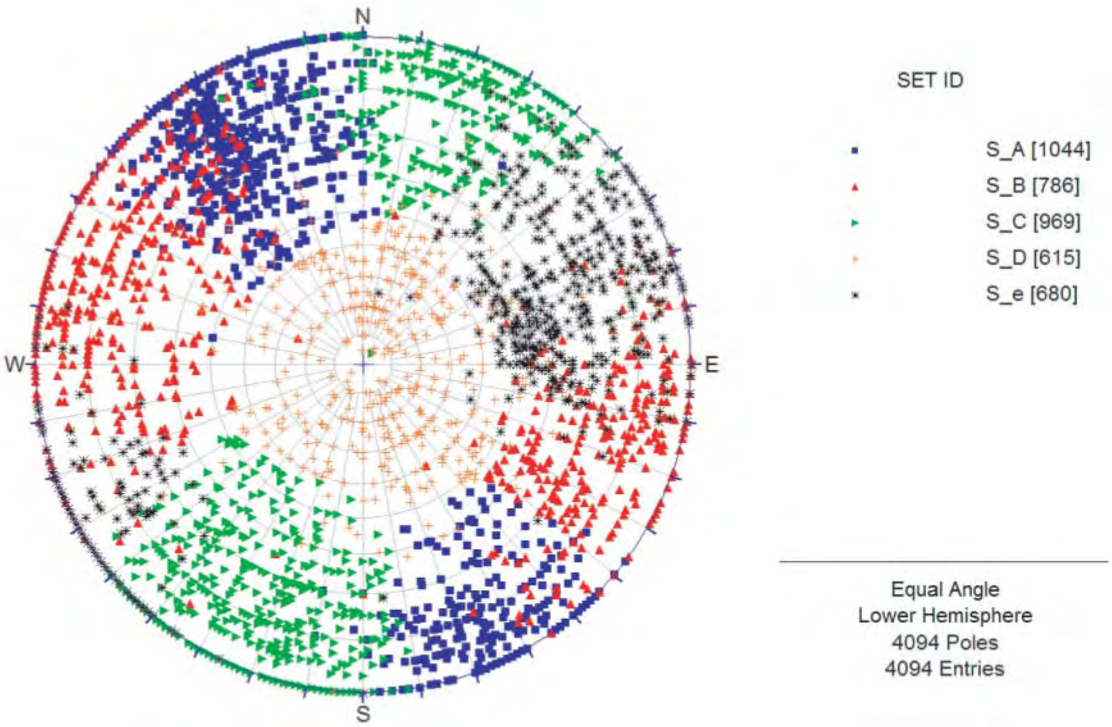

***Figure 4-36.** Simpevarp model sub-domain global fracture sets, Alternative 2.*

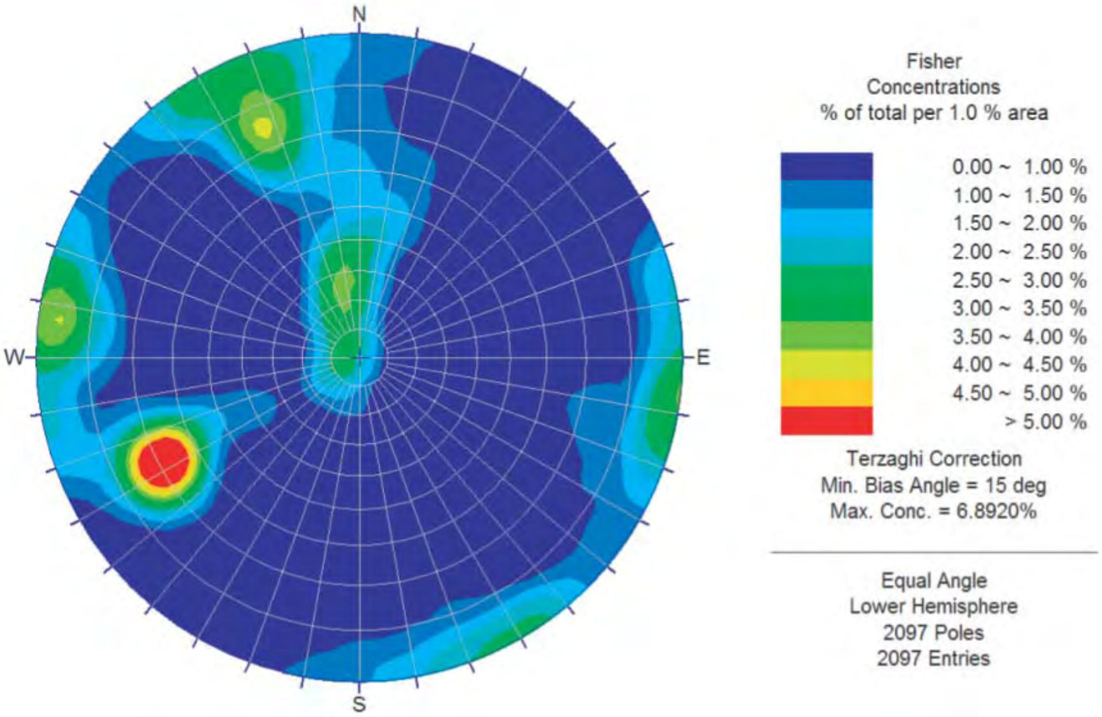

Figure 4-37. *Fisher contoured polar stereoplot of all fractures recorded during detailed outcrop mapping within the Laxemar subarea.*

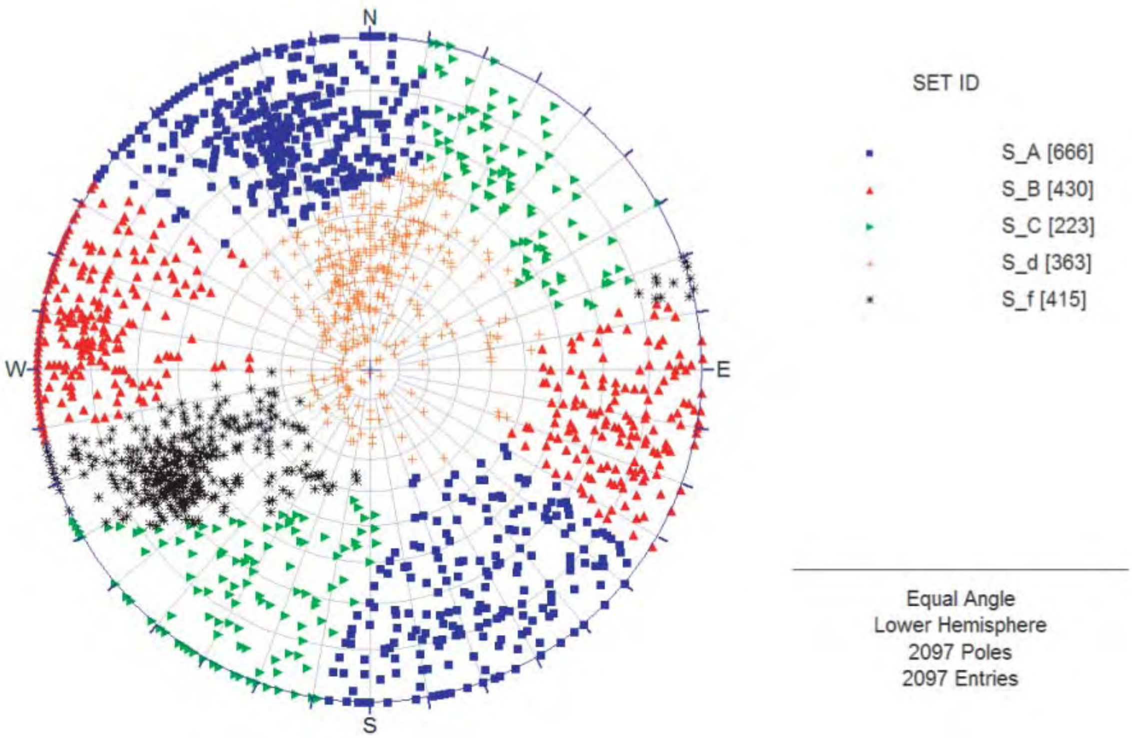

Figure 4-38. *Polar stereoplot of Laxemar model sub-domain global fracture sets, Alternative 1.*

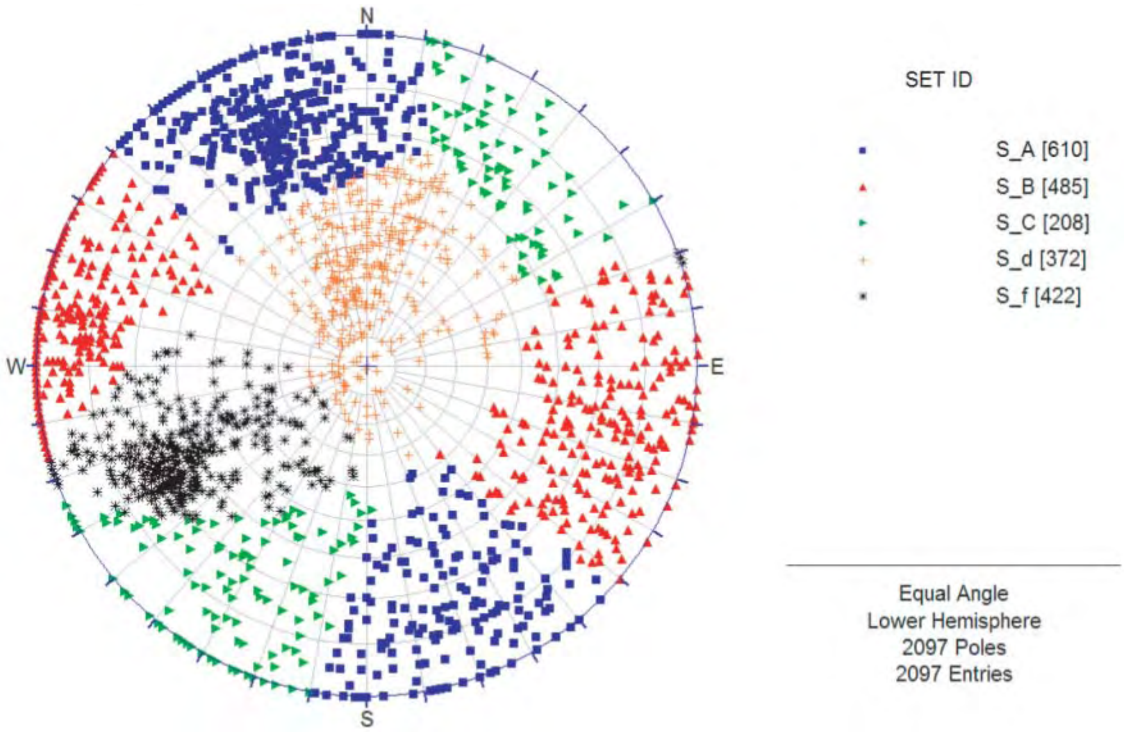

Figure 4-39. *Polar stereoplot of Laxemar model sub-domain global fracture sets, Altenative 2.*

4.9 Deformation zone orientations

Three general patterns were noted in the mapped deformation zones; a set of north-south trending zones, a strong set of north-northeast trending zones, and a weaker set of north-northwest trending zones. These zones, albeit more disperse than their outcrop-scale counterparts, roughly mimic the three identified regional fracture set orientations (Sets S_A, S_B, and S_C), cf Figure 4-40 and Figure 4-41.

This version of the SDM Laxemar DFN model makes the assumption that these deformation zones represent the largest structures of a continuous distribution of fractures (a 'tectonic continuum'). By classifying both the high- and low-confidence deformation zones as members of the three identified regional sets, a power-law scaling relationship (see Section 3.4.2) can be used to model the regional set size distributions.

The global set orientation divisions of the Laxemar sub-domain (S_A, S_B, and S_C), were imposed on all deformation zones within the Laxemar 1.2 regional model area (both Simpevarp and Laxemar subareas). Deformation zones were divided into sets using the ISIS algorithm; deformation zone strike and dips were obtained from two places:

- High-confidence deformation zones: Zone strikes and dips taken directly from Simpevarp_1.2_deformation zone model /SKB, 2004/.
- Lower-confidence deformation zones: ESRI shapefiles were imported into Manifold GIS, where the bearing (strike) of each deformation zone was approximated as the bearing of a straight line between the start and endpoints of the polyline segment. All lower-confidence deformation zones were assumed vertical.

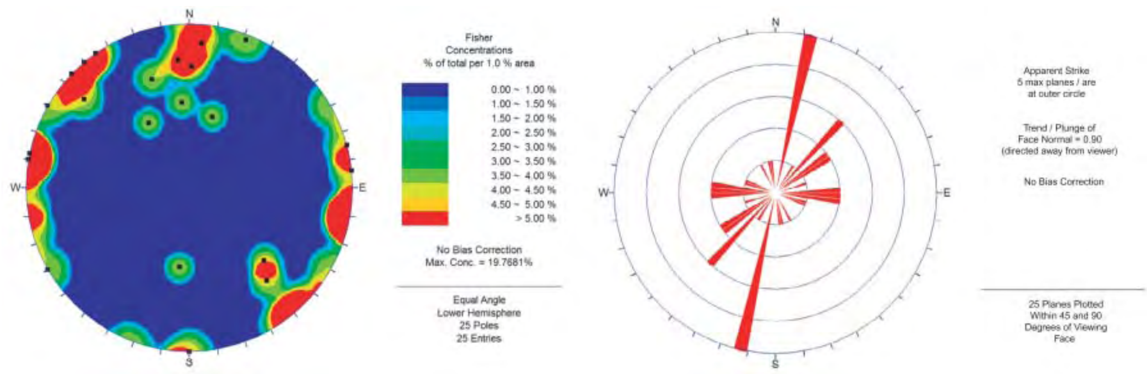

Figure 4-40. *Orientations of high-confidence deformation zones within the SDM Laxemar 1.2 model region. Orientations are taken from the SDM Simpevarp 1.2 model.*

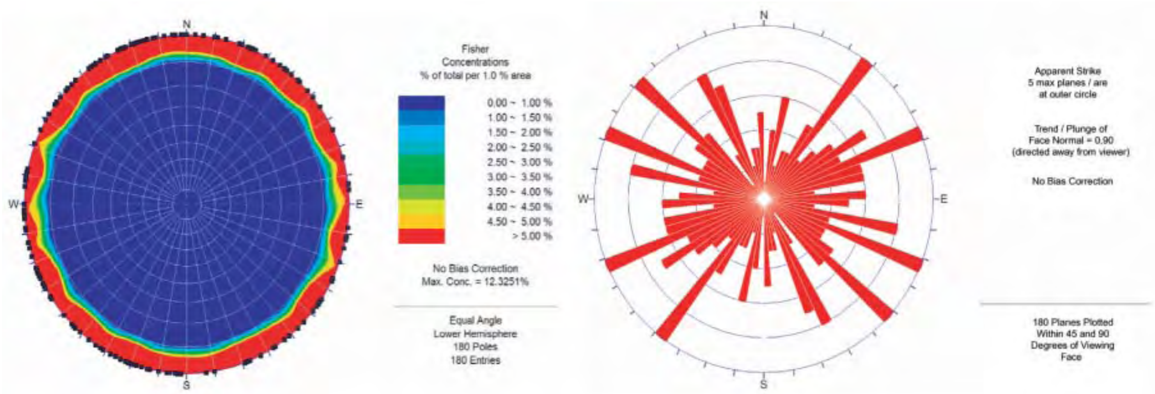

Figure 4-41. *Orientations of low-confidence deformation zones within the SDM Laxemar 1.2 model region. Orientations are taken from the SDM Simpevarp 1.2 model.*

Figure 4-42 through Figure 4-45 illustrate the global set divisions for deformation zones.

Once the set divisions were imposed on the existing deformation zone shape files, a new set of shapefiles (one for each Laxemar global set) was created. These new shapefiles were used to create 2D tracemaps for each global set. Next, deformation zone geometries were extracted from RVS as AutoCAD drawing interchange format files (.DXF). The .DXF files were imported into FracWorks XP, which converted the deformation zones to tesselated fractures. The tesselated fractures were then divided into global sets, based on the orientation of their fracture traces when intersected by a horizontal traceplane at elevation 0 m. The set division was accomplished by graphically comparing the FracWorks-derived traces to the global fracture set traces computed in ArcGIS.

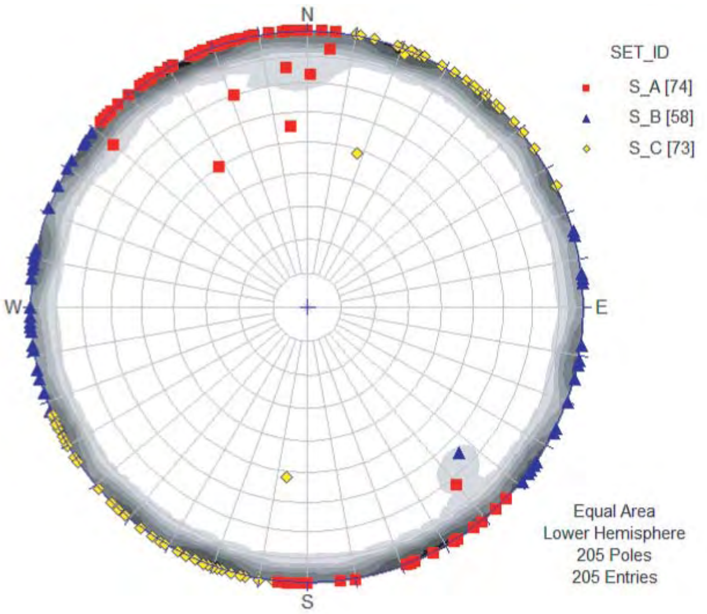

Figure 4-42. *Pole plot of prientations of all deformation zones, subdivided into global sets S_A, S_B, and S_C.*

Figure 4-43. *Global set S_A deformation zones.*

Figure 4-44. *Global set S_B deformation zones.*

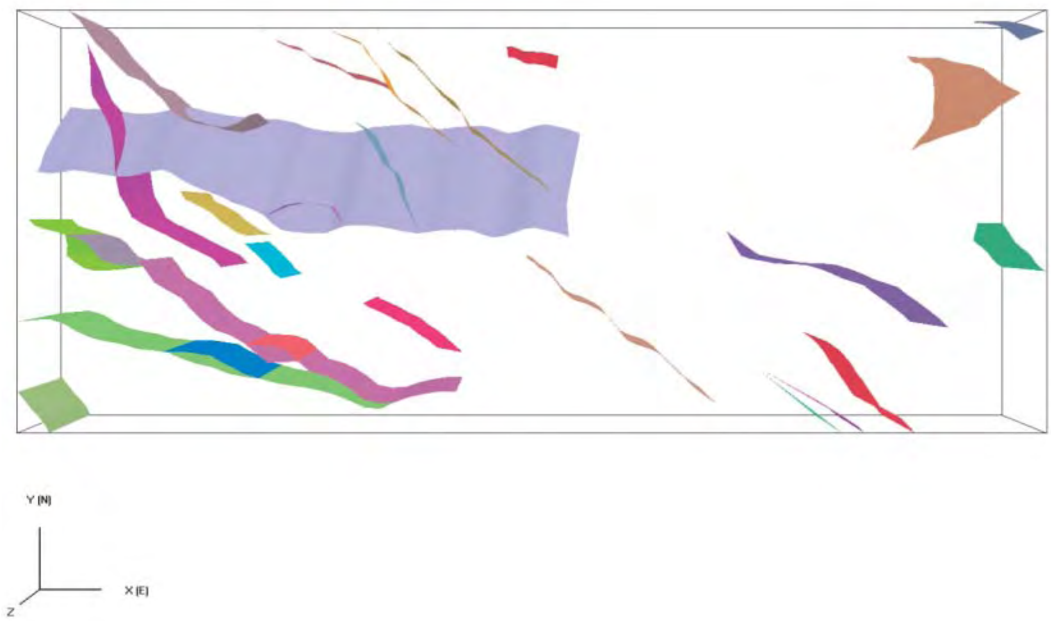

Figure 4-45. *Global set S_C deformation zones.*

5 Analysis of borehole data

5.1 Analysis of borehole data in Laxemar sub-domain

Four cored boreholes (KLX01 through KLX04) and one percussion-drilled borehole (HLX15) were used to analyze the three-dimensional characteristics of fracturing within the Laxemar model sub-domain. Fracture orientation data (strike/dip) was not available for borehole KLX01. In addition, pre-binned (1 m, 3 m, 5 m, 10 m, and 30 m intervals) fracture intensity data for the aforementioned cored boreholes was used to generate the moving-average fracture intensity (MAFI) plots. Borehole data was used primarily to constrain fracture intensities and to evaluate the suitability of the orientation model at depth. Fractures were assigned to global orientation sets based on a single-iteration hard-sector search within FracSys/ISIS; set definitions and parameters were not free to change. The boundaries of some sets within the borehole data may appear inconsistent with the contoured stereoplots; this is an artifact of the hard-sectoring algorithm used to partition borehole fractures into the orientation sets identified from surface trace data. In this iteration (SDM Laxemar 1.2), set orientations are not free to vary with depth or location once specified for a modeling subdomain. This may result in the apparent overlap of sets that, if an orientation analysis were run on a single borehole, might partition out as separate sets. In addition, note that in many of the stereoplots, the set names (i.e. S_d, S_e) are capitalized. This is due to limitations present within the DIPS software package.

5.1.1 Borehole fracture orientations and set assignment

Figure 5-1 through Figure 5-14 illustrate the orientation of fracture poles taken from drill core or borehole image logs. Fracture sets are assigned through a hard-sector process; they have not been fitted through an optimization or clustering routine.

The HLX15 data set is neither large enough nor complete enough to draw any significant conclusions with respect to the presence or absence of the fracture sets identified through outcrop analysis. No distinction was made between open and sealed fractures in the SICADA core data.

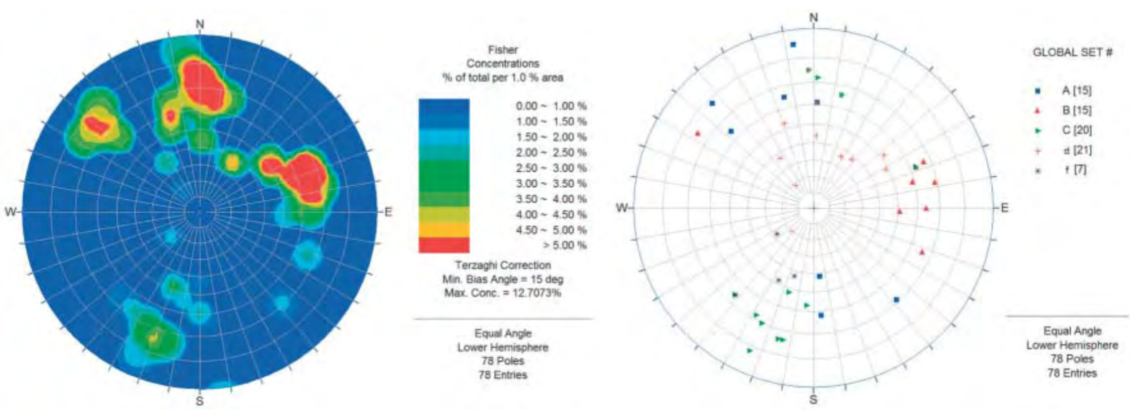

Figure 5-1. *HLX 15 fracture orientations.*

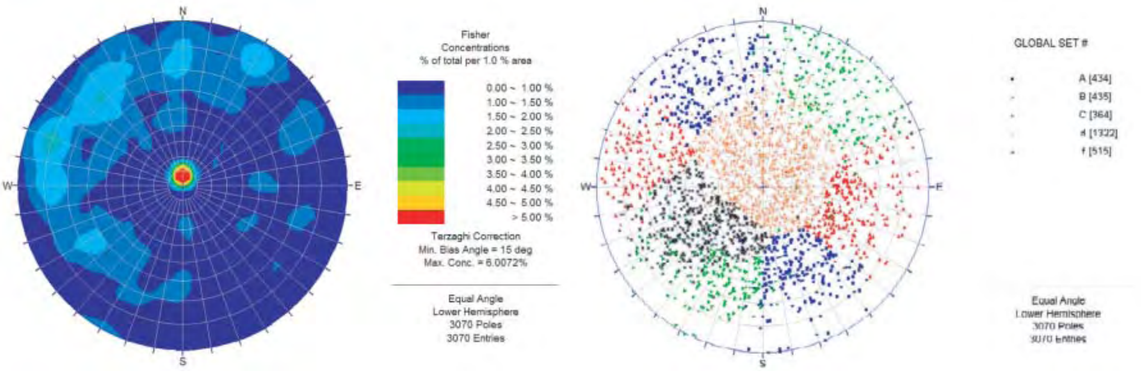

Figure 5-2. *KLX02 fracture orientations.*

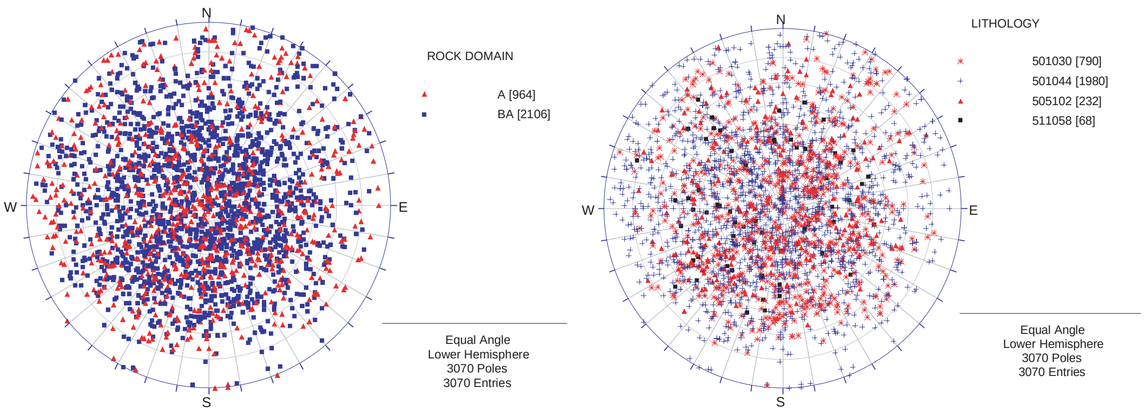

Figure 5-3. *KLX02 fracture orientations as a function of lithology and rock domain.*

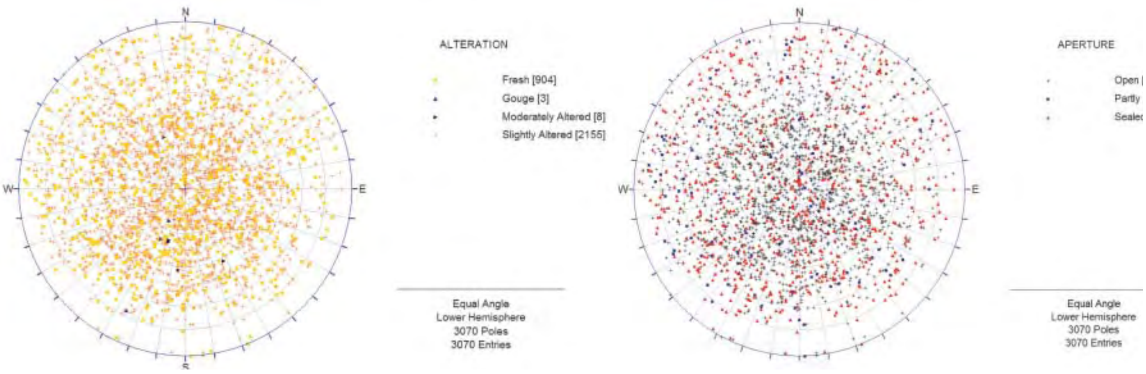

Figure 5-4. *KLX02 fracture orientations as a function of aperture and degree of alteration.*

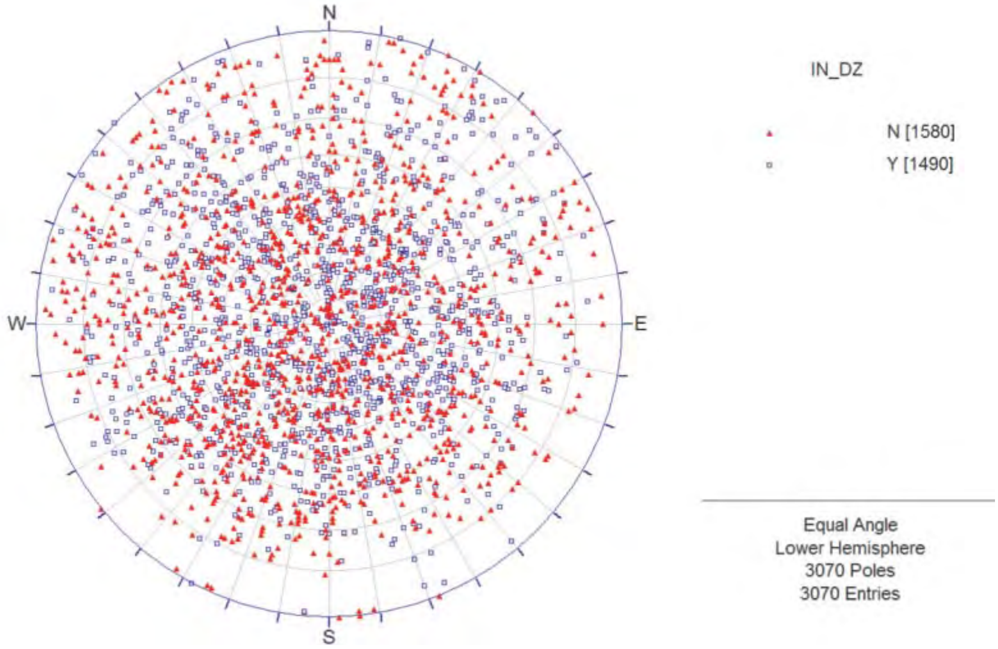

***Figure 5-5.** KLX02 fracture orientations inside and outside of mapped deformation zones.*

As a whole, Borehole KLX02 shows pole clusters that generally match the global subvertical fracture sets identified in the Laxemar detailed outcrop maps. The intensity of the subhorizontal set, however, is orders of magnitude larger than that observed in outcrop. In general, fracture orientations in KLX02 appear to be independent of rock domain. The sole exception is for subhorizontal fractures; the fine-grained granite (511058) seems to preferentially host subhorizontal to less-steeply dipping fractures. Set membership appears to be relatively independent of degree of fracture alteration, aperture, and presence inside or outside of a mapped deformation zone.

Though all three Laxemar global fracture sets are visible in Borehole KLX03, there are some notable differences from KLX02 and the outcrop patterns. Set S_f, the moderately-dipping northwest-trending set, appears to be absent from KLX03. Also, though global fracture sets S_B and S_C appear correctly positioned relative to each other, their stereonet pole cluster patterns appear to be rotated counterclockwise by approximately 20 degrees. Finally, the intensity of global fracture set S_A is much less than in outcrop or in KLX02. It is only weakly visible outside of deformation zones, but does appear slightly stronger inside deformation zones (Figure 5-9).

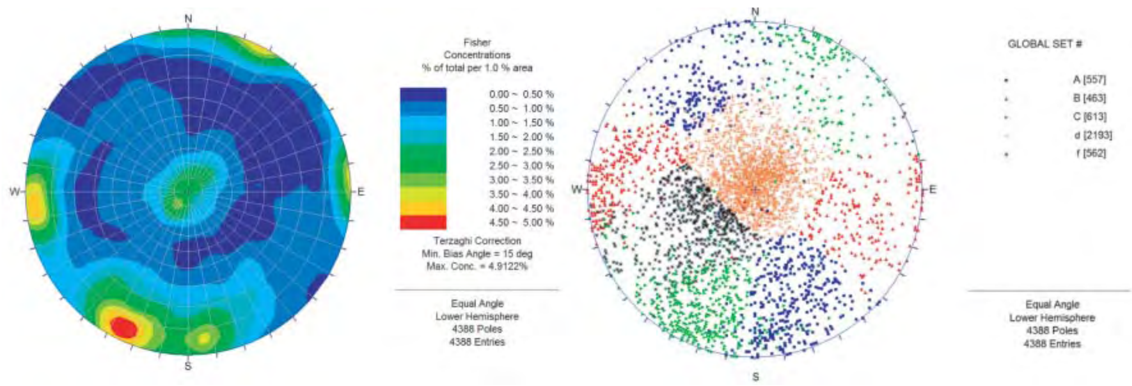

***Figure 5-6.** KLX03 fracture orientations.*

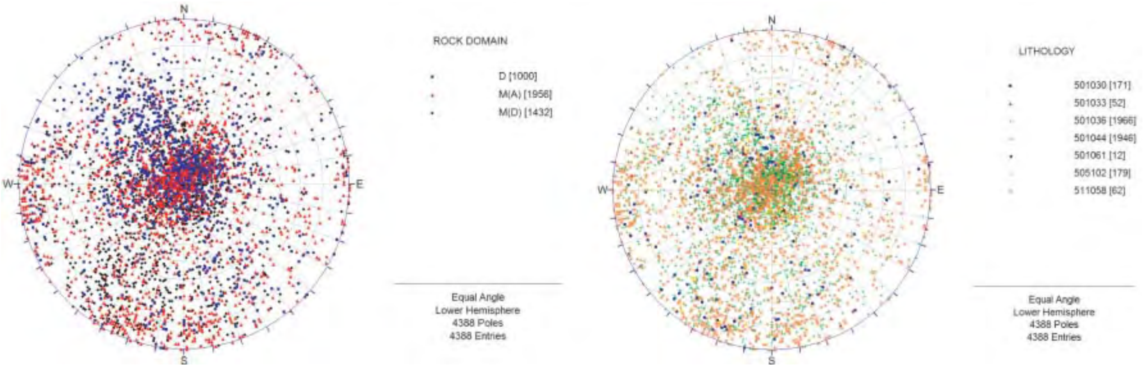

Figure 5-7. *KLX03 fracture orientations as a function of rock domain and core lithology.*

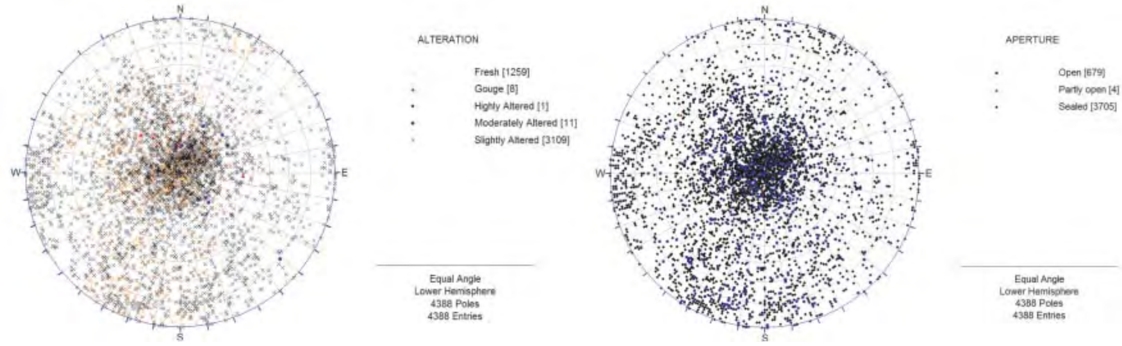

Figure 5-8. *KLX03 fracture orientations as a function of aperture and degree of alteration.*

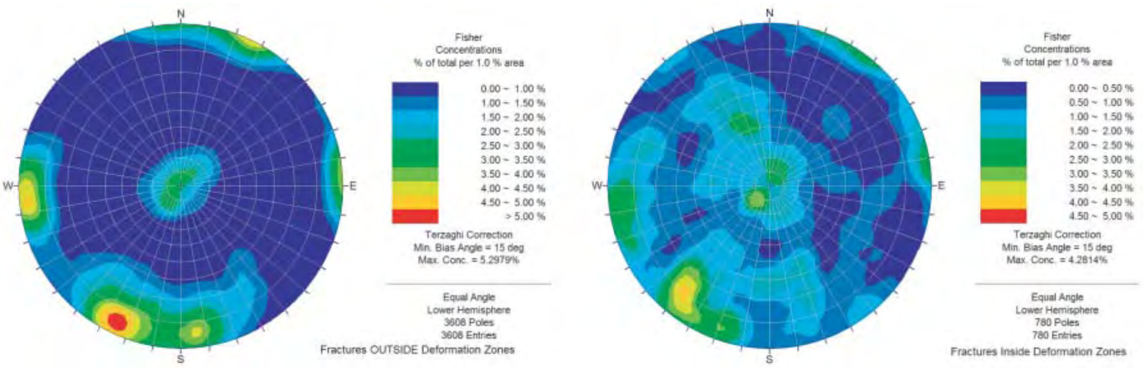

Figure 5-9. *KLX03 fracture orientations inside and outside of mapped deformation zones.*

Stereoplot observations (Figure 5-7) suggest that in KLX02, both fracture orientations are independent of both rock domain and core lithology. In addition, fracture aperture appears to be independent of set or orientation. A slight bias towards moderate alteration along subhorizontally-oriented fractures (Figure 5-8) was noted. However, the small sample size (11 fractures were recorded as having moderate alteration) relative to the large number of subhorizontal fractures makes it difficult to qualitatively prove causation.

Stereoplot analysis of borehole KLX04 suggests that, unlike in other Laxemar subarea boreholes, lithology does control fracture set alteration to a slight degree. Fractures in the Avro granite (501044), which makes up the majority of the rock encountered during drilling, appear to be spread uniformly among the sets visible in the borehole. Fractures within the diorite to gabbro units (501033) tend to have west-northwest or subhorizontal trends. Fractures within the fine-grained dioritic rocks (501030) appear to be predominantly subhorizontal.

Fracturing within the quartz monzodiorite units (501036) appears to be spread out across all sets, much like the fractures hosted in Ävrö granite. However, fractures within the fine-grained mafic rock units (505102) are grouped in a similar manner to those in the dioritic layers; they predominantly trend west-northwest, or are part of the subhorizontal set. The same trend is not observed in neither the fine-grained (511058) nor medium-grained (501058) granites.

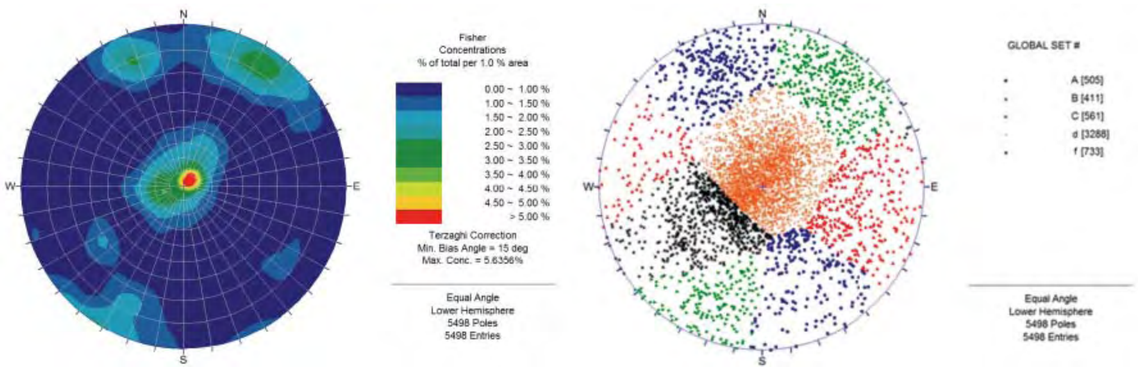

Figure 5-10. KLX04 fracture orientations.

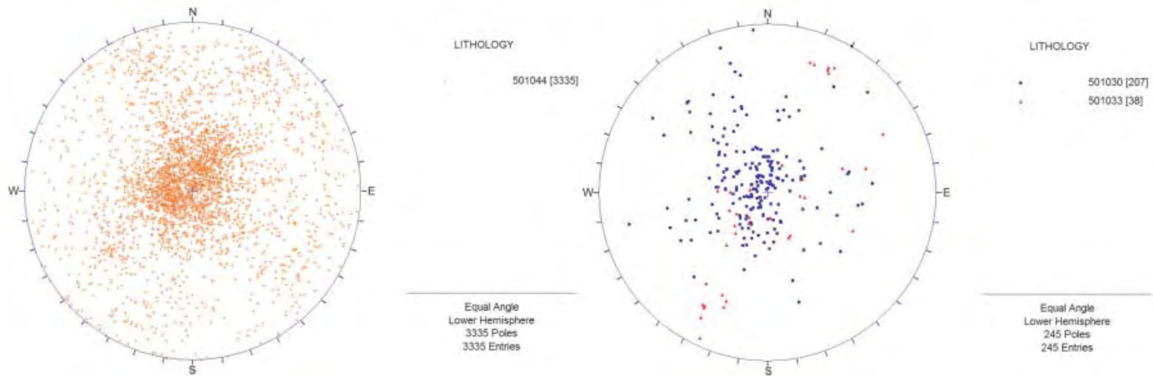

***Figure 5-11.** KLX04 fracture orientations within Ävrö granite (501044), fine grained dioritoid (501030), and within diorite to gabbro (501033).*

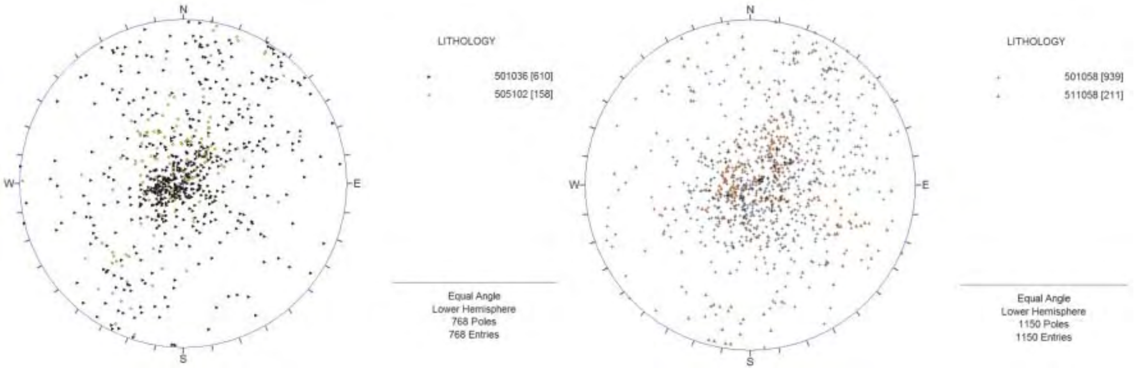

Figure 5-12. *KLX04 fracture orientations within Äspö diorite/quartz monzodiorite (501036), fine-grained mafic rock (505102), fine- to medium-grained granite (511058), and coarse- to medium-grained granite (501058).*

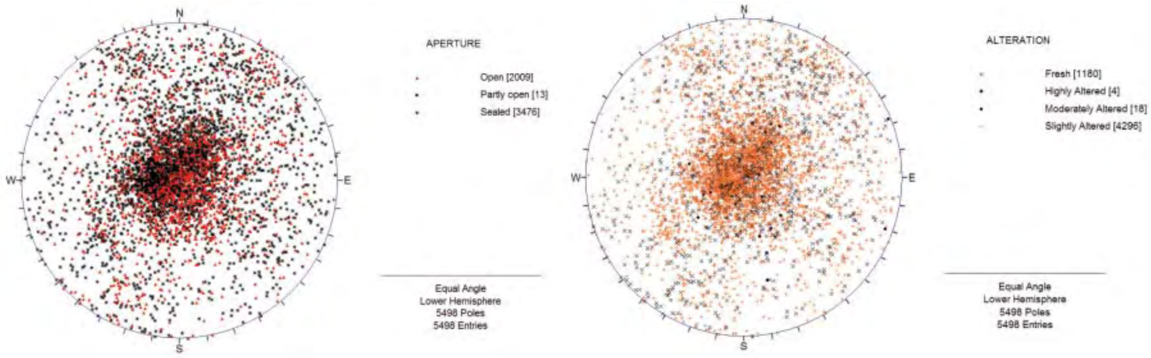

Figure 5-13. *KLX04 fracture orientations as a function of aperture and alteration.*

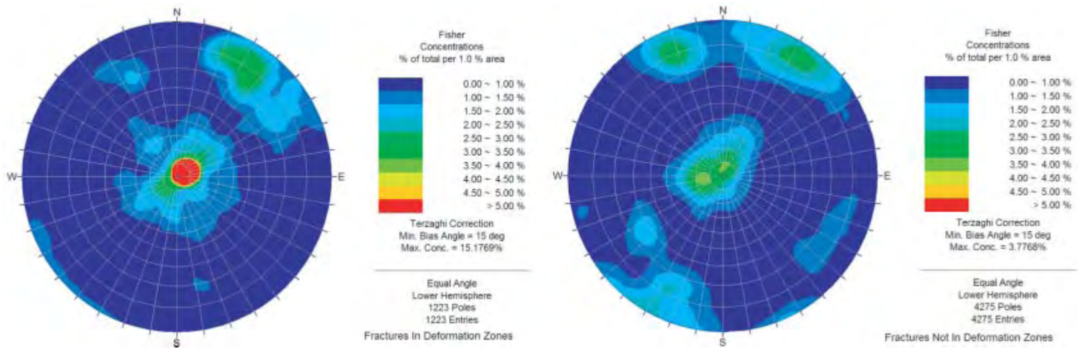

Figure 5-14. *KLX04 fracture orientations inside and outside of mapped deformation zones.*

Within borehole KLX04, fracture aperture appears to be independent of orientation or set membership. However, as in KLX02 and KLX03, the subhorizontal fracture sets tend to be the only ones that show alteration to a moderate or high degree. Unlike the other Laxemar boreholes, KLX04 does suggest that deformation zones may control intensity of certain sets. The east-west trending fracture set is much less intense (Figure 5-14) within deformation zones, compared to areas in KLX04 outside the mapped deformation zones.

5.1.2 Variation of fracture orientation with borehole depth

A key question in analyzing borehole fracture data is to assess how well the set divisions determined from outcrops describe fracture orientations at depth. Fracture orientations (and, more importantly, set intensity) can change as a function of depth; it is crucial to understand orientation anisotropy as it can influence both fluid flow and rock mechanical properties. Orientation variation with depth was evaluated in Laxemar subarea boreholes in two ways:

1. Construction of scatter plots of the trend and the plunge of the fracture poles as a function of measured borehole elevation (as opposed to length along the borehole).
2. Construction of polar trend and plunge density plots using ArcMap. The density plots highlight areas of the boreholes with 'clustered' fracture orientations, and also graphically illustrate areas of relatively low fracture intensity. The density plots are constructed using both the kernel density function within ArcMap's Geostatistical Toolbox and using a manual grid-cell point count (fundamentally, a quadrat analysis), /Cressie, 1993/ to output a custom (6 degree by 6 m) raster.

Both sets of plots are only truly usable qualitatively; the combination of different measurement systems on the horizontal (degrees; fundamentally an arc-length) and vertical (meters) makes statistical comparisons difficult.

Figures 5-15 through 5-17 illustrate fracture pole trends in borehole KLX02. The most prominent feature in KLX02 is the 'linear' set of fracture poles with plunges approximately 83° (nearly horizontal), at an approximate right angle to the general deviation of the well (7°). We interpret these structures to be core-discing or mechanically-induced borehole fractures produced during drilling. These structures should be confirmed by re-examination of BIPS image logs and drillcores, and, if found, removed from the SICADA database as they have the potential to skew the statistics of sets fitting natural fractures.

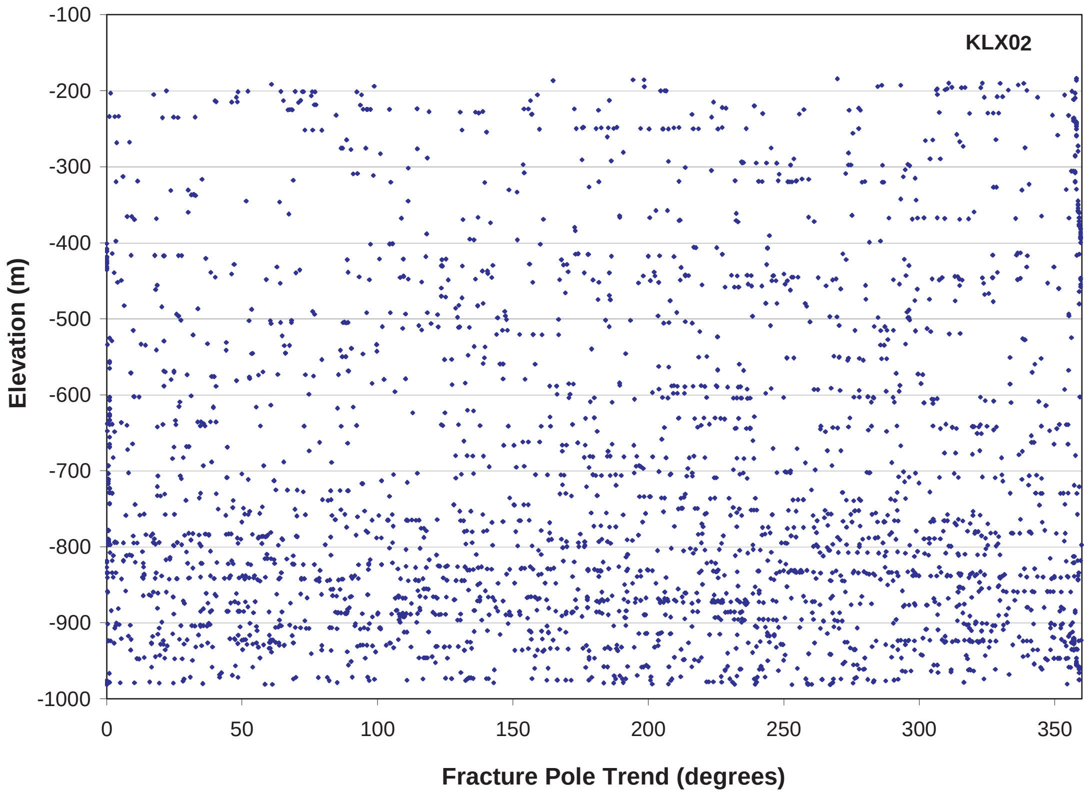

Figure 5-15. Fracture pole trend as a function of elevation, borehole KLX02, Laxemar subarea.

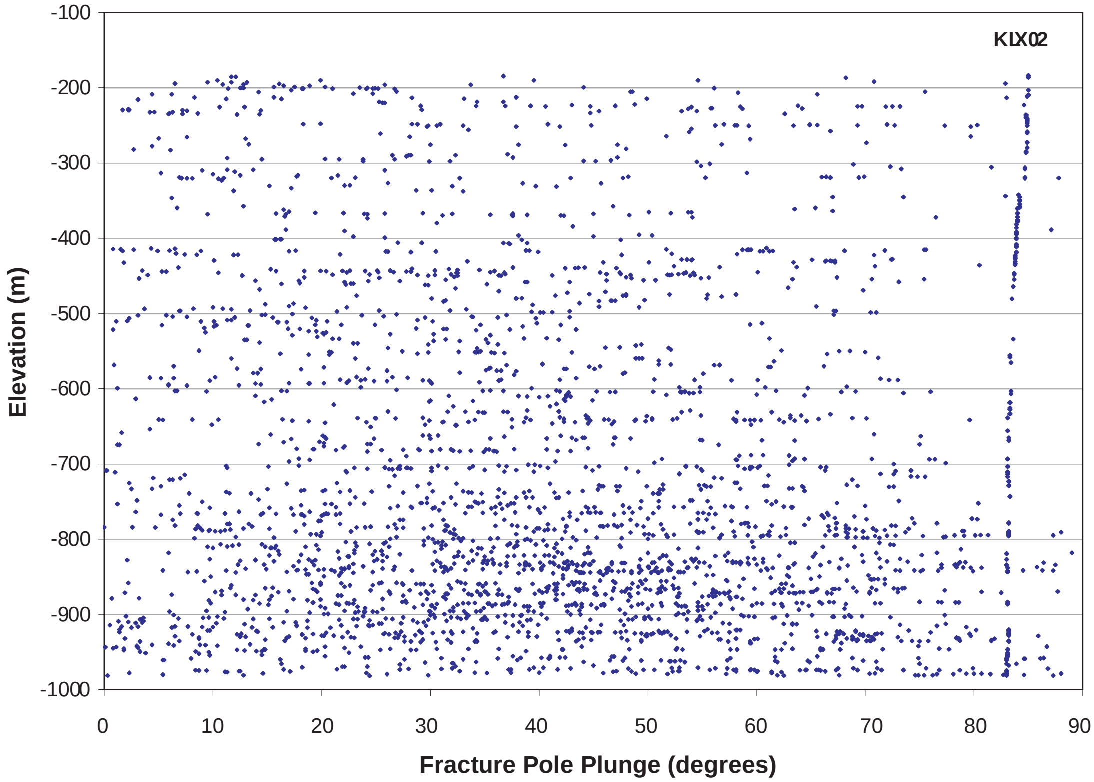

Figure 5-16. Fracture pole plunge as a function of elevation, borehole KLX02, Laxemar subarea.

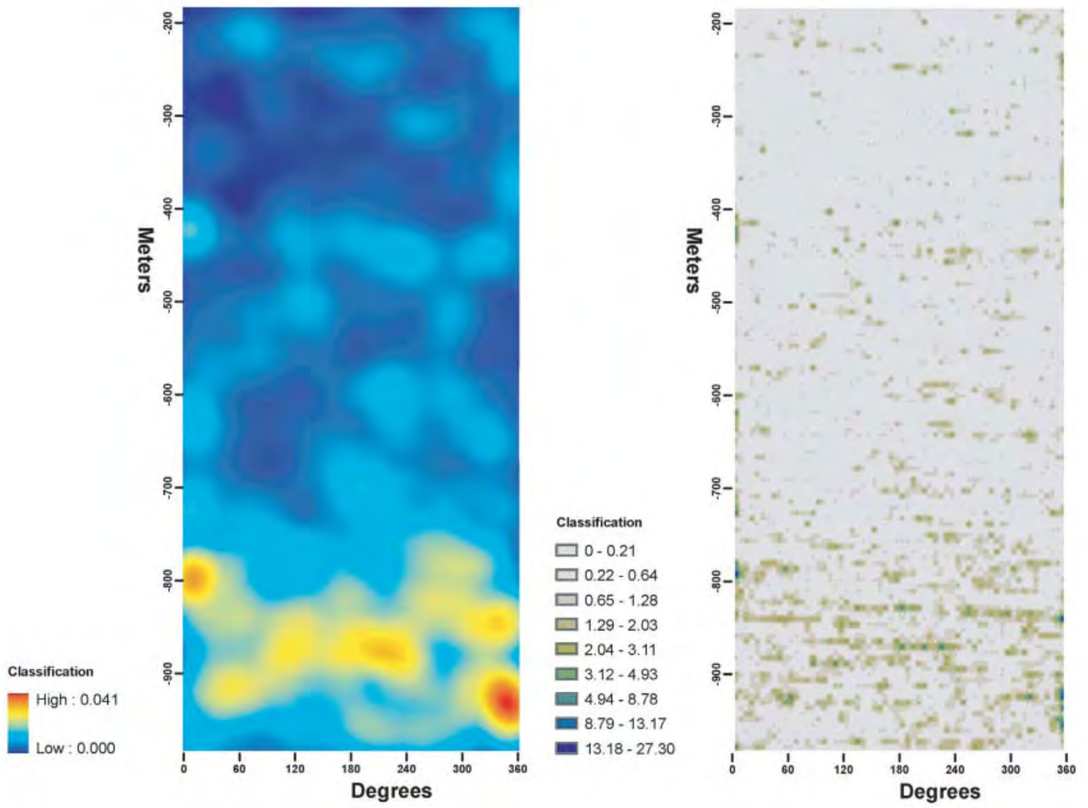

Figure 5-17. Kernel density (left) and raster point density (right) plots of fracture pole trends, borehole KLX02, Laxemar subarea. Plot illustrates the number of fracture poles lying within a 6 m by 6 degree 'bin'.

The orientation-depth plots for KLX02 illustrate a general increase in fracture intensity with depth. No specific pole trend clustering is noted; however, the intensity of moderately-dipping (25°–60°) fractures appears to increase between elevations –800 and –900 m; this is the lower portion of mapped deformation zone DZ1 in KXL02.

Fracture pole trend plots (Figure 5-18 through Figure 5-20) from borehole KLX03 show more features than those from KLX02. The same set of possibly induced fractures is clearly visible in the scatter diagrams; though since KLX03 has generally higher fracture intensity than KLX02 the effect of the induced fractures on borehole statistics may be less serious. Most curious is the large 'hole' between –400 m and –600 m that appears to exhibit generally low intensity, and appears to only contain nearly vertical or nearly horizontal fractures. There also appears to be some variation in fracture pole trends with depth, suggesting that the set orientations established at the surface in the Laxemar subarea may not be sufficient to model fracturing at depth, especially below –600 m.

Again, borehole KLX04 appears to exhibit the same degree of induced fracturing as KLX02 and KLX03. However, unlike KLX02 and KLX03, borehole KLX04 shows a significant number of subhorizontally-dipping (pole plunges greater than 60°) fractures at all depth intervals (see Figure 5-22).

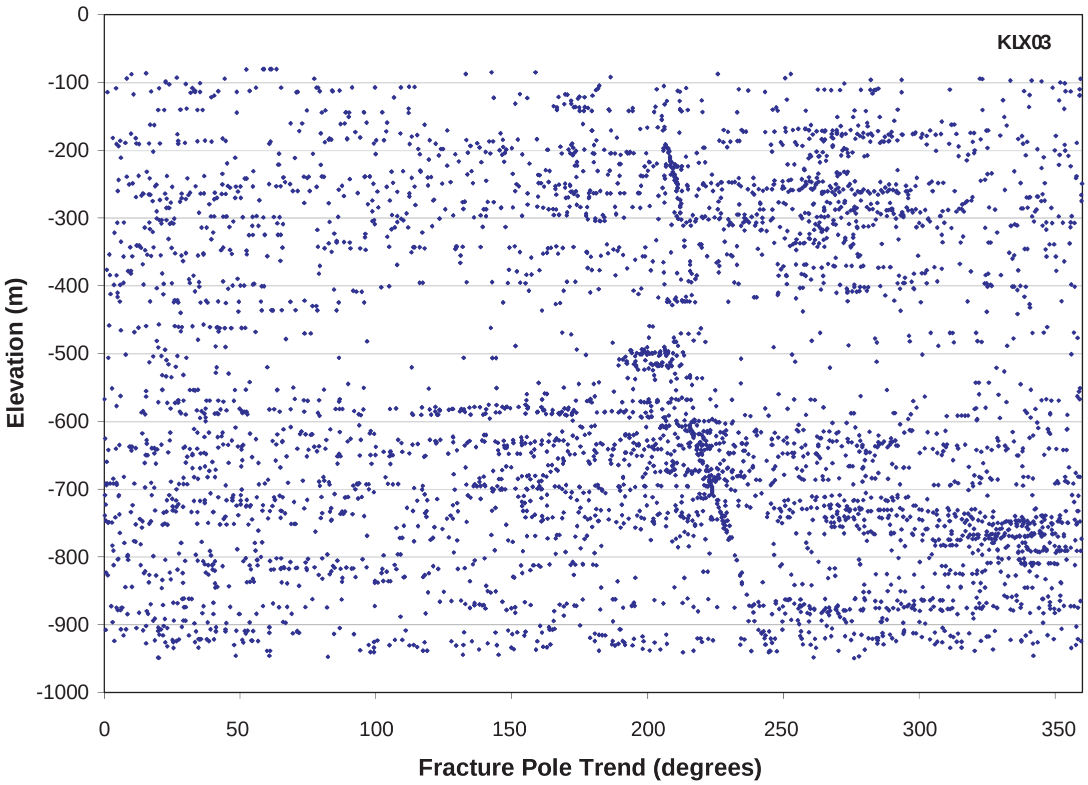

Figure 5-18. *Fracture pole trend as a function of elevation, borehole KLX03, Laxemar subarea.*

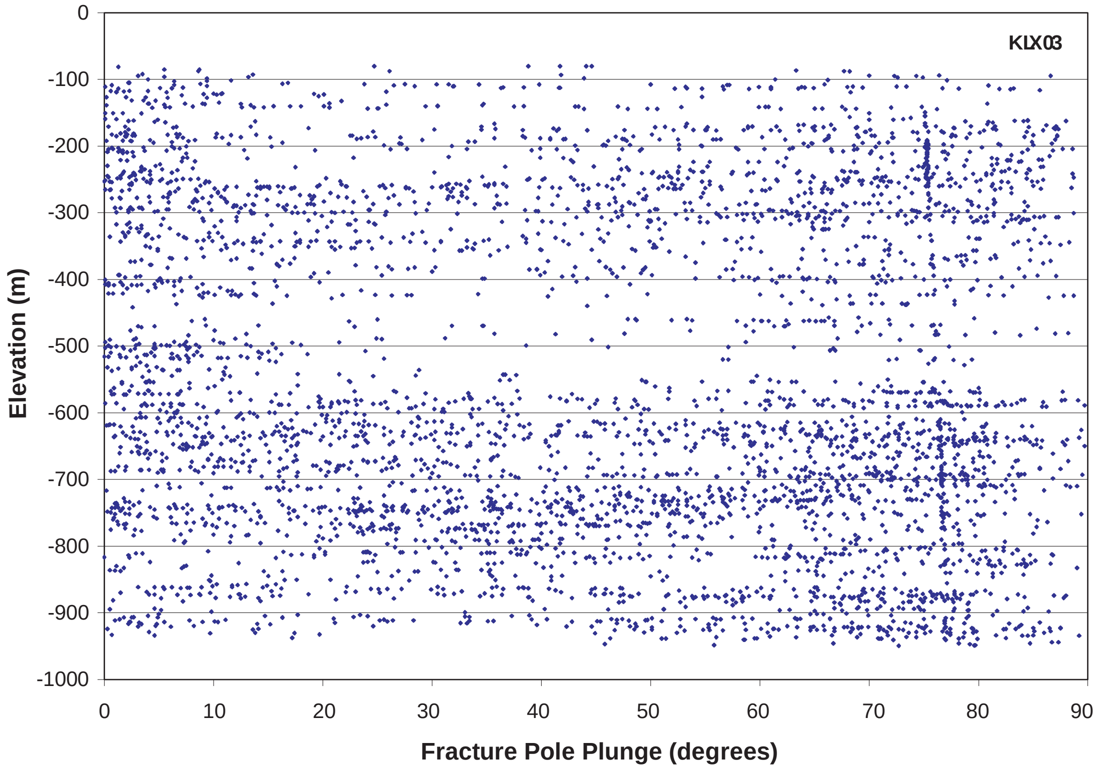

Figure 5-19. *Fracture pole plunge as a function of elevation, borehole KLX03, Laxemar subarea.*

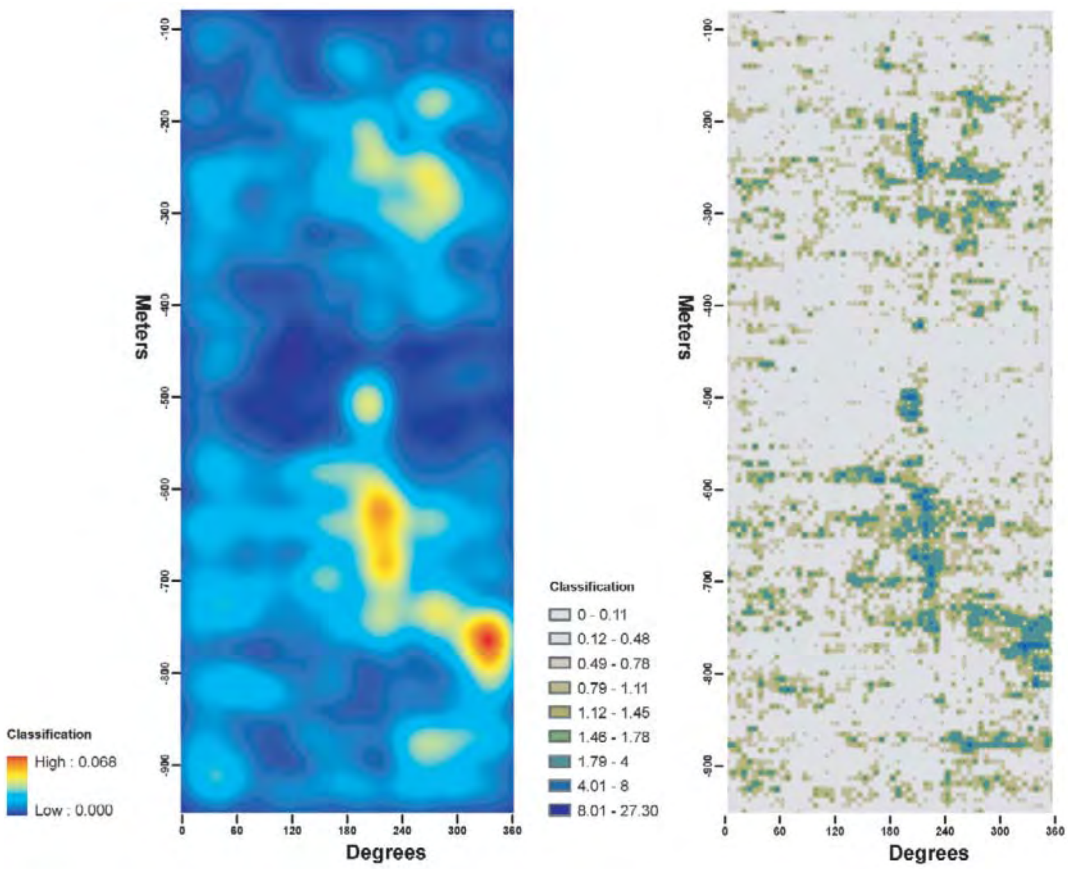

Figure 5-20. *Kernel density (left) and raster point density (right) plots of fracture pole trends, borehole KLX03, Laxemar subarea. Plot illustrates the number of fracture poles lying within a 6 m by 6 degree 'bin'.*

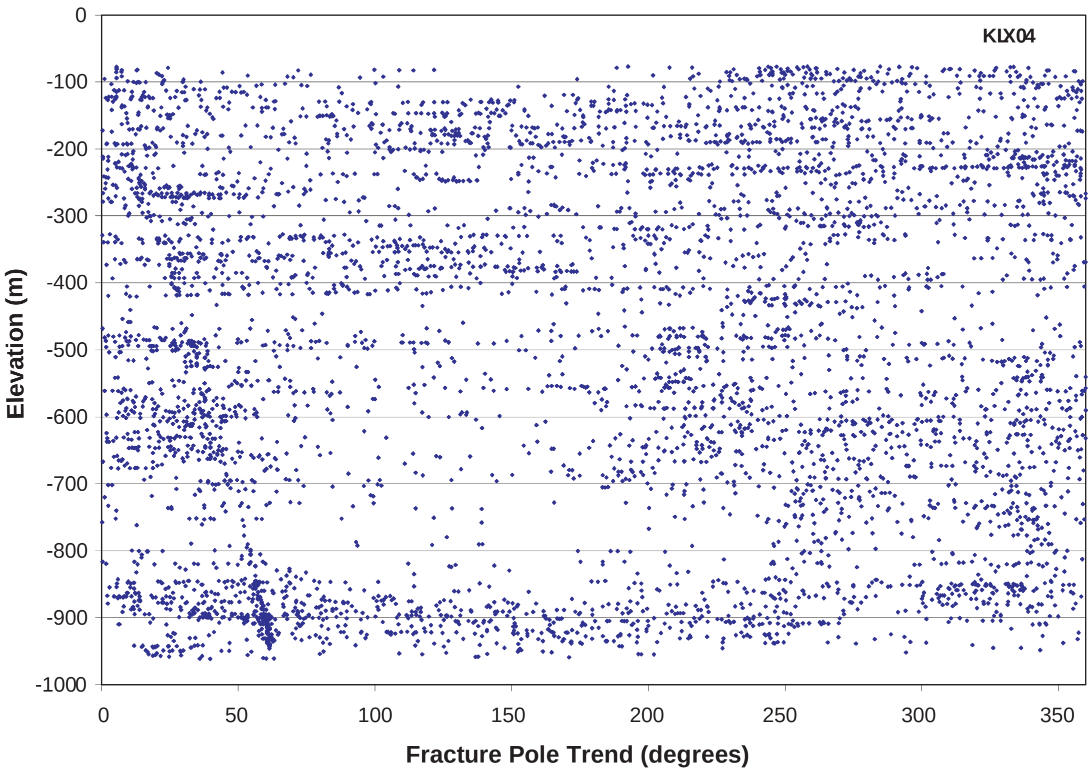

Figure 5-21. *Fracture pole trend as a function of elevation, borehole KLX04, Laxemar subarea.*

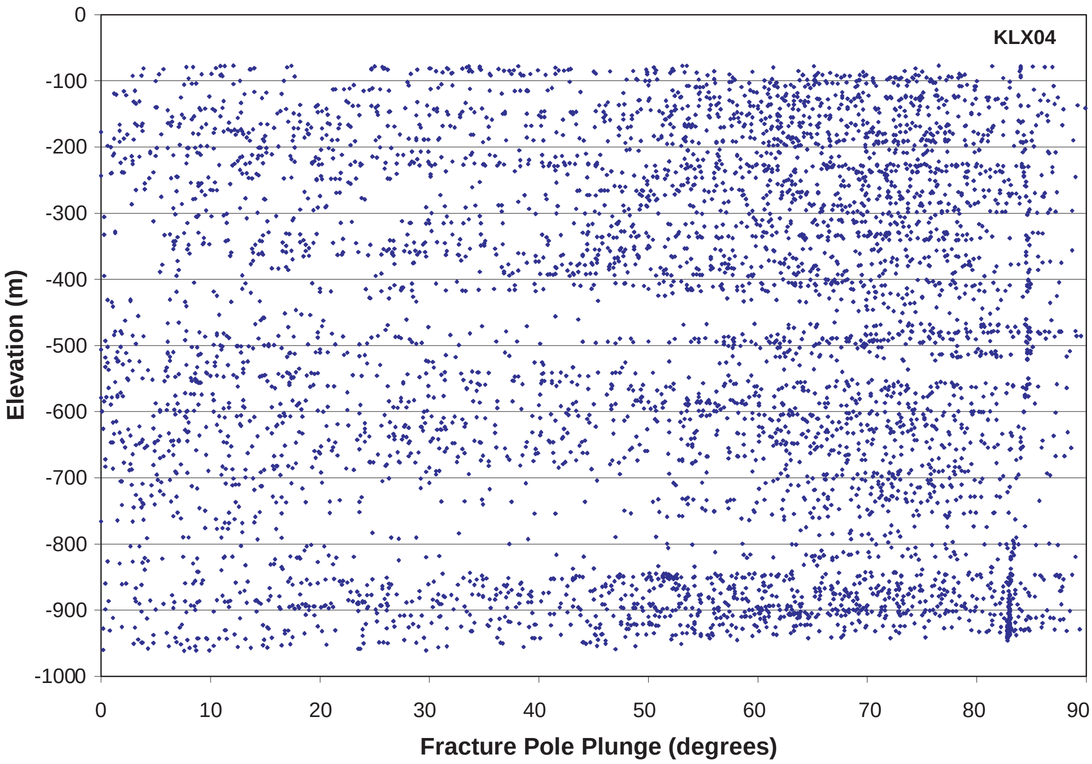

Figure 5-22. *Fracture pole plunge as a function of elevation, borehole KLX04, Laxemar subarea.*

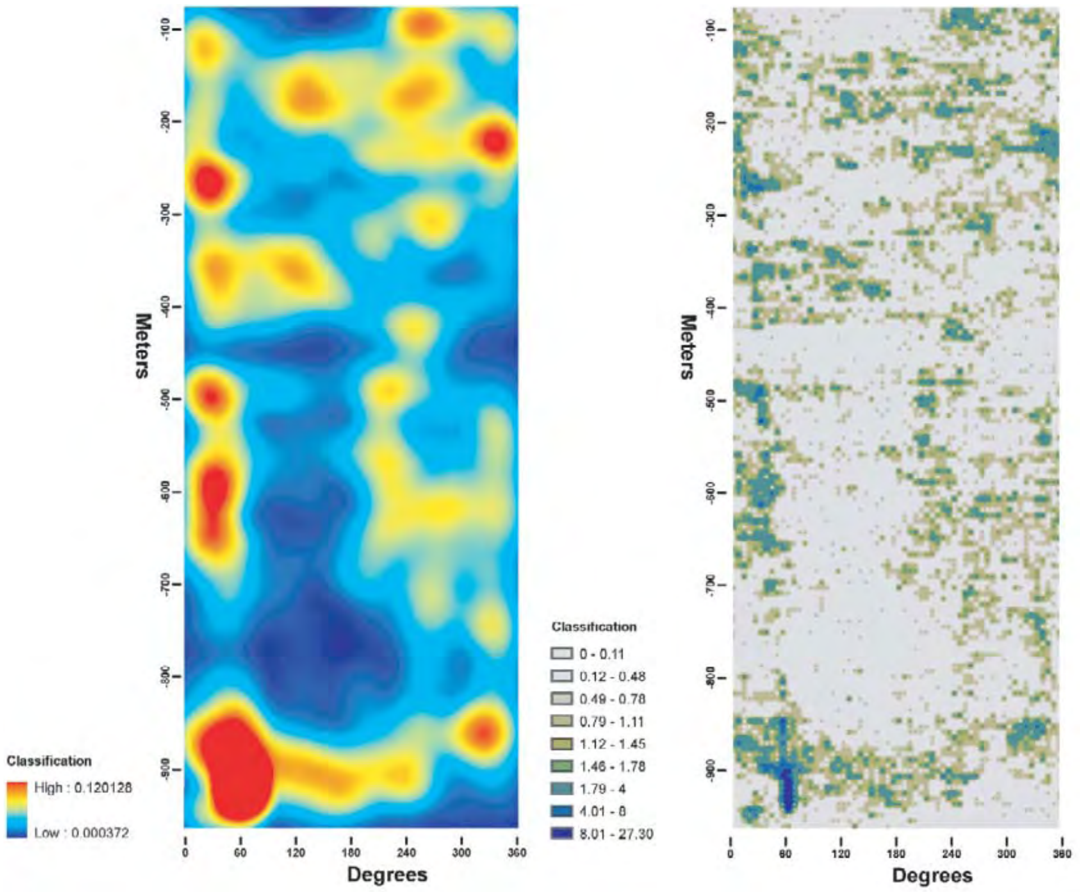

Figure 5-23. *Kernel density (left) and raster point density (right) plots of fracture pole trends, borehole KLX04, Laxemar subarea. Plot illustrates the number of fracture poles lying within a 6 m by 6 degree 'bin'.*

5.1.3 Intensity

Fracture intensity within the Laxemar series of cored boreholes (KLX01–KLX04) was initially analyzed through the use of cumulative fracture intensity (CFI) and moving-average fracture intensity (MAFI) plots. A 5-meter window (symmetric around the observation depth) was used to plot 1-meter fracture intensity (P_{10}) data from SICADA; the resulting graphs contain significantly less noise without adversely widening intensity peaks. The moving-average fracture plots are useful for identifying specific depth ranges where fracture intensity experiences significant variation.

The CFI plots, on the other hand, are most useful for identifying larger-scale fracture intensity relationships, such as the dependence of intensity on borehole depth or lithology. Zones of constant slope represent relatively constant intensity; slope breaks indicate boundaries between regions where the fracture intensity significantly differs. Note that fractures within deformation zones are removed from the CFI plots (as they will skew the view of the data), but are present within the moving average plots.

All plots were overlain with rock alteration and borehole lithology data from SICADA. The MAFI plots are correlated to borehole length (ADJUSTED_SECUP), as detailed coordinate data (elevation) was not available in the SICADA tables shipped before the data freeze. CFI plots, which are based off of the borehole core logs, are correlated to borehole elevation.

A moving average intensity plot was not constructed for borehole HLX-15 (a hammer-drill hole for which a BIPS log was completed) as the 1-m fracture intensity data was too sparse to produce a meaningful figure. In addition, fracture core data was not available for borehole KLX01. As such, only a MAFI plot was produced.

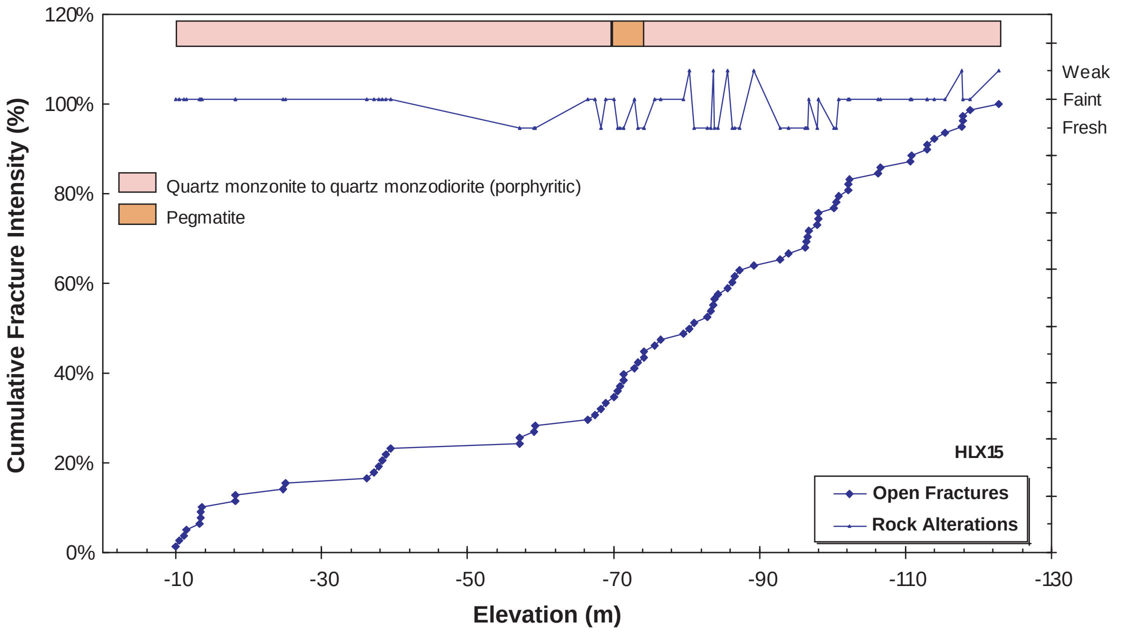

Figure 5-24. *CFI plot for borehole HLX15. Flat areas represent relatively low fracture frequency, while steeper slopes represent higher fracture intensity. Fracture data taken from cored borehole and BIPS logs. Plot excludes data based on fractures contained within mapped deformation zones.*

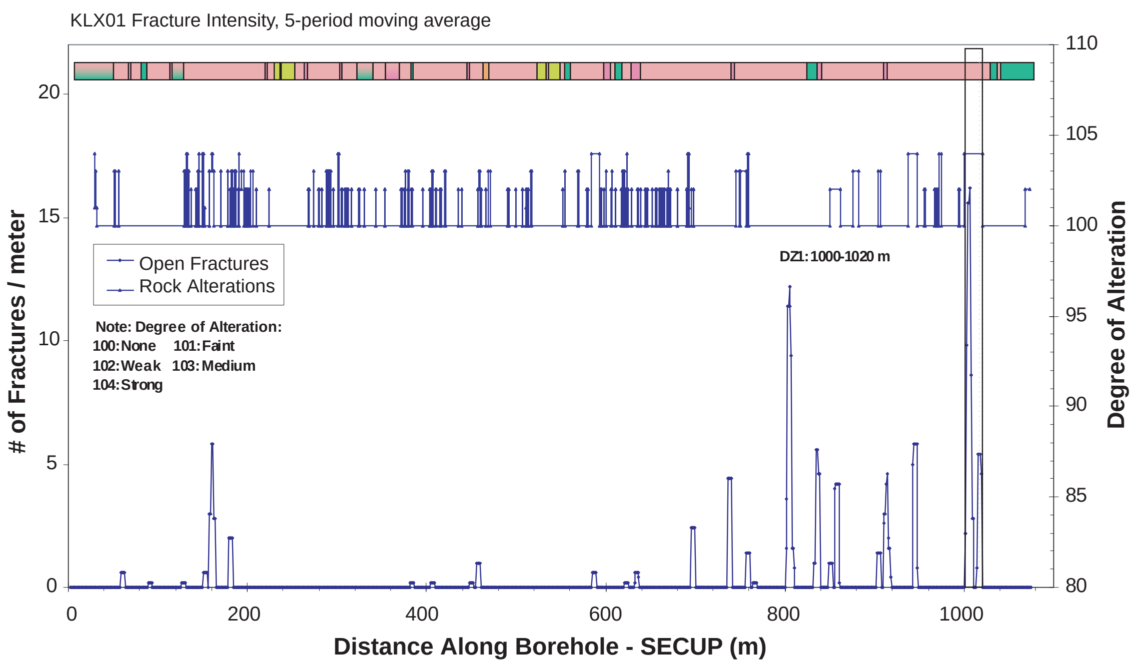

Figure 5-25. *Moving average fracture intensity (MAFI) for borehole KLX01 utilizing 1 m binned data. The moving average function utilizes a five-meter sliding window centered on the value of interest.*

The CFI plot for borehole HLX15 suggests relatively low fracture frequencies within approximately 70 m of the surface. An increase in fracture intensity is accompanied by a zone of highly variable rock alteration (70–95 m). The most predominant changes in slope appear to be correlated to zones of weak alteration within the host rock.

The MAFI plot for borehole KLX01 shows several interesting trends. First, though several zones of increased fracture intensity appear to be correlated with zones of moderately-altered bedrock, there are several zones that are clearly not correlated with increased alteration. These zones appear to be correlated with small regions of different lithologies (pegmatite, fine-grained mafic rock, and diorite-gabbro) within a matrix of granite to quartz monzonite. Curiously, though, the second largest intensity spike (at approximately 810 m) shows no visible correlation to either alteration degree or lithology in the MAFI plot.

The MAFI plot for borehole KLX02 (Figure 5-26) also suggests a strong relationship between open fracture intensity and rock alteration. The relationship between fracture intensity and lithology is less clear, however, largely due to the large numbers of small rock zones beginning at approximately 525 feet along the borehole. Zones of lower-intensity sealed fractures also seem to be associated with faint to no rock alteration; however, it is impossible to determine which result is causative without further investigation of fracture mineral assemblages. An interesting note is that borehole KLX02 is the only one in the Laxemar data set for which the open fracture intensity exceeds that of the sealed fracture intensity on a regular basis.

The CFI plot for KLX02 (Figure 5-27) shows several additional quirks not visible on the MAFI plots. First, the intensity spike at 275 m occurs only in the vertically-oriented fracture sets, and not in the subhorizontal fractures. Second is a zone (approximately 440 m to 540 m) where sealed fracture intensity varies quite significantly from open fracture intensity; a similar zone (albeit with the pattern reversed) is present from 660–720 m. These zones appear to be loosely associated with areas of faint to no rock alteration. Third, the relative strength of the subhorizontal fracturing at the start of the fracture log is interesting; this pattern is not seen elsewhere in the Laxemar cored borehole data. Finally, the relative intensity of open to sealed fractures within KLX02 is opposite that of the other cored boreholes for which reliable aperture information is available.

No rock alteration data was available for borehole KLX03 at the time of this report. However, both the MAFI (Figure 5-28) and the CFI (Figure 5-29) plots for this borehole show similar characteristics. Both indicate a significant fall-off in open fracture intensity below the mapped deformation zone DZ1. This drop off is not observed in either the sealed or the subhorizontal fractures. In addition, the average sealed fracture intensity appears to decrease between approximately 350 m to 650 m. This interval ends at the contact between granite to quartz monzonite (dark pink) rock units and those composed largely of quartz monzonite to monzodiorite (lighter pink). This might suggest a weak correlation to lithology; however, this pattern is not observed in the other Laxemar boreholes. The average open fracture intensity appears to remain relatively constant throughout this interval, and throughout the entire hole (with the exceptions of isolated peaks and areas within deformation zones).

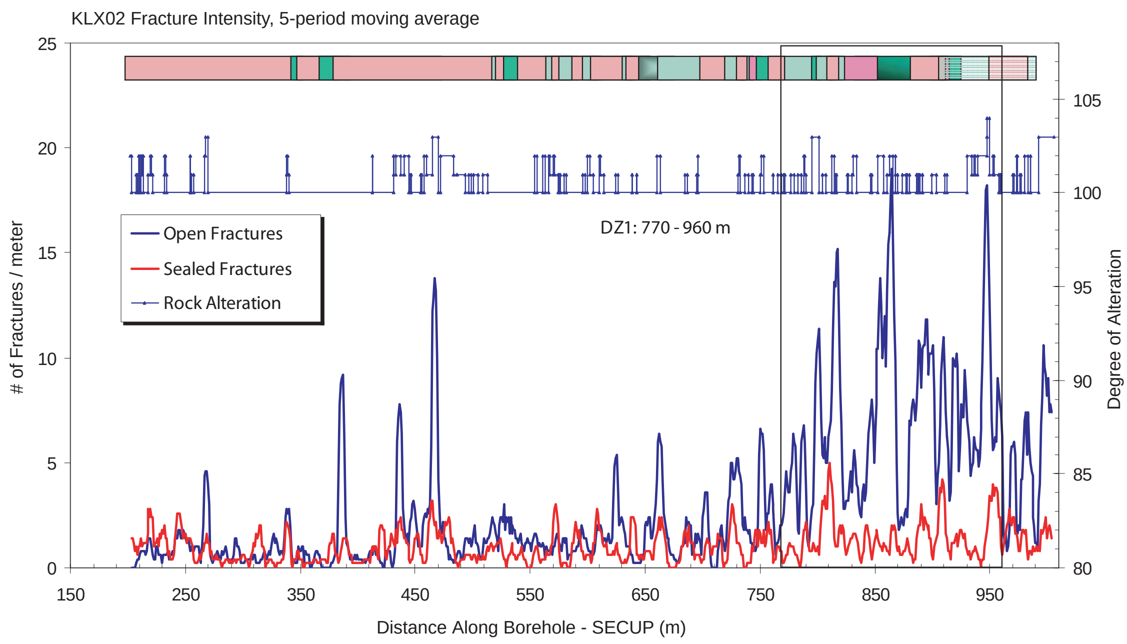

Figure 5-26. Moving average fracture intensity (MAFI) plot of 1 m binned data for borehole KLX02. The moving average function utilizes a five-meter sliding window centered on the value of interest.

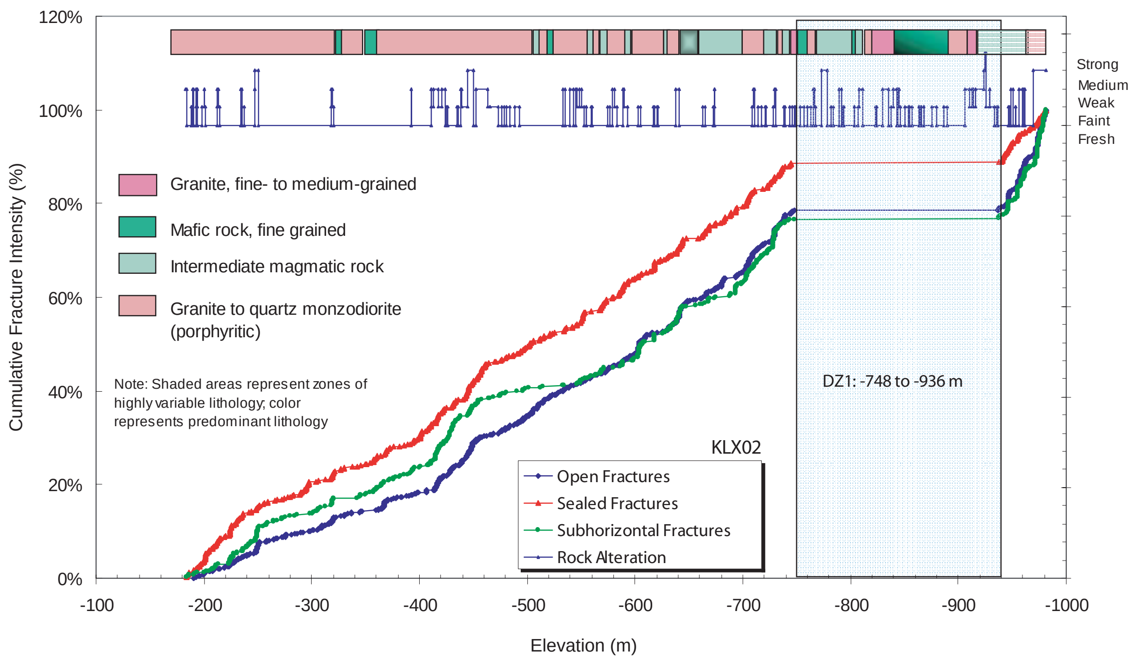

Figure 5-27. CFI plot for borehole KLX02. Flat areas represent relatively low fracture frequency, while steeper slopes represent higher fracture intensity. Fracture data taken from cored borehole and BIPS logs. Plot excludes data based on fractures contained within mapped deformation zones.

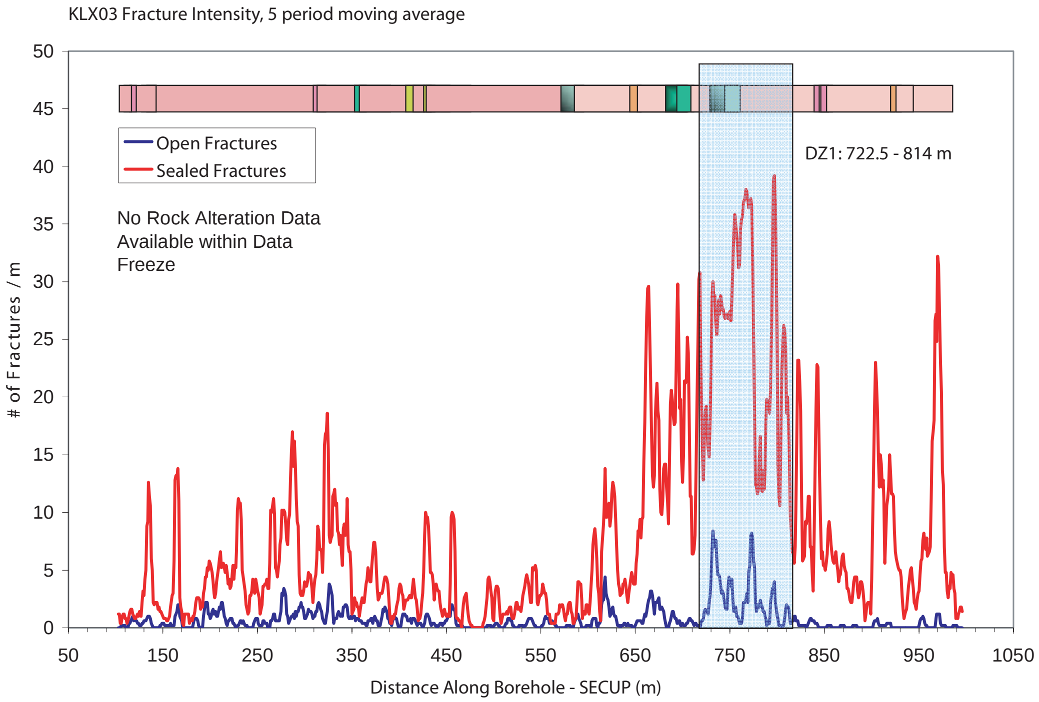

Figure 5-28. *Moving average fracture intensity (MAFI) plot of 1 m binned fracture data for borehole KLX03. The moving average function utilizes a five-meter sliding window centered on the value of interest.*

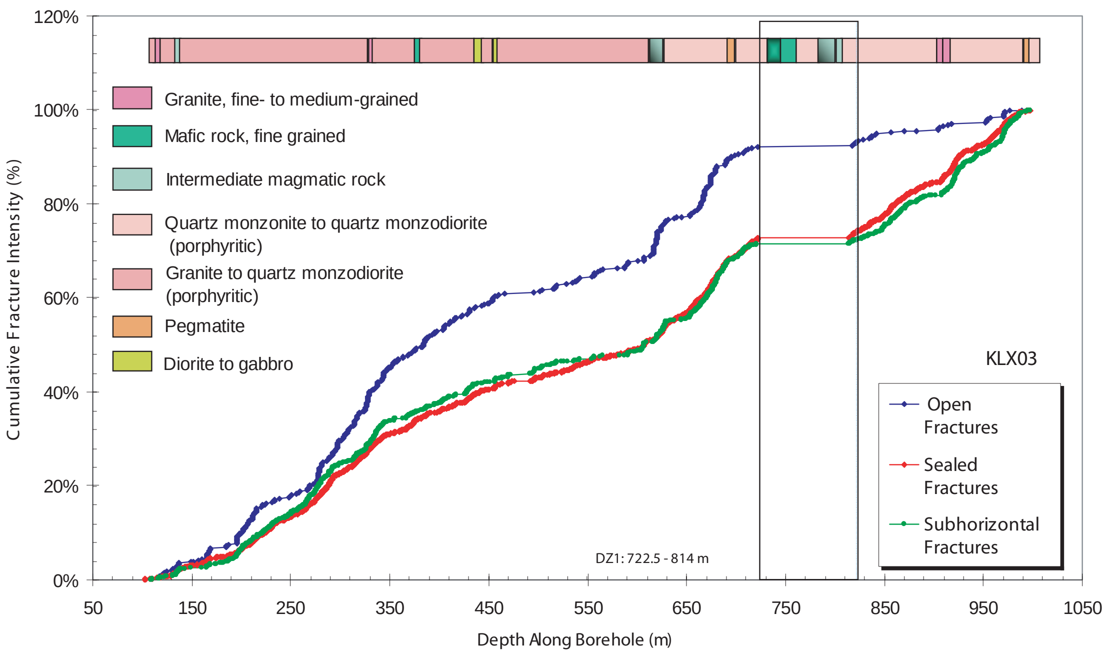

Figure 5-29. *CFI plot for borehole KLX03. Flat areas represent relatively low fracture frequency, while steeper slopes represent higher fracture intensity. Fracture data taken from cored borehole and BIPS logs. Plot excludes data based on fractures contained within mapped deformation zones.*

Borehole KXL04 exhibits a significant degree of lithological complexity; whether this is due to actual site conditions or a change in mapping protocol is unknown. Nevertheless, the presence of so many different small units makes identifying lithological correlations graphically difficult. However, the CFI plot (Figure 5-31) suggests a very strong correlation between fracture alteration degree and intensity; note the significant slope breaks at –420 m, –540 m, –715 m, and –760 m. These slope breaks occur at locations where the degree of rock alteration is faint to none.

The MAFI plot (Figure 5-30) indicates higher intensities of both sealed and open fractures within mapped deformation zones, but also suggests a good correlation between sealed and open fracture intensity throughout the rest of the borehole. There are several zones (most notably at ~500 m and ~590 m) that exhibit relatively high sealed fracture intensities, but are not explicitly mapped as deformation zones. The high sealed intensities do not appear to be accompanied by a drastic increase in open fracture intensities, with the exception of the spike noted at ~590 m. The nature of these zones are unknown; further re-examination of drill hole logs and the core itself might provide more insight, but the fracture logs by themselves are not sufficient to draw any conclusions.

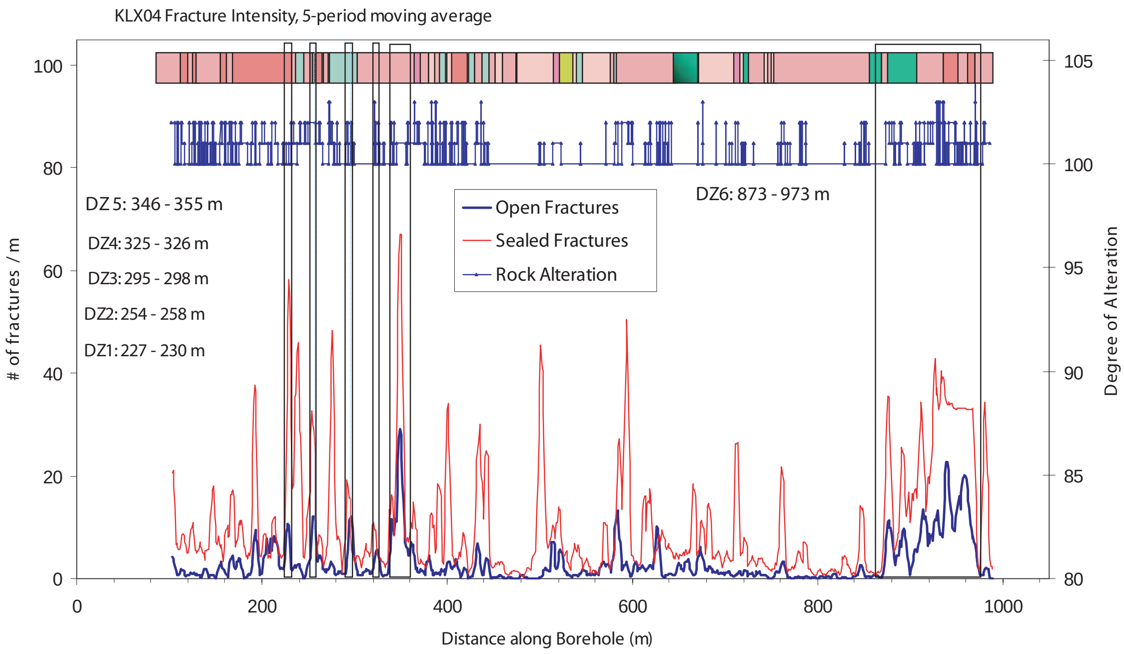

Figure 5-30. *Moving average fracture intensity (MAFI) plot of 1 m binned fracture data for borehole KLX04. Moving average function utilizes a five-meter sliding window centered on the value of interest.*

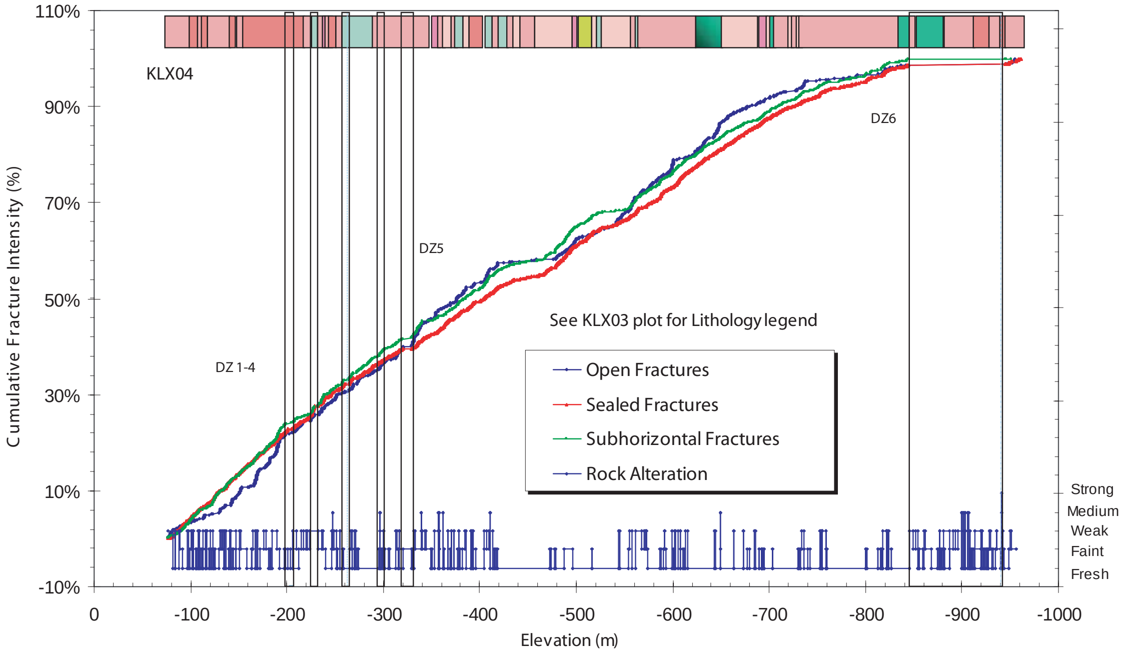

***Figure 5-31.** CFI plot for borehole KLX04. Flat areas represent relatively low fracture frequency, while steeper slopes represent higher fracture intensity. Fracture data taken from cored borehole and BIPS logs. Plot excludes data based on fractures contained within mapped deformation zones.*

5.2 Geological controls on fracture Intensity in Laxemar boreholes

5.2.1 Lithology

The variation of fracture intensity as a function of lithology was evaluated from data in the three cored boreholes at Laxemar in which there was fracture data: KLX02, KLX03 and KLX04. Fracture intensity, expressed as P_{10}, was calculated for open, sealed and total fractures separately. The value of intensity was calculated for each contiguous lithologic interval identified in the portion of the borehole over which fracture data was measured and recorded. An illustration of the calculation of P_{10} is shown in Figure 5-32.

The mean P_{10} for the blue rock would then be calculated as the arithmetic mean of 0.5 and 0.17, or 0.33. The standard deviation would be 0.23.

In this manner, P_{10} values for every lithologic interval were calculated. In addition, intervals were designated as being entirely within identified deformation zones, entirely outside of identified deformation zones, or in mixed intervals contained both deformation zone and non-deformation zone rock. These mixed zones constituted an insignificant amount of the data, and were excluded from all analyses.

The first series of tables (Table 5-1 and Table 5-2) show the mean and median P_{10} values, respectively, sorted from smallest to largest for each fracture aperture category and lithologic category. The value of n shown in these tables refers to the number of intervals in the three boreholes. Mean values are very sensitive to outliers, and so if n is small, the mean value may be highly uncertain. In this situation, the median is preferable.

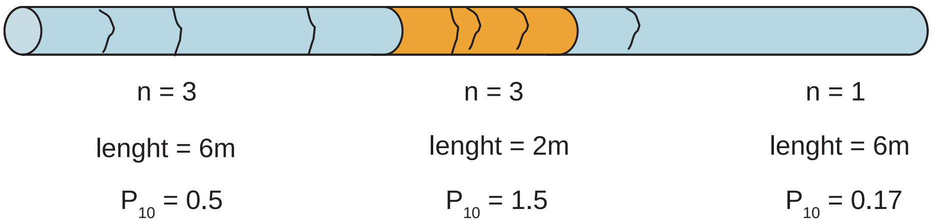

Figure 5-32. *Calculating P_{10} intensity for lithological intervals within a cored borehole.*

These tables show distinct differences in fracture intensity among lithologies. An additional series of tables (Table 5-4 and Table 5-5) showing the ratio of open to sealed fractures, further shows that the ratio of open to sealed fractures also varies according to lithology.

These tabulations show that it is not possible to combine any of the lithologic categories for any of the fracture types in terms of intensity in order to simplify the DFN model without introducing additional uncertainty. As different lithologies are combined to produce the rock domain model (see Section 1.2.3), it is difficult (if not impossible) to provide detailed fracture parameters for the rock domains without introducing additional uncertainty. Any group of lithologies that have similar Open fracture P_{10} do not have similar Sealed fracture P_{10}. Even when only total P_{10} values are considered, the groupings of total intensity have different ratios of open to sealed, as a comparison of Table 5-2 to Table 5-5 illustrates.

Further statistical testing of the association between intensity and lithology (Table 5-3) showed that the variable lithology accounts for approximately 18% (the Eta-squared value) of the variation for open fracture intensity, and about 11% for sealed fracture intensity. Overall, lithology accounts for about 16% of the variation. The differences between the values for eta squared and r-squared shown in this table also indicate that the relation is highly non-linear.

Table 5-1. Fracture intensity in cored boreholes sorted by aperture and mean P_{10}.

Fracture aperture	Sorted by mean P10 lithology	n	Mean	SD
Open	Pegmatite	3	0.2778	0.48113
Open	Quartz monzonite to monzodiorite, equigranular to weakly porphyritic	25	1.0272	0.79217
Open	Diorite to gabbro	3	1.1946	1.45819
Open	Granite to quartz monzodiorite, generally porphyritic	157	1.8530	2.16902
Open	Fine-grained dioritoid (Metavolcanite, volcanite)	48	3.1405	2.73619
Open	Granite, fine- to medium-grained	14	4.1174	4.97587
Open	Granite, medium- to coarse-grained	12	4.8666	3.85296
Open	Mafic rock, fine-grained	24	5.3461	4.35108
Sealed	Mafic rock, fine-grained	24	2.0127	2.18731
Sealed	Granite to quartz monzodiorite, generally porphyritic	157	2.0143	2.48459
Sealed	Fine-grained dioritoid (Metavolcanite, volcanite)	48	2.9752	3.05909
Sealed	Granite, fine- to medium-grained	14	3.5437	2.43283
Sealed	Diorite to gabbro	3	3.7964	2.24641
Sealed	Pegmatite	3	3.8095	2.06197
Sealed	Quartz monzonite to monzodiorite, equigranular to weakly porphyritic	25	4.5804	3.26318
Sealed	Granite, medium- to coarse-grained	12	4.8040	4.03940

Fracture aperture	Sorted by mean P10 lithology	n	Mean	SD
Total	Granite to quartz monzodiorite, generally porphyritic	157	3.8673	3.59946
Total	Pegmatite	3	4.0873	2.33992
Total	Diorite to gabbro	3	4.9910	3.18406
Total	Quartz monzonite to monzodiorite, equigranular to weakly porphyritic	25	5.6076	3.63062
Total	Fine-grained dioritoid (metavolcanite, volcanite)	48	6.1157	4.05980
Total	Mafic rock, fine-grained	24	7.3588	4.15778
Total	Granite, fine- to medium-grained	14	7.6611	4.09641
Total	Granite, medium- to coarse-grained	12	9.6706	4.03987

Table 5-2. Fracture intensity in cored boreholes sorted by aperture and median P_{10}.

Fracture aperture	Sorted by median P10 lithology	n	Median
Open	Pegmatite	3	0.0000
Open	Diorite to gabbro	3	0.7643
Open	Quartz monzonite to monzodiorite, equigranular to weakly porphyritic	25	1.0000
Open	Granite to quartz monzodiorite, generally porphyritic	157	1.1662
Open	Granite, fine- to medium-grained	14	1.7492
Open	Fine-grained dioritoid (metavolcanite, volcanite)	48	2.2650
Open	Granite, medium- to coarse-grained	12	2.7799
Open	Granite to quartz monzodiorite, generally porphyritic	157	1.1905
Sealed	Mafic rock, fine-grained	24	1.3642
Sealed	Fine-grained dioritoid (metavolcanite, volcanite)	48	1.9536
Sealed	Granite, fine- to medium-grained	14	3.2841
Sealed	Mafic rock, fine-grained	24	4.0166
Sealed	Quartz monzonite to monzodiorite, equigranular to weakly porphyritic	25	4.1348
Sealed	Diorite to gabbro	3	4.3233
Sealed	Granite, medium- to coarse-grained	12	4.3995
Sealed	Pegmatite	3	5.0000
Total	Granite to quartz monzodiorite, generally porphyritic	157	3.0303
Total	Pegmatite	3	5.0000
Total	Quartz monzonite to monzodiorite, equigranular to weakly porphyritic	25	5.2720
Total	Mafic rock, fine-grained	24	6.1180
Total	Granite, fine- to medium-grained	14	6.3898
Total	Diorite to gabbro	3	6.4968
Total	Fine-grained dioritoid (metavolcanite, volcanite)	48	7.1997
Total	Granite, medium- to coarse-grained	12	9.2546

Table 5-3. Evaluation of lithological controls on fracture intensity variations.

Measures of association	R	R squared	Eta	Eta squared
OpenP10 * Lith_Code	.252	.064	.429	.184
SealP10 * Lith_Code	.035	.001	.328	.108
TotalP10 * Lith_Code	.208	.043	.403	.162

Table 5-4. Ratio of open to sealed fractures as a function of lithology, sorted by mean ratio.

Sorted by mean ratio ratio O/S by lithology	n	Mean	SD	SE	95% CI of mean
Pegmatite	3	0.0556	0.09623	0.05556	–0.1835 to 0.2946
Diorite to gabbro	3	0.2618	0.34455	0.19893	–0.5941 to 1.1178
Quartz monzonite to monzodiorite, equigranular to weakly porphyritic	25	0.2772	0.25241	0.05048	0.1730 to 0.3813
Granite to quartz monzodiorite, generally porphyritic	149	1.4804	2.26801	0.18580	1.1132 to 1.8476
Fine-grained dioritoid (metavolcanite, volcanite)	45	1.9006	1.83296	0.27324	1.3499 to 2.4513
Granite, fine- to medium-grained	14	1.9470	3.07861	0.82279	0.1694 to 3.7245
Mafic rock, fine-grained	24	3.0172	3.39617	0.69324	1.5831 to 4.4513
Granite, medium- to coarse-grained	12	11.4121	29.98613	8.65625	–7.6401 to 30.4644

Table 5-5. Ratio of open to sealed fractures (sorted by median ratio) as a function of lithology.

Sorted by median ratio ratio O/S by lithology	n	Median	IQR	95% CI of median
Pegmatite	3	0.0000	0.0833	– to –
Diorite to gabbro	3	0.1333	0.3261	– to –
Quartz monzonite to monzodiorite, equigranular to weakly porphyritic	25	0.2000	0.3873	0.1176 to 0.3333
Granite, fine- to medium-grained	14	0.3030	1.0846	0.1111 to 6.5000
Granite, medium- to coarse-grained	12	0.5917	5.9202	0.3333 to 8.0000
Granite to quartz monzodiorite, generally porphyritic	149	1.0000	1.3461	0.8000 to 1.0000
Mafic rock, fine-grained	24	1.2100	3.7125	1.0000 to 3.6000
Fine-grained dioritoid (metavolcanite, volcanite)	45	1.6000	1.8056	0.7647 to 2.0588

The tables of open vs sealed fractures are calculated from ratios in individual intervals of the same lithology. In essence, these tables report the mean ratio of the intervals for each lithology. Another way to examine the data is to plot the ratio of the mean intensities, which has the effect of reducing the impact of local variations and examines the global ratios of mean open and sealed intensity. Figure 1-2 shows a cross plot of mean open P_{10} intensity vs the mean sealed P_{10} intensity. This plot shows that it may be possible to group the diorite to gabbro, pegmatite and quartz monzonite categories globally without introducing excessive uncertainty, but the remaining rock types, if combined, will introduce greater uncertainty in intensity.

Interestingly, there appears to be a trend line for the remaining granitic and dioritoid rocks that has a slope of about 1.0 (shown as a dashed line on the figure). This indicates that the global mean open intensity is approximately equal to the global mean sealed intensity for these lithologies. It may also be indicative of the fracture potential as a function of factors like grain size or mineralogy of these largely granitic rocks. If so, it may be possible to relate absolute fracture intensity, as well as sealed and open fracture intensity, to some compositional or textural variable. This could greatly simplify DFN model construction, reduce the need for additional samples, and help to reduce model uncertainty.

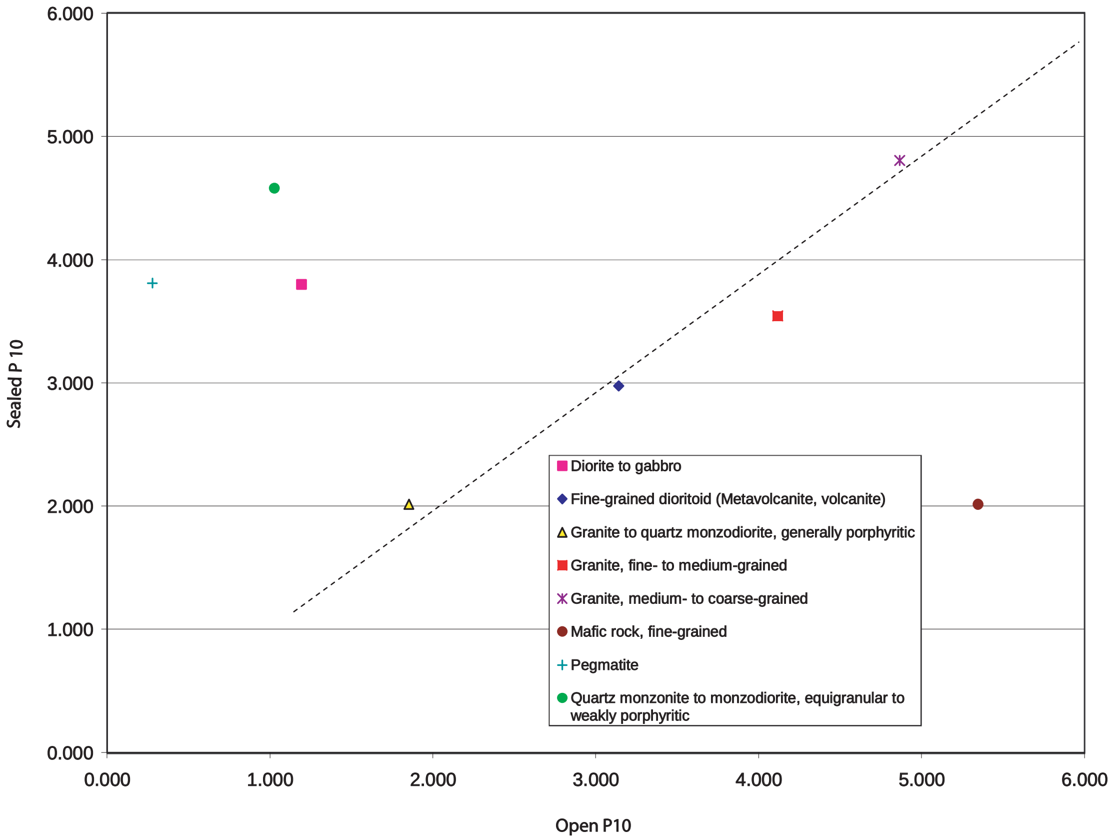

Figure 5-33. *Cross plot of open P_{10} vs sealed P_{10}, mean values for lithologies.*

Figure 5-34 and Figure 5-35 show the difference in intensities and intensity ratios for fractures inside and outside of deformation zone as a function of rock type category. In these figures, the intensities of fractures outside of deformation zones are shown by triangle symbols, while those inside are shown by circles. The dashed line indicates equal open and sealed fracture intensity.

This figure shows that the majority of rock types outside of deformation zones have a predominance of sealed fractures, as the symbols plot above the dashed line, while the majority of rock types in deformation zones have a predominance of open fractures, as the symbols mostly plot below the dashed line. The exception to this is for pegmatites and quartz monzonites in deformation zones, which plot above the line.

Figure 5-35 shows the direction of change for each lithology category from outside to inside deformation zones. The tail of the arrow represents the open and sealed intensity for a specific rock type for rock outside identified deformation zones. The tip of the arrow indicates the open and sealed intensities inside identified deformation zones. If the arrow's tip is farther away from the origin than its starting point, then the total sealed and open fracture intensity inside of deformation zones is greater than the total intensity outside of deformation zones. This is true for all rock types except medium to coarse-grained granite.

The slope of the line indicates whether the increase (or decrease) comes about because there are more open fractures in the deformation zones, more sealed fractures, or more of both relative to the same rock type outside of deformation zones. A negative slope, such as the blue arrows have, indicates a decrease in sealed fracture intensity but an increase in open fracture intensity. The red arrows indicate an increase in both sealed and open intensity.

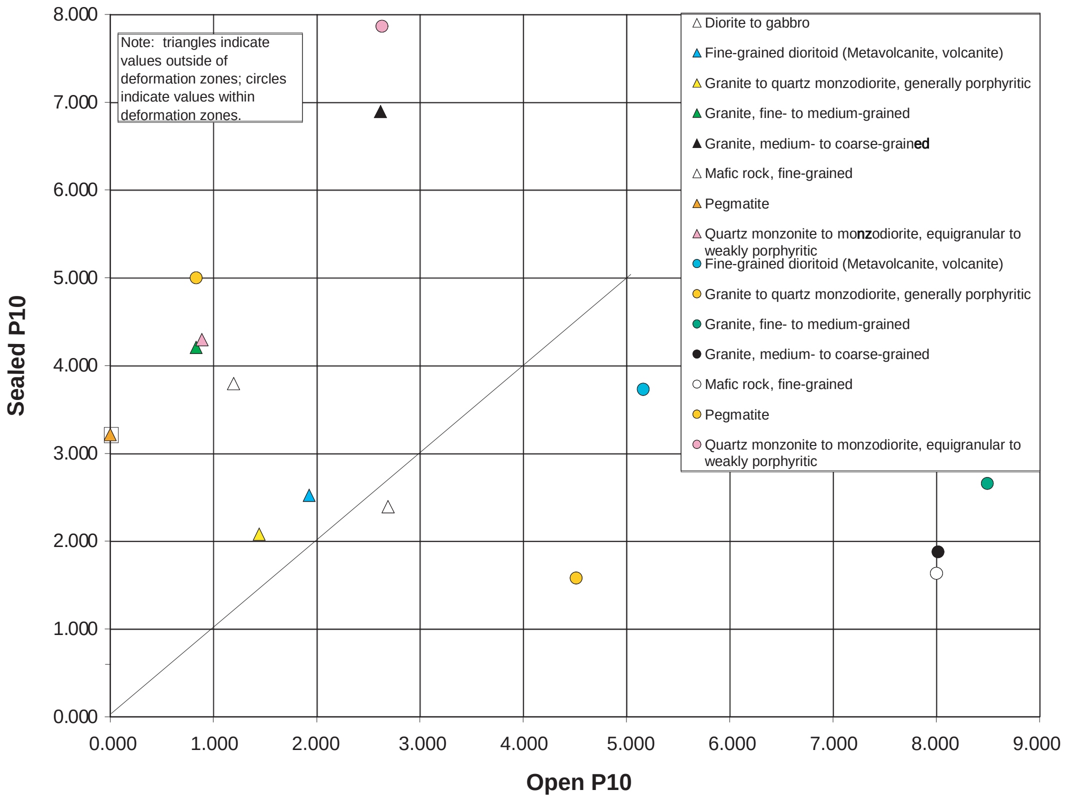

Figure 5-34. *Cross plot of open P_{10} vs sealed P_{10}, mean values, for fractures exclusively inside of deformation zones (circles), and fractures exclusively outside deformation zones (triangles). Dashed line indicates equal open and sealed fracture intensity.*

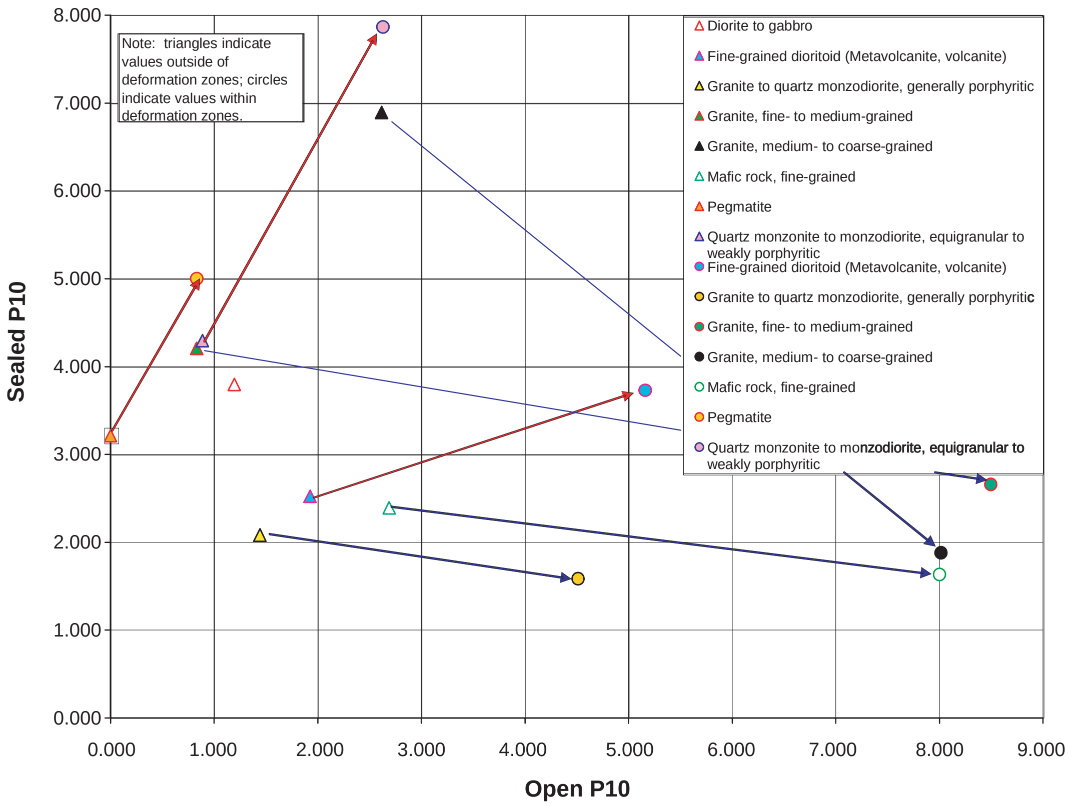

Figure 5-35. *Cross plot using same data as Figure 5-34, with arrows showing the change in intensity between fractures outside of deformation zones, to fractures inside of deformation zones.*

There are no examples of an increase in sealed intensity and a simultaneous decrease in open intensity. Thus, there appear to be two families of lithologies; one, shown by blue arrows, where intensity increases inside of deformation zones due to the absolute increase in open fracture intensity and the absolute decrease in sealed fracture intensity; and the other, shown by red arrows, in which both types of fractures increase in absolute intensity. The medium to coarse-grained granite is similar to the first category, as its sealed intensity decreases, and its open fracture intensity increases in deformation zones, although the overall intensity slightly decreases.

It is interesting to note that the slope of the arrows is similar for the pegmatite and quartz monzonite categories, and also for the fine grained mafic rock, the porphyritic quartz monzodiorite to granite, and the fine- to medium-grained granite. Although not as close in slope, the arrow for the medium to coarse grained granite is not too different. These similarities in slopes may indicate common controls on fracture enhancement in these rock types, even though the absolute values differ among the lithologies.

Overall, the intensity differences are greatest for the open fractures (Table 5-6). This table shows that approximately 38% of the total observed fracture intensity differences for the open fractures are accounted for by the deformation zones, while the differences for sealed fractures are statistically insignificant.

Table 5-6. Evaluation of deformation zones on fracture intensity variations.

Measures of association	Eta	Eta squared
OpenP10 * DZ=0(FILTER)	.618	.382
SealP10 * DZ=0 (FILTER)	.014	.000
TotalP10 * DZ=0 (FILTER)	.439	.193

5.2.2 Rock alteration

Alteration degree might be associated with differences in fracture intensity, because alteration zones may have been zones of weakness in the past that preferentially localized fracture development, or alternatively, zones of more intense fracturing may have promoted alteration due to higher fracture network permeability and fracture surface area. In either case, an association between the degree of alteration and the intensity of fracturing could improve the local accuracy of a DFN model, and also provide some insight into the geological processes that have produced fracturing in the Laxemar site.

Alteration degree was been categorized into four classes: none, faint, weak and medium. One of these alteration states has been assigned in terms of measured depth to contiguous intervals of the boreholes. The relation between alteration state of the rock and fracturing was examined in the three cored boreholes, KLX02, KLX03 and KLX04. As in the case of lithology, these three boreholes were selected because they:

1. Have both alteration information and fracture logs;
2. Are situated within the Laxemar subarea region;
3. Are cored boreholes, and it is presumed that the data quality is higher in cored boreholes than in percussion boreholes; and
4. Extend to depths from near the surface to the base (approx 1,000 m below the surface) of the repository block flow models.

The summary statistical tables (Table 5-7 through Table 5-9) and box-and-whisker plots (Figure 5-36 through Figure 5-38) show the intensity of fracturing in terms of fracture aperture and alteration category. These figures and tables are based upon only those intervals in the three boreholes that are not part of identified deformation zones.

Table 5-7. Summary statistics for open fracture intensity as a function of alteration category in Laxemar subarea cored boreholes.

	n	Mean	SD	SE	95% CI of mean	Median	IQR	95% CI of median
None – Open	137	1.426	1.5083	0.1289	1.171 to 1.681	1.071	1.441	0.792 to 1.357
Faint – Open	59	1.393	1.2852	0.1673	1.058 to 1.727	1.053	1.362	0.688 to 1.235
Weak – Open	21	2.076	2.4655	0.5380	0.954 to 3.198	1.031	2.756	0.556 to 3.311
Medium – Open	2	5.006	3.2053	2.2665	–23.792 to 33.805	5.006	0.000	– to –

Table 5-8. Summary statistics for sealed fracture intensity as a function of alteration category in Laxemar subarea cored boreholes.

	n	Mean	SD	SE	95% CI of mean	Median	IQR	95% CI of median
None – Sealed	137	3.314	2.6975	0.2305	2.858 to 3.769	2.907	3.438	2.392 to 3.343
Faint – Sealed	59	1.247	1.3584	0.1769	0.893 to 1.601	0.680	1.300	0.527 to 1.136
Weak – Sealed	21	2.338	4.2884	0.9358	0.386 to 4.29	0.833	2.722	0.37 to 3.093
Medium – Sealed	2	1.364	1.9285	1.3636	–15.963 to 18.69	1.364	0.000	– to –

Table 5-9. Summary statistics for total fracture intensity as a function of alteration category in Laxemar subarea cored boreholes.

	n	Mean	SD	SE	95% CI of Mean	Median	IQR	95% CI of Median
None	137	4.7397	3.31583	0.28329	4.179 to 5.3	4.3884	4.4843	3.571 to 5
Faint	59	2.6399	1.95618	0.25467	2.13 to 3.15	2.0455	2.2488	1.667 to 3.109
Weak	21	4.4137	6.31456	1.37795	1.539 to 7.288	2.6984	4.3372	0.926 to 5.263
Medium	2	6.3699	5.13379	3.63014	–39.755 to 52.495	6.3699	0.0000	– to –

Table 5-10. Evaluation of alteration degree on fracture intensity variations.

Measures of association	R	R squared	Eta	Eta squared
OpenP10 * Int_Code	.070	.005	.240	.058
SealedP10 * Int_Code	-.314	.099	.332	.110
TotalP10 * Int_Code	-.212	.045	.266	.071

These results show that the intensity for medium alteration zones is the highest for both open and total fractures, while zones with no alteration have the highest sealed fracture intensity. It should be noted that there are only two intervals designated as “medium” outside of the deformation zones, and as a result, the statistics for this category are highly uncertain relative to the other categories.

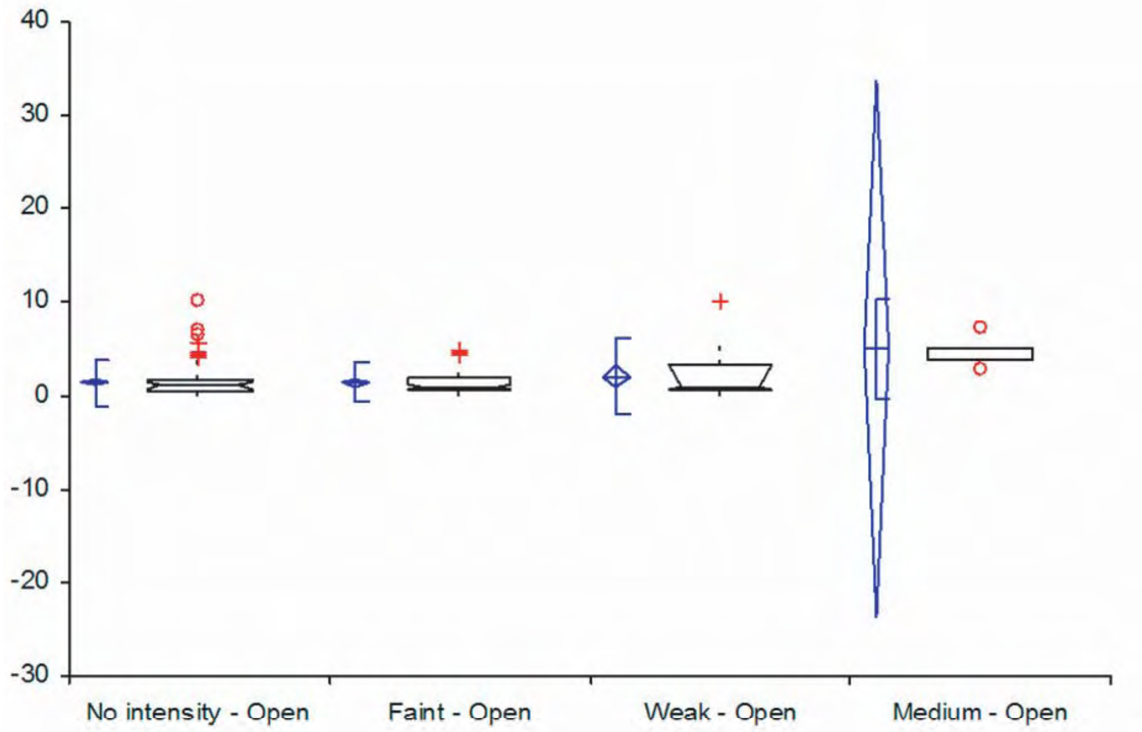

Figure 5-36. *Box-and-whisker plot of open fracture intensity classified by alteration category in Laxemar subarea cored boreholes*

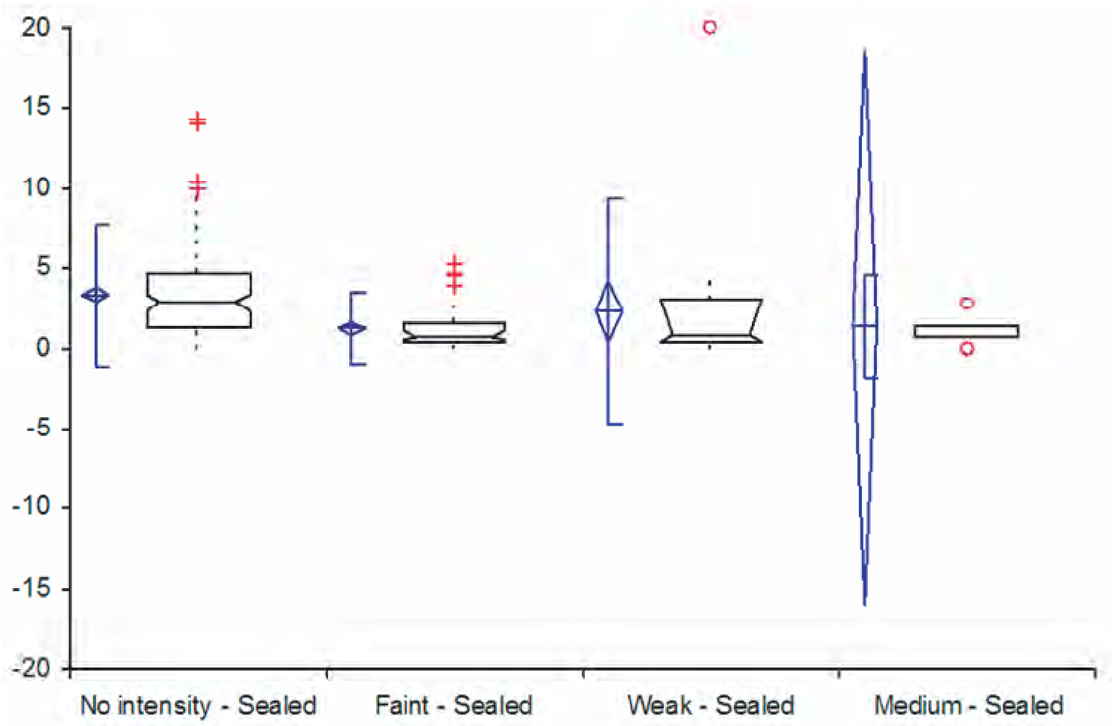

Figure 5-37. *Box-and-whisker plot of sealed fracture intensity classified by alteration category in Laxemar subarea cored boreholes.*

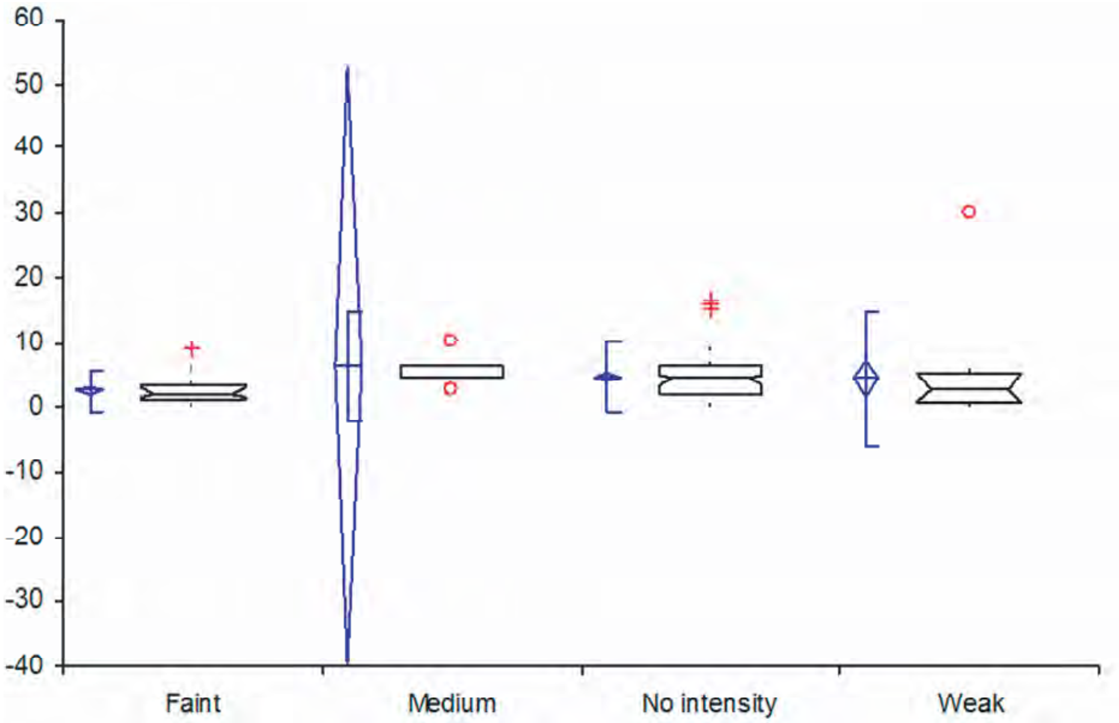

Figure 5-38. *Box-and-whisker plot of total fracture intensity classified by alteration category in Laxemar subarea cored boreholes.*

The Faint alteration category has the lowest mean fracture intensity for all three aperture classes. The Weak category shows intensity values vary by the aperture type.

Although there is not a unequivocal correlation between alteration and fracture intensity, open fracture intensity is either insensitive to alteration degree, if the results for the Medium category are largely due to the small sample size, or insensitive with the exception of the zones of medium alteration. One the other hand, sealed fractures are definitely more intense in zones that show no alteration. This relation becomes clearer in Table 5-10 and Figure 5-39. The table shows that only about 6% of the intensity variation for open fractures is explained by alteration degree, while about 11% of sealed fracture intensity is explained by alteration degree.

Figure 5-39 shows the ratio of open to sealed fracture intensity. The line indicates an equal ratio of open to sealed intensity. Data has been plotted in several ways: mean intensities for all fractures, including those in deformation zones (squares); mean intensities for only fractures outside of deformation zones (triangles); and median intensities for only fractures outside of deformation zones (circles). The colors of the symbols correspond to the alteration category. Both means and medians were plotted for the fractures outside of deformation zones to assess the impact of outliers on small data sets.

This graph clearly shows that:

1. The mean intensities are relatively robust, as they do not different markedly from the medians.
2. The zones with no alteration tend to have the highest ratios of sealed to open fracture intensity, and there is not much difference either in ratios or absolute intensity when deformation zones are included.

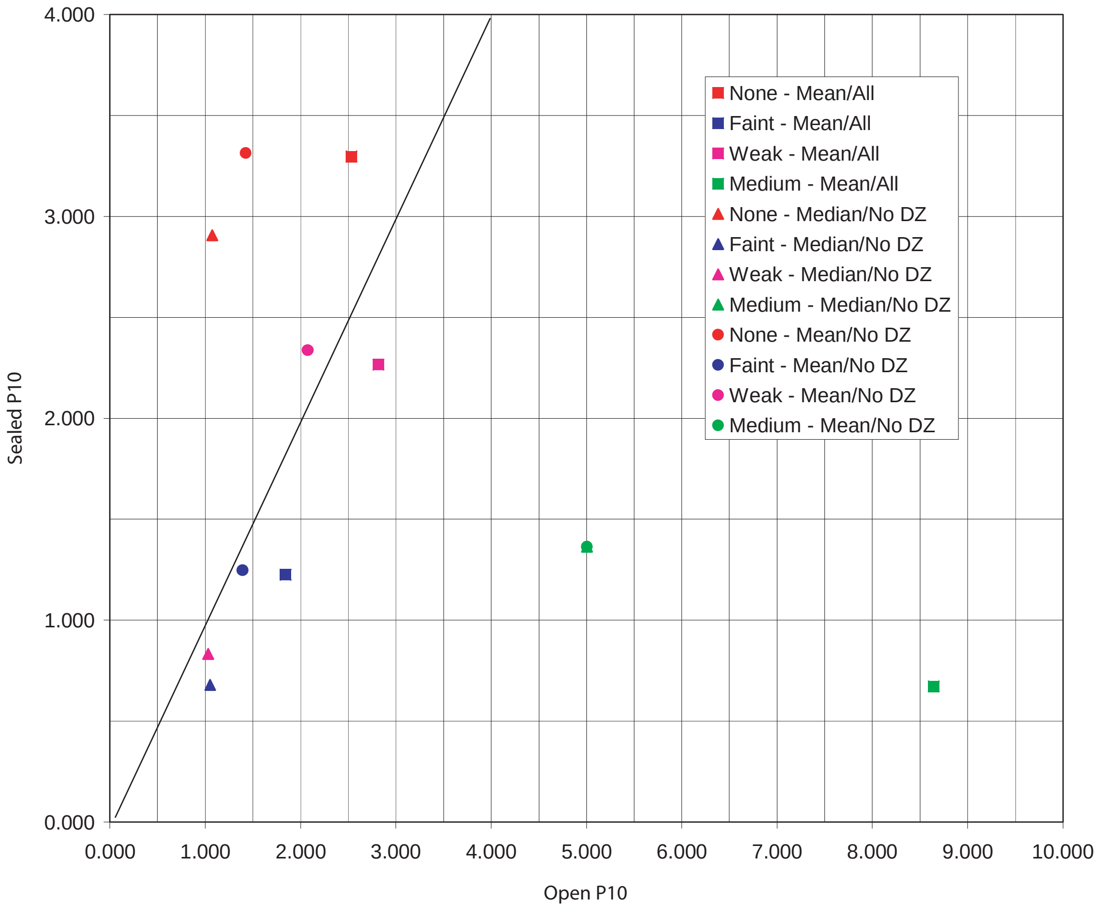

Figure 5-39. *Ratio of open to sealed fracture intensity as a function of alteration category for different subsets of fractures.*

3. The ratio of open to sealed fractures is considerably higher for Medium alteration zones than for any other alteration category.
4. The average intensity of sealed fractures decreases, while the average intensity of open fractures greatly increases, if deformation zones are included.
5. The ratio of open to sealed fractures is approximately 1.0 for Faint and Weak alteration classes.
6. Tthe absolute intensity of fracturing in Weak zones is greater than the absolute intensity in Faint zones.

This analysis supports the previous finding that there tend to be both numerically more fractures in the most highly altered zones (the Medium zones in this data set), and a higher ratio of open to sealed fractures. This is particularly accentuated in deformation zones, where an increase of open fractures apparently more than offsets a decrease in sealed fractures. On the other hand, sealed fractures predominate in the unaltered zones, and it makes very little difference whether deformation zones are included or not. One interpretation of these results might be that:

1. Some significant fracturing formed before hydrothermal alteration. /Tullborg, 2004 in Bäckblom and others, 2004; pg. 82–84/ describes several epochs of hydrothermal alteration, which occur after at least some of the fracturing developed.

2. These fractures formed preferential pathways for hydrothermal alteration.
3. As a result, alteration is associated with open fracturing, particularly in deformation zones. Sealed fractures did not provide any preferential pathways, and so there degree of alteration is not accentuated.

Overall, the variations in open and sealed fracture intensity outside of deformation zones are still not well understood. Somewhere on the order of 10% to 20% of the variation is explained by lithology and alteration, leaving about 80% of the variation unexplained. This result implies that the current state of understanding is possibly inadequate for making accurate local predictions of fracture intensity at the borehole scale or outcrop scale for flow or mechanical modeling.

5.3 Analysis of borehole data in Simpevarp sub-domain

Seven cored boreholes (KAV01A, KAV04A, KAV04B, KSH01A, KSH02, KSH03A, and KSH03B) were used to analyze the three-dimensional characteristics of fracturing within the Laxemar model sub-domain. Due to time constraints and questions regarding data collection procedures, data from percussion drilled holes was not used. Borehole data was used primarily to constrain fracture intensities and to evaluate the suitability of the orientation model at depth. Fractures were assigned to global orientation sets based on a single-iteration hard-sector search within FracSys/ISIS; set definitions and parameters were not free to change.

5.3.1 Borehole fracture orientations

Figure 5-40 through Figure 5-70 illustrate the orientation of fracture poles taken from drill core or borehole image logs. Fracture sets are assigned through a hard-sector process; they have not been fitted through an optimization or clustering routine.

The contoured stereonet plots of fracturing within borehole KAV01 (Figure 5-40) clearly illustrates two of the three (Sets S_A and S_C) regional fracture sets identified through outcrop trace map analysis. However, regional sets S_B and S_C appear in the pole plots as representing one large and disperse set. In addition, the subhorizontal regional fracture set (S_d) is much more intense than in outcrop.

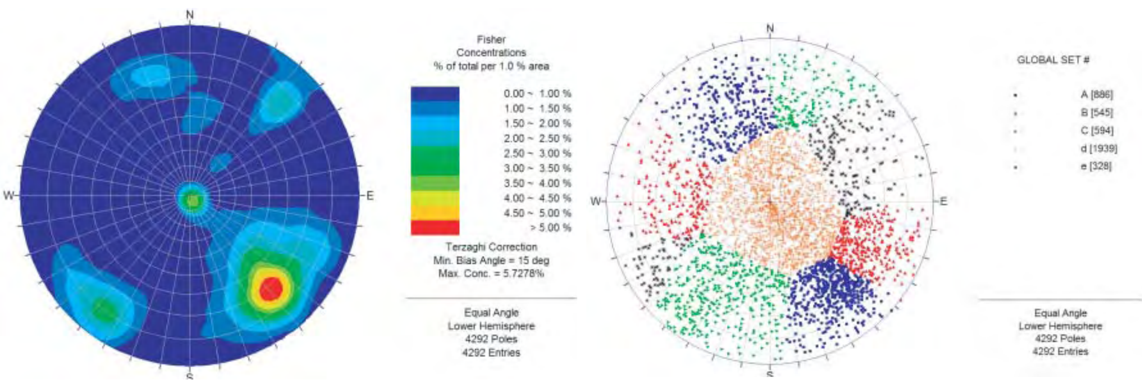

Figure 5-40. *Borehole KAV01A fracture orientations, Simpevarp subarea.*

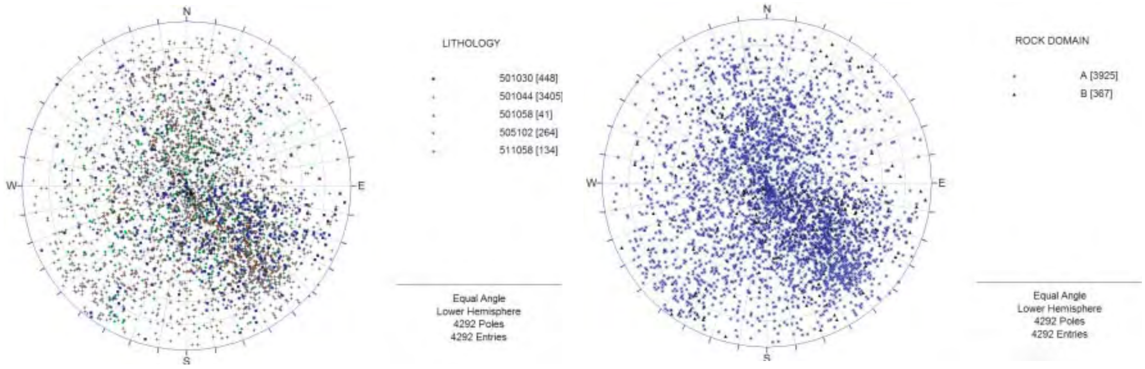

Figure 5-41. *KAV01A fracture orientations as a function of lithology and rock domain.*

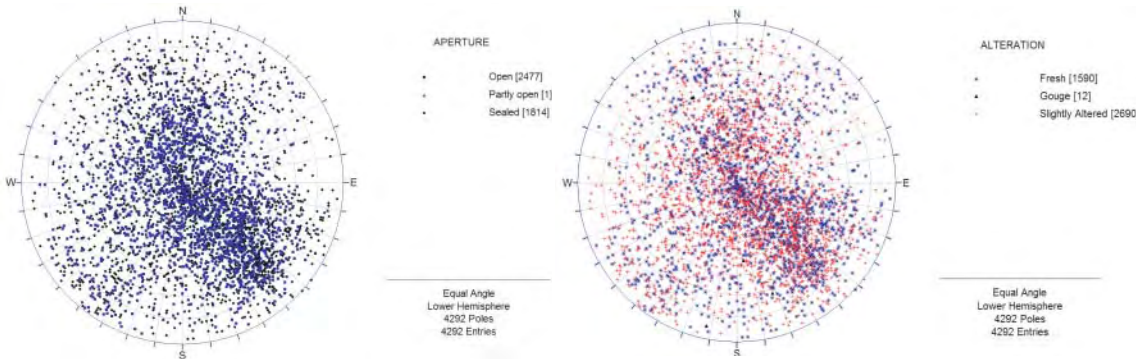

Figure 5-42. *KAV01A fracture orientations as a function of aperture and degree of alteration.*

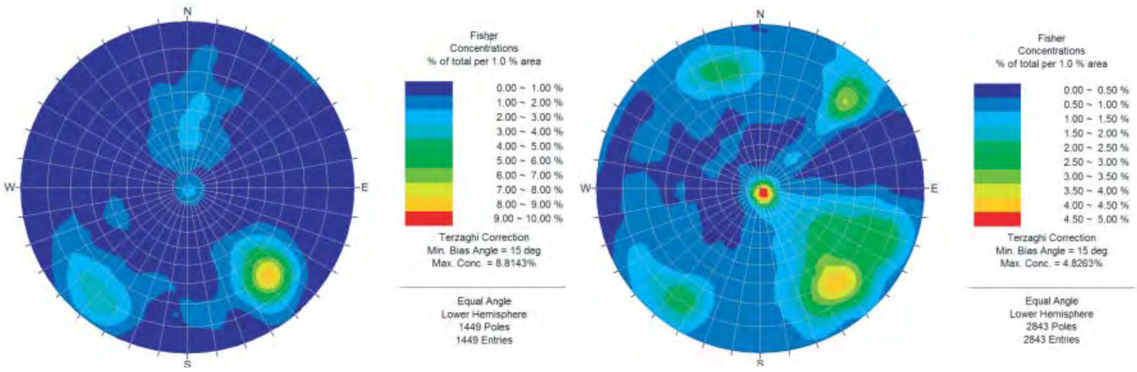

Figure 5-43. *KAV01A fracture orientations inside and outside of mapped deformation zones.*

Fracture aperture and degree of alteration (Figure 5-42) do not appear to be correlated to fracture orientation. Fractures hosted within Äspö diorite (501044) appear to have orientations scattered throughout the identified fracture sets. Fractures within lithologic zones identified as intermediate magmatic rock (501030) or fine- to medium-grained granite (511058) tend to be concentrated in the northeast-trending fracture set (Set S_A). Fractures hosted in all other lithologies appear to be spread out among. Orientation does appear, however, to be largely independent of rock domain (at least as they are currently constructed).

Fractures hosted inside mapped deformation zones tend to have similar orientations to those outside the zone; however, there is a notable concentration of east-west striking, moderately dipping (40°–50°) fractures seen inside deformation zones that is not noted in the rest of the borehole.

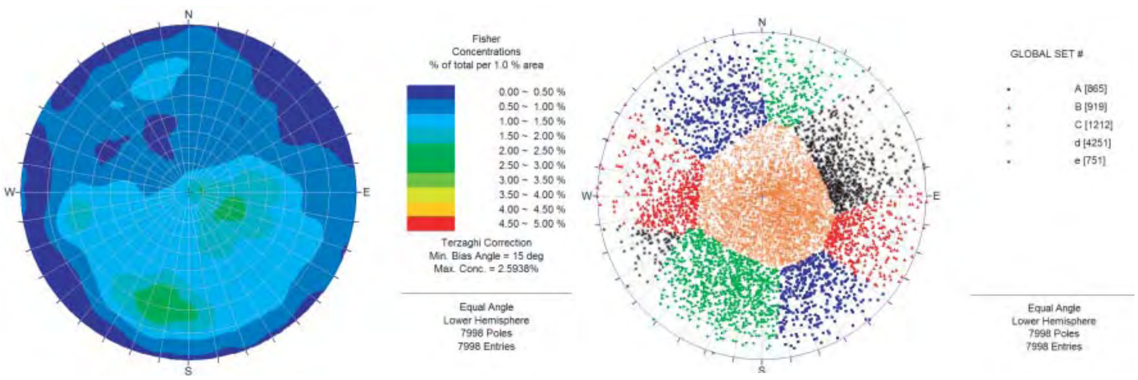

Figure 5-44. *KAV04A fracture orientations, Simpevarp subarea.*

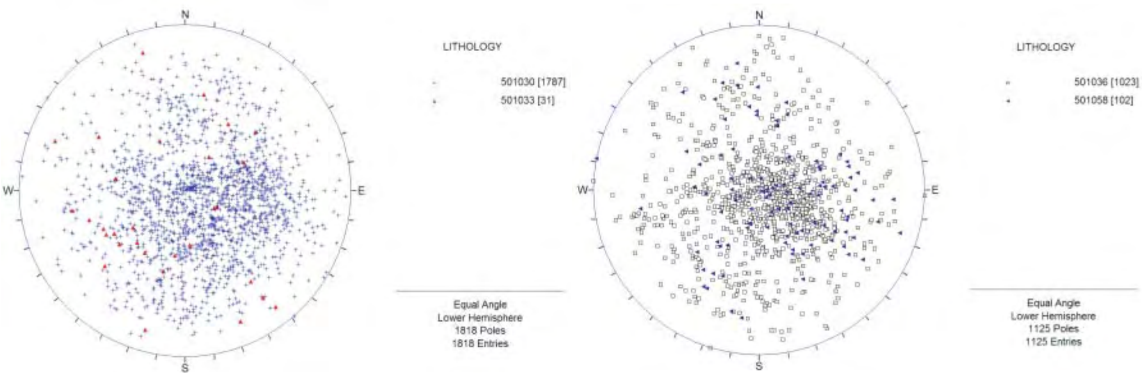

Figure 5-45. *KAV04A fracture orientations as a function of lithology: 501030 (intermediate magmatic rock), 501033 (diorite to gabbro), 501036 (quartz monzonite to monzodiorite), and 501058 (medium- to coarse-grained granite).*

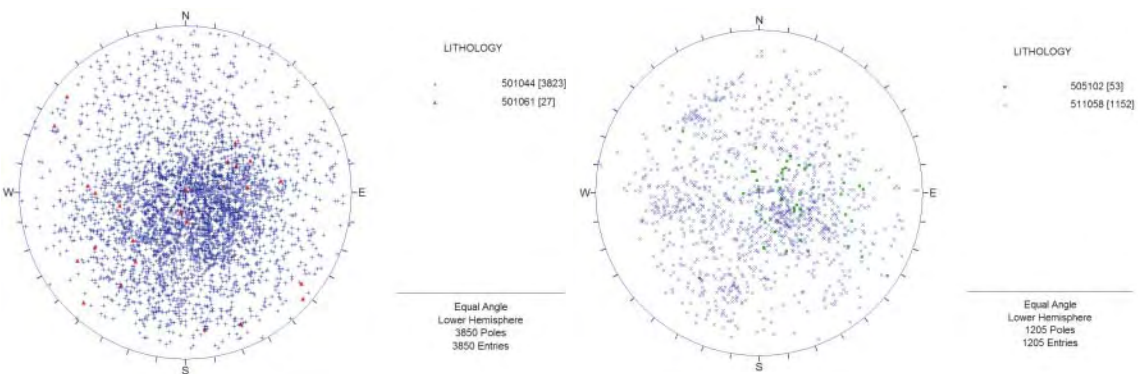

Figure 5-46. *KAV04A fracture orientations as a function of lithology: 501044 (Äspö diorite), 501061 (pegmatite), 505102 (fine-grained mafic rock), and 511058 (fine- to medium-grained granite).*

Cored borehole KAV04A is dominated by subhorizontal fracturing; it is difficult to pick out any of the steeply-dipping regional fracture sets (S_A, S_B, and S_C). Since the set assignment was done by imposing a definition on top of the borehole data, all five 'sets' are present in the pole plots. However, the contoured stereonet (Figure 5-44) clearly does not show the same sets as seen in the Simpevarp outcrops.

The large number of subhorizontal fractures in borehole KAV04A makes classification based on lithology difficult, but several trends are visible in the polar stereoplots above. Fractures hosted in dioritic to gabbroic rocks (501033) tend to be concentrated within regional set S_C (northwest-striking); fractures hosted in pegmatite (501061) also appear to follow this pattern to a limited extent. Fractures hosted within fine-grained mafic rock units are almost universally dipping westwards at low angles (Figure 5-46). Finally, most of the fracturing within KAV04A appears to be spread out uniformly with respect to rock domain (Figure 5-47).

Again, fracture aperture and the degree of alteration appear to have little control over or association with fracture orientations. In a change from borehole KAV01A, fractures within mapped deformation zones in borehole appear to have orientations quite similar (Figure 5-49) to those outside the zones.

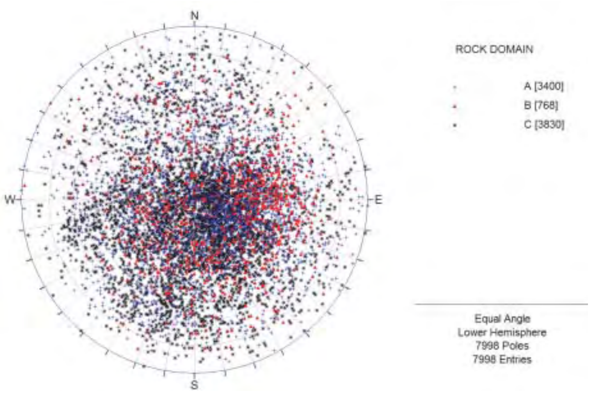

Figure 5-47. *KAV04A fracture orientations based on rock domain.*

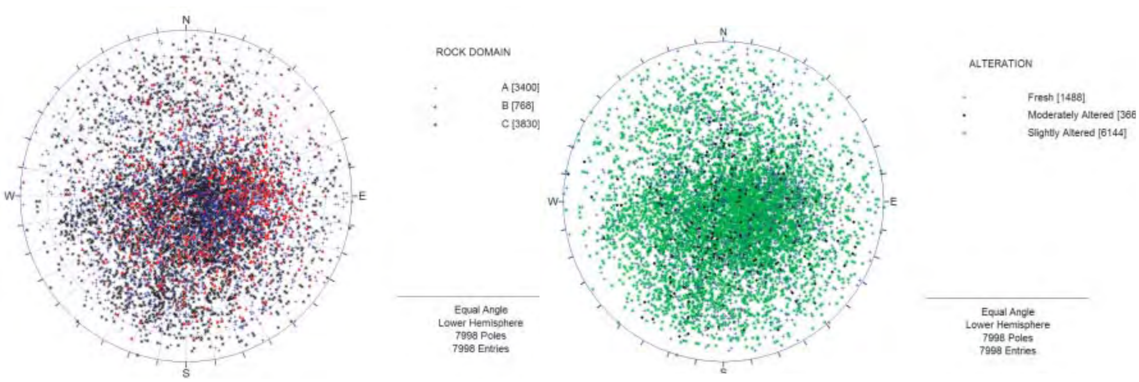

Figure 5-48. *KAV04A fracture orientations based on fracture aperture and degree of alteration.*

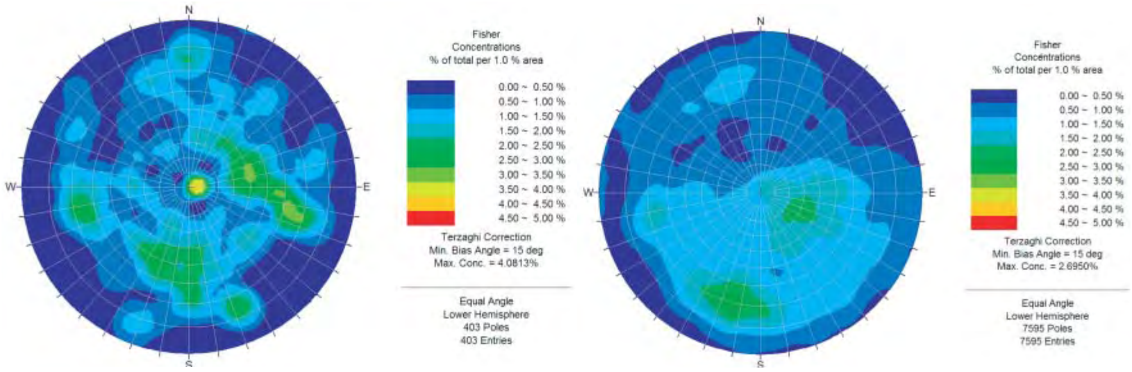

Figure 5-49. *KAV04A fracture orientations inside and outside mapped deformation zones.*

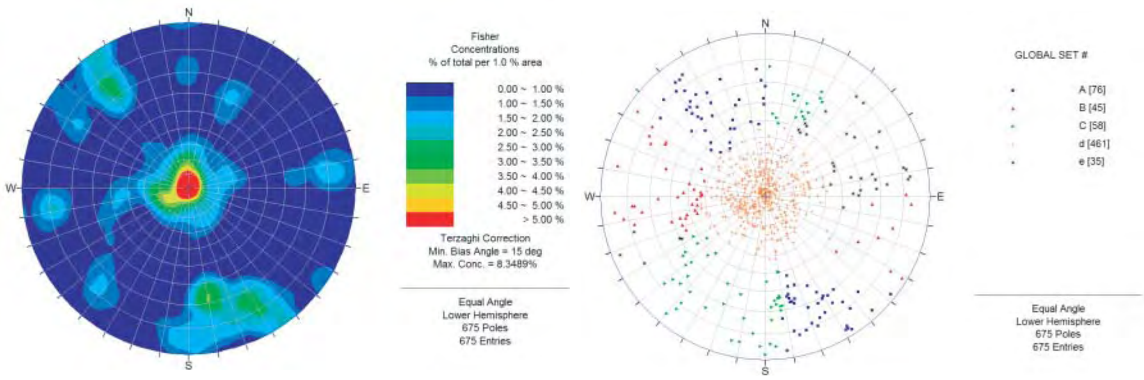

Figure 5-50. *KAV04B fracture orientations, Simpevarp subarea.*

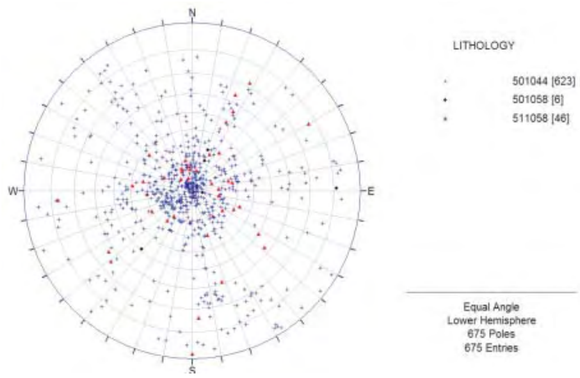

Figure 5-51. *KAV04B fracture orientations as a function of lithology. Note that the entire borehole is within rock domain B.*

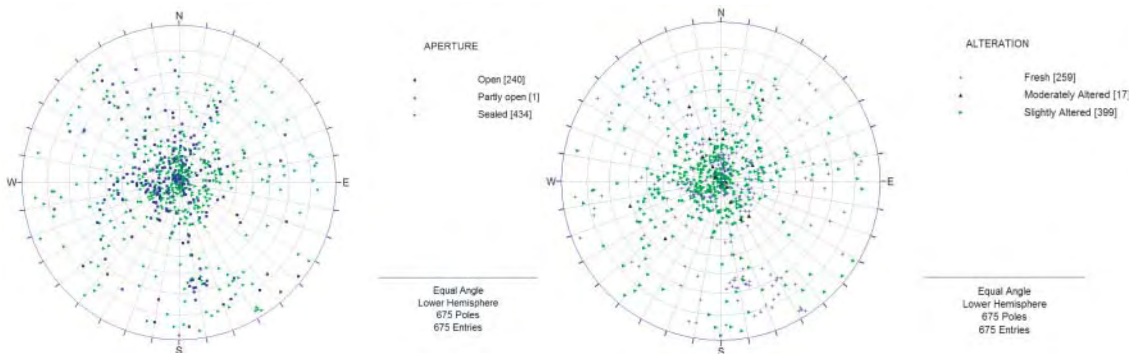

Figure 5-52. *KAV04B fracture orientations as a function of fracture aperture or degree of alteration.*

Cored borehole KAV04B is a short drilled hole designed to capture information in an approximately 100 m zone that was not sampled during the drilling of KAV04A. KAV04B exhibits a significant amount of subhorizontally-oriented fracturing in a pattern that is similar to that observed in Simpevarp subarea outcrops. No significant orientation/lithology or rock domain correlation was noted in KAV04B, though a slight propensity towards moderate degrees of alteration within the subhorizontally-dipping fracture set (S_d) was noted.

Cored borehole KSH01A exhibits a fracture pattern similar to that of KAV04; a significant number of subhorizontally- to moderately-dipping fractures and few, if any, discrete fracture sets visible on contoured stereonets (Figure 5-53). Few solid lithological correlations can be seen in the above stereoplots. Fractures hosted in medium- to coarse-grained granite (501058) appeared to largely strike west-northwest, and generally dipped either north or west (Figure 5-54). Though only nine recorded fractures occurred within dioritic to gabbroic rocks, almost all of them had dips less than 30° (subhorizontal).

As in most other cored boreholes within the Simpevarp subarea, fracture orientations appeared to be unrelated to either rock domain membership or fracture aperture. However, a distinct correlation between subhorizontal fracturing and moderate to severe (gouge) degrees of alteration was noted (Figure 5-57).

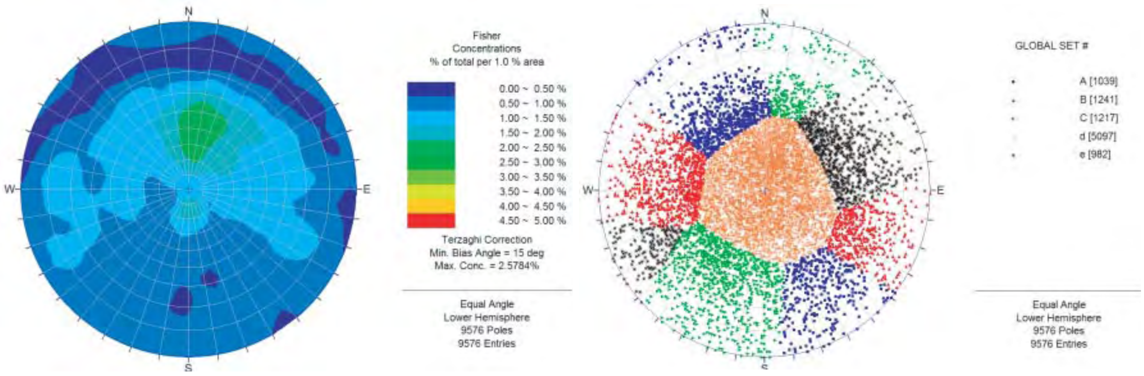

Figure 5-53. *KSH01A fracture orientations, Simpevarp subarea.*

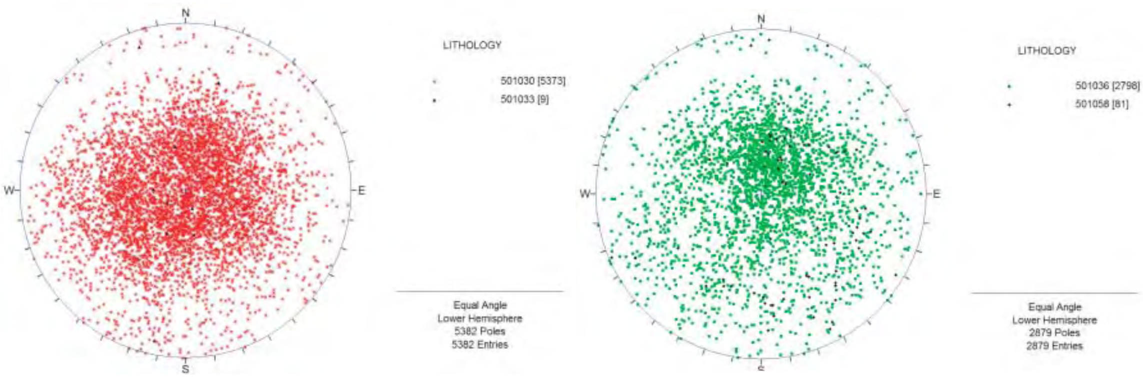

Figure 5-54. *KSH01A fracture orientations as a function of lithology: 501030 (intermediate magmatic rock), 501033 (diorite to gabbro), 501036 (quartz monzonite to monzodiorite), and 501058 (medium- to coarse-grained granite).*

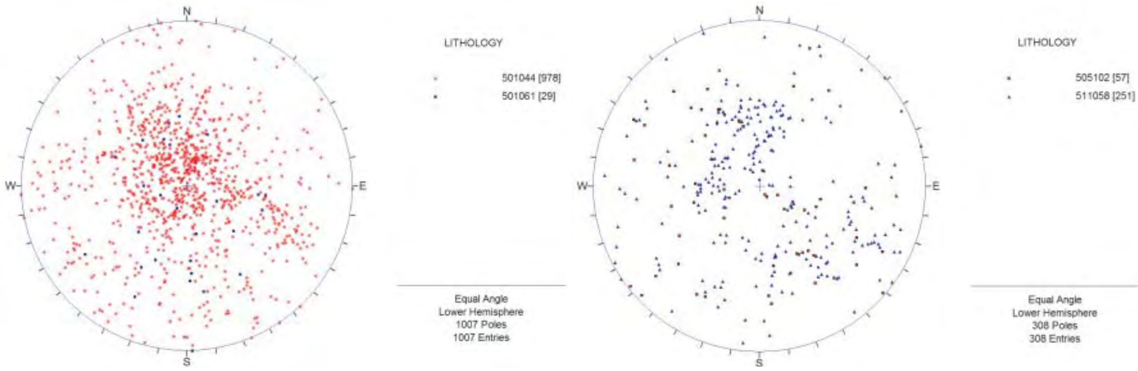

Figure 5-55. *KSH01A fracture orientations as a function of lithology: 501044 (Äspö diorite), 501061 (pegmatite), 505102 (fine-grained mafic rock), and 511058 (fine- to medium-grained granite).*

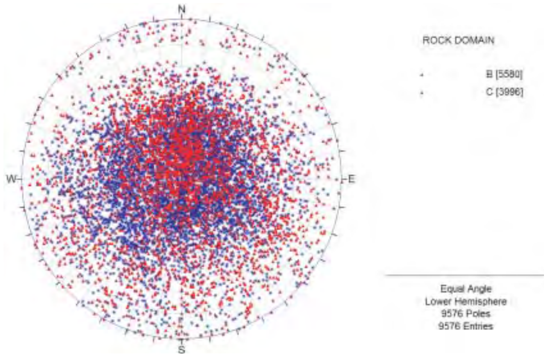

Figure 5-56. *KSH01A fracture orientations based on rock domain.*

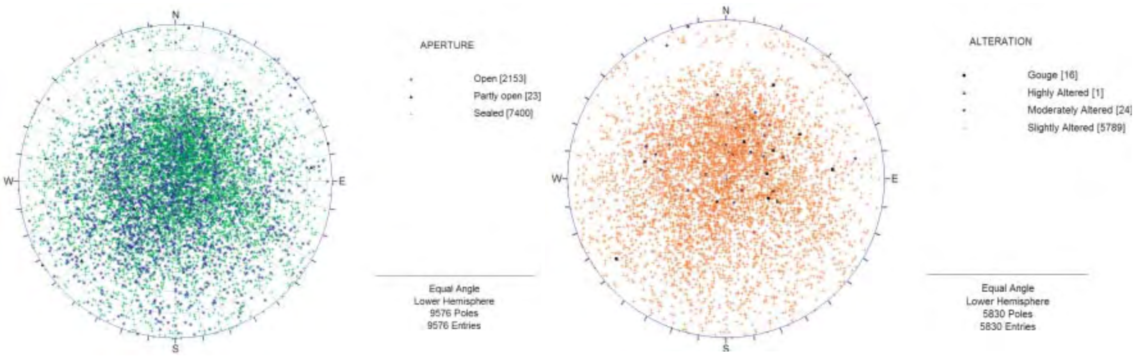

Figure 5-57. *KSH01A fracture orientations based on fracture aperture and degree of alteration. Due to sheer volume, all fractures with a degree of alteration of 'Fresh' have been removed from the stereonet.*

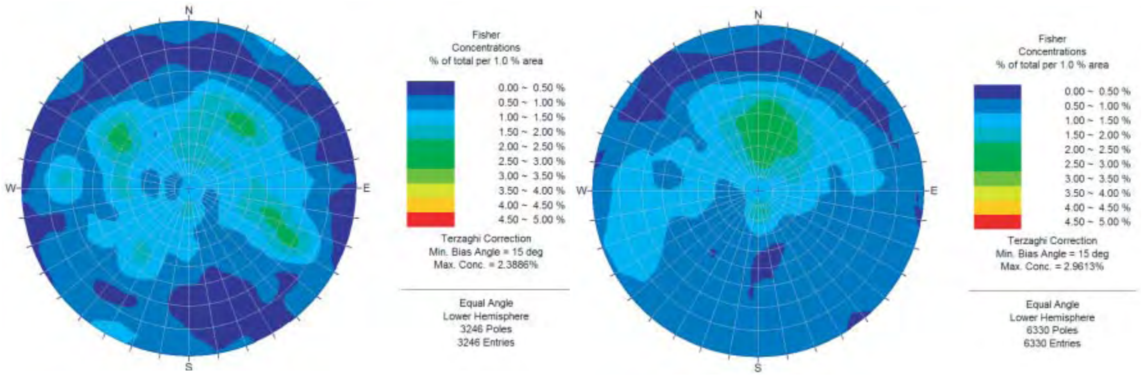

__Figure 5-58.__ KSH01A fracture orientations inside and outside mapped deformation zones.

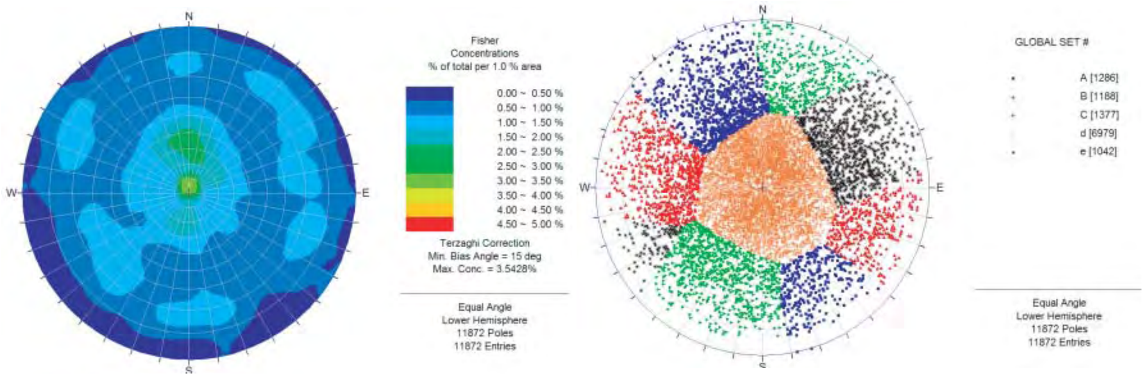

__Figure 5-59.__ KSH02 fracture orientations, Simpevarp subarea.

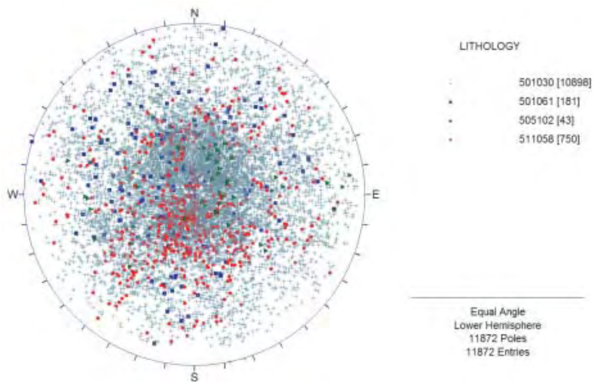

__Figure 5-60.__ KSH02 fracture orientations as a function of lithology. Note that KSH02 is entirely within rock domain B.

Contoured stereonets of fractures logged in cored borehole KSH02 appear to form patterns similar to those observed in the Simpevarp subarea detailed outcrops. Though the hole is largely dominated by subhorizontal fracturing, three distinct subvertical sets are visible. However, relative to the outcrop patterns of regional sets S_A, S_B, and S_C, the sets in KSH02 appear to be rotated approximately 20 degrees clockwise. It is impossible to tell from the data at hand whether this pattern represents a rotation of the local stress field, or a post-fracturing tectonic movement.

Borehole KSH02 is entirely within rock domain B (dominated by diorite to gabbro); the only strong lithologic association noted is within layers of fine-grained mafic rock (505102). Fractures here tend to have shallow (< 30°) westward dips (Figure 5-61). No association between fracture orientation and aperture was noted; however, as in most other Simpevarp boreholes, the subhorizontal fracture set tends to have the largest number of moderately to severely altered fractures. Finally, fracture patterns inside mapped deformation zones appear to be similar (at least on contoured stereonets) to those outside deformation zones (Figure 5-62).

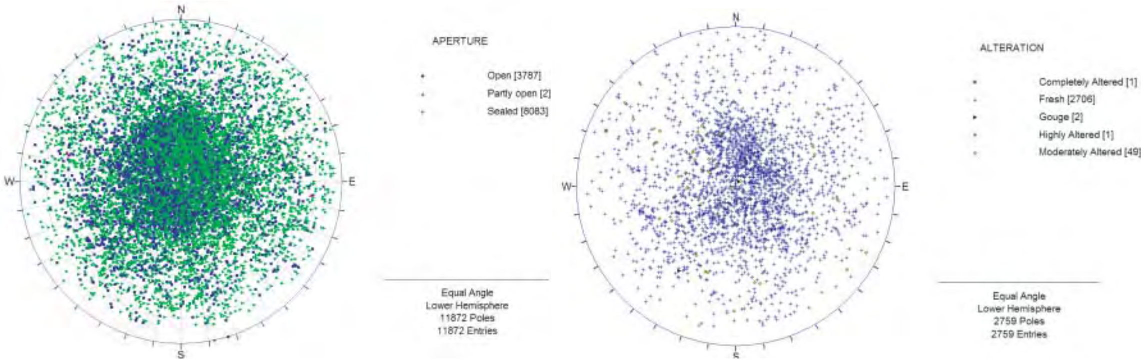

Figure 5-61. *KSH02 fracture orientations as a function of aperture and degree of alteration.*

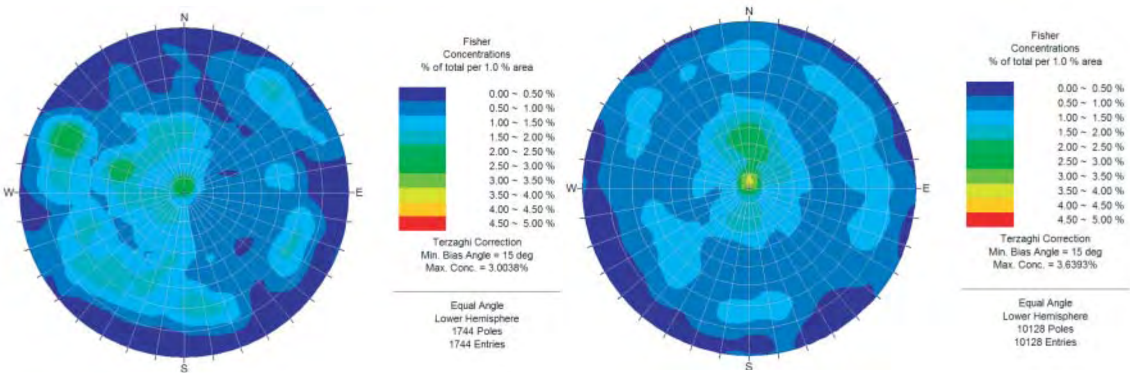

Figure 5-62. *KSH02 fracture orientations inside and outside of mapped deformation zones.*

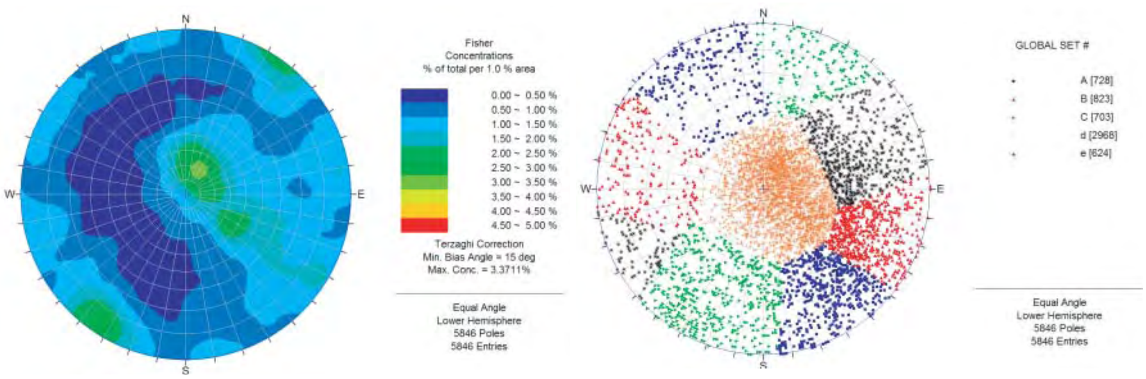

Figure 5-63. *KSH03A fracture orientations.*

Fracture patterns in cored borehole KSH03A appear to be quite similar to those observed in Simpevarp outcrops; all three regional sets (S_A, S_B, and S_C) are visible in the contoured stereoplot (Figure 5-63), along with a significantly more-intense subhorizontal fracture set (S_d). Some lithological-orientation associations are visible in the KSH03A core data. Fractures hosted in pegmatite dikes (501061) are largely west-dipping and belong to the subhorizontal fracture set (S_d). In addition, both the medium- to coarse-grained granite dikes and those units grouped as rock domain C host almost no northeast-trending fractures, when compared to the borehole at large (Figure 5-65).

No relationship between fracture aperture and orientation was observed in KSH03A; however, moderate to severe degrees of alteration were confined to the intense, moderately-dipping northeast trending fracture set (Figure 5-66). Significant differences in fracture orientations are noted inside and outside of mapped deformation zones; the strong northwest trending regional set (S_C) is almost completely absent, and a strong moderately dipping (40°–50°), relatively strongly clustered northeast-trending set stands out. This same set is visible throughout the rest of the hole; however, it appears to be most intense inside the mapped deformation zones.

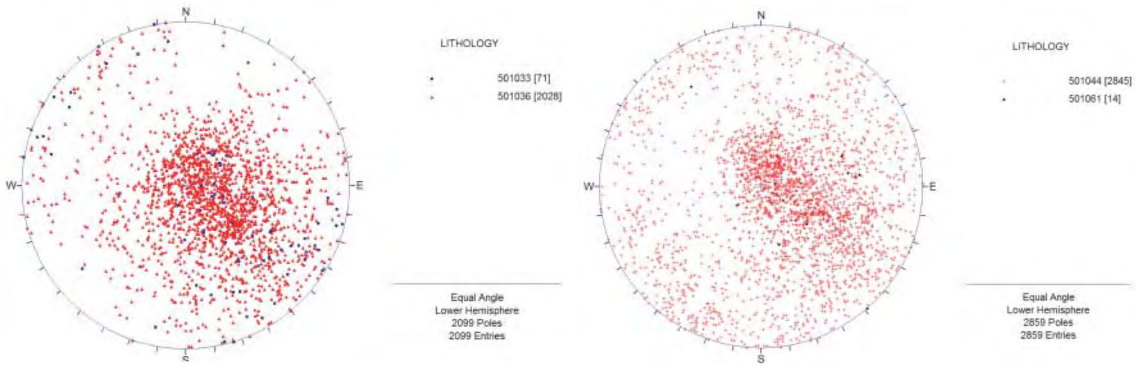

__Figure 5-64.__ KSH03A fracture orientations as a function of lithology: 501033 (diorite to gabbro), 501036 (quartz monzonite to monzodiorite), 501044 (Äspö diorite), and 501061 (pegmatite).

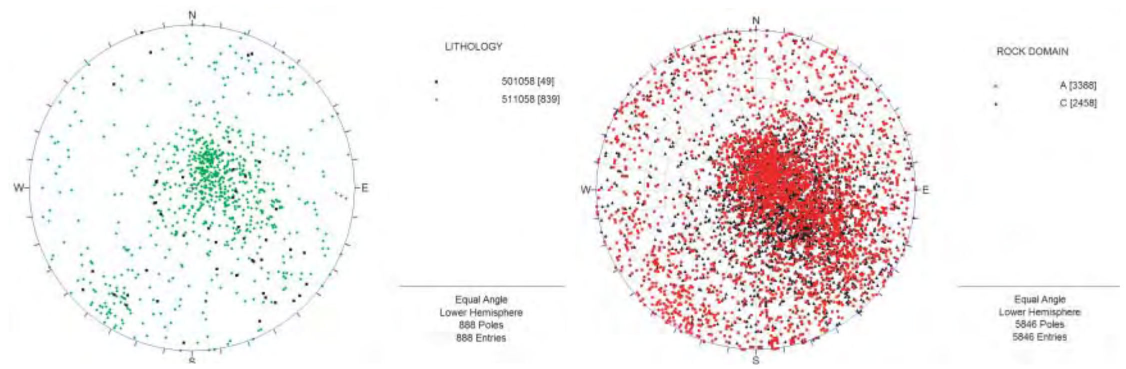

__Figure 5-65.__ KSH03A fracture orientations as a function of rock domain and lithology: 501058 (medium- to coarse-grained granite) and 511058 (fine- to medium-grained granite).

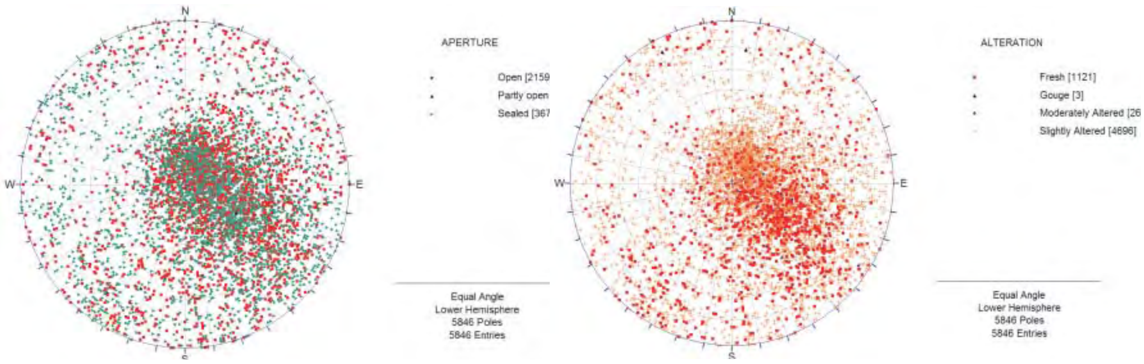

Figure 5-66. *KSH03A fracture orientations based on aperture and degree of alteration.*

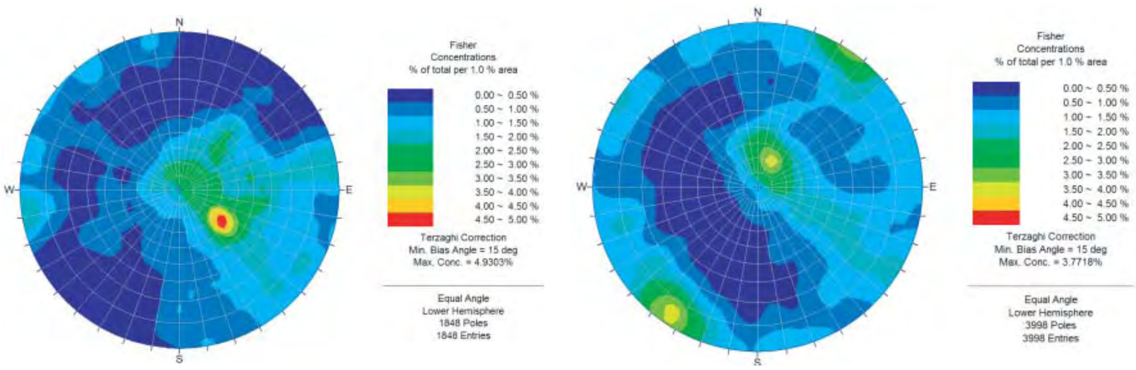

Figure 5-67. *KSH03A fracture orientations inside (left) and outside (right) of mapped deformation zones.*

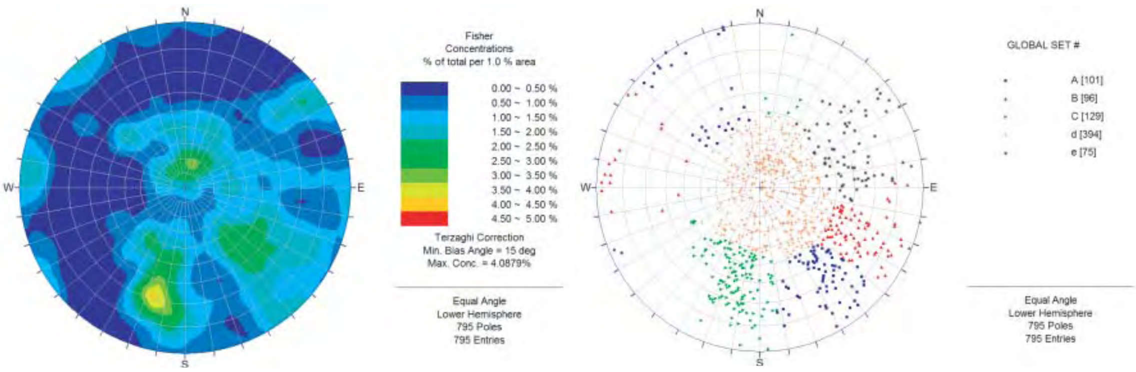

Figure 5-68. *KSH03B fracture orientations.*

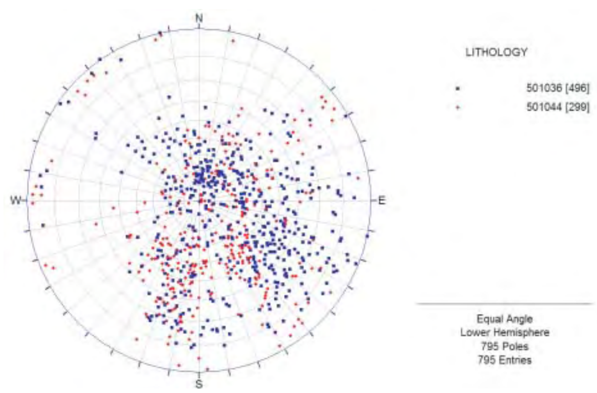

Figure 5-69. *KSH03B fracture orientations as a function of lithology.*

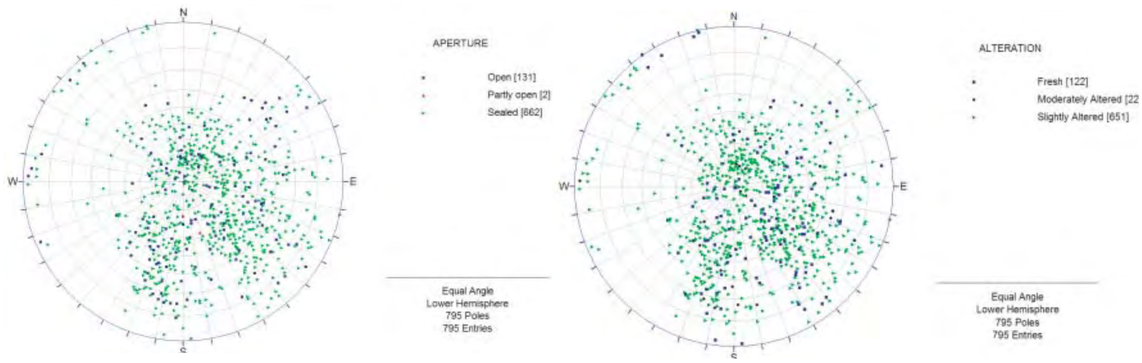

Figure 5-70. *KSH03B fracture orientations as a function of aperture and degree of alteration.*

Cored borehole KSH03B serves a similar role as borehole KAV04B; it fills in a data coverage gap near the ground surface not recorded initially during the drilling of KSH03A. No rock domain nor deformation zone information was available for this borehole. The patterns of fracture orientations observed are identical to those exposed in KSH03A.

In summary, though the regional subvertical fracture sets identified through the analysis of detailed Simpevarp subarea outcrop mapping are visible to some extent in most cored borehole, there is a degree of orientation variability noted in the core logs that is not captured by the current DFN model. In particular, the intensity of subvertical fracturing is much higher than noted in outcrop, and there may potentially be more than one subvertically-dipping fracture set. Significant variation in the intensity of the regional sets is noted between boreholes; a model based on surface outcrop fracture traces may not adequately capture the spatial variations in fracture orientations.

5.3.2 Variation of fracture orientation with depth in the Simpevarp subarea

Orientation variation with depth was evaluated in the Simpevarp subarea cored boreholes in two ways:

1. Construction of scatter plots of the trend and the plunge of the fracture poles as a function of measured borehole elevation (as opposed to length along the borehole).
2. Construction of polar trend and plunge density plots using ArcGIS and an inverse-distance weighted interpolation algorithm. The density plots highlight areas of the boreholes with ‘clustered’ fracture orientations, and also graphically illustrate areas of relatively low fracture intensity.

Both sets of plots are only truly usable qualitatively; the combination of different measurement systems on the horizontal (degrees; fundamentally an arc-length) and vertical (meters) makes statistical comparisons difficult. Note that in the pole density plots, a cell value of ‘Excluded’ indicates a zone of extremely high intensity (many fractures with pole trends of that orientation). These cells were excluded from the contouring algorithm to avoid adversely biasing the interpolation.

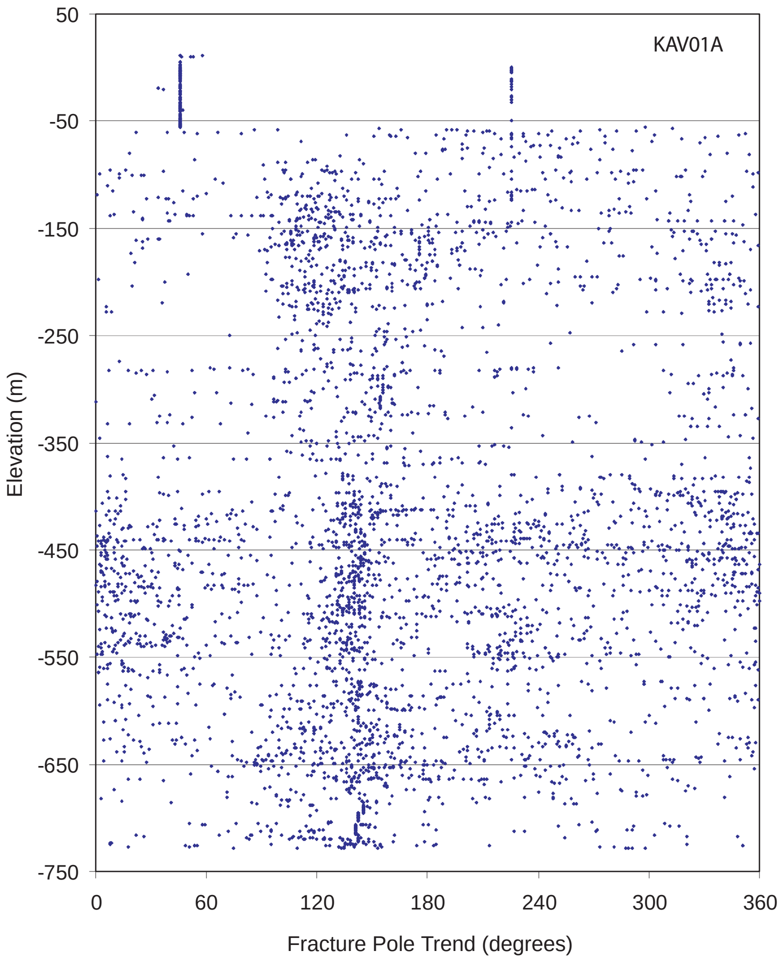

Figure 5-71. *KAV01A fracture pole trends as a function of depth.*

As in the Laxemar borehole data, KAV01A contains numerous fractures that appear to be non-natural; note the linear artifacts between elevation +20 and –55, and the general band of fracturing with poles oriented at or around the trend angle (149°) of the borehole. We interpret these structures to be core-discing or mechanically-induced borehole fractures produced during drilling. These structures should be confirmed by re-examination of BIPS image logs and drillcores, and, if found, removed from the SICADA database as they have the potential to skew the statistics of sets fitting natural fractures. Significant zones of variable set intensity are noted along the hole (–150 to –350, –700); however, the presence of core discing makes any more detailed interpretation risky.

Cored borehole KAV04A does not appear to exhibit the same amount of drilling-induced fractures as the rest of the Laxemar and Simpevarp subarea borings. Again, however, some variation in dominant fracture set trends and plunges with depth is seen. Northeast trending, moderately-dipping (20°–60°) fractures tend to dominate (Figure 5-75); however, intervals of increased east-west and west-northwest are noted (Figure 5-76) at several locations (–350 to –420 m, –550 to –625 m, and –750 to –800 m).

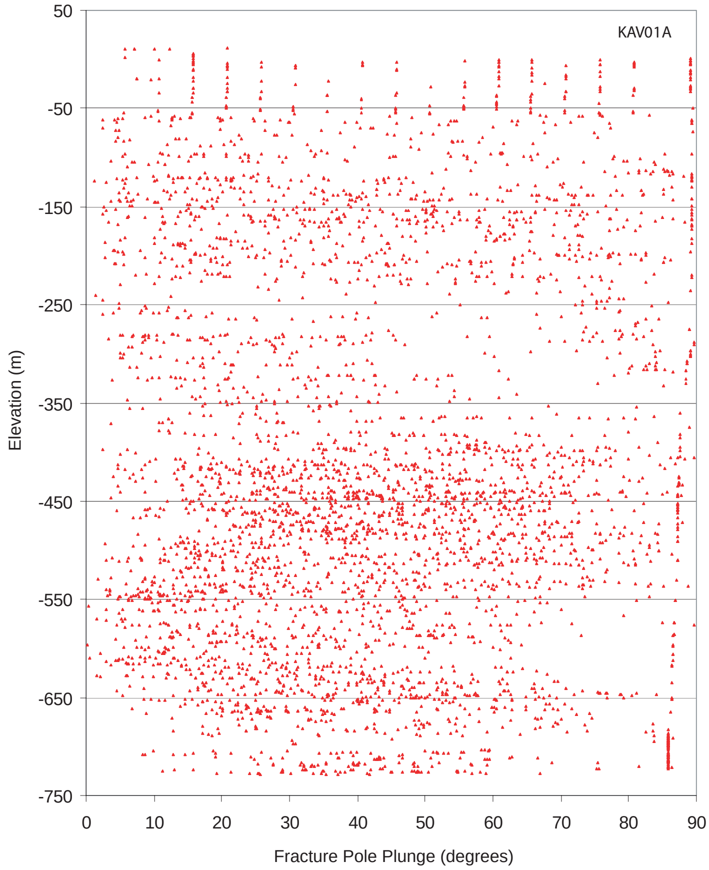

Figure 5-72. *KAV01A fracture pole plunges as a function of depth.*

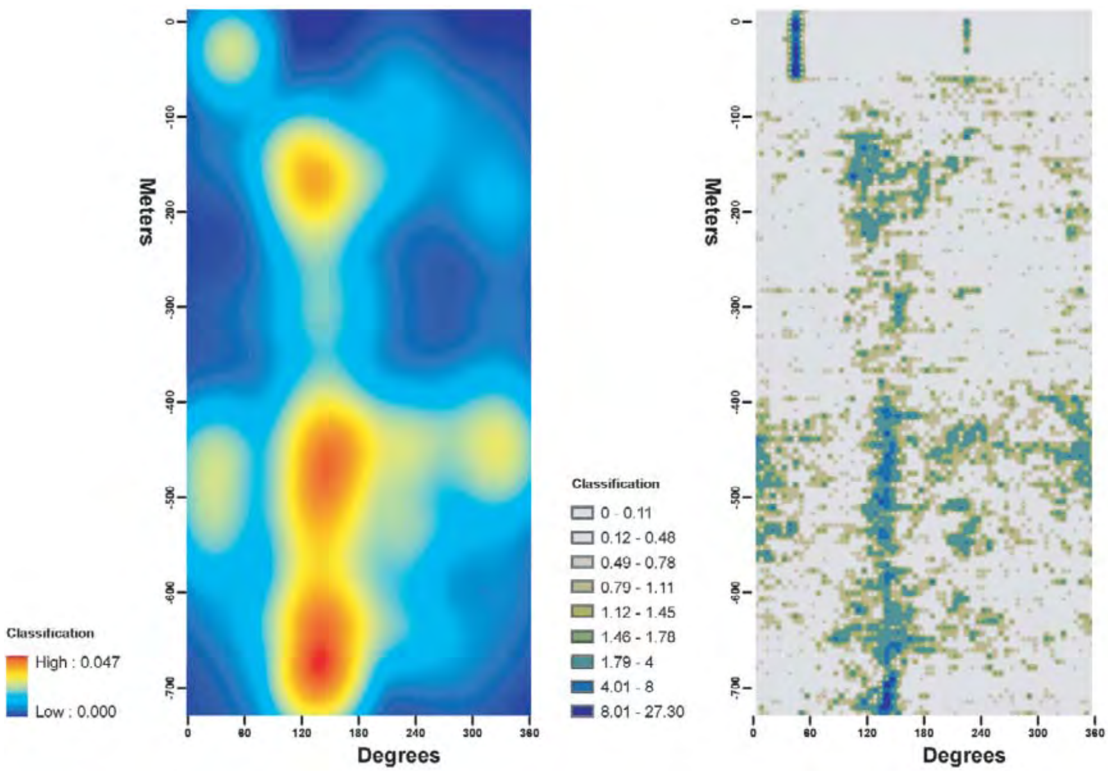

Figure 5-73. *Kernel density (left) and raster point density (right) plots of fracture pole trends, borehole KAV01A, Simpevarp subarea. Plot illustrates the number of fracture poles lying within a 6 m by 6 degree 'bin'.*

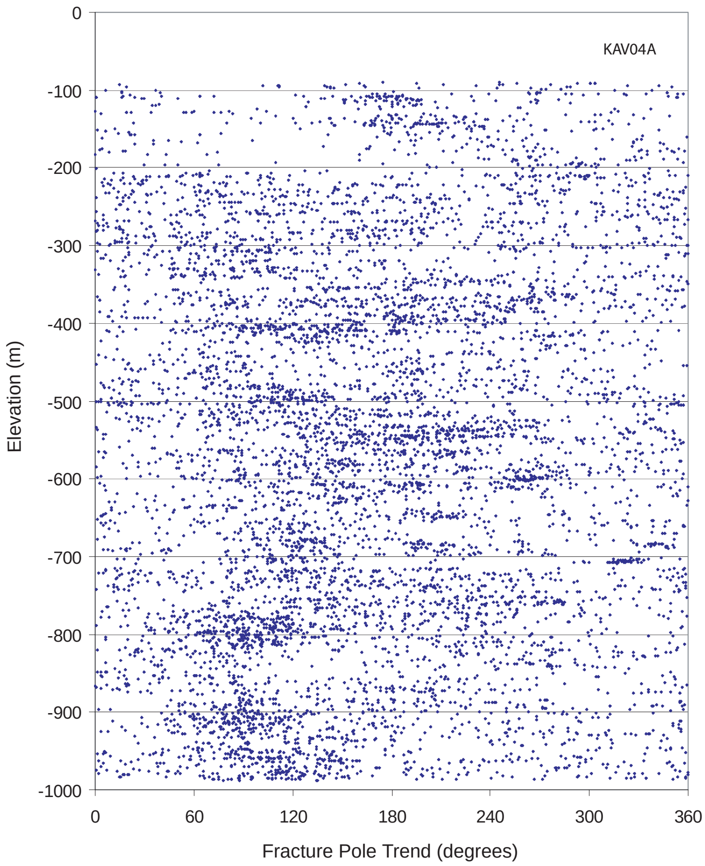

Figure 5-74. *KAV04A fracture pole trends as a function of depth.*

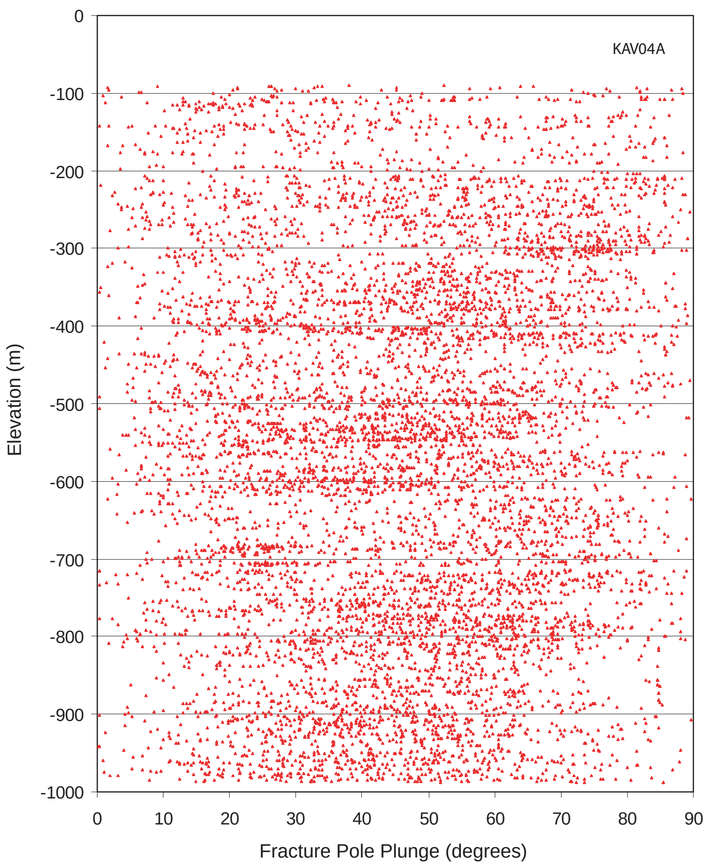

Figure 5-75. *KAV04A fracture pole plunges as a function of depth.*

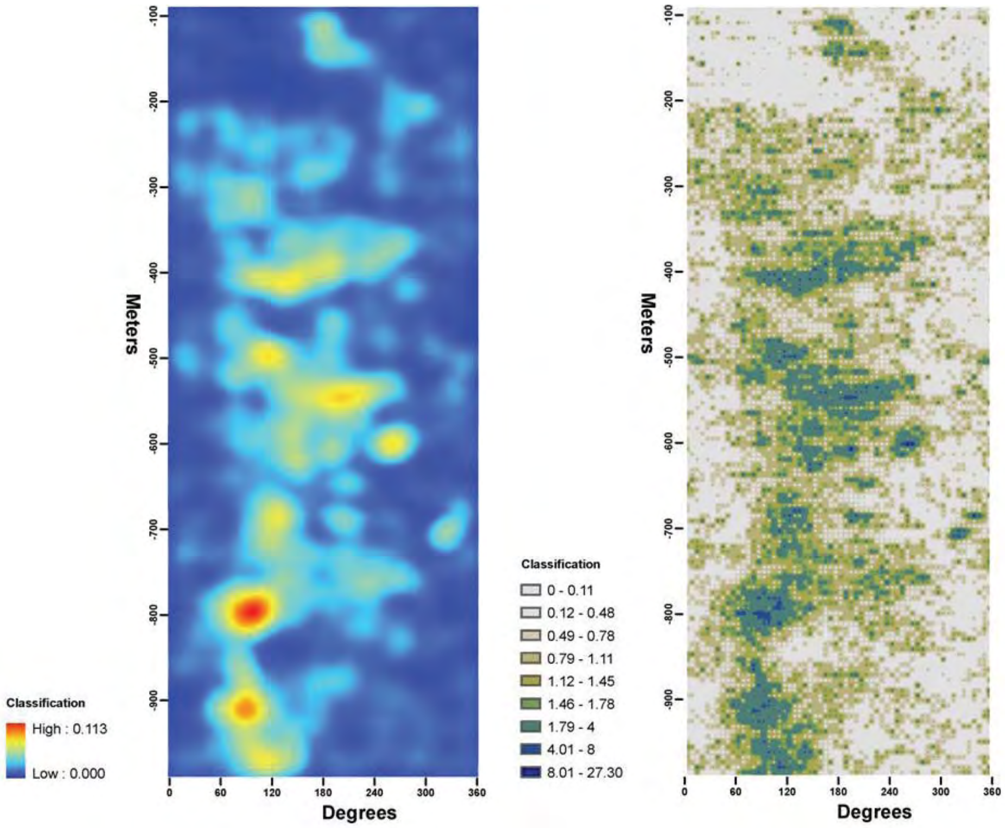

Figure 5-76. *Kernel density (left) and raster point density (right) plots of fracture pole trends, borehole KAV04A, Simpevarp subarea. Plot illustrates the number of fracture poles lying within a 6 m by 6 degree 'bin'.*

Borehole KSH01A also exhibits evidence of core discing or drilling-induced fracturing; well-defined linear zones that parallel the borehole deviation can be seen in Figure 5-77 and Figure 5-78. Other visible patterns include a zone of fewer northeast-trending fractures (~ –240 to –450 m), and a linear pattern of higher pole intensities from approximately elevation –770 m to –900 m (Figure 5-79). We hypothesize that these poles might represent the rotation of a local stress field along either a rheological contact or a subhorizontally-dipping plastic deformation zone. A similar linear 'zone' is visible on the pole trend scatterplot (Figure 5-77) from –700 m to –600 m, but obscured on the pole trend density plot.

Again, core discing or induced fracturing is visible in the KSH02 core data; it is most apparent when looking at the depth dependence of fracture pole plunges (Figure 5-81). Zones of higher fracture intensity are clearly visible on the pole trend scatterplot (Figure 5-80); the northeast-trending fracture sets appear to change substantially in intensity over approximately 100-meter depth intervals.

Core data from borehole KSH03A does not show the same amount of artificial fracturing that the other Simevarp subarea boreholes do. Scatterplots of pole trends and plunges (Figure 5-83 and Figure 5-84), however, do show large zones where the mean fracture orientation changes by approximately 90°. This is especially visible between elevations –350 and –450 m. A large zone of near-surface roughly north-south trending fractures is also visible (Figure 5-85); it appears to die out by approximately elevation –350 m.

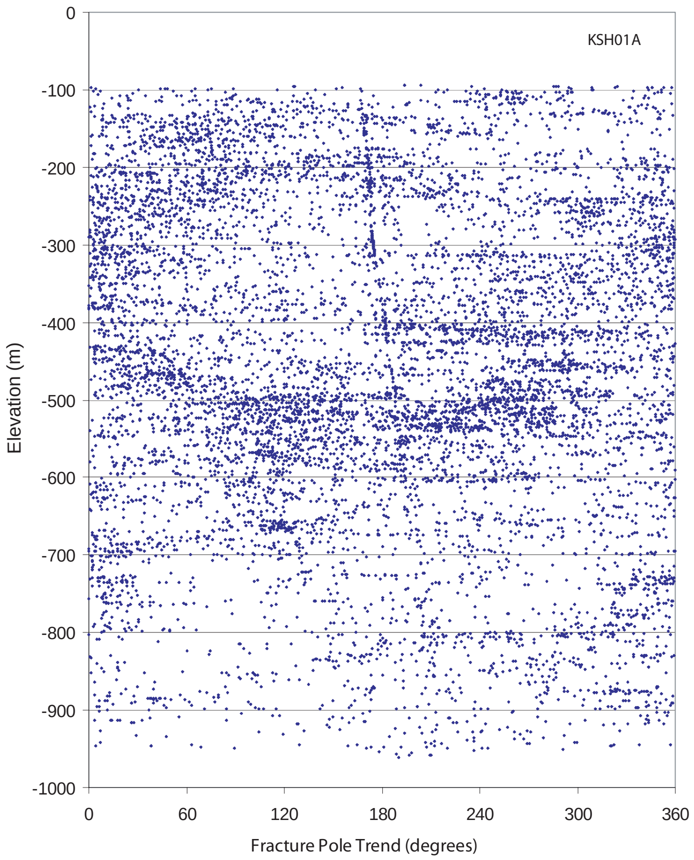

Figure 5-77. *KSH01A fracture pole trends as a function of depth.*

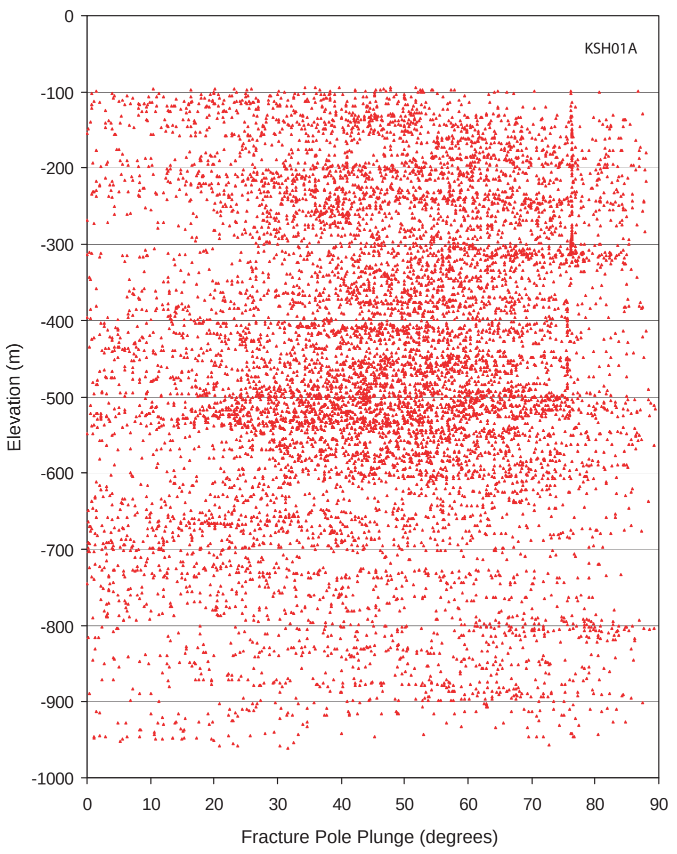

Figure 5-78. *KSH01A fracture pole plunges as a function of depth.*

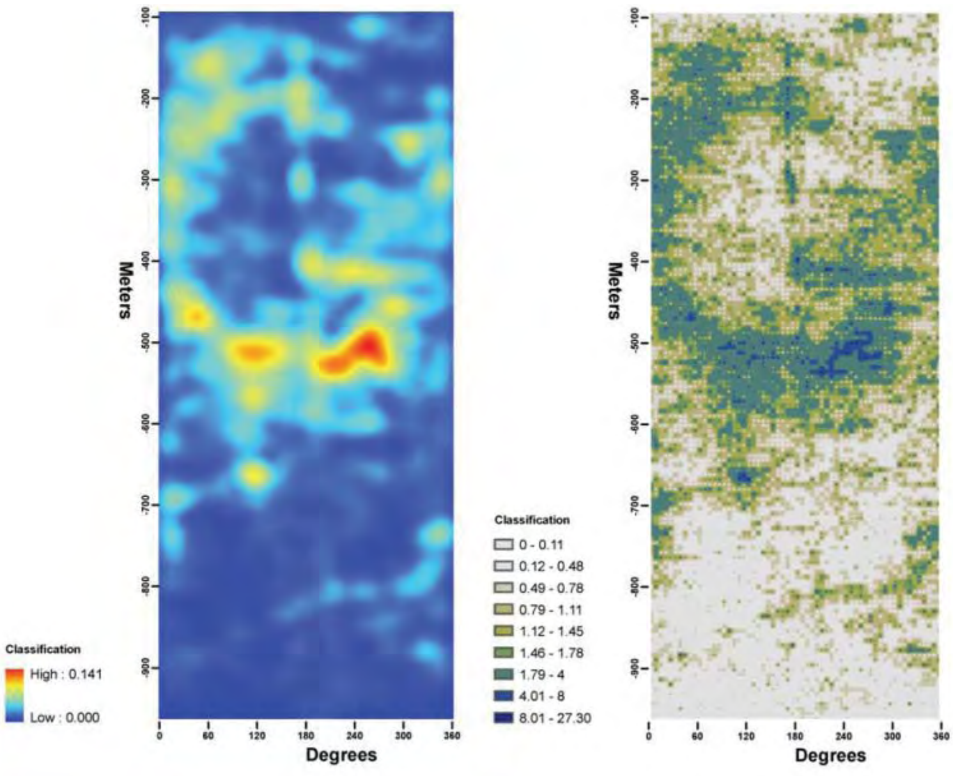

***Figure 5-79.** Kernel density (left) and raster point density (right) plots of fracture pole trends, borehole KSH01A, Simpevarp subarea. Plot illustrates the number of fracture poles lying within a 6 m by 6 degree 'bin'.*

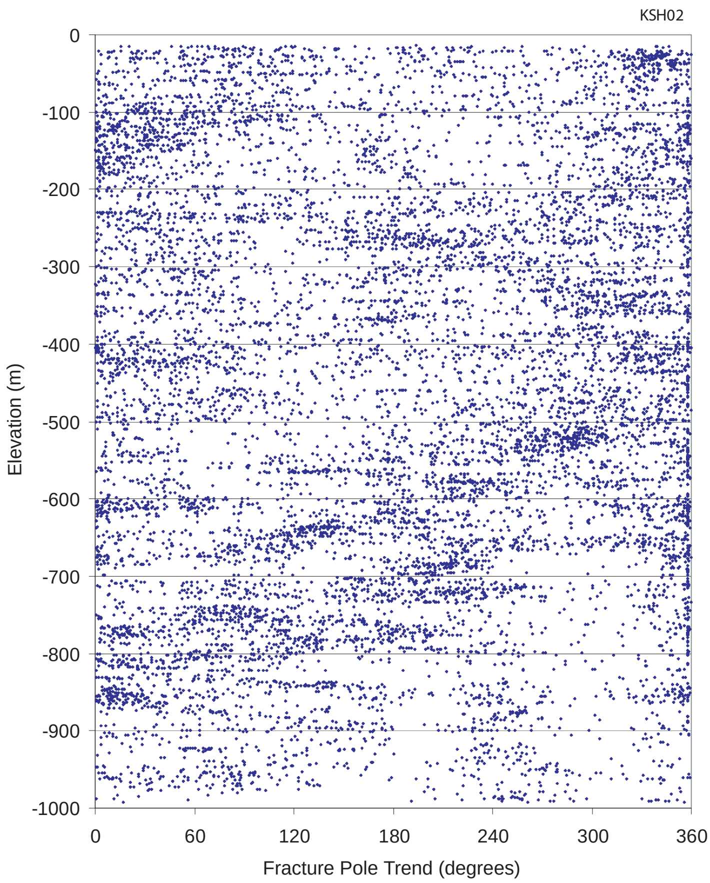

***Figure 5-80.** KSH02 fracture pole trends as a function of depth.*

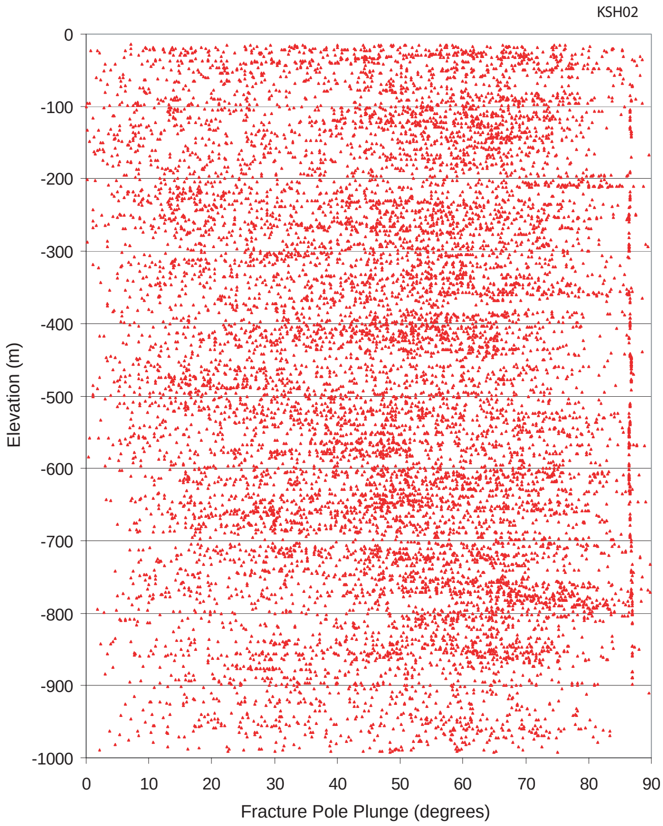

Figure 5-81. *KSH02 fracture pole plunges as a function of depth.*

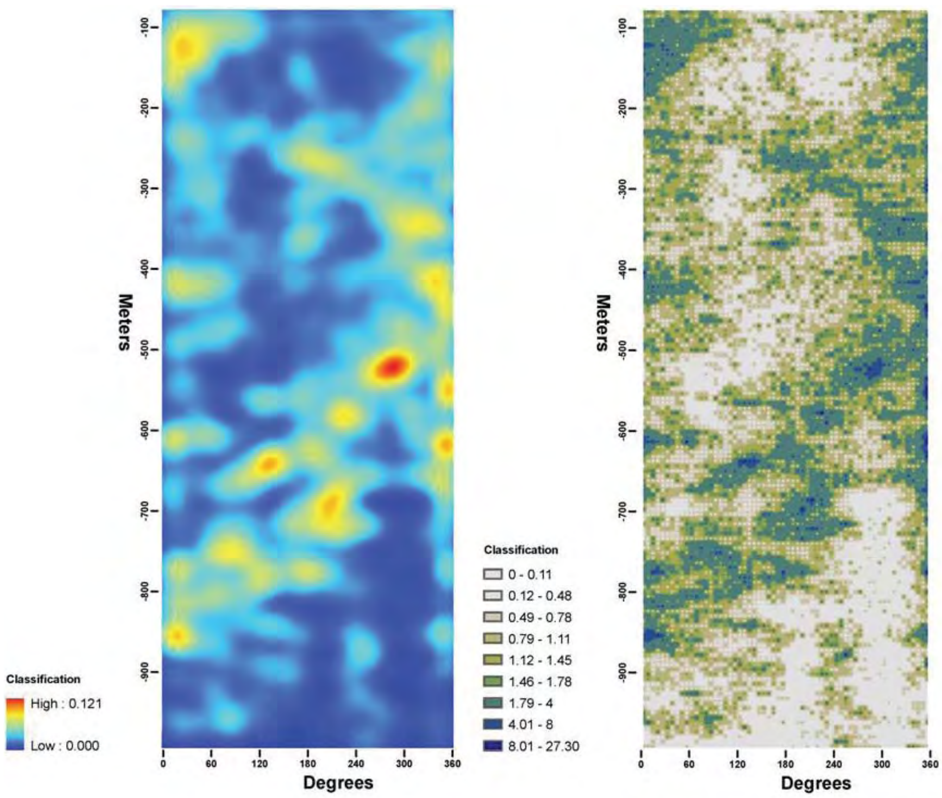

Figure 5-82. *Kernel density (left) and raster point density (right) plots of fracture pole trends, borehole KSH02, Simpevarp subarea. Plot illustrates the number of fracture poles lying within a 6 m by 6 degree 'bin'. Grey areas indicate no recorded fracture data or depths beyond the end of the borehole.*

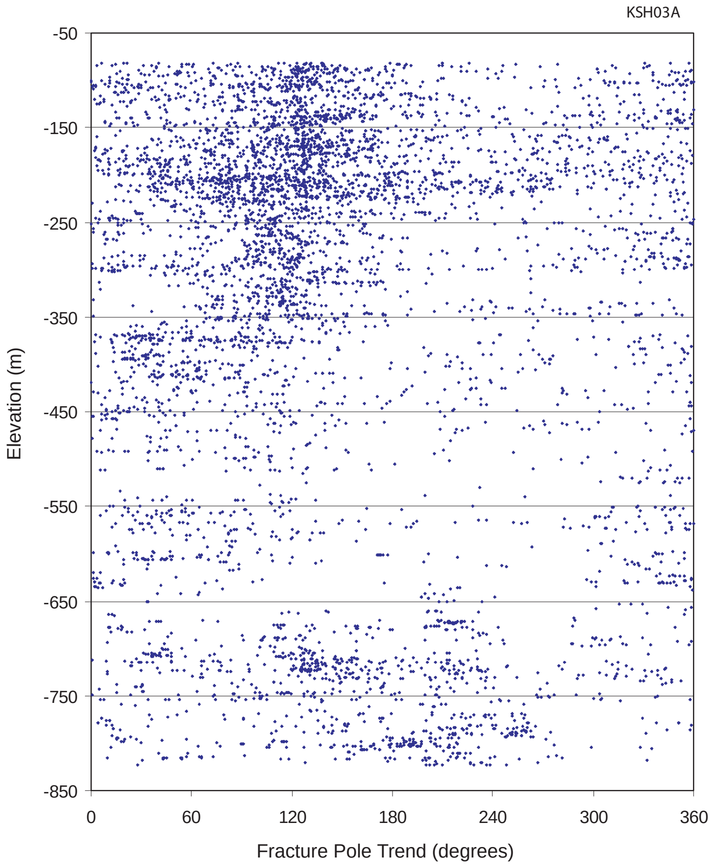

Figure 5-83. KSH03A fracture pole trends as a function of depth.

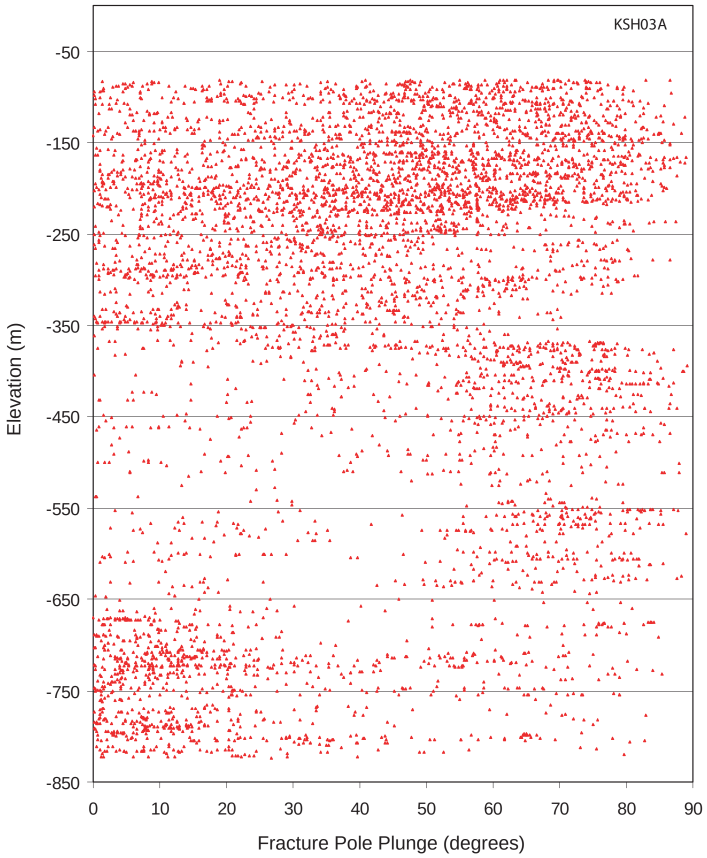

Figure 5-84. KSH03A fracture pole plunges as a function of depth.

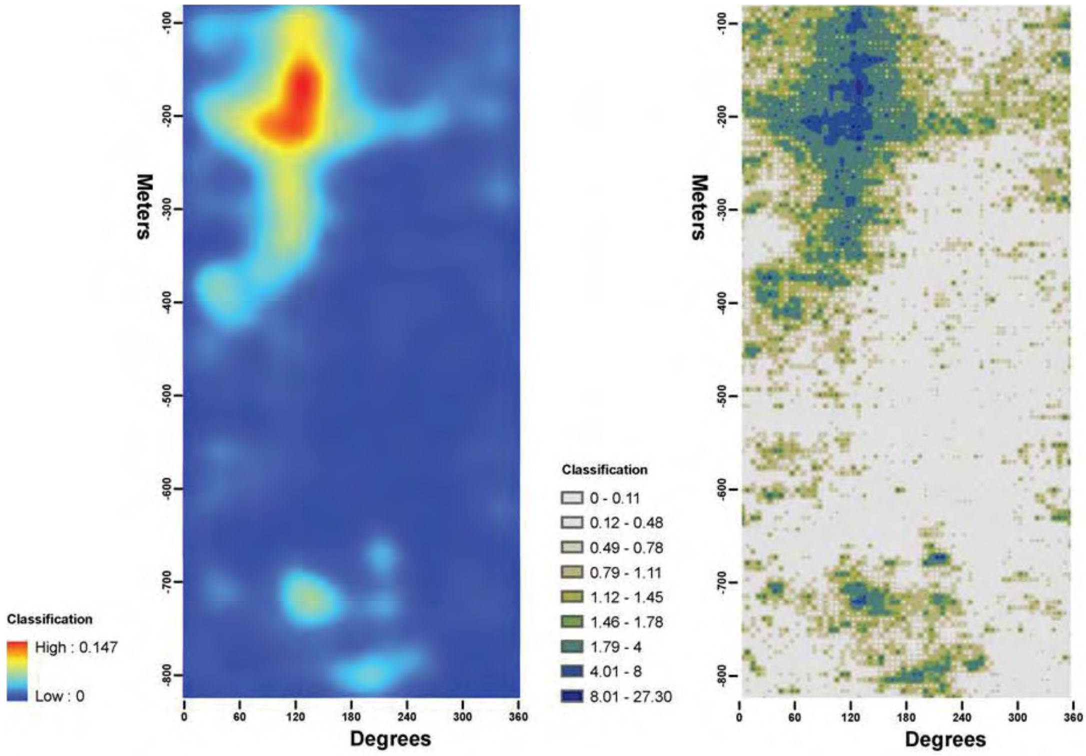

Figure 5-85. *Kernel density (left) and raster point density (right) plots of fracture pole trends, borehole KSH03A, Simpevarp subarea. Plot illustrates the number of fracture poles lying within a 6 m by 6 degree 'bin'.*

5.3.3 Intensity and geological controls in the Simpevarp subarea

An analysis of borehole fracture intensity within the Simpevarp sub-region was completed as a component of the SDM Simpevarp 1.2 modeling report /LaPointe and Hermanson, 2005/. Users are directed to that report for specific analysis results and model details.

However, studies during the SDM Simpevarp 1.2 modeling phase indicate similar results to those described in Section 5.2; namely, that fracture intensity appears to be a function of lithology and, to a lesser extent, of rock domain. Fracture intensity for the main cored boreholes in the Simpevarp subarea are presented below for completeness in Figure 5-86 through Figure 5-95. CFI plots constructed for Simpevarp 1.2 show a lack of near-surface stress-relief or alteration-enhanced fracturing similar to those in the Laxemar subarea. Overall fracture intensity in the Simpevarp boreholes is somewhat higher than in Laxemar. The effect of degree of alteration was also analyzed in the Simpevarp subarea and reported in the SDM Simpevarp 1.1 modeling report (see /La Pointe and Hermanson, 2005/), and showed that fracture intensity had a statistically significant dependence on alteration degree.

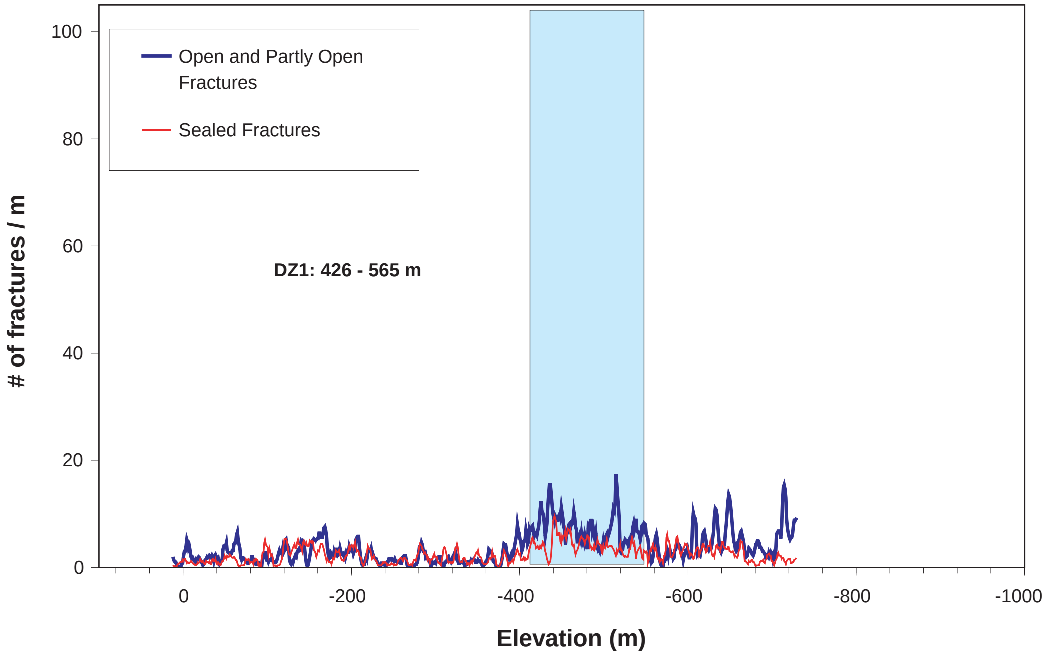

Figure 5-86. *Fracture intensity plot for borehole KAV01. Moving average function utilizes a five-meter sliding window centered on the value of interest.*

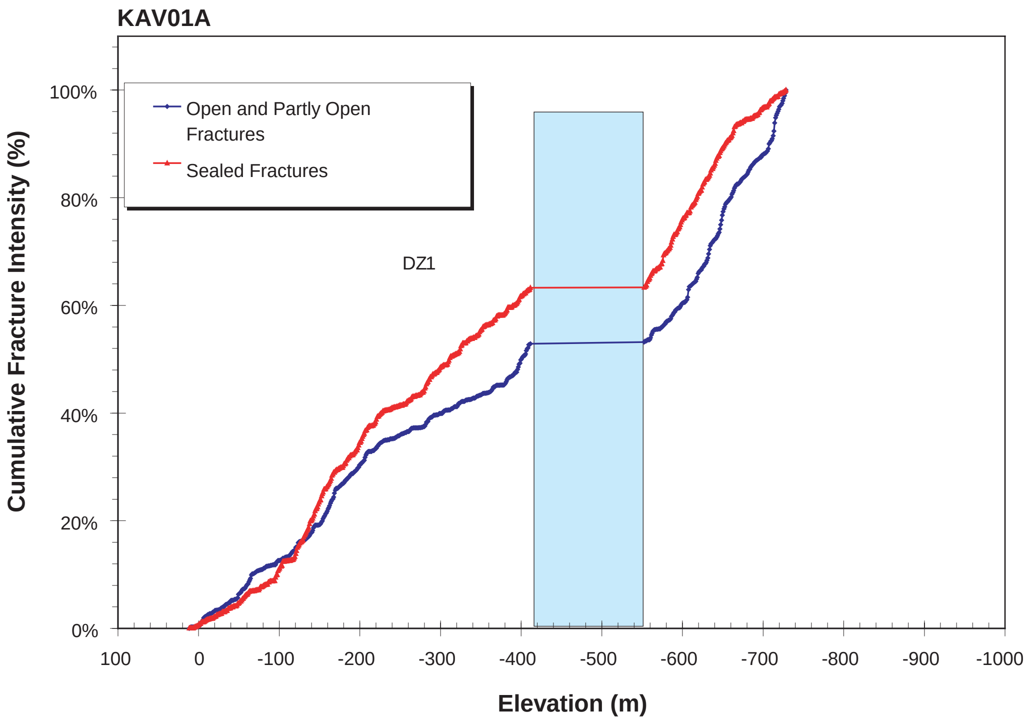

Figure 5-87. *CFI plot for borehole KAV01. Flat areas represent relatively low fracture frequency, while steeper slopes represent higher fracture intensity. Fracture data taken from cored borehole and BIPS logs. Plot excludes data based on fractures contained within mapped deformation zones.*

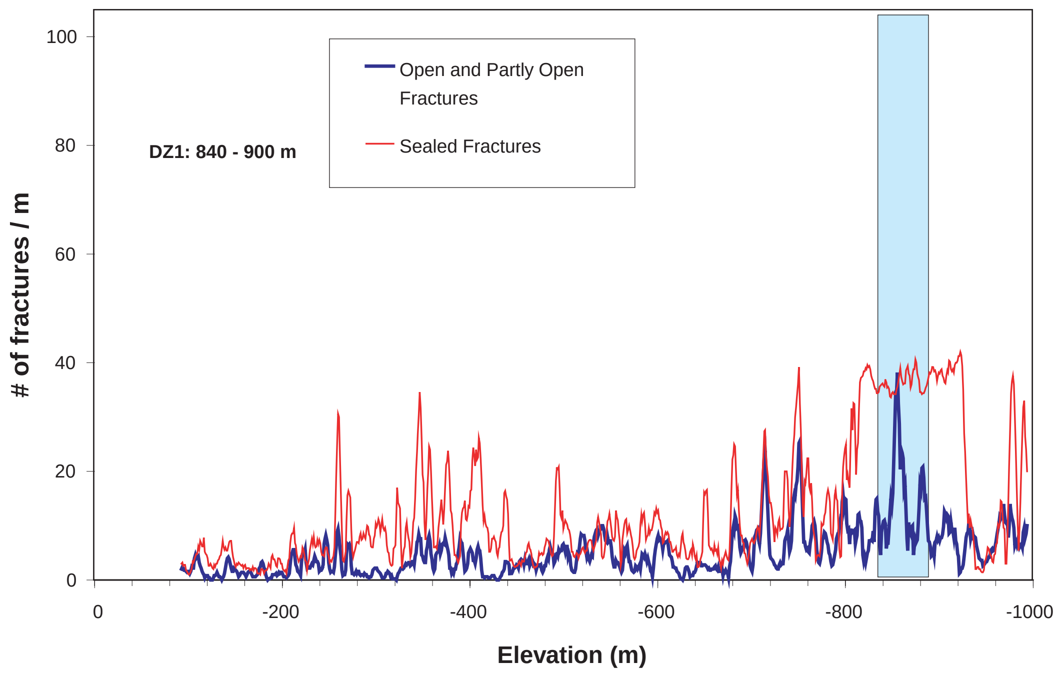

Figure 5-88. Fracture intensity plot for borehole KAV04A. Moving average function utilizes a five-meter sliding window centered on the value of interest.

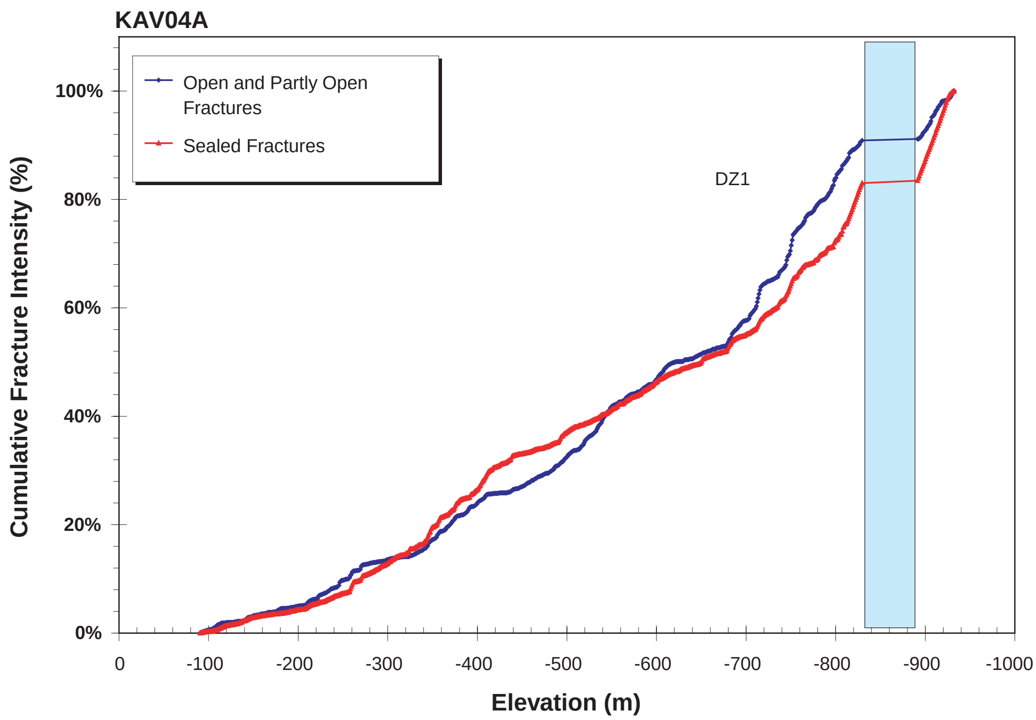

Figure 5-89. CFI plot for borehole KAV04A. Flat areas represent relatively low fracture frequency, while steeper slopes represent higher fracture intensity. Fracture data taken from cored borehole and BIPS logs. Plot excludes data based on fractures contained within mapped deformation zones.

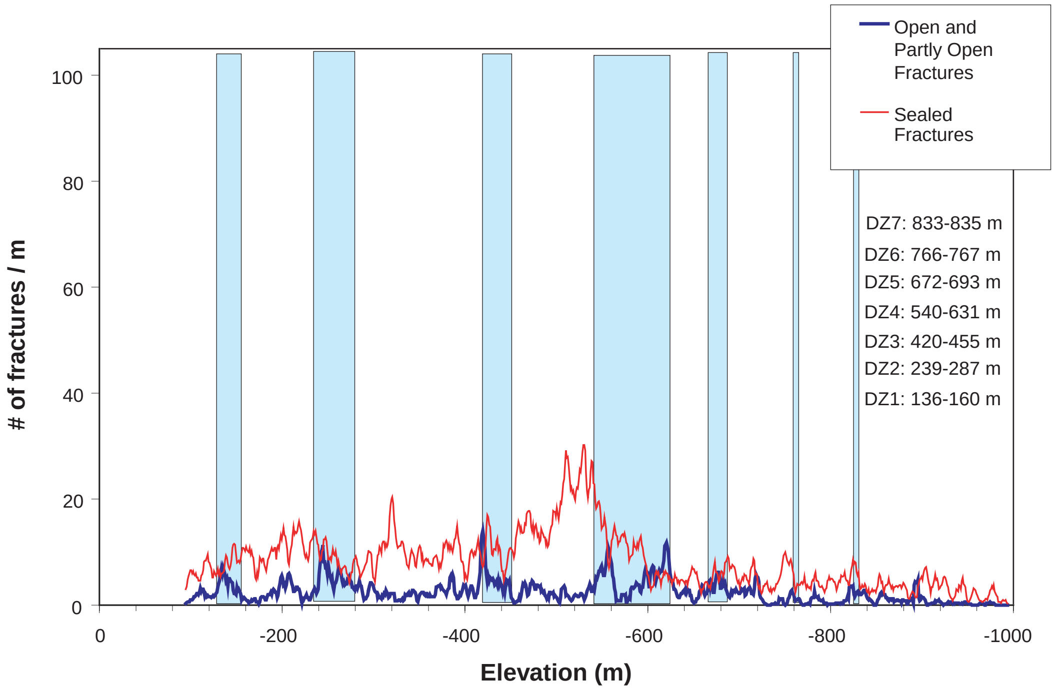

Figure 5-90. *Fracture intensity plot for borehole KSH01A. Moving average function utilizes a five-meter sliding window centered on the value of interest.*

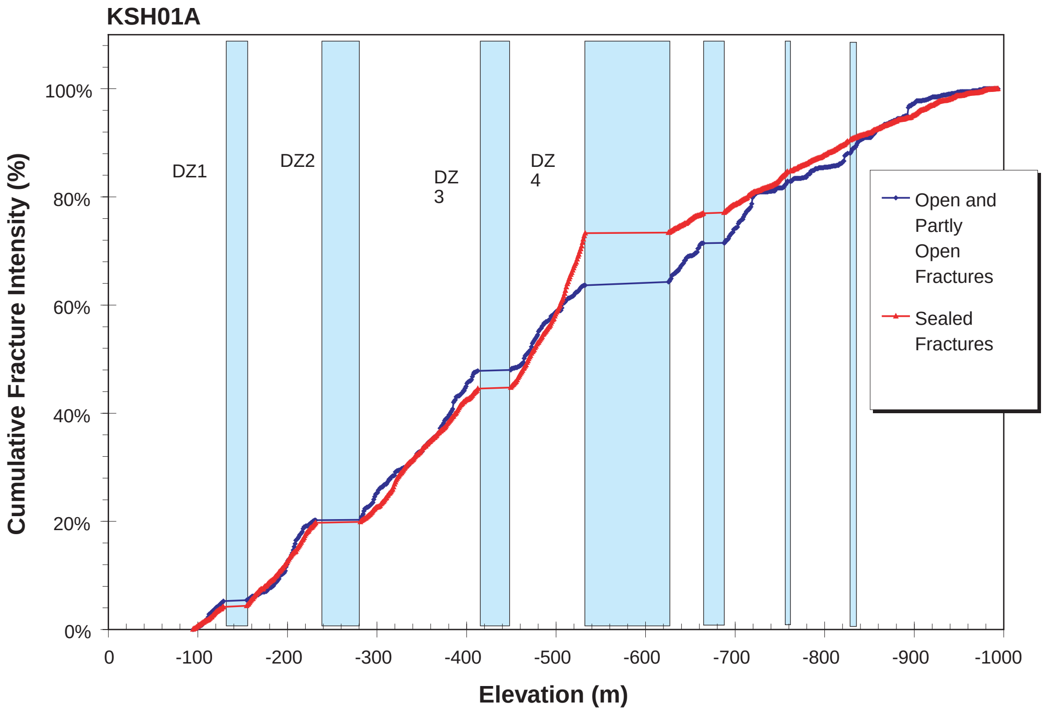

Figure 5-91. *CFI plot for borehole KSH01A. Flat areas represent relatively low fracture frequency, while steeper slopes represent higher fracture intensity. Fracture data taken from cored borehole and BIPS logs. Plot excludes data based on fractures contained within mapped deformation zones.*

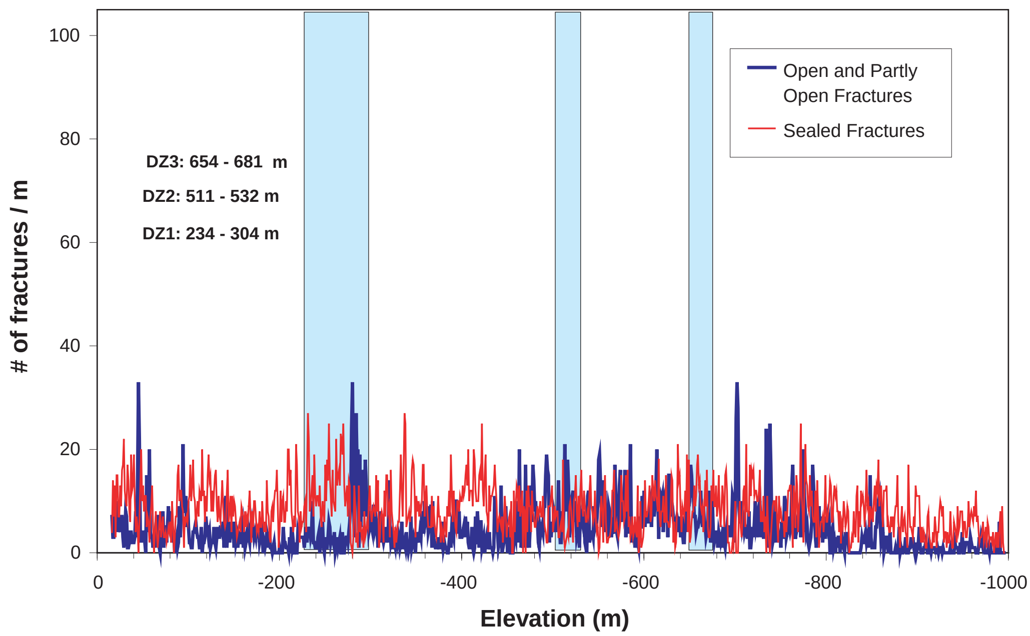

Figure 5-92. Fracture intensity plot for borehole KSH02A. Moving average function utilizes a five-meter sliding window centered on the value of interest.

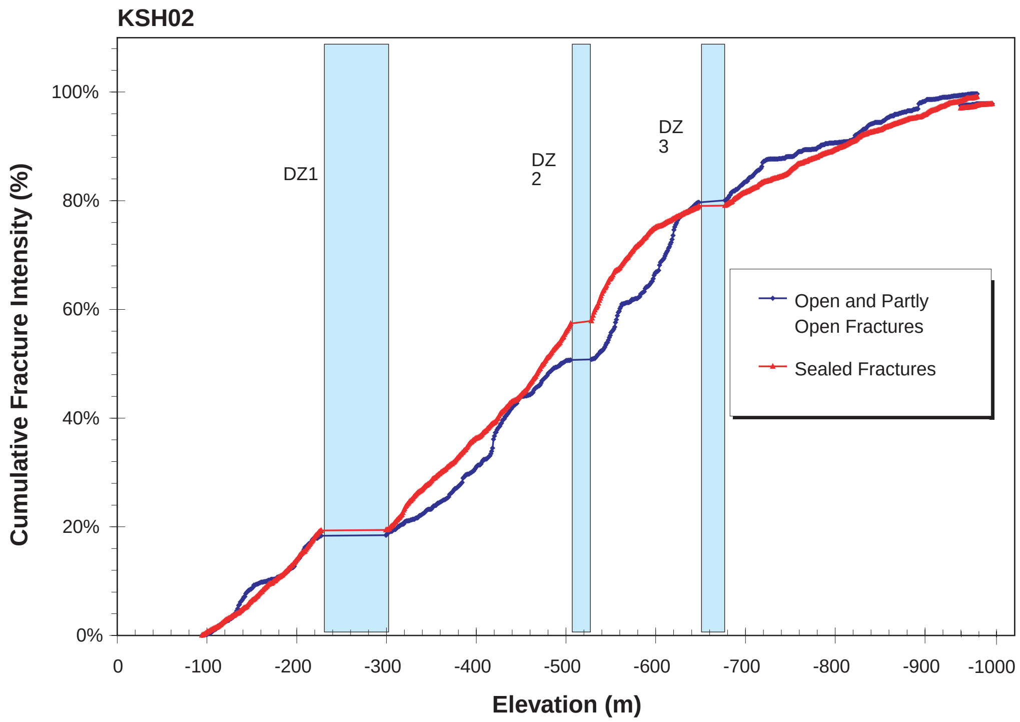

Figure 5-93. CFI plot for borehole KSH02A. Flat areas represent relatively low fracture frequency, while steeper slopes represent higher fracture intensity. Fracture data taken from cored borehole and BIPS logs. Plot excludes data based on fractures contained within mapped deformation zones.

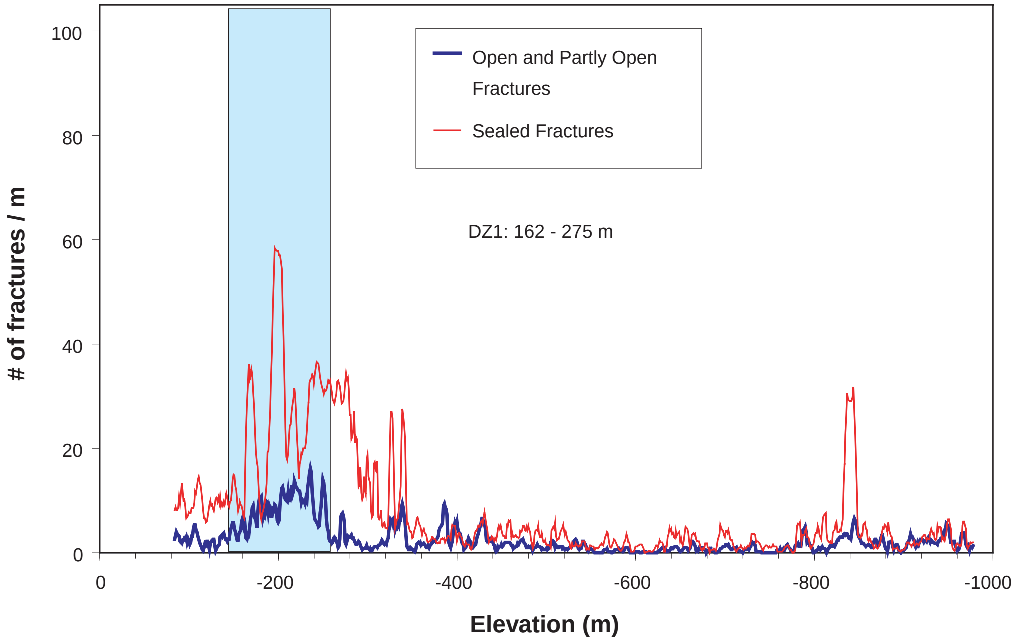

Figure 5-94. *Fracture intensity plot for borehole KSH03A. Moving average function utilizes a five-meter sliding window centered on the value of interest.*

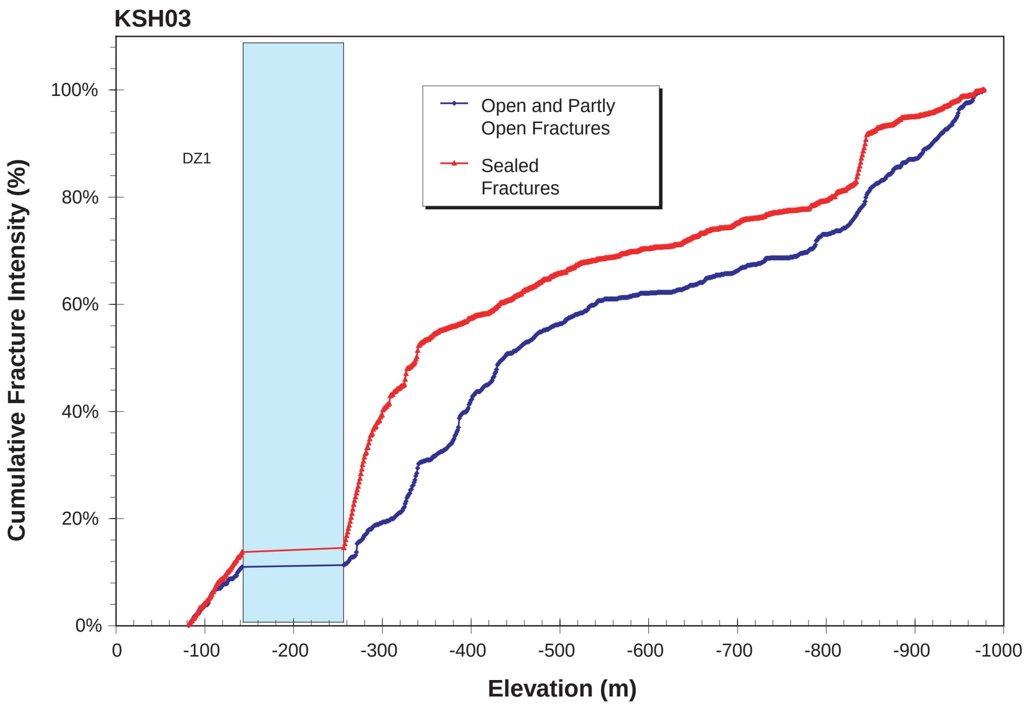

Figure 5-95. *CFI plot for borehole KSH03A. Flat areas represent relatively low fracture frequency, while steeper slopes represent higher fracture intensity. Fracture data taken from cored borehole and BIPS logs. Plot excludes data based on fractures contained within mapped deformation zones.*

6 Derivation of DFN statistical model

6.1 Orientation distributions

A detailed description of the derivation process for fracture sets is presented in Sections 3.3 and 4.8. The following models are summary tables of the chosen SDM Laxemar 1.2 fracture orientation model. These sets are based solely on univariate Fisher spherical probability distributions, and represent the 'best fit' to observed stereonet patterns. The distribution parameters were produced by entering amalgamated data from all outcrops in a particular subarea, applying a hard-sectored set division, and recording the results.

Table 6-1. Laxemar subarea fracture orientation set model.

Set name	Orientation model	Mean pole Trend	Plunge	Distribution details Dispersion	Relative intensity	Number of fractures	K-S Statistic	% Significance
S_A	Univariate Fisher	338.1	4.5	13.06	28.28%	593	0.031	55.60%
S_B	Univariate Fisher	100.4	0.2	19.62	26.90%	564	0.058	10.70%
S_C	Univariate Fisher	212.9	0.9	10.46	29.47%	618	0.076	15.70%
S_d	Univariate Fisher	3.3	62.1	10.13	9.63%	202	0.021	99.70%
S_f	Univariate Fisher	243	24.4	23.52	5.72%	120	0.216	Not Significant

Table 6-2. Simpevarp subarea fracture orientation set model.

Set name	Orientation model	Mean pole Trend	Plunge	Distribution details Dispersion	Relative intensity	Number of fractures	K-S Statistic	% Significance
S_A	Univariate Fisher	330.3	6.1	16.8	30.33%	1,190	0.091	Not Significant
S_B	Univariate Fisher	284.6	0.6	10.78	18.30%	718	0.076	0.02%
S_C	Univariate Fisher	201.8	3.7	14.6	31.12%	1,221	0.043	5.20%
S_d	Univariate Fisher	84.6	81.8	6.98	8.28%	325	0.053	6.90%
S_e	Univariate Fisher	67.1	15.5	11.73	11.98%	470	0.105	0.00%

6.2 Fracture size distribution parameters

6.2.1 Laxemar subarea

6.2.1.1 Laxemar subarea regional sets

The first step in deriving the size model for the regional sets is to calculate the trace length scaling plots for Euclidean and Mass Fractal scaling assumptions as previously described. The results for each set are shown in Figure 6-1 through Figure 6-6.

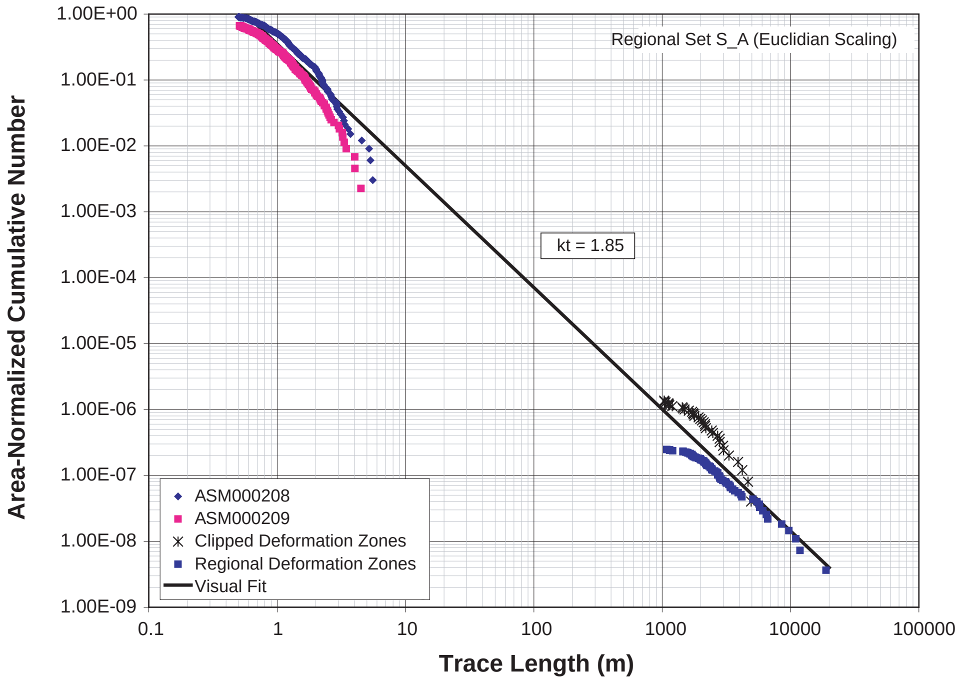

Figure 6-1. *Euclidean trace length scaling plot for regional set S_A, Laxemar subarea.*

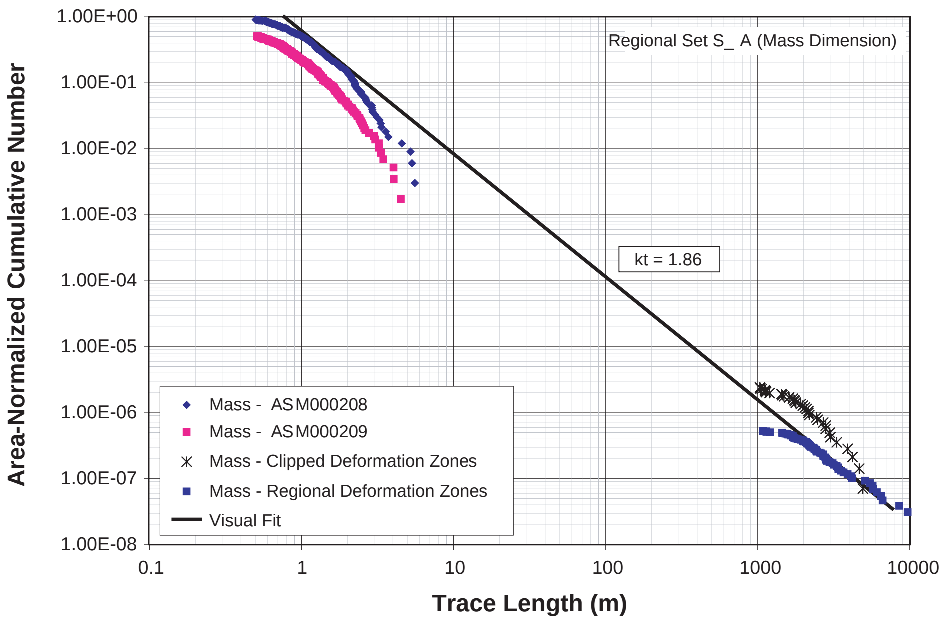

Figure 6-2. *Mass dimension trace length scaling plot for regional set S_A, Laxemar subarea.*

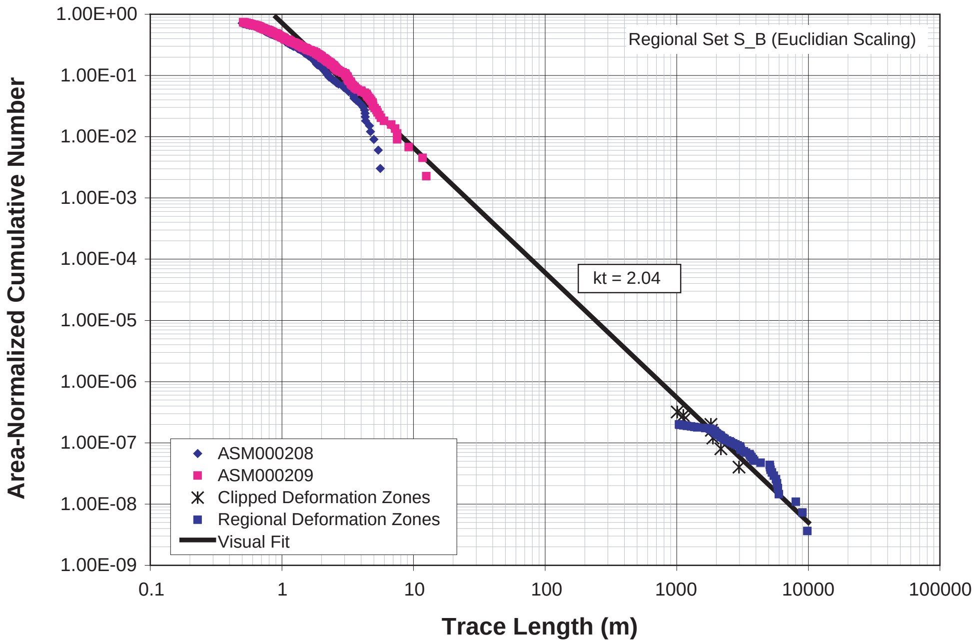

Figure 6-3. *Euclidean trace length scaling plot for regional set S_B, Laxemar subarea.*

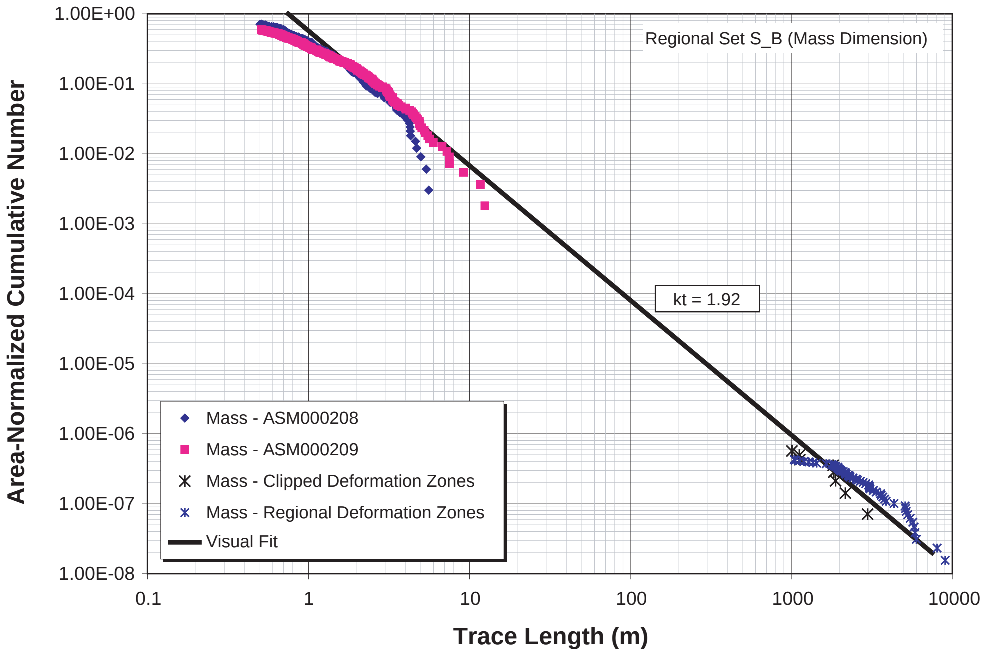

Figure 6-4. *Mass dimension trace length scaling plot for regional set S_B, Laxemar subarea.*

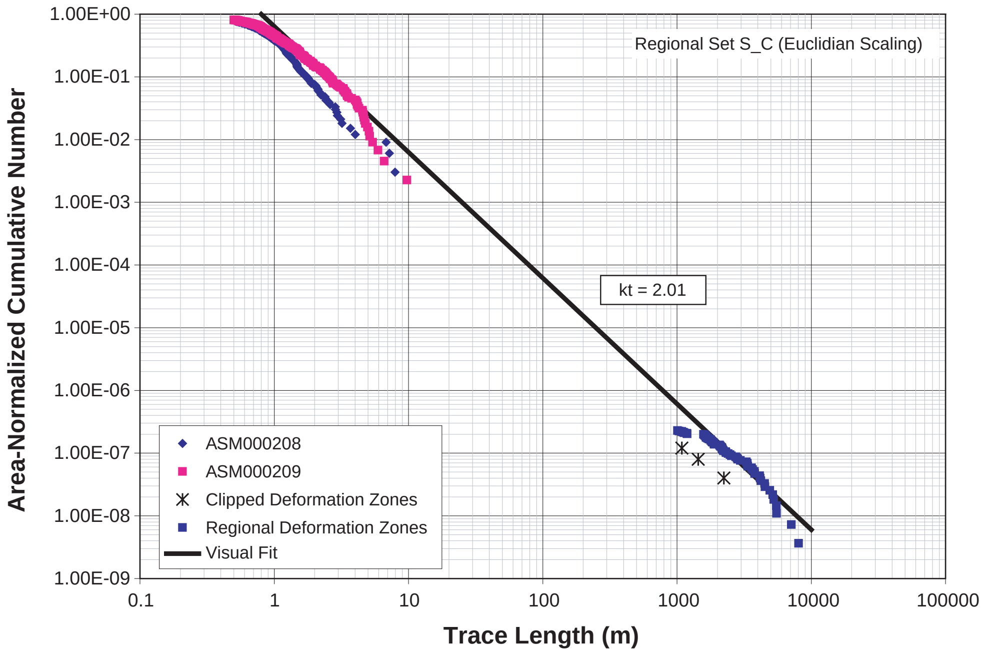

Figure 6-5. *Euclidean trace length scaling plot for regional set S_C, Laxemar subarea.*

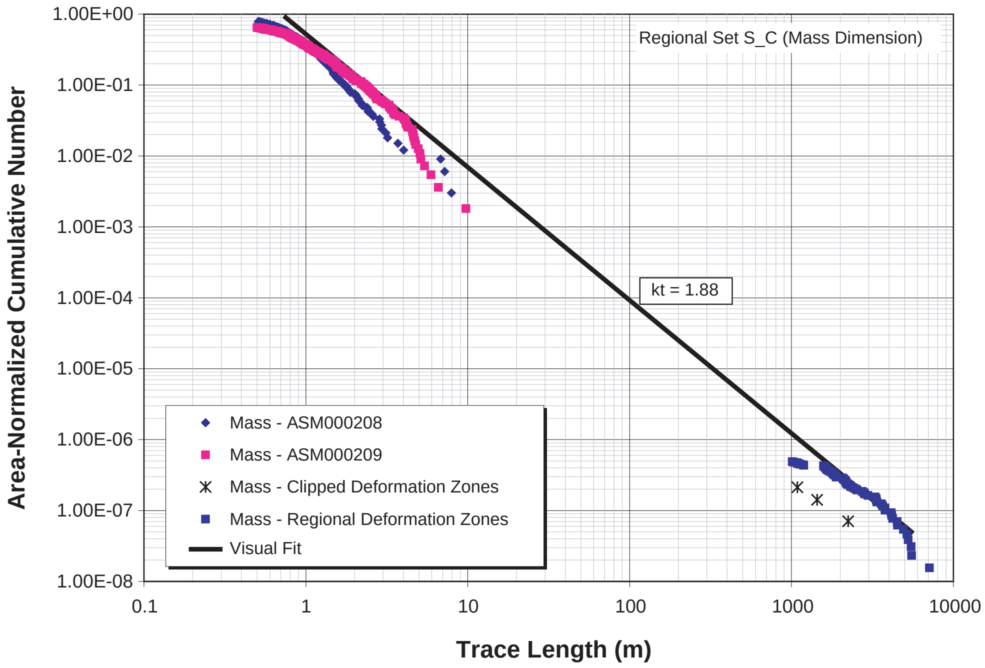

Figure 6-6. *Mass dimension trace length scaling plot for regional set S_C, Laxemar subarea.*

The size model for the Laxemar regional sets derives from the data in boreholes KLX02 and KLX04, outcrop ASM000208 and the deformation zone model. Both KLX02 and KLX04 are midway between mapped deformation zones. ASM000208 was selected because it was also in Domain A and the farther of the two outcrops from possible influence of identified deformation zones. While it is possible that fracture sizes vary by rock domain, there is insufficient data currently available at Laxemar to test this hypothesis. Previous work at Simpevarp /Bäckblom et al. 2004/ has suggested that fracture size differs slightly among some rock types, and also as a function of whether the fracture is open or sealed (fractures designated as "open" tend to have slightly longer traces in outcrop). However, the differences are relatively minor and likely to be overshadowed by other uncertainties. Likewise, the fracture intensity for the deformation zones in the Laxemar region have not been separated into groups based upon lithology, alteration degree or identified as open or sealed. For these reasons, the size model for each regional set was based upon the measures of total fracture intensity irrespective of lithology, aperture or alteration. The intensity for the borehole data was calculated for only those portions of the borehole not part of identified deformation zones. If additional data for Laxemar becomes available to allow for testing of size models in other domains, fracture size dependence on domain should be tested.

The percentiles of P_{32} were computed from the data listed in Appendix B for 25 m intervals. The P_{32} percentiles were calculated from only intervals that did not include identified deformation zones (shaded red in the appendix), and are reported separately in Table 6-3 through Table 6-5 and Figure 6-7 for each rock domain and regional set. Because it is assumed that the fractures identified in core are those which tend to cut all or most of the borehole cylinder, this represents a P_{10} value best approximated as an intersection of a line with the fracture system, rather than a value in which the finite borehole diameter is taken into account. As a consequence, the values of P_{32} determined from the P_{10} values are completely independent of fracture shape and of the type of size distribution. Thus, the derived values for P_{32} represent global values not affected by truncation or censoring effects, unlike the outcrop P_{21} and deformation zone P_{32} values.

Table 6-3. Cored borehole P_{32} percentiles – rock domain A set S_A, Laxemar subarea.

Percentiles	P_{32}	Percentiles	P_{32}	Percentiles	P_{32}	Percentiles	P_{32}
2.5%	0.276	27.5%	0.809	52.5%	1.452	77.5%	2.051
5.0%	0.390	30.0%	0.918	55.0%	1.494	80.0%	2.112
7.5%	0.398	32.5%	0.977	57.5%	1.532	82.5%	2.153
10.0%	0.456	35.0%	1.022	60.0%	1.546	85.0%	2.191
12.5%	0.560	37.5%	1.100	62.5%	1.595	87.5%	2.223
15.0%	0.683	40.0%	1.208	65.0%	1.715	90.0%	2.238
17.5%	0.708	42.5%	1.375	67.5%	1.866	92.5%	2.572
20.0%	0.752	45.0%	1.409	70.0%	1.950	95.0%	2.648
22.5%	0.770	47.5%	1.410	72.5%	1.955	97.5%	2.793
25.0%	0.770	50.0%	1.430	75.0%	1.975		

Table 6-4. Cored borehole P_{32} percentials – rock domain A set S_B, Laxemar subarea.

Percentiles	P_{32}	Percentiles	P_{32}	Percentiles	P_{32}	Percentiles	P_{32}
2.5%	0.017	27.5%	0.879	52.5%	1.374	77.5%	2.418
5.0%	0.348	30.0%	0.889	55.0%	1.434	80.0%	2.575
7.5%	0.381	32.5%	0.902	57.5%	1.598	82.5%	2.760
10.0%	0.513	35.0%	0.979	60.0%	1.604	85.0%	3.084
12.5%	0.532	37.5%	1.024	62.5%	1.653	87.5%	3.480
15.0%	0.590	40.0%	1.031	65.0%	1.721	90.0%	3.705
17.5%	0.683	42.5%	1.037	67.5%	1.737	92.5%	3.768
20.0%	0.717	45.0%	1.059	70.0%	1.779	95.0%	3.871
22.5%	0.803	47.5%	1.074	72.5%	1.933	97.5%	4.661
25.0%	0.865	50.0%	1.232	75.0%	2.250		

Table 6-5. Cored borehole P_{32} percentiles – rock domain A, set S_C, Laxemar subarea.

Percentiles	P_{32}	Percentiles	P_{32}	Percentiles	P_{32}	Percentiles	P_{32}
2.5%	0.006	27.5%	0.696	52.5%	1.134	77.5%	2.384
5.0%	0.123	30.0%	0.754	55.0%	1.213	80.0%	2.508
7.5%	0.124	32.5%	0.831	57.5%	1.283	82.5%	2.689
10.0%	0.150	35.0%	0.870	60.0%	1.541	85.0%	2.810
12.5%	0.245	37.5%	0.876	62.5%	1.638	87.5%	3.018
15.0%	0.249	40.0%	0.953	65.0%	1.779	90.0%	3.283
17.5%	0.380	42.5%	0.989	67.5%	1.886	92.5%	3.601
20.0%	0.618	45.0%	1.014	70.0%	1.995	95.0%	4.182
22.5%	0.620	47.5%	1.117	72.5%	2.136	0.975	4.353
25.0%	0.628	50.0%	1.123	75.0%	2.199		

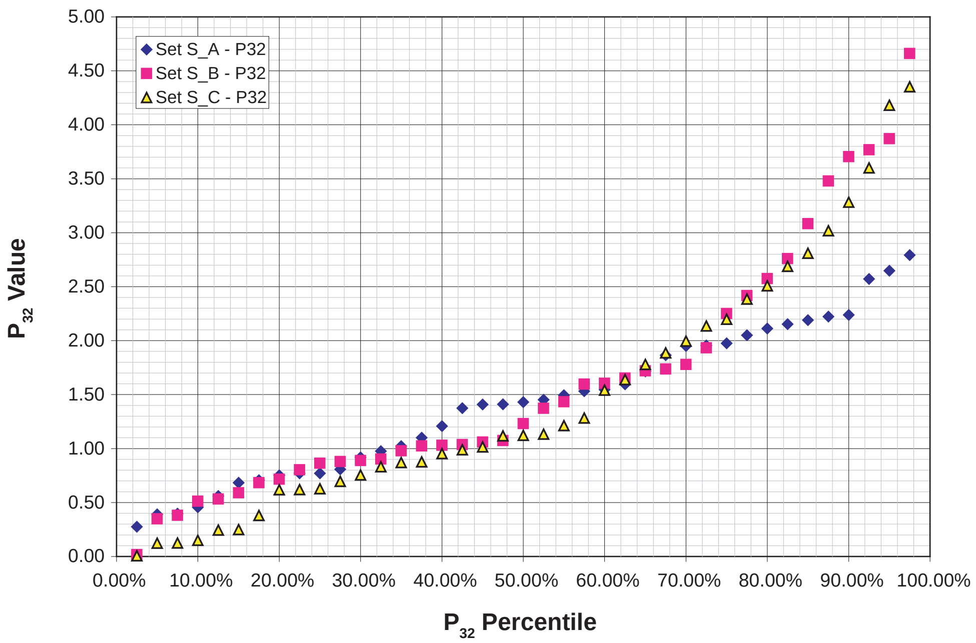

Figure 6-7. Cored borehole P_{32} values as a function of percentile for regional sets S_A, S_B and S_C, rock domain A, Laxemar subarea.

The next step was to calculate the deformation zone P_{32} values. This was done by importing the AutoCAD (.dxf) surfaces into FracWorksXP, converting them from into triangulated mesh fractures ('tesselated fractures'), and calculating their one-sided surface area (Figure 6-8). The volume used for the P_{32} calculation was based on a region that was 7,800 m by 3,200 m in horizontal extent and 1,100 m in vertical thickness, equivalent in scale to the local model volume.

The resulting deformation zone P_{32} values are given in Table 6-6.

Table 6-6. Values of P_{32} for deformation zones.

Fracture set	Total fracture area (m^2)	Target P_{32}
S_A	62,627,800	0.00228
S_B	33,077,900	0.00121
S_C	31,460,700	0.00120
Volume	27,456,000,000	

Now as described previously, in order to determine a set of exponent and minimum radius pairs that match both the borehole-derived P_{32} and the deformation zone P_{32}, a minimum fracture radius is estimated using the steps outlined in the workflow described in Section 3.4.2. Since the fractures in the deformation model are essentially rectangular rather than circular, and fully penetrate the thickness (1,100 m) of the modeling domain, a 1,000 m long surface fracture trace for a deformation zone fracture corresponds to a fracture area of 1,000 m × 1,100 m. A circular fracture of the same area would have a radius of:

$$Radius = \sqrt{\frac{1000*1100}{\pi}} \approx 591.73m \qquad \text{Equation 6-1}$$

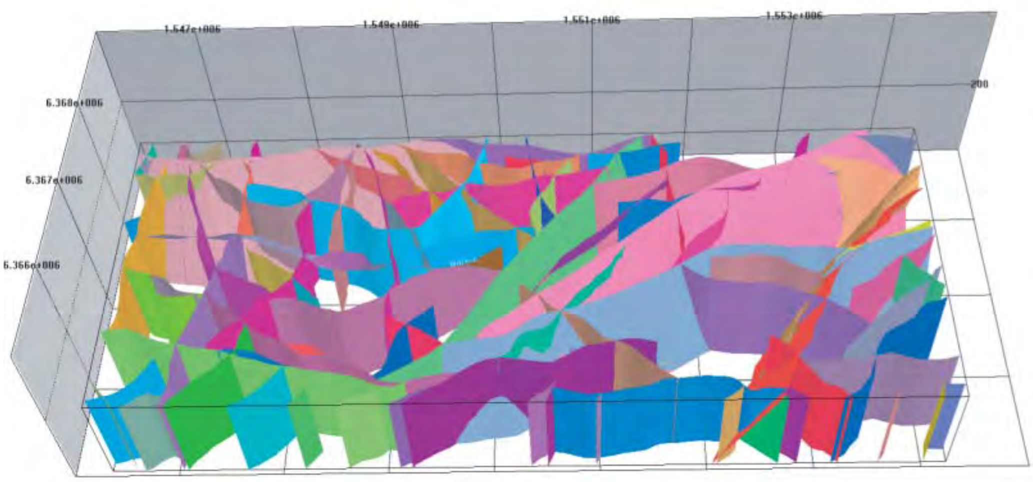

Figure 6-8. The Simpevarp 1.2 deformation zone model converted to tessellated (triangular elements) fracture surfaces in FracWorks XP.

The method for adjusting P_{32} based upon truncations is illustrated in Section 3.5.3. If a different value for the minimum size is needed for a particular application, for example the 1,000 m deformation zone limit, it is relatively straightforward to calculate the adjusted value of P_{32} that corresponds to this new value.

Values for several of the parameters in Equation 3-17 are known. $P_{32}(x_{0r},\infty)$ is equivalent to the values of P_{32} presented in Table 6-3 through Table 6-5 for each set. x_{2r} is taken to be infinity. x_{1r} is 591.73. $P_{32}(x_{1r},x_{2r})$ are the values given in Table 6-6. Values of k_r are equal to 1.0 plus the value of k_t given in Figure 6-1 through Figure 6-6. That leaves only x_{0r}, which can be calculated through Equation 3-17 from the fixed values of $P_{32}(x_{1r},x_{2r})$, x_{1r}, x_{2r} and k_r for each value of $P_{32}(x_{0r},\infty)$. These latter values are the percentiles shown in Table 6-3 through Table 6-5. A crossplot of the P_{32} percentiles vs x_{0r} is shown in Figure 6-9 for the Laxemar sets in Domain A.

Next, target values of fracture trace P_{21} were calculated excluding any fracture trace less than 0.5 m in length. The results are shown in Table 6-7.

Table 6-7. Values of P_{21} determined from observed fracture traces for each regional fracture set in outcrop ASM000208.

Regional set	P_{21}
S_A	1.18
S_B	1.02
S_C	0.95

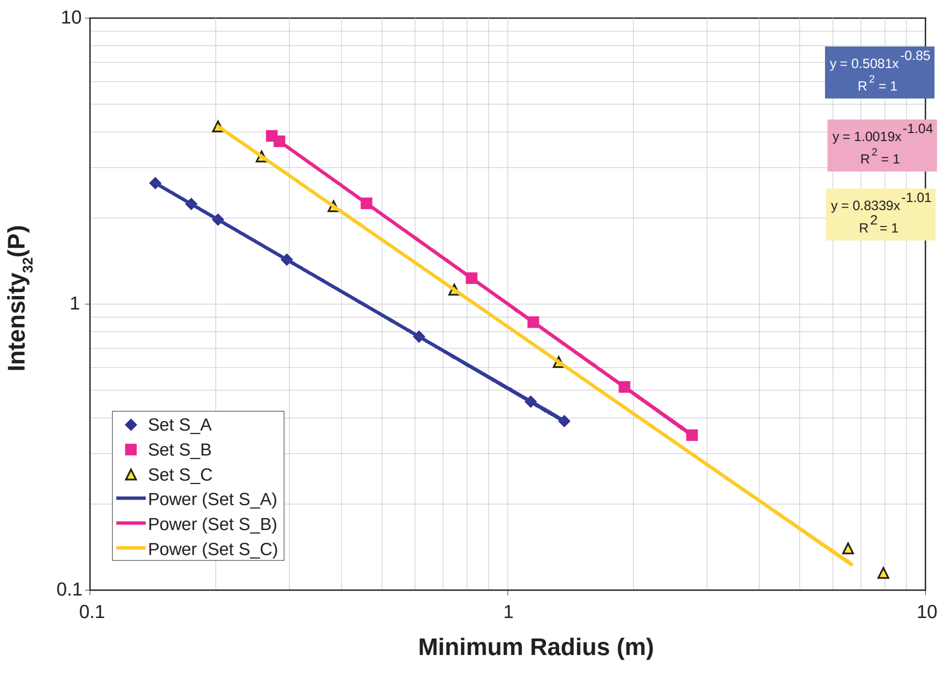

Figure 6-9. Calculated values of minimum radius as a function of P_{32} percentile, rock domain A, Laxemar subarea.

Figure 6-10 through Figure 6-12 show the results for various values of P_{32} percentile. In these crossplots, the red horizontal line represents the target truncated P_{21} value calculated from outcrops. The results from each realization is shown as an open purple square, while the mean of the realizations for a specific percentile is shown as a solid red circle. As long as trace length truncation effects are minimal, the relation between the P_{32} percentile and the truncated P_{21} are approximately linear, because the untruncated P_{21} has a linear relation with P_{32}, and the absolute value of P_{32} and P_{32} percentile are linear over large ranges, especially when the percentile is less than the 50^{th} percentile (Figure 6-7). When truncation effects are more pronounced, there will be a depature from this simple linearity.

It was possible to obtain matches for all three regional sets, as shown by the figures. Table 6-8 summarizes the matchpoint parameters for each set. It is interesting to note on this table that the match points correspond to the middle percentiles of the P_{32} distributions. This suggests that the fracture intensity values obtained from the cored boreholes in the Laxemar Domain A region may be a good representation for this domain in the Laxemar subarea. If the matching percentiles had been > 90^{th} or < 10^{th}, for example, this would suggest that either the boreholes or the outcrops were more highly fractured or less highly fractured than the remainder of the rock domain, and thus not representative of the "average" fracture intensity for the domain. The fact that the match for the Laxemar subarea occurred at percentiles for all three sets from the 37^{th} to the 46^{th} percentile suggests that the DFN parameters of size and intensity for the regional sets are likely to represent something like the "average" values for rock domain A in the Laxemar Subregion.

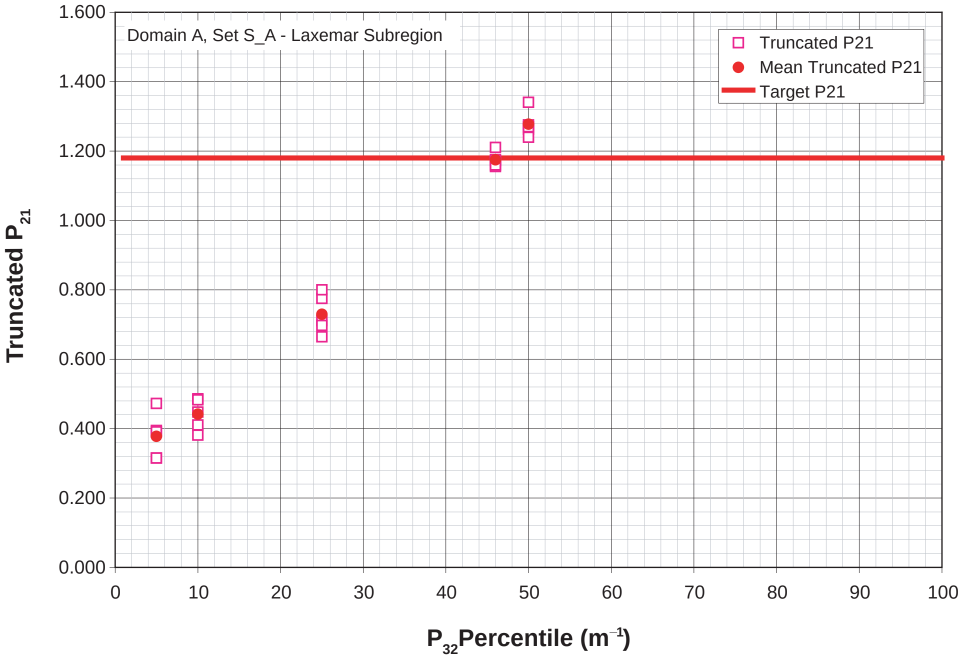

Figure 6-10. *Results from DFN simulations for regional set S_A, Laxemar subarea. The red horizontal line shows the target value of truncated P_{21}, while the symbols show the five realizations results (open squares) and mean value (red solid circles).*

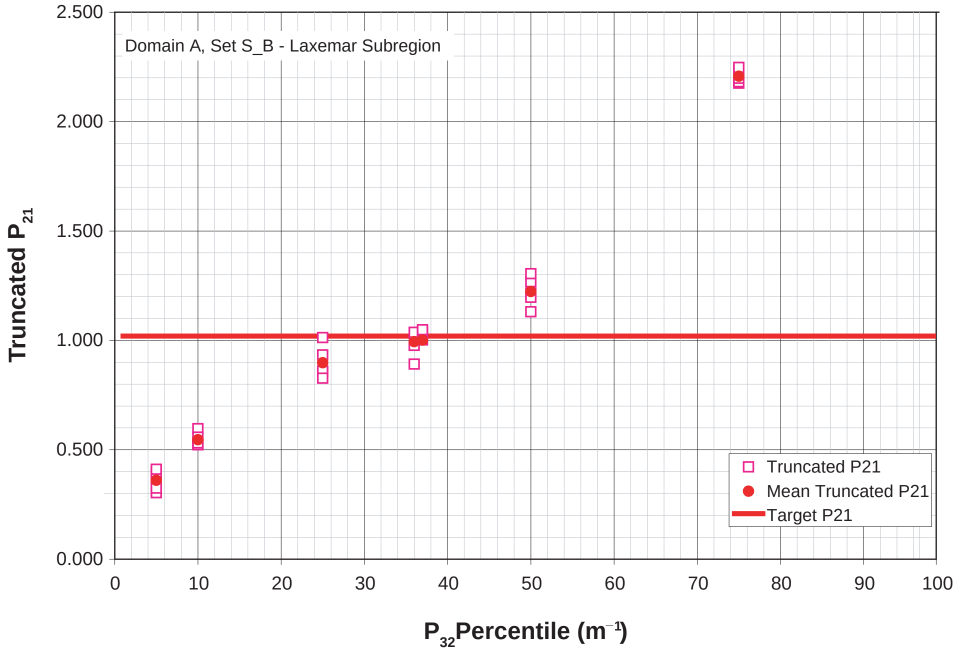

Figure 6-11. *Results from DFN simulations for regional set S_B, Laxemar subarea. The red horizontal line shows the target value of truncated P_{21}, while the symbols show the five realizations results (open squares) and mean value (red solid circles).*

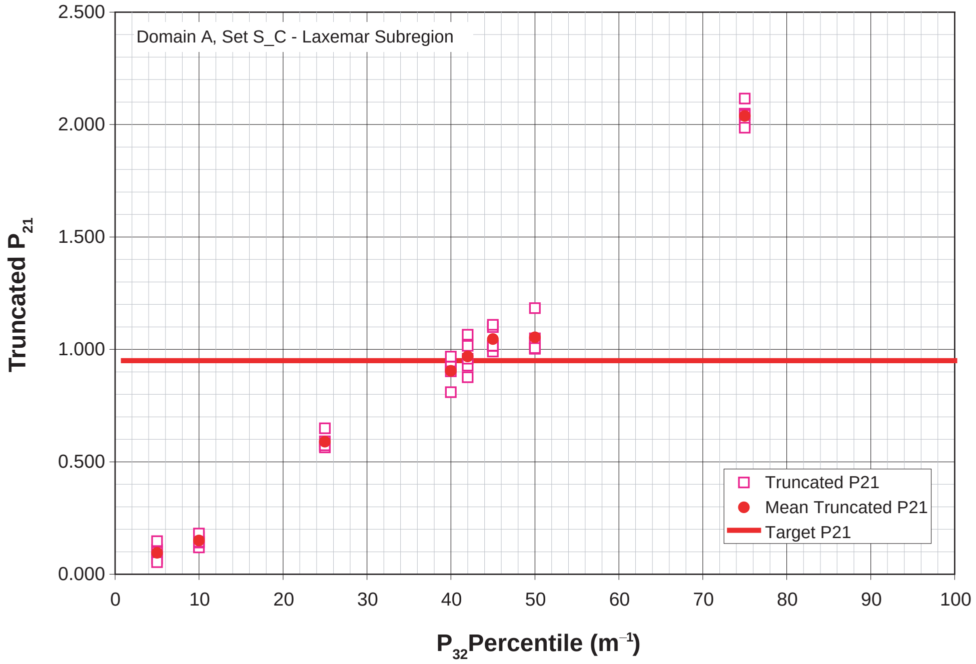

Figure 6-12. *Results from DFN simulations for regional set S_C, Laxemar subarea. The red horizontal line shows the target value of truncated P_{21}, while the symbols show the five realizations results (open squares) and mean value (red solid circles).*

Table 6-8. Match point fracture size parameter values for each regional set, rock domain A, Laxemar subarea. All sizes conform to a power law distribution.

Set	P_{32}	Minimum radius (m)	Scaling exponent	Borehole P_{32} percentile	Target truncated P_{21}	Simulation truncated P_{21}
S_A	1.310	0.328	2.85	46%	1.18	1.17
S_B	1.026	0.977	3.04	38%	1.02	1.00
S_C	0.974	0.858	3.01	42%	0.95	0.97

6.2.1.2 Laxemar subarea local sets

The FracSize approach (described further in Section 3.4.1) was used to choose appropriate size distributions for those fracture sets (S_d, S_f) without a visible component in the regional deformation zone model. Fractures were grouped by set membership, regardless of outcrop. A minimum size truncation of 0.5 m (equivalent radius) was used for all fits. The local set size models assume a sampling geometry of a single square trace plane with an area equal to that of the sum of the Laxemar detailed outcrop maps. A simulated annealing algorithm was used to select the optimum size distribution by minimizing the Kolmogrov-Smirnov test statistic. The results, as well as the preferred size alternative (highlighted in red), are presented below in Table 6-9.

Note that the minimum radius presented for power-law distributions is for the statistical distribution; the goodness of fit is only computed for fractures above the truncation threshold. In addition, though the fit statistics may be reasonably good, there is considerable uncertainty in the size model for subhorizontally-dipping fractures (local set S_d). This is due to the difficulty of accurately sampling subhorizontally-dipping features in subhorizontally-dipping outcrops.

Table 6-9. Size models for non-global fracture sets d and f, Laxemar subarea.

Set id	Size model	Mean, std dev or min radius, exp	Chi – squared salue, % sig	K-S value, % sig	# of fractures
S_d	Lognormal	0.169, 0.198	18.2, 25.0%	0.134, 5.42%	202
S_d	Exponential	0.250	4.81, 56.8%	0.059, 86.8%	202
S_d	Power Law	0.208, 2.90	8.73, 27.3%	0.094, 33.3%	202
S_f	Normal	0.280, 0.418	3.79, 70.5%	0.126, 18.5%	120
S_f	Lognormal	0.219, 0.255	12.4, 71.9%	0.107, 35%	120
S_f	Exponential	0.312	5.32, 50.4%	0.086, 63.2%	120
S_f	Power Law	0.400, 3.60	4.12, 84.6%	0.08, 71.6%	120

* Note: arithmetic mean and standard deviations presented for both normal and lognormal distributions.

6.2.2 Simpevarp subarea

6.2.2.1 Simpevarp subarea rock domain A regional sets

Trace length scaling plots were constructed for the Simpevarp outcrop and deformation zone trace data. As in the Laxemar subarea, the first step in deriving the size model for the regional sets is to calculate the trace length scaling plots based on Euclidean and Mass Fractal scaling assumptions as previously described. The results for each set are shown Figure 6-13 in through Figure 6-18.

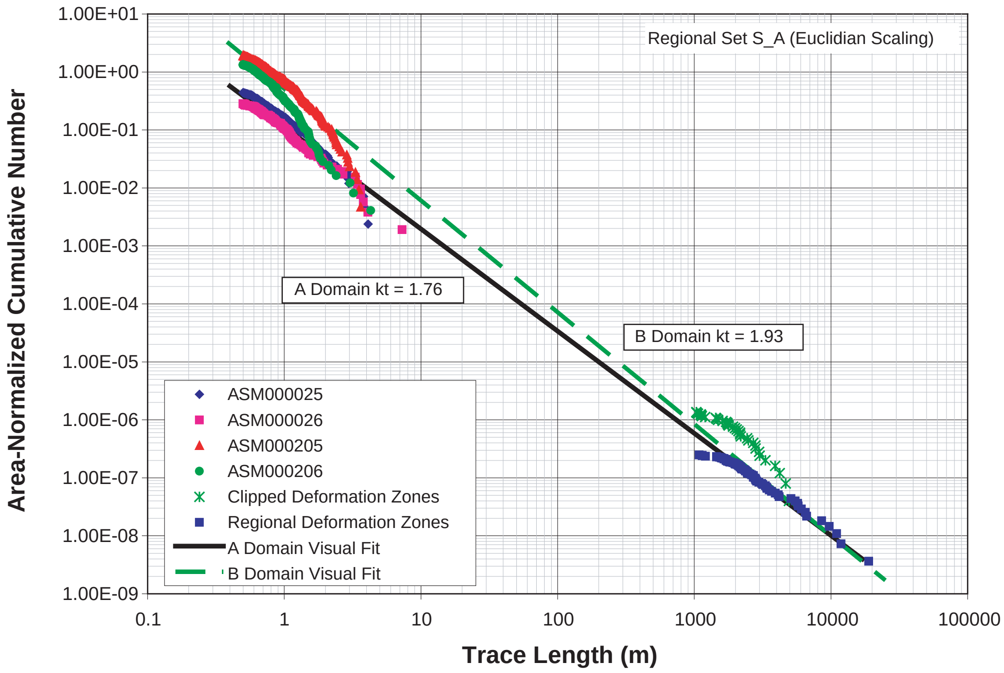

Figure 6-13. *Euclidean trace length scaling plot for regional set S_A, Simpevarp subarea, rock domains A and B.*

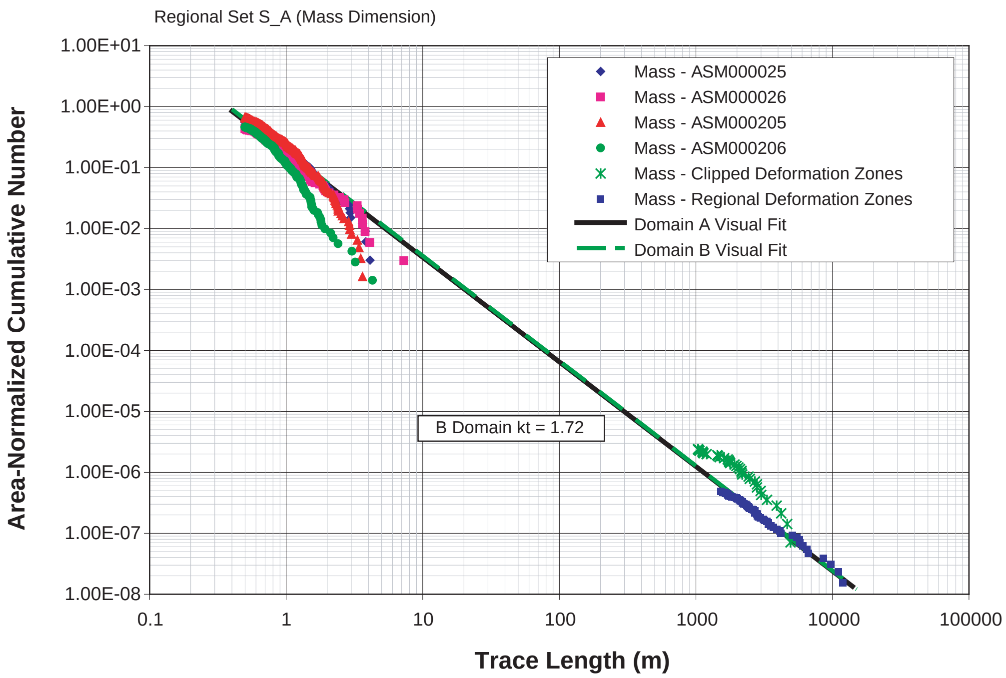

Figure 6-14. *Mass dimension trace length scaling plot for regional set S_A, Simpevarp subarea, rock domains A and B.*

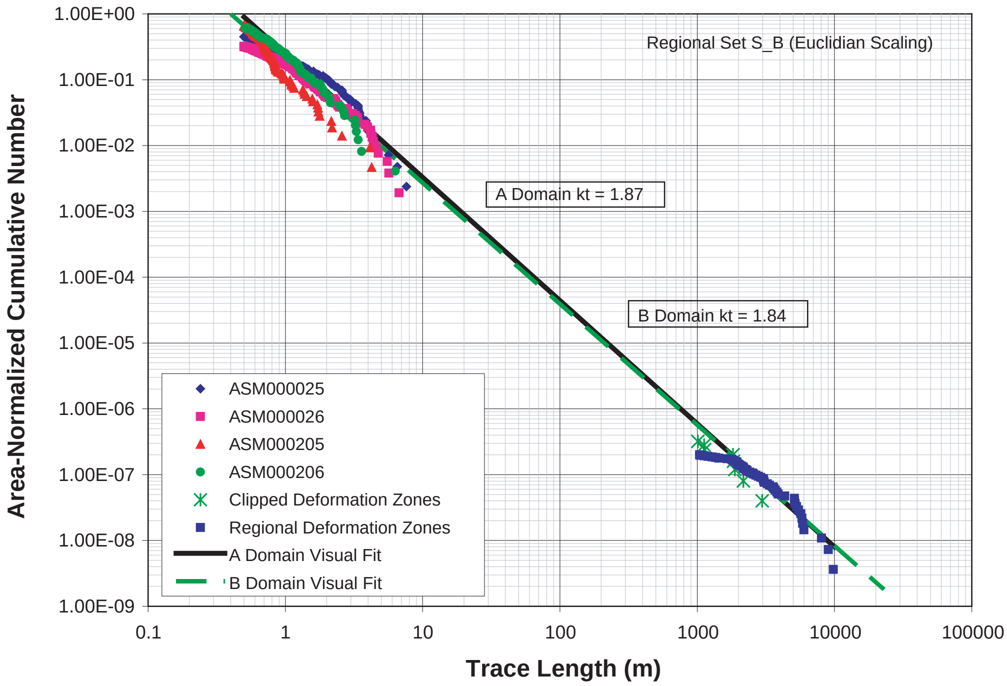

Figure 6-15. Euclidean trace length scaling plot for regional set S_B, Simpevarp subarea, rock domains A and B.

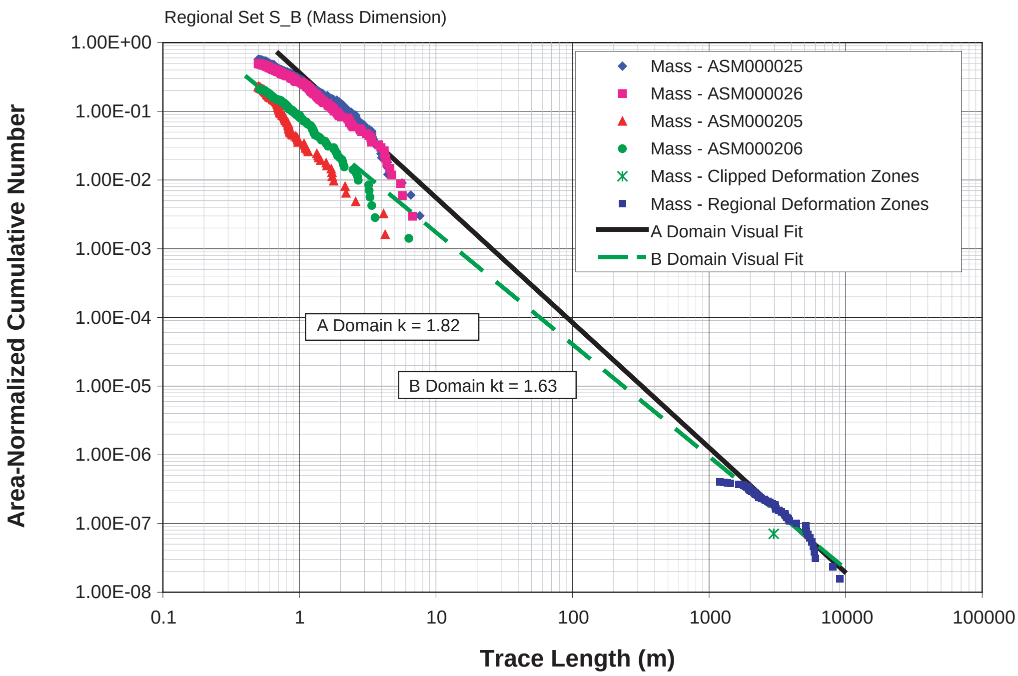

Figure 6-16. Mass dimension trace length scaling plot for regional set S_B, Simpevarp subarea, rock domains A and B.

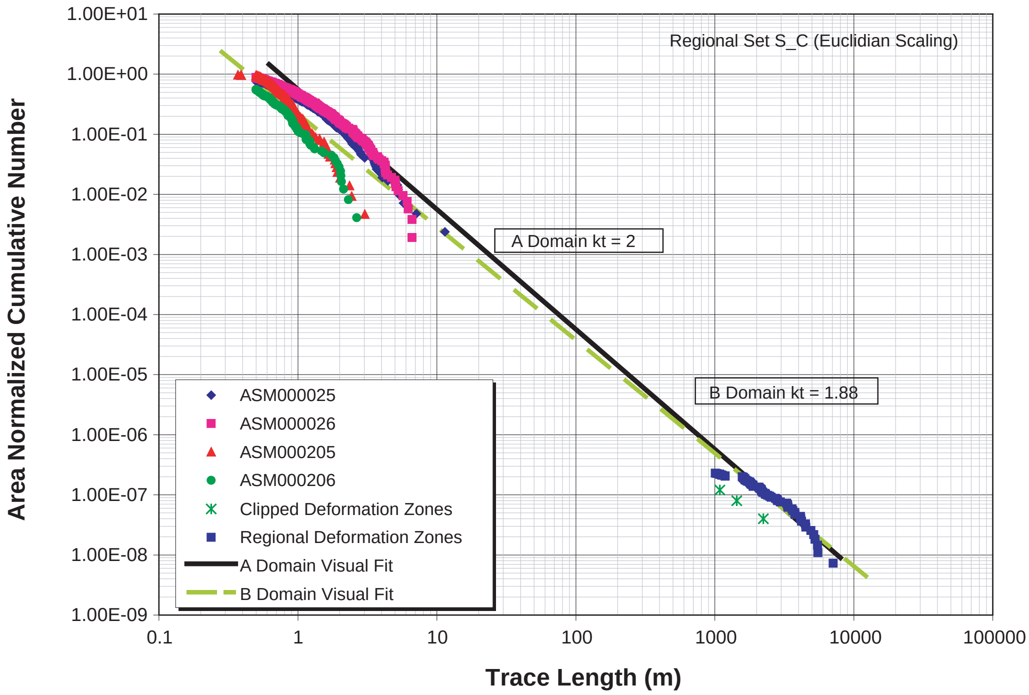

Figure 6-17. Euclidean trace length scaling plot for regional set S_C, Simpevarp subarea, rock domains A and B.

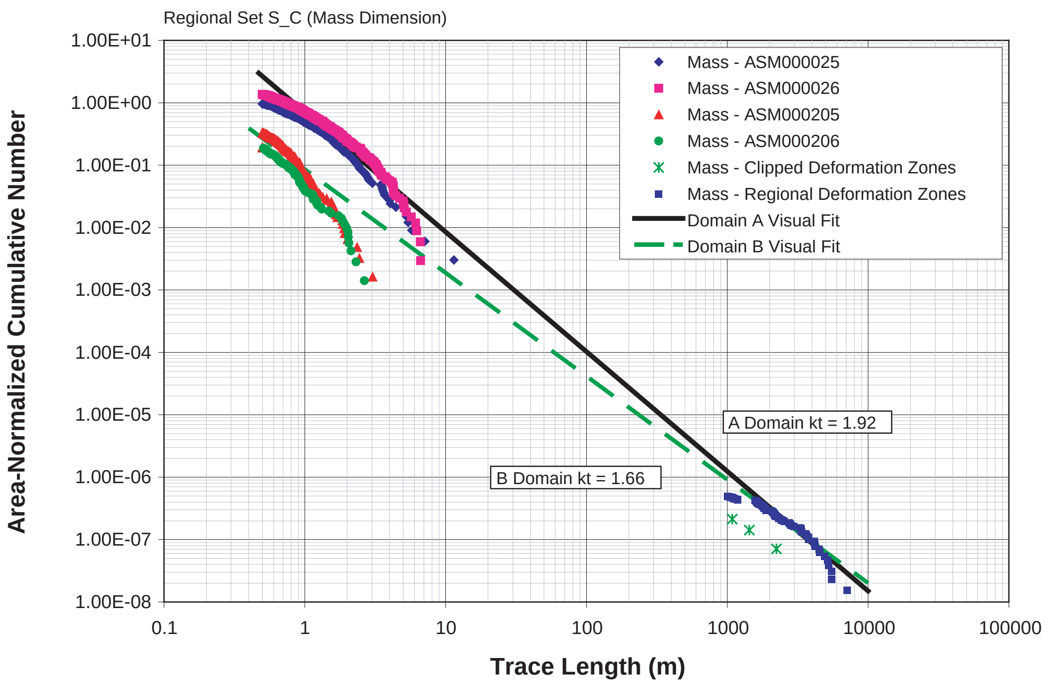

Figure 6-18. Mass dimension trace length scaling plot for regional set S_C, Simpevarp subarea, rock domains A and B.

It is interesting to note that the size model for set S_A does not seem to depend upon rock domain, while the size models for sets S_B and S_C differ between rock domains A and B. The steeper slope of the line for rock domain A for sets S_B and S_C indicates that the size distribution of these sets in rock domain A has a greater proportion of small fractures than they do in rock domain B. The reason for this is not known, but it might be related to grain size or mineralogy differences between the domains. It does indicate, however, that different size models for sets S_B and S_C exist for rock domains A and B. As a result, the analyses that follow are carried out separately for rock domains A and B.

The size model for the Simpevarp subarea regional sets within rock domain A is derived from cored boreholes KAV01, KAV04A, HSK03A and outcrop ASM000026 and the deformation zone model. The size model for the Simpevarp subarea regional sets within rock domain B is derived from cored boreholes KAV01, KAV04A, KSH01A, KSH02, outcrop ASM000205 and the deformation zone model. No size model was calculated for rock domain C due to lack of an outcrop data set, but the percentiles were calculated from boreholes KAV04A, KSH01A and KSH03A.

The values of P_{32} were estimated from the borehole P_{10} values through simulation, as described in Section 3.5.2. Because the fractures in the regional sets are nearly vertical with only moderate dispersion, the variability in the ratio of P_{32} to P_{10} is quite high, requiring the use of very high simulation P_{32} values in order to establish a good estimate of the ratio for each set. The calculated percentiles for each set and rock domain for the Simpevarp Subregion are shown in Figure 6-19.

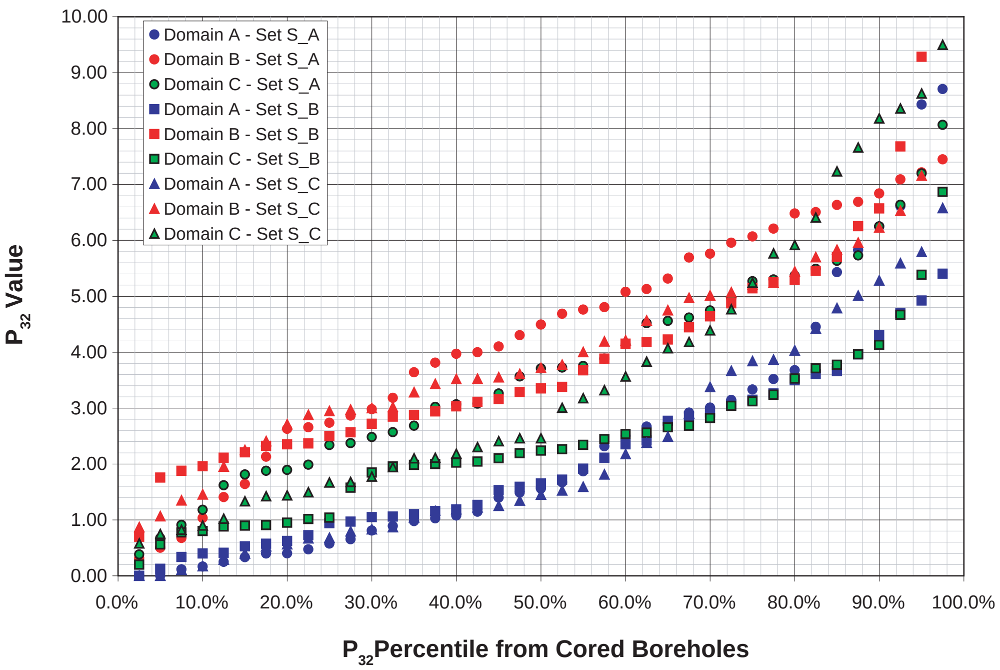

Figure 6-19. *P32 values as a function of percentile for regional sets S_A, S_B and S_C, rock domains A, B and C, Simpevarp subarea.*

This figure shows that the intensity of fracturing in rock domain B (red symbols) is much higher than the intensity in rock domain A (blue symbols), with rock domain C (green symbols) being intermediary. The figure also shows that within an individual rock domain, the relative intensity of a set can vary significantly with percentile. For example, Set S_B in rock domain B is the most prominent in the lower percentiles, while at about the 30th percentile, Set S_A becomes the most prominent. The closeness of the three sets in rock domain A also shows that the relative intensities of the three sets in rock domain A is much more uniform than in rock domain B, where Set S_A tends to dominate at percentiles greater than the 30th percentile. Rock domain C is typically intermediate between rock domains A and B. The percentile values are shown in Table 6-10 through Table 6-18.

Table 6-10. Cored borehole P_{32} percentiles – rock domain A, set S_A, Simpevarp subarea.

Percentiles	P_{32}	Percentiles	P_{32}	Percentiles	P_{32}	Percentiles	P_{32}
2.5%	0.000	27.5%	0.866	52.5%	2.388	77.5%	3.678
5.0%	0.000	30.0%	0.946	55.0%	2.504	80.0%	4.444
7.5%	0.160	32.5%	1.022	57.5%	2.654	82.5%	5.224
10.0%	0.256	35.0%	1.098	60.0%	2.716	85.0%	5.814
12.5%	0.320	37.5%	1.390	62.5%	2.890	87.5%	6.050
15.0%	0.400	40.0%	1.434	65.0%	2.970	90.0%	6.374
17.5%	0.400	42.5%	1.546	67.5%	3.026	92.5%	7.380
20.0%	0.434	45.0%	1.582	70.0%	3.202	95.0%	8.504
22.5%	0.504	47.5%	1.760	72.5%	3.400	97.5%	9.020
25.0%	0.640	50.0%	1.890	75.0%	3.520		

Table 6-11. Cored borehole P_{32} percentiles – rock domain A, set S_B, Simpevarp subarea.

Percentiles	P_{32}	Percentiles	P_{32}	Percentiles	P_{32}	Percentiles	P_{32}
2.5%	0.000	27.5%	0.968	52.5%	1.720	77.5%	3.262
5.0%	0.126	30.0%	1.050	55.0%	1.916	80.0%	3.498
7.5%	0.336	32.5%	1.060	57.5%	2.112	82.5%	3.610
10.0%	0.400	35.0%	1.104	60.0%	2.352	85.0%	3.658
12.5%	0.410	37.5%	1.160	62.5%	2.420	87.5%	3.960
15.0%	0.526	40.0%	1.186	65.0%	2.772	90.0%	4.304
17.5%	0.574	42.5%	1.266	67.5%	2.860	92.5%	4.702
20.0%	0.622	45.0%	1.532	70.0%	2.922	95.0%	4.924
22.5%	0.726	47.5%	1.592	72.5%	3.066	97.5%	5.402
25.0%	0.940	50.0%	1.650	75.0%	3.150		

Table 6-12. Cored borehole P_{32} percentiles – rock domain A, set S_C, Simpevarp Subarea.

Percentiles	P_{32}	Percentiles	P_{32}	Percentiles	P_{32}	Percentiles	P_{32}
2.5%	0.000	27.5%	0.794	52.5%	1.526	77.5%	3.866
5.0%	0.000	30.0%	0.832	55.0%	1.590	80.0%	4.030
7.5%	0.106	32.5%	0.868	57.5%	1.812	82.5%	4.422
10.0%	0.170	35.0%	1.042	60.0%	2.178	85.0%	4.788
12.5%	0.290	37.5%	1.160	62.5%	2.380	87.5%	5.010
15.0%	0.400	40.0%	1.190	65.0%	2.488	90.0%	5.282
17.5%	0.526	42.5%	1.224	67.5%	2.904	92.5%	5.590
20.0%	0.564	45.0%	1.252	70.0%	3.376	95.0%	5.792
22.5%	0.670	47.5%	1.344	72.5%	3.664	97.5%	6.578
25.0%	0.680	50.0%	1.450	75.0%	3.840		

Table 6-13. Cored borehole P_{32} percentiles – rock domain B, set S_A, Simpevarp subarea.

Percentiles	P_{32}	Percentiles	P_{32}	Percentiles	P_{32}	Percentiles	P_{32}
2.5%	0.319	27.5%	2.865	52.5%	4.688	77.5%	6.210
5.0%	0.500	30.0%	2.980	55.0%	4.763	80.0%	6.480
7.5%	0.676	32.5%	3.183	57.5%	4.805	82.5%	6.506
10.0%	1.035	35.0%	3.640	60.0%	5.080	85.0%	6.633
12.5%	1.406	37.5%	3.813	62.5%	5.130	87.5%	6.689
15.0%	1.643	40.0%	3.970	65.0%	5.315	90.0%	6.840
17.5%	2.130	42.5%	3.998	67.5%	5.694	92.5%	7.091
20.0%	2.630	45.0%	4.100	70.0%	5.760	95.0%	7.215
22.5%	2.658	47.5%	4.303	72.5%	5.958	97.5%	7.449
25.0%	2.738	50.0%	4.495	75.0%	6.070		

Table 6-14. Cored borehole P_{32} percentiles – rock domain B, set S_B, Simpevarp subarea.

Percentiles	P_{32}	Percentiles	P_{32}	Percentiles	P_{32}	Percentiles	P_{32}
2.5%	0.698	27.5%	2.568	52.5%	3.379	77.5%	5.251
5.0%	1.755	30.0%	2.720	55.0%	3.675	80.0%	5.290
7.5%	1.879	32.5%	2.848	57.5%	3.884	82.5%	5.453
10.0%	1.960	35.0%	2.878	60.0%	4.150	85.0%	5.703
12.5%	2.110	37.5%	2.941	62.5%	4.181	87.5%	6.254
15.0%	2.208	40.0%	3.030	65.0%	4.228	90.0%	6.570
17.5%	2.324	42.5%	3.113	67.5%	4.445	92.5%	7.680
20.0%	2.350	45.0%	3.163	70.0%	4.640	95.0%	9.285
22.5%	2.368	47.5%	3.290	72.5%	4.873	97.5%	12.711
25.0%	2.500	50.0%	3.350	75.0%	5.143		

Table 6-15. Cored borehole P_{32} percentiles – rock domain B, set S_C, Simpevarp Subregion.

Percentiles	P_{32}	Percentiles	P_{32}	Percentiles	P_{32}	Percentiles	P_{32}
2.5%	0.868	27.5%	2.971	52.5%	3.774	77.5%	5.240
5.0%	1.065	30.0%	3.000	55.0%	4.003	80.0%	5.440
7.5%	1.350	32.5%	3.016	57.5%	4.193	82.5%	5.699
10.0%	1.455	35.0%	3.283	60.0%	4.210	85.0%	5.830
12.5%	1.954	37.5%	3.431	62.5%	4.566	87.5%	5.958
15.0%	2.250	40.0%	3.520	65.0%	4.750	90.0%	6.230
17.5%	2.408	42.5%	3.524	67.5%	4.971	92.5%	6.528
20.0%	2.710	45.0%	3.550	70.0%	5.015	95.0%	7.158
22.5%	2.879	47.5%	3.610	72.5%	5.071	97.5%	10.208
25.0%	2.945	50.0%	3.720	75.0%	5.203		

Table 6-16. Cored borehole P_{32} percentiles – rock domain C, set S_A, Simpevarp subarea.

Percentiles	P_{32}	Percentiles	P_{32}	Percentiles	P_{32}	Percentiles	P_{32}
2.5%	0.384	27.5%	2.372	52.5%	3.726	77.5%	5.302
5.0%	0.672	30.0%	2.482	55.0%	3.754	80.0%	5.370
7.5%	0.908	32.5%	2.570	57.5%	3.882	82.5%	5.490
10.0%	1.180	35.0%	2.684	60.0%	4.144	85.0%	5.634
12.5%	1.620	37.5%	3.020	62.5%	4.520	87.5%	5.730
15.0%	1.812	40.0%	3.068	65.0%	4.560	90.0%	6.250
17.5%	1.878	42.5%	3.080	67.5%	4.618	92.5%	6.638
20.0%	1.894	45.0%	3.260	70.0%	4.746	95.0%	7.198
22.5%	1.988	47.5%	3.566	72.5%	4.966	97.5%	8.066
25.0%	2.340	50.0%	3.710	75.0%	5.270		

Table 6-17. Cored borehole P_{32} percentiles – domain C, set S_B, Simpevarp subarea.

Percentiles	P_{32}	Percentiles	P_{32}	Percentiles	P_{32}	Percentiles	P_{32}
2.5%	0.200	27.5%	1.576	52.5%	2.264	77.5%	3.240
5.0%	0.562	30.0%	1.848	55.0%	2.342	80.0%	3.528
7.5%	0.774	32.5%	1.956	57.5%	2.446	82.5%	3.712
10.0%	0.800	35.0%	1.984	60.0%	2.536	85.0%	3.776
12.5%	0.880	37.5%	2.000	62.5%	2.560	87.5%	3.960
15.0%	0.896	40.0%	2.024	65.0%	2.656	90.0%	4.128
17.5%	0.906	42.5%	2.042	67.5%	2.686	92.5%	4.668
20.0%	0.950	45.0%	2.102	70.0%	2.822	95.0%	5.384
22.5%	1.016	47.5%	2.192	72.5%	3.040	97.5%	6.868
25.0%	1.040	50.0%	2.240	75.0%	3.120		

Table 6-18. Cored borehole P_{32} percentiles – domain C, set S_C, Simpevarp subarea.

Percentiles	P_{32}	Percentiles	P_{32}	Percentiles	P_{32}	Percentiles	P_{32}
2.5%	0.578	27.5%	1.678	52.5%	3.004	77.5%	5.768
5.0%	0.746	30.0%	1.776	55.0%	3.176	80.0%	5.918
7.5%	0.822	32.5%	1.944	57.5%	3.320	82.5%	6.410
10.0%	0.900	35.0%	2.102	60.0%	3.566	85.0%	7.236
12.5%	1.020	37.5%	2.110	62.5%	3.830	87.5%	7.660
15.0%	1.332	40.0%	2.182	65.0%	4.070	90.0%	8.180
17.5%	1.422	42.5%	2.302	67.5%	4.184	92.5%	8.358
20.0%	1.438	45.0%	2.406	70.0%	4.392	95.0%	8.626
22.5%	1.494	47.5%	2.460	72.5%	4.768	97.5%	9.500
25.0%	1.670	50.0%	2.460	75.0%	5.240		

The values of P_{32} for the deformation zones were taken from Table 6-6.

The predicted values of x_{0r} as a function of borehole P_{32} percentile are shown in Figure 6-20. The parameters for the power law functions that describe this relation are shown in the bos to the right of the graph. As expected, the exponents are equal to $(2 - k_r)$. This graph also shows that Set S_C in rock domain A is very similar to Set S_A in rock domain B, and that Set S_B in rock domain A is similar to Set S_C in rock domain B. Set S_A in rock domain A and Set S_B in rock domain B are not similar to other sets. This suggests that the regional sets may not be sufficiently similar to the point that sets can be combined or that domains can be combined.

The triplets of minimum radius, scaling exponent and P_{32} percentile were used to generate five realizations. A plane approximating an outcrop in the domain was inserted into each DFN realization, and the P_{21} for all traces greater than or equal to 0.5 m was determined. Outcrop ASM000026 was used for Domain A. The calculated P_{21} values for this outcrop are shown in Table 6-19.

Table 6-19. Values of P_{21} determined for each regional fracture set in outcrop ASM000026, Simpevarp subarea (rock domain A).

Regional set #	P_{21}
S_A	0.318
S_B	0.455
S_C	1.239

The truncated P_{21} values calculated from the DFN simulations are shown in Figure 6-20.

It was possible to obtain matches for all three regional sets, as shown by Figure 6-21 through Figure 6-23. Table 6-20 summarizes the matchpoint parameters for each set. It is interesting to note that the match points for sets S_A and S_B correspond to relatively low percentiles of the P_{32} distributions, unlike their counterparts in rock domain A for the Laxemar subarea.

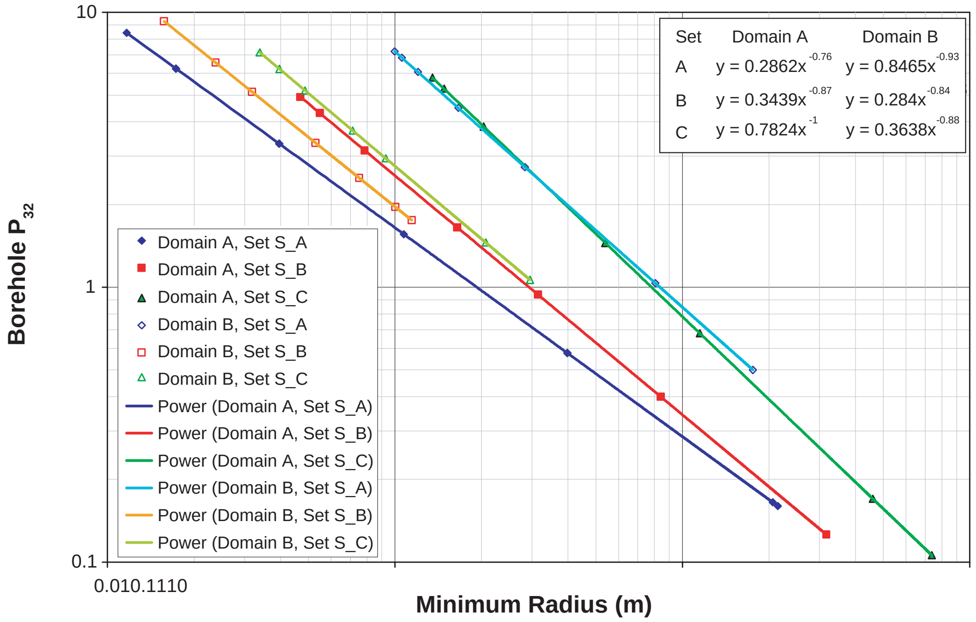

Figure 6-20. *Calculated values of minimum radius as a function of P_{32} percentile, rock domains A and B, Simpevarp subarea. The equations of the power law functions for minimum radius and P_{32} are shown in box to right of graph.*

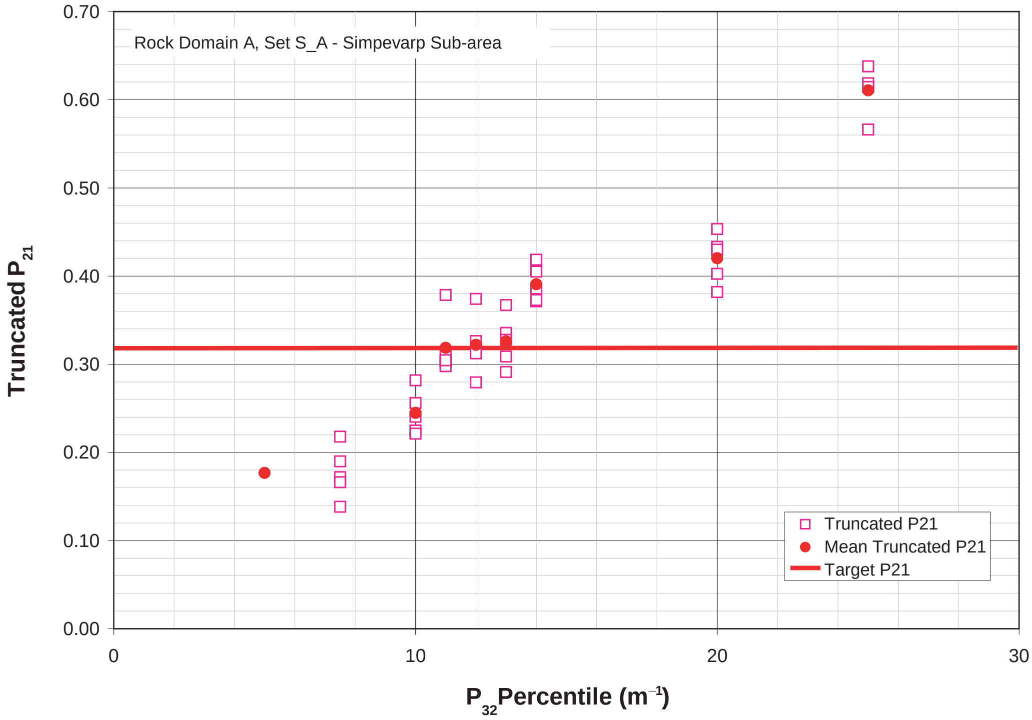

Figure 6-21. *Results from DFN simulations for regional set S_A, rock domain A, Simpevarp subarea. The red horizontal line shows the target value of truncated P_{21}, while the symbols show the five realizations results (open squares) and mean value (red solid circles).*

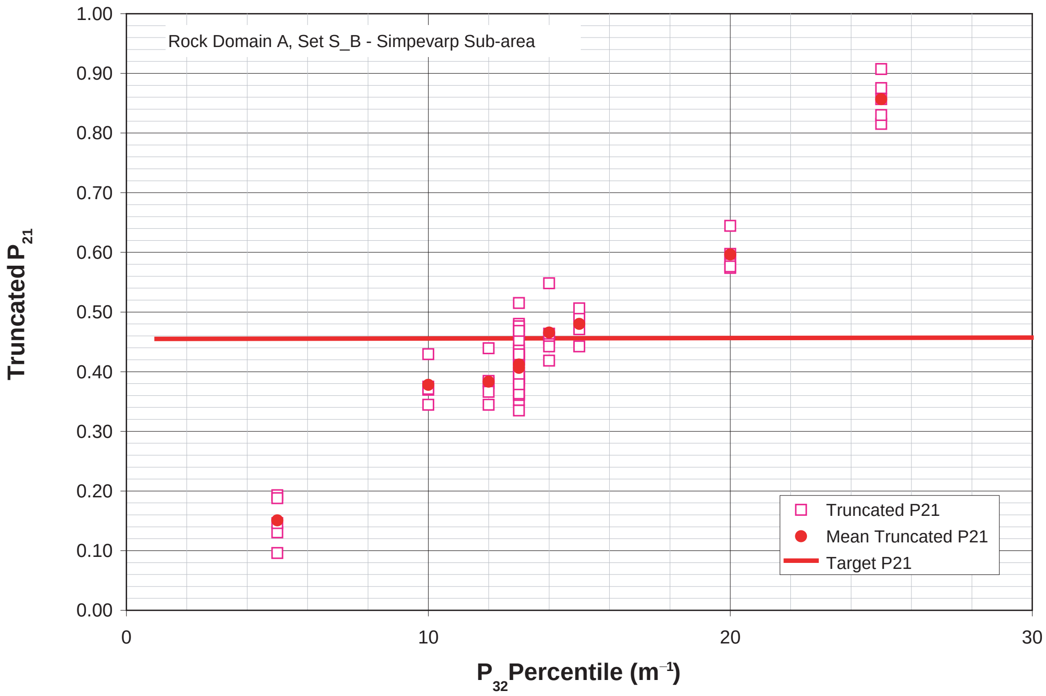

Figure 6-22. *Results from DFN simulations for regional set S_B, rock domain A, Simpevarp subarea. The red horizontal line shows the target value of truncated P_{21}, while the symbols show the five realizations results (open squares) and mean value (red solid circles).*

Table 6-20. Match point fracture size parameter values for each regional set, rock domain A, Simpevarp subarea. All sizes conform to a power law distribution.

Set	P_{32}	Minimum radius (m)	Scaling exponent	Borehole P_{32} percentile	Target truncated P_{21}	Simulation truncated P_{21}
S_A	0.320	0.864	2.760	12%	0.318	0.322
S_B	0.476	0.689	2.870	14%	0.455	0.466
S_C	1.312	0.596	3.000	47%	1.239	1.229

A possible explanation for this might be that the borehole data come from locations that could have higher-than-average intensities for these sets. Inspection of the borehole location map for the Simpevarp subregion (Figure 1-3) shows that borehole KAV04 is quite close to a major east-west deformation zone, and the borehole P_{32} fracture intensities for this borehole are typically higher than for other boreholes in the rock domain (Table 6-21). Outcrop ASM000026, on the other hand, is not near any mapped deformation zones, and so a lower percentile of the borehole P_{32} values may be required to match the outcrop data.

Table 6-21. Mean Borehole P_{32} values for rock domain A, Simpevarp subarea.

Borehole	Count	Set S_A	Set S_B	Set S_C
KAV01	27	1.06	0.63	0.69
KAV04A	16	0.81	1.01	1.17
KSH03A	30	0.11	0.21	0.07

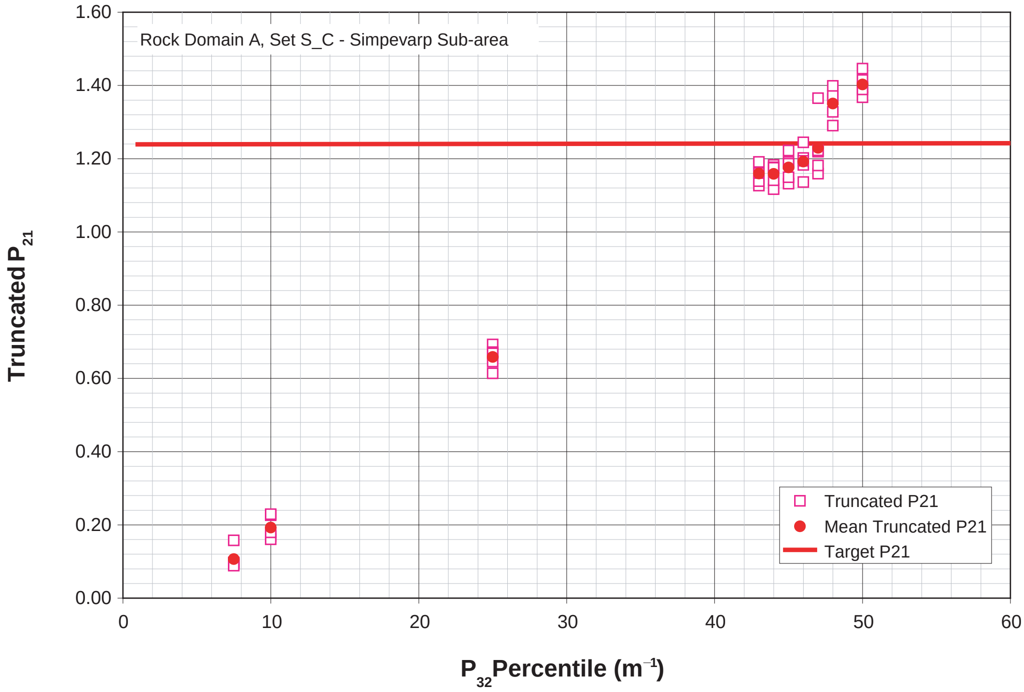

Figure 6-23. Results from DFN simulations for regional set S_C, rock domain A, Simpevarp subarea. The red horizontal line shows the target value of truncated P_{21}, while the symbols show the five realizations results (open squares) and mean value (red solid circles).

6.2.2.2 Domain B regional sets

The values of P_{32} were estimated from the borehole P_{10} values through simulation. Because the fractures in the regional sets are nearly vertical with only moderate dispersion, the variability in the ratio of P_{32} to P_{10} is quite high, requiring the use of very high simulation P_{32} values in order to establish a good estimate of the ratio for each set. The borehole P_{32} percentile values have previously been presented in Table 6-13 through Table 6-15. The target deformation zone P_{32} values were taken from Table 6-6. The calculated minimum radius values as a function of these parameters is shown in Figure 6-20. The calculated values of truncated P_{21} for outcrop ASM000205 are shown in Table 6-22.

Table 6-22. Values of P_{21} calculated for each regional fracture set, Outcrop ASM000205, Simpevarp subarea.

Regional set #	P_{21}
S_A	1.96
S_B	0.562
S_C	0.827

The simulation results are shown in Figure 6-24 through Figure 6-26. In all cases, it was possible to obtain a match point (Table 6-23).

The match points occur at very low borehole P_{32} percentiles, especially for sets S_B and S_C. The majority of the fracture data comes from borehole KSH02, which is very close to a major east-west deformation zone (Figure 5-93). This may explain why very low percentiles of the borehole P_{32} were required to obtain a match.

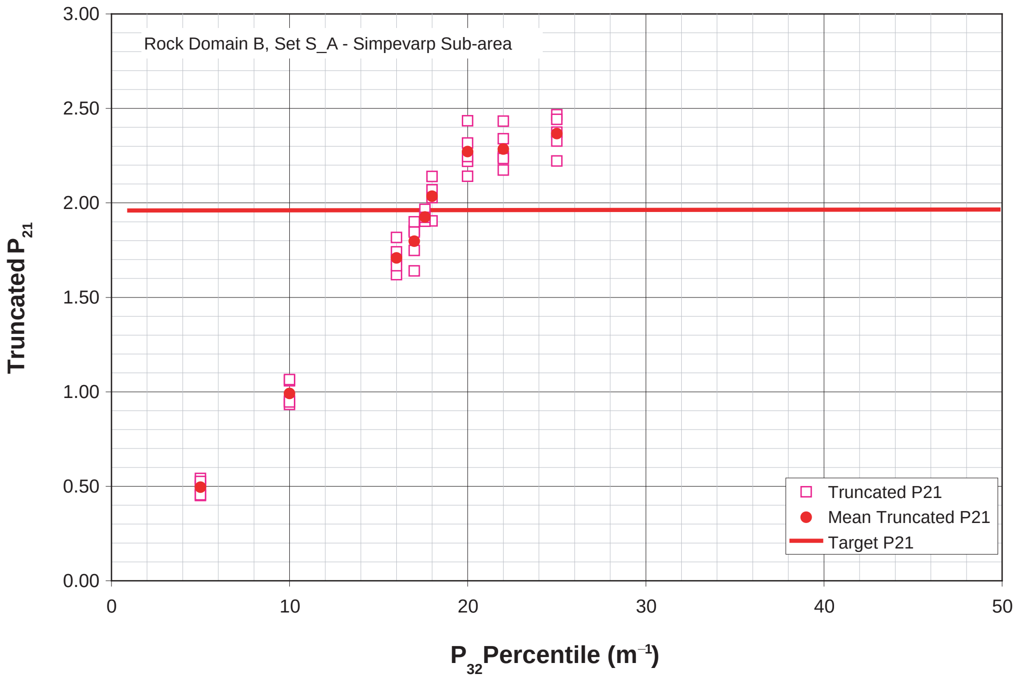

Figure 6-24. *Results from DFN simulations for regional set S_A, rock domain B. The red horizontal line shows the target value of truncated P_{21}, while the symbols show the five realizations results (open squares) and mean value (red solid circles).*

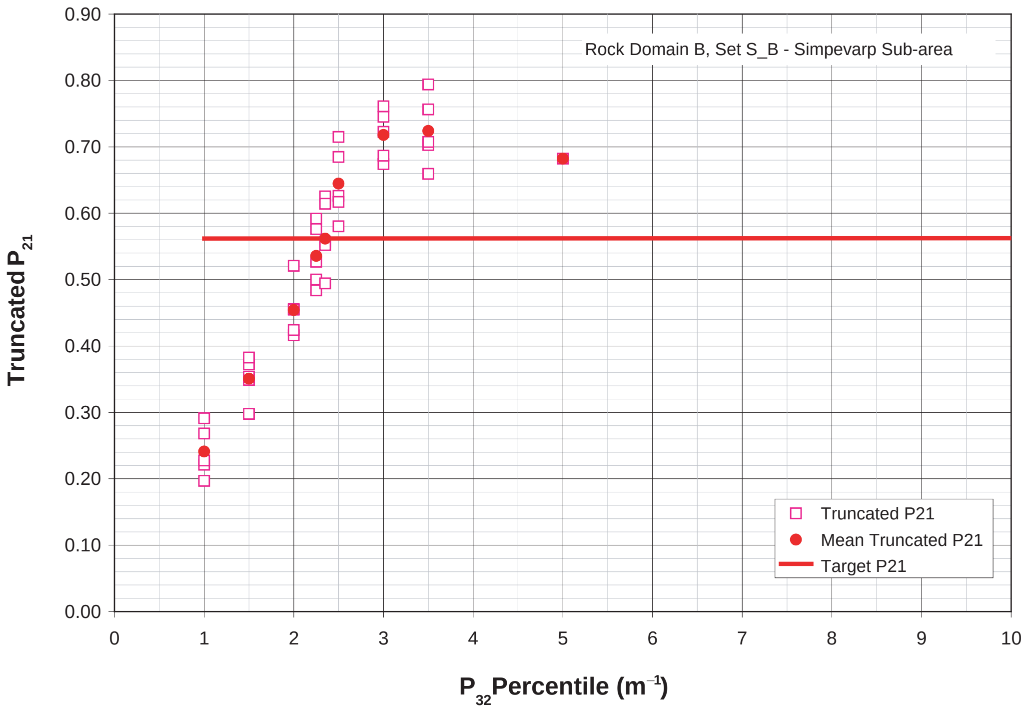

Figure 6-25. *Results from DFN simulations for regional set S_B, Domain B. The red horizontal line shows the target value of truncated P_{21}, while the symbols show the five realizations results (open squares) and mean value (red solid circles).*

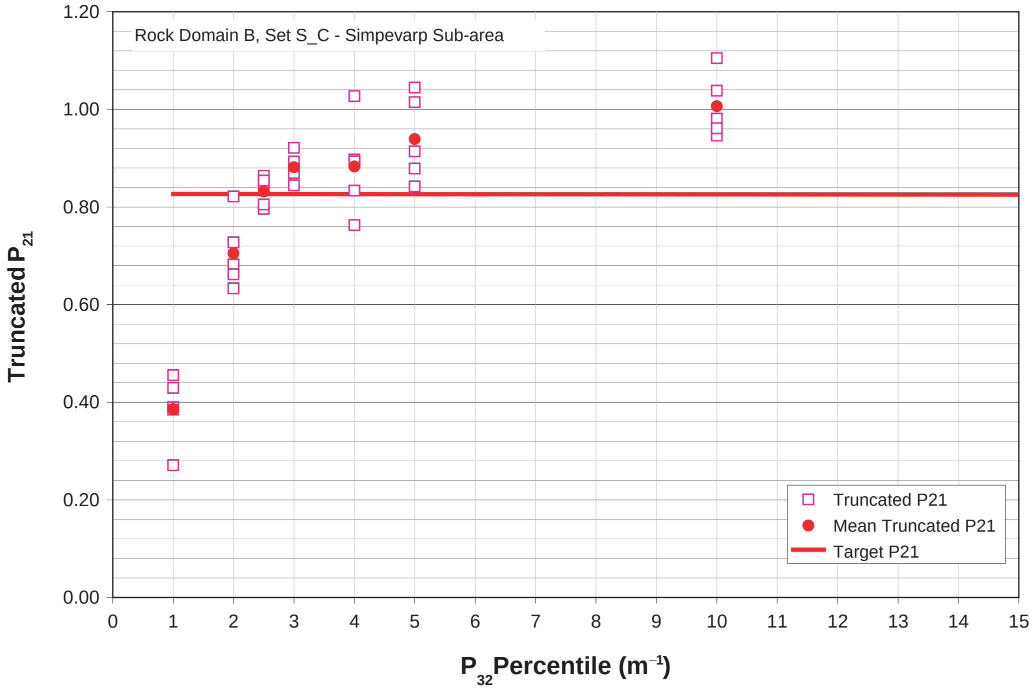

***Figure 6-26.** Results from DFN simulations for regional set S_C, rock domain B, Simpevarp subarea. The red horizontal line shows the target value of truncated P_{21}, while the symbols show the five realizations results (open squares) and mean value (red solid circles).*

Table 6-23. Match point fracture size parameter values for each regional set, Domain B, Simpevarp subregion. All sizes conform to a power law distribution.

Set	P_{32}	Minimum radius (m)	Scaling exponent	Borehole P_{32} percentile	Target truncated P_{21}	Simulation truncated P_{21}
S_A	2.152	0.367	2.93	17.60%	1.960	1.925
S_B	0.618	0.396	2.84	2.35%	0.562	0.562
S_C	0.868	0.372	2.88	2.50%	0.827	0.832

6.2.2.3 Local sets, Simpevarp subarea

The FracSize approach (Section 3.4.1) was used to specify size distributions for those fracture sets (S_d, S_e) in the Simpevarp modeling subarea without a visible component in the regional deformation zone model. Fractures were grouped by set membership, regardless of outcrop. A minimum size truncation of 0.5 m (equivalent radius) was used for all fits. The local set size models assume a sampling geometry of a single square trace plane with an area equal to that of the sum of the Simepvarp detailed outcrop maps. A simulated annealing algorithm was used to select the optimum size distribution by minimizing the Kolomogrov-Smirnov test statistic.

Note that the minimum radius presented for power-law distributions is for the statistical distribution; the goodness of fit is only computed for fractures above the truncation threshold. In addition, though the fit statistics may be reasonably good, there is considerable uncertainty in the size model for subhorizontally-dipping fractures (local set S_d). This is due to the difficulty of accurately sampling subhorizontally-dipping features in flat outcrops. The accumulated Simpevarp outcrop data is particularly bad; none of the analyzed size models produced a statistically significant fit to the recorded data.

Table 6-24. Size models for non-global fracture sets d and e, Simpevarp subarea.

Set id	Size model	Mean, std dev or min radius, exp	Chi – squared value, % sig	K-S value, % sig	# of fractures
S_d	Normal	0.141, 0.294	79.9, 0.0%	0.172, 0.02%	325
S_d	Lognormal	0.062, 0.122	50.1, 0.01%	0.16, 0.05%	325
S_d	Exponential	0.220	73, 0.0%	0.16, 0.05%	325
S_d	Power Law	0.150, 3.10	63.3, 0.0%	0.16, 0.05%	325
S_e	Normal	0.436, 0.251	95.7, 0.0%	0.222, 0.0%	472
S_e	Lognormal	0.231, 0.169	46.8, 0.04%	0.104, 1.24%	472
S_e	Exponential	0.222	76.7, 0.0%	0.161, 0.0%	472
S_e	Power Law	0.212, 3.27	54.7, 0.0%	0.106, 1%	472

* Note: arithmetic mean and standard deviations presented for both normal and lognormal distributions; only a mean is presented for the exponential distribution.

6.3 Spatial model

Cored borehole fracture data from both the Simpevarp and the Laxemar modeling subareas was analyzed to determine whether each set in each rock domain conformed to a Poisson, Fractal or Geostatistical model. This is done according to Equation 3-1 for the borehole data. In this calculation, the mean number of fractures for an interval of a specified length is calculated for interval lengths vary from much less than the average fracture spacing, to sizes approaching half the borehole length. Very small intervals contain fewer fractures than large intervals. As the interval size decreases, the mean number of fractures per interval tends towards 1.0, and as the size continues to decrease, the mean number in an interval becomes independent of interval size. This flattening is essentially an artifact of the measurement resolution of fractures in the BIPS log or core. Very small interval sizes are purposely included in the calculation to identify where this artifact is obscuring the actual mass dimension of the data, as they are in the mass dimension of the outcrop traces. The onset of a constant, non-zero slope in the log-log plot of interval length vs mean number of fractures is the portion of the plot that best describes the scaling properties of the data. If this portion of the curve has a slope of approximately 1.0, then the data scales in a Euclidian manner. If there is a constant slope but it has a slope other (typically less than) 1.0, then it scales in a fractal manner. If it is not linear, then it may scale as a geostatistical model with second order stationarity, or even according to other scaling functions. If it scales either in a Euclidian or fractal manner, then the data is not tested for additional models, as these will fail.

The plots for the mass dimension of the borehole data are grouped by rock domain. Domain A is represented by borehole KLX04 and by the “A” portion of KSH03A. Domain B is represented by borehole KSH02. The plots that follow were computed from the longest contiguous portions of the boreholes lying in the specified domain and not containing any deformation zones, as these would produce errors in the calculations. Table 6-25 shows the intervals analyzed.

Table 6-25. Borehole data used to compute DFN spatial model.

Borehole	Interval (measured depth – m)	Rock domain
KSH02	681–1,000	B
KSH03A	275–997	A
KLX04	355–873	A

The graphs of simulation results for each borehole (Figure 6-27 through Figure 6-29) suggest similar behaviors. On each graph there is a red and a green straight line. These lines have a constant slope of 1.0, and represent the slope of a data set that scale in a Euclidian manner. The red line is used to indicate where the subhorizontal set (S_d) scales in a Euclidian manner, while the green line is used to visually help distinguish where the other sets begin to scale in a Euclidean manner. In almost all cases for the regional sets, the onset of Euclidian scaling occurs around interval lengths of 20 m to 30 m; The onset of Euclidian scaling typically occurs at a smaller interval length for the subhorizontally-oriented fracture sets. Although the interval length is in measured depth, this is close to vertical depth for these boreholes. This implies that at scales greater than 20 m to 30 m, the intensity for a specific set within a single rock domain scales reasonably closely to a Euclidian (Poissonian) spatial pattern. The horizontal set (S_d) appears to scale in a Euclidian manner at intervals of 1 m or greater.

It has been shown previously that the outcrop trace patterns for the regional sets (sets S_A, S_B and S_C) have mass dimensions that are less than 2.0, indicating fractal and not Euclidian intensity scaling. However, the outcrop dimensions are on the order of 20 m to 30 m, and so it is not known if the trace pattern would have approached a Euclidian scaling pattern at much greater scales.

Whether or not the traces would have continued scaling in a fractal manner or approximated a Euclidian pattern creates some uncertainty in the model, but if the modeling discretization is on the order of tens of meters to perhaps a hundred meters (for example, if the finite difference or finite element sizes are on this scale), then the difference predicted from the fractal mass model and the Euclidian model is probably negligible relative to other uncertainties. Moreover, adoption of a Euclidian scaling law rather than a fractal scaling law will be slightly conservative, as the Euclidian model will predict a little higher intensity of fracturing. Therefore, it is reasonable to adopt a Poissonian spatial model for models discretized in the 10 m to 100 m range. Another alternative would be to fit a multifractal model to his data. The decision as to which type of model may be more useful depends upon whether there truly is a tectonic continuum in fracturing from meter-sized fractures to kilometer long deformation zones. The existence of a tectonic continuum remains an unanswered question with the current data available for analysis.

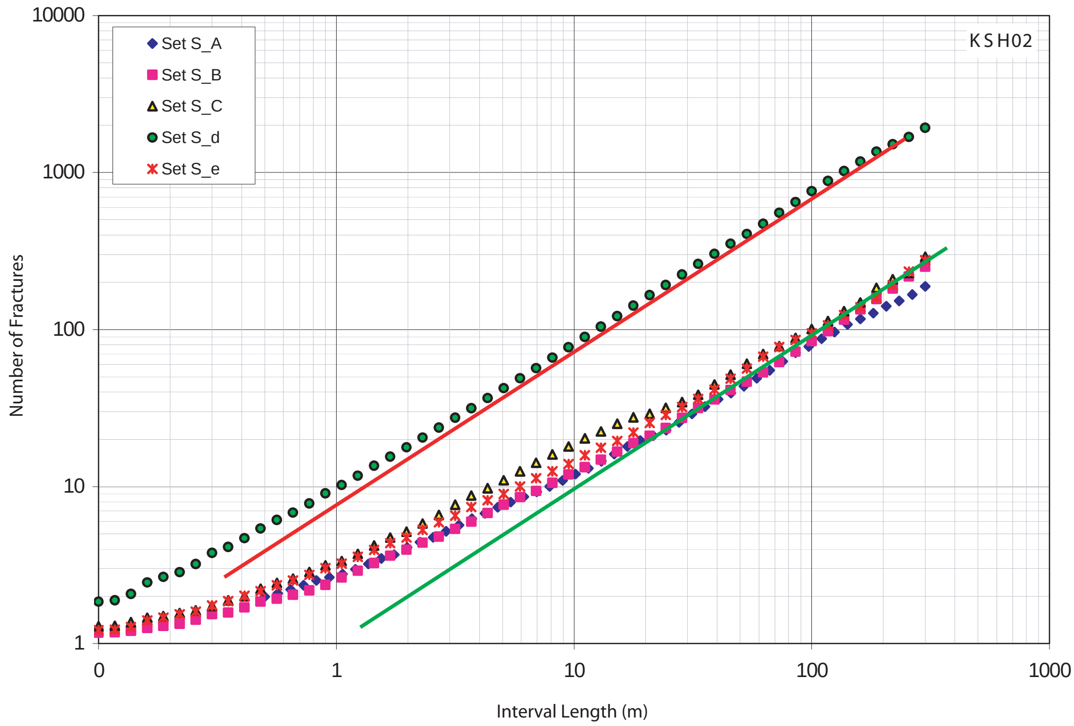

Figure 6-27. *Mass dimension plot of all fractures classified by set for borehole KSH02, Simpevarp subarea.*

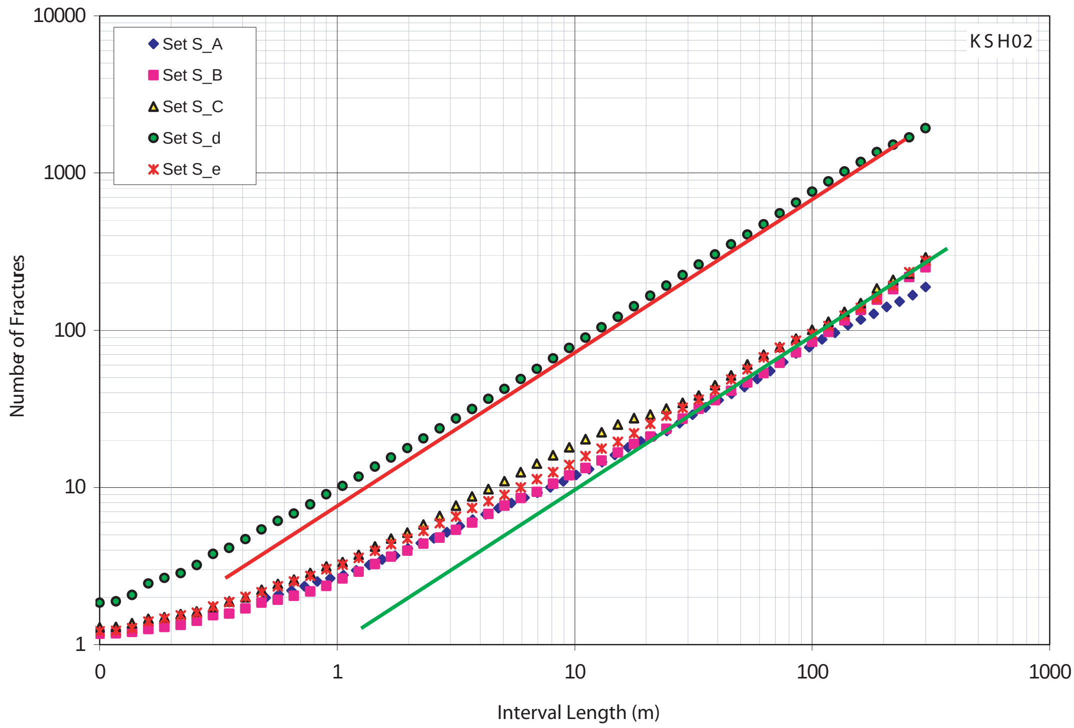

Figure 6-28. *Mass dimension plot of all fractures classified by set for borehole KSH03A, Simpevarp subarea.*

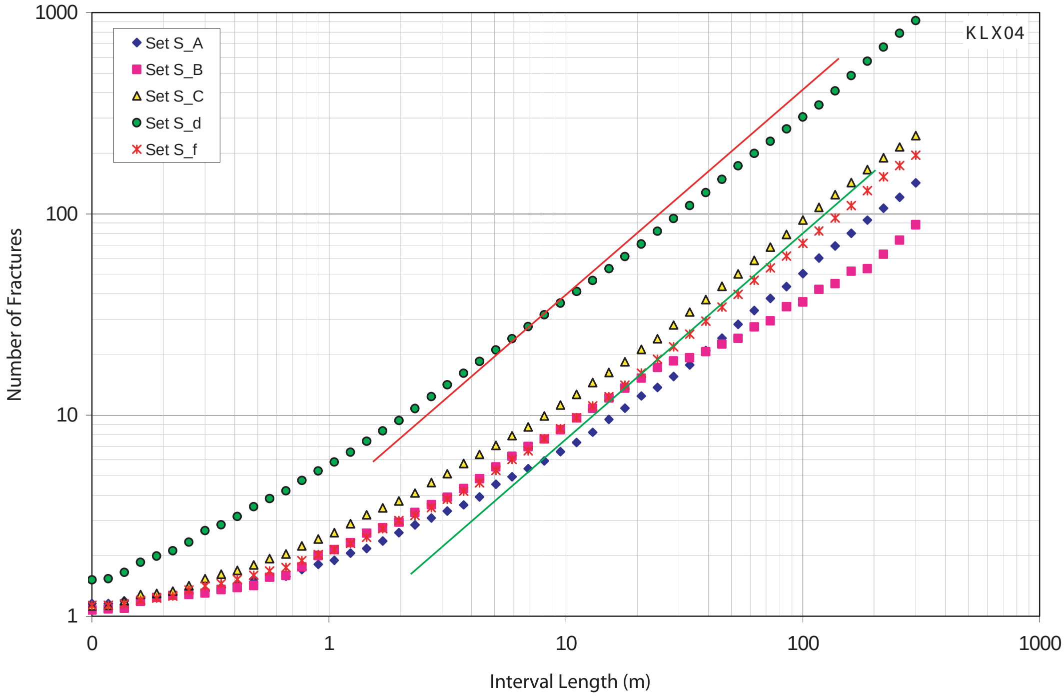

Figure 6-29. *Mass dimension plot of all fractures classified by set for borehole KLX04, Laxemar subarea.*

6.4 Fracture intensity distribution parameters

Fracture set intensity (P_{32}) is specified as a function of rock domain and model sub-domain, and is based on P_{10} intensities as recorded in drillcore logs. Though detailed analysis of fracture intensity trends (see Section 5.2 and the previous SDM Simpevarp 1.2 modeling report), there appear to be additional poorly-understood controls on fracture intensity at scales that may be significant for modeling. Thus, the data uncertainty reported for the fracture intensity in each domain and model subarea needs to be updated as additional data and understanding is obtained.

The fracture set intensity parameters for the SDM Laxemar 1.2 DFN model are based on borehole fracture intensity statistics (P_{10}) calculated for each orientation set and each identified rock domain. Calculation of P_{32} values was based on P_{10} intensities rather than P_{21} intensities (from detailed outcrop mapping) or a mixture of the two data sources for several reasons:

- Volumetric fracture intensities (P_{32}s) determined from borehole intersection data (P_{10}s) are independent of the size model chosen or of the shape of the fractures modeled (see Section 6.2.1.1. for more details). This offers modeling teams additional flexibility in implementing the DFN model.
- Availability of data: By far, the most spatially extensive data set for fracture intensities is the SICADA cored borehole database. By comparison, the detailed outcrop maps cover less area (and simulation volume), and constitute a more limited sample of all rock domains and lithologies in the model.
- Ease of implementation. As additional boreholes are completed, it is relatively simple to recalculate global P_{10} values and, by default, to adjust model P_{32}s.

The fracture set intensities were calculated for the SDM Laxemar 1.2 DFN through the following processes:

1. Construct sampling files (.SAB) that divide Simpevarp and Laxemar subarea cored boreholes into 25 m segments.
2. Generate several realizations of each fracture set using FracWorks XP. Fractures were generated within a cubic simulation region 100 m on a side. A total P_{32} of 20 (m^2/m^3) was specified, and a total of three Monte Carlo runs were carried out to ensure a robust estimation of the simulation P_{10}s and consequently, the P_{32}s/P_{10}s ratio for each 25 m borehole segment.
3. Calculate simulation P_{10}s through simulated exploration sampling using borehole geometries identical to those at Laxemar and Simpevarp. The results are presented in Appendix A
4. Using the methodology specified in Section 3.5.2, compute the P_{32} conversion factor C1 for each segment, in each borehole, using the simulation P_{32}s/P_{10}s ratio. The results are presented in Appendix A
5. Compute P_{10}s for each borehole interval based on core and BIPS logs. Zones containing mapped deformation zones are excluded from the analysis. The results are presented in Appendix B
6. Compute P_{32} for each borehole interval based on observed P_{10}s and the conversion factors for each interval obtained through simulation. The results are presented in Appendix B
7. The resulting P_{32} values are then aggregated by rock domain and by modeling subarea to determine mean and median P_{32}s and the associated standard deviations. The intensity model for the SDM Laxemar 1.2 DFN is presented below in Table 6-28 and Table 6-29. All statistical quantities reported are based on 25 m intervals. Accordingly, the user should scale the variance and other moments for intervals of other lengths.

Model users are encouraged to carefully review Section 5.2, Appendix A, and Appendix B of this report, and determine if the level of uncertainty in the intensity estimates presented in this section are sufficiently small to be adequate.

No distinction between open and sealed fractures is made during the intensity assignment; the average observed open/sealed ratio calculated for each rock domain from the detailed core logging data (p_fract_core.xls) was applied to the total intensity to estimate open and sealed fracture intensities. Cored boreholes KLX02, KLX03, and KLX04 were used to calculate the open-sealed fracture intensity for the Laxemar subarea, while fracture logs from cored boreholes KAV01A, KAV04A, KSH01A, KSH02, and KSH03A were used to calculate the open and sealed fracture intensities for the Simpevarp subarea.

Fractures labeled as ‘partially open’ were considered to be open fractures. In addition, it appears that a number of crush zones and dense zones of small fractures have not been included in the core logs, but broken out as separate SICADA tables. The intensity parameters do not represent either of these types of features, as it was not possible to assign these features to fracture sets using the methodologies set forth for this report. In addition, data from percussion-drilled boreholes was not used to determine DFN fracture set intensities.

Table 6-26. Simpevarp subarea open and sealed fracture ratios.

Rock domain A				
Regional set #	**Open fractures**	**Sealed fractures**	**Total fractures**	**Open percentage**
S_A	738	884	1,622	45.50%
S_B	587	840	1,427	41.14%
S_C	700	869	1,569	44.61%
S_d	2,593	2,470	5,063	51.21%
S_e	464	568	1,032	44.96%

Rock domain B				
Regional set #	**Open fractures**	**Sealed fractures**	**Total fractures**	**Open percentage**
S_A	505	1,394	1,899	26.59%
S_B	553	1,565	2,118	26.11%
S_C	666	1,582	2,248	29.63%
S_d	3,376	7,197	10,573	31.93%
S_e	401	1,348	1,749	22.93%

Rock domain C				
Regional set #	**Open fractures**	**Sealed fractures**	**Total fractures**	**Open percentage**
S_A	420	863	1,283	32.74%
S_B	362	809	1,171	30.91%
S_C	462	824	1,286	35.93%
S_d	1,730	3,868	5,598	30.90%
S_e	298	648	946	31.50%

Table 6-27. Laxemar subarea open and sealed fracture ratios.

Rock domain A				
Regional set #	**Open fractures**	**Sealed fractures**	**Total fractures**	**Open percentage**
S_A	271	367	638	42.48%
S_B	215	353	568	37.85%
S_C	283	403	686	41.25%
S_d	1,477	2,206	3,683	40.10%
S_f	373	514	887	42.05%

Rock domain BA				
Regional set #	Open fractures	Sealed fractures	Total fractures	Open percentage
S_A	203	98	301	67.44%
S_B	205	73	278	73.74%
S_C	145	94	239	60.67%
S_d	770	157	927	83.06%
S_f	288	73	361	79.78%

Rock domain D				
Regional set #	Open fractures	Sealed fractures	Total fractures	Open percentage
S_A	10	146	156	6.41%
S_B	1	93	94	1.06%
S_C	10	52	62	16.13%
S_d	24	582	606	3.96%
S_f	2	80	82	2.44%

Rock domain M(A)				
Regional set #	Open fractures	Sealed fractures	Total fractures	Open percentage
S_A	42	195	237	17.72%
S_B	30	236	266	11.28%
S_C	32	283	315	10.16%
S_d	188	700	888	21.17%
S_f	37	213	250	14.80%

Rock domain M(D)				
Regional set #	Open fractures	Sealed fractures	Total fractures	Open percentage
S_A	25	139	164	15.24%
S_B	15	88	103	14.56%
S_C	37	199	236	15.68%
S_d	189	510	699	27.04%
S_f	41	189	230	17.83%

A comparison of the open-sealed fracture ratios shows good consistency between the two subareas for Domain A, which is the only domain common to both modeling subareas in which there is fracture data. This suggests that the controls on open versus sealed fracture intensity exist independently of domain, although it would increase the confidence in this conclusion if more domains could be tested. One of the other observations that these tables show is that the ratio seems to be largely set independent for a specific subarea and domain. This can be seen in the consistency of the open percentage among the five sets for each subarea and domain. In some instances, the horizontal set S_d has a slightly higher intensity, although this might be due to the apparent inclusion of drilling-induced subhorizontal fractures into the data base (see Section 5.3.2).

Table 6-28. SDM Laxemar 1.2 DFN intensity model, Simpevarp subarea.

Regional set S_A				
Rock domain	Number of sections	P_{32} Mean	Median	Std dev
A	73	2.73	1.89	2.61
B	46	4.39	4.50	2.47
C	32	3.75	3.71	2.12

Regional set S_B				
Rock domain	Number of sections	P_{32} Mean	Median	Std dev
A	73	2.13	1.65	1.72
B	46	4.23	3.35	3.05
C	32	2.55	2.24	1.96

Regional set S_C				
Rock domain	Number of sections	P_{32} Mean	Median	Std dev
A	73	2.25	1.45	1.98
B	46	4.12	3.72	2.22
C	32	3.71	2.46	2.85

Local set S_d (subhorizontal)				
Rock domain	Number of sections	P_{32} Mean	Median	Std dev
A	73	2.75	2.31	1.73
B	46	7.05	7.02	3.12
C	32	4.37	4.69	2.40

Local set S_e				
Rock domain	Number of sections	P_{32} Mean	Median	Std dev
A	73	1.31	0.93	1.25
B	46	2.84	2.59	1.58
C	32	1.60	1.18	1.18

Table 6-29. SDM Laxemar 1.2 DFN intensity model, Laxemar subarea.

Regional set S_A				
Rock domain	Number of sections	P_{32} Mean	Median	Std dev
A	43	1.43	1.43	0.73
BA	7	1.20	1.28	0.56
M(A)	21	1.73	1.17	1.38
M(D)	3	3.60	3.67	0.18
D	8	2.00	1.91	1.41

Regional Set S_B				
Rock domain	Number of sections	P_{32} Mean	Median	Std dev
A	43	1.69	1.23	1.34
BA	7	1.51	1.24	0.78
M(A)	21	2.25	1.71	2.12
M(D)	3	2.27	2.03	1.55
D	8	1.45	1.39	1.14

Regional Set S_C				
Rock domain	Number of sections	P_{32} Mean	Median	Std dev
A	43	1.52	1.12	1.23
BA	7	1.05	0.90	0.43
M(A)	21	1.64	1.27	1.31
M(D)	3	3.81	3.88	0.94
D	8	0.71	0.51	0.74

Local Set S_d				
Rock domain	Number of sections	P_{32} Mean	Median	Std dev
A	43	2.32	1.89	1.58
BA	7	1.16	0.86	0.45
M(A)	21	2.17	1.87	1.29
M(D)	3	4.12	4.15	1.70
D	8	3.14	3.19	1.72

Local Set S_f				
Rock domain	Number of sections	P_{32} Mean	Median	Std dev
A	43	1.40	0.98	1.15
BA	7	1.26	1.17	0.77
M(A)	21	0.71	0.55	0.71
M(D)	3	2.08	1.92	1.44
D	8	0.53	0.32	0.55

The intensity model presented above can be implemented in several ways, depending upon use and whether the set is a regional or local set:

For local sets:

- As a single global intensity value for each rock domain, for each set, utilizing either the mean or median P_{32} value presented above in Table 6-28 and Table 6-29. A modeling team would first determine what rock domain(s) their model region lie within. Fracture sets, using the orientation and size distributions described earlier, would need to be created within each rock domain element separately, using the chosen intensity value.
- As a probability distribution for each fracture set within each rock domain, utilizing the means and standard deviations described above in Table 6-28 and Table 6-29. The end result would be a series of discrete fracture network models, rather than a single unified model.

For regional sets:

- P_{32} for regional sets is associated with the parameters of the fracture size model (see Section 6.2) in rock domains where both outcrop and borehole data were available. One option is to use the intensity which provides the best match with the size model parameters (Tables 6-8, 6-20 and 6-24, respectively) for rock domain A in the Laxemar subregion, and with domains A and B in the Simpevarp subregion.
- For other rock domains, the two alternatives listed for the local sets can be used. In fact, these two options could also be used for rock domain A in Laxemar or domains A and B in Simpevarp as well if the end usage did not require a strict coupling with the size model.

The summary tables for each model sub-region (Section 7.2. and 1.1) contain fracture intensity parameters for open and sealed fractures as a function of rock domain, rather than a single estimate of P_{32}. These values were obtained by multiplying the mean P_{32} intensity in Table 6-28 and Table 6-29 by the open and sealed fracture ratios in Table 6-26 and Table 6-27. If a modeling team chooses to use a different open-sealed ratio, merely use the mean or median P_{32}s presented in Table 6-28 and Table 6-29.

As an example for a local set, the value for intensity for the Simpevarp subarea, rock domain A, regional fracture set S_d for open fractures by obtaining two values from Table 6-26 and Table 6-28. First, the total P_{32} is selected from Table 6-28. The appropriate value is 2.75 m^{-1}. Table 6-26 shows that the percentage of open fractures is 51.21%. Therefore, a mean value of P_{32} for open fractures is 1.41 m^{-1}.

As an example for a regional set for the same domain and subarea, regional set S_C for open fractures could be obtained through the size model match point P_{32} value in Table 6-20 (1.312 m^{-1}). Table 6-26 shows that the percentage of open fractures in this domain is 44.61%. Multiplying the match point P_{32} value by 44.61% yields a value of P_{32} for open fractures of 0.59 m^{-1}.

Alternatively, regional set S_C intensity could be obtained in the exact same fashion as the local sets if the coupling with the size model parameters is not needed. In this option, the total P_{32} is selected from Table 6-28. The appropriate value is 3.75 m^{-1}. Table 6-26 shows that the percentage of open fractures is 44.61%. Therefore, a mean value of P_{32} for open fractures is 1.67 m^{-1}.

As described previously, this value of P_{32} is not necessarily the final value that should be used for a particular model. There are two additional considerations: the scale of the model, and whether fractures above or below a certain size will be excluded.

With regards to model scale, the mass dimension analyses indicated that the intensity of fracturing scales according to a power law function characterized by parameter values presented in Appendix C. For domains on the scale of 100 m or less, the difference between the Euclidean and fractal intensity scaling predictions will be minimal compared to the magnitude of other uncertainties.

If much larger domains are being simulated, then the P_{32} value should be scaled by multiply the value by the ratio of the fractal to the Euclidean scaling functions at the scale of interest. For example, the match point P_{32} for open fractures in set S_C in domain A is 0.59 m^{-1}. There are 320 fractures belonging to regional set S_C in outcrop ASM000025. The area of this outcrop is 418.98 m^2. The mass dimension from Appendix C for this subarea, outcrop and fracture set is 1.915, and the constant term (prefactor) is 3.117. This equation predicts that there would be 338 fractures in the outcrop, which is in good agreement with the actual number of 320 in the database, the difference coming from the model approximation. In an outcrop of 1 km by 2 km (which has an effective radius of 798 m), the equation predicts 1,124,481 fractures over 0.5 m in trace length. A Euclidean model would have predicted an amount proportional to the ratios of the two surface areas, in this case, 1,613,442. The ratio of the predictions is approximately 0.70. Since the ratios between intensity measures like P_{10}, P_{21} and P_{32} are described by constants, this proportion is also valid for scaling P_{32} values. This would imply that the correct P_{32} value would be 0.70 × 0.59 m^{-1} or 0.41 m^{-1}.

If different radius values for the fractures are needed for the model, then the final P_{32} is adjusted according to Equation 6-8.

6.5 Model validation

6.5.1 Discussion

Appendix D summarises verification demonstrations of how size, orientation and intensity is reproduced in a) outcrops and boreholes used for determining DFN parameters b) outcrops and boreholes in each studied rock domain.

The results for the size analyses for the three regional sets indicates that the model reproduces the fracture intensities for these sets, although the match point may occur at very low percentiles of the borehole-derived fracture intensity. This reason this may occur is as follows:

1. There are domains of homogeneous fracture intensity at the scale of tens and hundreds of meters.
2. Adjacent domains can have fracture intensities that differ up to an order of magnitude, which is significant from the standpoint of hydrological or mechanical modeling.
3. The variations exist within the same rock domain and are only partially explained (probably no more than 20%) by factors such as lithology and alteration. The factors that control the variations are largely unknown at this point, as they do not seem to relate to any variables measured and recorded in the fracture or borehole logs.
4. This gives rise to inconsistencies in trying to fit a regional model, since the borehole data may have come from a domain or domains with higher than average fracture intensity, while the outcrop data might lie in a domain of lower or average intensity. Unless there is extensive borehole and outcrop data from which to estimate the mean borehole and outcrop fracture intensities with a much higher degree of confidence than at present, the size model and its associated P_{32} match point contain uncertainty as to whether the size parameters are mean values or something else.

5. Even if it were possible to fit a robust mean size/intensity model, because the factors that control approximately 80% of the observed fracture intensity variations remain unknown, it may prove difficult to create a local model that has a sufficiently accurate combined fracture size/intensity characteristics for local hydrological or mechanical modeling.

What needs to be done in order to address this latter situation is to proceed in one or both of two ways:

1. Determine, in fact, what level of fracture intensity uncertainty is tolerable from the standpoint of hydrological and geomechanical modeling.
2. Carry out a more focused study of the core. Now that intensity domains have been defined through CFI plots, it would be possible to analyze the core to see what geological changes occur at domain boundaries and whether those changes persist through the remainder of the domain. In this way, it may be possible to develop a more accurate predictive model for fracture intensity.

6.5.2 Verification demonstration using KBH02 data

Despite the uncertainties, one borehole, KBH02 in the Simpevarp subarea, was chosen as a test case for verification of the model parameters. This borehole has not been used in the derivation of the model parameters and is one of very few gently dipping long cored boreholes outside of the Äspö Laboratory.

The data from KBH02 /SICADA, 2004a/ contains fractures that have not been interpreted according to the site investigation standard, and thus open and sealed fractures are not distinguished. Also, other additional data such as sections with crush or identified deformation zones are missing in this data set. The borehole fracture data was still considered to be of good quality and a simple frequency measure was calculated using all mapped fractures (both natural and sealed, according to the "old" terminology), cf Table 6-30.

The DFN model parameters used for this test case are shown in Table 6-31.

The verification demonstration were performed in two alternative ways;

Alternative 1: Intensity was deduced for all sets from Table 7-3.
Alternative 2: Intensity for regional sets was deduced from Table 7-2 and for local sets from Table 7-3.

All other input data to both alternatives are identical.

Alternative 1 aims to test the outcome based on what is known from borehole intensity only. In this alternative it is shown that the size distributions (k_r and x_{0r} values) does not effect P_{10} predictions given that sampling is performed with a zero-width borehole.

Alternative 2 aims to test the outcome using the exact parameters given in Table 7-2 and Table 7-3, including the best match k_r, x_{0r} and P_{32} for the regional sets.

Table 6-30. Fracture data from KBH02. P_{10} is calculated based on the mapped borehole length (705.0 m).

Fracture type	Number	P_{10}
Natural	3030	4.29
Sealed	1022	1.44
Total	4052	5.74

Table 6-31. DFN parameters used for the test case.

DFN parameter	Reference	Comments
Orientation	Table 7-1	All sets.
Size	Table 7-2	See text for specifications of k_r and x_{0r} values.
Intensity	Table 7-2 and Table 7-3	Two alternatives presented for rock domain A: Alternative 1 used intensity from Table 7-3 for all sets. Alternative 2 used "match" intensity for regional sets from Table 7-2 and intensity for local sets from Table 7-3.
Spatial model	Poissonian	See Section 6.3.
Model size	50 m × 50 m × 50 m	
Sampling borehole	KBH02 Orientation: 341/13.6 Length: 30 m radius 0 m (line sampling)	15 parallel boreholes were used in the model box to speed up sampling time.
Monte Carlo realizations	25	25 realisations for each set of x_{0r} values in alternative 1 and 7 realisations for the 700 m borehole in alternative 2.

6.5.2.1 Alternative 1

In this alternative, the aim is to test whether the SDM Laxemar 1.2 DFN model produces borehole P_{10} values similar to those observed in borehole KBH02; local variations in the bedrock make exact matches unlikely (see discussion of uncertainties in Section 6.6). Borehole P_{10} is in this case calculated through simulated sampling of the DFN model using a zero-width borehole with an orientation identical to that of KBH02. In this test case, this is considered an analogue to borehole fracture mapping.

In theory, when utilizing line sampling, P_{10} is not related to the size distribution. To show this independence three different x_{0r} values were tested for all powerlaw sets; 0.3, 0.5 and 1. P_{32} values were deduced from Table 7-3 for all sets.

Figure 6-30 shows the results of 25 realizations for each x_{0r} value. The results suggest that P_{10} values obtained from the simulated sampling of a test DFN built from the SDM Laxemar 1.2 model are constant within the limits of this size truncation, given a) that P_{32} is kept constant for each set as in Table 7-3 and b) sampling is performed using a zero-width borehole.

Results for this simulation also suggest that the average simulated P_{10} value is around 6.25 fractures per meter. This result is within 10% of the observed fracture frequency in KBH02. The simulated fracture frequency is, on average, higher than the observed fracture frequency recorded during the 'old' mapping of borehole KBH02. The disparity could possibly be due to the more detailed mapping technique used in the newer boreholes drilled during the site investigation.

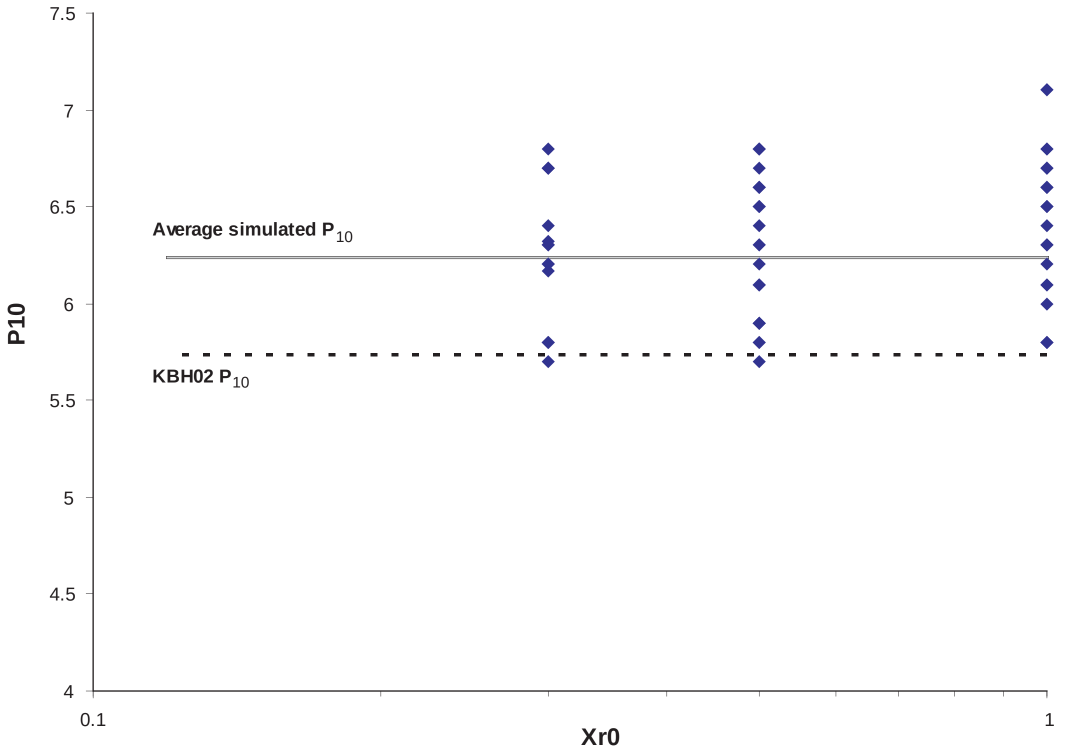

Figure 6-30. *Sampled P_{10} in 3×25 realizations using size estimates as presented above with x_{0r} values ranging between 0.3 to 1. The dashed line shows the mean observed fracture frequency in KBH02 and the gray line shows the mean simulated frequency. The blue dots represent results from each of the 75 realizations*

6.5.2.2 Alternative 2

In this alternative, the aim is to test whether the derived matchpoints for the regional sets (k_r, x_{0r} and P_{32}) in Table 7-2 can be verified in an inclined borehole (KBH02). This alternative is using the exact parameters as given in Table 7-2 for the regional sets, with the best match k_r, x_{0r} and P_{32}, the size distributions for the local sets from Table 7-2 and local set intensity from Table 7-3.

The matchpoint process behind the values in Table 7-2 is described in Section 6.2. This process is based on deformation zones, outcrop fractures and steeply inclined boreholes and aims to replicate the behaviour at all scales at once. However, the borehole intensity of sub-vertical sets is low in steeply inclined boreholes and is difficult to match against due to the severe orientation bias in these sets. It is therefore anticipated from the onset that a verification with an inclined borehole will be difficult.

Results in Figure 6-31 show that the simulated borehole P_{10} is considerably lower than the observed P_{10} in KBH02. The observed P_{10} in KBH02 as well as the simulated sampling has been averaged over 25 m sections. The variability in observed P_{10} span between 1.84 to 10 fractures per meter with a median P_{10} at 5.78 m^{-1} and a mean of 5.74 m^{-1}. The simulated P_{10} span between 0.3 to 5.3 fractures per meter with a P_{10} median at 2.3 m^{-1} and a mean of 2.6 m^{-1}.

The comparatively small span of the simulated data can be explained by the generation process, where only a single P_{32} value have been utilized for each fracture set. In reality, fracture intensity varies within the rock domains and between the different fracture sets. Table 6-29 shows that the standard deviation in P_{32} for each set is between 0.73 to 1.58.

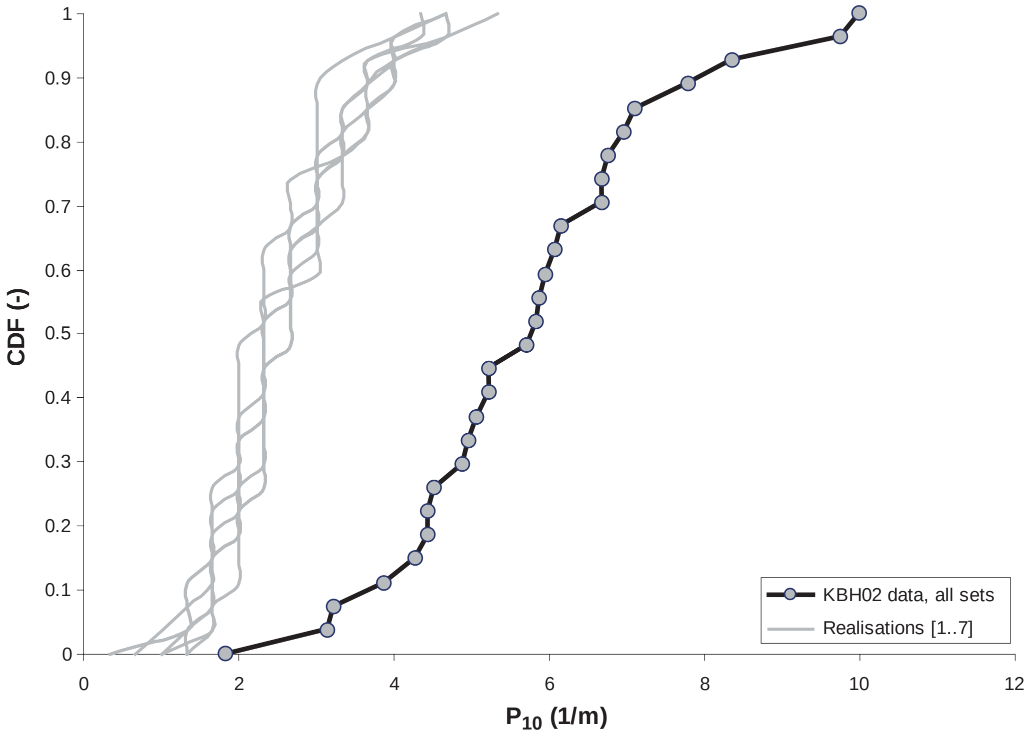

Figure 6-31. *Cumulative density plot of simulated and observed P_{10} in KBH02. P_{10} is sampled in 25 m sections in both simulated and observed borehole.*

Including this variance in the simulation would produce a CDF which would have a much larger span in sampled P_{10} values. Still, the simulated data contain a certain variability in sampled P_{10} which can be attributed to the orientation variability (Fisher kappa) of the different fracture sets.

The generally lower simulated P_{10} values can be explained by the fact that the match point intensity values for the regional sets S_A and S_B given in Table 7-2 represent the 12th to 14th intensity percentiles of the sub-vertical boreholes in the Simpevarp subarea. As KBH02 is an inclined borehole, sub-vertical set intensity will have a large impact on simulated data.

Clearly, this verification demonstrates that the current DFN model is developed on primarily sub-vertical borehole data which has difficulties in reproducing fracture intensity values which are universally valid. To calibrate the model further, more inclined boreholes are necessary in conjunction with detailed outcrop fracture maps.

6.6 Evaluation of DFN model uncertainties

6.6.1 Orientation

The use of spherical probability distributions with associated dispersions and goodness-of-fit statistics leads to a quantifiable level of dispersion uncertainty on fracture orientation. However, an evaluation of the chosen fracture set orientations indicates that none of the fitted fracture sets are statistically significant within a reasonable ($\alpha = 0.1$) confidence level. Whether the current model will accurately predict outcrop patterns at locations not already sampled is unknown.

Several outcrops (ASM000026, ASM000205, ASM000209) possessed fractures, though identified as members of a single set through analysis of contoured polar stereonets, that may actually belong to separate sets (see Figure 4-5 and Figure 4-22). Because these sets overlap to a significant degree, they are difficult to distinguish through contouring. Since orientation set membership impacts both fracture size and intensity calculations, this conceptual model uncertainty in fracture orientations is inherent in the DFN model.

In addition, a limited evaluation of fracture orientation variation with depth (Section 5.1.2 and Section 5.3.2) suggests that set memberships (and perhaps set mean orientations) are not constant with depth. Since the DFN orientation model is based on fracture orientations in surface outcrops, this leads to an additional, non-quantifiable conceptual uncertainty: are the set divisions used producing a model whose fracture orientations are reasonable at repository depths?

6.6.2 Intensity

The most significant uncertainties in the overall are in fracture size and intensity. The analyses have shown that there are substantial variations in fracture intensity at a scale important for modeling. The uncertainty in intensity largely revolves around the issues of intensity extrapolation between scales, spatial variability (especially with depth), and with the presence of censored data. It is not know if the magnitude of these variations would have a significant impact on the flow or mechanical modeling, but since they span at least an order of magnitude and are not predictable, it is likely that they are significant for the downstream models.

6.6.3 Size

The uncertainties in the intensity are the primary causes for the uncertainties in the size model for the regional sets. Currently, the range of possible size parameter values is a direct result of the uncertainty in the outcrop, borehole and deformation zone intensity uncertainties. This is due to both spatial variability in the size and intensity data, and also the lack of comprehensive fracture data in some of the rock domains. If it were possible to obtain accurate regional estimates of fracture intensity for all domains, then the uncertainty of the size models would be commensurately reduced for the regional sets. Moreover, if the uncertainty regarding local (borehole scale) variations in intensity were reduced, the local uncertainty of the size models would also be reduced accordingly.

Another uncertainty concerns the size of the horizontal sets. As it is unlikely that horizontal deformation zones, if they exist, will be easily detected through deformation zone analysis, it is uncertain at present as to whether the horizontal fracture sets found in outcrop and borehole are part of a parent fracture set that has some members with radii of hundreds or thousands of meters, like the regional vertical sets. Since the horizontal fractures do not show mineralogical or morphological differences with the vertical sets, it seems more likely than not that these horizontal fractures do extend in size to hundreds or even thousands of meters. A hydrological model that contains subhorizontal fractures at this scale will behave very differently than one that does not.

7 DFN model summary and conclusions

7.1 Conclusions

Fracture intensity is highly variable across both the Laxemar and Simpevarp model subareas, and appears to be subject to a number of different geological controls. These appear to include host lithology, host rock domain, fracture age, degree of alteration, and presence of ductile or brittle deformation zones. The current level of understanding may be inadequate to characterize fracture intensity controls at either a regional scale or a local scale. Of particular concern are changes in intensity at depth, especially where spikes are noted and no deformation zone has been identified.

For rock domain A in both the Laxemar and especially for most regional sets in domains A and B in the Simpevarp subregion, the P_{32} percentile derived from cored borehole fracture data that allows for a match with the outcrop intensity is typically below the median value. In the case of the Simpevarp subregion, the percentile can be a very low value. This may be due to the spatial heterogeneity in fracture intensity (or perhaps size). The outcrop intensity may represent something other than the mean or median fracture intensity, and so the resulting P_{32} and size model parameters for the regional sets include this uncertainty. Mapped outcrops mapped may not contain a broad enough sample from which to estimate mean fracture intensity with much confidence. The boreholes, on the other hand, contain a much more thorough and comprehensive sample, and so the estimates of the mean intensity from borehole may provide more robust statistical characterization of fracture intensity.

The current DFN orientation distribution model may not be accurate enough for local-scale site studies. The five major aggregated fracture sets for each model subarea are likely a good enough match to regional fracture trends as to allow for a reasonable regional flow and transport model. They are, however, most likely too simple for detailed shaft or tunnel stability analyses or canister failure evaluations. The presence of two or more additional subsets (visible in detailed outcrop trace maps) should be studied further; it may be necessary to further subdivide fracture sets, change set geometries, or change the set statistical distributions in subsequent versions of the SDM.

A limited analysis of borehole fracture orientation data suggests that, like intensity, fracture set orientations are not a static function and vary significantly with depth. The SDM Laxemar 1.2 orientation model is based solely on fracture patterns observed in outcrop, and it may not necessarily match conditions found at depth.

Below follows parameters necessary to implement the SDM Laxemar 1.2 DFN model. The actual implementation is highly dependent on the study area chosen, the level of acceptable uncertainty for the model, and the software tools utilized to complete the simulation. However, a suggested set of modeling steps is presented below:

- Determine the location of the model volume within the greater Simpevarp study region. If the model falls within either the Laxemar or Simpevarp modeling subareas use the tables below relevant to that subarea. The SDM Laxemar 1.2 DFN model has not been developed with significant data from other locations (with the exception of several boreholes from Ävrö Island), and so may not be valid for locations outside of the designated sub-regions.
- Determine several key factors: model scale, fracture size cut-offs, the location and extent of mapped rock domains within the desired modeling regions, the subareas for each domain, and whether open, sealed or total fracturing is to be simulated.

- For each regional fracture set (S_A, S_B, or S_C), generate a fracture population within each rock domain model present within the model volume based on the parameters presented in Sections 7.2 and 7.3. An example is presented below:
  – A model volume 2,000 m × 2,000 m by 2,000 m is chosen within the Laxemar subarea. The model volume contains two rock domains, A and D, of roughly equal size. Two separate iterations will need to be completed to generate a single realization of regional set S_A:
  – Regional set S_A within Rock Domain A: Utilizes the orientation model and dispersion for regional set S_A in the Laxemar subarea, the size model for regional set S_A in the Laxemar subarea, and the intensity model for regional set S_A within rock domain A. Orientations depend upon subarea and set.
  – Regional set S_A within Rock Domain B: Utilizes the orientation model and dispersion for regional set S_A in the Laxemar subarea, the size model for regional set S_A in the Laxemar subarea, and the intensity model for regional set S_A within rock domain B.. Orientations depend upon subarea and set.
- For regional fracture sets S_A, S_B and S_C in the Laxemar subarea and for regional set S_A in the Simpevarp subarea, specific values for x_{0r} and k_r and P_{32} are presented. Different minimum or maximum size cut-offs may be required for downstream modeling purposes, and if so, the P_{32} needs to be adjusted. It is up to individual modeling teams to choose values appropriate for their specific model volume from the parameters presented in Sections 6.2.1.1, 6.2.2.1 and 6.2.2.2. The size parameters depend upon subarea, rock domain and set.
- Specify an intensity value for each fracture set. This depends upon model scale, subarea, domain, set and any size cut-offs. Refer to the example in Section 6.4 for this calculation.
- For each 'local' fracture set (S_d, S_e, S_f), generate a fracture population within each rock domain model present within the model volume based on the parameters presented in Sections 7.2 and 7.3. The methodology is identical as that for the regional sets, except that a specific set of size model parameters is specified for the local fracture sets.

If a different size truncation value for a specific orientation set or rock domain is desired, Equation 6-8 can be used to compute a new volumetric intensity based on a revised truncation threshold (P_{32t}). Additional model parameters, such as termination percentages, modifications of open-sealed ratios, and fracture hydraulic parameters are left to the discretion of the individual modeling teams.

7.2 DFN model summary: Simpevarp subarea

Table 7-1. Orientation statistics for fracture sets in the Laxemar 1.2 DFN model: Simpevarp subarea.

Simpevarp subarea						
Set name	Probability distribution	Mean pole trend	plunge	Dispersion (k)	Goodness of fit K-S	% sig
S_A	Univ Fisher	330.3	6.1	16.80	0.091	N/S
S_B	Univ Fisher	284.6	0.6	10.78	0.076	N/S
S_C	Univ Fisher	201.8	3.7	14.60	0.043	5.20%
S_d	Univ Fisher	84.6	81.8	6.98	0.053	6.90%
S_e	Univ Fisher	67.1	15.5	11.73	0.105	N/S

Table 7-2. Size statistics for fracture sets in the Laxemar 1.2 DFN model: Simpevarp subarea. P_{32} values are for all fractures (open and sealed). See text for explanation of how to use the data.

Simpevarp subarea					
Set name	**Probability distribution**	**Mean radius or exponent (mass)**	**Mean radius or exponent (euclidian)**	**Standard deviation or min radius**	**Match point P_{32} (for regional sets only)**
Domain A					
S_A	Power Law	2.72	2.76	0.864	0.320
S_B	Power Law	2.82	2.87	0.689	0.476
S_C	Power Law	2.92	3.00	0.596	1.312
S_d	Power Law	N/A	3.10	0.150	N/A
S_e	Lognormal	0.23	N/A	0.169	N/A
Domain B					
S_A	Power Law	2.72	2.93	0.367	2.152
S_B	Power Law	2.63	2.84	0.396	0.618
S_C	Power Law	2.66	2.88	0.372	0.868
S_d	Power Law	N/A	3.10	0.150	N/A
S_e	Lognormal	0.23	N/A	0.169	N/A

Table 7-3. Intensity (P_{32}) and spatial model for fracture sets in the Laxemar 1.2 DFN model: Simpevarp subarea. The intended scale of modeling for these intensity values is 30–100 m. See text for explanation of how to use the data.

Spatial Model: Poissonian for model discretization regions of 30–100 m.

P_{32} intensity (m^{-1})**	**Set name**	**Mean P_{32}***	**Open P_{32}**	**Sealed P_{32}**	**% Open fractures**
Domain A	S_A	2.73	1.24	1.49	45.50%
	S_B	2.13	0.87	1.26	41.14%
	S_C	2.25	1.00	1.25	44.61%
	S_d	2.75	1.41	1.34	51.21%
	S_e	1.31	0.59	0.72	44.96%
Domain B	S_A	4.39	1.17	3.22	26.59%
	S_B	4.23	1.10	3.13	26.11%
	S_C	4.12	1.22	2.90	29.63%
	S_d	7.05	2.25	4.80	31.93%
	S_e	2.84	0.65	2.19	22.93%
Domain C	S_A	3.75	1.23	2.52	32.74%
	S_B	2.55	0.79	1.76	30.91%
	S_C	3.71	1.33	2.38	35.93%
	S_d	4.37	1.35	3.02	30.90%
	S_e	1.60	0.50	1.10	31.50%

* See Section 6.4 for explanation. The intensity values calculated here are based on the mean P_{32} reported in Table 6-28. If a coupled size/intensity alternative is preferred, the match point value of P_{32} shown in Table 7-2 should be substituted for the Mean P_{32} for regional sets in Domains A and B. The open and sealed intensity values should also be adjusted accordingly by the ratio shown in this table.

** Note: Rock Domains BA, D, E, F, G, M(A), M(D), and P are not defined within the cored boreholes used to assign DFN intensities.

7.3 DFN model summary: Laxemar subarea

Table 7-4. Orientation statistics for fracture sets in the Laxemar 1.2 DFN model: Laxemar subarea.

Laxemar subarea						
Set name	**Probability distribution**	**Mean pole trend**	**plunge**	**Dispersion (k)**	**Goodness of fit K–S**	**% sig**
S_A	Univ Fisher	338.1	4.5	13.06	0.031	55.60%
S_B	Univ Fisher	100.4	0.2	19.62	0.058	10.70%
S_C	Univ Fisher	212.9	0.9	10.46	0.076	15.70%
S_d	Univ Fisher	3.3	62.1	10.13	0.021	99.70%
S_f	Univ Fisher	243.0	24.4	23.52	0.216	N/S

Table 7-5. Size statistics for fracture sets in the Laxemar 1.2 DFN model: Laxemar subarea. See text for explanation of how to use the data.

Laxemar subarea					
Set name	**Probability distribution**	**Mean radius or exponent (mass)**	**Mean radius or exponent (euclidian)**	**Standard deviation or min radius**	**Match point P_{32} (for regional sets only)**
Domain A					
S_A	Power Law	2.86	2.85	0.328	1.310
S_B	Power Law	2.92	3.04	0.977	1.026
S_C	Power Law	2.88	3.01	0.858	0.974
S_d	Exponential	N/A	0.25	0.250	N/A
S_f	Power Law	3.60	N/A	0.400	N/A

Table 7-6. Intensity (P_{32}) for fracture sets in the Laxemar 1.2 DFN model: Laxemar subarea. P_{32} values are for all fractures (open and sealed). The intended scale of modeling for these intensity values is 30–100 m. See text for explanation of how to use the data.

Spatial Model: Poissonian for model discretization regions of 30–100 m.

P_{32}** intensity (m^{-1})	Set name	Mean P_{32}*	Open P_{32}	Sealed P_{32}	% Open fractures
Domain A	S_A	1.43	0.61	0.82	42.48%
	S_B	1.69	0.64	1.05	37.85%
	S_C	1.52	0.63	0.89	41.25%
	S_d	2.32	0.93	1.39	40.10%
	S_f	1.40	0.59	0.81	42.05%
Domain BA	S_A	1.20	0.81	0.39	67.44%
	S_B	1.51	1.11	0.40	73.74%
	S_C	1.05	0.64	0.41	60.67%
	S_d	1.16	0.97	0.20	83.06%
	S_f	1.26	1.01	0.25	79.78%
Domain D	S_A	2.00	0.13	1.87	6.41%
	S_B	1.45	0.02	1.43	1.06%
	S_C	0.71	0.12	0.59	16.13%
	S_d	3.14	0.13	3.01	3.96%
	S_f	0.53	0.01	0.52	2.44%
Domain M (A)	S_A	1.73	0.31	1.42	17.72%
	S_B	2.25	0.25	1.99	11.28%
	S_C	1.64	0.17	1.48	10.16%
	S_d	2.17	0.46	1.71	21.17%
	S_f	0.71	0.10	0.61	14.80%
Domain M (D)	S_A	3.60	0.55	3.05	15.24%
	S_B	2.27	0.33	1.94	14.56%
	S_C	3.81	0.60	3.21	15.68%
	S_d	4.12	1.11	3.01	27.04%
	S_f	2.08	0.37	1.71	17.83%

* See Section 6.4 for explanation. The intensity values calculated here are based on the mean P_{32}s reported in Table 6-29. If a coupled size/intensity alternative is preferred, the match point value of P_{32} shown in Table 7-5 should be substituted for the Mean P_{32} for regional sets in Domains A and B. The open and sealed intensity values should also be adjusted accordingly by the ratio shown in this table.

** Note: Rock domains B, C, E, F, G, and P not sampled in Laxemar boreholes.

8 Recommendations

The construction of the present DFN model has brought to light several data gaps and areas where the process of constructing and refining future models could be improved. These recommendations consist of acquiring additional data to address some data gaps in the existing model, and also some procedures that can improve the transparency and traceability of the model and its basis. Recommendations in this section have been numbered for reference.

8.1 Data gaps

Several data gaps have been identified in the course of the DFN model development. These gaps relate to the following unresolved questions that appear to have significant impacts on hydrological and mechanical modeling:

- Do the subvertical, meter-scale fracture sets identified in outcrop trace maps form a tectonic continuum with the kilometer-scale deformation zones?
- What formed the subhorizontal fracture sets? What is their maximum size?
- What controls measured fracture intensity variations both in terms of depth and laterally within a specific subarea and rock domain?
- What controls measured fracture orientation variations both in terms of depth and laterally within a specific subarea and rock domain?

8.1.1 Tectonic continuum for vertical fractures

With regards to question 1, fracture data used in this model consisted of meter- to ten meter-scale fracture traces, and traces of kilometer-scale deformation zones. Deformation zones may well be composed predominantly of secondary or anatomizing faults, while the traces in outcrop appear to be primarily individual joints. There was no data available on fractures between these two scales, although the existence of lack thereof would fundamentally change both the hydrological model and the risk associated with future earthquakes. The current model has assumed that this tectonic continuum exists, as it is the more conservative assumption. Future work needs to specifically address the size gap of observed subvertical fractures through geophysical or other means.

- Analysis of the new geophysical, outcrop and borehole data currently being obtained in the Laxemar area would provide the basis for this analysis.

8.1.2 Subhorizontal fracture size

While the problem of subhorizontal fracture size resembles the previous problem for vertical fractures, it contains both additional issues and possibly has an even greater impact on hydrology and earthquake risk. Large horizontal fractures would have a greater impact on earthquake risk as there probability for intersecting vertical canisters is much higher than for a vertical fracture, and also enhance lateral dispersion of radionuclides.

Like the vertical fractures, it is not currently known how large they may become. Unlike the vertical fractures, however, there were no equivalent data sets for horizontal deformation zones available for the DFN model on which to anchor the size distribution even if the tectonic continuum assumption were true. Observation of subhorizontal features in a crystalline rock mass is a more challenging problem as the surface expression of such features is greatly reduced relative to vertical features. It is not clear how to efficiently address this data gap, but it is important to consider for future models because of its importance in hydrology and earthquake risk.

- One way to address this data gap is to more closely study the horizontal fractures in outcrop and core to determine their origin. It is possible that improved understanding of their formation will make it possible to place reasonable limits on their size.

8.1.3 Fracture intensity controls

The inability to derive a size/intensity model that consistently matches borehole and outcrop fracture data in many instances indicates that the current data are inadequate to derive a model that predicts intensity in every subarea and domain. It is clear from the data analysis that intensity within a rock domain is variable, and that the variations can be large. Moreover, the scale of these variations is at the scale of hydrological modeling discretization – tens of meters to hundreds of meters. Pending hydrological sensitivity analyses to determine what level of uncertainty is tolerable, it appears that the variations would have a significant hydrological impact. Moreover, the ability to more accurately specify intensity would greatly increase confidence in the public and regulatory acceptance of the model and calculations based upon it.

This data gap could be reduced in two ways: re-analysis of core/image logs and increased spatial data coverage.

1. Zones of homogeneous fracture intensity have been identified from CFI plots. A re-examination of the core or image log for each of these zones might be useful for identifying what factors remain constant over these zones, or what geological factors change at zone boundariess
2. There is little or no fracture data in several of the rock domains. Additional outcrop and/or borehole data would be very useful to improve the state of knowledge about all rock domains in the SDM, and also additional data in the domains in which the most favorable repository blocks are located.

8.1.4 Fracture orientation controls

Plots of fracture orientation with depth for individual boreholes, as well as contoured stereoplots of fracture poles for individual wells, indicate that there are spatial variations in fracture orientation. The plots of orientation as a function of depth show that there are contiguous zones along the borehole on the order of tens to hundreds of meters where the fracture orientations are similar, and that there can be relatively abrupt changes in the orientations between zones. A comparison among all of the wells shows that the zones are not easily traceable laterally between wells.

This data gap could be reduced in two ways: re-analysis of core/image logs and increased spatial data coverage.

1. This data gap could be narrowed by re-examining the core or image logs for each zone of homogeneous fracture orientations to identify what geological factors appear to remain constant over the zones, but appear to change sharply when orientation zone boundaries are also sharply defined.
2. Another way to reduce the gap would be to obtain and analyze additional data in other rock domains, and to increase the amount of data in the rock domains in which the repository is likely to be located.

8.2 QA improvements

8.2.1 Enhanced transparency and traceability

When the public or regulators review the DFN model, they may find it useful to evaluate for themselves calculations performed as part of the model development. Currently, the final model parameters and the model report will be maintained under SKB QA procedures and be available without recourse to the developer or any of the individuals responsible for analyzing the data and constructing the DFN model. All other project files are not under as rigorous a system. A large number of files have been produced as part of the development of the DFN model, but they are not tracked as rigorously as the input data from Sicada or SDE, or as the final model parameters and report. The current practice followed in this model was to archive all files utilized in the preparation of this model. However, individual intermediate files do not have a standard nomenclature or reference system, and as a result, are not specifically referred to in the text of the report. As matters stand at present, it would be nearly impossible for a person to find the desired files in the archives without recourse to project personnel. This reduces the traceability and transparency of the DFN model development, and could ultimately undermine the acceptance of the model results and results of calculations or decisions based upon the model. This could be improved by:

1. Establishing within SKB a QA procedure for maintaining and archiving all files produced as part of model development.
2. Establishing a tracking system so that these data sets can be easily referenced in reports. This would include development of a file naming convention and a tracking number system.

8.2.2 Data quality review

Over the course of the development of DFN models for Simpevarp, Laxemar and Forsmark, there have been many different types of data errors that have been found and documented. These include, but are not limited to: data that is outside the range of acceptable values or has codes that are not listed as being among the options for the variable of interest; blank fields; inconsistencies in orientation data between the GIS outcrop traces and the orientations contained in Sicada for the same fractures; fractures identified as natural when in fact there are strong indications that they are drilling induced; layers with 0.0 thickness, and so on. Prior to the development of the next generation of models, these generic problems should be corrected. The specific types of tests that could be carried out include:

1. Check that no parameter in the data bases used to prepare the DFN model contains values outside the acceptable range for the parameter.

2. Ensure that there are no blank fields anywhere in the database. If a value was not measured, then a missing value flag should be used. If the parameter is absent, then a flag indicating "absence" should be used. If the field is a comment field and there are no comments, then a "No Comments" flag should be used. All blank fields should be eliminated.
3. Codes for a particular parameter should be of the same data type. An example of a mixed data type is the ISRM Alteration Degree Coding which has acceptable values of 0, 1, 2, r and rr. Mixed data types are an opportunity to mis-use a nominal variable as a continuous variable.
4. Review the borehole data for possible mis-labeling of artificial fractures as natural ones.
5. Perform a rigorous comparison of the GIS and Sicada data bases for outcrop fracture traces to assess the consistency of the number, orientations and trace lengths of fractures between the two data sources, and to resolve any inconsistencies that are found.

9 References

Aitchison J, Brown J A C, 1963. The Lognormal Distribution. University of Cambridge, Dept. of Applied Economics Monograph 5, Cambridge University Press. 176 p.

Bäckblom G, La Pointe P, Tullborg E-L, 2004. Preliminary studies for developing a practical, stepwise field methodology for determining the acceptable proximity of canisters to fracture zones in consideration of future earthquakes. SKB, IPR-04-44, 108 p. Svensk Kärnbränslehantering AB.

Cressie N A C, 1993. Statistics for Spatial Data, Revised Edition, John Wiley and Sons, New York, New York.

Dershowitz W, Lee G, Geier J, Foxford T, LaPointe P, Thomas A, 1998. FracMan Interactive Discrete Feature Data Analysis, Geometric Modeling, and Exploration Simulation User Documentation, Version 2.6, Golder Associates Inc.

Ericsson L, 1987. Programme GH 1a and GH 2c. Fracture mapping on outcrops. Findings of detailed and regional survey. SKB, PR-28-87-05. Svensk Kärnbränslehantering AB.

Fisher R, 1953. Dispersion on a sphere, Royal Soc. London, Proc, Ser A, vol 217, p 295–305.

Garson D, 2004. Nominal-by-Interval Association, Eta, the Correlation Ratio, Course Notes for PA 765: Quantitative Research in Public Administration, http://www2.chass.ncsu.edu/garson/pa765/eta.htm, last accessed 6/6/2005.

La Pointe P, Hudson J, 1985. Characterization and Interpretation of Rock Mass Joint Patterns, Geological Society of America Special Paper No 199.

La Pointe P, Hermanson J, 2005. Statistical model of fractures and deformation zones (SDM Simpevarp 1.2 DFN model), in review.

Mattsson H, Stanfors R, Wahlgren C-H, Stenberg L, 2004a. Oskarshamn site investigation. Geological single-hole interpretation of KSH01A, KSH01B, HSH01, HSH02, and HSH03. SKB P-04-32. Svensk Kärnbränslehantering AB.

Mattsson H, Stanfors R, Wahlgren C-H, Stenberg L, 2004b. Oskarshamn site investigation. Geological single-hole interpretation of KSH02 and KAV01. SKB P-04-133. Svensk Kärnbränslehantering AB.

Munier R, 1989. Brittle tectonics on Äspö, SE Sweden. SKB HRL Progress report 25-89-15. Svensk Kärnbränslehantering AB.

Munier R, 2004. Statistical analysis of fracture data adapted for modelling Discrete Fracture Networks-Version 2. SKB R-04-66. Svensk Kärnbränslehantering AB.

Press W, Flannery B, Teukolsky S, Vetterling W, 1992. Numerical Recipes in C: The Art of Scientific Computing. Cambridge University Press, Cambridge, UK.

SDE, 2004a. SKB GIS Data Delivery 04-86.

SDE, 2004b. SKB GIS Data Delivery 04-88.

SDE, 2004c. SKB GIS Data Delivery 04-90.

SDE, 2004d. SKB GIS Data Delivery, Reference AP PS 400-03-020.

SICADA, 2004a. SKB SICADA Database Delivery 04-04.

SICADA, 2004b. SKB SICADA Database Delivery 04-232.

SICADA, 2004c. SKB SICADA Database Delivery 04-253.

SICADA, 2005a. SKB Data Delivery 05-001.

SICADA, 2005b. SKB Data Delivery 05-002, reference number F51P Sicada_05_002.

SKB, 2004. Preliminary site description, Simpevarp Area – Version 1.1. SKB R-04-25, Svensk Kärnbränslehantering AB.

Tullborg E-L, Larson S Å, Stiberg J-P, 1996. Subsidence and uplift of the present land surface in the southeastern part of the Fennoscandian Shield. GFF, 118: 126–128.

Wahlgren C-H, 2005. Rock type that defines domains, email to afox@golder.com, sent 2/24/2005.

Appendix A

Simulated P_{10}s and Conversion Factors for Laxemar and Simpevarp Boreholes

Laxemar regional set A
Interval length 25 m
Simulated P_{32} 20 1/m

Borehole	Start length (m)	End length (m)	Run 1 # of fracs	Sim P_{10} (1/m)	Run 2 # of fracs	Sim P_{10} (1/m)	Run 3 # of fracs	Sim P_{10} (1/m)	Average # of fracs	Ave sim P_{10} (1/m)	Conversion factor C1
KLX02	200	225	143	5.72	164	6.56	148	5.92	151.67	6.067	3.297
KLX02	225	250	142	5.68	168	6.72	148	5.92	152.67	6.107	3.275
KLX02	250	275	141	5.64	168	6.72	152	6.08	153.67	6.147	3.254
KLX02	275	300	143	5.72	163	6.52	149	5.96	151.67	6.067	3.297
KLX02	300	325	142	5.68	168	6.72	149	5.96	153.00	6.120	3.268
KLX02	325	350	142	5.68	167	6.68	156	6.24	155.00	6.200	3.226
KLX02	350	375	144	5.76	165	6.60	155	6.20	154.67	6.187	3.233
KLX02	375	400	145	5.80	166	6.64	155	6.20	155.33	6.213	3.219
KLX02	400	425	128	5.12	130	5.20	147	5.88	135.00	5.400	3.704
KLX02	425	450	147	5.88	165	6.60	155	6.20	155.67	6.227	3.212
KLX02	450	475	147	5.88	168	6.72	155	6.20	156.67	6.267	3.191
KLX02	475	500	147	5.88	168	6.72	154	6.16	156.33	6.253	3.198
KLX02	500	525	151	6.04	165	6.60	153	6.12	156.33	6.253	3.198
KLX02	525	550	151	6.04	165	6.60	153	6.12	156.33	6.253	3.198
KLX02	550	575	149	5.96	164	6.56	154	6.16	155.67	6.227	3.212
KLX02	575	600	150	6.00	164	6.56	156	6.24	156.67	6.267	3.191
KLX02	600	625	148	5.92	165	6.60	154	6.16	155.67	6.227	3.212
KLX02	625	650	149	5.96	164	6.56	154	6.16	155.67	6.227	3.212
KLX02	650	675	151	6.04	165	6.60	161	6.44	159.00	6.360	3.145
KLX02	675	700	151	6.04	165	6.60	161	6.44	159.00	6.360	3.145
KLX02	700	725	151	6.04	165	6.60	161	6.44	159.00	6.360	3.145
KLX02	725	750	151	6.04	165	6.60	161	6.44	159.00	6.360	3.145
KLX02	750	775	150	6.00	164	6.56	156	6.24	156.67	6.267	3.191
KLX02	775	800	150	6.00	164	6.56	156	6.24	156.67	6.267	3.191
KLX02	800	825	151	6.04	166	6.64	161	6.44	159.33	6.373	3.138
KLX02	825	850	154	6.16	164	6.56	162	6.48	160.00	6.400	3.125
KLX02	850	875	154	6.16	166	6.64	163	6.52	161.00	6.440	3.106
KLX02	875	900	153	6.12	165	6.60	162	6.48	160.00	6.400	3.125
KLX02	900	925	155	6.20	165	6.60	163	6.52	161.00	6.440	3.106
KLX02	925	950	154	6.16	167	6.68	163	6.52	161.33	6.453	3.099
KLX02	950	975	154	6.16	167	6.68	163	6.52	161.33	6.453	3.099
KLX02	975	1,000	155	6.20	164	6.56	163	6.52	160.67	6.427	3.112
KLX02	1,000	1,025	132	5.28	124	4.96	150	6.00	135.33	5.413	3.695
KLX03	100	125	146	5.84	126	5.04	148	5.92	140.00	5.600	3.571
KLX03	125	150	146	5.84	126	5.04	146	5.84	139.33	5.573	3.589
KLX03	150	175	146	5.84	126	5.04	144	5.76	138.67	5.547	3.606
KLX03	175	200	146	5.84	118	4.72	146	5.84	136.67	5.467	3.659

Borehole	Start length (m)	End length (m)	Run 1 # of fracs	Sim P_{10} (1/m)	Run 2 # of fracs	Sim P_{10} (1/m)	Run 3 # of fracs	Sim P_{10} (1/m)	Average # of fracs	Ave sim P_{10} (1/m)	Conversion factor C1
KLX03	200	225	146	5.84	119	4.76	146	5.84	137.00	5.480	3.650
KLX03	225	250	146	5.84	117	4.68	146	5.84	136.33	5.453	3.667
KLX03	250	275	144	5.76	117	4.68	148	5.92	136.33	5.453	3.667
KLX03	275	300	140	5.60	116	4.64	147	5.88	134.33	5.373	3.722
KLX03	300	325	139	5.56	115	4.60	149	5.96	134.33	5.373	3.722
KLX03	325	350	137	5.48	114	4.56	148	5.92	133.00	5.320	3.759
KLX03	350	375	132	5.28	113	4.52	144	5.76	129.67	5.187	3.856
KLX03	375	400	137	5.48	114	4.56	142	5.68	131.00	5.240	3.817
KLX03	400	425	134	5.36	115	4.60	140	5.60	129.67	5.187	3.856
KLX03	425	450	136	5.44	114	4.56	141	5.64	130.33	5.213	3.836
KLX03	450	475	132	5.28	115	4.60	144	5.76	130.33	5.213	3.836
KLX03	475	500	131	5.24	116	4.64	146	5.84	131.00	5.240	3.817
KLX03	500	525	134	5.36	114	4.56	148	5.92	132.00	5.280	3.788
KLX03	525	550	141	5.64	118	4.72	145	5.80	134.67	5.387	3.713
KLX03	550	575	143	5.72	116	4.64	148	5.92	135.67	5.427	3.686
KLX03	575	600	140	5.60	112	4.48	147	5.88	133.00	5.320	3.759
KLX03	600	625	133	5.32	114	4.56	144	5.76	130.33	5.213	3.836
KLX03	625	650	132	5.28	112	4.48	141	5.64	128.33	5.133	3.896
KLX03	650	675	132	5.28	116	4.64	144	5.76	130.67	5.227	3.827
KLX03	675	700	133	5.32	124	4.96	149	5.96	135.33	5.413	3.695
KLX03	700	725	140	5.60	129	5.16	148	5.92	139.00	5.560	3.597
KLX03	725	750	138	5.52	128	5.12	142	5.68	136.00	5.440	3.676
KLX03	750	775	140	5.60	137	5.48	141	5.64	139.33	5.573	3.589
KLX03	775	800	142	5.68	139	5.56	145	5.80	142.00	5.680	3.521
KLX03	800	825	143	5.72	141	5.64	149	5.96	144.33	5.773	3.464
KLX03	825	850	142	5.68	138	5.52	151	6.04	143.67	5.747	3.480
KLX03	850	875	135	5.40	142	5.68	146	5.84	141.00	5.640	3.546
KLX03	875	900	134	5.36	136	5.44	142	5.68	137.33	5.493	3.641
KLX03	900	925	130	5.20	135	5.40	141	5.64	135.33	5.413	3.695
KLX03	925	950	132	5.28	140	5.60	141	5.64	137.67	5.507	3.632
KLX03	950	975	127	5.08	139	5.56	138	5.52	134.67	5.387	3.713
KLX03	975	1,000	133	5.32	138	5.52	136	5.44	135.67	5.427	3.686
KLX03	1,000	1,025	134	5.36	138	5.52	134	5.36	135.33	5.413	3.695
KLX04	100	125	142	5.68	167	6.68	152	6.08	153.67	6.147	3.254
KLX04	125	150	142	5.68	165	6.60	152	6.08	153.00	6.120	3.268
KLX04	150	175	142	5.68	166	6.64	152	6.08	153.33	6.133	3.261
KLX04	175	200	145	5.80	159	6.36	154	6.16	152.67	6.107	3.275
KLX04	200	225	145	5.80	158	6.32	154	6.16	152.33	6.093	3.282
KLX04	225	250	143	5.72	158	6.32	153	6.12	151.33	6.053	3.304
KLX04	250	275	141	5.64	156	6.24	155	6.20	150.67	6.027	3.319
KLX04	275	300	141	5.64	156	6.24	154	6.16	150.33	6.013	3.326
KLX04	300	325	142	5.68	154	6.16	148	5.92	148.00	5.920	3.378
KLX04	325	350	144	5.76	152	6.08	148	5.92	148.00	5.920	3.378
KLX04	350	375	140	5.60	153	6.12	146	5.84	146.33	5.853	3.417
KLX04	375	400	142	5.68	153	6.12	144	5.76	146.33	5.853	3.417

Borehole	Start length (m)	End length (m)	Run 1 # of fracs	Sim P_{10} (1/m)	Run 2 # of fracs	Sim P_{10} (1/m)	Run 3 # of fracs	Sim P_{10} (1/m)	Average # of fracs	Ave sim P_{10} (1/m)	Conversion factor C1
KLX04	400	425	141	5.64	154	6.16	142	5.68	145.67	5.827	3.432
KLX04	425	450	143	5.72	153	6.12	142	5.68	146.00	5.840	3.425
KLX04	450	475	142	5.68	155	6.20	142	5.68	146.33	5.853	3.417
KLX04	475	500	142	5.68	153	6.12	142	5.68	145.67	5.827	3.432
KLX04	500	525	144	5.76	148	5.92	141	5.64	144.33	5.773	3.464
KLX04	525	550	144	5.76	146	5.84	138	5.52	142.67	5.707	3.505
KLX04	550	575	145	5.80	148	5.92	138	5.52	143.67	5.747	3.480
KLX04	575	600	144	5.76	149	5.96	138	5.52	143.67	5.747	3.480
KLX04	600	625	144	5.76	148	5.92	138	5.52	143.33	5.733	3.488
KLX04	625	650	144	5.76	148	5.92	138	5.52	143.33	5.733	3.488
KLX04	650	675	144	5.76	146	5.84	139	5.56	143.00	5.720	3.497
KLX04	675	700	144	5.76	146	5.84	137	5.48	142.33	5.693	3.513
KLX04	700	725	145	5.80	144	5.76	139	5.56	142.67	5.707	3.505
KLX04	725	750	145	5.80	143	5.72	140	5.60	142.67	5.707	3.505
KLX04	750	775	144	5.76	143	5.72	142	5.68	143.00	5.720	3.497
KLX04	775	800	142	5.68	143	5.72	140	5.60	141.67	5.667	3.529
KLX04	800	825	140	5.60	144	5.76	139	5.56	141.00	5.640	3.546
KLX04	825	850	142	5.68	146	5.84	142	5.68	143.33	5.733	3.488
KLX04	850	875	140	5.60	149	5.96	140	5.60	143.00	5.720	3.497
KLX04	875	900	143	5.72	147	5.88	140	5.60	143.33	5.733	3.488
KLX04	900	925	142	5.68	147	5.88	142	5.68	143.67	5.747	3.480
KLX04	925	950	146	5.84	144	5.76	143	5.72	144.33	5.773	3.464
KLX04	950	975	145	5.80	143	5.72	141	5.64	143.00	5.720	3.497
KLX04	975	1,000	146	5.84	142	5.68	143	5.72	143.67	5.747	3.480

Laxemar regional set B
Interval length **25** **m**
Simulated P_{32} (1/m) **20** **1/m**

Borehole	Start length (m)	End length (m)	Run 1 # of fracs	Sim P_{10} (1/m)	Run 2 # of fracs	Sim P_{10} (1/m)	Run 3 # of fracs	Sim P_{10} (1/m)	Ave # of fracs	Simulated P_{10} (1/m)	Conversion factor C1
KLX02	200	225	119	4.76	114	4.56	115	4.60	116.00	4.64	4.31
KLX02	225	250	121	4.84	113	4.52	115	4.60	116.33	4.65	4.30
KLX02	250	275	120	4.80	113	4.52	116	4.64	116.33	4.65	4.30
KLX02	275	300	118	4.72	111	4.44	116	4.64	115.00	4.60	4.35
KLX02	300	325	120	4.80	114	4.56	116	4.64	116.67	4.67	4.29
KLX02	325	350	119	4.76	113	4.52	116	4.64	116.00	4.64	4.31
KLX02	350	375	120	4.80	113	4.52	116	4.64	116.33	4.65	4.30
KLX02	375	400	119	4.76	113	4.52	118	4.72	116.67	4.67	4.29
KLX02	400	425	104	4.16	108	4.32	120	4.80	110.67	4.43	4.52
KLX02	425	450	117	4.68	113	4.52	119	4.76	116.33	4.65	4.30
KLX02	450	475	117	4.68	111	4.44	119	4.76	115.67	4.63	4.32
KLX02	475	500	117	4.68	112	4.48	118	4.72	115.67	4.63	4.32
KLX02	500	525	116	4.64	112	4.48	117	4.68	115.00	4.60	4.35
KLX02	525	550	114	4.56	109	4.36	117	4.68	113.33	4.53	4.41

Borehole	Start length (m)	End length (m)	Run 1 # of fracs	Sim P_{10} (1/m)	Run 2 # of fracs	Sim P_{10} (1/m)	Run 3 # of fracs	Sim P_{10} (1/m)	Ave # of fracs	Simulated P_{10} (1/m)	Conversion factor C1
KLX02	550	575	113	4.52	112	4.48	117	4.68	114.00	4.56	4.39
KLX02	575	600	113	4.52	111	4.44	117	4.68	113.67	4.55	4.40
KLX02	600	625	112	4.48	113	4.52	117	4.68	114.00	4.56	4.39
KLX02	625	650	113	4.52	112	4.48	117	4.68	114.00	4.56	4.39
KLX02	650	675	111	4.44	112	4.48	116	4.64	113.00	4.52	4.42
KLX02	675	700	111	4.44	112	4.48	116	4.64	113.00	4.52	4.42
KLX02	700	725	111	4.44	111	4.44	116	4.64	112.67	4.51	4.44
KLX02	725	750	111	4.44	112	4.48	116	4.64	113.00	4.52	4.42
KLX02	750	775	113	4.52	111	4.44	117	4.68	113.67	4.55	4.40
KLX02	775	800	113	4.52	111	4.44	117	4.68	113.67	4.55	4.40
KLX02	800	825	111	4.44	111	4.44	116	4.64	112.67	4.51	4.44
KLX02	825	850	110	4.40	112	4.48	115	4.60	112.33	4.49	4.45
KLX02	850	875	113	4.52	108	4.32	116	4.64	112.33	4.49	4.45
KLX02	875	900	116	4.64	108	4.32	116	4.64	113.33	4.53	4.41
KLX02	900	925	116	4.64	108	4.32	116	4.64	113.33	4.53	4.41
KLX02	925	950	118	4.72	108	4.32	116	4.64	114.00	4.56	4.39
KLX02	950	975	118	4.72	108	4.32	116	4.64	114.00	4.56	4.39
KLX02	975	1,000	113	4.52	107	4.28	117	4.68	112.33	4.49	4.45
KLX02	1,000	1,025	109	4.36	108	4.32	118	4.72	111.67	4.47	4.48
KLX03	100	125	107	4.28	100	4.00	113	4.52	106.67	4.27	4.69
KLX03	125	150	107	4.28	100	4.00	113	4.52	106.67	4.27	4.69
KLX03	150	175	113	4.52	99	3.96	116	4.64	109.33	4.37	4.57
KLX03	175	200	114	4.56	103	4.12	120	4.80	112.33	4.49	4.45
KLX03	200	225	115	4.60	101	4.04	122	4.88	112.67	4.51	4.44
KLX03	225	250	120	4.80	101	4.04	122	4.88	114.33	4.57	4.37
KLX03	250	275	119	4.76	101	4.04	121	4.84	113.67	4.55	4.40
KLX03	275	300	117	4.68	104	4.16	123	4.92	114.67	4.59	4.36
KLX03	300	325	117	4.68	104	4.16	122	4.88	114.33	4.57	4.37
KLX03	325	350	119	4.76	102	4.08	123	4.92	114.67	4.59	4.36
KLX03	350	375	120	4.80	107	4.28	127	5.08	118.00	4.72	4.24
KLX03	375	400	119	4.76	106	4.24	126	5.04	117.00	4.68	4.27
KLX03	400	425	120	4.80	107	4.28	127	5.08	118.00	4.72	4.24
KLX03	425	450	120	4.80	108	4.32	127	5.08	118.33	4.73	4.23
KLX03	450	475	121	4.84	106	4.24	124	4.96	117.00	4.68	4.27
KLX03	475	500	121	4.84	107	4.28	123	4.92	117.00	4.68	4.27
KLX03	500	525	120	4.80	101	4.04	120	4.80	113.67	4.55	4.40
KLX03	525	550	117	4.68	101	4.04	120	4.80	112.67	4.51	4.44
KLX03	550	575	117	4.68	101	4.04	120	4.80	112.67	4.51	4.44
KLX03	575	600	121	4.84	102	4.08	121	4.84	114.67	4.59	4.36
KLX03	600	625	121	4.84	106	4.24	123	4.92	116.67	4.67	4.29
KLX03	625	650	122	4.88	104	4.16	125	5.00	117.00	4.68	4.27
KLX03	650	675	120	4.80	106	4.24	125	5.00	117.00	4.68	4.27
KLX03	675	700	122	4.88	106	4.24	126	5.04	118.00	4.72	4.24
KLX03	700	725	118	4.72	101	4.04	129	5.16	116.00	4.64	4.31
KLX03	725	750	121	4.84	102	4.08	132	5.28	118.33	4.73	4.23
KLX03	750	775	126	5.04	102	4.08	131	5.24	119.67	4.79	4.18
KLX03	775	800	130	5.20	102	4.08	131	5.24	121.00	4.84	4.13

Borehole	Start length (m)	End length (m)	Run 1 # of fracs	Sim P_{10} (1/m)	Run 2 # of fracs	Sim P_{10} (1/m)	Run 3 # of fracs	Sim P_{10} (1/m)	Ave # of fracs	Simulated P_{10} (1/m)	Conversion factor C1
KLX03	800	825	135	5.40	104	4.16	133	5.32	124.00	4.96	4.03
KLX03	825	850	134	5.36	105	4.20	133	5.32	124.00	4.96	4.03
KLX03	850	875	134	5.36	107	4.28	139	5.56	126.67	5.07	3.95
KLX03	875	900	137	5.48	110	4.40	141	5.64	129.33	5.17	3.87
KLX03	900	925	134	5.36	108	4.32	144	5.76	128.67	5.15	3.89
KLX03	925	950	134	5.36	113	4.52	144	5.76	130.33	5.21	3.84
KLX03	950	975	129	5.16	115	4.60	149	5.96	131.00	5.24	3.82
KLX03	975	1,000	131	5.24	113	4.52	147	5.88	130.33	5.21	3.84
KLX03	1,000	1,025	130	5.20	113	4.52	145	5.80	129.33	5.17	3.87
KLX04	100	125	114	4.56	109	4.36	113	4.52	112.00	4.48	4.46
KLX04	125	150	115	4.60	108	4.32	115	4.60	112.67	4.51	4.44
KLX04	150	175	115	4.60	108	4.32	114	4.56	112.33	4.49	4.45
KLX04	175	200	115	4.60	103	4.12	115	4.60	111.00	4.44	4.50
KLX04	200	225	115	4.60	105	4.20	116	4.64	112.00	4.48	4.46
KLX04	225	250	112	4.48	108	4.32	115	4.60	111.67	4.47	4.48
KLX04	250	275	110	4.40	102	4.08	115	4.60	109.00	4.36	4.59
KLX04	275	300	103	4.12	104	4.16	112	4.48	106.33	4.25	4.70
KLX04	300	325	100	4.00	104	4.16	113	4.52	105.67	4.23	4.73
KLX04	325	350	99	3.96	104	4.16	113	4.52	105.33	4.21	4.75
KLX04	350	375	101	4.04	106	4.24	113	4.52	106.67	4.27	4.69
KLX04	375	400	99	3.96	103	4.12	117	4.68	106.33	4.25	4.70
KLX04	400	425	100	4.00	100	4.00	118	4.72	106.00	4.24	4.72
KLX04	425	450	101	4.04	104	4.16	116	4.64	107.00	4.28	4.67
KLX04	450	475	103	4.12	104	4.16	119	4.76	108.67	4.35	4.60
KLX04	475	500	105	4.20	105	4.20	120	4.80	110.00	4.40	4.55
KLX04	500	525	104	4.16	107	4.28	120	4.80	110.33	4.41	4.53
KLX04	525	550	105	4.20	108	4.32	122	4.88	111.67	4.47	4.48
KLX04	550	575	109	4.36	105	4.20	124	4.96	112.67	4.51	4.44
KLX04	575	600	112	4.48	104	4.16	125	5.00	113.67	4.55	4.40
KLX04	600	625	111	4.44	104	4.16	122	4.88	112.33	4.49	4.45
KLX04	625	650	111	4.44	104	4.16	124	4.96	113.00	4.52	4.42
KLX04	650	675	111	4.44	105	4.20	123	4.92	113.00	4.52	4.42
KLX04	675	700	110	4.40	106	4.24	122	4.88	112.67	4.51	4.44
KLX04	700	725	106	4.24	108	4.32	127	5.08	113.67	4.55	4.40
KLX04	725	750	105	4.20	111	4.44	127	5.08	114.33	4.57	4.37
KLX04	750	775	107	4.28	111	4.44	130	5.20	116.00	4.64	4.31
KLX04	775	800	105	4.20	113	4.52	131	5.24	116.33	4.65	4.30
KLX04	800	825	103	4.12	112	4.48	131	5.24	115.33	4.61	4.34
KLX04	825	850	105	4.20	116	4.64	132	5.28	117.67	4.71	4.25
KLX04	850	875	105	4.20	120	4.80	128	5.12	117.67	4.71	4.25
KLX04	875	900	104	4.16	120	4.80	129	5.16	117.67	4.71	4.25
KLX04	900	925	106	4.24	119	4.76	128	5.12	117.67	4.71	4.25
KLX04	925	950	108	4.32	119	4.76	128	5.12	118.33	4.73	4.23
KLX04	950	975	109	4.36	119	4.76	127	5.08	118.33	4.73	4.23
KLX04	975	1,000	111	4.44	117	4.68	129	5.16	119.00	4.76	4.20

Laxemar regional set C
Interval length **25** **m**
Simulated P_{32} (1/m) **20** **1/m**

Borehole	Start length (m)	End length (m)	Run 1 # of fracs	Sim P_{10} (1/m)	Run 2 # of fracs	Sim P_{10} (1/m)	Run 3 # of fracs	Sim P_{10} (1/m)	Ave # of fracs	Ave sim P_{10} (1/m)	Conversion factor C1
KLX02	200	225	172	6.88	149	5.96	163	6.52	161.33	6.45	3.10
KLX02	225	250	173	6.92	149	5.96	163	6.52	161.67	6.47	3.09
KLX02	250	275	171	6.84	147	5.88	163	6.52	160.33	6.41	3.12
KLX02	275	300	173	6.92	148	5.92	164	6.56	161.67	6.47	3.09
KLX02	300	325	171	6.84	149	5.96	165	6.60	161.67	6.47	3.09
KLX02	325	350	172	6.88	149	5.96	161	6.44	160.67	6.43	3.11
KLX02	350	375	176	7.04	150	6.00	160	6.40	162.00	6.48	3.09
KLX02	375	400	183	7.32	150	6.00	161	6.44	164.67	6.59	3.04
KLX02	400	425	153	6.12	169	6.76	165	6.60	162.33	6.49	3.08
KLX02	425	450	184	7.36	151	6.04	161	6.44	165.33	6.61	3.02
KLX02	450	475	183	7.32	141	5.64	162	6.48	162.00	6.48	3.09
KLX02	475	500	184	7.36	146	5.84	162	6.48	164.00	6.56	3.05
KLX02	500	525	182	7.28	140	5.60	159	6.36	160.33	6.41	3.12
KLX02	525	550	183	7.32	138	5.52	157	6.28	159.33	6.37	3.14
KLX02	550	575	183	7.32	136	5.44	155	6.20	158.00	6.32	3.16
KLX02	575	600	183	7.32	134	5.36	155	6.20	157.33	6.29	3.18
KLX02	600	625	182	7.28	137	5.48	157	6.28	158.67	6.35	3.15
KLX02	625	650	183	7.32	136	5.44	155	6.20	158.00	6.32	3.16
KLX02	650	675	180	7.20	134	5.36	155	6.20	156.33	6.25	3.20
KLX02	675	700	180	7.20	134	5.36	155	6.20	156.33	6.25	3.20
KLX02	700	725	180	7.20	134	5.36	154	6.16	156.00	6.24	3.21
KLX02	725	750	180	7.20	134	5.36	155	6.20	156.33	6.25	3.20
KLX02	750	775	183	7.32	134	5.36	155	6.20	157.33	6.29	3.18
KLX02	775	800	183	7.32	134	5.36	155	6.20	157.33	6.29	3.18
KLX02	800	825	180	7.20	135	5.40	154	6.16	156.33	6.25	3.20
KLX02	825	850	181	7.24	133	5.32	156	6.24	156.67	6.27	3.19
KLX02	850	875	182	7.28	135	5.40	154	6.16	157.00	6.28	3.18
KLX02	875	900	182	7.28	136	5.44	155	6.20	157.67	6.31	3.17
KLX02	900	925	183	7.32	137	5.48	156	6.24	158.67	6.35	3.15
KLX02	925	950	182	7.28	138	5.52	158	6.32	159.33	6.37	3.14
KLX02	950	975	182	7.28	138	5.52	158	6.32	159.33	6.37	3.14
KLX02	975	1,000	181	7.24	136	5.44	155	6.20	157.33	6.29	3.18
KLX02	1,000	1,025	149	5.96	168	6.72	167	6.68	161.33	6.45	3.10
KLX03	100	125	187	7.48	197	7.88	189	7.56	191.00	7.64	2.62
KLX03	125	150	189	7.56	197	7.88	191	7.64	192.33	7.69	2.60
KLX03	150	175	190	7.60	200	8.00	191	7.64	193.67	7.75	2.58
KLX03	175	200	190	7.60	201	8.04	192	7.68	194.33	7.77	2.57
KLX03	200	225	189	7.56	201	8.04	196	7.84	195.33	7.81	2.56
KLX03	225	250	187	7.48	204	8.16	194	7.76	195.00	7.80	2.56
KLX03	250	275	190	7.60	204	8.16	196	7.84	196.67	7.87	2.54
KLX03	275	300	191	7.64	203	8.12	197	7.88	197.00	7.88	2.54
KLX03	300	325	188	7.52	199	7.96	194	7.76	193.67	7.75	2.58
KLX03	325	350	187	7.48	195	7.80	192	7.68	191.33	7.65	2.61

Borehole	Start length (m)	End length (m)	Run 1 # of fracs	Sim P_{10} (1/m)	Run 2 # of fracs	Sim P_{10} (1/m)	Run 3 # of fracs	Sim P_{10} (1/m)	Ave # of fracs	Ave sim P_{10} (1/m)	Conversion factor C1
KLX03	350	375	186	7.44	194	7.76	192	7.68	190.67	7.63	2.62
KLX03	375	400	185	7.40	195	7.80	190	7.60	190.00	7.60	2.63
KLX03	400	425	184	7.36	195	7.80	189	7.56	189.33	7.57	2.64
KLX03	425	450	186	7.44	193	7.72	186	7.44	188.33	7.53	2.65
KLX03	450	475	184	7.36	187	7.48	189	7.56	186.67	7.47	2.68
KLX03	475	500	185	7.40	190	7.60	189	7.56	188.00	7.52	2.66
KLX03	500	525	180	7.20	191	7.64	191	7.64	187.33	7.49	2.67
KLX03	525	550	178	7.12	187	7.48	190	7.60	185.00	7.40	2.70
KLX03	550	575	180	7.20	189	7.56	189	7.56	186.00	7.44	2.69
KLX03	575	600	182	7.28	190	7.60	191	7.64	187.67	7.51	2.66
KLX03	600	625	182	7.28	191	7.64	187	7.48	186.67	7.47	2.68
KLX03	625	650	184	7.36	190	7.60	186	7.44	186.67	7.47	2.68
KLX03	650	675	184	7.36	187	7.48	185	7.40	185.33	7.41	2.70
KLX03	675	700	182	7.28	184	7.36	185	7.40	183.67	7.35	2.72
KLX03	700	725	178	7.12	180	7.20	188	7.52	182.00	7.28	2.75
KLX03	725	750	177	7.08	178	7.12	188	7.52	181.00	7.24	2.76
KLX03	750	775	174	6.96	176	7.04	192	7.68	180.67	7.23	2.77
KLX03	775	800	170	6.80	176	7.04	192	7.68	179.33	7.17	2.79
KLX03	800	825	170	6.80	174	6.96	190	7.60	178.00	7.12	2.81
KLX03	825	850	167	6.68	173	6.92	192	7.68	177.33	7.09	2.82
KLX03	850	875	165	6.60	173	6.92	187	7.48	175.00	7.00	2.86
KLX03	875	900	165	6.60	174	6.96	183	7.32	174.00	6.96	2.87
KLX03	900	925	162	6.48	172	6.88	186	7.44	173.33	6.93	2.88
KLX03	925	950	160	6.40	170	6.80	184	7.36	171.33	6.85	2.92
KLX03	950	975	157	6.28	169	6.76	185	7.40	170.33	6.81	2.94
KLX03	975	1,000	158	6.32	174	6.96	184	7.36	172.00	6.88	2.91
KLX03	1,000	1,025	156	6.24	177	7.08	183	7.32	172.00	6.88	2.91
KLX04	100	125	183	7.32	143	5.72	157	6.28	161.00	6.44	3.11
KLX04	125	150	183	7.32	143	5.72	156	6.24	160.67	6.43	3.11
KLX04	150	175	183	7.32	144	5.76	156	6.24	161.00	6.44	3.11
KLX04	175	200	183	7.32	144	5.76	156	6.24	161.00	6.44	3.11
KLX04	200	225	183	7.32	145	5.80	155	6.20	161.00	6.44	3.11
KLX04	225	250	182	7.28	146	5.84	155	6.20	161.00	6.44	3.11
KLX04	250	275	180	7.20	145	5.80	155	6.20	160.00	6.40	3.13
KLX04	275	300	180	7.20	147	5.88	155	6.20	160.67	6.43	3.11
KLX04	300	325	178	7.12	148	5.92	155	6.20	160.33	6.41	3.12
KLX04	325	350	177	7.08	146	5.84	151	6.04	158.00	6.32	3.16
KLX04	350	375	180	7.20	147	5.88	152	6.08	159.67	6.39	3.13
KLX04	375	400	180	7.20	148	5.92	150	6.00	159.33	6.37	3.14
KLX04	400	425	181	7.24	150	6.00	154	6.16	161.67	6.47	3.09
KLX04	425	450	181	7.24	149	5.96	153	6.12	161.00	6.44	3.11
KLX04	450	475	179	7.16	146	5.84	149	5.96	158.00	6.32	3.16
KLX04	475	500	179	7.16	144	5.76	149	5.96	157.33	6.29	3.18
KLX04	500	525	179	7.16	145	5.80	150	6.00	158.00	6.32	3.16
KLX04	525	550	182	7.28	146	5.84	149	5.96	159.00	6.36	3.14

Borehole	Start length (m)	End length (m)	Run 1 # of fracs	Sim P_{10} (1/m)	Run 2 # of fracs	Sim P_{10} (1/m)	Run 3 # of fracs	Sim P_{10} (1/m)	Ave # of fracs	Ave sim P_{10} (1/m)	Conversion factor C1
KLX04	550	575	182	7.28	149	5.96	150	6.00	160.33	6.41	3.12
KLX04	575	600	180	7.20	145	5.80	147	5.88	157.33	6.29	3.18
KLX04	600	625	178	7.12	143	5.72	148	5.92	156.33	6.25	3.20
KLX04	625	650	178	7.12	142	5.68	148	5.92	156.00	6.24	3.21
KLX04	650	675	178	7.12	140	5.60	150	6.00	156.00	6.24	3.21
KLX04	675	700	176	7.04	139	5.56	153	6.12	156.00	6.24	3.21
KLX04	700	725	175	7.00	141	5.64	151	6.04	155.67	6.23	3.21
KLX04	725	750	174	6.96	144	5.76	152	6.08	156.67	6.27	3.19
KLX04	750	775	176	7.04	146	5.84	150	6.00	157.33	6.29	3.18
KLX04	775	800	176	7.04	147	5.88	150	6.00	157.67	6.31	3.17
KLX04	800	825	179	7.16	146	5.84	149	5.96	158.00	6.32	3.16
KLX04	825	850	179	7.16	148	5.92	149	5.96	158.67	6.35	3.15
KLX04	850	875	179	7.16	148	5.92	151	6.04	159.33	6.37	3.14
KLX04	875	900	179	7.16	148	5.92	151	6.04	159.33	6.37	3.14
KLX04	900	925	177	7.08	149	5.96	152	6.08	159.33	6.37	3.14
KLX04	925	950	177	7.08	150	6.00	151	6.04	159.33	6.37	3.14
KLX04	950	975	178	7.12	149	5.96	151	6.04	159.33	6.37	3.14
KLX04	975	1,000	181	7.24	147	5.88	151	6.04	159.67	6.39	3.13

Laxemar local set D (subhorizontal)
Interval length 25 m
Simulated P_{32} (1/m) 20 1/m

Borehole	Start length (m)	End length (m)	Run 1 # of fracs	Sim P_{10} (1/m)	Run 2 # of fracs	Sim P_{10} (1/m)	Run 3 # of fracs	Sim P_{10} (1/m)	Ave # of fracs	Ave sim P_{10} (1/m)	Conversion factor C1
KLX02	200	225	504	20.16	476	19.04	470	18.80	483.33	19.33	1.034
KLX02	225	250	505	20.20	476	19.04	473	18.92	484.67	19.39	1.032
KLX02	250	275	504	20.16	476	19.04	471	18.84	483.67	19.35	1.034
KLX02	275	300	504	20.16	475	19.00	467	18.68	482.00	19.28	1.037
KLX02	300	325	504	20.16	476	19.04	470	18.80	483.33	19.33	1.034
KLX02	325	350	504	20.16	476	19.04	470	18.80	483.33	19.33	1.034
KLX02	350	375	507	20.28	476	19.04	466	18.64	483.00	19.32	1.035
KLX02	375	400	513	20.52	477	19.08	468	18.72	486.00	19.44	1.029
KLX02	400	425	448	17.92	427	17.08	427	17.08	434.00	17.36	1.152
KLX02	425	450	513	20.52	478	19.12	467	18.68	486.00	19.44	1.029
KLX02	450	475	514	20.56	477	19.08	469	18.76	486.67	19.47	1.027
KLX02	475	500	515	20.60	477	19.08	471	18.84	487.67	19.51	1.025
KLX02	500	525	516	20.64	478	19.12	470	18.80	488.00	19.52	1.025
KLX02	525	550	517	20.68	473	18.92	470	18.80	486.67	19.47	1.027
KLX02	550	575	519	20.76	478	19.12	468	18.72	488.33	19.53	1.024
KLX02	575	600	519	20.76	473	18.92	467	18.68	486.33	19.45	1.028
KLX02	600	625	516	20.64	477	19.08	469	18.76	487.33	19.49	1.026
KLX02	625	650	519	20.76	478	19.12	468	18.72	488.33	19.53	1.024

Borehole	Start length (m)	End length (m)	Run 1 # of fracs	Sim P_{10} (1/m)	Run 2 # of fracs	Sim P_{10} (1/m)	Run 3 # of fracs	Sim P_{10} (1/m)	Ave # of fracs	Ave sim P_{10} (1/m)	Conversion factor C1
KLX02	650	675	521	20.84	472	18.88	467	18.68	486.67	19.47	1.027
KLX02	675	700	521	20.84	472	18.88	467	18.68	486.67	19.47	1.027
KLX02	700	725	520	20.80	471	18.84	468	18.72	486.33	19.45	1.028
KLX02	725	750	521	20.84	472	18.88	467	18.68	486.67	19.47	1.027
KLX02	750	775	519	20.76	473	18.92	467	18.68	486.33	19.45	1.028
KLX02	775	800	519	20.76	473	18.92	467	18.68	486.33	19.45	1.028
KLX02	800	825	520	20.80	471	18.84	467	18.68	486.00	19.44	1.029
KLX02	825	850	520	20.80	470	18.80	466	18.64	485.33	19.41	1.030
KLX02	850	875	521	20.84	470	18.80	470	18.80	487.00	19.48	1.027
KLX02	875	900	523	20.92	473	18.92	473	18.92	489.67	19.59	1.021
KLX02	900	925	522	20.88	473	18.92	473	18.92	489.33	19.57	1.022
KLX02	925	950	519	20.76	478	19.12	473	18.92	490.00	19.60	1.020
KLX02	950	975	519	20.76	478	19.12	473	18.92	490.00	19.60	1.020
KLX02	975	1,000	520	20.80	470	18.80	469	18.76	486.33	19.45	1.028
KLX02	1,000	1,025	447	17.88	417	16.68	414	16.56	426.00	17.04	1.174
KLX03	100	125	416	16.64	381	15.24	390	15.60	395.67	15.83	1.264
KLX03	125	150	414	16.56	382	15.28	394	15.76	396.67	15.87	1.261
KLX03	150	175	417	16.68	384	15.36	394	15.76	398.33	15.93	1.255
KLX03	175	200	417	16.68	384	15.36	393	15.72	398.00	15.92	1.256
KLX03	200	225	416	16.64	386	15.44	396	15.84	399.33	15.97	1.252
KLX03	225	250	417	16.68	385	15.40	395	15.80	399.00	15.96	1.253
KLX03	250	275	420	16.80	387	15.48	395	15.80	400.67	16.03	1.248
KLX03	275	300	419	16.76	386	15.44	395	15.80	400.00	16.00	1.250
KLX03	300	325	423	16.92	391	15.64	398	15.92	404.00	16.16	1.238
KLX03	325	350	424	16.96	393	15.72	398	15.92	405.00	16.20	1.235
KLX03	350	375	426	17.04	393	15.72	397	15.88	405.33	16.21	1.234
KLX03	375	400	424	16.96	394	15.76	401	16.04	406.33	16.25	1.231
KLX03	400	425	424	16.96	394	15.76	401	16.04	406.33	16.25	1.231
KLX03	425	450	423	16.92	394	15.76	401	16.04	406.00	16.24	1.232
KLX03	450	475	427	17.08	392	15.68	404	16.16	407.67	16.31	1.226
KLX03	475	500	430	17.20	393	15.72	403	16.12	408.67	16.35	1.223
KLX03	500	525	422	16.88	393	15.72	404	16.16	406.33	16.25	1.231
KLX03	525	550	426	17.04	391	15.64	396	15.84	404.33	16.17	1.237
KLX03	550	575	419	16.76	392	15.68	398	15.92	403.00	16.12	1.241
KLX03	575	600	422	16.88	394	15.76	405	16.20	407.00	16.28	1.229
KLX03	600	625	428	17.12	390	15.60	405	16.20	407.67	16.31	1.226
KLX03	625	650	428	17.12	392	15.68	406	16.24	408.67	16.35	1.223
KLX03	650	675	431	17.24	394	15.76	403	16.12	409.33	16.37	1.221
KLX03	675	700	431	17.24	395	15.80	405	16.20	410.33	16.41	1.219
KLX03	700	725	426	17.04	388	15.52	409	16.36	407.67	16.31	1.226
KLX03	725	750	425	17.00	395	15.80	410	16.40	410.00	16.40	1.220
KLX03	750	775	427	17.08	396	15.84	410	16.40	411.00	16.44	1.217
KLX03	775	800	425	17.00	396	15.84	413	16.52	411.33	16.45	1.216
KLX03	800	825	432	17.28	403	16.12	408	16.32	414.33	16.57	1.207

Borehole	Start length (m)	End length (m)	Run 1 # of fracs	Sim P_{10} (1/m)	Run 2 # of fracs	Sim P_{10} (1/m)	Run 3 # of fracs	Sim P_{10} (1/m)	Ave # of fracs	Ave sim P_{10} (1/m)	Conversion factor C1
KLX03	825	850	430	17.20	404	16.16	413	16.52	415.67	16.63	1.203
KLX03	850	875	435	17.40	402	16.08	416	16.64	417.67	16.71	1.197
KLX03	875	900	436	17.44	404	16.16	423	16.92	421.00	16.84	1.188
KLX03	900	925	435	17.40	405	16.20	425	17.00	421.67	16.87	1.186
KLX03	925	950	436	17.44	411	16.44	425	17.00	424.00	16.96	1.179
KLX03	950	975	441	17.64	410	16.40	431	17.24	427.33	17.09	1.170
KLX03	975	1,000	439	17.56	414	16.56	435	17.40	429.33	17.17	1.165
KLX03	1,000	1,025	444	17.76	417	16.68	436	17.44	432.33	17.29	1.157
KLX04	100	125	511	20.44	479	19.16	465	18.60	485.00	19.40	1.031
KLX04	125	150	510	20.40	480	19.20	465	18.60	485.00	19.40	1.031
KLX04	150	175	510	20.40	481	19.24	465	18.60	485.33	19.41	1.030
KLX04	175	200	509	20.36	482	19.28	466	18.64	485.67	19.43	1.030
KLX04	200	225	509	20.36	482	19.28	466	18.64	485.67	19.43	1.030
KLX04	225	250	509	20.36	482	19.28	468	18.72	486.33	19.45	1.028
KLX04	250	275	511	20.44	481	19.24	466	18.64	486.00	19.44	1.029
KLX04	275	300	513	20.52	479	19.16	467	18.68	486.33	19.45	1.028
KLX04	300	325	513	20.52	480	19.20	469	18.76	487.33	19.49	1.026
KLX04	325	350	514	20.56	479	19.16	467	18.68	486.67	19.47	1.027
KLX04	350	375	515	20.60	476	19.04	463	18.52	484.67	19.39	1.032
KLX04	375	400	514	20.56	476	19.04	463	18.52	484.33	19.37	1.032
KLX04	400	425	513	20.52	473	18.92	466	18.64	484.00	19.36	1.033
KLX04	425	450	513	20.52	472	18.88	467	18.68	484.00	19.36	1.033
KLX04	450	475	513	20.52	474	18.96	461	18.44	482.67	19.31	1.036
KLX04	475	500	510	20.40	473	18.92	461	18.44	481.33	19.25	1.039
KLX04	500	525	505	20.20	471	18.84	464	18.56	480.00	19.20	1.042
KLX04	525	550	504	20.16	471	18.84	462	18.48	479.00	19.16	1.044
KLX04	550	575	504	20.16	470	18.80	463	18.52	479.00	19.16	1.044
KLX04	575	600	501	20.04	470	18.80	463	18.52	478.00	19.12	1.046
KLX04	600	625	503	20.12	472	18.88	464	18.56	479.67	19.19	1.042
KLX04	625	650	503	20.12	471	18.84	462	18.48	478.67	19.15	1.045
KLX04	650	675	502	20.08	473	18.92	461	18.44	478.67	19.15	1.045
KLX04	675	700	500	20.00	469	18.76	458	18.32	475.67	19.03	1.051
KLX04	700	725	498	19.92	471	18.84	455	18.20	474.67	18.99	1.053
KLX04	725	750	496	19.84	470	18.80	456	18.24	474.00	18.96	1.055
KLX04	750	775	499	19.96	470	18.80	456	18.24	475.00	19.00	1.053
KLX04	775	800	496	19.84	467	18.68	457	18.28	473.33	18.93	1.056
KLX04	800	825	497	19.88	464	18.56	456	18.24	472.33	18.89	1.059
KLX04	825	850	499	19.96	464	18.56	455	18.20	472.67	18.91	1.058
KLX04	850	875	496	19.84	465	18.60	453	18.12	471.33	18.85	1.061
KLX04	875	900	497	19.88	462	18.48	455	18.20	471.33	18.85	1.061
KLX04	900	925	495	19.80	461	18.44	458	18.32	471.33	18.85	1.061
KLX04	925	950	496	19.84	461	18.44	458	18.32	471.67	18.87	1.060
KLX04	950	975	498	19.92	459	18.36	458	18.32	471.67	18.87	1.060
KLX04	975	1,000	497	19.88	457	18.28	457	18.28	470.33	18.81	1.063

Laxemar local set F
Interval length **25** **m**
Simulated P_{32} (1/m) **20** **1/m**

Borehole	Start length (m)	End length (m)	Run 1 # of fracs	Sim P_{10} (1/m)	Run 2 # of fracs	Sim P_{10} (1/m)	Run 3 # of fracs	Sim P_{10} (1/m)	Ave # of fracs	Ave sim P_{10} (1/m)	Conversion factor C1
KLX02	200	225	241	9.64	224	8.96	219	8.76	228.00	9.12	2.19
KLX02	225	250	241	9.64	224	8.96	219	8.76	228.00	9.12	2.19
KLX02	250	275	241	9.64	222	8.88	219	8.76	227.33	9.09	2.20
KLX02	275	300	241	9.64	222	8.88	221	8.84	228.00	9.12	2.19
KLX02	300	325	241	9.64	222	8.88	220	8.80	227.67	9.11	2.20
KLX02	325	350	239	9.56	222	8.88	218	8.72	226.33	9.05	2.21
KLX02	350	375	239	9.56	218	8.72	217	8.68	224.67	8.99	2.23
KLX02	375	400	240	9.60	217	8.68	217	8.68	224.67	8.99	2.23
KLX02	400	425	258	10.32	254	10.16	262	10.48	258.00	10.32	1.94
KLX02	425	450	240	9.60	216	8.64	216	8.64	224.00	8.96	2.23
KLX02	450	475	238	9.52	216	8.64	217	8.68	223.67	8.95	2.24
KLX02	475	500	239	9.56	216	8.64	215	8.60	223.33	8.93	2.24
KLX02	500	525	239	9.56	217	8.68	216	8.64	224.00	8.96	2.23
KLX02	525	550	239	9.56	214	8.56	215	8.60	222.67	8.91	2.25
KLX02	550	575	238	9.52	214	8.56	214	8.56	222.00	8.88	2.25
KLX02	575	600	237	9.48	212	8.48	215	8.60	221.33	8.85	2.26
KLX02	600	625	238	9.52	215	8.60	215	8.60	222.67	8.91	2.25
KLX02	625	650	238	9.52	214	8.56	214	8.56	222.00	8.88	2.25
KLX02	650	675	236	9.44	213	8.52	216	8.64	221.67	8.87	2.26
KLX02	675	700	236	9.44	213	8.52	216	8.64	221.67	8.87	2.26
KLX02	700	725	236	9.44	213	8.52	215	8.60	221.33	8.85	2.26
KLX02	725	750	236	9.44	213	8.52	216	8.64	221.67	8.87	2.26
KLX02	750	775	237	9.48	212	8.48	215	8.60	221.33	8.85	2.26
KLX02	775	800	237	9.48	212	8.48	215	8.60	221.33	8.85	2.26
KLX02	800	825	237	9.48	213	8.52	215	8.60	221.67	8.87	2.26
KLX02	825	850	235	9.40	213	8.52	214	8.56	220.67	8.83	2.27
KLX02	850	875	236	9.44	215	8.60	214	8.56	221.67	8.87	2.26
KLX02	875	900	237	9.48	218	8.72	215	8.60	223.33	8.93	2.24
KLX02	900	925	236	9.44	220	8.80	214	8.56	223.33	8.93	2.24
KLX02	925	950	237	9.48	221	8.84	214	8.56	224.00	8.96	2.23
KLX02	950	975	237	9.48	221	8.84	214	8.56	224.00	8.96	2.23
KLX02	975	1,000	236	9.44	215	8.60	213	8.52	221.33	8.85	2.26
KLX02	1,000	1,025	262	10.48	256	10.24	267	10.68	261.67	10.47	1.91
KLX03	100	125	325	13.00	313	12.52	340	13.60	326.00	13.04	1.53
KLX03	125	150	327	13.08	316	12.64	336	13.44	326.33	13.05	1.53
KLX03	150	175	329	13.16	317	12.68	338	13.52	328.00	13.12	1.52
KLX03	175	200	329	13.16	320	12.80	340	13.60	329.67	13.19	1.52
KLX03	200	225	331	13.24	321	12.84	339	13.56	330.33	13.21	1.51
KLX03	225	250	333	13.32	322	12.88	347	13.88	334.00	13.36	1.50
KLX03	250	275	339	13.56	323	12.92	351	14.04	337.67	13.51	1.48
KLX03	275	300	343	13.72	327	13.08	350	14.00	340.00	13.60	1.47
KLX03	300	325	341	13.64	326	13.04	348	13.92	338.33	13.53	1.48

Borehole	Start length (m)	End length (m)	Run 1 # of fracs	Sim P_{10} (1/m)	Run 2 # of fracs	Sim P_{10} (1/m)	Run 3 # of fracs	Sim P_{10} (1/m)	Ave # of fracs	Ave sim P_{10} (1/m)	Conversion factor C1
KLX03	325	350	340	13.60	327	13.08	346	13.84	337.67	13.51	1.48
KLX03	350	375	342	13.68	324	12.96	348	13.92	338.00	13.52	1.48
KLX03	375	400	342	13.68	325	13.00	347	13.88	338.00	13.52	1.48
KLX03	400	425	341	13.64	324	12.96	345	13.80	336.67	13.47	1.49
KLX03	425	450	341	13.64	322	12.88	346	13.84	336.33	13.45	1.49
KLX03	450	475	343	13.72	324	12.96	343	13.72	336.67	13.47	1.49
KLX03	475	500	342	13.68	323	12.92	345	13.80	336.67	13.47	1.49
KLX03	500	525	333	13.32	318	12.72	337	13.48	329.33	13.17	1.52
KLX03	525	550	328	13.12	312	12.48	334	13.36	324.67	12.99	1.54
KLX03	550	575	329	13.16	316	12.64	341	13.64	328.67	13.15	1.52
KLX03	575	600	331	13.24	321	12.84	338	13.52	330.00	13.20	1.52
KLX03	600	625	336	13.44	320	12.80	334	13.36	330.00	13.20	1.52
KLX03	625	650	334	13.36	318	12.72	336	13.44	329.33	13.17	1.52
KLX03	650	675	339	13.56	320	12.80	341	13.64	333.33	13.33	1.50
KLX03	675	700	340	13.60	317	12.68	341	13.64	332.67	13.31	1.50
KLX03	700	725	339	13.56	317	12.68	351	14.04	335.67	13.43	1.49
KLX03	725	750	339	13.56	319	12.76	352	14.08	336.67	13.47	1.49
KLX03	750	775	337	13.48	323	12.92	355	14.20	338.33	13.53	1.48
KLX03	775	800	342	13.68	326	13.04	359	14.36	342.33	13.69	1.46
KLX03	800	825	345	13.80	327	13.08	361	14.44	344.33	13.77	1.45
KLX03	825	850	348	13.92	332	13.28	358	14.32	346.00	13.84	1.45
KLX03	850	875	347	13.88	337	13.48	357	14.28	347.00	13.88	1.44
KLX03	875	900	347	13.88	336	13.44	360	14.40	347.67	13.91	1.44
KLX03	900	925	349	13.96	335	13.40	358	14.32	347.33	13.89	1.44
KLX03	925	950	350	14.00	332	13.28	355	14.20	345.67	13.83	1.45
KLX03	950	975	355	14.20	333	13.32	356	14.24	348.00	13.92	1.44
KLX03	975	1,000	354	14.16	332	13.28	348	13.92	344.67	13.79	1.45
KLX03	1,000	1,025	359	14.36	331	13.24	347	13.88	345.67	13.83	1.45
KLX04	100	125	241	9.64	218	8.72	218	8.72	225.67	9.03	2.22
KLX04	125	150	242	9.68	219	8.76	219	8.76	226.67	9.07	2.21
KLX04	150	175	242	9.68	219	8.76	219	8.76	226.67	9.07	2.21
KLX04	175	200	243	9.72	220	8.80	218	8.72	227.00	9.08	2.20
KLX04	200	225	243	9.72	221	8.84	219	8.76	227.67	9.11	2.20
KLX04	225	250	241	9.64	220	8.80	217	8.68	226.00	9.04	2.21
KLX04	250	275	237	9.48	219	8.76	213	8.52	223.00	8.92	2.24
KLX04	275	300	237	9.48	219	8.76	214	8.56	223.33	8.93	2.24
KLX04	300	325	237	9.48	219	8.76	214	8.56	223.33	8.93	2.24
KLX04	325	350	234	9.36	220	8.80	212	8.48	222.00	8.88	2.25
KLX04	350	375	232	9.28	216	8.64	213	8.52	220.33	8.81	2.27
KLX04	375	400	229	9.16	216	8.64	211	8.44	218.67	8.75	2.29
KLX04	400	425	228	9.12	219	8.76	211	8.44	219.33	8.77	2.28
KLX04	425	450	229	9.16	218	8.72	211	8.44	219.33	8.77	2.28
KLX04	450	475	228	9.12	214	8.56	207	8.28	216.33	8.65	2.31
KLX04	475	500	229	9.16	213	8.52	208	8.32	216.67	8.67	2.31

Borehole	Start length (m)	End length (m)	Run 1 # of fracs	Sim P_{10} (1/m)	Run 2 # of fracs	Sim P_{10} (1/m)	Run 3 # of fracs	Sim P_{10} (1/m)	Ave # of fracs	Ave sim P_{10} (1/m)	Conversion factor C1
KLX04	500	525	228	9.12	213	8.52	208	8.32	216.33	8.65	2.31
KLX04	525	550	227	9.08	213	8.52	207	8.28	215.67	8.63	2.32
KLX04	550	575	227	9.08	214	8.56	207	8.28	216.00	8.64	2.31
KLX04	575	600	227	9.08	211	8.44	204	8.16	214.00	8.56	2.34
KLX04	600	625	227	9.08	206	8.24	200	8.00	211.00	8.44	2.37
KLX04	625	650	224	8.96	206	8.24	197	7.88	209.00	8.36	2.39
KLX04	650	675	225	9.00	204	8.16	196	7.84	208.33	8.33	2.40
KLX04	675	700	223	8.92	202	8.08	192	7.68	205.67	8.23	2.43
KLX04	700	725	219	8.76	201	8.04	190	7.60	203.33	8.13	2.46
KLX04	725	750	219	8.76	198	7.92	184	7.36	200.33	8.01	2.50
KLX04	750	775	217	8.68	199	7.96	185	7.40	200.33	8.01	2.50
KLX04	775	800	216	8.64	200	8.00	181	7.24	199.00	7.96	2.51
KLX04	800	825	219	8.76	196	7.84	178	7.12	197.67	7.91	2.53
KLX04	825	850	220	8.80	192	7.68	176	7.04	196.00	7.84	2.55
KLX04	850	875	220	8.80	194	7.76	176	7.04	196.67	7.87	2.54
KLX04	875	900	218	8.72	193	7.72	175	7.00	195.33	7.81	2.56
KLX04	900	925	217	8.68	190	7.60	174	6.96	193.67	7.75	2.58
KLX04	925	950	216	8.64	191	7.64	174	6.96	193.67	7.75	2.58
KLX04	950	975	218	8.72	191	7.64	173	6.92	194.00	7.76	2.58
KLX04	975	1,000	217	8.68	190	7.60	171	6.84	192.67	7.71	2.60

Simpevarp regional set A
Interval length **25** **m**
Simulated P_{32} (1/m) **20** **1/m**

Borehole	Start length (m)	End length (m)	Run 1 # of fracs	Sim P_{10} (1/m)	Run 2 # of fracs	Sim P_{10} (1/m)	Run 3 # of fracs	Sim P_{10} (1/m)	Ave # of fracs	Ave sim P_{10} (1/m)	Conversion factor C1
KAV01	0	25	121	4.84	139	5.56	129	5.16	129.67	5.19	3.86
KAV01	25	50	121	4.84	138	5.52	128	5.12	129.00	5.16	3.88
KAV01	50	75	120	4.80	139	5.56	129	5.16	129.33	5.17	3.87
KAV01	75	100	120	4.80	139	5.56	129	5.16	129.33	5.17	3.87
KAV01	100	125	120	4.80	139	5.56	129	5.16	129.33	5.17	3.87
KAV01	125	150	120	4.80	139	5.56	129	5.16	129.33	5.17	3.87
KAV01	150	175	117	4.68	137	5.48	124	4.96	126.00	5.04	3.97
KAV01	175	200	118	4.72	135	5.40	123	4.92	125.33	5.01	3.99
KAV01	200	225	118	4.72	135	5.40	122	4.88	125.00	5.00	4.00
KAV01	225	250	118	4.72	135	5.40	123	4.92	125.33	5.01	3.99
KAV01	250	275	119	4.76	138	5.52	119	4.76	125.33	5.01	3.99
KAV01	275	300	116	4.64	139	5.56	121	4.84	125.33	5.01	3.99
KAV01	300	325	121	4.84	138	5.52	121	4.84	126.67	5.07	3.95
KAV01	325	350	114	4.56	138	5.52	123	4.92	125.00	5.00	4.00
KAV01	350	375	113	4.52	136	5.44	125	5.00	124.67	4.99	4.01
KAV01	375	400	119	4.76	133	5.32	130	5.20	127.33	5.09	3.93
KAV01	400	425	119	4.76	133	5.32	130	5.20	127.33	5.09	3.93

Borehole	Start length (m)	End length (m)	Run 1 # of fracs	Sim P_{10} (1/m)	Run 2 # of fracs	Sim P_{10} (1/m)	Run 3 # of fracs	Sim P_{10} (1/m)	Ave # of fracs	Ave sim P_{10} (1/m)	Conversion factor C1
KAV01	425	450	119	4.76	133	5.32	130	5.20	127.33	5.09	3.93
KAV01	450	475	121	4.84	125	5.00	134	5.36	126.67	5.07	3.95
KAV01	475	500	121	4.84	127	5.08	132	5.28	126.67	5.07	3.95
KAV01	500	525	120	4.80	128	5.12	130	5.20	126.00	5.04	3.97
KAV01	525	550	121	4.84	128	5.12	132	5.28	127.00	5.08	3.94
KAV01	550	575	113	4.52	120	4.80	132	5.28	121.67	4.87	4.11
KAV01	575	600	113	4.52	120	4.80	134	5.36	122.33	4.89	4.09
KAV01	600	625	115	4.60	121	4.84	135	5.40	123.67	4.95	4.04
KAV01	625	650	116	4.64	122	4.88	133	5.32	123.67	4.95	4.04
KAV01	650	675	115	4.60	122	4.88	132	5.28	123.00	4.92	4.07
KAV01	675	700	123	4.92	119	4.76	130	5.20	124.00	4.96	4.03
KAV01	700	725	123	4.92	118	4.72	131	5.24	124.00	4.96	4.03
KAV01	725	750	123	4.92	118	4.72	131	5.24	124.00	4.96	4.03
KAV01	750	775	123	4.92	118	4.72	131	5.24	124.00	4.96	4.03
KAV04A	100	125	131	5.24	137	5.48	123	4.92	130.33	5.21	3.84
KAV04A	125	150	130	5.20	139	5.56	123	4.92	130.67	5.23	3.83
KAV04A	150	175	130	5.20	138	5.52	124	4.96	130.67	5.23	3.83
KAV04A	175	200	130	5.20	139	5.56	123	4.92	130.67	5.23	3.83
KAV04A	200	225	133	5.32	139	5.56	122	4.88	131.33	5.25	3.81
KAV04A	225	250	131	5.24	139	5.56	122	4.88	130.67	5.23	3.83
KAV04A	250	275	131	5.24	139	5.56	122	4.88	130.67	5.23	3.83
KAV04A	275	300	131	5.24	139	5.56	122	4.88	130.67	5.23	3.83
KAV04A	300	325	132	5.28	139	5.56	122	4.88	131.00	5.24	3.82
KAV04A	325	350	130	5.20	138	5.52	123	4.92	130.33	5.21	3.84
KAV04A	350	375	125	5.00	138	5.52	123	4.92	128.67	5.15	3.89
KAV04A	375	400	126	5.04	138	5.52	123	4.92	129.00	5.16	3.88
KAV04A	400	425	125	5.00	137	5.48	122	4.88	128.00	5.12	3.91
KAV04A	425	450	126	5.04	136	5.44	122	4.88	128.00	5.12	3.91
KAV04A	450	475	122	4.88	138	5.52	121	4.84	127.00	5.08	3.94
KAV04A	475	500	120	4.80	139	5.56	119	4.76	126.00	5.04	3.97
KAV04A	500	525	120	4.80	139	5.56	119	4.76	126.00	5.04	3.97
KAV04A	525	550	119	4.76	138	5.52	122	4.88	126.33	5.05	3.96
KAV04A	550	575	119	4.76	137	5.48	122	4.88	126.00	5.04	3.97
KAV04A	575	600	119	4.76	135	5.40	122	4.88	125.33	5.01	3.99
KAV04A	600	625	118	4.72	134	5.36	124	4.96	125.33	5.01	3.99
KAV04A	625	650	118	4.72	131	5.24	123	4.92	124.00	4.96	4.03
KAV04A	650	675	118	4.72	133	5.32	123	4.92	124.67	4.99	4.01
KAV04A	675	700	117	4.68	133	5.32	124	4.96	124.67	4.99	4.01
KAV04A	700	725	118	4.72	132	5.28	123	4.92	124.33	4.97	4.02
KAV04A	725	750	118	4.72	132	5.28	125	5.00	125.00	5.00	4.00
KAV04A	750	775	119	4.76	132	5.28	126	5.04	125.67	5.03	3.98
KAV04A	775	800	117	4.68	132	5.28	127	5.08	125.33	5.01	3.99
KAV04A	800	825	116	4.64	133	5.32	128	5.12	125.67	5.03	3.98
KAV04A	825	850	115	4.60	135	5.40	129	5.16	126.33	5.05	3.96
KAV04A	850	875	114	4.56	133	5.32	129	5.16	125.33	5.01	3.99

Borehole	Start length (m)	End length (m)	Run 1 # of fracs	Sim P_{10} (1/m)	Run 2 # of fracs	Sim P_{10} (1/m)	Run 3 # of fracs	Sim P_{10} (1/m)	Ave # of fracs	Ave sim P_{10} (1/m)	Conversion factor C1
KAV04A	875	900	114	4.56	132	5.28	129	5.16	125.00	5.00	4.00
KAV04A	900	925	113	4.52	133	5.32	130	5.20	125.33	5.01	3.99
KAV04A	925	950	111	4.44	134	5.36	129	5.16	124.67	4.99	4.01
KAV04A	950	975	113	4.52	135	5.40	130	5.20	126.00	5.04	3.97
KAV04A	975	1,000	117	4.68	136	5.44	130	5.20	127.67	5.11	3.92
KSH01A	97	122	134	5.36	123	4.92	140	5.60	132.33	5.29	3.78
KSH01A	122	147	134	5.36	122	4.88	141	5.64	132.33	5.29	3.78
KSH01A	147	172	132	5.28	117	4.68	142	5.68	130.33	5.21	3.84
KSH01A	172	197	131	5.24	120	4.80	137	5.48	129.33	5.17	3.87
KSH01A	197	222	128	5.12	119	4.76	137	5.48	128.00	5.12	3.91
KSH01A	222	247	130	5.20	117	4.68	137	5.48	128.00	5.12	3.91
KSH01A	247	272	129	5.16	119	4.76	137	5.48	128.33	5.13	3.90
KSH01A	272	297	130	5.20	119	4.76	138	5.52	129.00	5.16	3.88
KSH01A	297	322	130	5.20	121	4.84	139	5.56	130.00	5.20	3.85
KSH01A	322	347	126	5.04	121	4.84	138	5.52	128.33	5.13	3.90
KSH01A	347	372	124	4.96	121	4.84	135	5.40	126.67	5.07	3.95
KSH01A	372	397	126	5.04	124	4.96	135	5.40	128.33	5.13	3.90
KSH01A	397	422	124	4.96	125	5.00	136	5.44	128.33	5.13	3.90
KSH01A	422	447	124	4.96	124	4.96	135	5.40	127.67	5.11	3.92
KSH01A	447	472	127	5.08	129	5.16	135	5.40	130.33	5.21	3.84
KSH01A	472	497	128	5.12	125	5.00	136	5.44	129.67	5.19	3.86
KSH01A	497	522	128	5.12	126	5.04	133	5.32	129.00	5.16	3.88
KSH01A	522	547	132	5.28	126	5.04	132	5.28	130.00	5.20	3.85
KSH01A	547	572	131	5.24	125	5.00	132	5.28	129.33	5.17	3.87
KSH01A	572	597	130	5.20	126	5.04	129	5.16	128.33	5.13	3.90
KSH01A	597	622	129	5.16	121	4.84	127	5.08	125.67	5.03	3.98
KSH01A	622	647	131	5.24	122	4.88	128	5.12	127.00	5.08	3.94
KSH01A	647	672	134	5.36	121	4.84	127	5.08	127.33	5.09	3.93
KSH01A	672	697	135	5.40	118	4.72	131	5.24	128.00	5.12	3.91
KSH01A	697	722	136	5.44	118	4.72	131	5.24	128.33	5.13	3.90
KSH01A	722	747	135	5.40	119	4.76	131	5.24	128.33	5.13	3.90
KSH01A	747	772	136	5.44	118	4.72	130	5.20	128.00	5.12	3.91
KSH01A	772	797	133	5.32	118	4.72	130	5.20	127.00	5.08	3.94
KSH01A	797	822	131	5.24	115	4.60	131	5.24	125.67	5.03	3.98
KSH01A	822	847	135	5.40	118	4.72	131	5.24	128.00	5.12	3.91
KSH01A	847	872	136	5.44	113	4.52	131	5.24	126.67	5.07	3.95
KSH01A	872	897	133	5.32	111	4.44	132	5.28	125.33	5.01	3.99
KSH01A	897	922	132	5.28	111	4.44	134	5.36	125.67	5.03	3.98
KSH01A	922	947	134	5.36	109	4.36	134	5.36	125.67	5.03	3.98
KSH01A	947	972	130	5.20	108	4.32	133	5.32	123.67	4.95	4.04
KSH01A	972	997	129	5.16	108	4.32	135	5.40	124.00	4.96	4.03
KSH01A	997	1,022	131	5.24	108	4.32	136	5.44	125.00	5.00	4.00
KSH02	0	25	143	5.72	165	6.60	156	6.24	154.67	6.19	3.23
KSH02	25	50	143	5.72	165	6.60	158	6.32	155.33	6.21	3.22

Borehole	Start length (m)	End length (m)	Run 1 # of fracs	Sim P_{10} (1/m)	Run 2 # of fracs	Sim P_{10} (1/m)	Run 3 # of fracs	Sim P_{10} (1/m)	Ave # of fracs	Ave sim P_{10} (1/m)	Conversion factor C1
KSH02	50	75	144	5.76	165	6.60	156	6.24	155.00	6.20	3.23
KSH02	75	100	136	5.44	158	6.32	144	5.76	146.00	5.84	3.42
KSH02	100	125	135	5.40	157	6.28	146	5.84	146.00	5.84	3.42
KSH02	125	150	132	5.28	158	6.32	145	5.80	145.00	5.80	3.45
KSH02	150	175	132	5.28	158	6.32	145	5.80	145.00	5.80	3.45
KSH02	175	200	133	5.32	158	6.32	144	5.76	145.00	5.80	3.45
KSH02	200	225	131	5.24	158	6.32	145	5.80	144.67	5.79	3.46
KSH02	225	250	132	5.28	157	6.28	144	5.76	144.33	5.77	3.46
KSH02	250	275	131	5.24	157	6.28	149	5.96	145.67	5.83	3.43
KSH02	275	300	132	5.28	157	6.28	146	5.84	145.00	5.80	3.45
KSH02	300	325	132	5.28	157	6.28	149	5.96	146.00	5.84	3.42
KSH02	325	350	131	5.24	157	6.28	145	5.80	144.33	5.77	3.46
KSH02	350	375	131	5.24	155	6.20	145	5.80	143.67	5.75	3.48
KSH02	375	400	131	5.24	150	6.00	145	5.80	142.00	5.68	3.52
KSH02	400	425	126	5.04	137	5.48	132	5.28	131.67	5.27	3.80
KSH02	425	450	133	5.32	149	5.96	145	5.80	142.33	5.69	3.51
KSH02	450	475	133	5.32	150	6.00	145	5.80	142.67	5.71	3.50
KSH02	475	500	132	5.28	148	5.92	146	5.84	142.00	5.68	3.52
KSH02	500	525	131	5.24	147	5.88	146	5.84	141.33	5.65	3.54
KSH02	525	550	132	5.28	147	5.88	146	5.84	141.67	5.67	3.53
KSH02	550	575	132	5.28	148	5.92	145	5.80	141.67	5.67	3.53
KSH02	575	600	132	5.28	147	5.88	145	5.80	141.33	5.65	3.54
KSH02	600	625	132	5.28	147	5.88	145	5.80	141.33	5.65	3.54
KSH02	625	650	131	5.24	148	5.92	146	5.84	141.67	5.67	3.53
KSH02	650	675	131	5.24	146	5.84	145	5.80	140.67	5.63	3.55
KSH02	675	700	130	5.20	147	5.88	145	5.80	140.67	5.63	3.55
KSH02	700	725	130	5.20	145	5.80	145	5.80	140.00	5.60	3.57
KSH02	725	750	129	5.16	145	5.80	143	5.72	139.00	5.56	3.60
KSH02	750	775	130	5.20	146	5.84	144	5.76	140.00	5.60	3.57
KSH02	775	800	131	5.24	142	5.68	144	5.76	139.00	5.56	3.60
KSH02	800	825	132	5.28	140	5.60	143	5.72	138.33	5.53	3.61
KSH02	825	850	131	5.24	141	5.64	139	5.56	137.00	5.48	3.65
KSH02	850	875	131	5.24	136	5.44	140	5.60	135.67	5.43	3.69
KSH02	875	900	131	5.24	134	5.36	138	5.52	134.33	5.37	3.72
KSH02	900	925	130	5.20	133	5.32	136	5.44	133.00	5.32	3.76
KSH02	925	950	129	5.16	134	5.36	137	5.48	133.33	5.33	3.75
KSH02	950	975	128	5.12	134	5.36	136	5.44	132.67	5.31	3.77
KSH02	975	1,000	125	5.00	135	5.40	137	5.48	132.33	5.29	3.78
KSH02	1,000	1,025	126	5.04	136	5.44	136	5.44	132.67	5.31	3.77
KSH03A	100	125	233	9.32	219	8.76	230	9.20	227.33	9.09	2.20
KSH03A	125	150	237	9.48	215	8.60	230	9.20	227.33	9.09	2.20
KSH03A	150	175	240	9.60	217	8.68	231	9.24	229.33	9.17	2.18
KSH03A	175	200	238	9.52	219	8.76	234	9.36	230.33	9.21	2.17
KSH03A	200	225	237	9.48	222	8.88	236	9.44	231.67	9.27	2.16

Borehole	Start length (m)	End length (m)	Run 1 # of fracs	Sim P_{10} (1/m)	Run 2 # of fracs	Sim P_{10} (1/m)	Run 3 # of fracs	Sim P_{10} (1/m)	Ave # of fracs	Ave sim P_{10} (1/m)	Conversion factor C1
KSH03A	225	250	238	9.52	222	8.88	234	9.36	231.33	9.25	2.16
KSH03A	250	275	237	9.48	219	8.76	233	9.32	229.67	9.19	2.18
KSH03A	275	300	236	9.44	220	8.80	230	9.20	228.67	9.15	2.19
KSH03A	300	325	234	9.36	226	9.04	231	9.24	230.33	9.21	2.17
KSH03A	325	350	235	9.40	230	9.20	231	9.24	232.00	9.28	2.16
KSH03A	350	375	238	9.52	232	9.28	240	9.60	236.67	9.47	2.11
KSH03A	375	400	239	9.56	239	9.56	244	9.76	240.67	9.63	2.08
KSH03A	400	425	243	9.72	241	9.64	249	9.96	244.33	9.77	2.05
KSH03A	425	450	243	9.72	248	9.92	251	10.04	247.33	9.89	2.02
KSH03A	450	475	244	9.76	245	9.80	256	10.24	248.33	9.93	2.01
KSH03A	475	500	240	9.60	244	9.76	260	10.40	248.00	9.92	2.02
KSH03A	500	525	240	9.60	247	9.88	259	10.36	248.67	9.95	2.01
KSH03A	525	550	239	9.56	246	9.84	264	10.56	249.67	9.99	2.00
KSH03A	550	575	236	9.44	250	10.00	259	10.36	248.33	9.93	2.01
KSH03A	575	600	234	9.36	248	9.92	258	10.32	246.67	9.87	2.03
KSH03A	600	625	231	9.24	246	9.84	259	10.36	245.33	9.81	2.04
KSH03A	625	650	235	9.40	245	9.80	257	10.28	245.67	9.83	2.04
KSH03A	650	675	236	9.44	245	9.80	263	10.52	248.00	9.92	2.02
KSH03A	675	700	235	9.40	251	10.04	262	10.48	249.33	9.97	2.01
KSH03A	700	725	233	9.32	247	9.88	258	10.32	246.00	9.84	2.03
KSH03A	725	750	233	9.32	248	9.92	259	10.36	246.67	9.87	2.03
KSH03A	750	775	240	9.60	249	9.96	260	10.40	249.67	9.99	2.00
KSH03A	775	800	242	9.68	256	10.24	260	10.40	252.67	10.11	1.98
KSH03A	800	825	246	9.84	262	10.48	262	10.48	256.67	10.27	1.95
KSH03A	825	850	251	10.04	261	10.44	268	10.72	260.00	10.40	1.92
KSH03A	850	875	253	10.12	273	10.92	271	10.84	265.67	10.63	1.88
KSH03A	875	900	264	10.56	276	11.04	281	11.24	273.67	10.95	1.83
KSH03A	900	925	268	10.72	287	11.48	291	11.64	282.00	11.28	1.77
KSH03A	925	950	275	11.00	285	11.40	299	11.96	286.33	11.45	1.75
KSH03A	950	975	267	10.68	285	11.40	304	12.16	285.33	11.41	1.75
KSH03A	975	1,000	263	10.52	290	11.60	312	12.48	288.33	11.53	1.73
KSH03A	1,000	1,025	267	10.68	289	11.56	316	12.64	290.67	11.63	1.72

Simpevarp regional set B
Interval length **25** **m**
Simulated P_{32} (1/m) **20** **1/m**

Borehole	Start length (m)	End length (m)	Run 1 # of fracs	Sim P_{10} (1/m)	Run 1 # of fracs	Sim P_{10} (1/m)	Run 1 # of fracs	Sim P_{10} (1/m)	Ave # of fracs	Ave sim P_{10} (1/m)	Conversion factor C1
KAV01	0	25	147	5.88	141	5.64	163	6.52	150.33	6.01	3.33
KAV01	25	50	147	5.88	142	5.68	163	6.52	150.67	6.03	3.32
KAV01	50	75	147	5.88	140	5.60	163	6.52	150.00	6.00	3.33
KAV01	75	100	148	5.92	140	5.60	163	6.52	150.33	6.01	3.33
KAV01	100	125	148	5.92	140	5.60	163	6.52	150.33	6.01	3.33

Borehole	Start length (m)	End length (m)	Run 1 # of fracs	Sim P_{10} (1/m)	Run 1 # of fracs	Sim P_{10} (1/m)	Run 1 # of fracs	Sim P_{10} (1/m)	Ave # of fracs	Ave sim P_{10} (1/m)	Conversion factor C1
KAV01	125	150	148	5.92	140	5.60	163	6.52	150.33	6.01	3.33
KAV01	150	175	150	6.00	137	5.48	161	6.44	149.33	5.97	3.35
KAV01	175	200	150	6.00	137	5.48	163	6.52	150.00	6.00	3.33
KAV01	200	225	149	5.96	138	5.52	162	6.48	149.67	5.99	3.34
KAV01	225	250	149	5.96	137	5.48	162	6.48	149.33	5.97	3.35
KAV01	250	275	153	6.12	139	5.56	165	6.60	152.33	6.09	3.28
KAV01	275	300	152	6.08	135	5.40	167	6.68	151.33	6.05	3.30
KAV01	300	325	151	6.04	137	5.48	167	6.68	151.67	6.07	3.30
KAV01	325	350	151	6.04	139	5.56	174	6.96	154.67	6.19	3.23
KAV01	350	375	150	6.00	137	5.48	175	7.00	154.00	6.16	3.25
KAV01	375	400	149	5.96	139	5.56	176	7.04	154.67	6.19	3.23
KAV01	400	425	151	6.04	138	5.52	171	6.84	153.33	6.13	3.26
KAV01	425	450	150	6.00	139	5.56	172	6.88	153.67	6.15	3.25
KAV01	450	475	148	5.92	138	5.52	175	7.00	153.67	6.15	3.25
KAV01	475	500	147	5.88	137	5.48	173	6.92	152.33	6.09	3.28
KAV01	500	525	147	5.88	137	5.48	174	6.96	152.67	6.11	3.28
KAV01	525	550	147	5.88	137	5.48	173	6.92	152.33	6.09	3.28
KAV01	550	575	150	6.00	137	5.48	171	6.84	152.67	6.11	3.28
KAV01	575	600	148	5.92	138	5.52	169	6.76	151.67	6.07	3.30
KAV01	600	625	147	5.88	138	5.52	169	6.76	151.33	6.05	3.30
KAV01	625	650	143	5.72	137	5.48	171	6.84	150.33	6.01	3.33
KAV01	650	675	143	5.72	138	5.52	169	6.76	150.00	6.00	3.33
KAV01	675	700	143	5.72	138	5.52	167	6.68	149.33	5.97	3.35
KAV01	700	725	141	5.64	138	5.52	168	6.72	149.00	5.96	3.36
KAV01	725	750	142	5.68	137	5.48	170	6.80	149.67	5.99	3.34
KAV01	750	775	143	5.72	137	5.48	172	6.88	150.67	6.03	3.32
KAV04A	100	125	146	5.84	136	5.44	171	6.84	151.00	6.04	3.31
KAV04A	125	150	146	5.84	135	5.40	172	6.88	151.00	6.04	3.31
KAV04A	150	175	146	5.84	136	5.44	173	6.92	151.67	6.07	3.30
KAV04A	175	200	144	5.76	135	5.40	172	6.88	150.33	6.01	3.33
KAV04A	200	225	143	5.72	134	5.36	172	6.88	149.67	5.99	3.34
KAV04A	225	250	143	5.72	134	5.36	172	6.88	149.67	5.99	3.34
KAV04A	250	275	143	5.72	135	5.40	172	6.88	150.00	6.00	3.33
KAV04A	275	300	144	5.76	135	5.40	172	6.88	150.33	6.01	3.33
KAV04A	300	325	145	5.80	135	5.40	171	6.84	150.33	6.01	3.33
KAV04A	325	350	145	5.80	135	5.40	170	6.80	150.00	6.00	3.33
KAV04A	350	375	143	5.72	134	5.36	170	6.80	149.00	5.96	3.36
KAV04A	375	400	145	5.80	135	5.40	170	6.80	150.00	6.00	3.33
KAV04A	400	425	143	5.72	133	5.32	170	6.80	148.67	5.95	3.36
KAV04A	425	450	143	5.72	132	5.28	170	6.80	148.33	5.93	3.37
KAV04A	450	475	145	5.80	133	5.32	171	6.84	149.67	5.99	3.34
KAV04A	475	500	139	5.56	135	5.40	170	6.80	148.00	5.92	3.38
KAV04A	500	525	139	5.56	133	5.32	171	6.84	147.67	5.91	3.39
KAV04A	525	550	141	5.64	133	5.32	170	6.80	148.00	5.92	3.38

Borehole	Start length (m)	End length (m)	Run 1 # of fracs	Sim P_{10} (1/m)	Run 1 # of fracs	Sim P_{10} (1/m)	Run 1 # of fracs	Sim P_{10} (1/m)	Ave # of fracs	Ave sim P_{10} (1/m)	Conversion factor C1
KAV04A	550	575	140	5.60	131	5.24	168	6.72	146.33	5.85	3.42
KAV04A	575	600	139	5.56	131	5.24	167	6.68	145.67	5.83	3.43
KAV04A	600	625	141	5.64	132	5.28	167	6.68	146.67	5.87	3.41
KAV04A	625	650	141	5.64	133	5.32	166	6.64	146.67	5.87	3.41
KAV04A	650	675	142	5.68	132	5.28	166	6.64	146.67	5.87	3.41
KAV04A	675	700	143	5.72	132	5.28	166	6.64	147.00	5.88	3.40
KAV04A	700	725	141	5.64	133	5.32	166	6.64	146.67	5.87	3.41
KAV04A	725	750	142	5.68	134	5.36	164	6.56	146.67	5.87	3.41
KAV04A	750	775	142	5.68	136	5.44	163	6.52	147.00	5.88	3.40
KAV04A	775	800	142	5.68	138	5.52	164	6.56	148.00	5.92	3.38
KAV04A	800	825	144	5.76	139	5.56	163	6.52	148.67	5.95	3.36
KAV04A	825	850	142	5.68	138	5.52	170	6.80	150.00	6.00	3.33
KAV04A	850	875	143	5.72	138	5.52	170	6.80	150.33	6.01	3.33
KAV04A	875	900	147	5.88	139	5.56	165	6.60	150.33	6.01	3.33
KAV04A	900	925	146	5.84	140	5.60	160	6.40	148.67	5.95	3.36
KAV04A	925	950	145	5.80	140	5.60	161	6.44	148.67	5.95	3.36
KAV04A	950	975	143	5.72	141	5.64	164	6.56	149.33	5.97	3.35
KAV04A	975	1,000	140	5.60	138	5.52	163	6.52	147.00	5.88	3.40
KSH01A	97	122	151	6.04	159	6.36	163	6.52	157.67	6.31	3.17
KSH01A	122	147	151	6.04	158	6.32	164	6.56	157.67	6.31	3.17
KSH01A	147	172	143	5.72	157	6.28	164	6.56	154.67	6.19	3.23
KSH01A	172	197	142	5.68	158	6.32	163	6.52	154.33	6.17	3.24
KSH01A	197	222	138	5.52	156	6.24	162	6.48	152.00	6.08	3.29
KSH01A	222	247	139	5.56	155	6.20	164	6.56	152.67	6.11	3.28
KSH01A	247	272	139	5.56	155	6.20	166	6.64	153.33	6.13	3.26
KSH01A	272	297	137	5.48	155	6.20	165	6.60	152.33	6.09	3.28
KSH01A	297	322	140	5.60	153	6.12	164	6.56	152.33	6.09	3.28
KSH01A	322	347	136	5.44	149	5.96	164	6.56	149.67	5.99	3.34
KSH01A	347	372	131	5.24	151	6.04	167	6.68	149.67	5.99	3.34
KSH01A	372	397	128	5.12	150	6.00	166	6.64	148.00	5.92	3.38
KSH01A	397	422	128	5.12	148	5.92	166	6.64	147.33	5.89	3.39
KSH01A	422	447	126	5.04	148	5.92	169	6.76	147.67	5.91	3.39
KSH01A	447	472	129	5.16	149	5.96	166	6.64	148.00	5.92	3.38
KSH01A	472	497	126	5.04	150	6.00	166	6.64	147.33	5.89	3.39
KSH01A	497	522	132	5.28	148	5.92	167	6.68	149.00	5.96	3.36
KSH01A	522	547	128	5.12	146	5.84	173	6.92	149.00	5.96	3.36
KSH01A	547	572	137	5.48	150	6.00	171	6.84	152.67	6.11	3.28
KSH01A	572	597	142	5.68	150	6.00	174	6.96	155.33	6.21	3.22
KSH01A	597	622	144	5.76	154	6.16	174	6.96	157.33	6.29	3.18
KSH01A	622	647	140	5.60	156	6.24	175	7.00	157.00	6.28	3.18
KSH01A	647	672	140	5.60	154	6.16	174	6.96	156.00	6.24	3.21
KSH01A	672	697	144	5.76	147	5.88	175	7.00	155.33	6.21	3.22
KSH01A	697	722	148	5.92	142	5.68	180	7.20	156.67	6.27	3.19
KSH01A	722	747	151	6.04	141	5.64	182	7.28	158.00	6.32	3.16

Borehole	Start length (m)	End length (m)	Run 1 # of fracs	Sim P_{10} (1/m)	Run 1 # of fracs	Sim P_{10} (1/m)	Run 1 # of fracs	Sim P_{10} (1/m)	Ave # of fracs	Ave sim P_{10} (1/m)	Conversion factor C1
KSH01A	747	772	147	5.88	139	5.56	183	7.32	156.33	6.25	3.20
KSH01A	772	797	150	6.00	138	5.52	178	7.12	155.33	6.21	3.22
KSH01A	797	822	148	5.92	138	5.52	180	7.20	155.33	6.21	3.22
KSH01A	822	847	149	5.96	139	5.56	174	6.96	154.00	6.16	3.25
KSH01A	847	872	149	5.96	137	5.48	175	7.00	153.67	6.15	3.25
KSH01A	872	897	150	6.00	142	5.68	173	6.92	155.00	6.20	3.23
KSH01A	897	922	151	6.04	140	5.60	170	6.80	153.67	6.15	3.25
KSH01A	922	947	157	6.28	141	5.64	173	6.92	157.00	6.28	3.18
KSH01A	947	972	156	6.24	143	5.72	175	7.00	158.00	6.32	3.16
KSH01A	972	997	158	6.32	141	5.64	176	7.04	158.33	6.33	3.16
KSH01A	997	1,022	159	6.36	144	5.76	172	6.88	158.33	6.33	3.16
KSH02	0	25	150	6.00	136	5.44	150	6.00	145.33	5.81	3.44
KSH02	25	50	150	6.00	135	5.40	151	6.04	145.33	5.81	3.44
KSH02	50	75	150	6.00	135	5.40	151	6.04	145.33	5.81	3.44
KSH02	75	100	151	6.04	134	5.36	150	6.00	145.00	5.80	3.45
KSH02	100	125	150	6.00	134	5.36	150	6.00	144.67	5.79	3.46
KSH02	125	150	152	6.08	135	5.40	151	6.04	146.00	5.84	3.42
KSH02	150	175	156	6.24	136	5.44	152	6.08	148.00	5.92	3.38
KSH02	175	200	155	6.20	138	5.52	151	6.04	148.00	5.92	3.38
KSH02	200	225	155	6.20	140	5.60	151	6.04	148.67	5.95	3.36
KSH02	225	250	158	6.32	142	5.68	153	6.12	151.00	6.04	3.31
KSH02	250	275	158	6.32	143	5.72	151	6.04	150.67	6.03	3.32
KSH02	275	300	156	6.24	144	5.76	149	5.96	149.67	5.99	3.34
KSH02	300	325	155	6.20	142	5.68	148	5.92	148.33	5.93	3.37
KSH02	325	350	155	6.20	140	5.60	148	5.92	147.67	5.91	3.39
KSH02	350	375	158	6.32	144	5.76	146	5.84	149.33	5.97	3.35
KSH02	375	400	157	6.28	144	5.76	151	6.04	150.67	6.03	3.32
KSH02	400	425	156	6.24	138	5.52	171	6.84	155.00	6.20	3.23
KSH02	425	450	159	6.36	147	5.88	154	6.16	153.33	6.13	3.26
KSH02	450	475	158	6.32	148	5.92	156	6.24	154.00	6.16	3.25
KSH02	475	500	159	6.36	141	5.64	160	6.40	153.33	6.13	3.26
KSH02	500	525	159	6.36	139	5.56	160	6.40	152.67	6.11	3.28
KSH02	525	550	160	6.40	139	5.56	160	6.40	153.00	6.12	3.27
KSH02	550	575	160	6.40	140	5.60	160	6.40	153.33	6.13	3.26
KSH02	575	600	162	6.48	141	5.64	159	6.36	154.00	6.16	3.25
KSH02	600	625	160	6.40	139	5.56	160	6.40	153.00	6.12	3.27
KSH02	625	650	160	6.40	139	5.56	161	6.44	153.33	6.13	3.26
KSH02	650	675	160	6.40	139	5.56	163	6.52	154.00	6.16	3.25
KSH02	675	700	159	6.36	138	5.52	165	6.60	154.00	6.16	3.25
KSH02	700	725	158	6.32	137	5.48	165	6.60	153.33	6.13	3.26
KSH02	725	750	158	6.32	138	5.52	164	6.56	153.33	6.13	3.26
KSH02	750	775	158	6.32	138	5.52	164	6.56	153.33	6.13	3.26
KSH02	775	800	156	6.24	136	5.44	169	6.76	153.67	6.15	3.25
KSH02	800	825	156	6.24	137	5.48	165	6.60	152.67	6.11	3.28

Borehole	Start length (m)	End length (m)	Run 1 # of fracs	Sim P_{10} (1/m)	Run 1 # of fracs	Sim P_{10} (1/m)	Run 1 # of fracs	Sim P_{10} (1/m)	Ave # of fracs	Ave sim P_{10} (1/m)	Conversion factor C1
KSH02	825	850	155	6.20	136	5.44	166	6.64	152.33	6.09	3.28
KSH02	850	875	156	6.24	136	5.44	167	6.68	153.00	6.12	3.27
KSH02	875	900	154	6.16	134	5.36	167	6.68	151.67	6.07	3.30
KSH02	900	925	151	6.04	134	5.36	166	6.64	150.33	6.01	3.33
KSH02	925	950	150	6.00	135	5.40	166	6.64	150.33	6.01	3.33
KSH02	950	975	154	6.16	136	5.44	169	6.76	153.00	6.12	3.27
KSH02	975	1,000	154	6.16	137	5.48	168	6.72	153.00	6.12	3.27
KSH02	1,000	1,025	153	6.12	136	5.44	168	6.72	152.33	6.09	3.28
KSH03A	100	125	291	11.64	272	10.88	287	11.48	283.33	11.33	1.76
KSH03A	125	150	288	11.52	265	10.60	279	11.16	277.33	11.09	1.80
KSH03A	150	175	288	11.52	266	10.64	276	11.04	276.67	11.07	1.81
KSH03A	175	200	287	11.48	265	10.60	270	10.80	274.00	10.96	1.82
KSH03A	200	225	288	11.52	267	10.68	270	10.80	275.00	11.00	1.82
KSH03A	225	250	286	11.44	264	10.56	272	10.88	274.00	10.96	1.82
KSH03A	250	275	285	11.40	264	10.56	274	10.96	274.33	10.97	1.82
KSH03A	275	300	283	11.32	262	10.48	274	10.96	273.00	10.92	1.83
KSH03A	300	325	278	11.12	261	10.44	268	10.72	269.00	10.76	1.86
KSH03A	325	350	272	10.88	255	10.20	263	10.52	263.33	10.53	1.90
KSH03A	350	375	271	10.84	257	10.28	257	10.28	261.67	10.47	1.91
KSH03A	375	400	268	10.72	248	9.92	261	10.44	259.00	10.36	1.93
KSH03A	400	425	260	10.40	243	9.72	254	10.16	252.33	10.09	1.98
KSH03A	425	450	255	10.20	240	9.60	248	9.92	247.67	9.91	2.02
KSH03A	450	475	253	10.12	238	9.52	244	9.76	245.00	9.80	2.04
KSH03A	475	500	250	10.00	239	9.56	231	9.24	240.00	9.60	2.08
KSH03A	500	525	243	9.72	241	9.64	227	9.08	237.00	9.48	2.11
KSH03A	525	550	237	9.48	236	9.44	218	8.72	230.33	9.21	2.17
KSH03A	550	575	233	9.32	233	9.32	216	8.64	227.33	9.09	2.20
KSH03A	575	600	236	9.44	231	9.24	211	8.44	226.00	9.04	2.21
KSH03A	600	625	230	9.20	224	8.96	210	8.40	221.33	8.85	2.26
KSH03A	625	650	223	8.92	223	8.92	197	7.88	214.33	8.57	2.33
KSH03A	650	675	219	8.76	211	8.44	192	7.68	207.33	8.29	2.41
KSH03A	675	700	215	8.60	200	8.00	190	7.60	201.67	8.07	2.48
KSH03A	700	725	211	8.44	195	7.80	197	7.88	201.00	8.04	2.49
KSH03A	725	750	208	8.32	192	7.68	195	7.80	198.33	7.93	2.52
KSH03A	750	775	196	7.84	189	7.56	189	7.56	191.33	7.65	2.61
KSH03A	775	800	188	7.52	168	6.72	193	7.72	183.00	7.32	2.73
KSH03A	800	825	191	7.64	171	6.84	199	7.96	187.00	7.48	2.67
KSH03A	825	850	191	7.64	162	6.48	196	7.84	183.00	7.32	2.73
KSH03A	850	875	188	7.52	165	6.60	198	7.92	183.67	7.35	2.72
KSH03A	875	900	190	7.60	163	6.52	192	7.68	181.67	7.27	2.75
KSH03A	900	925	188	7.52	161	6.44	189	7.56	179.33	7.17	2.79
KSH03A	925	950	182	7.28	161	6.44	182	7.28	175.00	7.00	2.86
KSH03A	950	975	174	6.96	160	6.40	183	7.32	172.33	6.89	2.90
KSH03A	975	1,000	173	6.92	157	6.28	179	7.16	169.67	6.79	2.95
KSH03A	1,000	1,025	175	7.00	159	6.36	180	7.20	171.33	6.85	2.92

Simpevarp regional set C
Interval length 25 m
Simulated P_{32} (1/m) 20 1/m

Borehole	Start length (m)	End length (m)	Run 1 # of fracs	Sim P_{10} (1/m)	Run 2 # of fracs	Sim P_{10} (1/m)	Run 3 # of fracs	Sim P_{10} (1/m)	Ave # of fracs	Ave sim P_{10} (1/m)	Conversion factor C1
KAV01	0	25	151	6.04	152	6.08	149	5.96	150.67	6.03	3.32
KAV01	25	50	153	6.12	152	6.08	149	5.96	151.33	6.05	3.30
KAV01	50	75	153	6.12	152	6.08	149	5.96	151.33	6.05	3.30
KAV01	75	100	153	6.12	152	6.08	149	5.96	151.33	6.05	3.30
KAV01	100	125	152	6.08	154	6.16	149	5.96	151.67	6.07	3.30
KAV01	125	150	152	6.08	154	6.16	149	5.96	151.67	6.07	3.30
KAV01	150	175	154	6.16	150	6.00	147	5.88	150.33	6.01	3.33
KAV01	175	200	151	6.04	149	5.96	147	5.88	149.00	5.96	3.36
KAV01	200	225	153	6.12	149	5.96	148	5.92	150.00	6.00	3.33
KAV01	225	250	154	6.16	149	5.96	147	5.88	150.00	6.00	3.33
KAV01	250	275	155	6.20	150	6.00	149	5.96	151.33	6.05	3.30
KAV01	275	300	154	6.16	150	6.00	149	5.96	151.00	6.04	3.31
KAV01	300	325	150	6.00	149	5.96	148	5.92	149.00	5.96	3.36
KAV01	325	350	153	6.12	150	6.00	150	6.00	151.00	6.04	3.31
KAV01	350	375	156	6.24	151	6.04	146	5.84	151.00	6.04	3.31
KAV01	375	400	160	6.40	151	6.04	147	5.88	152.67	6.11	3.28
KAV01	400	425	155	6.20	150	6.00	146	5.84	150.33	6.01	3.33
KAV01	425	450	155	6.20	148	5.92	145	5.80	149.33	5.97	3.35
KAV01	450	475	161	6.44	151	6.04	144	5.76	152.00	6.08	3.29
KAV01	475	500	162	6.48	153	6.12	145	5.80	153.33	6.13	3.26
KAV01	500	525	157	6.28	154	6.16	144	5.76	151.67	6.07	3.30
KAV01	525	550	161	6.44	153	6.12	145	5.80	153.00	6.12	3.27
KAV01	550	575	160	6.40	155	6.20	146	5.84	153.67	6.15	3.25
KAV01	575	600	160	6.40	154	6.16	146	5.84	153.33	6.13	3.26
KAV01	600	625	161	6.44	157	6.28	146	5.84	154.67	6.19	3.23
KAV01	625	650	161	6.44	158	6.32	145	5.80	154.67	6.19	3.23
KAV01	650	675	162	6.48	158	6.32	146	5.84	155.33	6.21	3.22
KAV01	675	700	163	6.52	156	6.24	147	5.88	155.33	6.21	3.22
KAV01	700	725	162	6.48	155	6.20	149	5.96	155.33	6.21	3.22
KAV01	725	750	165	6.60	156	6.24	150	6.00	157.00	6.28	3.18
KAV01	750	775	165	6.60	156	6.24	148	5.92	156.33	6.25	3.20
KAV04A	100	125	142	5.68	137	5.48	140	5.60	139.67	5.59	3.58
KAV04A	125	150	143	5.72	137	5.48	140	5.60	140.00	5.60	3.57
KAV04A	150	175	144	5.76	140	5.60	138	5.52	140.67	5.63	3.55
KAV04A	175	200	143	5.72	139	5.56	140	5.60	140.67	5.63	3.55
KAV04A	200	225	144	5.76	140	5.60	139	5.56	141.00	5.64	3.55
KAV04A	225	250	142	5.68	139	5.56	139	5.56	140.00	5.60	3.57
KAV04A	250	275	146	5.84	142	5.68	138	5.52	142.00	5.68	3.52
KAV04A	275	300	146	5.84	142	5.68	138	5.52	142.00	5.68	3.52
KAV04A	300	325	147	5.88	142	5.68	138	5.52	142.33	5.69	3.51
KAV04A	325	350	142	5.68	141	5.64	138	5.52	140.33	5.61	3.56
KAV04A	350	375	142	5.68	141	5.64	138	5.52	140.33	5.61	3.56
KAV04A	375	400	142	5.68	141	5.64	138	5.52	140.33	5.61	3.56
KAV04A	400	425	142	5.68	141	5.64	138	5.52	140.33	5.61	3.56

Borehole	Start length (m)	End length (m)	Run 1 # of fracs	Sim P_{10} (1/m)	Run 2 # of fracs	Sim P_{10} (1/m)	Run 3 # of fracs	Sim P_{10} (1/m)	Ave # of fracs	Ave sim P_{10} (1/m)	Conversion factor C1
KAV04A	425	450	145	5.80	142	5.68	138	5.52	141.67	5.67	3.53
KAV04A	450	475	143	5.72	142	5.68	138	5.52	141.00	5.64	3.55
KAV04A	475	500	143	5.72	143	5.72	138	5.52	141.33	5.65	3.54
KAV04A	500	525	144	5.76	143	5.72	138	5.52	141.67	5.67	3.53
KAV04A	525	550	141	5.64	141	5.64	140	5.60	140.67	5.63	3.55
KAV04A	550	575	142	5.68	143	5.72	140	5.60	141.67	5.67	3.53
KAV04A	575	600	142	5.68	144	5.76	140	5.60	142.00	5.68	3.52
KAV04A	600	625	143	5.72	145	5.80	139	5.56	142.33	5.69	3.51
KAV04A	625	650	144	5.76	144	5.76	140	5.60	142.67	5.71	3.50
KAV04A	650	675	144	5.76	144	5.76	139	5.56	142.33	5.69	3.51
KAV04A	675	700	143	5.72	144	5.76	139	5.56	142.00	5.68	3.52
KAV04A	700	725	144	5.76	143	5.72	140	5.60	142.33	5.69	3.51
KAV04A	725	750	143	5.72	137	5.48	139	5.56	139.67	5.59	3.58
KAV04A	750	775	143	5.72	139	5.56	139	5.56	140.33	5.61	3.56
KAV04A	775	800	142	5.68	143	5.72	138	5.52	141.00	5.64	3.55
KAV04A	800	825	143	5.72	140	5.60	138	5.52	140.33	5.61	3.56
KAV04A	825	850	142	5.68	140	5.60	137	5.48	139.67	5.59	3.58
KAV04A	850	875	143	5.72	140	5.60	137	5.48	140.00	5.60	3.57
KAV04A	875	900	144	5.76	138	5.52	139	5.56	140.33	5.61	3.56
KAV04A	900	925	145	5.80	138	5.52	137	5.48	140.00	5.60	3.57
KAV04A	925	950	143	5.72	139	5.56	140	5.60	140.67	5.63	3.55
KAV04A	950	975	146	5.84	138	5.52	144	5.76	142.67	5.71	3.50
KAV04A	975	1,000	146	5.84	138	5.52	143	5.72	142.33	5.69	3.51
KSH01A	97	122	185	7.40	184	7.36	169	6.76	179.33	7.17	2.79
KSH01A	122	147	186	7.44	184	7.36	168	6.72	179.33	7.17	2.79
KSH01A	147	172	185	7.40	185	7.40	169	6.76	179.67	7.19	2.78
KSH01A	172	197	185	7.40	182	7.28	171	6.84	179.33	7.17	2.79
KSH01A	197	222	184	7.36	184	7.36	169	6.76	179.00	7.16	2.79
KSH01A	222	247	183	7.32	184	7.36	169	6.76	178.67	7.15	2.80
KSH01A	247	272	185	7.40	186	7.44	168	6.72	179.67	7.19	2.78
KSH01A	272	297	186	7.44	187	7.48	169	6.76	180.67	7.23	2.77
KSH01A	297	322	188	7.52	185	7.40	170	6.80	181.00	7.24	2.76
KSH01A	322	347	191	7.64	189	7.56	171	6.84	183.67	7.35	2.72
KSH01A	347	372	195	7.80	195	7.80	169	6.76	186.33	7.45	2.68
KSH01A	372	397	196	7.84	200	8.00	172	6.88	189.33	7.57	2.64
KSH01A	397	422	199	7.96	202	8.08	175	7.00	192.00	7.68	2.60
KSH01A	422	447	200	8.00	204	8.16	173	6.92	192.33	7.69	2.60
KSH01A	447	472	203	8.12	202	8.08	176	7.04	193.67	7.75	2.58
KSH01A	472	497	203	8.12	203	8.12	178	7.12	194.67	7.79	2.57
KSH01A	497	522	205	8.20	205	8.20	177	7.08	195.67	7.83	2.56
KSH01A	522	547	201	8.04	205	8.20	176	7.04	194.00	7.76	2.58
KSH01A	547	572	201	8.04	207	8.28	177	7.08	195.00	7.80	2.56
KSH01A	572	597	200	8.00	205	8.20	180	7.20	195.00	7.80	2.56
KSH01A	597	622	202	8.08	203	8.12	184	7.36	196.33	7.85	2.55
KSH01A	622	647	200	8.00	203	8.12	182	7.28	195.00	7.80	2.56
KSH01A	647	672	197	7.88	205	8.20	185	7.40	195.67	7.83	2.56
KSH01A	672	697	205	8.20	212	8.48	187	7.48	201.33	8.05	2.48

Borehole	Start length (m)	End length (m)	Run 1 # of fracs	Sim P_{10} (1/m)	Run 2 # of fracs	Sim P_{10} (1/m)	Run 3 # of fracs	Sim P_{10} (1/m)	Ave # of fracs	Ave sim P_{10} (1/m)	Conversion factor C1
KSH01A	697	722	213	8.52	219	8.76	195	7.80	209.00	8.36	2.39
KSH01A	722	747	217	8.68	220	8.80	198	7.92	211.67	8.47	2.36
KSH01A	747	772	222	8.88	224	8.96	201	8.04	215.67	8.63	2.32
KSH01A	772	797	225	9.00	227	9.08	204	8.16	218.67	8.75	2.29
KSH01A	797	822	229	9.16	224	8.96	204	8.16	219.00	8.76	2.28
KSH01A	822	847	234	9.36	225	9.00	208	8.32	222.33	8.89	2.25
KSH01A	847	872	238	9.52	222	8.88	217	8.68	225.67	9.03	2.22
KSH01A	872	897	240	9.60	222	8.88	222	8.88	228.00	9.12	2.19
KSH01A	897	922	242	9.68	225	9.00	226	9.04	231.00	9.24	2.16
KSH01A	922	947	248	9.92	229	9.16	229	9.16	235.33	9.41	2.12
KSH01A	947	972	250	10.00	228	9.12	229	9.16	235.67	9.43	2.12
KSH01A	972	997	251	10.04	230	9.20	232	9.28	237.67	9.51	2.10
KSH01A	997	1,022	253	10.12	229	9.16	231	9.24	237.67	9.51	2.10
KSH02	0	25	140	5.60	128	5.12	142	5.68	136.67	5.47	3.66
KSH02	25	50	141	5.64	125	5.00	144	5.76	136.67	5.47	3.66
KSH02	50	75	141	5.64	131	5.24	145	5.80	139.00	5.56	3.60
KSH02	75	100	142	5.68	141	5.64	145	5.80	142.67	5.71	3.50
KSH02	100	125	142	5.68	142	5.68	144	5.76	142.67	5.71	3.50
KSH02	125	150	143	5.72	142	5.68	143	5.72	142.67	5.71	3.50
KSH02	150	175	143	5.72	136	5.44	147	5.88	142.00	5.68	3.52
KSH02	175	200	141	5.64	135	5.40	147	5.88	141.00	5.64	3.55
KSH02	200	225	143	5.72	131	5.24	149	5.96	141.00	5.64	3.55
KSH02	225	250	144	5.76	129	5.16	148	5.92	140.33	5.61	3.56
KSH02	250	275	145	5.80	128	5.12	148	5.92	140.33	5.61	3.56
KSH02	275	300	147	5.88	127	5.08	147	5.88	140.33	5.61	3.56
KSH02	300	325	146	5.84	127	5.08	148	5.92	140.33	5.61	3.56
KSH02	325	350	147	5.88	127	5.08	148	5.92	140.67	5.63	3.55
KSH02	350	375	147	5.88	126	5.04	148	5.92	140.33	5.61	3.56
KSH02	375	400	146	5.84	127	5.08	145	5.80	139.33	5.57	3.59
KSH02	400	425	142	5.68	142	5.68	139	5.56	141.00	5.64	3.55
KSH02	425	450	146	5.84	127	5.08	146	5.84	139.67	5.59	3.58
KSH02	450	475	146	5.84	128	5.12	146	5.84	140.00	5.60	3.57
KSH02	475	500	147	5.88	129	5.16	146	5.84	140.67	5.63	3.55
KSH02	500	525	149	5.96	129	5.16	145	5.80	141.00	5.64	3.55
KSH02	525	550	146	5.84	128	5.12	145	5.80	139.67	5.59	3.58
KSH02	550	575	145	5.80	129	5.16	146	5.84	140.00	5.60	3.57
KSH02	575	600	145	5.80	128	5.12	147	5.88	140.00	5.60	3.57
KSH02	600	625	146	5.84	127	5.08	145	5.80	139.33	5.57	3.59
KSH02	625	650	146	5.84	127	5.08	146	5.84	139.67	5.59	3.58
KSH02	650	675	145	5.80	130	5.20	145	5.80	140.00	5.60	3.57
KSH02	675	700	146	5.84	131	5.24	145	5.80	140.67	5.63	3.55
KSH02	700	725	146	5.84	132	5.28	146	5.84	141.33	5.65	3.54
KSH02	725	750	146	5.84	130	5.20	146	5.84	140.67	5.63	3.55
KSH02	750	775	145	5.80	132	5.28	146	5.84	141.00	5.64	3.55
KSH02	775	800	146	5.84	132	5.28	146	5.84	141.33	5.65	3.54
KSH02	800	825	146	5.84	133	5.32	146	5.84	141.67	5.67	3.53
KSH02	825	850	145	5.80	134	5.36	146	5.84	141.67	5.67	3.53

Borehole	Start length (m)	End length (m)	Run 1 # of fracs	Sim P_{10} (1/m)	Run 2 # of fracs	Sim P_{10} (1/m)	Run 3 # of fracs	Sim P_{10} (1/m)	Ave # of fracs	Ave sim P_{10} (1/m)	Conversion factor C1
KSH02	850	875	143	5.72	135	5.40	146	5.84	141.33	5.65	3.54
KSH02	875	900	144	5.76	136	5.44	146	5.84	142.00	5.68	3.52
KSH02	900	925	144	5.76	136	5.44	146	5.84	142.00	5.68	3.52
KSH02	925	950	144	5.76	138	5.52	144	5.76	142.00	5.68	3.52
KSH02	950	975	144	5.76	138	5.52	143	5.72	141.67	5.67	3.53
KSH02	975	1,000	141	5.64	136	5.44	142	5.68	139.67	5.59	3.58
KSH02	1,000	1,025	143	5.72	136	5.44	141	5.64	140.00	5.60	3.57
KSH03A	100	125	168	6.72	157	6.28	138	5.52	154.33	6.17	3.24
KSH03A	125	150	172	6.88	163	6.52	153	6.12	162.67	6.51	3.07
KSH03A	150	175	176	7.04	168	6.72	151	6.04	165.00	6.60	3.03
KSH03A	175	200	176	7.04	169	6.76	149	5.96	164.67	6.59	3.04
KSH03A	200	225	176	7.04	169	6.76	148	5.92	164.33	6.57	3.04
KSH03A	225	250	180	7.20	166	6.64	148	5.92	164.67	6.59	3.04
KSH03A	250	275	185	7.40	166	6.64	147	5.88	166.00	6.64	3.01
KSH03A	275	300	183	7.32	167	6.68	156	6.24	168.67	6.75	2.96
KSH03A	300	325	181	7.24	176	7.04	160	6.40	172.33	6.89	2.90
KSH03A	325	350	180	7.20	187	7.48	167	6.68	178.00	7.12	2.81
KSH03A	350	375	186	7.44	191	7.64	166	6.64	181.00	7.24	2.76
KSH03A	375	400	194	7.76	204	8.16	184	7.36	194.00	7.76	2.58
KSH03A	400	425	196	7.84	200	8.00	186	7.44	194.00	7.76	2.58
KSH03A	425	450	201	8.04	203	8.12	195	7.80	199.67	7.99	2.50
KSH03A	450	475	213	8.52	208	8.32	196	7.84	205.67	8.23	2.43
KSH03A	475	500	213	8.52	209	8.36	204	8.16	208.67	8.35	2.40
KSH03A	500	525	217	8.68	219	8.76	210	8.40	215.33	8.61	2.32
KSH03A	525	550	226	9.04	217	8.68	221	8.84	221.33	8.85	2.26
KSH03A	550	575	228	9.12	219	8.76	234	9.36	227.00	9.08	2.20
KSH03A	575	600	238	9.52	225	9.00	234	9.36	232.33	9.29	2.15
KSH03A	600	625	239	9.56	229	9.16	242	9.68	236.67	9.47	2.11
KSH03A	625	650	236	9.44	229	9.16	258	10.32	241.00	9.64	2.07
KSH03A	650	675	244	9.76	237	9.48	263	10.52	248.00	9.92	2.02
KSH03A	675	700	242	9.68	243	9.72	274	10.96	253.00	10.12	1.98
KSH03A	700	725	249	9.96	244	9.76	285	11.40	259.33	10.37	1.93
KSH03A	725	750	264	10.56	251	10.04	291	11.64	268.67	10.75	1.86
KSH03A	750	775	290	11.60	253	10.12	296	11.84	279.67	11.19	1.79
KSH03A	775	800	305	12.20	269	10.76	309	12.36	294.33	11.77	1.70
KSH03A	800	825	311	12.44	279	11.16	321	12.84	303.67	12.15	1.65
KSH03A	825	850	320	12.80	291	11.64	326	13.04	312.33	12.49	1.60
KSH03A	850	875	331	13.24	302	12.08	337	13.48	323.33	12.93	1.55
KSH03A	875	900	338	13.52	311	12.44	350	14.00	333.00	13.32	1.50
KSH03A	900	925	351	14.04	318	12.72	357	14.28	342.00	13.68	1.46
KSH03A	925	950	364	14.56	331	13.24	357	14.28	350.67	14.03	1.43
KSH03A	950	975	369	14.76	341	13.64	369	14.76	359.67	14.39	1.39
KSH03A	975	1,000	380	15.20	351	14.04	371	14.84	367.33	14.69	1.36
KSH03A	1,000	1,025	382	15.28	358	14.32	382	15.28	374.00	14.96	1.34

Simpevarp local set D
Interval length **25** **m**
Simulated P_{32} (1/m) **20** **1/m**

Borehole	Start length (m)	End length (m)	Run 1 # of fracs	Sim P_{10} (1/m)	Run 2 # of fracs	Sim P_{10} (1/m)	Run 3 # of fracs	Sim P_{10} (1/m)	Ave # of fracs	Ave sim P_{10} (1/m)	Conversion factor C1
KAV01	0	25	518	20.72	490	19.60	468	18.72	492.00	19.68	1.02
KAV01	25	50	518	20.72	490	19.60	469	18.76	492.33	19.69	1.02
KAV01	50	75	518	20.72	489	19.56	468	18.72	491.67	19.67	1.02
KAV01	75	100	518	20.72	489	19.56	468	18.72	491.67	19.67	1.02
KAV01	100	125	518	20.72	488	19.52	468	18.72	491.33	19.65	1.02
KAV01	125	150	518	20.72	488	19.52	468	18.72	491.33	19.65	1.02
KAV01	150	175	522	20.88	489	19.56	465	18.60	492.00	19.68	1.02
KAV01	175	200	520	20.80	488	19.52	467	18.68	491.67	19.67	1.02
KAV01	200	225	524	20.96	489	19.56	467	18.68	493.33	19.73	1.01
KAV01	225	250	523	20.92	489	19.56	467	18.68	493.00	19.72	1.01
KAV01	250	275	521	20.84	492	19.68	467	18.68	493.33	19.73	1.01
KAV01	275	300	523	20.92	495	19.80	466	18.64	494.67	19.79	1.01
KAV01	300	325	523	20.92	488	19.52	471	18.84	494.00	19.76	1.01
KAV01	325	350	521	20.84	493	19.72	473	18.92	495.67	19.83	1.01
KAV01	350	375	521	20.84	495	19.80	472	18.88	496.00	19.84	1.01
KAV01	375	400	518	20.72	496	19.84	472	18.88	495.33	19.81	1.01
KAV01	400	425	516	20.64	495	19.80	472	18.88	494.33	19.77	1.01
KAV01	425	450	515	20.60	497	19.88	472	18.88	494.67	19.79	1.01
KAV01	450	475	517	20.68	491	19.64	471	18.84	493.00	19.72	1.01
KAV01	475	500	515	20.60	491	19.64	472	18.88	492.67	19.71	1.01
KAV01	500	525	516	20.64	496	19.84	474	18.96	495.33	19.81	1.01
KAV01	525	550	516	20.64	491	19.64	472	18.88	493.00	19.72	1.01
KAV01	550	575	516	20.64	492	19.68	474	18.96	494.00	19.76	1.01
KAV01	575	600	514	20.56	492	19.68	472	18.88	492.67	19.71	1.01
KAV01	600	625	513	20.52	492	19.68	471	18.84	492.00	19.68	1.02
KAV01	625	650	509	20.36	494	19.76	472	18.88	491.67	19.67	1.02
KAV01	650	675	509	20.36	496	19.84	472	18.88	492.33	19.69	1.02
KAV01	675	700	514	20.56	494	19.76	471	18.84	493.00	19.72	1.01
KAV01	700	725	517	20.68	495	19.80	469	18.76	493.67	19.75	1.01
KAV01	725	750	517	20.68	495	19.80	470	18.80	494.00	19.76	1.01
KAV01	750	775	517	20.68	496	19.84	471	18.84	494.67	19.79	1.01
KAV04A	100	125	517	20.68	485	19.40	464	18.56	488.67	19.55	1.02
KAV04A	125	150	515	20.60	485	19.40	464	18.56	488.00	19.52	1.02
KAV04A	150	175	514	20.56	484	19.36	465	18.60	487.67	19.51	1.03
KAV04A	175	200	517	20.68	484	19.36	464	18.56	488.33	19.53	1.02
KAV04A	200	225	517	20.68	484	19.36	464	18.56	488.33	19.53	1.02
KAV04A	225	250	520	20.80	484	19.36	464	18.56	489.33	19.57	1.02
KAV04A	250	275	516	20.64	484	19.36	465	18.60	488.33	19.53	1.02
KAV04A	275	300	517	20.68	484	19.36	465	18.60	488.67	19.55	1.02
KAV04A	300	325	516	20.64	485	19.40	464	18.56	488.33	19.53	1.02
KAV04A	325	350	516	20.64	485	19.40	464	18.56	488.33	19.53	1.02
KAV04A	350	375	516	20.64	485	19.40	465	18.60	488.67	19.55	1.02
KAV04A	375	400	515	20.60	488	19.52	465	18.60	489.33	19.57	1.02
KAV04A	400	425	515	20.60	485	19.40	465	18.60	488.33	19.53	1.02

Borehole	Start length (m)	End length (m)	Run 1 # of fracs	Sim P_{10} (1/m)	Run 2 # of fracs	Sim P_{10} (1/m)	Run 3 # of fracs	Sim P_{10} (1/m)	Ave # of fracs	Ave sim P_{10} (1/m)	Conversion factor C1
KAV04A	425	450	515	20.60	485	19.40	466	18.64	488.67	19.55	1.02
KAV04A	450	475	516	20.64	485	19.40	466	18.64	489.00	19.56	1.02
KAV04A	475	500	517	20.68	484	19.36	467	18.68	489.33	19.57	1.02
KAV04A	500	525	516	20.64	483	19.32	468	18.72	489.00	19.56	1.02
KAV04A	525	550	516	20.64	486	19.44	468	18.72	490.00	19.60	1.02
KAV04A	550	575	517	20.68	488	19.52	469	18.76	491.33	19.65	1.02
KAV04A	575	600	516	20.64	486	19.44	469	18.76	490.33	19.61	1.02
KAV04A	600	625	519	20.76	487	19.48	468	18.72	491.33	19.65	1.02
KAV04A	625	650	519	20.76	488	19.52	465	18.60	490.67	19.63	1.02
KAV04A	650	675	518	20.72	487	19.48	466	18.64	490.33	19.61	1.02
KAV04A	675	700	518	20.72	487	19.48	466	18.64	490.33	19.61	1.02
KAV04A	700	725	517	20.68	487	19.48	465	18.60	489.67	19.59	1.02
KAV04A	725	750	516	20.64	486	19.44	466	18.64	489.33	19.57	1.02
KAV04A	750	775	517	20.68	488	19.52	466	18.64	490.33	19.61	1.02
KAV04A	775	800	518	20.72	488	19.52	464	18.56	490.00	19.60	1.02
KAV04A	800	825	517	20.68	488	19.52	465	18.60	490.00	19.60	1.02
KAV04A	825	850	516	20.64	490	19.60	468	18.72	491.33	19.65	1.02
KAV04A	850	875	516	20.64	490	19.60	469	18.76	491.67	19.67	1.02
KAV04A	875	900	513	20.52	490	19.60	470	18.80	491.00	19.64	1.02
KAV04A	900	925	510	20.40	493	19.72	469	18.76	490.67	19.63	1.02
KAV04A	925	950	510	20.40	493	19.72	469	18.76	490.67	19.63	1.02
KAV04A	950	975	512	20.48	492	19.68	468	18.72	490.67	19.63	1.02
KAV04A	975	1,000	515	20.60	493	19.72	470	18.80	492.67	19.71	1.01
KSH01A	97	122	490	19.60	484	19.36	464	18.56	479.33	19.17	1.04
KSH01A	122	147	492	19.68	481	19.24	464	18.56	479.00	19.16	1.04
KSH01A	147	172	493	19.72	482	19.28	467	18.68	480.67	19.23	1.04
KSH01A	172	197	490	19.60	482	19.28	468	18.72	480.00	19.20	1.04
KSH01A	197	222	490	19.60	482	19.28	464	18.56	478.67	19.15	1.04
KSH01A	222	247	490	19.60	483	19.32	466	18.64	479.67	19.19	1.04
KSH01A	247	272	492	19.68	482	19.28	463	18.52	479.00	19.16	1.04
KSH01A	272	297	491	19.64	481	19.24	464	18.56	478.67	19.15	1.04
KSH01A	297	322	491	19.64	480	19.20	469	18.76	480.00	19.20	1.04
KSH01A	322	347	493	19.72	481	19.24	472	18.88	482.00	19.28	1.04
KSH01A	347	372	493	19.72	483	19.32	471	18.84	482.33	19.29	1.04
KSH01A	372	397	493	19.72	481	19.24	470	18.80	481.33	19.25	1.04
KSH01A	397	422	494	19.76	478	19.12	472	18.88	481.33	19.25	1.04
KSH01A	422	447	493	19.72	482	19.28	474	18.96	483.00	19.32	1.04
KSH01A	447	472	494	19.76	479	19.16	477	19.08	483.33	19.33	1.03
KSH01A	472	497	496	19.84	473	18.92	476	19.04	481.67	19.27	1.04
KSH01A	497	522	493	19.72	471	18.84	472	18.88	478.67	19.15	1.04
KSH01A	522	547	490	19.60	471	18.84	472	18.88	477.67	19.11	1.05
KSH01A	547	572	492	19.68	471	18.84	472	18.88	478.33	19.13	1.05
KSH01A	572	597	491	19.64	471	18.84	475	19.00	479.00	19.16	1.04
KSH01A	597	622	489	19.56	466	18.64	476	19.04	477.00	19.08	1.05
KSH01A	622	647	488	19.52	462	18.48	475	19.00	475.00	19.00	1.05
KSH01A	647	672	488	19.52	461	18.44	476	19.04	475.00	19.00	1.05
KSH01A	672	697	494	19.76	458	18.32	478	19.12	476.67	19.07	1.05

Borehole	Start length (m)	End length (m)	Run 1 # of fracs	Sim P_{10} (1/m)	Run 2 # of fracs	Sim P_{10} (1/m)	Run 3 # of fracs	Sim P_{10} (1/m)	Ave # of fracs	Ave sim P_{10} (1/m)	Conversion factor C1
KSH01A	697	722	492	19.68	457	18.28	474	18.96	474.33	18.97	1.05
KSH01A	722	747	493	19.72	449	17.96	474	18.96	472.00	18.88	1.06
KSH01A	747	772	487	19.48	448	17.92	474	18.96	469.67	18.79	1.06
KSH01A	772	797	490	19.60	446	17.84	471	18.84	469.00	18.76	1.07
KSH01A	797	822	490	19.60	435	17.40	465	18.60	463.33	18.53	1.08
KSH01A	822	847	484	19.36	431	17.24	463	18.52	459.33	18.37	1.09
KSH01A	847	872	486	19.44	427	17.08	465	18.60	459.33	18.37	1.09
KSH01A	872	897	480	19.20	424	16.96	467	18.68	457.00	18.28	1.09
KSH01A	897	922	474	18.96	424	16.96	463	18.52	453.67	18.15	1.10
KSH01A	922	947	475	19.00	415	16.60	458	18.32	449.33	17.97	1.11
KSH01A	947	972	471	18.84	414	16.56	458	18.32	447.67	17.91	1.12
KSH01A	972	997	462	18.48	412	16.48	454	18.16	442.67	17.71	1.13
KSH01A	997	1,022	462	18.48	411	16.44	455	18.20	442.67	17.71	1.13
KSH02	0	25	521	20.84	484	19.36	474	18.96	493.00	19.72	1.01
KSH02	25	50	520	20.80	484	19.36	475	19.00	493.00	19.72	1.01
KSH02	50	75	521	20.84	485	19.40	473	18.92	493.00	19.72	1.01
KSH02	75	100	524	20.96	491	19.64	470	18.80	495.00	19.80	1.01
KSH02	100	125	523	20.92	488	19.52	470	18.80	493.67	19.75	1.01
KSH02	125	150	525	21.00	488	19.52	468	18.72	493.67	19.75	1.01
KSH02	150	175	524	20.96	481	19.24	469	18.76	491.33	19.65	1.02
KSH02	175	200	526	21.04	479	19.16	469	18.76	491.33	19.65	1.02
KSH02	200	225	526	21.04	481	19.24	472	18.88	493.00	19.72	1.01
KSH02	225	250	524	20.96	481	19.24	471	18.84	492.00	19.68	1.02
KSH02	250	275	523	20.92	483	19.32	470	18.80	492.00	19.68	1.02
KSH02	275	300	524	20.96	483	19.32	471	18.84	492.67	19.71	1.01
KSH02	300	325	523	20.92	484	19.36	473	18.92	493.33	19.73	1.01
KSH02	325	350	524	20.96	485	19.40	474	18.96	494.33	19.77	1.01
KSH02	350	375	526	21.04	484	19.36	474	18.96	494.67	19.79	1.01
KSH02	375	400	523	20.92	481	19.24	476	19.04	493.33	19.73	1.01
KSH02	400	425	518	20.72	483	19.32	468	18.72	489.67	19.59	1.02
KSH02	425	450	522	20.88	480	19.20	476	19.04	492.67	19.71	1.01
KSH02	450	475	520	20.80	479	19.16	476	19.04	491.67	19.67	1.02
KSH02	475	500	524	20.96	479	19.16	475	19.00	492.67	19.71	1.01
KSH02	500	525	523	20.92	479	19.16	474	18.96	492.00	19.68	1.02
KSH02	525	550	523	20.92	476	19.04	476	19.04	491.67	19.67	1.02
KSH02	550	575	522	20.88	476	19.04	475	19.00	491.00	19.64	1.02
KSH02	575	600	522	20.88	477	19.08	475	19.00	491.33	19.65	1.02
KSH02	600	625	522	20.88	476	19.04	476	19.04	491.33	19.65	1.02
KSH02	625	650	523	20.92	478	19.12	475	19.00	492.00	19.68	1.02
KSH02	650	675	524	20.96	478	19.12	474	18.96	492.00	19.68	1.02
KSH02	675	700	523	20.92	479	19.16	472	18.88	491.33	19.65	1.02
KSH02	700	725	522	20.88	480	19.20	470	18.80	490.67	19.63	1.02
KSH02	725	750	523	20.92	479	19.16	470	18.80	490.67	19.63	1.02
KSH02	750	775	522	20.88	479	19.16	470	18.80	490.33	19.61	1.02
KSH02	775	800	522	20.88	480	19.20	469	18.76	490.33	19.61	1.02
KSH02	800	825	521	20.84	483	19.32	466	18.64	490.00	19.60	1.02
KSH02	825	850	521	20.84	483	19.32	466	18.64	490.00	19.60	1.02

Borehole	Start length (m)	End length (m)	Run 1 # of fracs	Sim P_{10} (1/m)	Run 2 # of fracs	Sim P_{10} (1/m)	Run 3 # of fracs	Sim P_{10} (1/m)	Ave # of fracs	Ave sim P_{10} (1/m)	Conversion factor C1
KSH02	850	875	519	20.76	483	19.32	465	18.60	489.00	19.56	1.02
KSH02	875	900	518	20.72	483	19.32	466	18.64	489.00	19.56	1.02
KSH02	900	925	519	20.76	482	19.28	468	18.72	489.67	19.59	1.02
KSH02	925	950	518	20.72	484	19.36	468	18.72	490.00	19.60	1.02
KSH02	950	975	516	20.64	483	19.32	468	18.72	489.00	19.56	1.02
KSH02	975	1,000	519	20.76	484	19.36	466	18.64	489.67	19.59	1.02
KSH02	1,000	1,025	520	20.80	482	19.28	468	18.72	490.00	19.60	1.02
KSH03A	100	125	470	18.80	407	16.28	433	17.32	436.67	17.47	1.15
KSH03A	125	150	471	18.84	404	16.16	436	17.44	437.00	17.48	1.14
KSH03A	150	175	475	19.00	399	15.96	436	17.44	436.67	17.47	1.15
KSH03A	175	200	473	18.92	404	16.16	437	17.48	438.00	17.52	1.14
KSH03A	200	225	472	18.88	407	16.28	436	17.44	438.33	17.53	1.14
KSH03A	225	250	472	18.88	408	16.32	437	17.48	439.00	17.56	1.14
KSH03A	250	275	473	18.92	410	16.40	435	17.40	439.33	17.57	1.14
KSH03A	275	300	474	18.96	410	16.40	440	17.60	441.33	17.65	1.13
KSH03A	300	325	469	18.76	412	16.48	438	17.52	439.67	17.59	1.14
KSH03A	325	350	467	18.68	416	16.64	435	17.40	439.33	17.57	1.14
KSH03A	350	375	467	18.68	419	16.76	433	17.32	439.67	17.59	1.14
KSH03A	375	400	467	18.68	422	16.88	440	17.60	443.00	17.72	1.13
KSH03A	400	425	467	18.68	420	16.80	441	17.64	442.67	17.71	1.13
KSH03A	425	450	464	18.56	420	16.80	436	17.44	440.00	17.60	1.14
KSH03A	450	475	461	18.44	425	17.00	437	17.48	441.00	17.64	1.13
KSH03A	475	500	458	18.32	419	16.76	440	17.60	439.00	17.56	1.14
KSH03A	500	525	458	18.32	417	16.68	441	17.64	438.67	17.55	1.14
KSH03A	525	550	450	18.00	418	16.72	435	17.40	434.33	17.37	1.15
KSH03A	550	575	446	17.84	413	16.52	438	17.52	432.33	17.29	1.16
KSH03A	575	600	449	17.96	407	16.28	441	17.64	432.33	17.29	1.16
KSH03A	600	625	451	18.04	406	16.24	444	17.76	433.67	17.35	1.15
KSH03A	625	650	455	18.20	402	16.08	440	17.60	432.33	17.29	1.16
KSH03A	650	675	461	18.44	404	16.16	442	17.68	435.67	17.43	1.15
KSH03A	675	700	462	18.48	401	16.04	449	17.96	437.33	17.49	1.14
KSH03A	700	725	452	18.08	393	15.72	455	18.20	433.33	17.33	1.15
KSH03A	725	750	450	18.00	391	15.64	451	18.04	430.67	17.23	1.16
KSH03A	750	775	442	17.68	379	15.16	445	17.80	422.00	16.88	1.18
KSH03A	775	800	421	16.84	371	14.84	440	17.60	410.67	16.43	1.22
KSH03A	800	825	417	16.68	366	14.64	437	17.48	406.67	16.27	1.23
KSH03A	825	850	410	16.40	361	14.44	429	17.16	400.00	16.00	1.25
KSH03A	850	875	402	16.08	363	14.52	420	16.80	395.00	15.80	1.27
KSH03A	875	900	399	15.96	357	14.28	413	16.52	389.67	15.59	1.28
KSH03A	900	925	399	15.96	351	14.04	401	16.04	383.67	15.35	1.30
KSH03A	925	950	392	15.68	343	13.72	382	15.28	372.33	14.89	1.34
KSH03A	950	975	388	15.52	342	13.68	377	15.08	369.00	14.76	1.36
KSH03A	975	1,000	383	15.32	337	13.48	362	14.48	360.67	14.43	1.39
KSH03A	1,000	1,025	378	15.12	335	13.40	359	14.36	357.33	14.29	1.40

Simpevarp local set E
Interval length 25 m
Simulated P_{32} 20 1/m

Borehole	Start length (m)	End length (m)	Run 1 # of fracs	Sim P_{10} (1/m)	Run 2 # of fracs	Sim P_{10} (1/m)	Run 3 # of fracs	Sim P_{10} (1/m)	Ave # of fracs	Ave sim P_{10} (1/m)	Conversion factor C1
KAV01	0	25	183	7.32	194	7.76	182	7.28	186.33	7.45	2.68
KAV01	25	50	183	7.32	194	7.76	183	7.32	186.67	7.47	2.68
KAV01	50	75	185	7.40	194	7.76	182	7.28	187.00	7.48	2.67
KAV01	75	100	185	7.40	194	7.76	183	7.32	187.33	7.49	2.67
KAV01	100	125	185	7.40	194	7.76	181	7.24	186.67	7.47	2.68
KAV01	125	150	185	7.40	194	7.76	181	7.24	186.67	7.47	2.68
KAV01	150	175	187	7.48	197	7.88	184	7.36	189.33	7.57	2.64
KAV01	175	200	187	7.48	197	7.88	185	7.40	189.67	7.59	2.64
KAV01	200	225	186	7.44	199	7.96	183	7.32	189.33	7.57	2.64
KAV01	225	250	186	7.44	199	7.96	183	7.32	189.33	7.57	2.64
KAV01	250	275	186	7.44	199	7.96	182	7.28	189.00	7.56	2.65
KAV01	275	300	189	7.56	197	7.88	184	7.36	190.00	7.60	2.63
KAV01	300	325	192	7.68	197	7.88	184	7.36	191.00	7.64	2.62
KAV01	325	350	185	7.40	196	7.84	186	7.44	189.00	7.56	2.65
KAV01	350	375	188	7.52	199	7.96	182	7.28	189.67	7.59	2.64
KAV01	375	400	190	7.60	195	7.80	185	7.40	190.00	7.60	2.63
KAV01	400	425	195	7.80	196	7.84	183	7.32	191.33	7.65	2.61
KAV01	425	450	196	7.84	193	7.72	183	7.32	190.67	7.63	2.62
KAV01	450	475	189	7.56	196	7.84	186	7.44	190.33	7.61	2.63
KAV01	475	500	193	7.72	195	7.80	185	7.40	191.00	7.64	2.62
KAV01	500	525	196	7.84	197	7.88	186	7.44	193.00	7.72	2.59
KAV01	525	550	195	7.80	196	7.84	185	7.40	192.00	7.68	2.60
KAV01	550	575	191	7.64	194	7.76	189	7.56	191.33	7.65	2.61
KAV01	575	600	193	7.72	195	7.80	189	7.56	192.33	7.69	2.60
KAV01	600	625	194	7.76	195	7.80	188	7.52	192.33	7.69	2.60
KAV01	625	650	193	7.72	193	7.72	188	7.52	191.33	7.65	2.61
KAV01	650	675	194	7.76	193	7.72	188	7.52	191.67	7.67	2.61
KAV01	675	700	193	7.72	196	7.84	189	7.56	192.67	7.71	2.60
KAV01	700	725	193	7.72	198	7.92	189	7.56	193.33	7.73	2.59
KAV01	725	750	193	7.72	197	7.88	189	7.56	193.00	7.72	2.59
KAV01	750	775	193	7.72	197	7.88	189	7.56	193.00	7.72	2.59
KAV04A	100	125	213	8.52	215	8.60	207	8.28	211.67	8.47	2.36
KAV04A	125	150	212	8.48	213	8.52	208	8.32	211.00	8.44	2.37
KAV04A	150	175	212	8.48	214	8.56	208	8.32	211.33	8.45	2.37
KAV04A	175	200	213	8.52	213	8.52	207	8.28	211.00	8.44	2.37
KAV04A	200	225	212	8.48	215	8.60	206	8.24	211.00	8.44	2.37
KAV04A	225	250	212	8.48	214	8.56	207	8.28	211.00	8.44	2.37
KAV04A	250	275	212	8.48	215	8.60	207	8.28	211.33	8.45	2.37
KAV04A	275	300	212	8.48	215	8.60	207	8.28	211.33	8.45	2.37
KAV04A	300	325	213	8.52	215	8.60	207	8.28	211.67	8.47	2.36
KAV04A	325	350	214	8.56	215	8.60	206	8.24	211.67	8.47	2.36
KAV04A	350	375	212	8.48	215	8.60	205	8.20	210.67	8.43	2.37

Borehole	Start length (m)	End length (m)	Run 1 # of fracs	Sim P_{10} (1/m)	Run 2 # of fracs	Sim P_{10} (1/m)	Run 3 # of fracs	Sim P_{10} (1/m)	Ave # of fracs	Ave sim P_{10} (1/m)	Conversion factor C1
KAV04A	375	400	213	8.52	217	8.68	206	8.24	212.00	8.48	2.36
KAV04A	400	425	213	8.52	216	8.64	205	8.20	211.33	8.45	2.37
KAV04A	425	450	213	8.52	215	8.60	207	8.28	211.67	8.47	2.36
KAV04A	450	475	214	8.56	217	8.68	209	8.36	213.33	8.53	2.34
KAV04A	475	500	216	8.64	219	8.76	209	8.36	214.67	8.59	2.33
KAV04A	500	525	218	8.72	218	8.72	211	8.44	215.67	8.63	2.32
KAV04A	525	550	219	8.76	219	8.76	210	8.40	216.00	8.64	2.31
KAV04A	550	575	219	8.76	219	8.76	210	8.40	216.00	8.64	2.31
KAV04A	575	600	219	8.76	218	8.72	211	8.44	216.00	8.64	2.31
KAV04A	600	625	221	8.84	218	8.72	210	8.40	216.33	8.65	2.31
KAV04A	625	650	221	8.84	217	8.68	210	8.40	216.00	8.64	2.31
KAV04A	650	675	222	8.88	216	8.64	210	8.40	216.00	8.64	2.31
KAV04A	675	700	222	8.88	217	8.68	210	8.40	216.33	8.65	2.31
KAV04A	700	725	222	8.88	218	8.72	209	8.36	216.33	8.65	2.31
KAV04A	725	750	222	8.88	220	8.80	209	8.36	217.00	8.68	2.30
KAV04A	750	775	222	8.88	219	8.76	210	8.40	217.00	8.68	2.30
KAV04A	775	800	224	8.96	217	8.68	212	8.48	217.67	8.71	2.30
KAV04A	800	825	224	8.96	217	8.68	212	8.48	217.67	8.71	2.30
KAV04A	825	850	225	9.00	217	8.68	213	8.52	218.33	8.73	2.29
KAV04A	850	875	224	8.96	217	8.68	212	8.48	217.67	8.71	2.30
KAV04A	875	900	223	8.92	216	8.64	212	8.48	217.00	8.68	2.30
KAV04A	900	925	222	8.88	218	8.72	209	8.36	216.33	8.65	2.31
KAV04A	925	950	221	8.84	217	8.68	208	8.32	215.33	8.61	2.32
KAV04A	950	975	217	8.68	218	8.72	205	8.20	213.33	8.53	2.34
KAV04A	975	1,000	217	8.68	218	8.72	203	8.12	212.67	8.51	2.35
KSH01A	97	122	185	7.40	181	7.24	176	7.04	180.67	7.23	2.77
KSH01A	122	147	185	7.40	179	7.16	176	7.04	180.00	7.20	2.78
KSH01A	147	172	182	7.28	175	7.00	172	6.88	176.33	7.05	2.84
KSH01A	172	197	180	7.20	168	6.72	177	7.08	175.00	7.00	2.86
KSH01A	197	222	182	7.28	164	6.56	177	7.08	174.33	6.97	2.87
KSH01A	222	247	182	7.28	164	6.56	179	7.16	175.00	7.00	2.86
KSH01A	247	272	180	7.20	164	6.56	179	7.16	174.33	6.97	2.87
KSH01A	272	297	180	7.20	166	6.64	180	7.20	175.33	7.01	2.85
KSH01A	297	322	180	7.20	168	6.72	181	7.24	176.33	7.05	2.84
KSH01A	322	347	175	7.00	172	6.88	177	7.08	174.67	6.99	2.86
KSH01A	347	372	170	6.80	167	6.68	174	6.96	170.33	6.81	2.94
KSH01A	372	397	168	6.72	164	6.56	178	7.12	170.00	6.80	2.94
KSH01A	397	422	169	6.76	163	6.52	180	7.20	170.67	6.83	2.93
KSH01A	422	447	171	6.84	162	6.48	182	7.28	171.67	6.87	2.91
KSH01A	447	472	174	6.96	165	6.60	181	7.24	173.33	6.93	2.88
KSH01A	472	497	167	6.68	170	6.80	182	7.28	173.00	6.92	2.89
KSH01A	497	522	165	6.60	170	6.80	184	7.36	173.00	6.92	2.89
KSH01A	522	547	165	6.60	166	6.64	185	7.40	172.00	6.88	2.91
KSH01A	547	572	162	6.48	164	6.56	181	7.24	169.00	6.76	2.96
KSH01A	572	597	161	6.44	161	6.44	177	7.08	166.33	6.65	3.01

Borehole	Start length (m)	End length (m)	Run 1 # of fracs	Sim P_{10} (1/m)	Run 2 # of fracs	Sim P_{10} (1/m)	Run 3 # of fracs	Sim P_{10} (1/m)	Ave # of fracs	Ave sim P_{10} (1/m)	Conversion factor C1
KSH01A	597	622	159	6.36	157	6.28	179	7.16	165.00	6.60	3.03
KSH01A	622	647	156	6.24	157	6.28	175	7.00	162.67	6.51	3.07
KSH01A	647	672	156	6.24	152	6.08	172	6.88	160.00	6.40	3.13
KSH01A	672	697	154	6.16	153	6.12	174	6.96	160.33	6.41	3.12
KSH01A	697	722	155	6.20	154	6.16	166	6.64	158.33	6.33	3.16
KSH01A	722	747	156	6.24	156	6.24	167	6.68	159.67	6.39	3.13
KSH01A	747	772	161	6.44	155	6.20	163	6.52	159.67	6.39	3.13
KSH01A	772	797	162	6.48	153	6.12	163	6.52	159.33	6.37	3.14
KSH01A	797	822	158	6.32	148	5.92	167	6.68	157.67	6.31	3.17
KSH01A	822	847	159	6.36	143	5.72	171	6.84	157.67	6.31	3.17
KSH01A	847	872	161	6.44	139	5.56	174	6.96	158.00	6.32	3.16
KSH01A	872	897	154	6.16	139	5.56	172	6.88	155.00	6.20	3.23
KSH01A	897	922	152	6.08	135	5.40	169	6.76	152.00	6.08	3.29
KSH01A	922	947	156	6.24	136	5.44	155	6.20	149.00	5.96	3.36
KSH01A	947	972	151	6.04	136	5.44	154	6.16	147.00	5.88	3.40
KSH01A	972	997	149	5.96	138	5.52	152	6.08	146.33	5.85	3.42
KSH01A	997	1,022	148	5.92	135	5.40	149	5.96	144.00	5.76	3.47
KSH02	0	25	188	7.52	189	7.56	186	7.44	187.67	7.51	2.66
KSH02	25	50	189	7.56	189	7.56	186	7.44	188.00	7.52	2.66
KSH02	50	75	187	7.48	190	7.60	183	7.32	186.67	7.47	2.68
KSH02	75	100	191	7.64	193	7.72	183	7.32	189.00	7.56	2.65
KSH02	100	125	193	7.72	193	7.72	185	7.40	190.33	7.61	2.63
KSH02	125	150	193	7.72	193	7.72	180	7.20	188.67	7.55	2.65
KSH02	150	175	197	7.88	196	7.84	179	7.16	190.67	7.63	2.62
KSH02	175	200	197	7.88	197	7.88	180	7.20	191.33	7.65	2.61
KSH02	200	225	196	7.84	201	8.04	183	7.32	193.33	7.73	2.59
KSH02	225	250	194	7.76	206	8.24	183	7.32	194.33	7.77	2.57
KSH02	250	275	191	7.64	206	8.24	183	7.32	193.33	7.73	2.59
KSH02	275	300	193	7.72	204	8.16	182	7.28	193.00	7.72	2.59
KSH02	300	325	191	7.64	204	8.16	183	7.32	192.67	7.71	2.60
KSH02	325	350	191	7.64	204	8.16	183	7.32	192.67	7.71	2.60
KSH02	350	375	191	7.64	204	8.16	186	7.44	193.67	7.75	2.58
KSH02	375	400	195	7.80	205	8.20	187	7.48	195.67	7.83	2.56
KSH02	400	425	207	8.28	215	8.60	197	7.88	206.33	8.25	2.42
KSH02	425	450	194	7.76	205	8.20	188	7.52	195.67	7.83	2.56
KSH02	450	475	195	7.80	208	8.32	188	7.52	197.00	7.88	2.54
KSH02	475	500	199	7.96	208	8.32	189	7.56	198.67	7.95	2.52
KSH02	500	525	201	8.04	207	8.28	191	7.64	199.67	7.99	2.50
KSH02	525	550	202	8.08	207	8.28	192	7.68	200.33	8.01	2.50
KSH02	550	575	204	8.16	206	8.24	192	7.68	200.67	8.03	2.49
KSH02	575	600	203	8.12	207	8.28	192	7.68	200.67	8.03	2.49
KSH02	600	625	203	8.12	208	8.32	192	7.68	201.00	8.04	2.49
KSH02	625	650	202	8.08	207	8.28	192	7.68	200.33	8.01	2.50
KSH02	650	675	204	8.16	207	8.28	190	7.60	200.33	8.01	2.50
KSH02	675	700	205	8.20	207	8.28	190	7.60	200.67	8.03	2.49

Borehole	Start length (m)	End length (m)	Run 1 # of fracs	Sim P_{10} (1/m)	Run 2 # of fracs	Sim P_{10} (1/m)	Run 3 # of fracs	Sim P_{10} (1/m)	Ave # of fracs	Ave sim P_{10} (1/m)	Conversion factor C1
KSH02	700	725	205	8.20	208	8.32	189	7.56	200.67	8.03	2.49
KSH02	725	750	205	8.20	208	8.32	189	7.56	200.67	8.03	2.49
KSH02	750	775	206	8.24	208	8.32	190	7.60	201.33	8.05	2.48
KSH02	775	800	207	8.28	208	8.32	192	7.68	202.33	8.09	2.47
KSH02	800	825	207	8.28	206	8.24	194	7.76	202.33	8.09	2.47
KSH02	825	850	207	8.28	208	8.32	194	7.76	203.00	8.12	2.46
KSH02	850	875	207	8.28	208	8.32	194	7.76	203.00	8.12	2.46
KSH02	875	900	208	8.32	212	8.48	196	7.84	205.33	8.21	2.44
KSH02	900	925	206	8.24	215	8.60	196	7.84	205.67	8.23	2.43
KSH02	925	950	204	8.16	214	8.56	195	7.80	204.33	8.17	2.45
KSH02	950	975	204	8.16	215	8.60	197	7.88	205.33	8.21	2.44
KSH02	975	1,000	205	8.20	216	8.64	196	7.84	205.67	8.23	2.43
KSH02	1,000	1,025	206	8.24	216	8.64	195	7.80	205.67	8.23	2.43
KSH03A	100	125	318	12.72	284	11.36	267	10.68	289.67	11.59	1.73
KSH03A	125	150	311	12.44	285	11.40	266	10.64	287.33	11.49	1.74
KSH03A	150	175	300	12.00	278	11.12	261	10.44	279.67	11.19	1.79
KSH03A	175	200	302	12.08	271	10.84	262	10.48	278.33	11.13	1.80
KSH03A	200	225	305	12.20	270	10.80	263	10.52	279.33	11.17	1.79
KSH03A	225	250	301	12.04	273	10.92	260	10.40	278.00	11.12	1.80
KSH03A	250	275	294	11.76	269	10.76	261	10.44	274.67	10.99	1.82
KSH03A	275	300	291	11.64	266	10.64	259	10.36	272.00	10.88	1.84
KSH03A	300	325	284	11.36	260	10.40	245	9.80	263.00	10.52	1.90
KSH03A	325	350	274	10.96	253	10.12	241	9.64	256.00	10.24	1.95
KSH03A	350	375	266	10.64	244	9.76	240	9.60	250.00	10.00	2.00
KSH03A	375	400	256	10.24	241	9.64	227	9.08	241.33	9.65	2.07
KSH03A	400	425	242	9.68	236	9.44	227	9.08	235.00	9.40	2.13
KSH03A	425	450	243	9.72	235	9.40	226	9.04	234.67	9.39	2.13
KSH03A	450	475	232	9.28	233	9.32	216	8.64	227.00	9.08	2.20
KSH03A	475	500	229	9.16	221	8.84	208	8.32	219.33	8.77	2.28
KSH03A	500	525	215	8.60	203	8.12	205	8.20	207.67	8.31	2.41
KSH03A	525	550	209	8.36	198	7.92	198	7.92	201.67	8.07	2.48
KSH03A	550	575	204	8.16	194	7.76	195	7.80	197.67	7.91	2.53
KSH03A	575	600	201	8.04	186	7.44	191	7.64	192.67	7.71	2.60
KSH03A	600	625	190	7.60	180	7.20	190	7.60	186.67	7.47	2.68
KSH03A	625	650	183	7.32	171	6.84	188	7.52	180.67	7.23	2.77
KSH03A	650	675	177	7.08	164	6.56	188	7.52	176.33	7.05	2.84
KSH03A	675	700	181	7.24	163	6.52	180	7.20	174.67	6.99	2.86
KSH03A	700	725	176	7.04	147	5.88	176	7.04	166.33	6.65	3.01
KSH03A	725	750	170	6.80	148	5.92	175	7.00	164.33	6.57	3.04
KSH03A	750	775	162	6.48	140	5.60	176	7.04	159.33	6.37	3.14
KSH03A	775	800	145	5.80	137	5.48	165	6.60	149.00	5.96	3.36
KSH03A	800	825	142	5.68	134	5.36	160	6.40	145.33	5.81	3.44
KSH03A	825	850	147	5.88	136	5.44	163	6.52	148.67	5.95	3.36
KSH03A	850	875	145	5.80	136	5.44	156	6.24	145.67	5.83	3.43
KSH03A	875	900	138	5.52	136	5.44	149	5.96	141.00	5.64	3.55

Borehole	Start length (m)	End length (m)	Run 1 # of fracs	Sim P_{10} (1/m)	Run 2 # of fracs	Sim P_{10} (1/m)	Run 3 # of fracs	Sim P_{10} (1/m)	Ave # of fracs	Ave sim P_{10} (1/m)	Conversion factor C1
KSH03A	900	925	131	5.24	131	5.24	147	5.88	136.33	5.45	3.67
KSH03A	925	950	130	5.20	130	5.20	155	6.20	138.33	5.53	3.61
KSH03A	950	975	139	5.56	136	5.44	155	6.20	143.33	5.73	3.49
KSH03A	975	1,000	141	5.64	137	5.48	151	6.04	143.00	5.72	3.50
KSH03A	1,000	1,025	146	5.84	133	5.32	152	6.08	143.67	5.75	3.48

Appendix B

Actual P_{10}s and P_{32}s for Simpevarp and Laxemar cored boreholes

Note: Yellow text within highlighted blocks represent borehole sections that span mapped deformation zones. These zones are not used to calculate rock domain intensity statistics.

Laxemar regional set A
Section length 25 m

Borehole	Start length (m)	End length (m)	Number of fractures	Observed P_{10} (1/m)	Rock domain	P_{10} > P_{32} conversion factor	DFN P_{32} (1/m)
KLX02	200	225	11	0.44	A	3.30	1.45
KLX02	225	250	12	0.48	A	3.28	1.57
KLX02	250	275	8	0.32	A	3.25	1.04
KLX02	275	300	2	0.08	A	3.30	0.26
KLX02	300	325	3	0.12	A	3.27	0.39
KLX02	325	350	6	0.24	A	3.23	0.77
KLX02	350	375	3	0.12	A	3.23	0.39
KLX02	375	400	6	0.24	A	3.22	0.77
KLX02	400	425	5	0.20	A	3.70	0.74
KLX02	425	450	11	0.44	A	3.21	1.41
KLX02	450	475	11	0.44	A	3.19	1.40
KLX02	475	500	6	0.24	A	3.20	0.77
KLX02	500	525	11	0.44	A	3.20	1.41
KLX02	525	550	17	0.68	A	3.20	2.17
KLX02	550	575	6	0.24	BA	3.21	0.77
KLX02	575	600	5	0.20	BA	3.19	0.64
KLX02	600	625	10	0.40	BA	3.21	1.28
KLX02	625	650	2	0.08	BA	3.21	0.26
KLX02	650	675	14	0.56	BA	3.14	1.76
KLX02	675	700	12	0.48	BA	3.14	1.51
KLX02	700	725	11	0.44	BA	3.14	1.38
KLX02	725	750	16	0.64	BA	3.14	2.01
KLX02	750	775	9	0.36	BA	3.19	1.15
KLX02	775	800	16	0.64	BA	3.19	2.04
KLX02	800	825	31	1.24	BA	3.14	3.89
KLX02	825	850	14	0.56	BA	3.13	1.75
KLX02	850	875	39	1.56	BA	3.11	4.84
KLX02	875	900	28	1.12	BA	3.13	3.50
KLX02	900	925	29	1.16	BA	3.11	3.60
KLX02	925	950	33	1.32	BA	3.10	4.09
KLX02	950	975	26	1.04	A	3.10	3.22
KLX02	975	1,000	18	0.72	A	3.11	2.24
KLX02	1,000	1,025	3	0.12	A	3.69	0.44
KLX03	100	125	2	0.08	M(A)	3.57	0.29
KLX03	125	150	19	0.76	M(A)	3.59	2.73

Borehole	Start length (m)	End length (m)	Number of fractures	Observed P_{10} (1/m)	Rock domain	P_{10} > P_{32} conversion factor	DFN P_{32} (1/m)
KLX03	150	175	17	0.68	M(A)	3.61	2.45
KLX03	175	200	4	0.16	M(A)	3.66	0.59
KLX03	200	225	16	0.64	M(A)	3.65	2.34
KLX03	225	250	23	0.92	M(A)	3.67	3.37
KLX03	250	275	8	0.32	M(A)	3.67	1.17
KLX03	275	300	33	1.32	M(A)	3.72	4.91
KLX03	300	325	26	1.04	M(A)	3.72	3.87
KLX03	325	350	8	0.32	M(A)	3.76	1.20
KLX03	350	375	7	0.28	M(A)	3.86	1.08
KLX03	375	400	12	0.48	M(A)	3.82	1.83
KLX03	400	425	7	0.28	M(A)	3.86	1.08
KLX03	425	450	7	0.28	M(A)	3.84	1.07
KLX03	450	475	4	0.16	M(A)	3.84	0.61
KLX03	475	500	3	0.12	M(A)	3.82	0.46
KLX03	500	525	5	0.20	M(A)	3.79	0.76
KLX03	525	550	4	0.16	M(A)	3.71	0.59
KLX03	550	575	1	0.04	M(A)	3.69	0.15
KLX03	575	600	11	0.44	M(A)	3.76	1.65
KLX03	600	625	27	1.08	M(A)	3.84	4.14
KLX03	625	650	24	0.96	M(D)	3.90	3.74
KLX03	650	675	24	0.96	M(D)	3.83	3.67
KLX03	675	700	23	0.92	M(D)	3.69	3.40
KLX03	700	725	15	0.60	M(D)	3.60	2.16
KLX03	725	750	17	0.68	M(D)	3.68	2.50
KLX03	750	775	9	0.36	M(D)	3.59	1.29
KLX03	775	800	45	1.80	M(D)	3.52	6.34
KLX03	800	825	45	1.80	D	3.46	6.24
KLX03	825	850	25	1.00	D	3.48	3.48
KLX03	850	875	24	0.96	D	3.55	3.40
KLX03	875	900	13	0.52	D	3.64	1.89
KLX03	900	925	25	1.00	D	3.69	3.69
KLX03	925	950	6	0.24	D	3.63	0.87
KLX03	950	975	13	0.52	D	3.71	1.93
KLX03	975	1,000	5	0.20	D	3.69	0.74
KLX03	1,000	1,025	0	0.00	D	3.69	0.00
KLX04	100	125	11	0.44	A	3.25	1.43
KLX04	125	150	4	0.16	A	3.27	0.52
KLX04	150	175	15	0.60	A	3.26	1.96
KLX04	175	200	17	0.68	A	3.28	2.23
KLX04	200	225	20	0.80	A	3.28	2.63
KLX04	225	250	34	1.36	A	3.30	4.49
KLX04	250	275	29	1.16	A	3.32	3.85
KLX04	275	300	10	0.40	A	3.33	1.33
KLX04	300	325	11	0.44	A	3.38	1.49
KLX04	325	350	5	0.20	A	3.38	0.68

Borehole	Start length (m)	End length (m)	Number of fractures	Observed P_{10} (1/m)	Rock domain	P_{10} > P_{32} conversion factor	DFN P_{32} (1/m)
KLX04	350	375	15	0.60	A	3.42	2.05
KLX04	375	400	9	0.36	A	3.42	1.23
KLX04	400	425	16	0.64	A	3.43	2.20
KLX04	425	450	5	0.20	A	3.42	0.68
KLX04	450	475	2	0.08	A	3.42	0.27
KLX04	475	500	5	0.20	A	3.43	0.69
KLX04	500	525	7	0.28	A	3.46	0.97
KLX04	525	550	11	0.44	A	3.50	1.54
KLX04	550	575	19	0.76	A	3.48	2.65
KLX04	575	600	11	0.44	A	3.48	1.53
KLX04	600	625	7	0.28	A	3.49	0.98
KLX04	625	650	14	0.56	A	3.49	1.95
KLX04	650	675	15	0.60	A	3.50	2.10
KLX04	675	700	6	0.24	A	3.51	0.84
KLX04	700	725	20	0.80	A	3.50	2.80
KLX04	725	750	13	0.52	A	3.50	1.82
KLX04	750	775	21	0.84	A	3.50	2.94
KLX04	775	800	15	0.60	A	3.53	2.12
KLX04	800	825	14	0.56	A	3.55	1.99
KLX04	825	850	14	0.56	A	3.49	1.95
KLX04	850	875	8	0.32	A	3.50	1.12
KLX04	875	900	22	0.88	A	3.49	3.07
KLX04	900	925	20	0.80	A	3.48	2.78
KLX04	925	950	20	0.80	A	3.46	2.77
KLX04	950	975	28	1.12	A	3.50	3.92
KLX04	975	1,000	12	0.48	A	3.48	1.67

Laxemar regional set B
Section length 25 m

Borehole	Start length (m)	End length (m)	Number of fractures	Observed P_{10} (1/m)	Rock domain	P_{10} > P_{32} conversion factor	DFN P_{32} (1/m)
KLX02	200	225	14	0.56	A	4.31	2.41
KLX02	225	250	10	0.40	A	4.30	1.72
KLX02	250	275	5	0.20	A	4.30	0.86
KLX02	275	300	5	0.20	A	4.35	0.87
KLX02	300	325	8	0.32	A	4.29	1.37
KLX02	325	350	10	0.40	A	4.31	1.72
KLX02	350	375	0	0.00	A	4.30	0.00
KLX02	375	400	6	0.24	A	4.29	1.03
KLX02	400	425	10	0.40	A	4.52	1.81
KLX02	425	450	6	0.24	A	4.30	1.03
KLX02	450	475	14	0.56	A	4.32	2.42

Borehole	Start length (m)	End length (m)	Number of fractures	Observed P_{10} (1/m)	Rock domain	P_{10} > P_{32} conversion factor	DFN P_{32} (1/m)
KLX02	475	500	6	0.24	A	4.32	1.04
KLX02	500	525	12	0.48	A	4.35	2.09
KLX02	525	550	22	0.88	A	4.41	3.88
KLX02	550	575	15	0.60	BA	4.39	2.63
KLX02	575	600	7	0.28	BA	4.40	1.23
KLX02	600	625	16	0.64	BA	4.39	2.81
KLX02	625	650	7	0.28	BA	4.39	1.23
KLX02	650	675	7	0.28	BA	4.42	1.24
KLX02	675	700	4	0.16	BA	4.42	0.71
KLX02	700	725	3	0.12	BA	4.44	0.53
KLX02	725	750	8	0.32	BA	4.42	1.42
KLX02	750	775	10	0.40	BA	4.40	1.76
KLX02	775	800	33	1.32	BA	4.40	5.81
KLX02	800	825	17	0.68	BA	4.44	3.02
KLX02	825	850	20	0.80	BA	4.45	3.56
KLX02	850	875	29	1.16	BA	4.45	5.16
KLX02	875	900	24	0.96	BA	4.41	4.24
KLX02	900	925	40	1.60	BA	4.41	7.06
KLX02	925	950	23	0.92	BA	4.39	4.04
KLX02	950	975	24	0.96	A	4.39	4.21
KLX02	975	1,000	18	0.72	A	4.45	3.20
KLX02	1,000	1,025	2	0.08	A	4.48	0.36
KLX03	100	125	5	0.20	M(A)	4.69	0.94
KLX03	125	150	10	0.40	M(A)	4.69	1.88
KLX03	150	175	3	0.12	M(A)	4.57	0.55
KLX03	175	200	14	0.56	M(A)	4.45	2.49
KLX03	200	225	30	1.20	M(A)	4.44	5.33
KLX03	225	250	14	0.56	M(A)	4.37	2.45
KLX03	250	275	17	0.68	M(A)	4.40	2.99
KLX03	275	300	36	1.44	M(A)	4.36	6.28
KLX03	300	325	37	1.48	M(A)	4.37	6.47
KLX03	325	350	22	0.88	M(A)	4.36	3.84
KLX03	350	375	30	1.20	M(A)	4.24	5.08
KLX03	375	400	10	0.40	M(A)	4.27	1.71
KLX03	400	425	6	0.24	M(A)	4.24	1.02
KLX03	425	450	22	0.88	M(A)	4.23	3.72
KLX03	450	475	1	0.04	M(A)	4.27	0.17
KLX03	475	500	0	0.00	M(A)	4.27	0.00
KLX03	500	525	2	0.08	M(A)	4.40	0.35
KLX03	525	550	3	0.12	M(A)	4.44	0.53
KLX03	550	575	0	0.00	M(A)	4.44	0.00
KLX03	575	600	1	0.04	M(A)	4.36	0.17
KLX03	600	625	7	0.28	M(A)	4.29	1.20
KLX03	625	650	5	0.20	M(D)	4.27	0.85
KLX03	650	675	23	0.92	M(D)	4.27	3.93

Borehole	Start length (m)	End length (m)	Number of fractures	Observed P_{10} (1/m)	Rock domain	P_{10} > P_{32} conversion factor	DFN P_{32} (1/m)
KLX03	675	700	12	0.48	M(D)	4.24	2.03
KLX03	700	725	9	0.36	M(D)	4.31	1.55
KLX03	725	750	9	0.36	M(D)	4.23	1.52
KLX03	750	775	10	0.40	M(D)	4.18	1.67
KLX03	775	800	31	1.24	M(D)	4.13	5.12
KLX03	800	825	19	0.76	D	4.03	3.06
KLX03	825	850	3	0.12	D	4.03	0.48
KLX03	850	875	14	0.56	D	3.95	2.21
KLX03	875	900	14	0.56	D	3.87	2.16
KLX03	900	925	18	0.72	D	3.89	2.80
KLX03	925	950	4	0.16	D	3.84	0.61
KLX03	950	975	18	0.72	D	3.82	2.75
KLX03	975	1,000	4	0.16	D	3.84	0.61
KLX03	1,000	1,025	0	0.00	D	3.87	0.00
KLX04	100	125	15	0.60	A	4.46	2.68
KLX04	125	150	5	0.20	A	4.44	0.89
KLX04	150	175	21	0.84	A	4.45	3.74
KLX04	175	200	35	1.40	A	4.50	6.31
KLX04	200	225	20	0.80	A	4.46	3.57
KLX04	225	250	15	0.60	A	4.48	2.69
KLX04	250	275	21	0.84	A	4.59	3.85
KLX04	275	300	3	0.12	A	4.70	0.56
KLX04	300	325	4	0.16	A	4.73	0.76
KLX04	325	350	7	0.28	A	4.75	1.33
KLX04	350	375	35	1.40	A	4.69	6.56
KLX04	375	400	25	1.00	A	4.70	4.70
KLX04	400	425	20	0.80	A	4.72	3.77
KLX04	425	450	15	0.60	A	4.67	2.80
KLX04	450	475	3	0.12	A	4.60	0.55
KLX04	475	500	5	0.20	A	4.55	0.91
KLX04	500	525	9	0.36	A	4.53	1.63
KLX04	525	550	6	0.24	A	4.48	1.07
KLX04	550	575	9	0.36	A	4.44	1.60
KLX04	575	600	10	0.40	A	4.40	1.76
KLX04	600	625	5	0.20	A	4.45	0.89
KLX04	625	650	8	0.32	A	4.42	1.42
KLX04	650	675	6	0.24	A	4.42	1.06
KLX04	675	700	9	0.36	A	4.44	1.60
KLX04	700	725	7	0.28	A	4.40	1.23
KLX04	725	750	3	0.12	A	4.37	0.52
KLX04	750	775	4	0.16	A	4.31	0.69
KLX04	775	800	0	0.00	A	4.30	0.00
KLX04	800	825	2	0.08	A	4.34	0.35
KLX04	825	850	3	0.12	A	4.25	0.51
KLX04	850	875	4	0.16	A	4.25	0.68

Borehole	Start length (m)	End length (m)	Number of fractures	Observed P_{10} (1/m)	Rock domain	$P_{10} > P_{32}$ conversion factor	DFN P_{32} (1/m)
KLX04	875	900	9	0.36	A	4.25	1.53
KLX04	900	925	33	1.32	A	4.25	5.61
KLX04	925	950	12	0.48	A	4.23	2.03
KLX04	950	975	17	0.68	A	4.23	2.87
KLX04	975	1,000	6	0.24	A	4.20	1.01

Laxemar regional set C
Section length 25 m

Borehole	Start length (m)	End length (m)	Number of fractures	Observed P_{10} (1/m)	Rock domain	$P_{10} > P_{32}$ conversion factor	DFN P_{32} (1/m)
KLX02	200	225	10	0.40	A	3.10	1.24
KLX02	225	250	5	0.20	A	3.09	0.62
KLX02	250	275	9	0.36	A	3.12	1.12
KLX02	275	300	2	0.08	A	3.09	0.25
KLX02	300	325	1	0.04	A	3.09	0.12
KLX02	325	350	6	0.24	A	3.11	0.75
KLX02	350	375	5	0.20	A	3.09	0.62
KLX02	375	400	8	0.32	A	3.04	0.97
KLX02	400	425	1	0.04	A	3.08	0.12
KLX02	425	450	10	0.40	A	3.02	1.21
KLX02	450	475	13	0.52	A	3.09	1.60
KLX02	475	500	2	0.08	A	3.05	0.24
KLX02	500	525	15	0.60	A	3.12	1.87
KLX02	525	550	9	0.36	A	3.14	1.13
KLX02	550	575	5	0.20	BA	3.16	0.63
KLX02	575	600	5	0.20	BA	3.18	0.64
KLX02	600	625	10	0.40	BA	3.15	1.26
KLX02	625	650	5	0.20	BA	3.16	0.63
KLX02	650	675	6	0.24	BA	3.20	0.77
KLX02	675	700	7	0.28	BA	3.20	0.90
KLX02	700	725	12	0.48	BA	3.21	1.54
KLX02	725	750	10	0.40	BA	3.20	1.28
KLX02	750	775	14	0.56	BA	3.18	1.78
KLX02	775	800	7	0.28	BA	3.18	0.89
KLX02	800	825	20	0.80	BA	3.20	2.56
KLX02	825	850	22	0.88	BA	3.19	2.81
KLX02	850	875	27	1.08	BA	3.18	3.44
KLX02	875	900	23	0.92	BA	3.17	2.92
KLX02	900	925	16	0.64	BA	3.15	2.02
KLX02	925	950	32	1.28	BA	3.14	4.02
KLX02	950	975	27	1.08	A	3.14	3.39
KLX02	975	1,000	12	0.48	A	3.18	1.53

Borehole	Start length (m)	End length (m)	Number of fractures	Observed P_{10} (1/m)	Rock domain	P_{10} > P_{32} conversion factor	DFN P_{32} (1/m)
KLX02	1,000	1,025	8	0.32	A	3.10	0.99
KLX03	100	125	7	0.28	M(A)	2.62	0.73
KLX03	125	150	15	0.60	M(A)	2.60	1.56
KLX03	150	175	21	0.84	M(A)	2.58	2.17
KLX03	175	200	2	0.08	M(A)	2.57	0.21
KLX03	200	225	7	0.28	M(A)	2.56	0.72
KLX03	225	250	11	0.44	M(A)	2.56	1.13
KLX03	250	275	9	0.36	M(A)	2.54	0.92
KLX03	275	300	22	0.88	M(A)	2.54	2.23
KLX03	300	325	14	0.56	M(A)	2.58	1.45
KLX03	325	350	5	0.20	M(A)	2.61	0.52
KLX03	350	375	12	0.48	M(A)	2.62	1.26
KLX03	375	400	14	0.56	M(A)	2.63	1.47
KLX03	400	425	10	0.40	M(A)	2.64	1.06
KLX03	425	450	12	0.48	M(A)	2.65	1.27
KLX03	450	475	18	0.72	M(A)	2.68	1.93
KLX03	475	500	2	0.08	M(A)	2.66	0.21
KLX03	500	525	8	0.32	M(A)	2.67	0.85
KLX03	525	550	49	1.96	M(A)	2.70	5.30
KLX03	550	575	37	1.48	M(A)	2.69	3.98
KLX03	575	600	15	0.60	M(A)	2.66	1.60
KLX03	600	625	37	1.48	M(A)	2.68	3.96
KLX03	625	650	44	1.76	M(D)	2.68	4.71
KLX03	650	675	36	1.44	M(D)	2.70	3.88
KLX03	675	700	26	1.04	M(D)	2.72	2.83
KLX03	700	725	36	1.44	M(D)	2.75	3.96
KLX03	725	750	16	0.64	M(D)	2.76	1.77
KLX03	750	775	20	0.80	M(D)	2.77	2.21
KLX03	775	800	46	1.84	M(D)	2.79	5.13
KLX03	800	825	13	0.52	D	2.81	1.46
KLX03	825	850	6	0.24	D	2.82	0.68
KLX03	850	875	3	0.12	D	2.86	0.34
KLX03	875	900	7	0.28	D	2.87	0.80
KLX03	900	925	15	0.60	D	2.88	1.73
KLX03	925	950	0	0.00	D	2.92	0.00
KLX03	950	975	16	0.64	D	2.94	1.88
KLX03	975	1,000	2	0.08	D	2.91	0.23
KLX03	1,000	1,025	0	0.00	D	2.91	0.00
KLX04	100	125	7	0.28	A	3.11	0.87
KLX04	125	150	17	0.68	A	3.11	2.12
KLX04	150	175	18	0.72	A	3.11	2.24
KLX04	175	200	14	0.56	A	3.11	1.74
KLX04	200	225	5	0.20	A	3.11	0.62
KLX04	225	250	13	0.52	A	3.11	1.61
KLX04	250	275	9	0.36	A	3.13	1.13

Borehole	Start length (m)	End length (m)	Number of fractures	Observed P_{10} (1/m)	Rock domain	P_{10} > P_{32} conversion factor	DFN P_{32} (1/m)
KLX04	275	300	11	0.44	A	3.11	1.37
KLX04	300	325	9	0.36	A	3.12	1.12
KLX04	325	350	12	0.48	A	3.16	1.52
KLX04	350	375	8	0.32	A	3.13	1.00
KLX04	375	400	20	0.80	A	3.14	2.51
KLX04	400	425	0	0.00	A	3.09	0.00
KLX04	425	450	7	0.28	A	3.11	0.87
KLX04	450	475	6	0.24	A	3.16	0.76
KLX04	475	500	8	0.32	A	3.18	1.02
KLX04	500	525	22	0.88	A	3.16	2.78
KLX04	525	550	29	1.16	A	3.14	3.65
KLX04	550	575	34	1.36	A	3.12	4.24
KLX04	575	600	17	0.68	A	3.18	2.16
KLX04	600	625	35	1.40	A	3.20	4.48
KLX04	625	650	22	0.88	A	3.21	2.82
KLX04	650	675	34	1.36	A	3.21	4.36
KLX04	675	700	26	1.04	A	3.21	3.33
KLX04	700	725	24	0.96	A	3.21	3.08
KLX04	725	750	15	0.60	A	3.19	1.91
KLX04	750	775	0	0.00	A	3.18	0.00
KLX04	775	800	5	0.20	A	3.17	0.63
KLX04	800	825	1	0.04	A	3.16	0.13
KLX04	825	850	2	0.08	A	3.15	0.25
KLX04	850	875	7	0.28	A	3.14	0.88
KLX04	875	900	12	0.48	A	3.14	1.51
KLX04	900	925	49	1.96	A	3.14	6.15
KLX04	925	950	17	0.68	A	3.14	2.13
KLX04	950	975	26	1.04	A	3.14	3.26
KLX04	975	1,000	20	0.80	A	3.13	2.51

Laxemar local set D
Section length 25 m

Borehole	Start length (m)	End length (m)	Number of fractures	Observed P_{10} (1/m)	Rock domain	P_{10} > P_{32} conversion factor	DFN P_{32} (1/m)
KLX02	200	225	14	0.56	A	1.03	0.58
KLX02	225	250	23	0.92	A	1.03	0.95
KLX02	250	275	27	1.08	A	1.03	1.12
KLX02	275	300	14	0.56	A	1.04	0.58
KLX02	300	325	7	0.28	A	1.03	0.29
KLX02	325	350	17	0.68	A	1.03	0.70
KLX02	350	375	9	0.36	A	1.04	0.37
KLX02	375	400	20	0.80	A	1.03	0.82
KLX02	400	425	13	0.52	A	1.15	0.60

Borehole	Start length (m)	End length (m)	Number of fractures	Observed P_{10} (1/m)	Rock domain	P_{10} > P_{32} conversion factor	DFN P_{32} (1/m)
KLX02	425	450	40	1.60	A	1.03	1.65
KLX02	450	475	46	1.84	A	1.03	1.89
KLX02	475	500	12	0.48	A	1.03	0.49
KLX02	500	525	10	0.40	A	1.02	0.41
KLX02	525	550	5	0.20	A	1.03	0.21
KLX02	550	575	17	0.68	BA	1.02	0.70
KLX02	575	600	21	0.84	BA	1.03	0.86
KLX02	600	625	19	0.76	BA	1.03	0.78
KLX02	625	650	30	1.20	BA	1.02	1.23
KLX02	650	675	43	1.72	BA	1.03	1.77
KLX02	675	700	21	0.84	BA	1.03	0.86
KLX02	700	725	21	0.84	BA	1.03	0.86
KLX02	725	750	42	1.68	BA	1.03	1.73
KLX02	750	775	41	1.64	BA	1.03	1.69
KLX02	775	800	36	1.44	BA	1.03	1.48
KLX02	800	825	133	5.32	BA	1.03	5.47
KLX02	825	850	57	2.28	BA	1.03	2.35
KLX02	850	875	125	5.00	BA	1.03	5.13
KLX02	875	900	82	3.28	BA	1.02	3.35
KLX02	900	925	60	2.40	BA	1.02	2.45
KLX02	925	950	116	4.64	BA	1.02	4.73
KLX02	950	975	91	3.64	A	1.02	3.71
KLX02	975	1,000	78	3.12	A	1.03	3.21
KLX02	1,000	1,025	32	1.28	A	1.17	1.50
KLX03	100	125	18	0.72	M(A)	1.26	0.91
KLX03	125	150	29	1.16	M(A)	1.26	1.46
KLX03	150	175	20	0.80	M(A)	1.26	1.00
KLX03	175	200	42	1.68	M(A)	1.26	2.11
KLX03	200	225	74	2.96	M(A)	1.25	3.71
KLX03	225	250	49	1.96	M(A)	1.25	2.46
KLX03	250	275	71	2.84	M(A)	1.25	3.54
KLX03	275	300	92	3.68	M(A)	1.25	4.60
KLX03	300	325	44	1.76	M(A)	1.24	2.18
KLX03	325	350	104	4.16	M(A)	1.23	5.14
KLX03	350	375	41	1.64	M(A)	1.23	2.02
KLX03	375	400	37	1.48	M(A)	1.23	1.82
KLX03	400	425	38	1.52	M(A)	1.23	1.87
KLX03	425	450	51	2.04	M(A)	1.23	2.51
KLX03	450	475	36	1.44	M(A)	1.23	1.77
KLX03	475	500	21	0.84	M(A)	1.22	1.03
KLX03	500	525	33	1.32	M(A)	1.23	1.62
KLX03	525	550	10	0.40	M(A)	1.24	0.49
KLX03	550	575	11	0.44	M(A)	1.24	0.55
KLX03	575	600	22	0.88	M(A)	1.23	1.08
KLX03	600	625	74	2.96	M(A)	1.23	3.63

Borehole	Start length (m)	End length (m)	Number of fractures	Observed P_{10} (1/m)	Rock domain	$P_{10} > P_{32}$ conversion factor	DFN P_{32} (1/m)
KLX03	625	650	49	1.96	M(D)	1.22	2.40
KLX03	650	675	85	3.40	M(D)	1.22	4.15
KLX03	675	700	119	4.76	M(D)	1.22	5.80
KLX03	700	725	66	2.64	M(D)	1.23	3.24
KLX03	725	750	123	4.92	M(D)	1.22	6.00
KLX03	750	775	118	4.72	M(D)	1.22	5.74
KLX03	775	800	110	4.40	M(D)	1.22	5.35
KLX03	800	825	76	3.04	D	1.21	3.67
KLX03	825	850	73	2.92	D	1.20	3.51
KLX03	850	875	102	4.08	D	1.20	4.88
KLX03	875	900	35	1.40	D	1.19	1.66
KLX03	900	925	92	3.68	D	1.19	4.36
KLX03	925	950	61	2.44	D	1.18	2.88
KLX03	950	975	109	4.36	D	1.17	5.10
KLX03	975	1,000	58	2.32	D	1.16	2.70
KLX03	1,000	1,025	0	0.00	D	1.16	0.00
KLX04	100	125	84	3.36	A	1.03	3.46
KLX04	125	150	109	4.36	A	1.03	4.49
KLX04	150	175	101	4.04	A	1.03	4.16
KLX04	175	200	91	3.64	A	1.03	3.75
KLX04	200	225	136	5.44	A	1.03	5.60
KLX04	225	250	74	2.96	A	1.03	3.04
KLX04	250	275	149	5.96	A	1.03	6.13
KLX04	275	300	128	5.12	A	1.03	5.26
KLX04	300	325	100	4.00	A	1.03	4.10
KLX04	325	350	56	2.24	A	1.03	2.30
KLX04	350	375	116	4.64	A	1.03	4.79
KLX04	375	400	88	3.52	A	1.03	3.63
KLX04	400	425	95	3.80	A	1.03	3.93
KLX04	425	450	101	4.04	A	1.03	4.17
KLX04	450	475	30	1.20	A	1.04	1.24
KLX04	475	500	36	1.44	A	1.04	1.50
KLX04	500	525	133	5.32	A	1.04	5.54
KLX04	525	550	70	2.80	A	1.04	2.92
KLX04	550	575	30	1.20	A	1.04	1.25
KLX04	575	600	98	3.92	A	1.05	4.10
KLX04	600	625	91	3.64	A	1.04	3.79
KLX04	625	650	100	4.00	A	1.04	4.18
KLX04	650	675	92	3.68	A	1.04	3.84
KLX04	675	700	79	3.16	A	1.05	3.32
KLX04	700	725	72	2.88	A	1.05	3.03
KLX04	725	750	61	2.44	A	1.05	2.57
KLX04	750	775	57	2.28	A	1.05	2.40
KLX04	775	800	38	1.52	A	1.06	1.61
KLX04	800	825	24	0.96	A	1.06	1.02

Borehole	Start length (m)	End length (m)	Number of fractures	Observed P_{10} (1/m)	Rock domain	$P_{10} > P_{32}$ conversion factor	DFN P_{32} (1/m)
KLX04	825	850	67	2.68	A	1.06	2.83
KLX04	850	875	43	1.72	A	1.06	1.82
KLX04	875	900	190	7.60	A	1.06	8.06
KLX04	900	925	154	6.16	A	1.06	6.53
KLX04	925	950	217	8.68	A	1.06	9.20
KLX04	950	975	171	6.84	A	1.06	7.25
KLX04	975	1,000	7	0.28	A	1.06	0.30

Laxemar local set F
Section length **25** **m**

Borehole	Start length (m)	End length (m)	Number of fractures	Observed P_{10} (1/m)	Rock domain	$P_{10} > P_{32}$ conversion factor	DFN P_{32} (1/m)
KLX02	200	225	1	0.04	A	2.19	0.09
KLX02	225	250	9	0.36	A	2.19	0.79
KLX02	250	275	11	0.44	A	2.20	0.97
KLX02	275	300	2	0.08	A	2.19	0.18
KLX02	300	325	11	0.44	A	2.20	0.97
KLX02	325	350	6	0.24	A	2.21	0.53
KLX02	350	375	1	0.04	A	2.23	0.09
KLX02	375	400	8	0.32	A	2.23	0.71
KLX02	400	425	1	0.04	A	1.94	0.08
KLX02	425	450	11	0.44	A	2.23	0.98
KLX02	450	475	20	0.80	A	2.24	1.79
KLX02	475	500	15	0.60	A	2.24	1.34
KLX02	500	525	7	0.28	A	2.23	0.63
KLX02	525	550	5	0.20	A	2.25	0.45
KLX02	550	575	9	0.36	BA	2.25	0.81
KLX02	575	600	5	0.20	BA	2.26	0.45
KLX02	600	625	16	0.64	BA	2.25	1.44
KLX02	625	650	12	0.48	BA	2.25	1.08
KLX02	650	675	21	0.84	BA	2.26	1.89
KLX02	675	700	3	0.12	BA	2.26	0.27
KLX02	700	725	16	0.64	BA	2.26	1.45
KLX02	725	750	13	0.52	BA	2.26	1.17
KLX02	750	775	31	1.24	BA	2.26	2.80
KLX02	775	800	26	1.04	BA	2.26	2.35
KLX02	800	825	20	0.80	BA	2.26	1.80
KLX02	825	850	16	0.64	BA	2.27	1.45
KLX02	850	875	50	2.00	BA	2.26	4.51
KLX02	875	900	55	2.20	BA	2.24	4.93
KLX02	900	925	40	1.60	BA	2.24	3.58
KLX02	925	950	17	0.68	BA	2.23	1.52
KLX02	950	975	17	0.68	A	2.23	1.52

Borehole	Start length (m)	End length (m)	Number of fractures	Observed P_{10} (1/m)	Rock domain	$P_{10} > P_{32}$ conversion factor	DFN P_{32} (1/m)
KLX02	975	1,000	31	1.24	A	2.26	2.80
KLX02	1,000	1,025	9	0.36	A	1.91	0.69
KLX03	100	125	2	0.08	M(A)	1.53	0.12
KLX03	125	150	5	0.20	M(A)	1.53	0.31
KLX03	150	175	4	0.16	M(A)	1.52	0.24
KLX03	175	200	12	0.48	M(A)	1.52	0.73
KLX03	200	225	17	0.68	M(A)	1.51	1.03
KLX03	225	250	15	0.60	M(A)	1.50	0.90
KLX03	250	275	18	0.72	M(A)	1.48	1.07
KLX03	275	300	40	1.60	M(A)	1.47	2.35
KLX03	300	325	33	1.32	M(A)	1.48	1.95
KLX03	325	350	39	1.56	M(A)	1.48	2.31
KLX03	350	375	12	0.48	M(A)	1.48	0.71
KLX03	375	400	11	0.44	M(A)	1.48	0.65
KLX03	400	425	14	0.56	M(A)	1.49	0.83
KLX03	425	450	7	0.28	M(A)	1.49	0.42
KLX03	450	475	4	0.16	M(A)	1.49	0.24
KLX03	475	500	1	0.04	M(A)	1.49	0.06
KLX03	500	525	1	0.04	M(A)	1.52	0.06
KLX03	525	550	4	0.16	M(A)	1.54	0.25
KLX03	550	575	2	0.08	M(A)	1.52	0.12
KLX03	575	600	0	0.00	M(A)	1.52	0.00
KLX03	600	625	9	0.36	M(A)	1.52	0.55
KLX03	625	650	12	0.48	M(D)	1.52	0.73
KLX03	650	675	60	2.40	M(D)	1.50	3.60
KLX03	675	700	32	1.28	M(D)	1.50	1.92
KLX03	700	725	31	1.24	M(D)	1.49	1.85
KLX03	725	750	19	0.76	M(D)	1.49	1.13
KLX03	750	775	44	1.76	M(D)	1.48	2.60
KLX03	775	800	32	1.28	M(D)	1.46	1.87
KLX03	800	825	8	0.32	D	1.45	0.46
KLX03	825	850	5	0.20	D	1.45	0.29
KLX03	850	875	4	0.16	D	1.44	0.23
KLX03	875	900	3	0.12	D	1.44	0.17
KLX03	900	925	30	1.20	D	1.44	1.73
KLX03	925	950	12	0.48	D	1.45	0.69
KLX03	950	975	14	0.56	D	1.44	0.80
KLX03	975	1,000	6	0.24	D	1.45	0.35
KLX03	1,000	1,025	0	0.00	D	1.45	0.00
KLX04	100	125	58	2.32	A	2.22	5.14
KLX04	125	150	24	0.96	A	2.21	2.12
KLX04	150	175	35	1.40	A	2.21	3.09
KLX04	175	200	44	1.76	A	2.20	3.88
KLX04	200	225	42	1.68	A	2.20	3.69
KLX04	225	250	11	0.44	A	2.21	0.97

Borehole	Start length (m)	End length (m)	Number of fractures	Observed P_{10} (1/m)	Rock domain	P_{10} > P_{32} conversion factor	DFN P_{32} (1/m)
KLX04	250	275	42	1.68	A	2.24	3.77
KLX04	275	300	9	0.36	A	2.24	0.81
KLX04	300	325	20	0.80	A	2.24	1.79
KLX04	325	350	40	1.60	A	2.25	3.60
KLX04	350	375	9	0.36	A	2.27	0.82
KLX04	375	400	11	0.44	A	2.29	1.01
KLX04	400	425	19	0.76	A	2.28	1.73
KLX04	425	450	25	1.00	A	2.28	2.28
KLX04	450	475	14	0.56	A	2.31	1.29
KLX04	475	500	9	0.36	A	2.31	0.83
KLX04	500	525	17	0.68	A	2.31	1.57
KLX04	525	550	13	0.52	A	2.32	1.21
KLX04	550	575	9	0.36	A	2.31	0.83
KLX04	575	600	23	0.92	A	2.34	2.15
KLX04	600	625	23	0.92	A	2.37	2.18
KLX04	625	650	34	1.36	A	2.39	3.25
KLX04	650	675	24	0.96	A	2.40	2.30
KLX04	675	700	20	0.80	A	2.43	1.94
KLX04	700	725	8	0.32	A	2.46	0.79
KLX04	725	750	3	0.12	A	2.50	0.30
KLX04	750	775	7	0.28	A	2.50	0.70
KLX04	775	800	9	0.36	A	2.51	0.90
KLX04	800	825	1	0.04	A	2.53	0.10
KLX04	825	850	3	0.12	A	2.55	0.31
KLX04	850	875	13	0.52	A	2.54	1.32
KLX04	875	900	18	0.72	A	2.56	1.84
KLX04	900	925	23	0.92	A	2.58	2.38
KLX04	925	950	41	1.64	A	2.58	4.23
KLX04	950	975	29	1.16	A	2.58	2.99
KLX04	975	1,000	3	0.12	A	2.60	0.31

Simpevarp regional set A
Section length 25 m

Borehole	Start length (m)	End length (m)	Number of fractures	Observed P_{10} (1/m)	Rock domain	P_{10} > P_{32} conversion factor	DFN P_{32} (1/m)
KAV01	0	25	0	0.00	A	3.86	0.00
KAV01	25	50	0	0.00	A	3.88	0.00
KAV01	50	75	0	0.00	A	3.87	0.00
KAV01	75	100	9	0.36	A	3.87	1.39
KAV01	100	125	10	0.40	A	3.87	1.55
KAV01	125	150	19	0.76	B	3.87	2.94
KAV01	150	175	32	1.28	B	3.97	5.08
KAV01	175	200	23	0.92	A	3.99	3.67
KAV01	200	225	40	1.60	A	4.00	6.40

Borehole	Start length (m)	End length (m)	Number of fractures	Observed P_{10} (1/m)	Rock domain	P_{10} > P_{32} conversion factor	DFN P_{32} (1/m)
KAV01	225	250	19	0.76	A	3.99	3.03
KAV01	250	275	10	0.40	A	3.99	1.60
KAV01	275	300	17	0.68	A	3.99	2.71
KAV01	300	325	28	1.12	A	3.95	4.42
KAV01	325	350	22	0.88	A	4.00	3.52
KAV01	350	375	18	0.72	A	4.01	2.89
KAV01	375	400	19	0.76	A	3.93	2.98
KAV01	400	425	35	1.40	A	3.93	5.50
KAV01	425	450	65	2.60	A	3.93	10.21
KAV01	450	475	57	2.28	A	3.95	9.00
KAV01	475	500	65	2.60	A	3.95	10.26
KAV01	500	525	65	2.60	A	3.97	10.32
KAV01	525	550	37	1.48	A	3.94	5.83
KAV01	550	575	53	2.12	A	4.11	8.71
KAV01	575	600	37	1.48	A	4.09	6.05
KAV01	600	625	41	1.64	A	4.04	6.63
KAV01	625	650	53	2.12	A	4.04	8.57
KAV01	650	675	52	2.08	A	4.07	8.46
KAV01	675	700	36	1.44	A	4.03	5.81
KAV01	700	725	7	0.28	A	4.03	1.13
KAV01	725	750	17	0.68	A	4.03	2.74
KAV01	750	775	0	0.00	A	4.03	0.00
KAV04A	100	125	21	0.84	A	3.84	3.22
KAV04A	125	150	12	0.48	A	3.83	1.84
KAV04A	150	175	16	0.64	A	3.83	2.45
KAV04A	175	200	14	0.56	A	3.83	2.14
KAV04A	200	225	7	0.28	A	3.81	1.07
KAV04A	225	250	16	0.64	A	3.83	2.45
KAV04A	250	275	22	0.88	A	3.83	3.37
KAV04A	275	300	23	0.92	A	3.83	3.52
KAV04A	300	325	17	0.68	C	3.82	2.60
KAV04A	325	350	7	0.28	C	3.84	1.07
KAV04A	350	375	24	0.96	C	3.89	3.73
KAV04A	375	400	30	1.20	C	3.88	4.65
KAV04A	400	425	34	1.36	C	3.91	5.31
KAV04A	425	450	15	0.60	C	3.91	2.34
KAV04A	450	475	12	0.48	C	3.94	1.89
KAV04A	475	500	12	0.48	C	3.97	1.90
KAV04A	500	525	58	2.32	C	3.97	9.21
KAV04A	525	550	43	1.72	C	3.96	6.81
KAV04A	550	575	49	1.96	C	3.97	7.78
KAV04A	575	600	33	1.32	C	3.99	5.27
KAV04A	600	625	40	1.60	C	3.99	6.38
KAV04A	625	650	23	0.92	C	4.03	3.71
KAV04A	650	675	22	0.88	C	4.01	3.53

Borehole	Start length (m)	End length (m)	Number of fractures	Observed P_{10} (1/m)	Rock domain	P_{10} > P_{32} conversion factor	DFN P_{32} (1/m)
KAV04A	675	700	35	1.40	C	4.01	5.61
KAV04A	700	725	49	1.96	A	4.02	7.88
KAV04A	725	750	23	0.92	A	4.00	3.68
KAV04A	750	775	28	1.12	A	3.98	4.46
KAV04A	775	800	20	0.80	A	3.99	3.19
KAV04A	800	825	4	0.16	A	3.98	0.64
KAV04A	825	850	11	0.44	A	3.96	1.74
KAV04A	850	875	6	0.24	B	3.99	0.96
KAV04A	875	900	25	1.00	B	4.00	4.00
KAV04A	900	925	25	1.00	B	3.99	3.99
KAV04A	925	950	30	1.20	B	4.01	4.81
KAV04A	950	975	19	0.76	A	3.97	3.02
KAV04A	975	1,000	40	1.60	A	3.92	6.27
KSH01A	97	122	20	0.80	C	3.78	3.02
KSH01A	122	147	36	1.44	C	3.78	5.44
KSH01A	147	172	8	0.32	C	3.84	1.23
KSH01A	172	197	12	0.48	C	3.87	1.86
KSH01A	197	222	43	1.72	B	3.91	6.72
KSH01A	222	247	30	1.20	B	3.91	4.69
KSH01A	247	272	59	2.36	C	3.90	9.19
KSH01A	272	297	35	1.40	C	3.88	5.43
KSH01A	297	322	20	0.80	C	3.85	3.08
KSH01A	322	347	26	1.04	B	3.90	4.05
KSH01A	347	372	30	1.20	B	3.95	4.74
KSH01A	372	397	37	1.48	B	3.90	5.77
KSH01A	397	422	17	0.68	B	3.90	2.65
KSH01A	422	447	34	1.36	B	3.92	5.33
KSH01A	447	472	30	1.20	B	3.84	4.60
KSH01A	472	497	42	1.68	B	3.86	6.48
KSH01A	497	522	43	1.72	B	3.88	6.67
KSH01A	522	547	47	1.88	B	3.85	7.23
KSH01A	547	572	45	1.80	B	3.87	6.96
KSH01A	572	597	35	1.40	B	3.90	5.45
KSH01A	597	622	20	0.80	B	3.98	3.18
KSH01A	622	647	10	0.40	C	3.94	1.57
KSH01A	647	672	24	0.96	C	3.93	3.77
KSH01A	672	697	45	1.80	C	3.91	7.03
KSH01A	697	722	29	1.16	C	3.90	4.52
KSH01A	722	747	26	1.04	C	3.90	4.05
KSH01A	747	772	56	2.24	C	3.91	8.75
KSH01A	772	797	29	1.16	C	3.94	4.57
KSH01A	797	822	36	1.44	C	3.98	5.73
KSH01A	822	847	16	0.64	C	3.91	2.50
KSH01A	847	872	31	1.24	C	3.95	4.89
KSH01A	872	897	5	0.20	C	3.99	0.80

Borehole	Start length (m)	End length (m)	Number of fractures	Observed P_{10} (1/m)	Rock domain	P_{10} > P_{32} conversion factor	DFN P_{32} (1/m)
KSH01A	897	922	34	1.36	C	3.98	5.41
KSH01A	922	947	16	0.64	C	3.98	2.55
KSH01A	947	972	10	0.40	C	4.04	1.62
KSH01A	972	997	3	0.12	C	4.03	0.48
KSH01A	997	1,022	0	0.00	C	4.00	0.00
KSH02	0	25	5	0.20	B	3.23	0.65
KSH02	25	50	101	4.04	B	3.22	13.00
KSH02	50	75	34	1.36	B	3.23	4.39
KSH02	75	100	16	0.64	B	3.42	2.19
KSH02	100	125	29	1.16	B	3.42	3.97
KSH02	125	150	41	1.64	B	3.45	5.66
KSH02	150	175	52	2.08	B	3.45	7.17
KSH02	175	200	44	1.76	B	3.45	6.07
KSH02	200	225	37	1.48	B	3.46	5.12
KSH02	225	250	29	1.16	B	3.46	4.02
KSH02	250	275	56	2.24	B	3.43	7.69
KSH02	275	300	20	0.80	B	3.45	2.76
KSH02	300	325	33	1.32	B	3.42	4.52
KSH02	325	350	54	2.16	B	3.46	7.48
KSH02	350	375	50	2.00	B	3.48	6.96
KSH02	375	400	20	0.80	B	3.52	2.82
KSH02	400	425	41	1.64	B	3.80	6.23
KSH02	425	450	37	1.48	B	3.51	5.20
KSH02	450	475	34	1.36	B	3.50	4.77
KSH02	475	500	47	1.88	B	3.52	6.62
KSH02	500	525	57	2.28	B	3.54	8.07
KSH02	525	550	37	1.48	B	3.53	5.22
KSH02	550	575	43	1.72	B	3.53	6.07
KSH02	575	600	30	1.20	B	3.54	4.25
KSH02	600	625	27	1.08	B	3.54	3.82
KSH02	625	650	46	1.84	B	3.53	6.49
KSH02	650	675	57	2.28	B	3.55	8.10
KSH02	675	700	24	0.96	B	3.55	3.41
KSH02	700	725	19	0.76	B	3.57	2.71
KSH02	725	750	21	0.84	B	3.60	3.02
KSH02	750	775	12	0.48	B	3.57	1.71
KSH02	775	800	10	0.40	B	3.60	1.44
KSH02	800	825	5	0.20	B	3.61	0.72
KSH02	825	850	18	0.72	B	3.65	2.63
KSH02	850	875	39	1.56	B	3.69	5.75
KSH02	875	900	22	0.88	B	3.72	3.28
KSH02	900	925	25	1.00	B	3.76	3.76
KSH02	925	950	9	0.36	B	3.75	1.35
KSH02	950	975	3	0.12	B	3.77	0.45
KSH02	975	1,000	2	0.08	B	3.78	0.30

Borehole	Start length (m)	End length (m)	Number of fractures	Observed P_{10} (1/m)	Rock domain	P_{10} > P_{32} conversion factor	DFN P_{32} (1/m)
KSH02	1,000	1,025	0	0.00	B	3.77	0.00
KSH03A	100	125	35	1.40	C	2.20	3.08
KSH03A	125	150	27	1.08	C	2.20	2.38
KSH03A	150	175	57	2.28	C	2.18	4.97
KSH03A	175	200	29	1.16	C	2.17	2.52
KSH03A	200	225	52	2.08	C	2.16	4.49
KSH03A	225	250	47	1.88	C	2.16	4.06
KSH03A	250	275	49	1.96	C	2.18	4.27
KSH03A	275	300	18	0.72	A	2.19	1.57
KSH03A	300	325	31	1.24	A	2.17	2.69
KSH03A	325	350	34	1.36	A	2.16	2.93
KSH03A	350	375	17	0.68	A	2.11	1.44
KSH03A	375	400	17	0.68	A	2.08	1.41
KSH03A	400	425	31	1.24	A	2.05	2.54
KSH03A	425	450	12	0.48	A	2.02	0.97
KSH03A	450	475	5	0.20	A	2.01	0.40
KSH03A	475	500	4	0.16	A	2.02	0.32
KSH03A	500	525	3	0.12	A	2.01	0.24
KSH03A	525	550	5	0.20	A	2.00	0.40
KSH03A	550	575	7	0.28	A	2.01	0.56
KSH03A	575	600	4	0.16	A	2.03	0.32
KSH03A	600	625	5	0.20	A	2.04	0.41
KSH03A	625	650	2	0.08	A	2.04	0.16
KSH03A	650	675	5	0.20	A	2.02	0.40
KSH03A	675	700	11	0.44	A	2.01	0.88
KSH03A	700	725	10	0.40	A	2.03	0.81
KSH03A	725	750	2	0.08	A	2.03	0.16
KSH03A	750	775	5	0.20	A	2.00	0.40
KSH03A	775	800	6	0.24	A	1.98	0.47
KSH03A	800	825	14	0.56	A	1.95	1.09
KSH03A	825	850	20	0.80	A	1.92	1.54
KSH03A	850	875	67	2.68	A	1.88	5.04
KSH03A	875	900	36	1.44	A	1.83	2.63
KSH03A	900	925	14	0.56	A	1.77	0.99
KSH03A	925	950	27	1.08	A	1.75	1.89
KSH03A	950	975	13	0.52	A	1.75	0.91
KSH03A	975	1,000	7	0.28	A	1.73	0.49
KSH03A	1,000	1,025	0	0.00	A	1.72	0.00

Simpevarp regional set B
Section length 25 m

Borehole	Start length (m)	End length (m)	Number of fractures	Observed P_{10} (1/m)	Rock domain	P_{10} > P_{32} conversion factor	DFN P_{32} (1/m)
KAV01	0	25	0	0.00	A	3.33	0.00
KAV01	25	50	0	0.00	A	3.32	0.00
KAV01	50	75	3	0.12	A	3.33	0.40
KAV01	75	100	8	0.32	A	3.33	1.06
KAV01	100	125	24	0.96	A	3.33	3.19
KAV01	125	150	39	1.56	B	3.33	5.19
KAV01	150	175	31	1.24	B	3.35	4.15
KAV01	175	200	28	1.12	A	3.33	3.73
KAV01	200	225	27	1.08	A	3.34	3.61
KAV01	225	250	7	0.28	A	3.35	0.94
KAV01	250	275	6	0.24	A	3.28	0.79
KAV01	275	300	12	0.48	A	3.30	1.59
KAV01	300	325	8	0.32	A	3.30	1.05
KAV01	325	350	9	0.36	A	3.23	1.16
KAV01	350	375	18	0.72	A	3.25	2.34
KAV01	375	400	13	0.52	A	3.23	1.68
KAV01	400	425	9	0.36	A	3.26	1.17
KAV01	425	450	22	0.88	A	3.25	2.86
KAV01	450	475	31	1.24	A	3.25	4.03
KAV01	475	500	24	0.96	A	3.28	3.15
KAV01	500	525	20	0.80	A	3.28	2.62
KAV01	525	550	33	1.32	A	3.28	4.33
KAV01	550	575	25	1.00	A	3.28	3.28
KAV01	575	600	12	0.48	A	3.30	1.58
KAV01	600	625	30	1.20	A	3.30	3.96
KAV01	625	650	36	1.44	A	3.33	4.79
KAV01	650	675	13	0.52	A	3.33	1.73
KAV01	675	700	21	0.84	A	3.35	2.81
KAV01	700	725	14	0.56	A	3.36	1.88
KAV01	725	750	22	0.88	A	3.34	2.94
KAV01	750	775	0	0.00	A	3.32	0.00
KAV04A	100	125	22	0.88	A	3.31	2.91
KAV04A	125	150	9	0.36	A	3.31	1.19
KAV04A	150	175	8	0.32	A	3.30	1.05
KAV04A	175	200	8	0.32	A	3.33	1.06
KAV04A	200	225	38	1.52	A	3.34	5.08
KAV04A	225	250	27	1.08	A	3.34	3.61
KAV04A	250	275	18	0.72	A	3.33	2.40
KAV04A	275	300	12	0.48	A	3.33	1.60
KAV04A	300	325	18	0.72	C	3.33	2.39
KAV04A	325	350	17	0.68	C	3.33	2.27
KAV04A	350	375	20	0.80	C	3.36	2.68
KAV04A	375	400	28	1.12	C	3.33	3.73

Borehole	Start length (m)	End length (m)	Number of fractures	Observed P_{10} (1/m)	Rock domain	$P_{10} > P_{32}$ conversion factor	DFN P_{32} (1/m)
KAV04A	400	425	31	1.24	C	3.36	4.17
KAV04A	425	450	19	0.76	C	3.37	2.56
KAV04A	450	475	15	0.60	C	3.34	2.00
KAV04A	475	500	15	0.60	C	3.38	2.03
KAV04A	500	525	23	0.92	C	3.39	3.12
KAV04A	525	550	37	1.48	C	3.38	5.00
KAV04A	550	575	29	1.16	C	3.42	3.96
KAV04A	575	600	22	0.88	C	3.43	3.02
KAV04A	600	625	77	3.08	C	3.41	10.50
KAV04A	625	650	24	0.96	C	3.41	3.27
KAV04A	650	675	15	0.60	C	3.41	2.05
KAV04A	675	700	16	0.64	C	3.40	2.18
KAV04A	700	725	21	0.84	A	3.41	2.86
KAV04A	725	750	21	0.84	A	3.41	2.86
KAV04A	750	775	39	1.56	A	3.40	5.31
KAV04A	775	800	16	0.64	A	3.38	2.16
KAV04A	800	825	34	1.36	A	3.36	4.57
KAV04A	825	850	25	1.00	A	3.33	3.33
KAV04A	850	875	16	0.64	B	3.33	2.13
KAV04A	875	900	18	0.72	B	3.33	2.39
KAV04A	900	925	46	1.84	B	3.36	6.19
KAV04A	925	950	29	1.16	B	3.36	3.90
KAV04A	950	975	36	1.44	A	3.35	4.82
KAV04A	975	1,000	70	2.80	A	3.40	9.52
KSH01A	97	122	47	1.88	C	3.17	5.96
KSH01A	122	147	52	2.08	C	3.17	6.60
KSH01A	147	172	17	0.68	C	3.23	2.20
KSH01A	172	197	7	0.28	C	3.24	0.91
KSH01A	197	222	40	1.60	B	3.29	5.26
KSH01A	222	247	18	0.72	B	3.28	2.36
KSH01A	247	272	35	1.40	C	3.26	4.57
KSH01A	272	297	25	1.00	C	3.28	3.28
KSH01A	297	322	13	0.52	C	3.28	1.71
KSH01A	322	347	21	0.84	B	3.34	2.81
KSH01A	347	372	25	1.00	B	3.34	3.34
KSH01A	372	397	41	1.64	B	3.38	5.54
KSH01A	397	422	32	1.28	B	3.39	4.34
KSH01A	422	447	64	2.56	B	3.39	8.67
KSH01A	447	472	37	1.48	B	3.38	5.00
KSH01A	472	497	71	2.84	B	3.39	9.64
KSH01A	497	522	130	5.20	B	3.36	17.45
KSH01A	522	547	98	3.92	B	3.36	13.15
KSH01A	547	572	93	3.72	B	3.28	12.18
KSH01A	572	597	51	2.04	B	3.22	6.57
KSH01A	597	622	41	1.64	B	3.18	5.21

Borehole	Start length (m)	End length (m)	Number of fractures	Observed P_{10} (1/m)	Rock domain	P_{10} > P_{32} conversion factor	DFN P_{32} (1/m)
KSH01A	622	647	36	1.44	C	3.18	4.59
KSH01A	647	672	21	0.84	C	3.21	2.69
KSH01A	672	697	89	3.56	C	3.22	11.46
KSH01A	697	722	29	1.16	C	3.19	3.70
KSH01A	722	747	20	0.80	C	3.16	2.53
KSH01A	747	772	14	0.56	C	3.20	1.79
KSH01A	772	797	6	0.24	C	3.22	0.77
KSH01A	797	822	7	0.28	C	3.22	0.90
KSH01A	822	847	15	0.60	C	3.25	1.95
KSH01A	847	872	8	0.32	C	3.25	1.04
KSH01A	872	897	15	0.60	C	3.23	1.94
KSH01A	897	922	6	0.24	C	3.25	0.78
KSH01A	922	947	2	0.08	C	3.18	0.25
KSH01A	947	972	8	0.32	C	3.16	1.01
KSH01A	972	997	7	0.28	C	3.16	0.88
KSH01A	997	1,022	0	0.00	C	3.16	0.00
KSH02	0	25	4	0.16	B	3.44	0.55
KSH02	25	50	22	0.88	B	3.44	3.03
KSH02	50	75	16	0.64	B	3.44	2.20
KSH02	75	100	16	0.64	B	3.45	2.21
KSH02	100	125	18	0.72	B	3.46	2.49
KSH02	125	150	34	1.36	B	3.42	4.66
KSH02	150	175	23	0.92	B	3.38	3.11
KSH02	175	200	31	1.24	B	3.38	4.19
KSH02	200	225	25	1.00	B	3.36	3.36
KSH02	225	250	44	1.76	B	3.31	5.83
KSH02	250	275	25	1.00	B	3.32	3.32
KSH02	275	300	15	0.60	B	3.34	2.00
KSH02	300	325	18	0.72	B	3.37	2.43
KSH02	325	350	25	1.00	B	3.39	3.39
KSH02	350	375	22	0.88	B	3.35	2.95
KSH02	375	400	41	1.64	B	3.32	5.44
KSH02	400	425	41	1.64	B	3.23	5.29
KSH02	425	450	18	0.72	B	3.26	2.35
KSH02	450	475	49	1.96	B	3.25	6.36
KSH02	475	500	63	2.52	B	3.26	8.22
KSH02	500	525	87	3.48	B	3.28	11.40
KSH02	525	550	98	3.92	B	3.27	12.81
KSH02	550	575	52	2.08	B	3.26	6.78
KSH02	575	600	29	1.16	B	3.25	3.77
KSH02	600	625	15	0.60	B	3.27	1.96
KSH02	625	650	22	0.88	B	3.26	2.87
KSH02	650	675	66	2.64	B	3.25	8.57
KSH02	675	700	14	0.56	B	3.25	1.82
KSH02	700	725	25	1.00	B	3.26	3.26

Borehole	Start length (m)	End length (m)	Number of fractures	Observed P_{10} (1/m)	Rock domain	P_{10} > P_{32} conversion factor	DFN P_{32} (1/m)
KSH02	725	750	24	0.96	B	3.26	3.13
KSH02	750	775	18	0.72	B	3.26	2.35
KSH02	775	800	18	0.72	B	3.25	2.34
KSH02	800	825	22	0.88	B	3.28	2.88
KSH02	825	850	20	0.80	B	3.28	2.63
KSH02	850	875	14	0.56	B	3.27	1.83
KSH02	875	900	35	1.40	B	3.30	4.62
KSH02	900	925	13	0.52	B	3.33	1.73
KSH02	925	950	19	0.76	B	3.33	2.53
KSH02	950	975	32	1.28	B	3.27	4.18
KSH02	975	1,000	15	0.60	B	3.27	1.96
KSH02	1,000	1,025	0	0.00	B	3.28	0.00
KSH03A	100	125	28	1.12	C	1.76	1.98
KSH03A	125	150	31	1.24	C	1.80	2.24
KSH03A	150	175	32	1.28	C	1.81	2.31
KSH03A	175	200	42	1.68	C	1.82	3.07
KSH03A	200	225	46	1.84	C	1.82	3.35
KSH03A	225	250	71	2.84	C	1.82	5.18
KSH03A	250	275	55	2.20	C	1.82	4.01
KSH03A	275	300	33	1.32	A	1.83	2.42
KSH03A	300	325	49	1.96	A	1.86	3.64
KSH03A	325	350	76	3.04	A	1.90	5.77
KSH03A	350	375	41	1.64	A	1.91	3.13
KSH03A	375	400	27	1.08	A	1.93	2.08
KSH03A	400	425	53	2.12	A	1.98	4.20
KSH03A	425	450	16	0.64	A	2.02	1.29
KSH03A	450	475	5	0.20	A	2.04	0.41
KSH03A	475	500	8	0.32	A	2.08	0.67
KSH03A	500	525	7	0.28	A	2.11	0.59
KSH03A	525	550	11	0.44	A	2.17	0.96
KSH03A	550	575	11	0.44	A	2.20	0.97
KSH03A	575	600	8	0.32	A	2.21	0.71
KSH03A	600	625	6	0.24	A	2.26	0.54
KSH03A	625	650	5	0.20	A	2.33	0.47
KSH03A	650	675	4	0.16	A	2.41	0.39
KSH03A	675	700	11	0.44	A	2.48	1.09
KSH03A	700	725	4	0.16	A	2.49	0.40
KSH03A	725	750	3	0.12	A	2.52	0.30
KSH03A	750	775	2	0.08	A	2.61	0.21
KSH03A	775	800	5	0.20	A	2.73	0.55
KSH03A	800	825	14	0.56	A	2.67	1.50
KSH03A	825	850	33	1.32	A	2.73	3.61
KSH03A	850	875	28	1.12	A	2.72	3.05
KSH03A	875	900	15	0.60	A	2.75	1.65
KSH03A	900	925	11	0.44	A	2.79	1.23

Borehole	Start length (m)	End length (m)	Number of fractures	Observed P_{10} (1/m)	Rock domain	P_{10} > P_{32} conversion factor	DFN P_{32} (1/m)
KSH03A	925	950	17	0.68	A	2.86	1.94
KSH03A	950	975	10	0.40	A	2.90	1.16
KSH03A	975	1,000	5	0.20	A	2.95	0.59
KSH03A	1,000	1,025	0	0.00	A	2.92	0.00

Simpevarp regional set C
Section length 25 m

Borehole	Start length (m)	End length (m)	Number of fractures	Observed P_{10} (1/m)	Rock domain	P_{10} > P_{32} conversion factor	DFN P_{32} (1/m)
KAV01	0	25	0	0.00	A	3.32	0.00
KAV01	25	50	3	0.12	A	3.30	0.40
KAV01	50	75	9	0.36	A	3.30	1.19
KAV01	75	100	15	0.60	A	3.30	1.98
KAV01	100	125	11	0.44	A	3.30	1.45
KAV01	125	150	11	0.44	B	3.30	1.45
KAV01	150	175	28	1.12	B	3.33	3.73
KAV01	175	200	12	0.48	A	3.36	1.61
KAV01	200	225	9	0.36	A	3.33	1.20
KAV01	225	250	5	0.20	A	3.33	0.67
KAV01	250	275	4	0.16	A	3.30	0.53
KAV01	275	300	18	0.72	A	3.31	2.38
KAV01	300	325	5	0.20	A	3.36	0.67
KAV01	325	350	10	0.40	A	3.31	1.32
KAV01	350	375	9	0.36	A	3.31	1.19
KAV01	375	400	13	0.52	A	3.28	1.70
KAV01	400	425	6	0.24	A	3.33	0.80
KAV01	425	450	28	1.12	A	3.35	3.75
KAV01	450	475	61	2.44	A	3.29	8.03
KAV01	475	500	43	1.72	A	3.26	5.61
KAV01	500	525	38	1.52	A	3.30	5.01
KAV01	525	550	31	1.24	A	3.27	4.05
KAV01	550	575	58	2.32	A	3.25	7.55
KAV01	575	600	20	0.80	A	3.26	2.61
KAV01	600	625	43	1.72	A	3.23	5.56
KAV01	625	650	37	1.48	A	3.23	4.78
KAV01	650	675	28	1.12	A	3.22	3.61
KAV01	675	700	25	1.00	A	3.22	3.22
KAV01	700	725	4	0.16	A	3.22	0.52
KAV01	725	750	10	0.40	A	3.18	1.27
KAV01	750	775	0	0.00	A	3.20	0.00
KAV04A	100	125	35	1.40	A	3.58	5.01
KAV04A	125	150	30	1.20	A	3.57	4.29

Borehole	Start length (m)	End length (m)	Number of fractures	Observed P_{10} (1/m)	Rock domain	P_{10} > P_{32} conversion factor	DFN P_{32} (1/m)
KAV04A	150	175	46	1.84	A	3.55	6.54
KAV04A	175	200	11	0.44	A	3.55	1.56
KAV04A	200	225	8	0.32	A	3.55	1.13
KAV04A	225	250	28	1.12	A	3.57	4.00
KAV04A	250	275	26	1.04	A	3.52	3.66
KAV04A	275	300	38	1.52	A	3.52	5.35
KAV04A	300	325	15	0.60	C	3.51	2.11
KAV04A	325	350	22	0.88	C	3.56	3.14
KAV04A	350	375	29	1.16	C	3.56	4.13
KAV04A	375	400	50	2.00	C	3.56	7.13
KAV04A	400	425	63	2.52	C	3.56	8.98
KAV04A	425	450	10	0.40	C	3.53	1.41
KAV04A	450	475	54	2.16	C	3.55	7.66
KAV04A	475	500	37	1.48	C	3.54	5.24
KAV04A	500	525	42	1.68	C	3.53	5.93
KAV04A	525	550	59	2.36	C	3.55	8.39
KAV04A	550	575	82	3.28	C	3.53	11.58
KAV04A	575	600	59	2.36	C	3.52	8.31
KAV04A	600	625	42	1.68	C	3.51	5.90
KAV04A	625	650	25	1.00	C	3.50	3.50
KAV04A	650	675	30	1.20	C	3.51	4.22
KAV04A	675	700	33	1.32	C	3.52	4.65
KAV04A	700	725	41	1.64	A	3.51	5.76
KAV04A	725	750	47	1.88	A	3.58	6.73
KAV04A	750	775	41	1.64	A	3.56	5.84
KAV04A	775	800	34	1.36	A	3.55	4.82
KAV04A	800	825	27	1.08	A	3.56	3.85
KAV04A	825	850	27	1.08	A	3.58	3.87
KAV04A	850	875	19	0.76	B	3.57	2.71
KAV04A	875	900	35	1.40	B	3.56	4.99
KAV04A	900	925	17	0.68	B	3.57	2.43
KAV04A	925	950	21	0.84	B	3.55	2.99
KAV04A	950	975	11	0.44	A	3.50	1.54
KAV04A	975	1,000	16	0.64	A	3.51	2.25
KSH01A	97	122	13	0.52	C	2.79	1.45
KSH01A	122	147	28	1.12	C	2.79	3.12
KSH01A	147	172	43	1.72	C	2.78	4.79
KSH01A	172	197	15	0.60	C	2.79	1.67
KSH01A	197	222	27	1.08	B	2.79	3.02
KSH01A	222	247	64	2.56	B	2.80	7.16
KSH01A	247	272	34	1.36	C	2.78	3.78
KSH01A	272	297	10	0.40	C	2.77	1.11
KSH01A	297	322	19	0.76	C	2.76	2.10
KSH01A	322	347	27	1.08	B	2.72	2.94
KSH01A	347	372	28	1.12	B	2.68	3.01

Borehole	Start length (m)	End length (m)	Number of fractures	Observed P_{10} (1/m)	Rock domain	P_{10} > P_{32} conversion factor	DFN P_{32} (1/m)
KSH01A	372	397	36	1.44	B	2.64	3.80
KSH01A	397	422	56	2.24	B	2.60	5.83
KSH01A	422	447	96	3.84	B	2.60	9.98
KSH01A	447	472	55	2.20	B	2.58	5.68
KSH01A	472	497	41	1.64	B	2.57	4.21
KSH01A	497	522	33	1.32	B	2.56	3.37
KSH01A	522	547	103	4.12	B	2.58	10.62
KSH01A	547	572	105	4.20	B	2.56	10.77
KSH01A	572	597	33	1.32	B	2.56	3.38
KSH01A	597	622	28	1.12	B	2.55	2.85
KSH01A	622	647	29	1.16	C	2.56	2.97
KSH01A	647	672	18	0.72	C	2.56	1.84
KSH01A	672	697	21	0.84	C	2.48	2.09
KSH01A	697	722	40	1.60	C	2.39	3.83
KSH01A	722	747	26	1.04	C	2.36	2.46
KSH01A	747	772	34	1.36	C	2.32	3.15
KSH01A	772	797	35	1.40	C	2.29	3.20
KSH01A	797	822	26	1.04	C	2.28	2.37
KSH01A	822	847	17	0.68	C	2.25	1.53
KSH01A	847	872	19	0.76	C	2.22	1.68
KSH01A	872	897	9	0.36	C	2.19	0.79
KSH01A	897	922	10	0.40	C	2.16	0.87
KSH01A	922	947	8	0.32	C	2.12	0.68
KSH01A	947	972	12	0.48	C	2.12	1.02
KSH01A	972	997	17	0.68	C	2.10	1.43
KSH01A	997	1,022	2	0.08	C	2.10	0.17
KSH02	0	25	10	0.40	B	3.66	1.46
KSH02	25	50	43	1.72	B	3.66	6.29
KSH02	50	75	35	1.40	B	3.60	5.04
KSH02	75	100	29	1.16	B	3.50	4.07
KSH02	100	125	44	1.76	B	3.50	6.17
KSH02	125	150	30	1.20	B	3.50	4.21
KSH02	150	175	25	1.00	B	3.52	3.52
KSH02	175	200	35	1.40	B	3.55	4.96
KSH02	200	225	33	1.32	B	3.55	4.68
KSH02	225	250	56	2.24	B	3.56	7.98
KSH02	250	275	73	2.92	B	3.56	10.40
KSH02	275	300	58	2.32	B	3.56	8.27
KSH02	300	325	59	2.36	B	3.56	8.41
KSH02	325	350	25	1.00	B	3.55	3.55
KSH02	350	375	35	1.40	B	3.56	4.99
KSH02	375	400	20	0.80	B	3.59	2.87
KSH02	400	425	47	1.88	B	3.55	6.67
KSH02	425	450	38	1.52	B	3.58	5.44
KSH02	450	475	19	0.76	B	3.57	2.71

Borehole	Start length (m)	End length (m)	Number of fractures	Observed P_{10} (1/m)	Rock domain	P_{10} > P_{32} conversion factor	DFN P_{32} (1/m)
KSH02	475	500	41	1.64	B	3.55	5.83
KSH02	500	525	24	0.96	B	3.55	3.40
KSH02	525	550	25	1.00	B	3.58	3.58
KSH02	550	575	26	1.04	B	3.57	3.71
KSH02	575	600	81	3.24	B	3.57	11.57
KSH02	600	625	51	2.04	B	3.59	7.32
KSH02	625	650	24	0.96	B	3.58	3.44
KSH02	650	675	43	1.72	B	3.57	6.14
KSH02	675	700	81	3.24	B	3.55	11.52
KSH02	700	725	36	1.44	B	3.54	5.09
KSH02	725	750	32	1.28	B	3.55	4.55
KSH02	750	775	25	1.00	B	3.55	3.55
KSH02	775	800	37	1.48	B	3.54	5.24
KSH02	800	825	21	0.84	B	3.53	2.96
KSH02	825	850	7	0.28	B	3.53	0.99
KSH02	850	875	37	1.48	B	3.54	5.24
KSH02	875	900	16	0.64	B	3.52	2.25
KSH02	900	925	25	1.00	B	3.52	3.52
KSH02	925	950	16	0.64	B	3.52	2.25
KSH02	950	975	6	0.24	B	3.53	0.85
KSH02	975	1,000	9	0.36	B	3.58	1.29
KSH02	1,000	1,025	0	0.00	B	3.57	0.00
KSH03A	100	125	17	0.68	C	3.24	2.20
KSH03A	125	150	20	0.80	C	3.07	2.46
KSH03A	150	175	18	0.72	C	3.03	2.18
KSH03A	175	200	12	0.48	C	3.04	1.46
KSH03A	200	225	18	0.72	C	3.04	2.19
KSH03A	225	250	51	2.04	C	3.04	6.19
KSH03A	250	275	48	1.92	C	3.01	5.78
KSH03A	275	300	31	1.24	A	2.96	3.68
KSH03A	300	325	10	0.40	A	2.90	1.16
KSH03A	325	350	11	0.44	A	2.81	1.24
KSH03A	350	375	13	0.52	A	2.76	1.44
KSH03A	375	400	8	0.32	A	2.58	0.82
KSH03A	400	425	12	0.48	A	2.58	1.24
KSH03A	425	450	6	0.24	A	2.50	0.60
KSH03A	450	475	7	0.28	A	2.43	0.68
KSH03A	475	500	3	0.12	A	2.40	0.29
KSH03A	500	525	9	0.36	A	2.32	0.84
KSH03A	525	550	6	0.24	A	2.26	0.54
KSH03A	550	575	0	0.00	A	2.20	0.00
KSH03A	575	600	2	0.08	A	2.15	0.17
KSH03A	600	625	0	0.00	A	2.11	0.00
KSH03A	625	650	2	0.08	A	2.07	0.17
KSH03A	650	675	2	0.08	A	2.02	0.16

Borehole	Start length (m)	End length (m)	Number of fractures	Observed P_{10} (1/m)	Rock domain	P_{10} > P_{32} conversion factor	DFN P_{32} (1/m)
KSH03A	675	700	5	0.20	A	1.98	0.40
KSH03A	700	725	10	0.40	A	1.93	0.77
KSH03A	725	750	1	0.04	A	1.86	0.07
KSH03A	750	775	12	0.48	A	1.79	0.86
KSH03A	775	800	15	0.60	A	1.70	1.02
KSH03A	800	825	47	1.88	A	1.65	3.10
KSH03A	825	850	23	0.92	A	1.60	1.47
KSH03A	850	875	62	2.48	A	1.55	3.84
KSH03A	875	900	36	1.44	A	1.50	2.16
KSH03A	900	925	15	0.60	A	1.46	0.88
KSH03A	925	950	44	1.76	A	1.43	2.51
KSH03A	950	975	83	3.32	A	1.39	4.62
KSH03A	975	1,000	44	1.76	A	1.36	2.40
KSH03A	1,000	1,025	0	0.00	A	1.34	0.00

Simpevarp local set D (subhorizontal)
Section length 25 m

Borehole	Start length (m)	End length (m)	Number of fractures	Observed P_{10} (1/m)	Rock domain	P10 > P32 conversion factor	DFN P_{32} (1/m)
KAV01	0	25	28	1.12	A	1.02	1.14
KAV01	25	50	37	1.48	A	1.02	1.50
KAV01	50	75	45	1.80	A	1.02	1.83
KAV01	75	100	32	1.28	A	1.02	1.30
KAV01	100	125	35	1.40	A	1.02	1.42
KAV01	125	150	53	2.12	B	1.02	2.16
KAV01	150	175	93	3.72	B	1.02	3.78
KAV01	175	200	83	3.32	A	1.02	3.38
KAV01	200	225	73	2.92	A	1.01	2.96
KAV01	225	250	45	1.80	A	1.01	1.83
KAV01	250	275	27	1.08	A	1.01	1.09
KAV01	275	300	31	1.24	A	1.01	1.25
KAV01	300	325	29	1.16	A	1.01	1.17
KAV01	325	350	32	1.28	A	1.01	1.29
KAV01	350	375	13	0.52	A	1.01	0.52
KAV01	375	400	41	1.64	A	1.01	1.66
KAV01	400	425	94	3.76	A	1.01	3.80
KAV01	425	450	112	4.48	A	1.01	4.53
KAV01	450	475	180	7.20	A	1.01	7.30
KAV01	475	500	118	4.72	A	1.01	4.79
KAV01	500	525	104	4.16	A	1.01	4.20
KAV01	525	550	85	3.40	A	1.01	3.45
KAV01	550	575	62	2.48	A	1.01	2.51

Borehole	Start length (m)	End length (m)	Number of fractures	Observed P_{10} (1/m)	Rock domain	P10 > P32 conversion factor	DFN P_{32} (1/m)
KAV01	575	600	50	2.00	A	1.01	2.03
KAV01	600	625	39	1.56	A	1.02	1.59
KAV01	625	650	49	1.96	A	1.02	1.99
KAV01	650	675	108	4.32	A	1.02	4.39
KAV01	675	700	53	2.12	A	1.01	2.15
KAV01	700	725	87	3.48	A	1.01	3.52
KAV01	725	750	101	4.04	A	1.01	4.09
KAV01	750	775	0	0.00	A	1.01	0.00
KAV04A	100	125	63	2.52	A	1.02	2.58
KAV04A	125	150	41	1.64	A	1.02	1.68
KAV04A	150	175	55	2.20	A	1.03	2.26
KAV04A	175	200	42	1.68	A	1.02	1.72
KAV04A	200	225	85	3.40	A	1.02	3.48
KAV04A	225	250	116	4.64	A	1.02	4.74
KAV04A	250	275	122	4.88	A	1.02	5.00
KAV04A	275	300	130	5.20	A	1.02	5.32
KAV04A	300	325	180	7.20	C	1.02	7.37
KAV04A	325	350	102	4.08	C	1.02	4.18
KAV04A	350	375	135	5.40	C	1.02	5.53
KAV04A	375	400	155	6.20	C	1.02	6.34
KAV04A	400	425	189	7.56	C	1.02	7.74
KAV04A	425	450	122	4.88	C	1.02	4.99
KAV04A	450	475	60	2.40	C	1.02	2.45
KAV04A	475	500	121	4.84	C	1.02	4.95
KAV04A	500	525	146	5.84	C	1.02	5.97
KAV04A	525	550	155	6.20	C	1.02	6.33
KAV04A	550	575	119	4.76	C	1.02	4.84
KAV04A	575	600	150	6.00	C	1.02	6.12
KAV04A	600	625	122	4.88	C	1.02	4.97
KAV04A	625	650	93	3.72	C	1.02	3.79
KAV04A	650	675	115	4.60	C	1.02	4.69
KAV04A	675	700	120	4.80	C	1.02	4.89
KAV04A	700	725	106	4.24	A	1.02	4.33
KAV04A	725	750	171	6.84	A	1.02	6.99
KAV04A	750	775	137	5.48	A	1.02	5.59
KAV04A	775	800	173	6.92	A	1.02	7.06
KAV04A	800	825	192	7.68	A	1.02	7.84
KAV04A	825	850	94	3.76	A	1.02	3.83
KAV04A	850	875	91	3.64	B	1.02	3.70
KAV04A	875	900	96	3.84	B	1.02	3.91
KAV04A	900	925	103	4.12	B	1.02	4.20
KAV04A	925	950	125	5.00	B	1.02	5.10
KAV04A	950	975	100	4.00	A	1.02	4.08
KAV04A	975	1,000	116	4.64	A	1.01	4.71
KSH01A	97	122	42	1.68	C	1.04	1.75

Borehole	Start length (m)	End length (m)	Number of fractures	Observed P_{10} (1/m)	Rock domain	P10 > P32 conversion factor	DFN P_{32} (1/m)
KSH01A	122	147	108	4.32	C	1.04	4.51
KSH01A	147	172	173	6.92	C	1.04	7.20
KSH01A	172	197	158	6.32	C	1.04	6.58
KSH01A	197	222	232	9.28	B	1.04	9.69
KSH01A	222	247	166	6.64	B	1.04	6.92
KSH01A	247	272	238	9.52	C	1.04	9.94
KSH01A	272	297	145	5.80	C	1.04	6.06
KSH01A	297	322	207	8.28	C	1.04	8.63
KSH01A	322	347	258	10.32	B	1.04	10.71
KSH01A	347	372	173	6.92	B	1.04	7.17
KSH01A	372	397	192	7.68	B	1.04	7.98
KSH01A	397	422	156	6.24	B	1.04	6.48
KSH01A	422	447	224	8.96	B	1.04	9.28
KSH01A	447	472	166	6.64	B	1.03	6.87
KSH01A	472	497	232	9.28	B	1.04	9.63
KSH01A	497	522	275	11.00	B	1.04	11.49
KSH01A	522	547	360	14.40	B	1.05	15.07
KSH01A	547	572	225	9.00	B	1.05	9.41
KSH01A	572	597	198	7.92	B	1.04	8.27
KSH01A	597	622	184	7.36	B	1.05	7.71
KSH01A	622	647	144	5.76	C	1.05	6.06
KSH01A	647	672	87	3.48	C	1.05	3.66
KSH01A	672	697	73	2.92	C	1.05	3.06
KSH01A	697	722	74	2.96	C	1.05	3.12
KSH01A	722	747	39	1.56	C	1.06	1.65
KSH01A	747	772	68	2.72	C	1.06	2.90
KSH01A	772	797	49	1.96	C	1.07	2.09
KSH01A	797	822	39	1.56	C	1.08	1.68
KSH01A	822	847	127	5.08	C	1.09	5.53
KSH01A	847	872	53	2.12	C	1.09	2.31
KSH01A	872	897	61	2.44	C	1.09	2.67
KSH01A	897	922	67	2.68	C	1.10	2.95
KSH01A	922	947	64	2.56	C	1.11	2.85
KSH01A	947	972	29	1.16	C	1.12	1.30
KSH01A	972	997	11	0.44	C	1.13	0.50
KSH01A	997	1,022	0	0.00	C	1.13	0.00
KSH02	0	25	40	1.60	B	1.01	1.62
KSH02	25	50	200	8.00	B	1.01	8.11
KSH02	50	75	142	5.68	B	1.01	5.76
KSH02	75	100	185	7.40	B	1.01	7.47
KSH02	100	125	220	8.80	B	1.01	8.91
KSH02	125	150	234	9.36	B	1.01	9.48
KSH02	150	175	151	6.04	B	1.02	6.15
KSH02	175	200	117	4.68	B	1.02	4.76
KSH02	200	225	159	6.36	B	1.01	6.45

Borehole	Start length (m)	End length (m)	Number of fractures	Observed P_{10} (1/m)	Rock domain	P10 > P32 conversion factor	DFN P_{32} (1/m)
KSH02	225	250	173	6.92	B	1.02	7.03
KSH02	250	275	216	8.64	B	1.02	8.78
KSH02	275	300	178	7.12	B	1.01	7.23
KSH02	300	325	177	7.08	B	1.01	7.18
KSH02	325	350	166	6.64	B	1.01	6.72
KSH02	350	375	235	9.40	B	1.01	9.50
KSH02	375	400	137	5.48	B	1.01	5.55
KSH02	400	425	224	8.96	B	1.02	9.15
KSH02	425	450	216	8.64	B	1.01	8.77
KSH02	450	475	131	5.24	B	1.02	5.33
KSH02	475	500	118	4.72	B	1.01	4.79
KSH02	500	525	141	5.64	B	1.02	5.73
KSH02	525	550	196	7.84	B	1.02	7.97
KSH02	550	575	241	9.64	B	1.02	9.82
KSH02	575	600	147	5.88	B	1.02	5.98
KSH02	600	625	296	11.84	B	1.02	12.05
KSH02	625	650	241	9.64	B	1.02	9.80
KSH02	650	675	244	9.76	B	1.02	9.92
KSH02	675	700	153	6.12	B	1.02	6.23
KSH02	700	725	193	7.72	B	1.02	7.87
KSH02	725	750	201	8.04	B	1.02	8.19
KSH02	750	775	218	8.72	B	1.02	8.89
KSH02	775	800	302	12.08	B	1.02	12.32
KSH02	800	825	212	8.48	B	1.02	8.65
KSH02	825	850	134	5.36	B	1.02	5.47
KSH02	850	875	230	9.20	B	1.02	9.41
KSH02	875	900	92	3.68	B	1.02	3.76
KSH02	900	925	83	3.32	B	1.02	3.39
KSH02	925	950	58	2.32	B	1.02	2.37
KSH02	950	975	111	4.44	B	1.02	4.54
KSH02	975	1,000	67	2.68	B	1.02	2.74
KSH02	1,000	1,025	0	0.00	B	1.02	0.00
KSH03A	100	125	179	7.16	C	1.15	8.20
KSH03A	125	150	200	8.00	C	1.14	9.15
KSH03A	150	175	178	7.12	C	1.15	8.15
KSH03A	175	200	184	7.36	C	1.14	8.40
KSH03A	200	225	269	10.76	C	1.14	12.27
KSH03A	225	250	227	9.08	C	1.14	10.34
KSH03A	250	275	262	10.48	C	1.14	11.93
KSH03A	275	300	114	4.56	A	1.13	5.17
KSH03A	300	325	68	2.72	A	1.14	3.09
KSH03A	325	350	54	2.16	A	1.14	2.46
KSH03A	350	375	98	3.92	A	1.14	4.46
KSH03A	375	400	56	2.24	A	1.13	2.53
KSH03A	400	425	43	1.72	A	1.13	1.94

Borehole	Start length (m)	End length (m)	Number of fractures	Observed P_{10} (1/m)	Rock domain	P10 > P32 conversion factor	DFN P_{32} (1/m)
KSH03A	425	450	81	3.24	A	1.14	3.68
KSH03A	450	475	116	4.64	A	1.13	5.26
KSH03A	475	500	111	4.44	A	1.14	5.06
KSH03A	500	525	57	2.28	A	1.14	2.60
KSH03A	525	550	80	3.20	A	1.15	3.68
KSH03A	550	575	41	1.64	A	1.16	1.90
KSH03A	575	600	29	1.16	A	1.16	1.34
KSH03A	600	625	26	1.04	A	1.15	1.20
KSH03A	625	650	20	0.80	A	1.16	0.93
KSH03A	650	675	72	2.88	A	1.15	3.31
KSH03A	675	700	59	2.36	A	1.14	2.70
KSH03A	700	725	50	2.00	A	1.15	2.31
KSH03A	725	750	43	1.72	A	1.16	2.00
KSH03A	750	775	30	1.20	A	1.18	1.42
KSH03A	775	800	8	0.32	A	1.22	0.39
KSH03A	800	825	42	1.68	A	1.23	2.07
KSH03A	825	850	20	0.80	A	1.25	1.00
KSH03A	850	875	53	2.12	A	1.27	2.68
KSH03A	875	900	27	1.08	A	1.28	1.39
KSH03A	900	925	22	0.88	A	1.30	1.15
KSH03A	925	950	10	0.40	A	1.34	0.54
KSH03A	950	975	31	1.24	A	1.36	1.68
KSH03A	975	1,000	8	0.32	A	1.39	0.44
KSH03A	1,000	1,025	0	0.00	A	1.40	0.00

Simpevarp local set E
Section length 25 m

Borehole	Start length (m)	End length (m)	Number of fractures	Observed P_{10} (1/m)	Rock domain	P_{10} > P_{32} conversion factor	DFN P_{32} (1/m)
KAV01	0	25	35	1.40	A	2.68	3.76
KAV01	25	50	18	0.72	A	2.68	1.93
KAV01	50	75	39	1.56	A	2.67	4.17
KAV01	75	100	9	0.36	A	2.67	0.96
KAV01	100	125	5	0.20	A	2.68	0.54
KAV01	125	150	7	0.28	B	2.68	0.75
KAV01	150	175	10	0.40	B	2.64	1.06
KAV01	175	200	8	0.32	A	2.64	0.84
KAV01	200	225	8	0.32	A	2.64	0.85
KAV01	225	250	1	0.04	A	2.64	0.11
KAV01	250	275	1	0.04	A	2.65	0.11
KAV01	275	300	10	0.40	A	2.63	1.05
KAV01	300	325	5	0.20	A	2.62	0.52

Borehole	Start length (m)	End length (m)	Number of fractures	Observed P_{10} (1/m)	Rock domain	P_{10} > P_{32} conversion factor	DFN P_{32} (1/m)
KAV01	325	350	9	0.36	A	2.65	0.95
KAV01	350	375	1	0.04	A	2.64	0.11
KAV01	375	400	1	0.04	A	2.63	0.11
KAV01	400	425	3	0.12	A	2.61	0.31
KAV01	425	450	27	1.08	A	2.62	2.83
KAV01	450	475	14	0.56	A	2.63	1.47
KAV01	475	500	16	0.64	A	2.62	1.68
KAV01	500	525	11	0.44	A	2.59	1.14
KAV01	525	550	16	0.64	A	2.60	1.67
KAV01	550	575	14	0.56	A	2.61	1.46
KAV01	575	600	13	0.52	A	2.60	1.35
KAV01	600	625	6	0.24	A	2.60	0.62
KAV01	625	650	14	0.56	A	2.61	1.46
KAV01	650	675	9	0.36	A	2.61	0.94
KAV01	675	700	6	0.24	A	2.60	0.62
KAV01	700	725	3	0.12	A	2.59	0.31
KAV01	725	750	9	0.36	A	2.59	0.93
KAV01	750	775	0	0.00	A	2.59	0.00
KAV04A	100	125	2	0.08	A	2.36	0.19
KAV04A	125	150	8	0.32	A	2.37	0.76
KAV04A	150	175	6	0.24	A	2.37	0.57
KAV04A	175	200	6	0.24	A	2.37	0.57
KAV04A	200	225	10	0.40	A	2.37	0.95
KAV04A	225	250	15	0.60	A	2.37	1.42
KAV04A	250	275	18	0.72	A	2.37	1.70
KAV04A	275	300	11	0.44	A	2.37	1.04
KAV04A	300	325	10	0.40	C	2.36	0.94
KAV04A	325	350	21	0.84	C	2.36	1.98
KAV04A	350	375	13	0.52	C	2.37	1.23
KAV04A	375	400	23	0.92	C	2.36	2.17
KAV04A	400	425	34	1.36	C	2.37	3.22
KAV04A	425	450	12	0.48	C	2.36	1.13
KAV04A	450	475	24	0.96	C	2.34	2.25
KAV04A	475	500	9	0.36	C	2.33	0.84
KAV04A	500	525	17	0.68	C	2.32	1.58
KAV04A	525	550	25	1.00	C	2.31	2.31
KAV04A	550	575	12	0.48	C	2.31	1.11
KAV04A	575	600	17	0.68	C	2.31	1.57
KAV04A	600	625	30	1.20	C	2.31	2.77
KAV04A	625	650	8	0.32	C	2.31	0.74
KAV04A	650	675	5	0.20	C	2.31	0.46
KAV04A	675	700	7	0.28	C	2.31	0.65
KAV04A	700	725	10	0.40	A	2.31	0.92
KAV04A	725	750	7	0.28	A	2.30	0.65

Borehole	Start length (m)	End length (m)	Number of fractures	Observed P_{10} (1/m)	Rock domain	$P_{10} > P_{32}$ conversion factor	DFN P_{32} (1/m)
KAV04A	750	775	10	0.40	A	2.30	0.92
KAV04A	775	800	45	1.80	A	2.30	4.13
KAV04A	800	825	66	2.64	A	2.30	6.06
KAV04A	825	850	40	1.60	A	2.29	3.66
KAV04A	850	875	20	0.80	B	2.30	1.84
KAV04A	875	900	18	0.72	B	2.30	1.66
KAV04A	900	925	69	2.76	B	2.31	6.38
KAV04A	925	950	48	1.92	B	2.32	4.46
KAV04A	950	975	43	1.72	A	2.34	4.03
KAV04A	975	1,000	30	1.20	A	2.35	2.82
KSH01A	97	122	29	1.16	C	2.77	3.21
KSH01A	122	147	35	1.40	C	2.78	3.89
KSH01A	147	172	59	2.36	C	2.84	6.69
KSH01A	172	197	41	1.64	C	2.86	4.69
KSH01A	197	222	45	1.80	B	2.87	5.16
KSH01A	222	247	76	3.04	B	2.86	8.69
KSH01A	247	272	33	1.32	C	2.87	3.79
KSH01A	272	297	46	1.84	C	2.85	5.25
KSH01A	297	322	26	1.04	C	2.84	2.95
KSH01A	322	347	20	0.80	B	2.86	2.29
KSH01A	347	372	13	0.52	B	2.94	1.53
KSH01A	372	397	31	1.24	B	2.94	3.65
KSH01A	397	422	32	1.28	B	2.93	3.75
KSH01A	422	447	23	0.92	B	2.91	2.68
KSH01A	447	472	37	1.48	B	2.88	4.27
KSH01A	472	497	51	2.04	B	2.89	5.90
KSH01A	497	522	58	2.32	B	2.89	6.71
KSH01A	522	547	44	1.76	B	2.91	5.12
KSH01A	547	572	51	2.04	B	2.96	6.04
KSH01A	572	597	20	0.80	B	3.01	2.40
KSH01A	597	622	31	1.24	B	3.03	3.76
KSH01A	622	647	30	1.20	C	3.07	3.69
KSH01A	647	672	18	0.72	C	3.13	2.25
KSH01A	672	697	22	0.88	C	3.12	2.74
KSH01A	697	722	38	1.52	C	3.16	4.80
KSH01A	722	747	13	0.52	C	3.13	1.63
KSH01A	747	772	16	0.64	C	3.13	2.00
KSH01A	772	797	7	0.28	C	3.14	0.88
KSH01A	797	822	5	0.20	C	3.17	0.63
KSH01A	822	847	2	0.08	C	3.17	0.25
KSH01A	847	872	2	0.08	C	3.16	0.25
KSH01A	872	897	9	0.36	C	3.23	1.16
KSH01A	897	922	4	0.16	C	3.29	0.53
KSH01A	922	947	4	0.16	C	3.36	0.54

Borehole	Start length (m)	End length (m)	Number of fractures	Observed P_{10} (1/m)	Rock domain	P_{10} > P_{32} conversion factor	DFN P_{32} (1/m)
KSH01A	947	972	4	0.16	C	3.40	0.54
KSH01A	972	997	7	0.28	C	3.42	0.96
KSH01A	997	1,022	0	0.00	C	3.47	0.00
KSH02	0	25	13	0.52	B	2.66	1.39
KSH02	25	50	32	1.28	B	2.66	3.40
KSH02	50	75	27	1.08	B	2.68	2.89
KSH02	75	100	20	0.80	B	2.65	2.12
KSH02	100	125	38	1.52	B	2.63	3.99
KSH02	125	150	21	0.84	B	2.65	2.23
KSH02	150	175	7	0.28	B	2.62	0.73
KSH02	175	200	8	0.32	B	2.61	0.84
KSH02	200	225	33	1.32	B	2.59	3.41
KSH02	225	250	37	1.48	B	2.57	3.81
KSH02	250	275	29	1.16	B	2.59	3.00
KSH02	275	300	28	1.12	B	2.59	2.90
KSH02	300	325	48	1.92	B	2.60	4.98
KSH02	325	350	27	1.08	B	2.60	2.80
KSH02	350	375	18	0.72	B	2.58	1.86
KSH02	375	400	21	0.84	B	2.56	2.15
KSH02	400	425	46	1.84	B	2.42	4.46
KSH02	425	450	44	1.76	B	2.56	4.50
KSH02	450	475	27	1.08	B	2.54	2.74
KSH02	475	500	38	1.52	B	2.52	3.83
KSH02	500	525	19	0.76	B	2.50	1.90
KSH02	525	550	12	0.48	B	2.50	1.20
KSH02	550	575	15	0.60	B	2.49	1.50
KSH02	575	600	21	0.84	B	2.49	2.09
KSH02	600	625	39	1.56	B	2.49	3.88
KSH02	625	650	19	0.76	B	2.50	1.90
KSH02	650	675	44	1.76	B	2.50	4.39
KSH02	675	700	40	1.60	B	2.49	3.99
KSH02	700	725	28	1.12	B	2.49	2.79
KSH02	725	750	39	1.56	B	2.49	3.89
KSH02	750	775	41	1.64	B	2.48	4.07
KSH02	775	800	14	0.56	B	2.47	1.38
KSH02	800	825	22	0.88	B	2.47	2.17
KSH02	825	850	20	0.80	B	2.46	1.97
KSH02	850	875	13	0.52	B	2.46	1.28
KSH02	875	900	15	0.60	B	2.44	1.46
KSH02	900	925	10	0.40	B	2.43	0.97
KSH02	925	950	25	1.00	B	2.45	2.45
KSH02	950	975	29	1.16	B	2.44	2.82
KSH02	975	1,000	15	0.60	B	2.43	1.46
KSH02	1,000	1,025	0	0.00	B	2.43	0.00

Borehole	Start length (m)	End length (m)	Number of fractures	Observed P_{10} (1/m)	Rock domain	$P_{10} > P_{32}$ conversion factor	DFN P_{32} (1/m)
KSH03A	100	125	24	0.96	C	1.73	1.66
KSH03A	125	150	17	0.68	C	1.74	1.18
KSH03A	150	175	14	0.56	C	1.79	1.00
KSH03A	175	200	30	1.20	C	1.80	2.16
KSH03A	200	225	24	0.96	C	1.79	1.72
KSH03A	225	250	69	2.76	C	1.80	4.96
KSH03A	250	275	75	3.00	C	1.82	5.46
KSH03A	275	300	39	1.56	A	1.84	2.87
KSH03A	300	325	33	1.32	A	1.90	2.51
KSH03A	325	350	20	0.80	A	1.95	1.56
KSH03A	350	375	34	1.36	A	2.00	2.72
KSH03A	375	400	25	1.00	A	2.07	2.07
KSH03A	400	425	44	1.76	A	2.13	3.74
KSH03A	425	450	34	1.36	A	2.13	2.90
KSH03A	450	475	4	0.16	A	2.20	0.35
KSH03A	475	500	6	0.24	A	2.28	0.55
KSH03A	500	525	6	0.24	A	2.41	0.58
KSH03A	525	550	2	0.08	A	2.48	0.20
KSH03A	550	575	6	0.24	A	2.53	0.61
KSH03A	575	600	11	0.44	A	2.60	1.14
KSH03A	600	625	3	0.12	A	2.68	0.32
KSH03A	625	650	0	0.00	A	2.77	0.00
KSH03A	650	675	1	0.04	A	2.84	0.11
KSH03A	675	700	3	0.12	A	2.86	0.34
KSH03A	700	725	3	0.12	A	3.01	0.36
KSH03A	725	750	0	0.00	A	3.04	0.00
KSH03A	750	775	2	0.08	A	3.14	0.25
KSH03A	775	800	1	0.04	A	3.36	0.13
KSH03A	800	825	5	0.20	A	3.44	0.69
KSH03A	825	850	18	0.72	A	3.36	2.42
KSH03A	850	875	13	0.52	A	3.43	1.78
KSH03A	875	900	3	0.12	A	3.55	0.43
KSH03A	900	925	10	0.40	A	3.67	1.47
KSH03A	925	950	18	0.72	A	3.61	2.60
KSH03A	950	975	13	0.52	A	3.49	1.81
KSH03A	975	1,000	14	0.56	A	3.50	1.96
KSH03A	1,000	1,025	0	0.00	A	3.48	0.00

Mass dimension plots for Simpevarp and Laxemar regional fracture sets

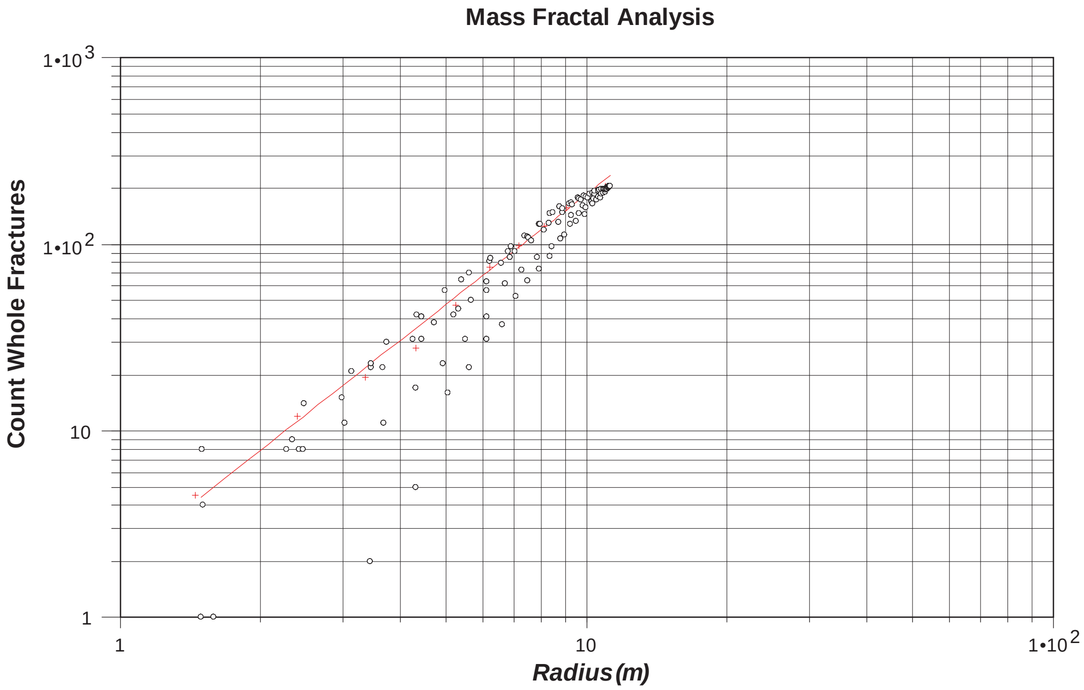

Outcrop ASM000025, Regional Set S_A Mass Dimension Plot

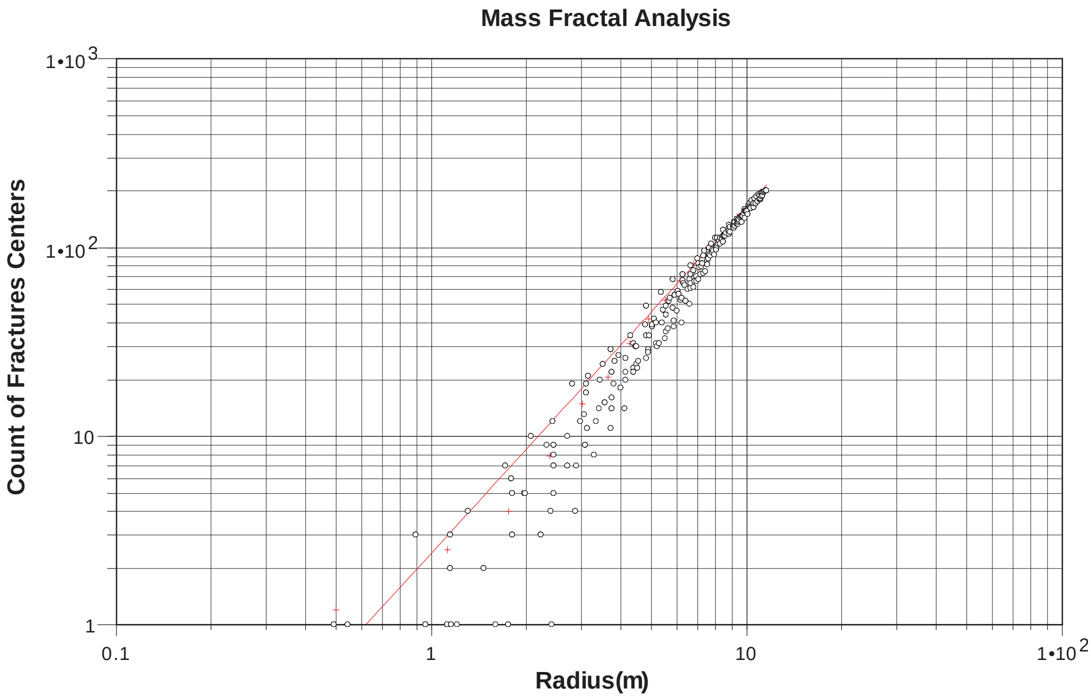

Outcrop ASM000025, Regional Set S_B Mass Dimension Plot

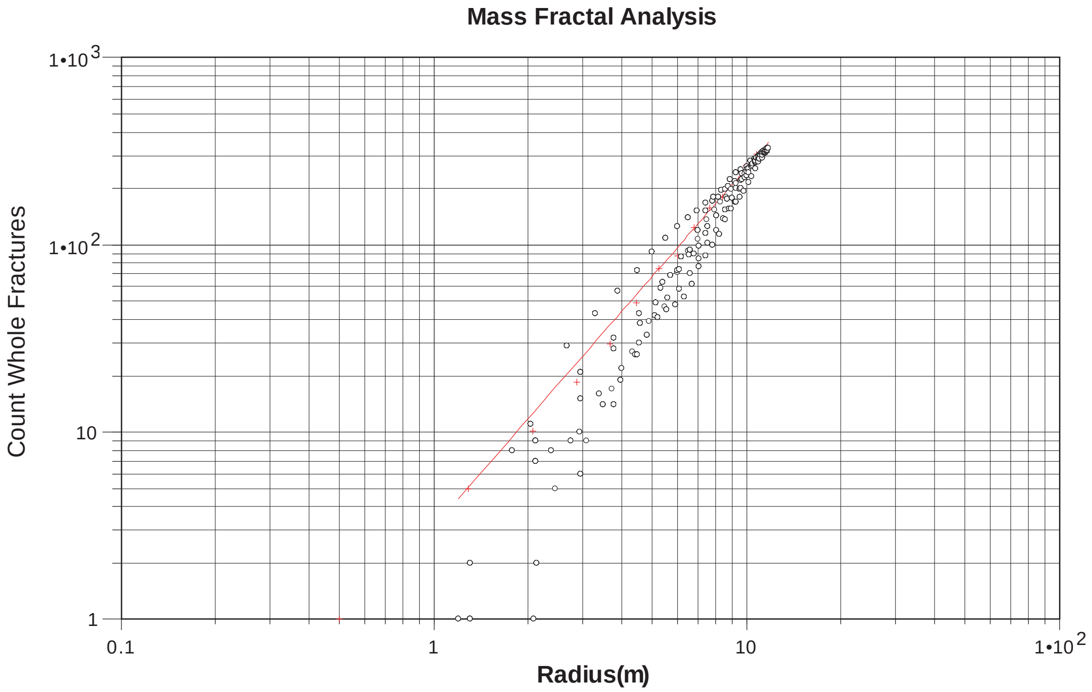

Outcrop ASM000025, Regional Set S_C Mass Dimension Plot

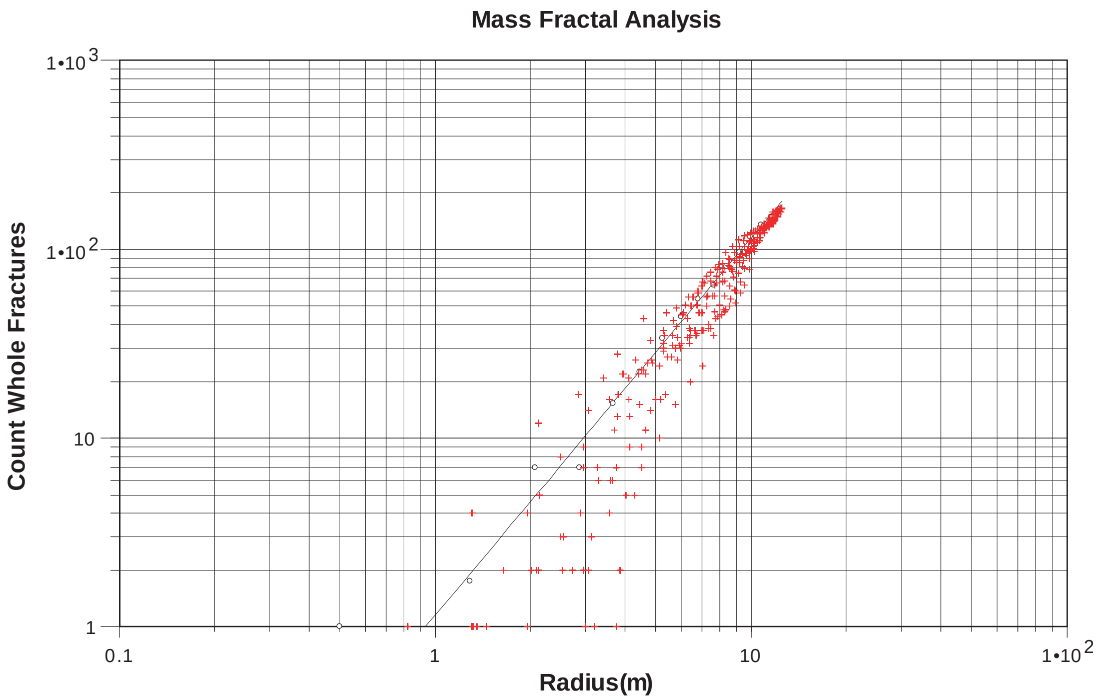

Outcrop ASM000026, Regional Set S_A Mass Dimension Plot

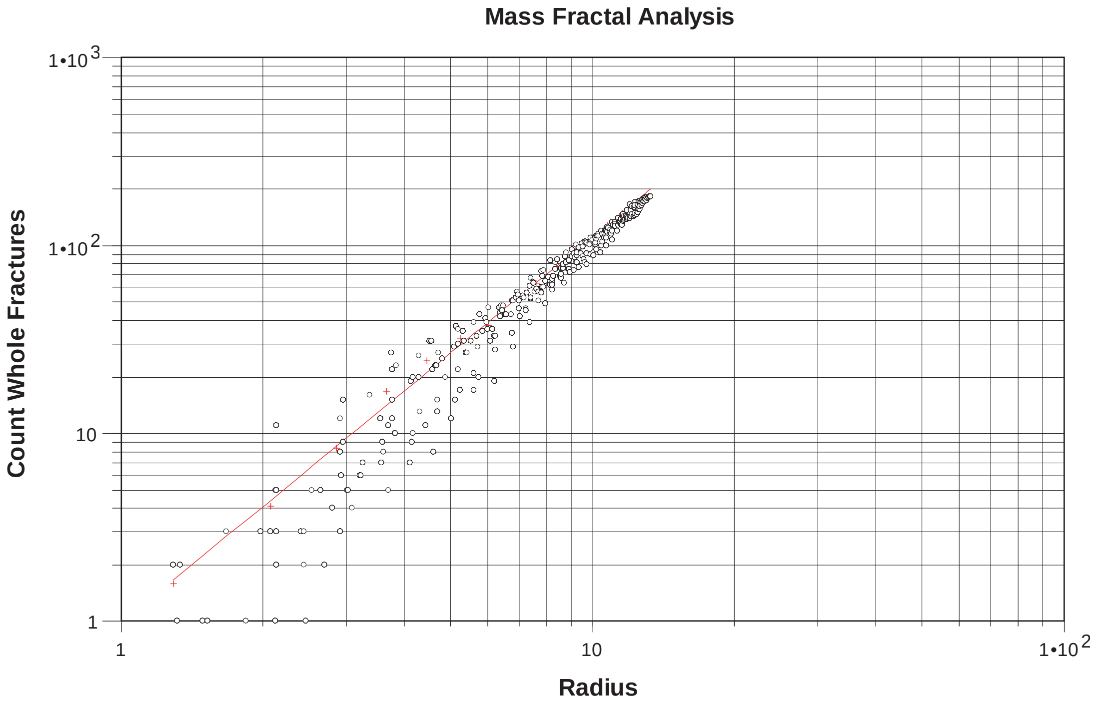

Outcrop ASM000026, Regional Set S_B Mass Dimension Plot

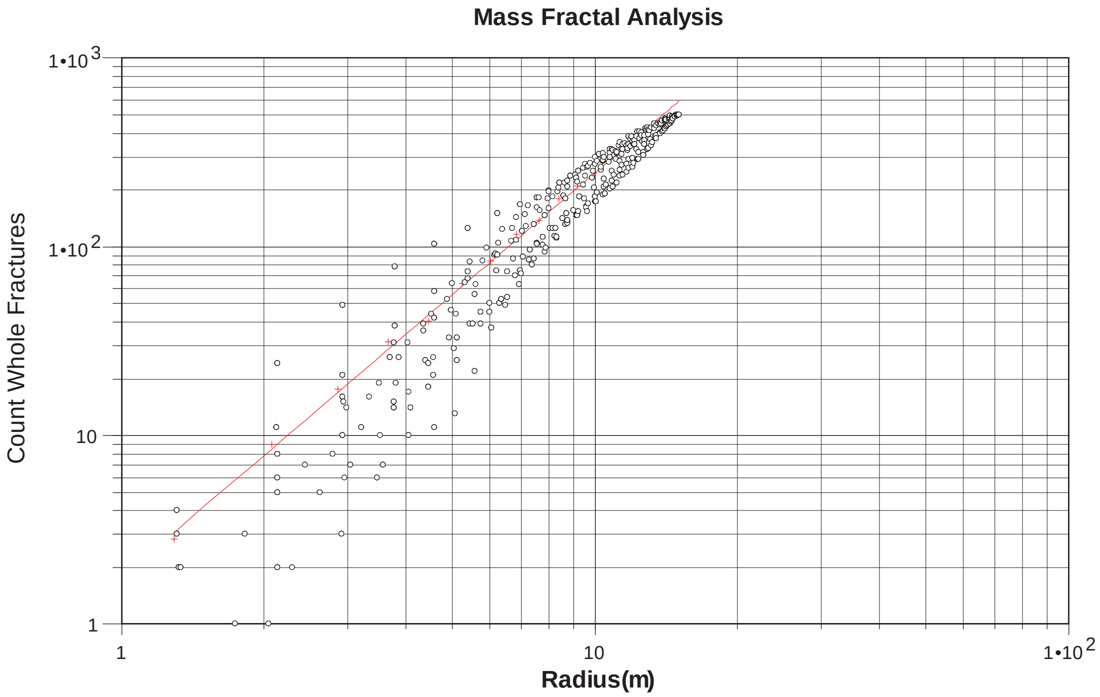

Outcrop ASM000026, Regional Set S_C Mass Dimension Plot

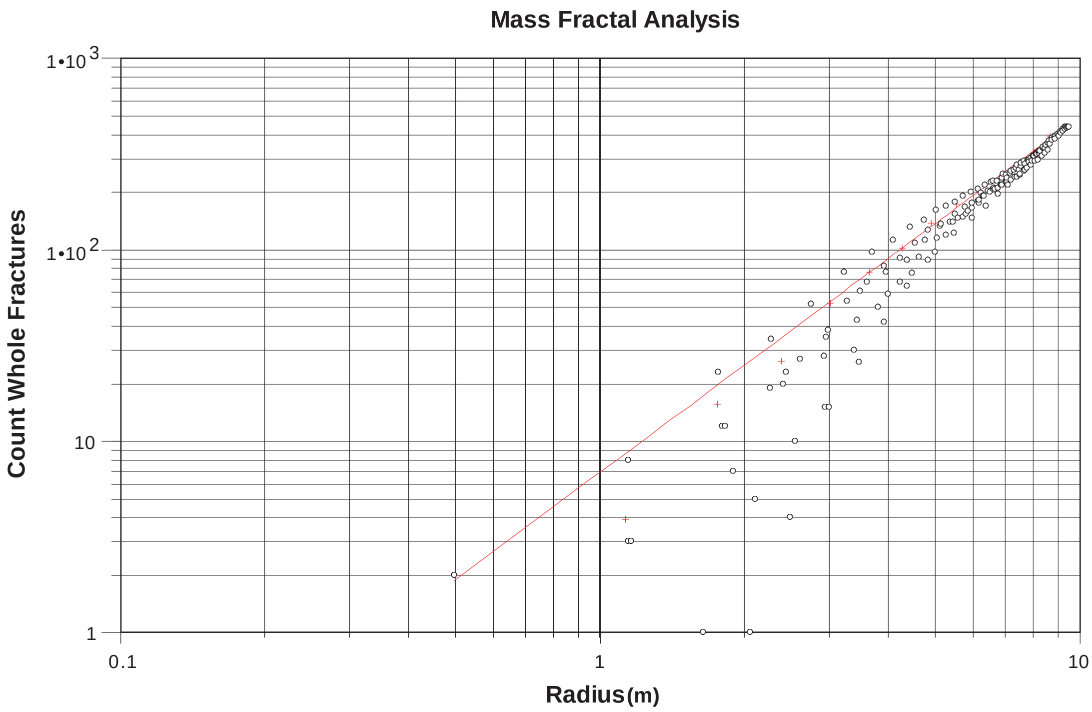

Outcrop ASM000205, Regional Set S_A Mass Dimension Plot

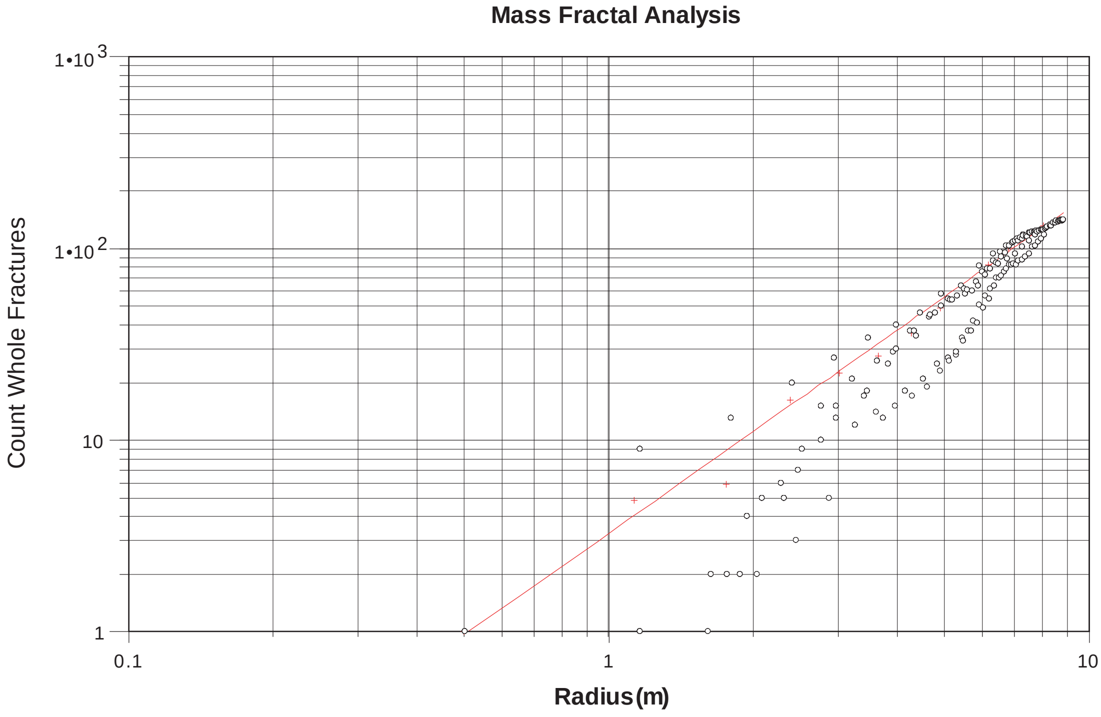

Outcrop ASM000205, Regional Set S_B Mass Dimension Plot

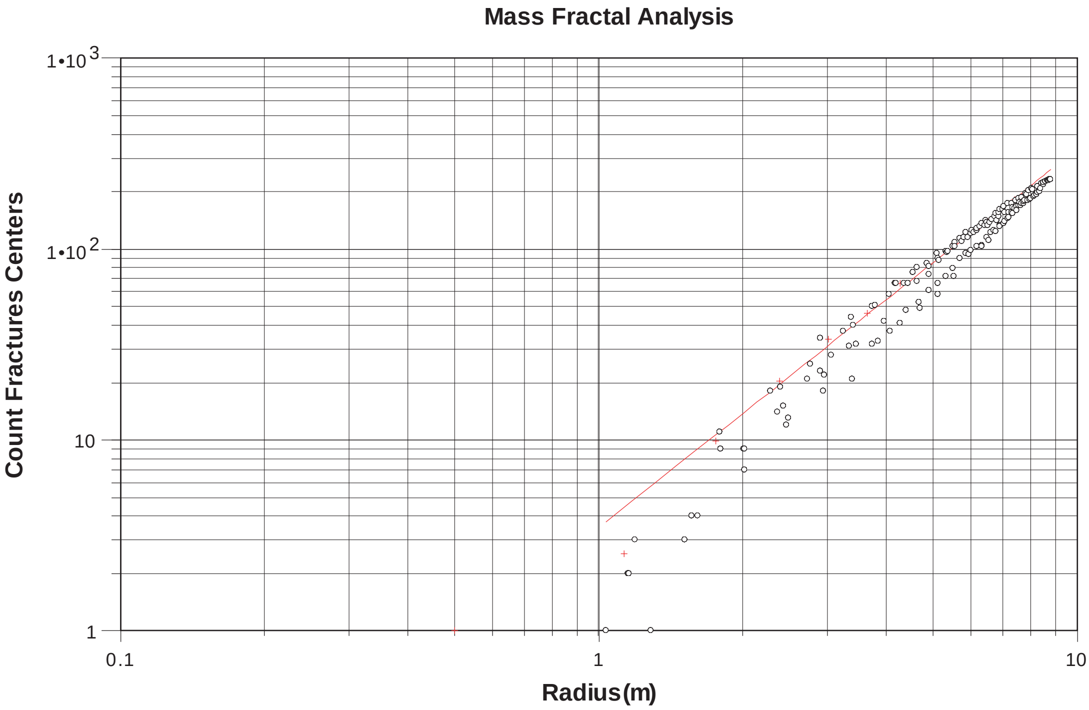

Outcrop ASM000205, Regional Set S_C Mass Dimension Plot

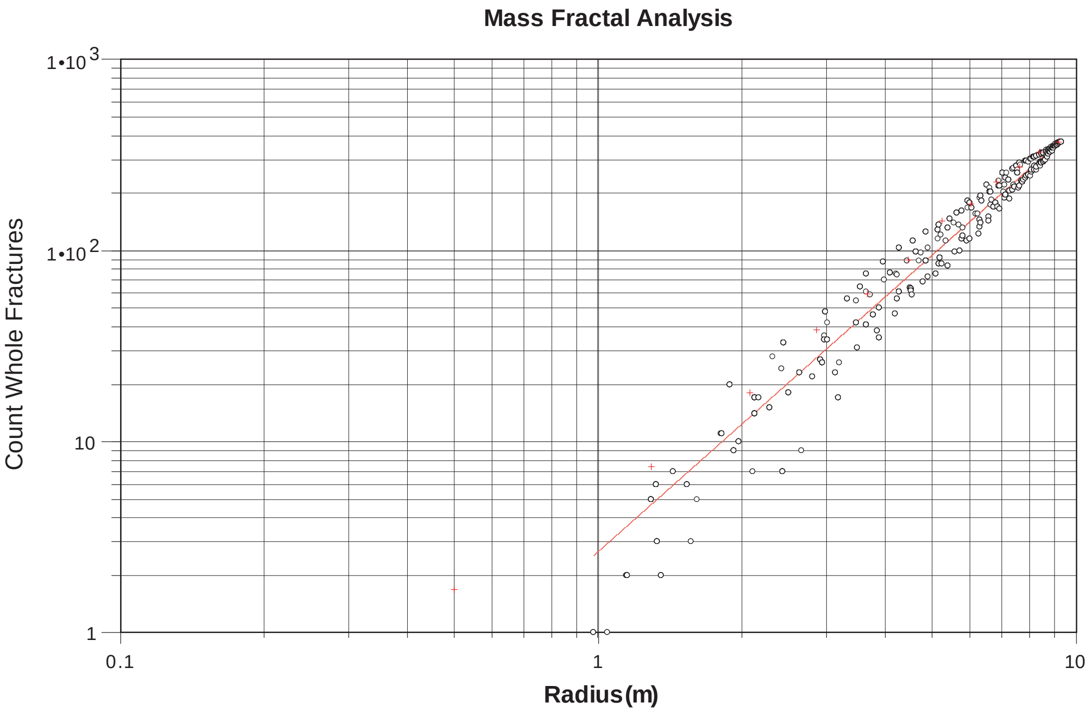

Outcrop ASM000206, Regional Set S_A Mass Dimension Plot

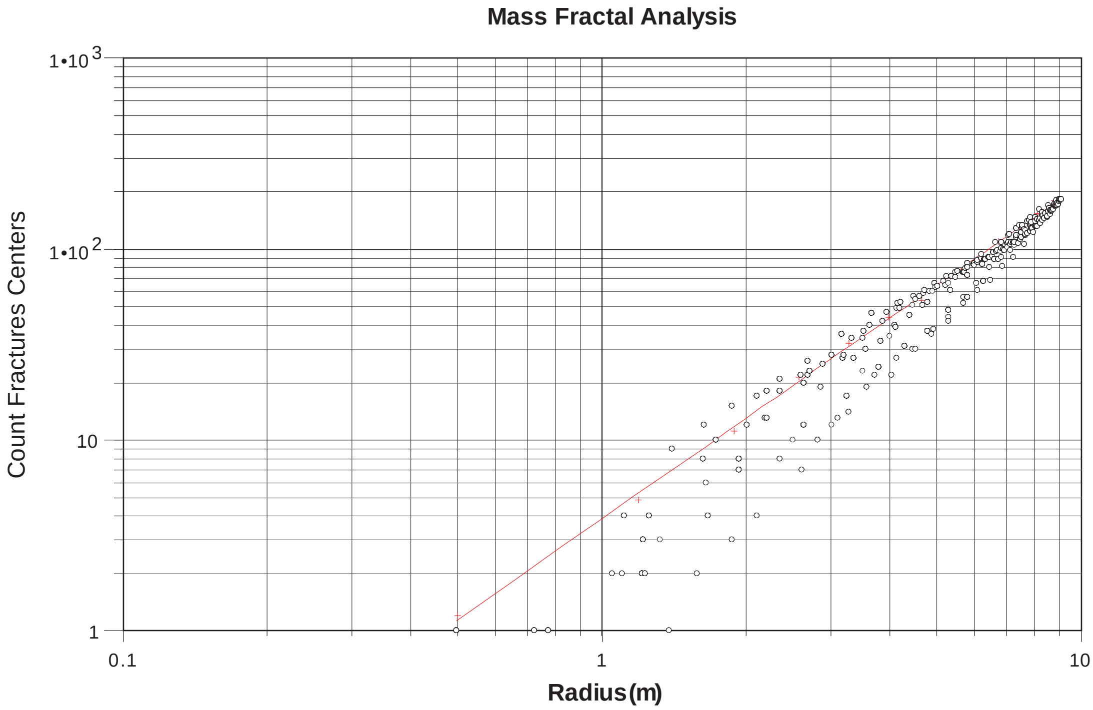

Outcrop ASM000206, Regional Set S_B Mass Dimension Plot

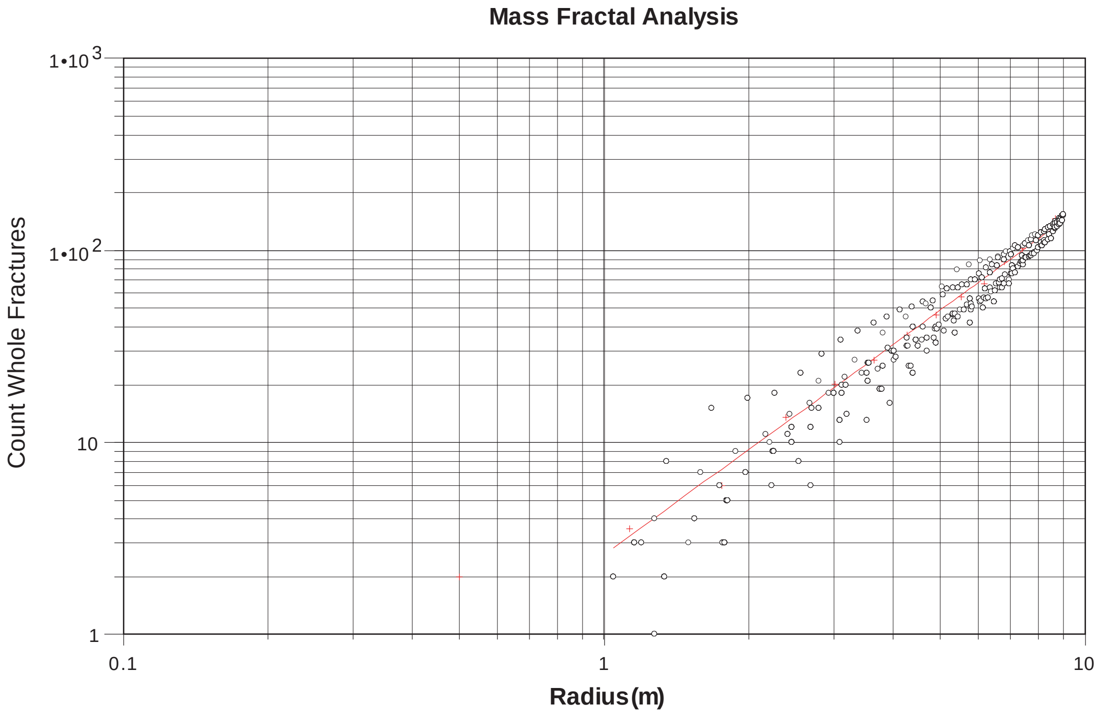

Outcrop ASM000206, Regional Set S_C Mass Dimension Plot

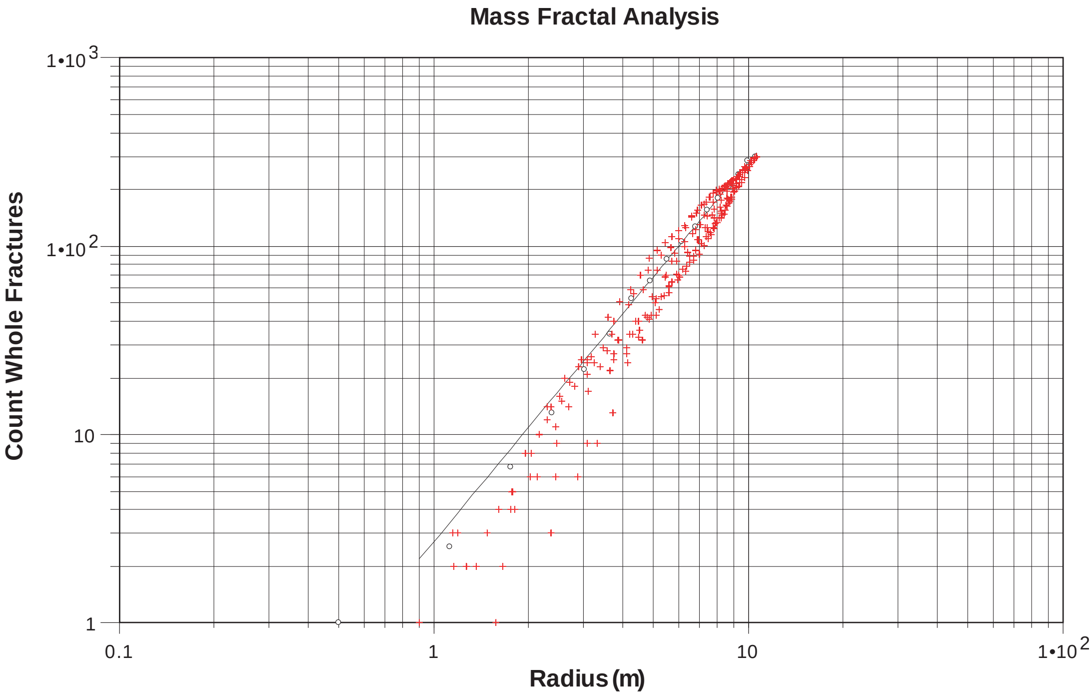

Outcrop ASM000208, Regional Set S_A Mass Dimension Plot

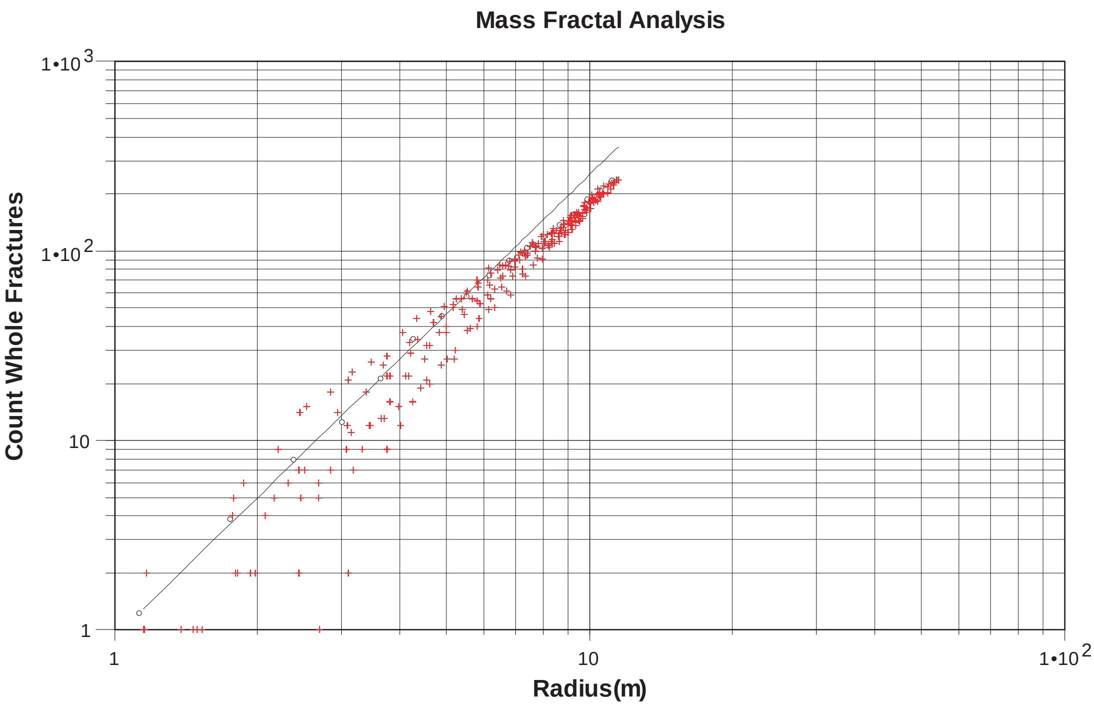

Outcrop ASM000208, Regional Set S_B Mass Dimension Plot

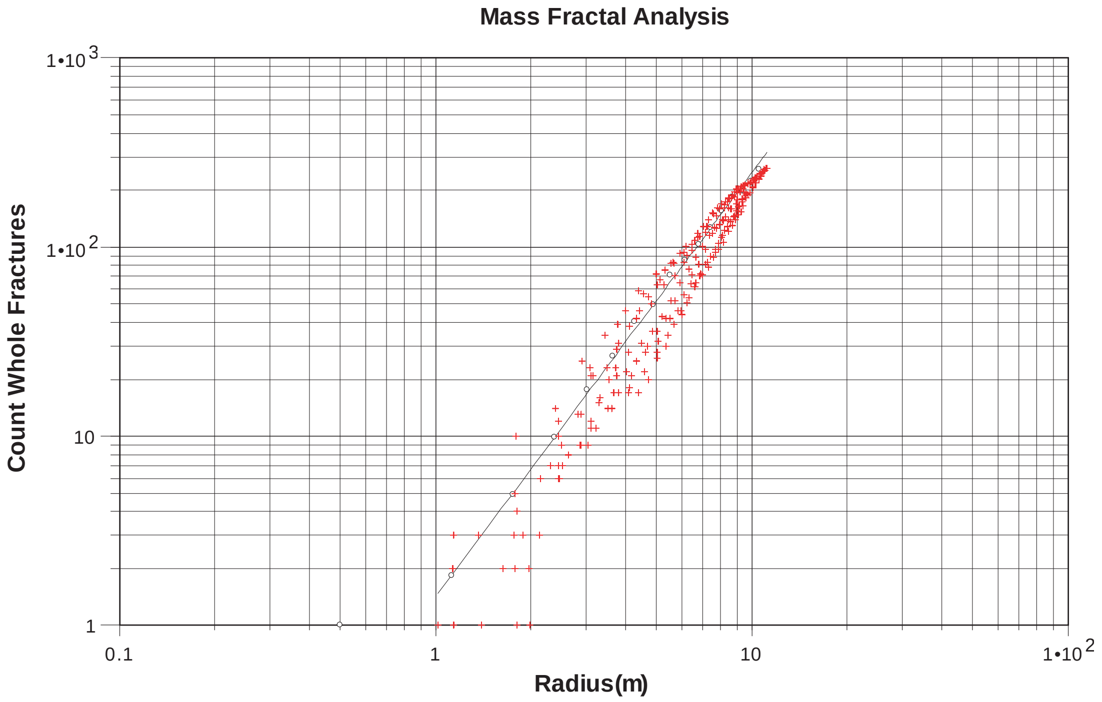

Outcrop ASM000208, Regional Set S_C Mass Dimension Plot

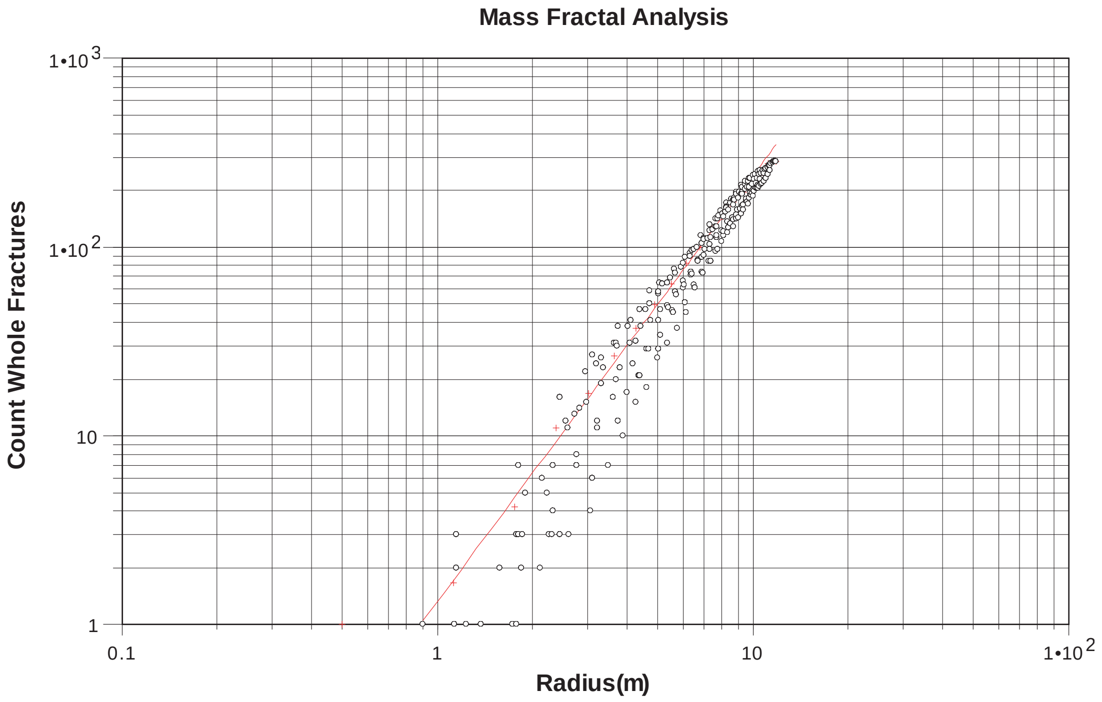

Outcrop ASM000209, Regional Set S_A Mass Dimension Plot

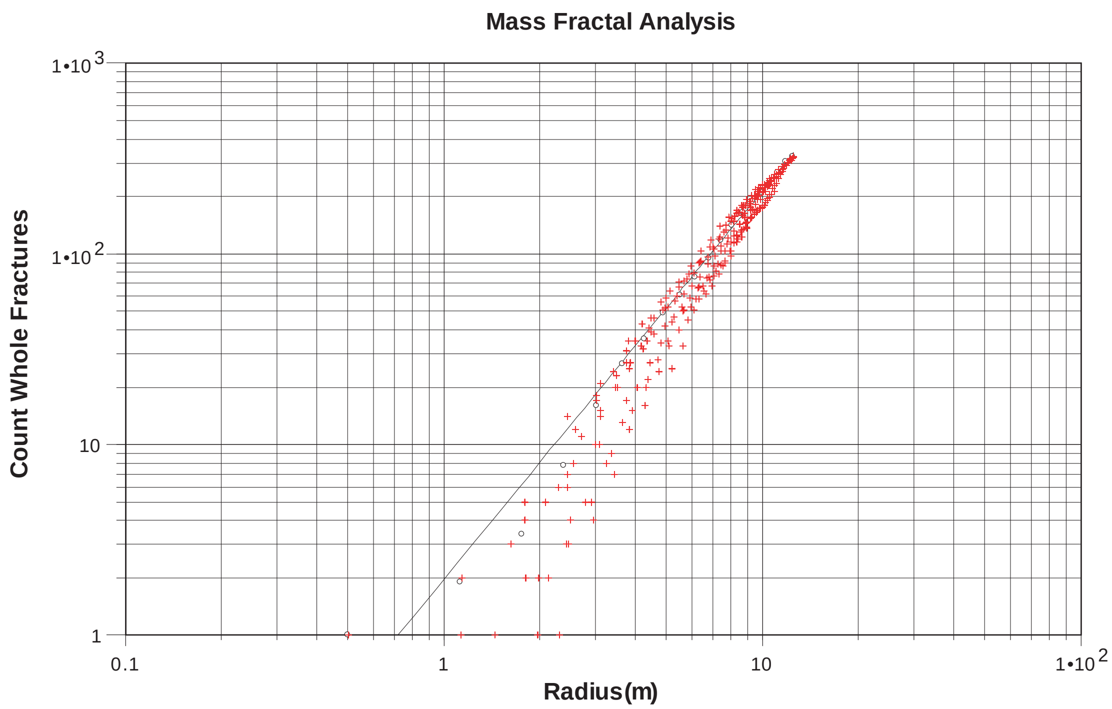

Outcrop ASM000209, Regional Set S_B Mass Dimension Plot

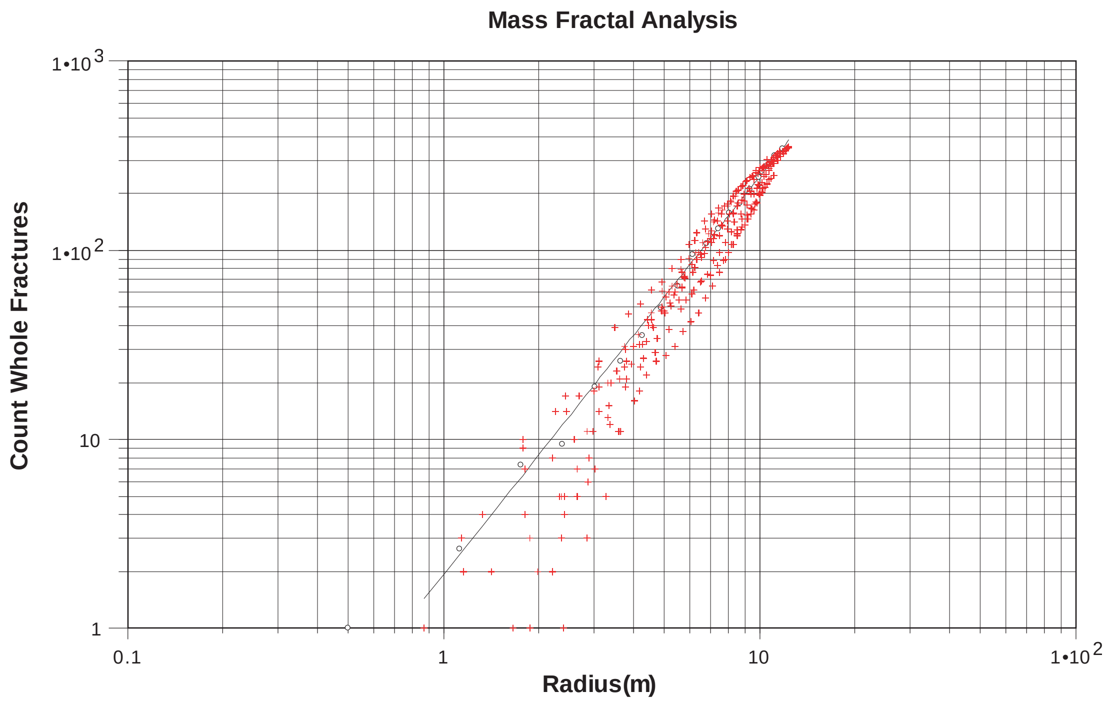

Outcrop ASM000209, Regional Set S_C Mass Dimension Plot

Appendix D

Verification of the Laxemar 1.2 DFN model

Purpose and objectives

The purpose of this section is to demonstrate that the discrete-fracture network (DFN) model for the local site domain model (SDM) Laxemar version 1.2 is consistent with outcrops and boreholes from where it was derived and evaluate if the model is consistent with broader field data in the Laxemar and Simpevarp sub areas. This task was divided into two phases, with objectives to state whether

1) the Laxemar 1.2 DFN model is consistent with the data from which it was derived,
2) the variability within the rock domains, as defined in the DFN model, is consistent with the variability in the data available for those rock domains.

Scope

This study was delimited to verify geometrical model parameters of the Laxemar 1.2 DFN model. More precisely, the consistency between the DFN model and field data was evaluated in terms of statistical distributions of the following four parameters:

1) fracture frequency (P_{10}, m^{-1}) in boreholes,
2) fracture intensity (P_{21}, m/m^2) in outcrops,
3) trace lengths in outcrops, and
4) fracture orientation in outcrops.

Furthermore, all three particular rock domains of the DFN model were evaluated:

- Laxemar subarea, rock domain A.
- Simpevarp subarea, rock domain A.
- Simpevarp subarea, rock domain B.

Approach

A stochastic approach was used for verifying the DFN model to its field data. This approach was based on simulated exploration of boreholes and outcrops in multiple DFN realizations of each rock domain. To make this study meaningful, the simulated exploration was performed as consistently as possible to the real field investigations, in terms of geometry, sample sizes, scales, sampling bias, etc.

Simulated borehole exploration

In the simulated borehole exploration, DFN realizations were sampled over 25 m borehole sections, as such P_{10}-data are already assembled in Appendix 1 and has been used in the derivation of DFN parameters in the report. Furthermore, the simulated exploration does not consider borehole radius, since it is assumed that the borehole fracture data does not include fractures which do not intersect the central axis of the borehole. This assumption has also been made in the derivation of DFN parameters in the report. When comparisons are made to field data, emphasis is also placed on consistency of sample sizes. P_{10} is available for 27 recorded 25 m-sections of borehole KLX04. Thus, 27 stochastic DFN realizations are generated and explored by a simulated 25 m borehole, which has an orientation equal to the approximated average orientation of KLX04. This provides one simulated data set, i.e. consisting of P_{10} values for 27 borehole sections, which can consistently be compared to the field data set. For each rock domain, and for each fracture set, 10 such simulated data sets (below simply referred to as "realizations") were generated and compared to field data.

Simulated outcrop exploration

Fracture traces were extracted from 3D DFN realizations using sampling trace planes (Figure D-1). These trace planes were assigned the mean orientation of the outcrop, in order to provide the same sampling bias of fracture orientations as that encountered in the field. Furthermore, the simulated exploration of outcrops used the same truncation of fracture traces as that in the field. These were: a) removing any part of fracture traces that extend beyond the boundary of the mapped outcrop, and b) discarding any below the truncation limit used in the field (0.5 m). Three distributions can be calculated from each such realization of fracture traces: fracture intensity (P_{21} m/m^2), trace lengths, and fracture orientations. For each rock domain, and for each fracture set, 20 fracture trace realizations were generated and compared to field data.

Implementation

The DFN model parameters were selected according to the recommendations in Sections 6 and 7 in the main report. The main report states that Fractal scaling is recommended for models smaller than 30 m (cf Section 6.3). Therefore fractal mass exponents given in Tables 7-2 and 7-5 are appropriate for this scale of model. Furthermore, the calibrated match-point P_{32} values were selected for the global sets S_A, S_B, and S_C (Table 7-2 and Table 7-5), while borehole mean P_{32} were used for the local sets S_d, S_e, and S_f (Table 7-3 and Table 7-6). Thus, P_{32} was assigned as constant values and did not include the observed variability of P_{32} (as given in Tables 6-28 and 6-29). The parameters used are summarized in Tables D-1 to D-3. Prior expectations were therefore that the global sets should match outcrop data well, and that the local sets should match their borehole-median P_{10} percentiles.

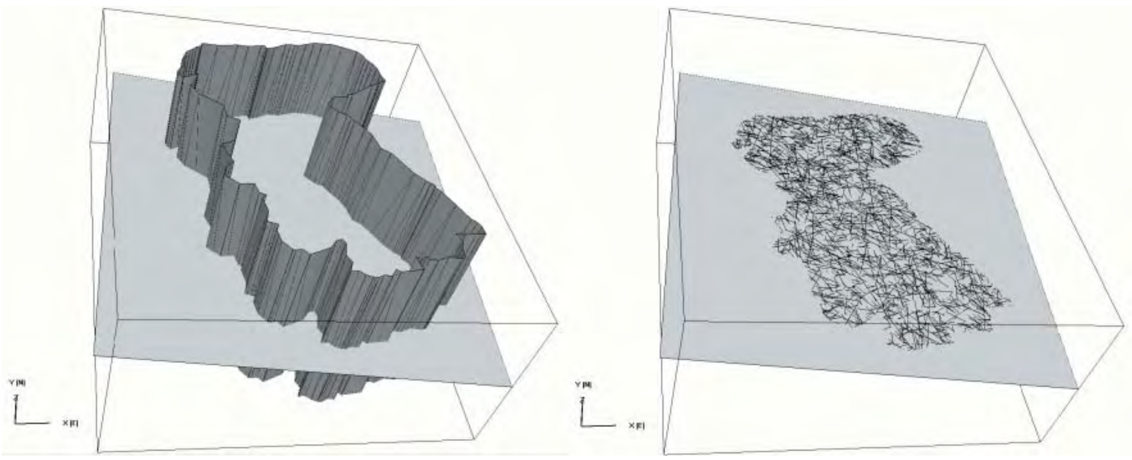

Figure D-1. Example of a simulated exploration of outcrop ASM000208. First, any portion of generated fractures extending beyond the mapped boundary of ASM000208 (dark grey shape; left) is truncated. Next, the traces of the remaining DFN are sampled by a plane (light grey; both figures), which has a mean orientation equal to that of the outcrop. In the final step, all traces shorter than the truncation limit used in the field were truncated from the realization.

Table D-1. Used DFN parameters for the Laxemar subarea, RSMA.

Set	Intensity	Size distribution[1)]			Orientation[3)]		
	P_{32}	Type	X_{ro} (m)	Radius exponent, k_r	Mean pole trend	plunge	Fisher dist κ
S_A	1.310[1)]	Power law	0.328	2.86	338.1	4.5	13.06
S_B	1.026[1)]	Power law	0.977	2.92	100.4	0.2	19.62
S_C	0.974[1)]	Power law	0.858	2.88	212.9	0.9	10.46
S_d	2.32[2)]	Exponential	μ = 0.25		3.3	62.1	10.13
S_f	1.40[2)]	Power law	0.400	3.60	243.0	24.4	23.52

[1)] Taken from Table 7-5. Note that only mean value is reported for the exponential distribution.

[2)] Taken from Table 7-6.

[3)] Taken from Table 7-4.

Table D-2. Used DFN parameters for the Simpevarp subarea, RSMA.

Set	Intensity	Size distribution[1)]			Orientation[3)]		
	P_{32}	Type	X_{ro} (m)	Radius exponent, k_r	Mean pole trend	plunge	Fisher dist κ
S_A	0.320[1)]	Power Law	0.864	2.72	330.3	6.1	16.8
S_B	0.476[1)]	Power Law	0.689	2.82	284.6	0.6	10.78
S_C	1.312[1)]	Power Law	0.596	2.92	201.8	3.7	14.6
S_d	2.75[2)]	Power Law	0.150	3.10	84.6	81.8	6.98
S_e	1.31[2)]	Lognormal	μ = 0.231	σ = 0.169	67.1	15.5	11.73

[1)] Taken from Table 7-2. Note that arithmetic mean and standard deviation is specified for the lognormal distribution.

[2)] Taken from Table 7-3.

[3)] Taken from Table 7-1.

Table D-3. DFN parameters used for the Simpevarp subarea, RSMB.

Set	Intensity	Size distribution[1)]			Orientation[3)]		
	P_{32}	Type	X_{ro} (m)	Radius exponent, k_r	Mean pole trend	plunge	Fisher dist κ
S_A	2.152[1)]	Power Law	0.367	2.72	330.3	6.1	16.8
S_B	0.618[1)]	Power Law	0.396	2.63	284.6	0.6	10.78
S_C	0.868[1)]	Power Law	0.372	2.66	201.8	3.7	14.6
S_d	7.05[2)]	Power Law	0.150	3.10	84.6	81.8	6.98
S_e	2.84[2)]	Lognormal	μ = 0.231	σ = 0.169	67.1	15.5	11.73

[1)] Taken from Table 7-2. Note that arithmetic mean and standard deviation is specified for the lognormal distribution.

[2)] Taken from Table 7-3.

[3)] Taken from Table 7-1.

The borehole validation data (P_{10} for 25 m sections) for each respective rock domain were taken from Appendix B. Those sections that span mapped deformation zones (Section 5.1; Appendix B), and those that extend beyond the actual borehole (e.g. section 1,000–1,025 m of KSH02; Appendix B) were excluded. The outcrops in Section 4 were all used as validation data, for respective rock domain, except for ASM000206, which belongs to rock domain C. The validation data used are summarized in Table D-4, below.

Table D-4. Verification field data for different rock domains and subareas used in phases I and II, respectively.

Phase I[1)]	Borehole	Number of 25 m sections	Orientation (trend/plunge)	Outcrop	Orientation (strike/dip)	Area (m^2)
Laxemar, RSMA	KLX04	27	35°/85°	ASM000208	94°/1.8°	331
Simpevarp, RSMA	KAV01	25	149°/88°	ASM000026	265°/4.4°	524
Simpevarp, RSMB	KSH02	31	0°/87°	ASM000205	138°/5.3°	215
Phase II[2)]	Borehole	Number of 25 m sections	Orientation (trend/plunge)	Outcrop	Orientation (strike/dip)	Area (m^2)
Laxemar, RSMA	KLX04	27	35°/85°	ASM000208	94°/1.8°	331
	KLX02	16	0°/85°	ASM000209	0°/1.4°	446
Simpevarp, RSMA	KAV01	25	149°/88°	ASM000026	265°/4.4°	524
	KAV04A	16	75°/85°	ASM000025	180°/5.3°	422.5
	KSH03A	29	151°/58°	–	–	–
Simpevarp, RSMB	KSH02	31	0°/87°	ASM000205	138°/5.3°	215
	KSH01A	9	191°/75°	–	–	–
	KAV04A	2	75°/85°	–	–	–
	KAV01	2	149°/88°	–	–	–

[1)] Phase I: Simulated exploration of the DFN model compared to its underlying field data (one borehole and one outcrop).

[2)] Phase II: Simulated exploration compared to all available data for each rock domain.

Results

The results of the simulated exploration are shown in the figures below. These figures are organized in the following manner:

- First, the results of phase I are presented (Figure D-2 to Figure D-22) these are followed by those of phase II (Figure D-23 to Figure D-37); in phase I, the simulated exploration is compared to one borehole and one outcrop for each rock domain, while in phase II, the simulated exploration is compared to all available data for each rock domain.
- The rock domains are ordered in the following way: 1) Laxemar subarea, RSMA, 2) Simpevarp subarea, RSMA, and 3) Simpevarp subarea, RSMB.
- The results of each rock domain, is subdivided into an evaluation for all fracture sets combined (e.g. Figure D-2) followed by each individual fracture set (e.g. Figure D-3 to Figure D-7). Finally, orientation distributions of traces are compared (e.g. Figure D-8).
- Each figure (e.g. Figure D-2) demonstrates a visual comparison between outcrop trace data and a simulated realization of its outcrop traces. Next, simulated exploration of fracture properties (grey lines) are compared to field data (blue) for a number of stochastic DFN realizations. The comparisons are made in terms of distributions of: fracture intensity, P_{21}, fracture frequency, P_{10}, and trace length.
- For Laxemar RSMA, each fracture trace realization was, first truncated at 0.5m trace length, then discretized into $(2\ m)^2$ cells, for which P_{21} was calculated as a distribution. These distributions were then compared to those of outcrop data (e.g. Figure D-2). However, results indicated that the simulated P_{21}-distributions are very similar, in terms of variance, to those from the field data. The main difference between simulated P_{21} and outcrop data is its mean or total value. Therefore only the total truncated P_{21} was compared for Simpevarp subarea RSMA and RSMB (cf Figure D-2 and Figure D-23).

Phase I: Simulated exploration of the DFN model compared to its underlying field data; Laxemar subarea, RSMA

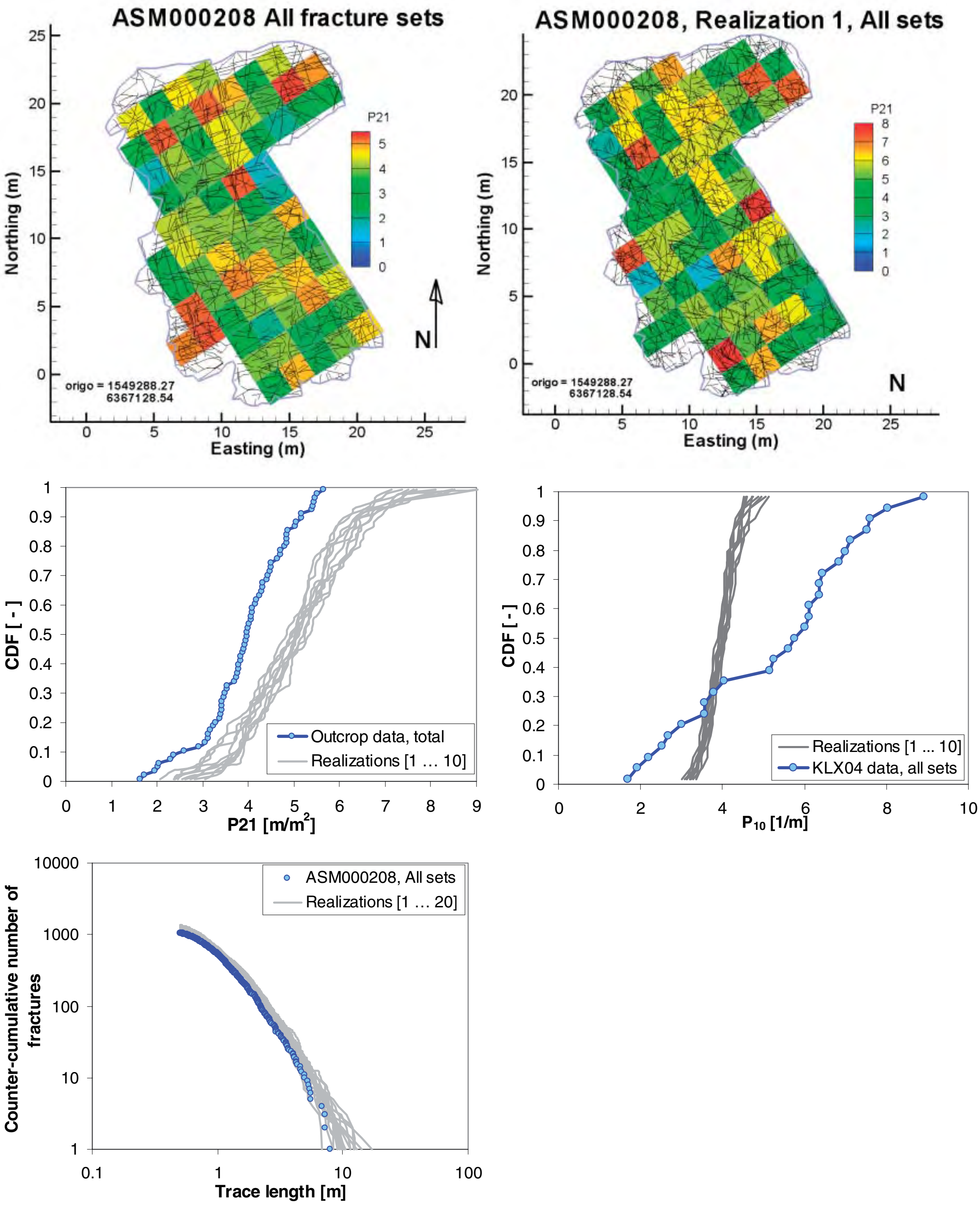

Figure D-2. Evaluation of Laxemar subarea, RSMA, all fracture sets. Traces of outcrop ASM000208 compared to one realization. Simulated fracture properties (grey lines) are compared to field data (blue), in terms of: fracture intensity, P_{21}, fracture frequency, P_{10}, and trace length distribution.

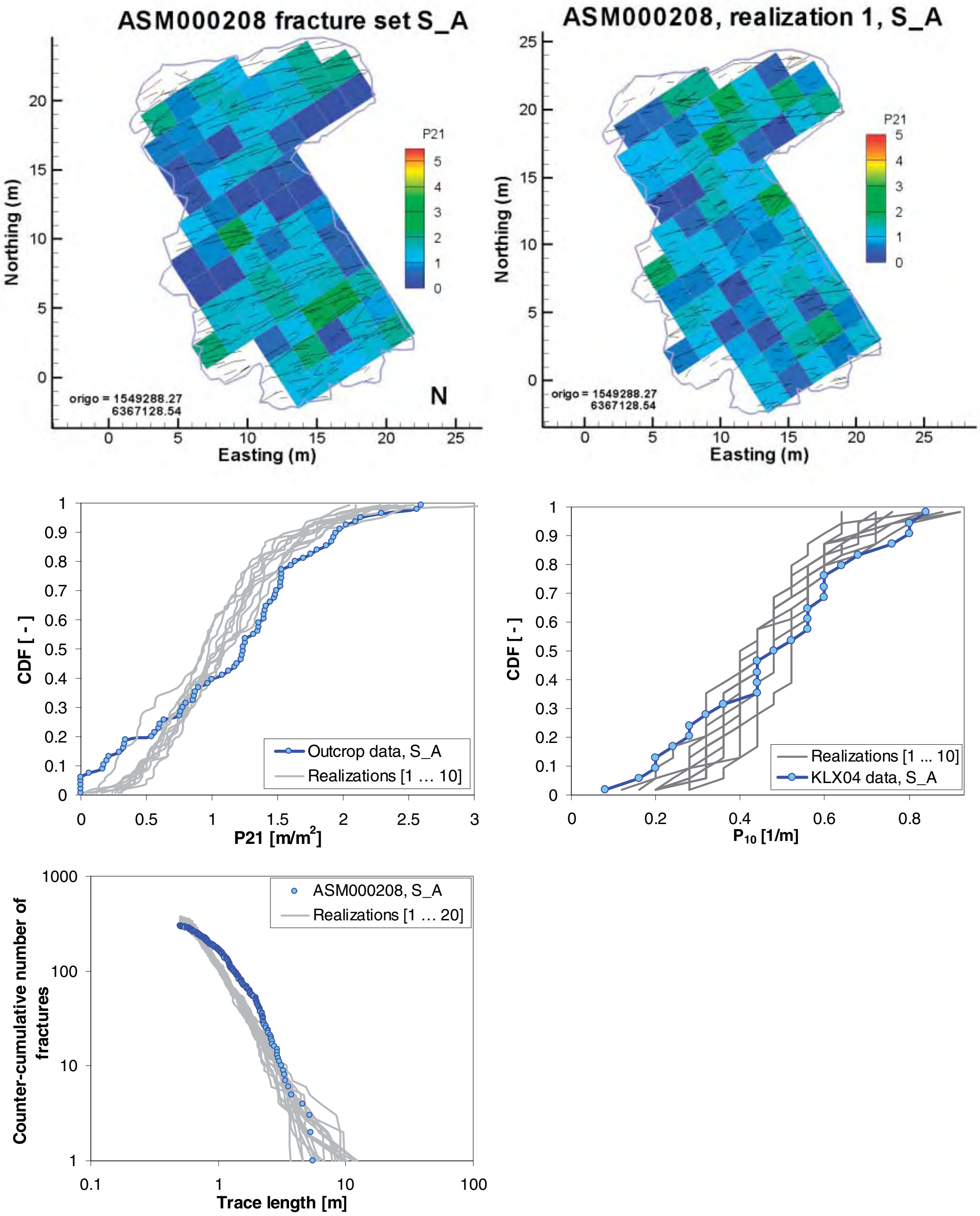

Figure D-3. *Evaluation of Laxemar subarea, RSMA, fracture set S_A. Traces of outcrop ASM000208 compared to one realization. Simulated fracture properties (grey lines) are compared to field data (blue), in terms of: fracture intensity, P_{21}, fracture frequency, P_{10}, and trace length distribution.*

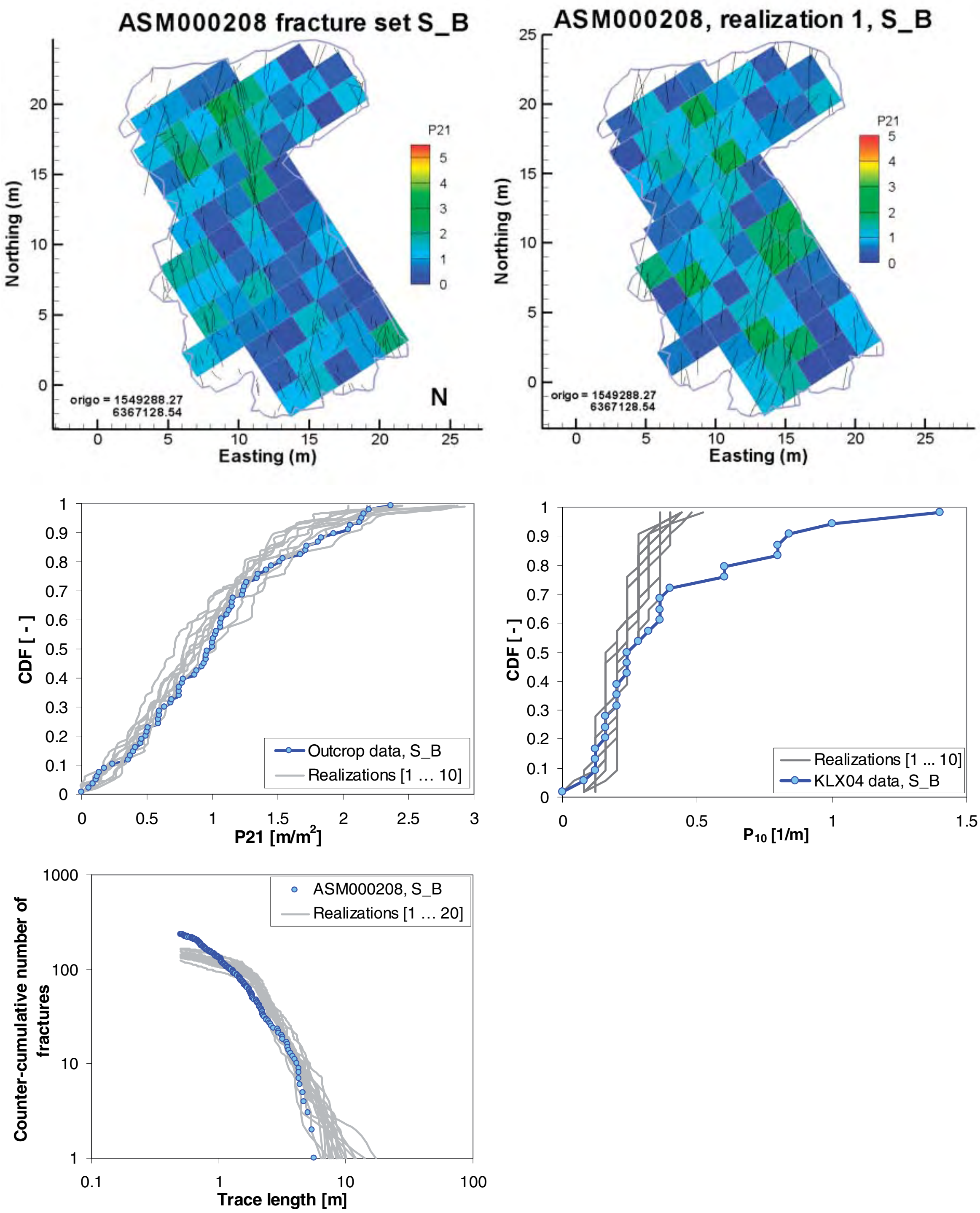

Figure D-4. *Evaluation of Laxemar subarea, RSMA, fracture set S_B. Traces of outcrop ASM000208 compared to one realization. Simulated fracture properties (grey lines) are compared to field data (blue), in terms of: fracture intensity,* P_{21}*, fracture frequency,* P_{10}*, and trace length distribution.*

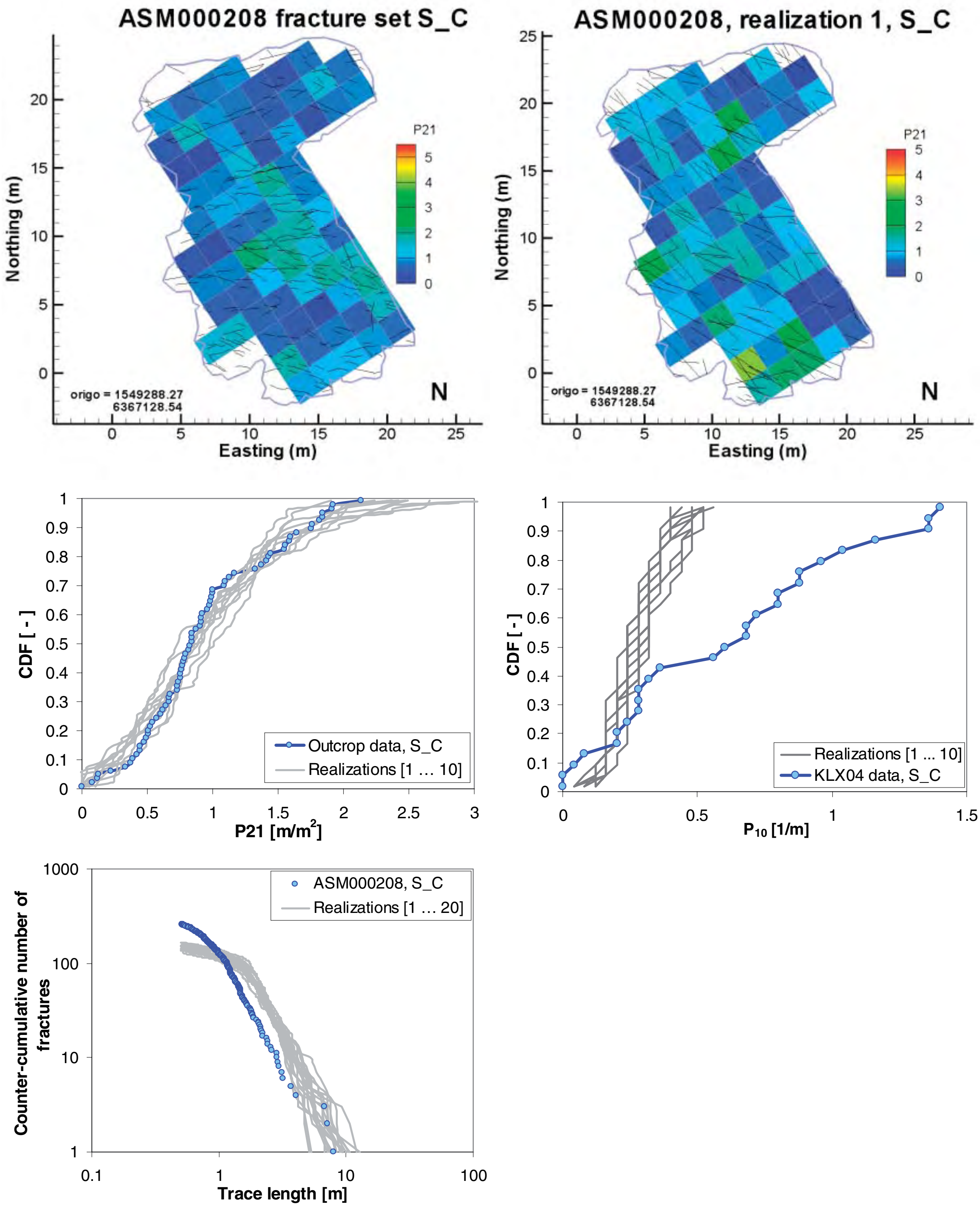

Figure D-5. *Evaluation of Laxemar subarea, RSMA, fracture set S_C. Traces of outcrop ASM000208 compared to one realization. Simulated fracture properties (grey lines) are compared to field data (blue), in terms of: fracture intensity,* P_{21}*, fracture frequency,* P_{10}*, and trace length distribution.*

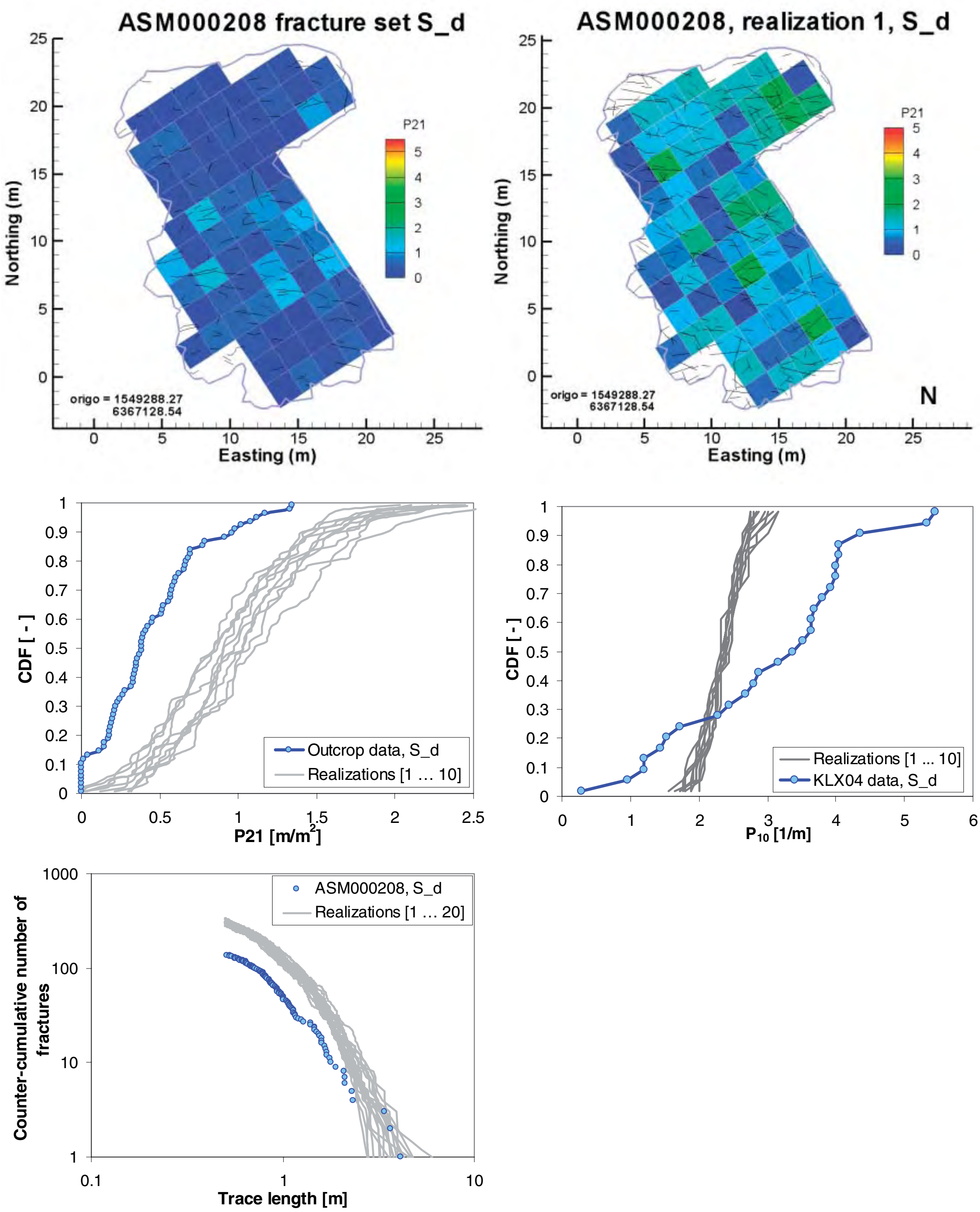

Figure D-6. *Evaluation of Laxemar subarea, RSMA, fracture set S_d. Traces of outcrop ASM000208 compared to one realization. Simulated fracture properties (grey lines) are compared to field data (blue), in terms of: fracture intensity,* P_{21}*, fracture frequency,* P_{10}*, and trace length distribution.*

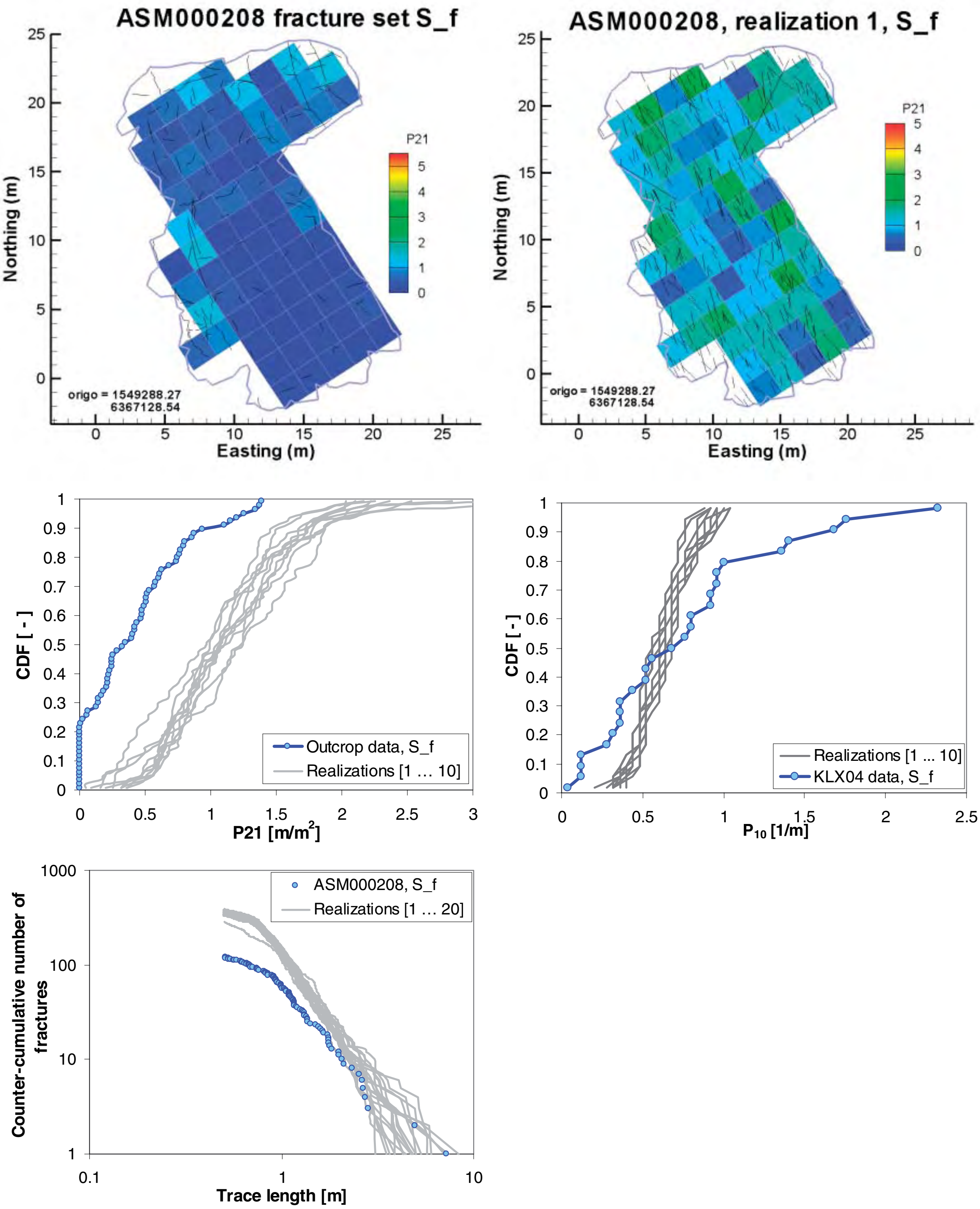

Figure D-7. Evaluation of Laxemar subarea, RSMA, fracture set S_f. Traces of outcrop ASM000208 compared to one realization. Simulated fracture properties (grey lines) are compared to field data (blue), in terms of: fracture intensity, P_{21}, fracture frequency, P_{10}, and trace length distribution.

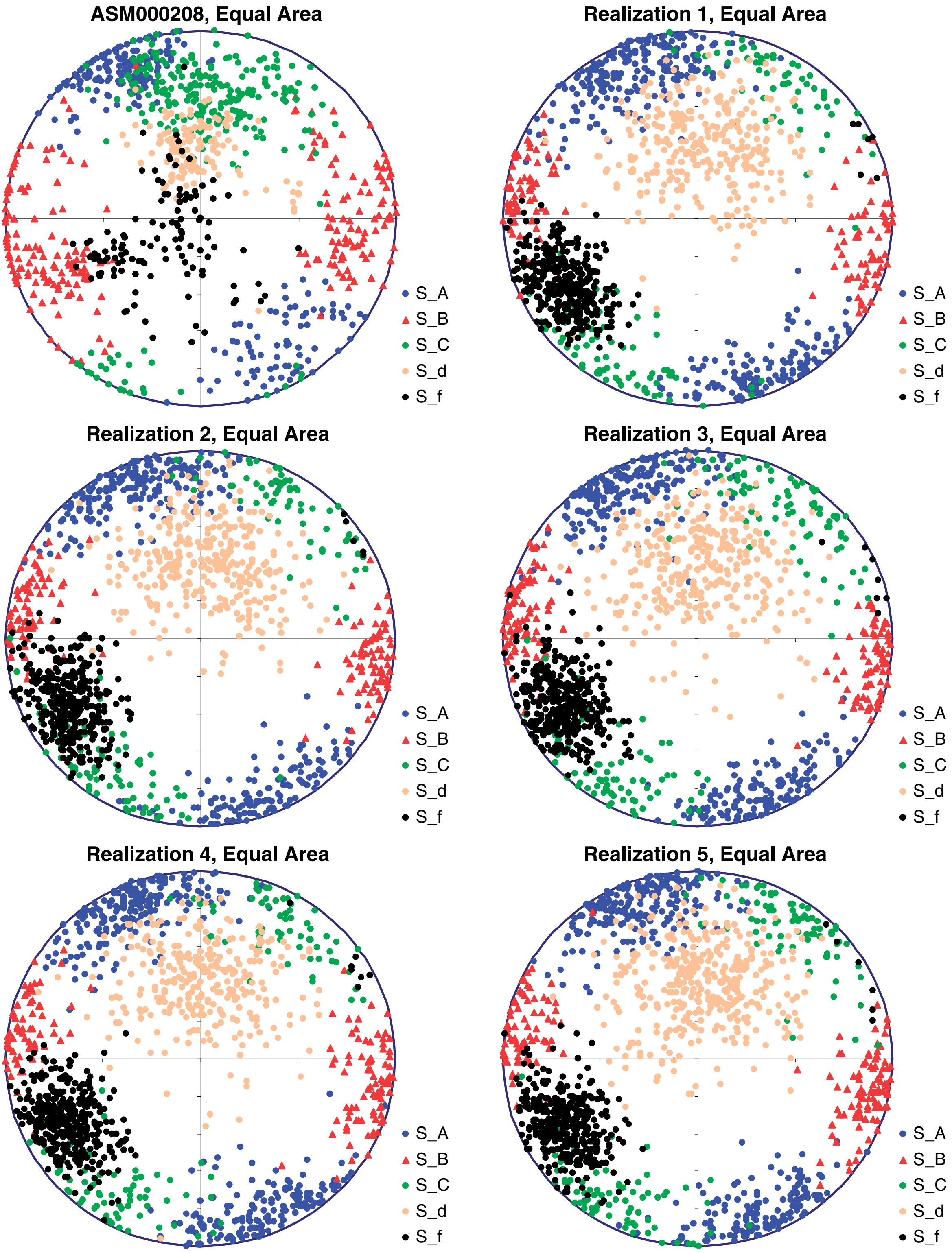

***Figure D-8.** Stereoplots of simulated traces for the Laxemar subarea, RSMA: outcrop ASM000208 data compared to five realizations.*

Simpevarp subarea, RSMA

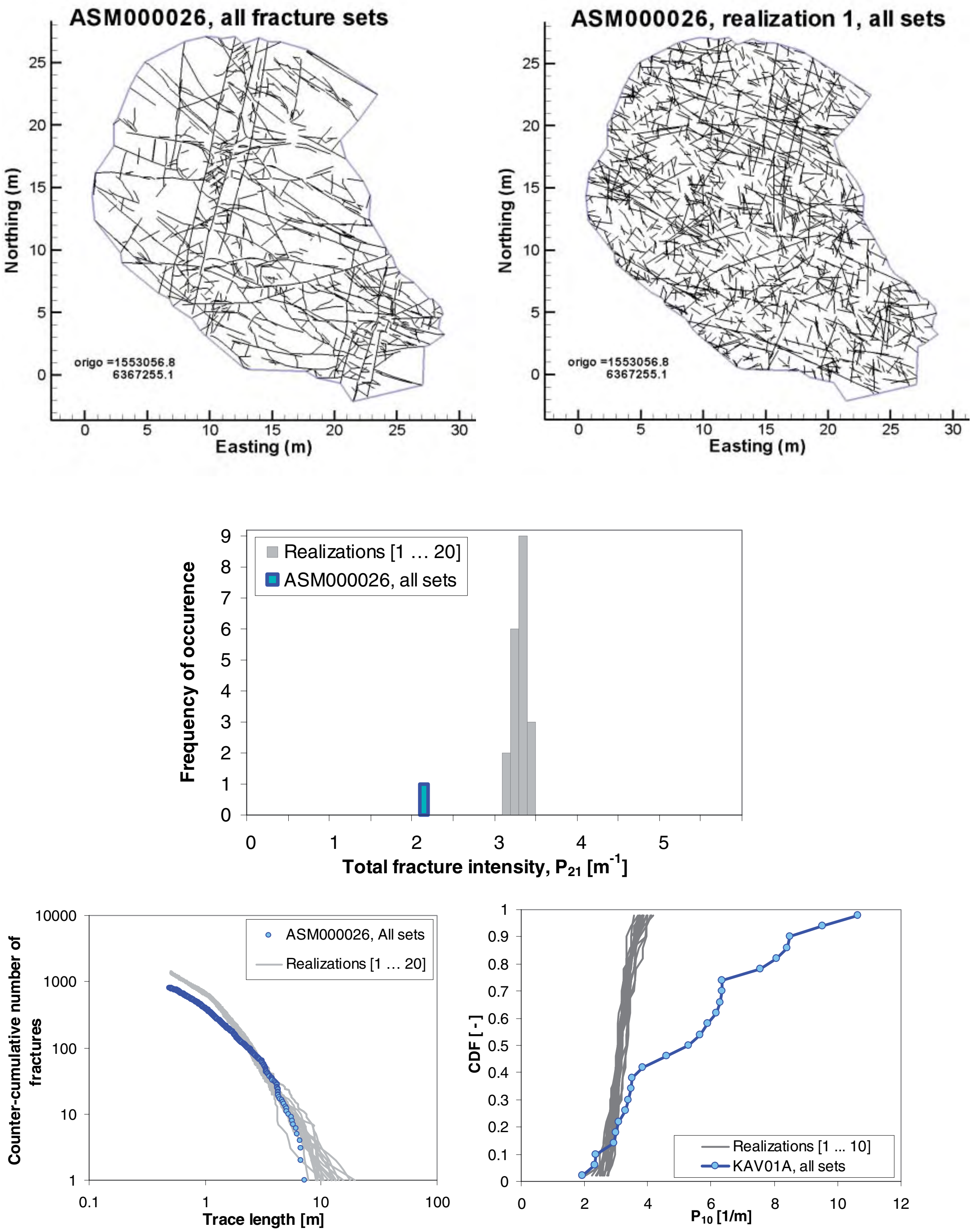

Figure D-9. *Evaluation of Simpevarp subarea, RSMA, all fracture sets. Traces of outcrop ASM000026 compared to one realization. Simulated fracture properties (grey lines) are compared to field data (blue), in terms of: fracture intensity, P_{21}, fracture frequency, P_{10}, and trace length distribution.*

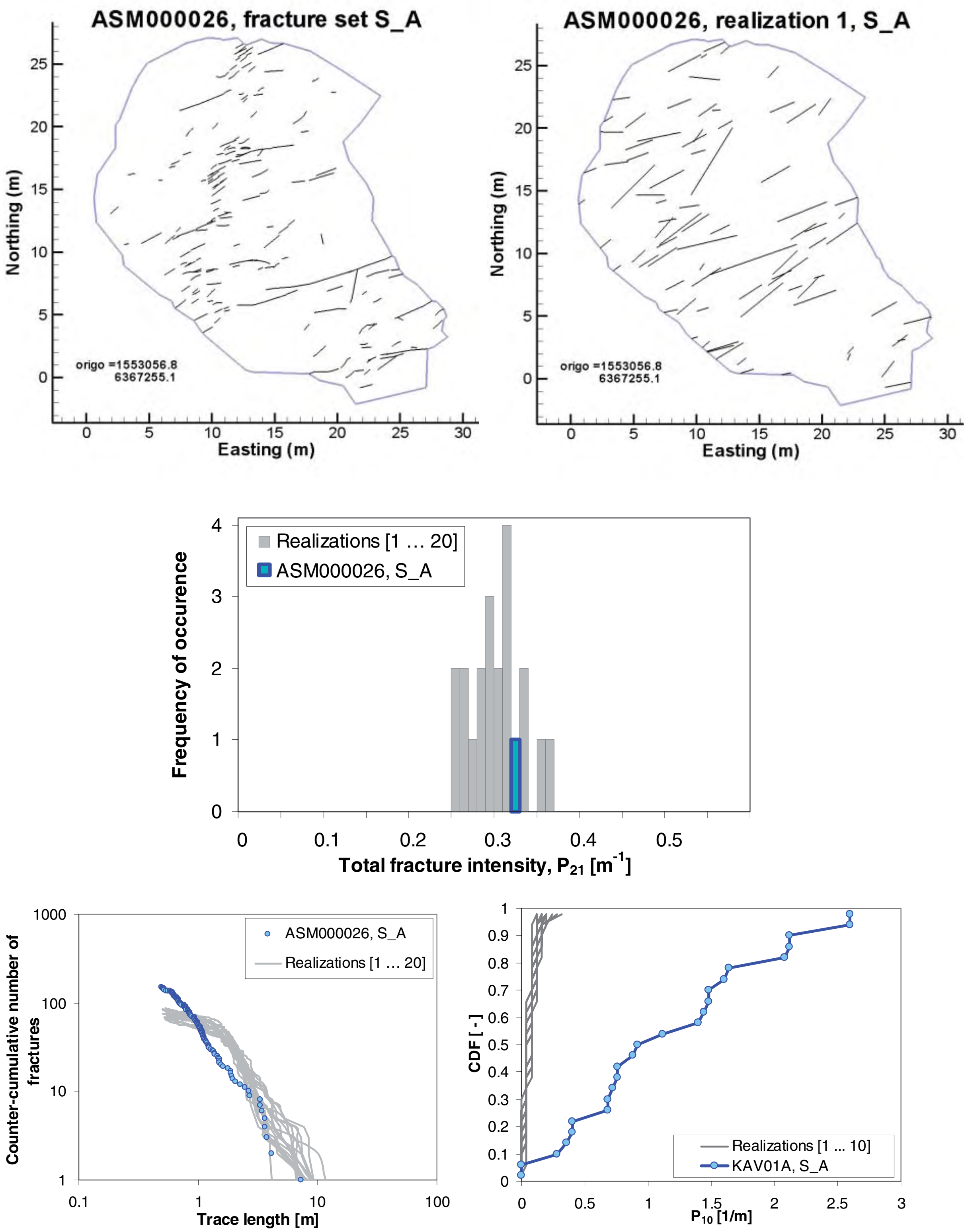

***Figure D-10.** Evaluation of Simpevarp subarea, RSMA, fracture set S_A. Traces of outcrop ASM000026 compared to one realization. Simulated fracture properties (grey lines) are compared to field data (blue), in terms of: fracture intensity, P_{21}, fracture frequency, P_{10}, and trace length distribution.*

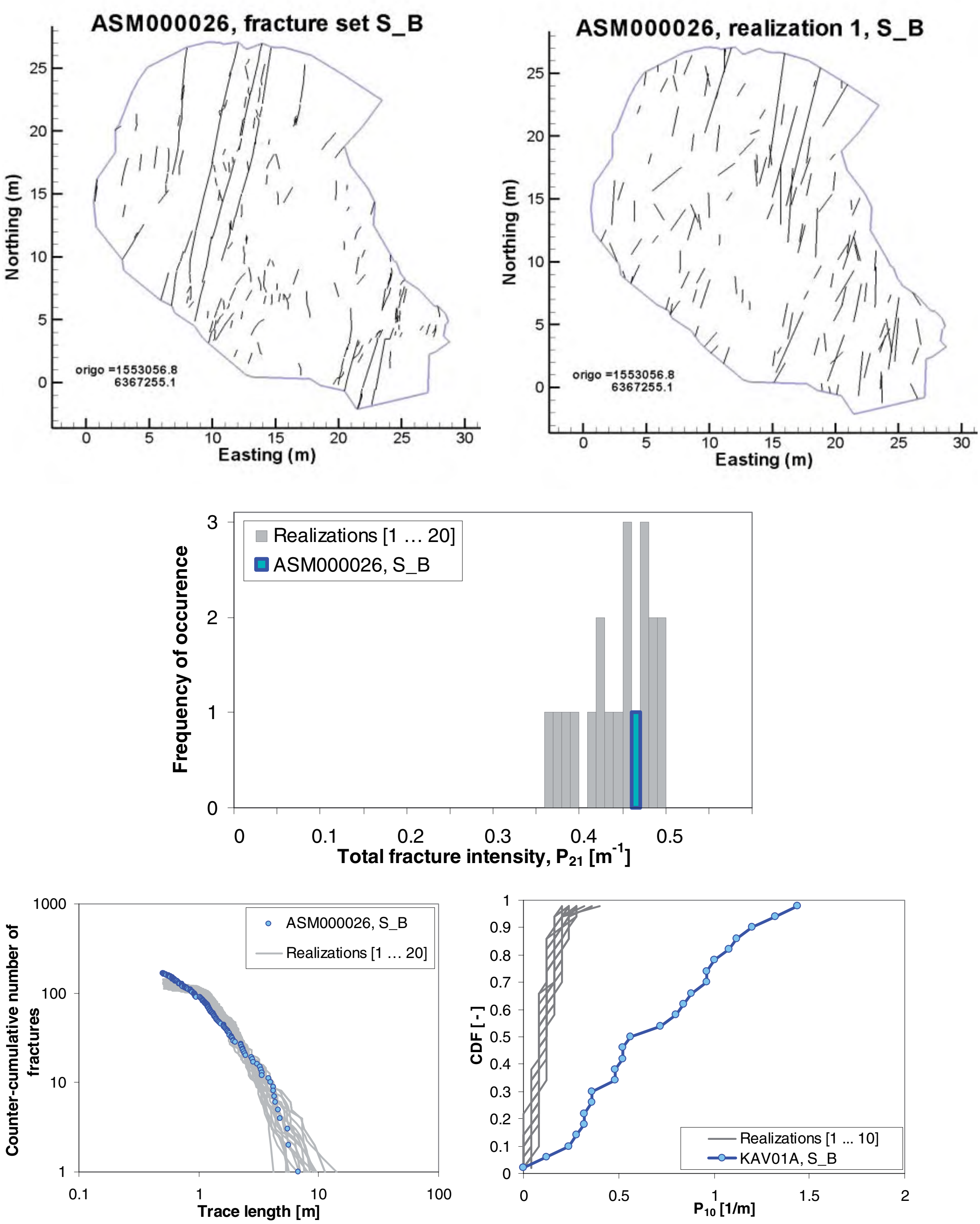

Figure D-11. *Evaluation of Simpevarp subarea, RSMA, fracture set S_B. Traces of outcrop ASM000026 compared to one realization. Simulated fracture properties (grey lines) are compared to field data (blue), in terms of: fracture intensity, P_{21}, fracture frequency, P_{10}, and trace length distribution.*

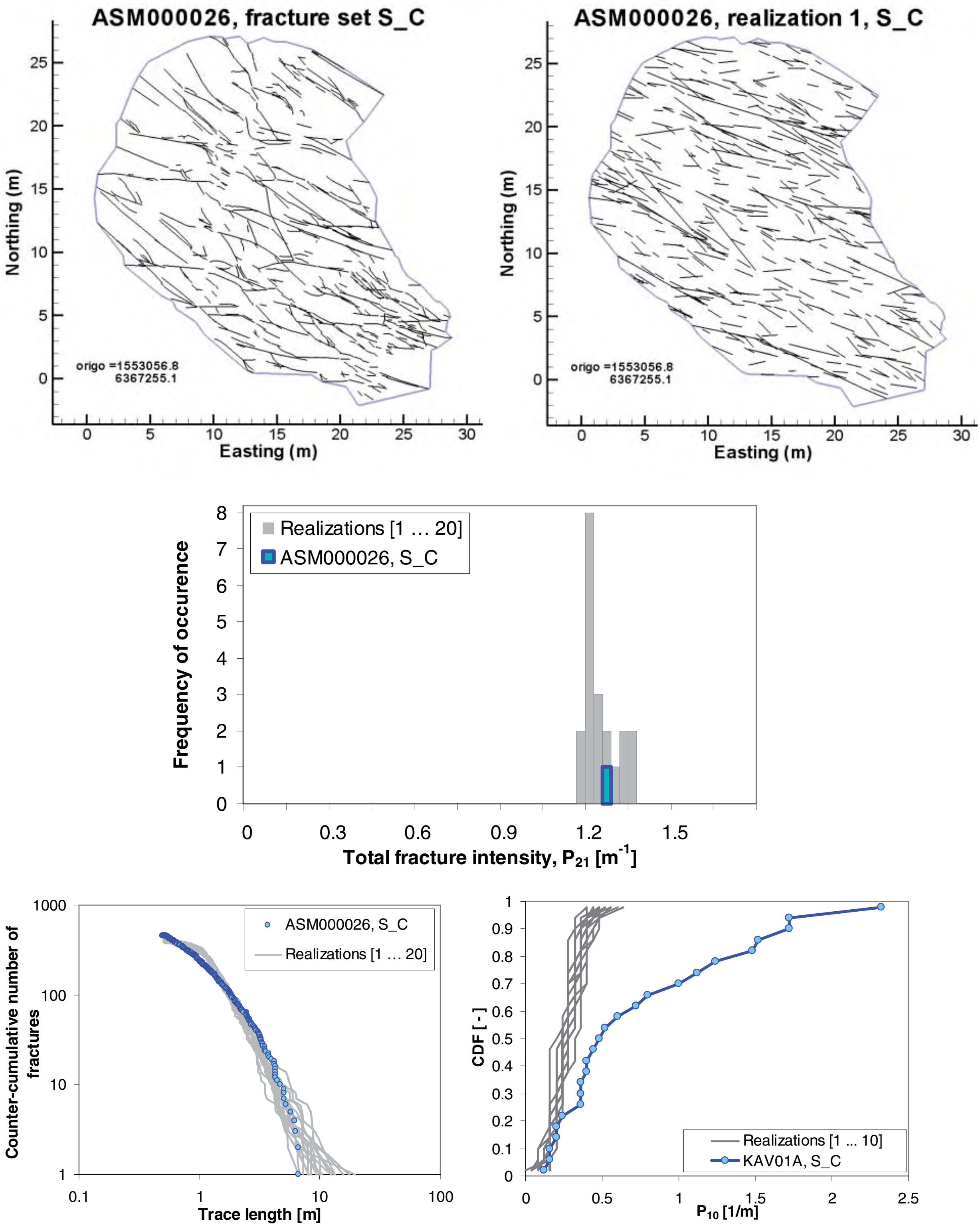

***Figure D-12.** Evaluation of Simpevarp subarea, RSMA, fracture set S_C. Traces of outcrop ASM000026 compared to one realization. Simulated fracture properties (grey lines) are compared to field data (blue), in terms of: fracture intensity, P_{21}, fracture frequency, P_{10}, and trace length distribution.*

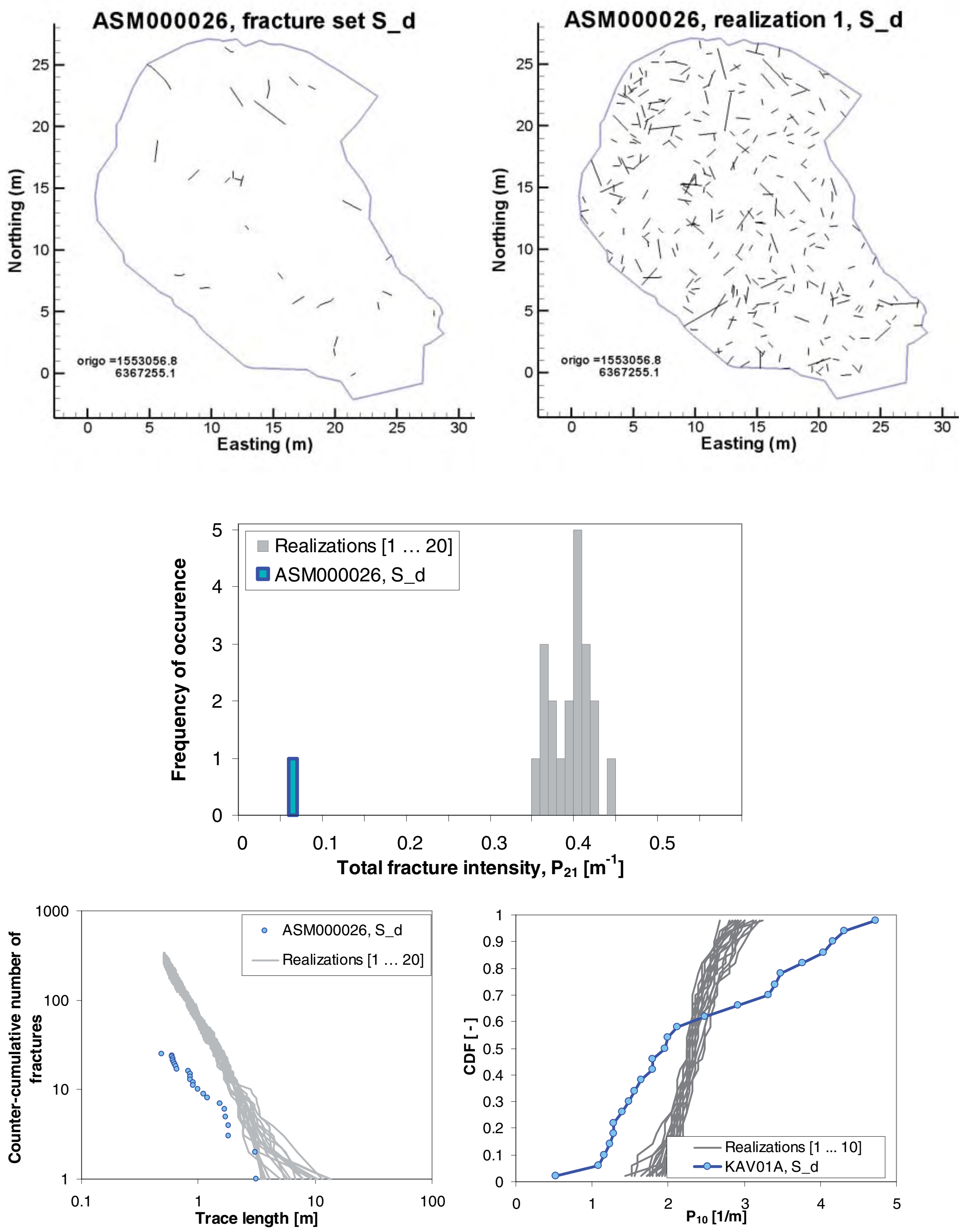

Figure D-13. Evaluation of Simpevarp subarea, RSMA, fracture set S_d. Traces of outcrop ASM000026 compared to one realization. Simulated fracture properties (grey lines) are compared to field data (blue), in terms of: fracture intensity, P_{21}, fracture frequency, P_{10}, and trace length distribution.

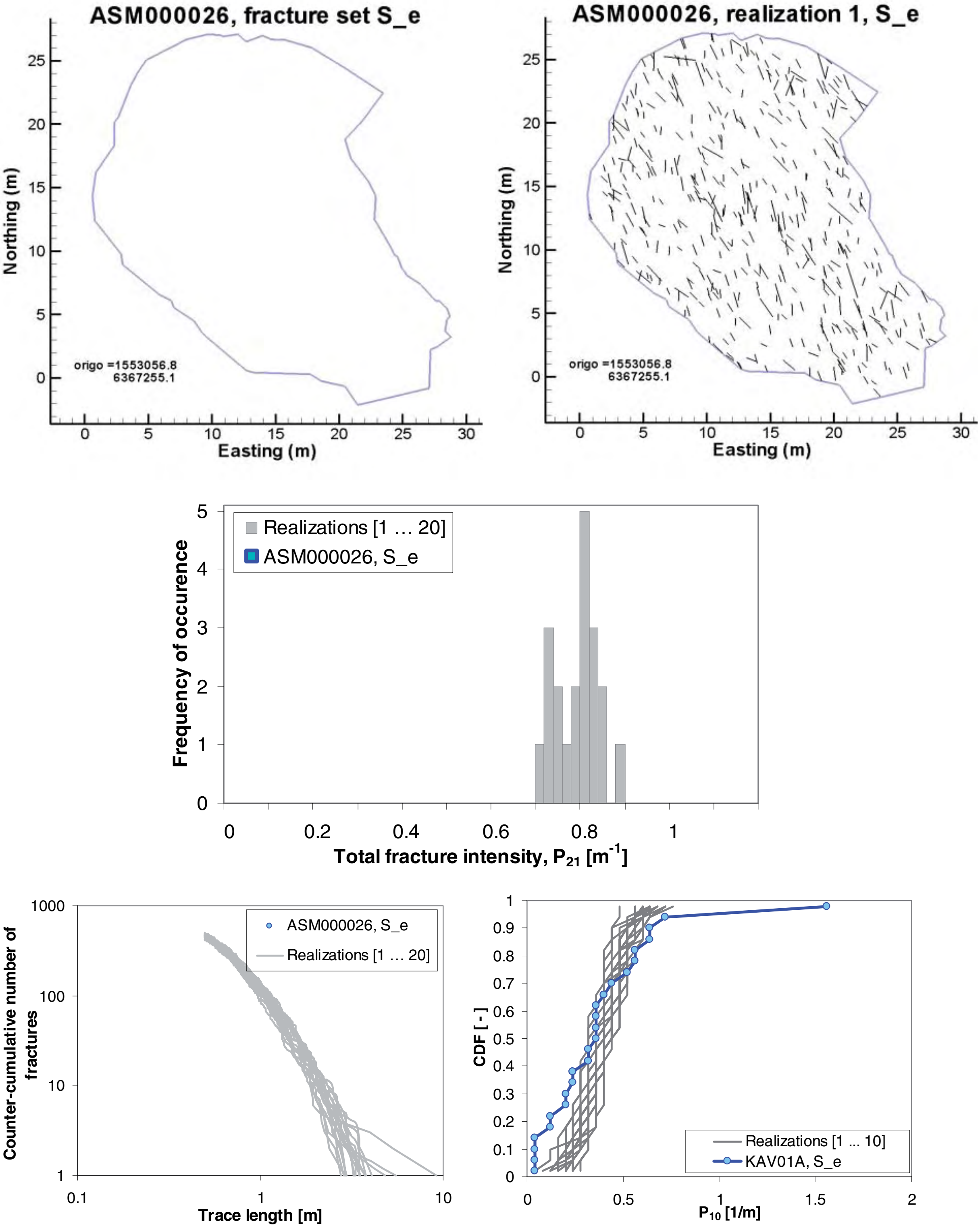

Figure D-14. *Evaluation of Simpevarp subarea, RSMA, fracture set S_e. Traces of outcrop ASM000026 compared to one realization. Simulated fracture properties (grey lines) are compared to field data (blue), in terms of: fracture intensity, P_{21}, fracture frequency, P_{10}, and trace length distribution.*

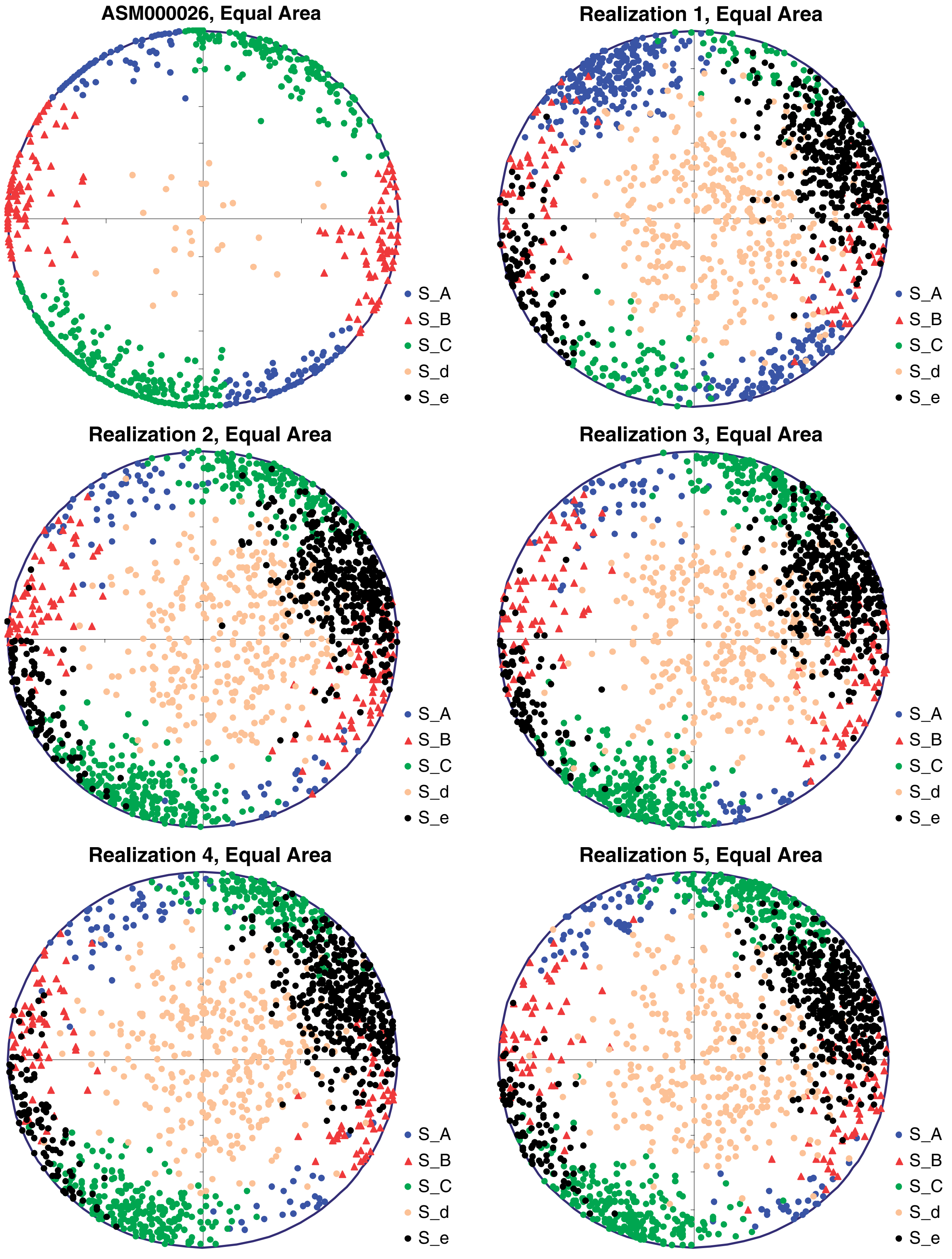

Figure D-15. *Stereoplots of simulated traces for the Simpevarp subarea, RSMA: outcrop ASM000026 data compared to five realizations.Simpevarp subarea, RSMB*

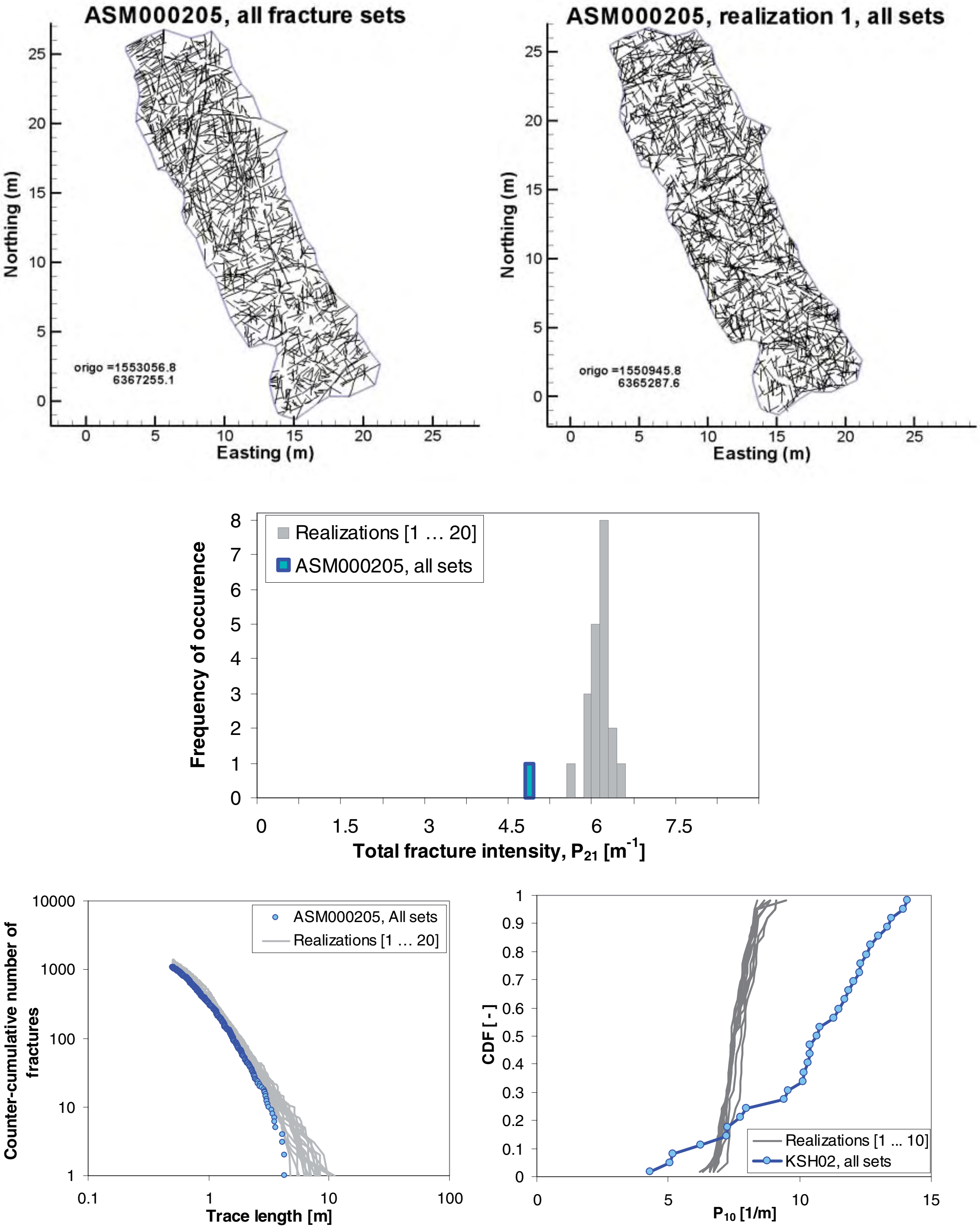

Figure D-16. *Evaluation of Simpevarp subarea, RSMB, all fracture sets. Traces of outcrop ASM000205 compared to one realization. Simulated fracture properties (grey lines) are compared to field data (blue), in terms of: fracture intensity, P_{21}, fracture frequency, P_{10}, and trace length distribution.*

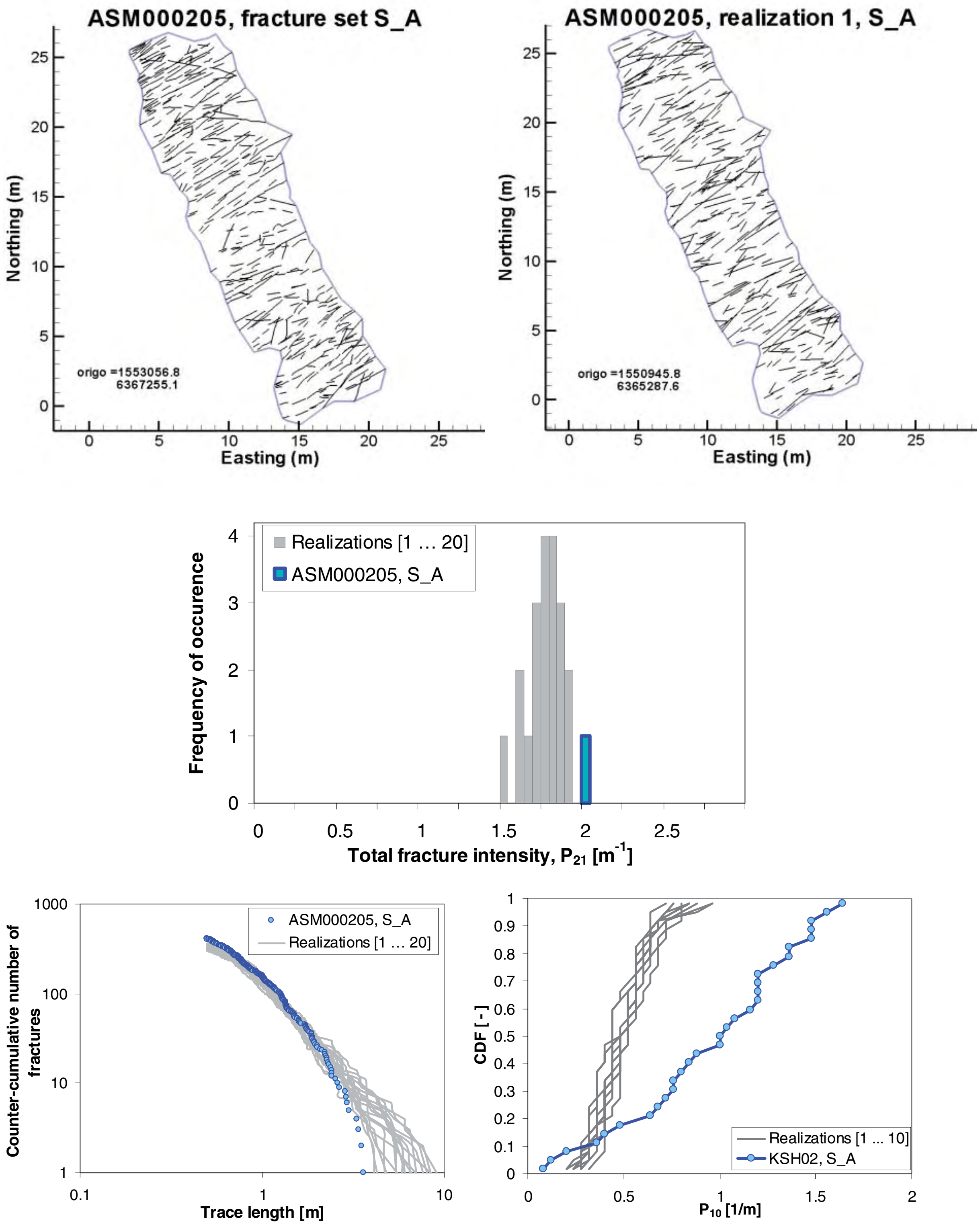

Figure D-17. *Evaluation of Simpevarp subarea, RSMB, fracture set S_A. Traces of outcrop ASM000205 compared to one realization. Simulated fracture properties (grey lines) are compared to field data (blue), in terms of: fracture intensity, P_{21}, fracture frequency, P_{10}, and trace length distribution.*

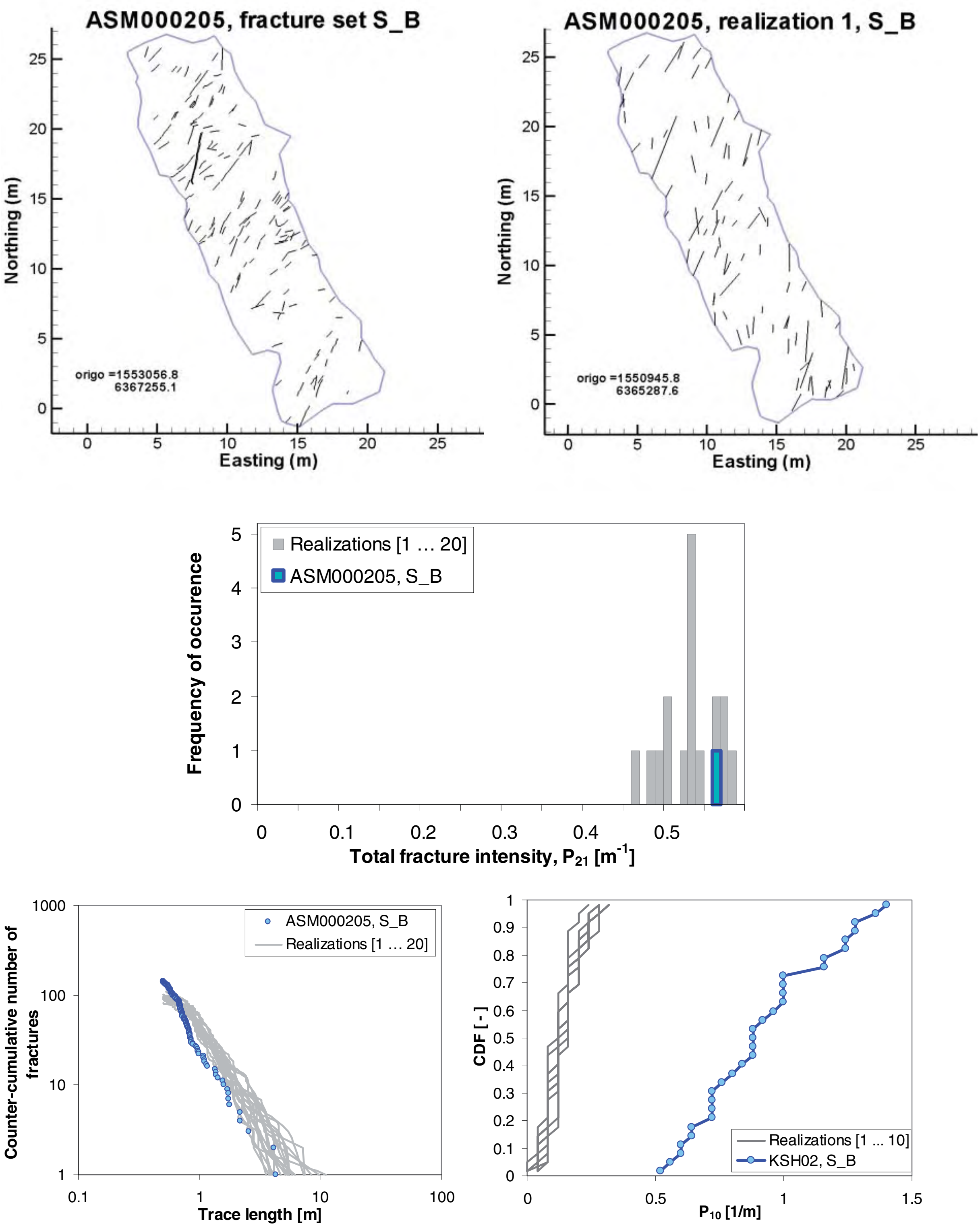

Figure D-18. Evaluation of Simpevarp subarea, RSMB, fracture set S_B. Traces of outcrop ASM000205 compared to one realization. Simulated fracture properties (grey lines) are compared to field data (blue), in terms of: fracture intensity, P_{21}, fracture frequency, P_{10}, and trace length distribution.

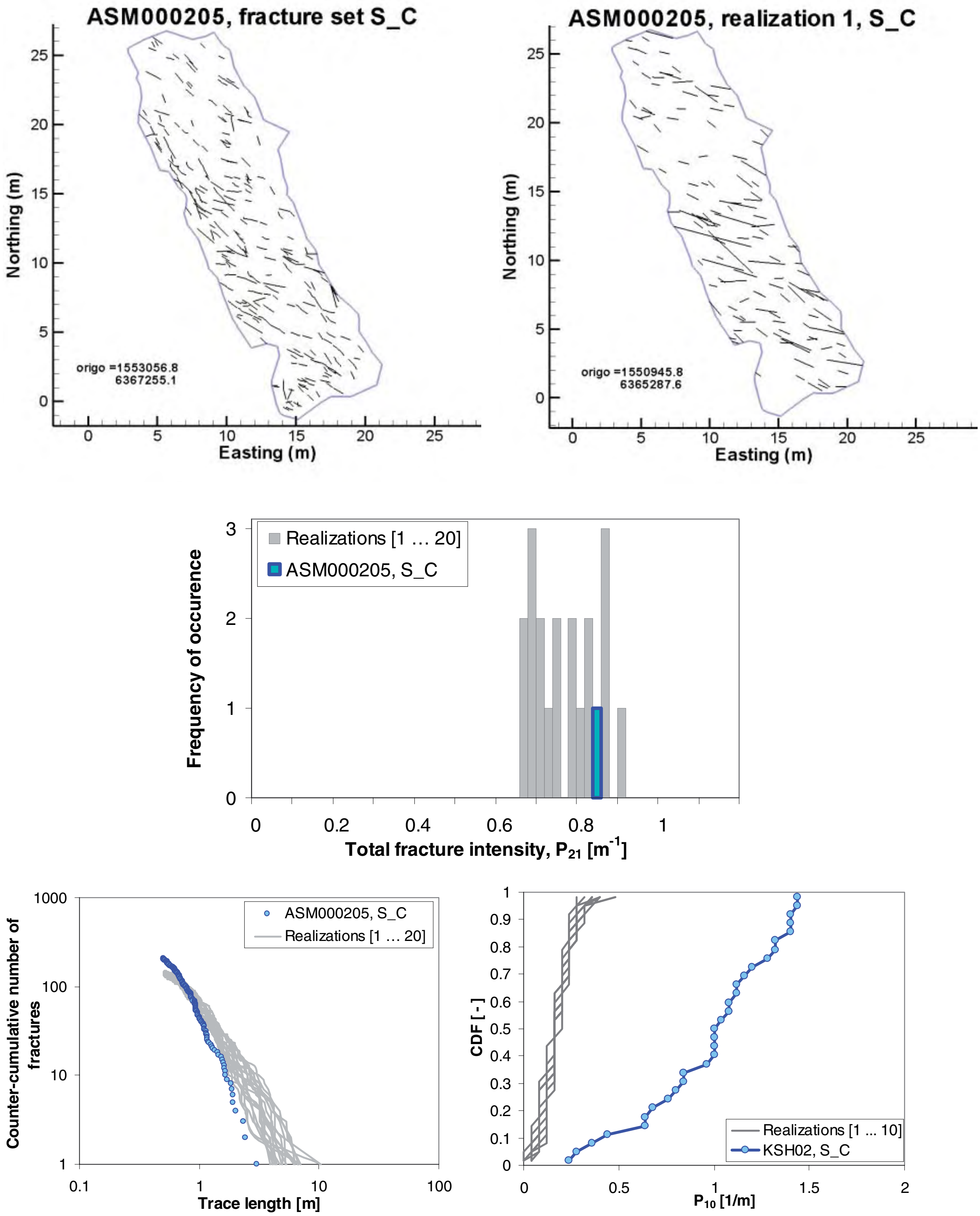

Figure D-19. *Evaluation of Simpevarp subarea, RSMB, fracture set S_C. Traces of outcrop ASM000205 compared to one realization. Simulated fracture properties (grey lines) are compared to field data (blue), in terms of: fracture intensity, P_{21}, fracture frequency, P_{10}, and trace length distribution.*

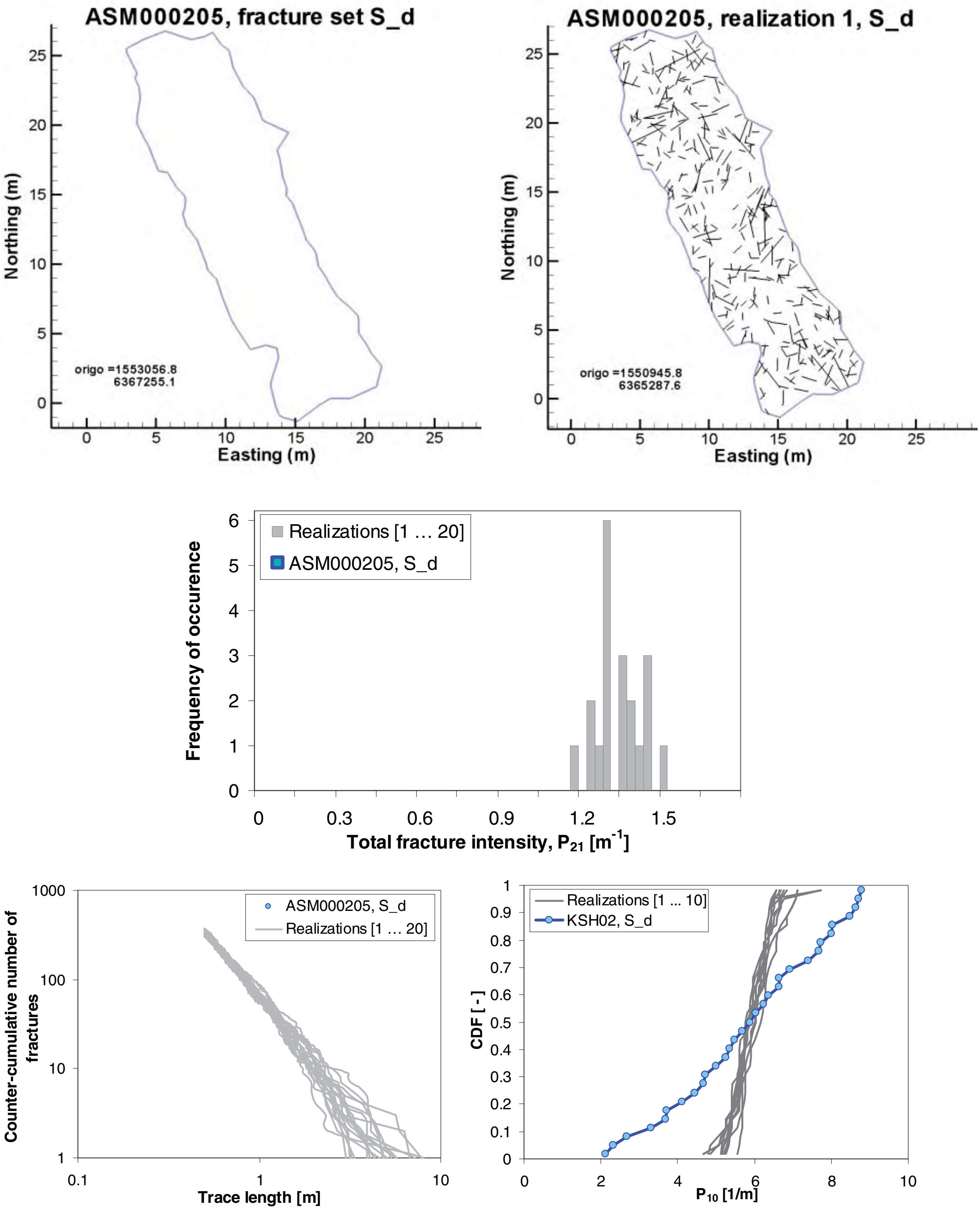

Figure D-20. Evaluation of Simpevarp subarea, RSMB, fracture set S_d. Traces of outcrop ASM000205 compared to one realization. Simulated fracture properties (grey lines) are compared to field data (blue), in terms of: fracture intensity, P_{21}, fracture frequency, P_{10}, and trace length distribution.

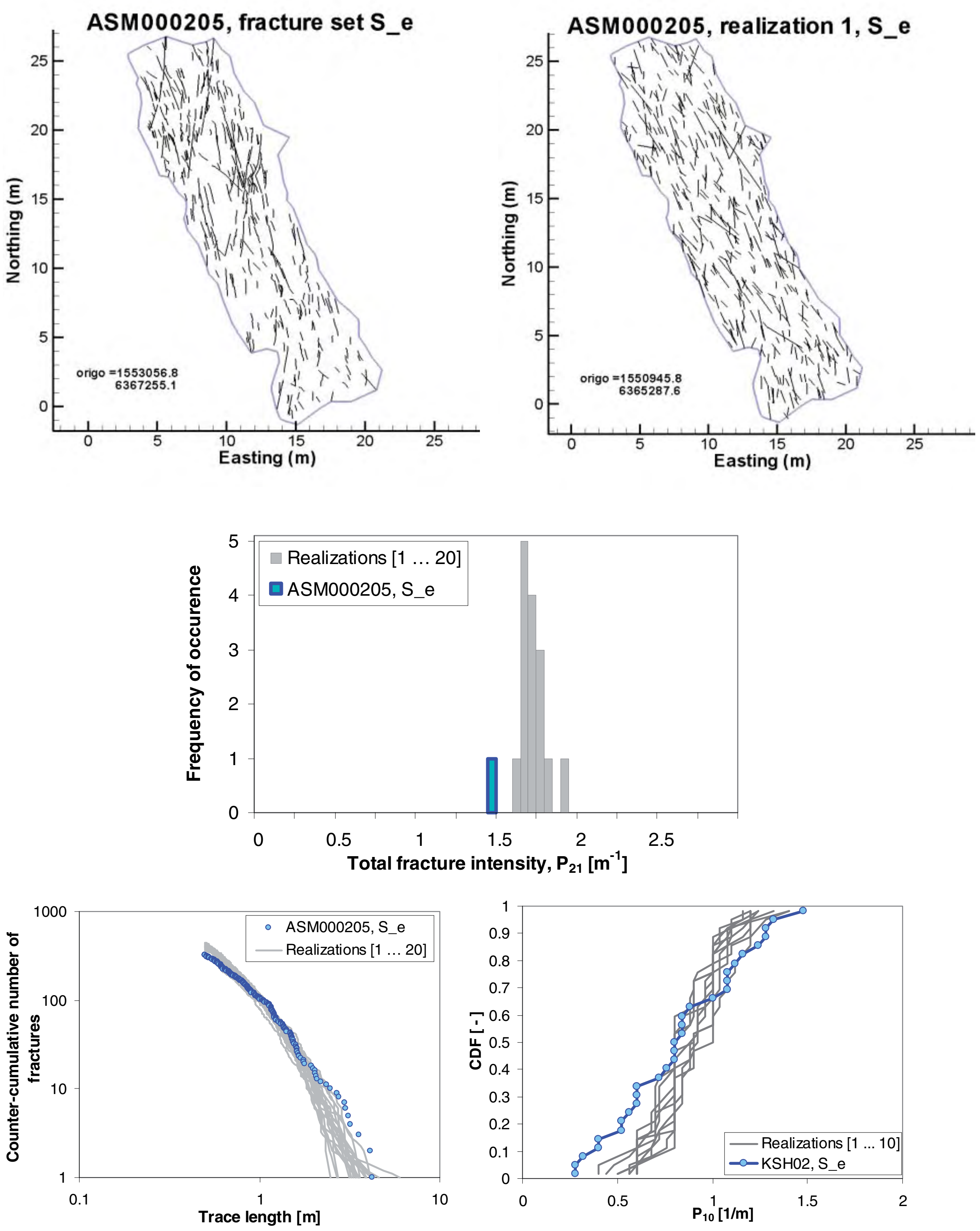

Figure D-21. *Evaluation of Simpevarp subarea, RSMB, fracture set S_e. Traces of outcrop ASM000205 compared to one realization. Simulated fracture properties (grey lines) are compared to field data (blue), in terms of: fracture intensity, P_{21}, fracture frequency, P_{10}, and trace length distribution.*

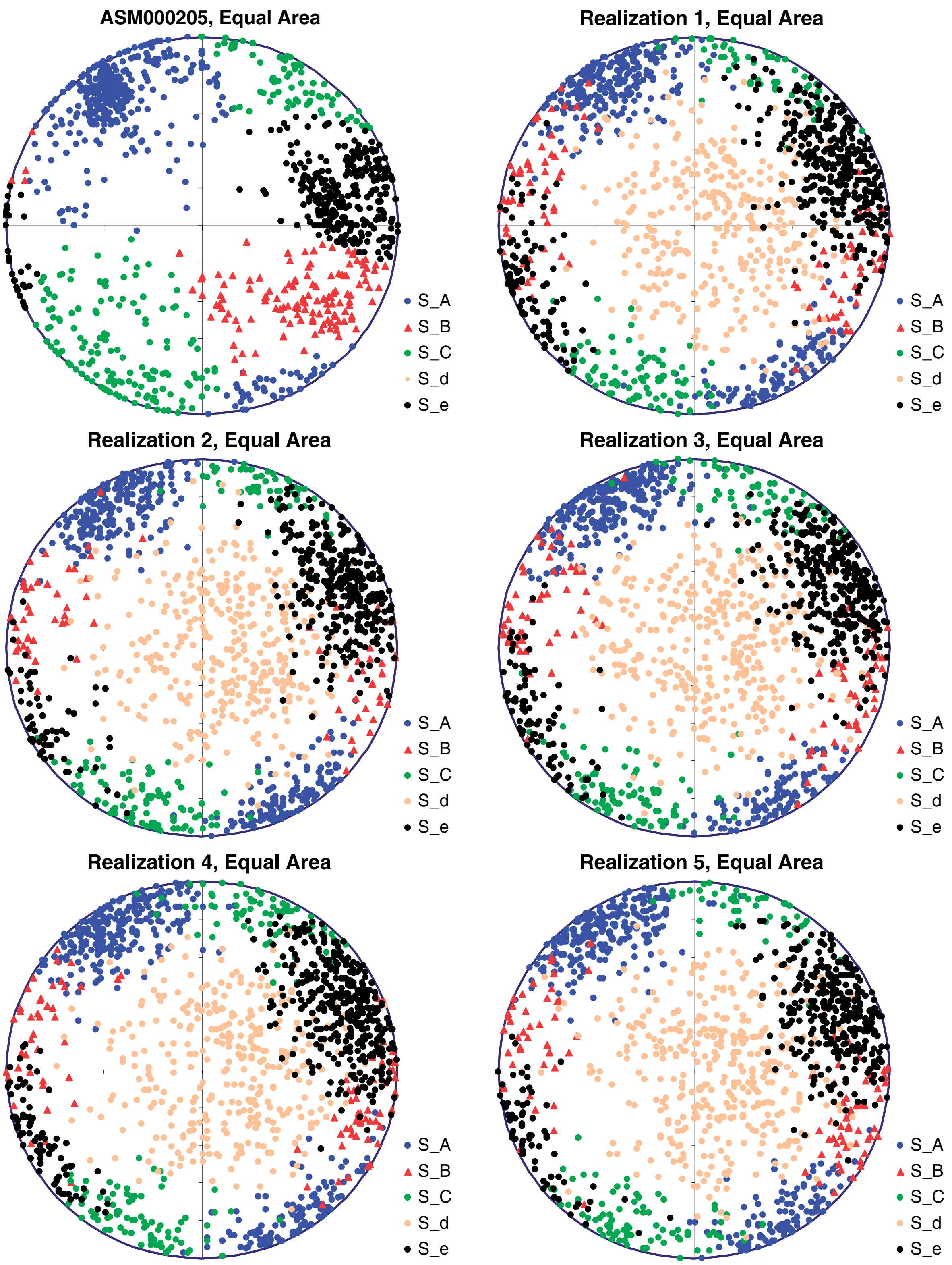

Figure D-22. *Stereoplots of simulated traces for the Simpevarp subarea, RSMB: outcrop ASM000205 data compared to five realizations.*

Phase II, variability within the rock domains; Laxemar Subarea, RSMA

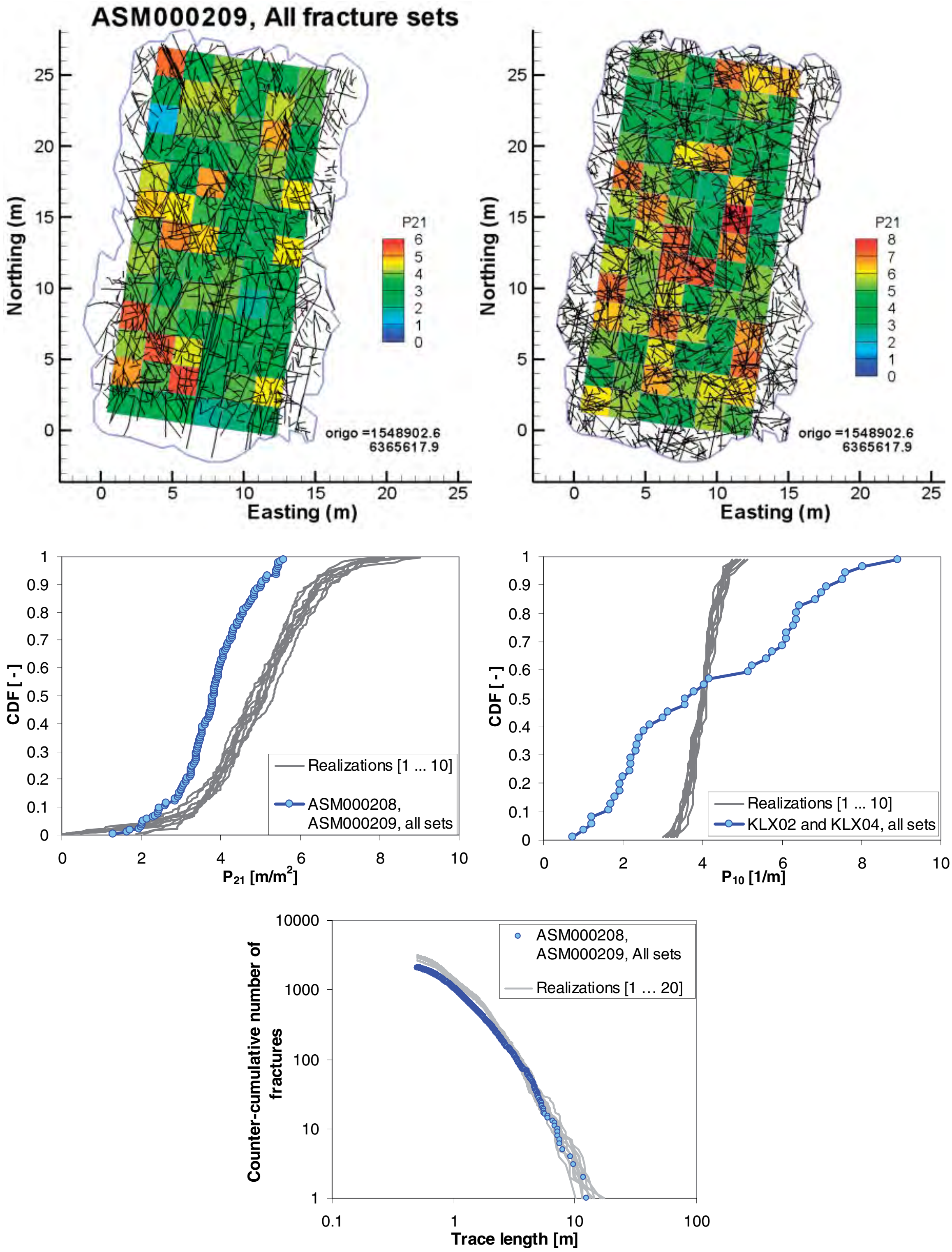

Figure D-23. Evaluation of Laxemar subarea, RSMA, all fracture sets. Traces of outcrop ASM000209 compared to one realization. Simulated fracture properties (grey lines) are compared to field data (blue), in terms of: fracture intensity, P_{21}, fracture frequency, P_{10}, and trace length distribution.

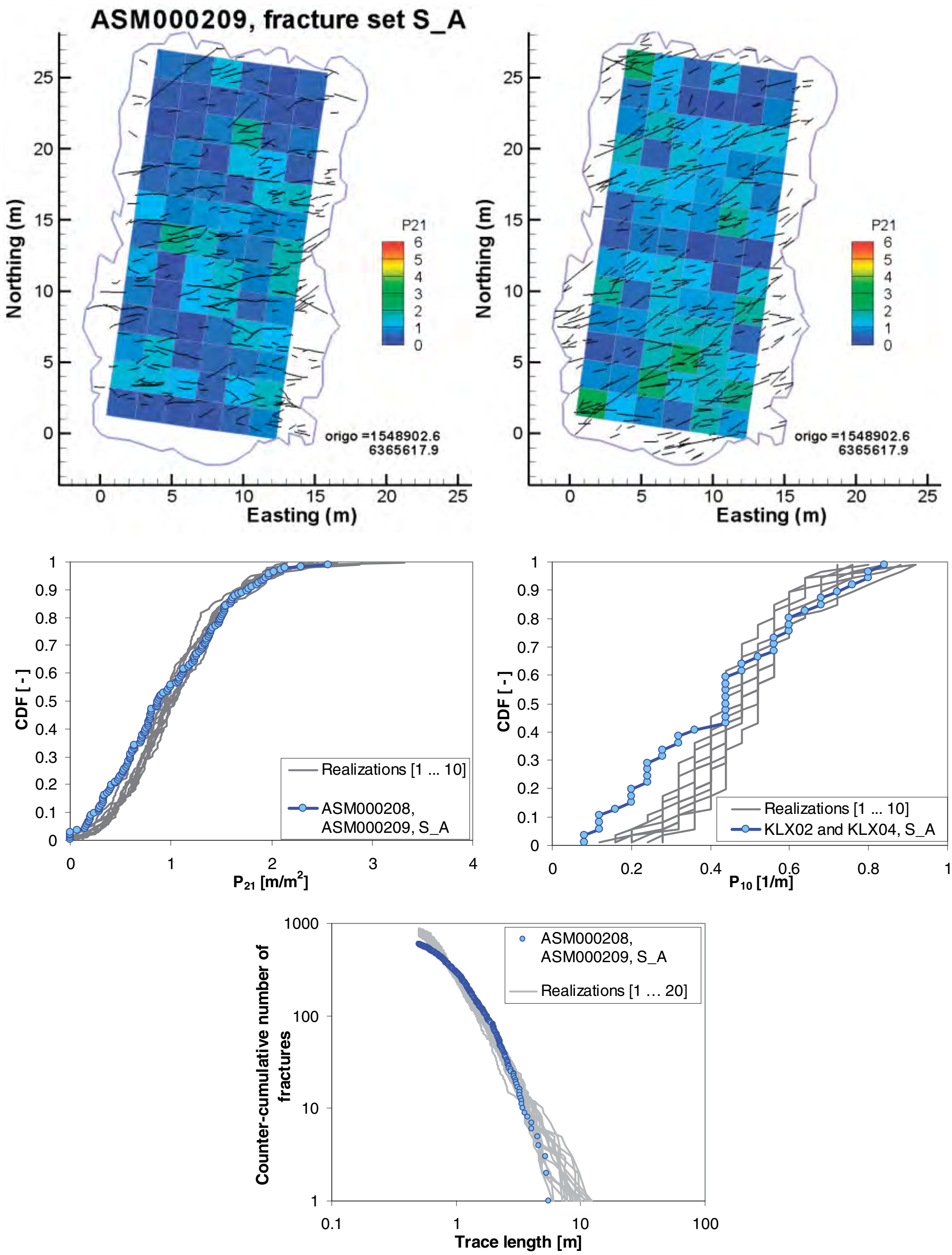

Figure D-24. Evaluation of Laxemar subarea, RSMA, fracture set S_A. Traces of outcrop ASM000209 compared to one realization. Simulated fracture properties (grey lines) are compared to field data (blue), in terms of: fracture intensity, P_{21}, fracture frequency, P_{10}, and trace length distribution.

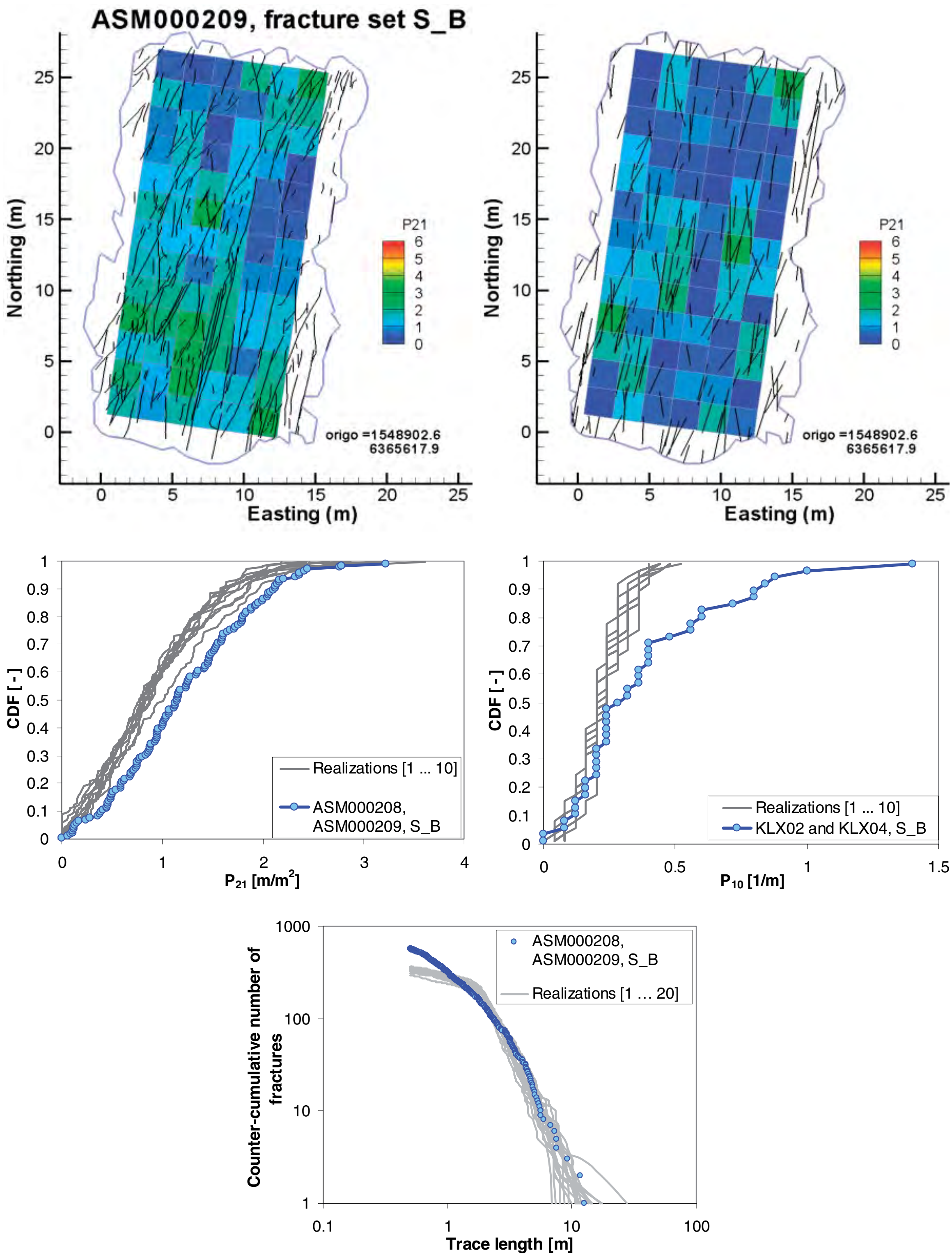

Figure D-25. *Evaluation of Laxemar subarea, RSMA, fracture set S_B. Traces of outcrop ASM000209 compared to one realization. Simulated fracture properties (grey lines) are compared to field data (blue), in terms of: fracture intensity, P_{21}, fracture frequency, P_{10}, and trace length distribution.*

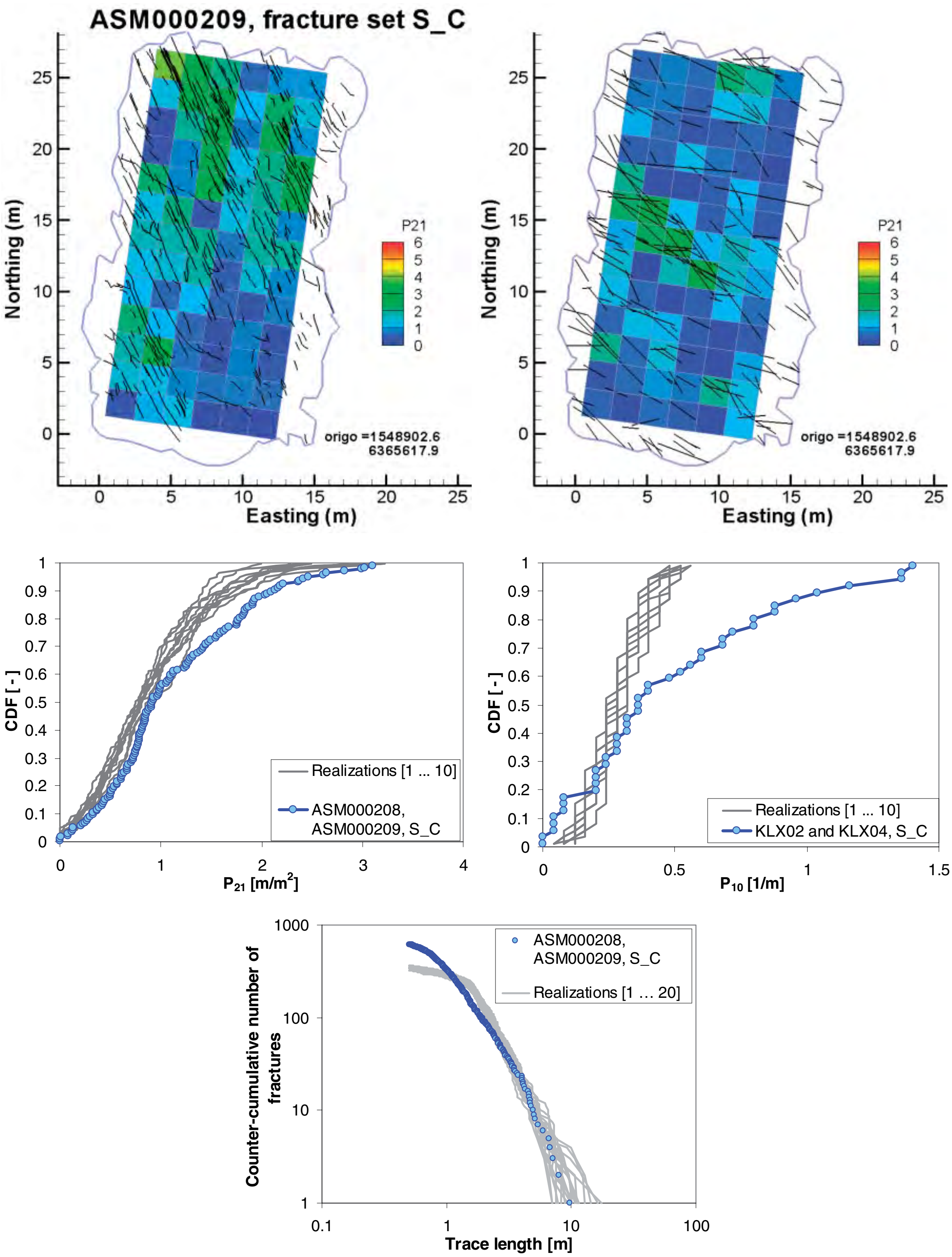

Figure D-26. *Evaluation of Laxemar subarea, RSMA, fracture set S_C. Traces of outcrop ASM000209 compared to one realization. Simulated fracture properties (grey lines) are compared to field data (blue), in terms of: fracture intensity,* P_{21}*, fracture frequency,* P_{10}*, and trace length distribution.*

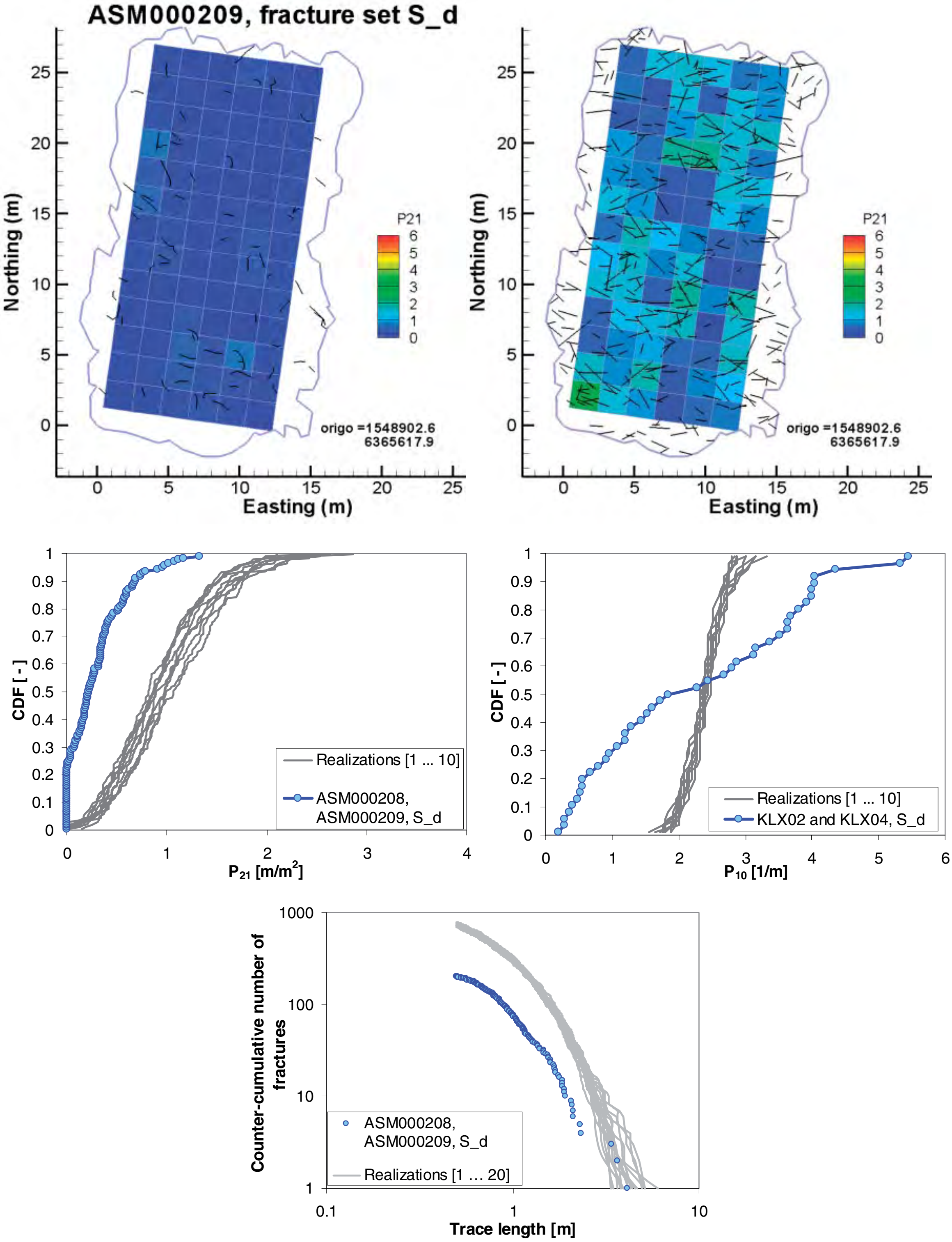

Figure D-27. *Evaluation of Laxemar subarea, RSMA, fracture set S_d. Traces of outcrop ASM000209 compared to one realization. Simulated fracture properties (grey lines) are compared to field data (blue), in terms of: fracture intensity, P_{21}, fracture frequency, P_{10}, and trace length distribution.*

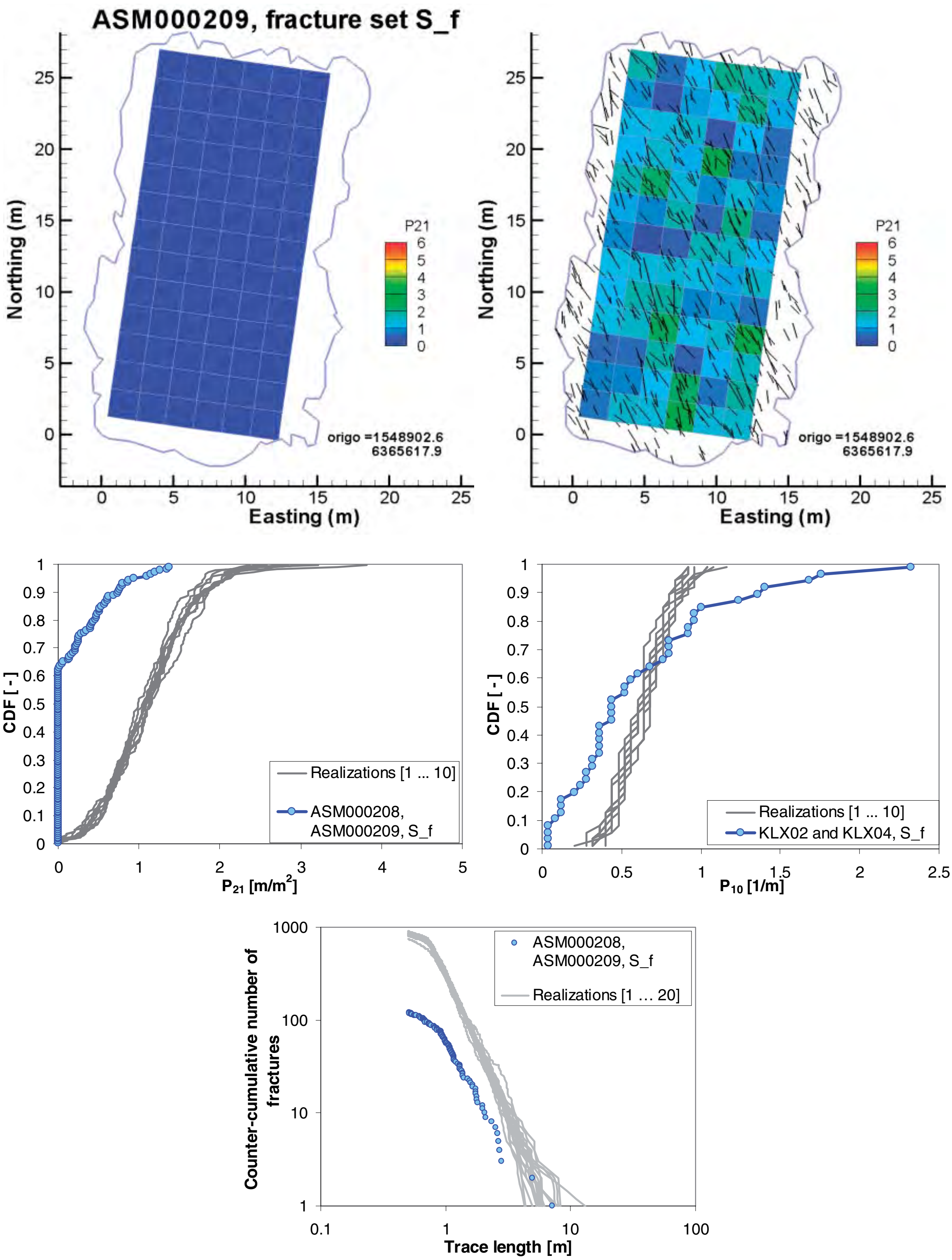

Figure D-28. *Evaluation of Laxemar subarea, RSMA, fracture set S_f. Traces of outcrop ASM000209 compared to one realization. Simulated fracture properties (grey lines) are compared to field data (blue), in terms of: fracture intensity, P_{21}, fracture frequency, P_{10}, and trace length distribution.*

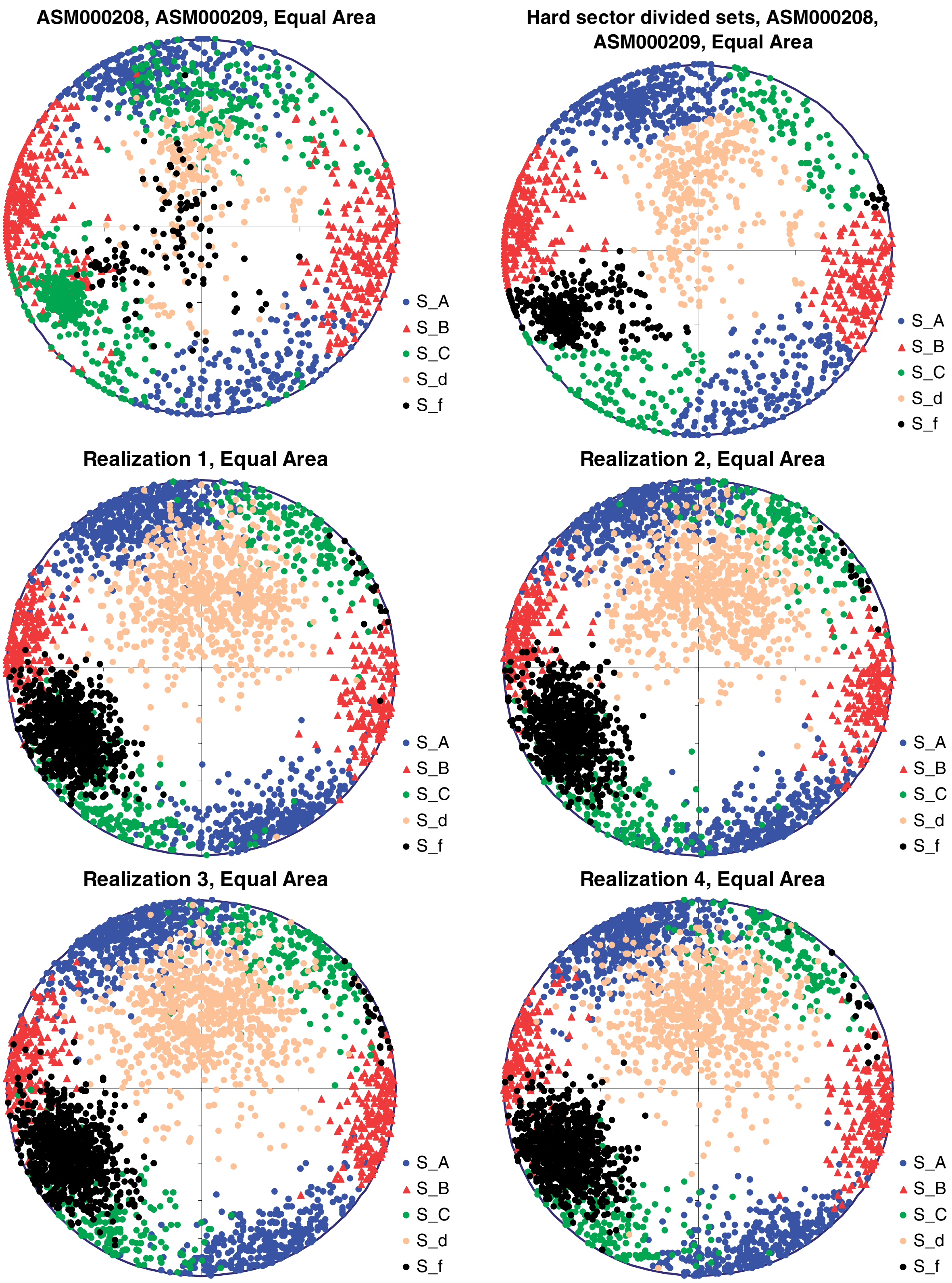

Figure D-29. Stereoplots of simulated traces for the Laxemar subarea, RSMA: outcrop ASM000208 and ASM000209 data compared to five realizations.

Simpevarp subarea, RSMA

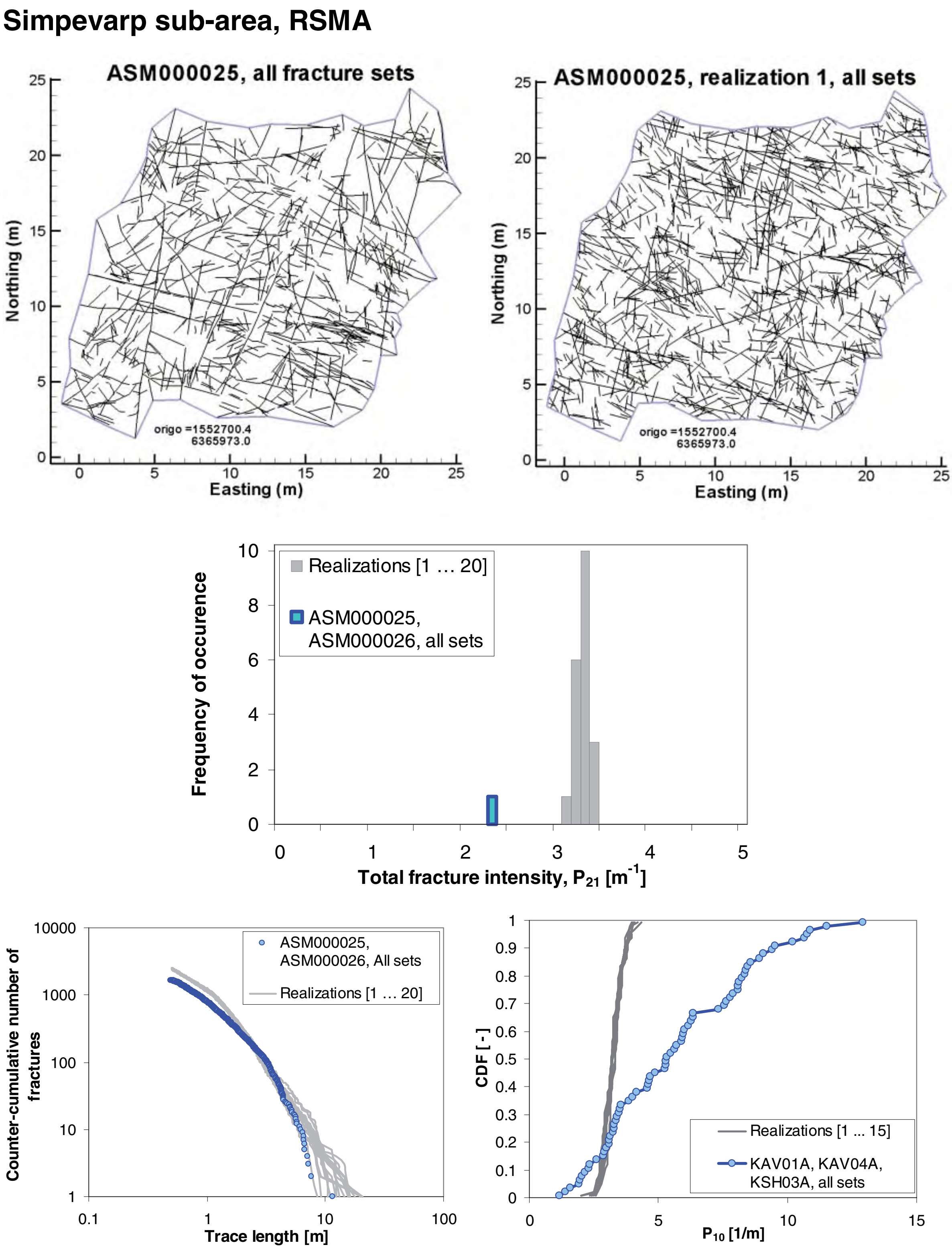

Figure D-30. *Evaluation of Simpevarp subarea, RSMA, all fracture sets. Traces of outcrop ASM000025 compared to one realization. Simulated fracture properties (grey lines) are compared to field data (blue), in terms of: fracture intensity, P_{21}, fracture frequency, P_{10}, and trace length distribution.*

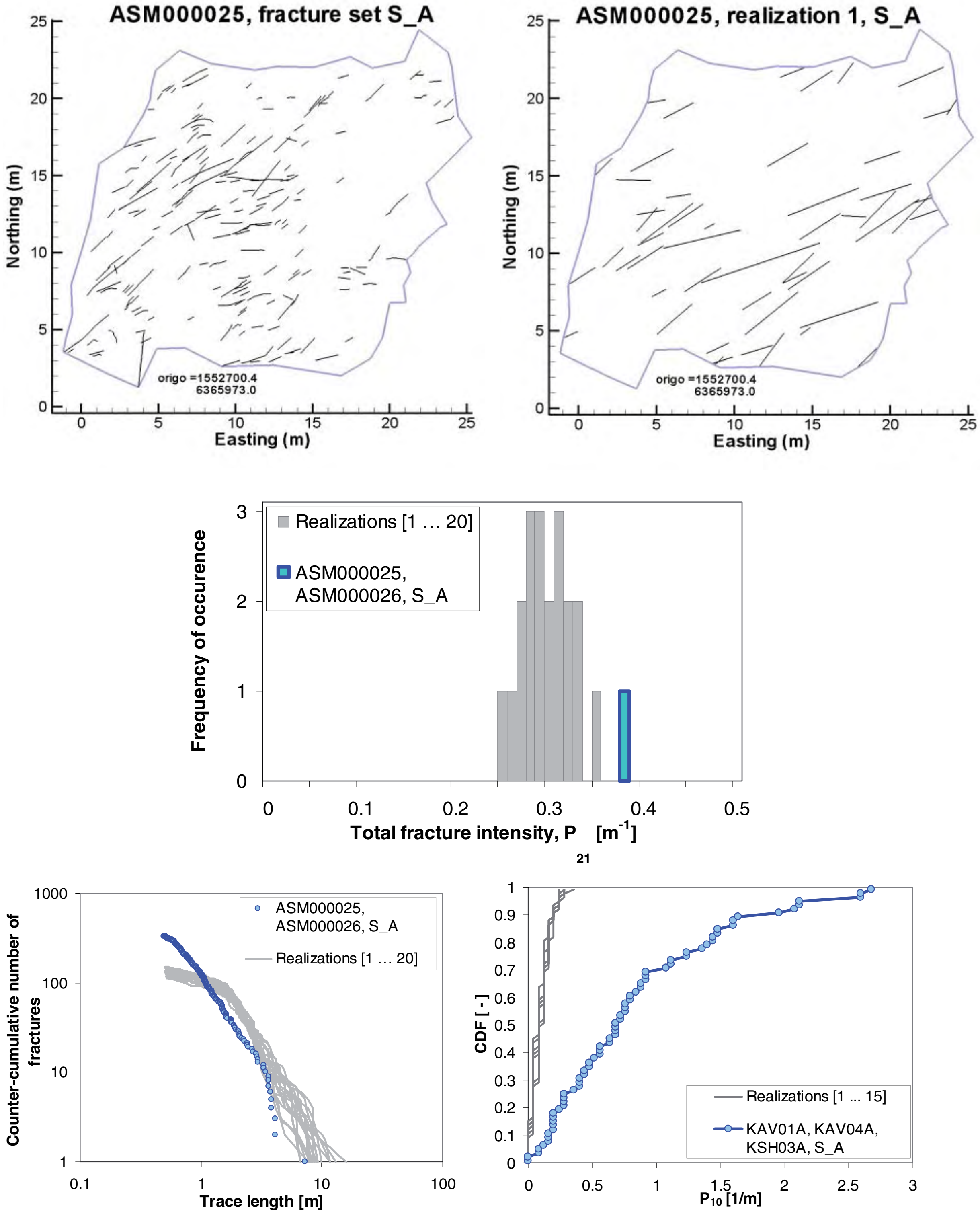

Figure D-31. *Evaluation of Simpevarp subarea, RSMA, fracture set S_A. Traces of outcrop ASM000025 compared to one realization. Simulated fracture properties (grey lines) are compared to field data (blue), in terms of: fracture intensity, P_{21}, fracture frequency, P_{10}, and trace length distribution.*

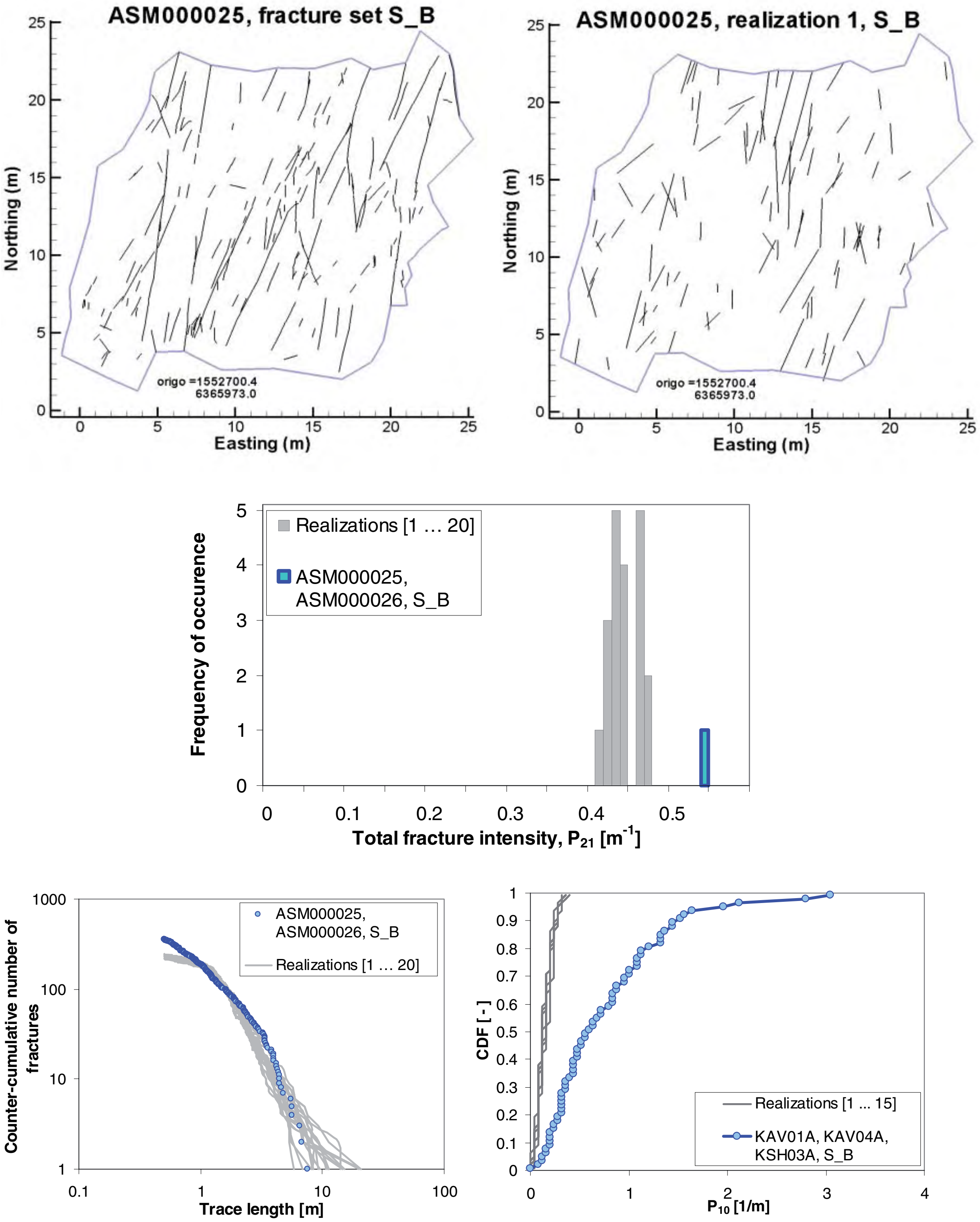

Figure D-32. *Evaluation of Simpevarp subarea, RSMA, fracture set S_B. Traces of outcrop ASM000025 compared to one realization. Simulated fracture properties (grey lines) are compared to field data (blue), in terms of: fracture intensity, P_{21}, fracture frequency, P_{10}, and trace length distribution.*

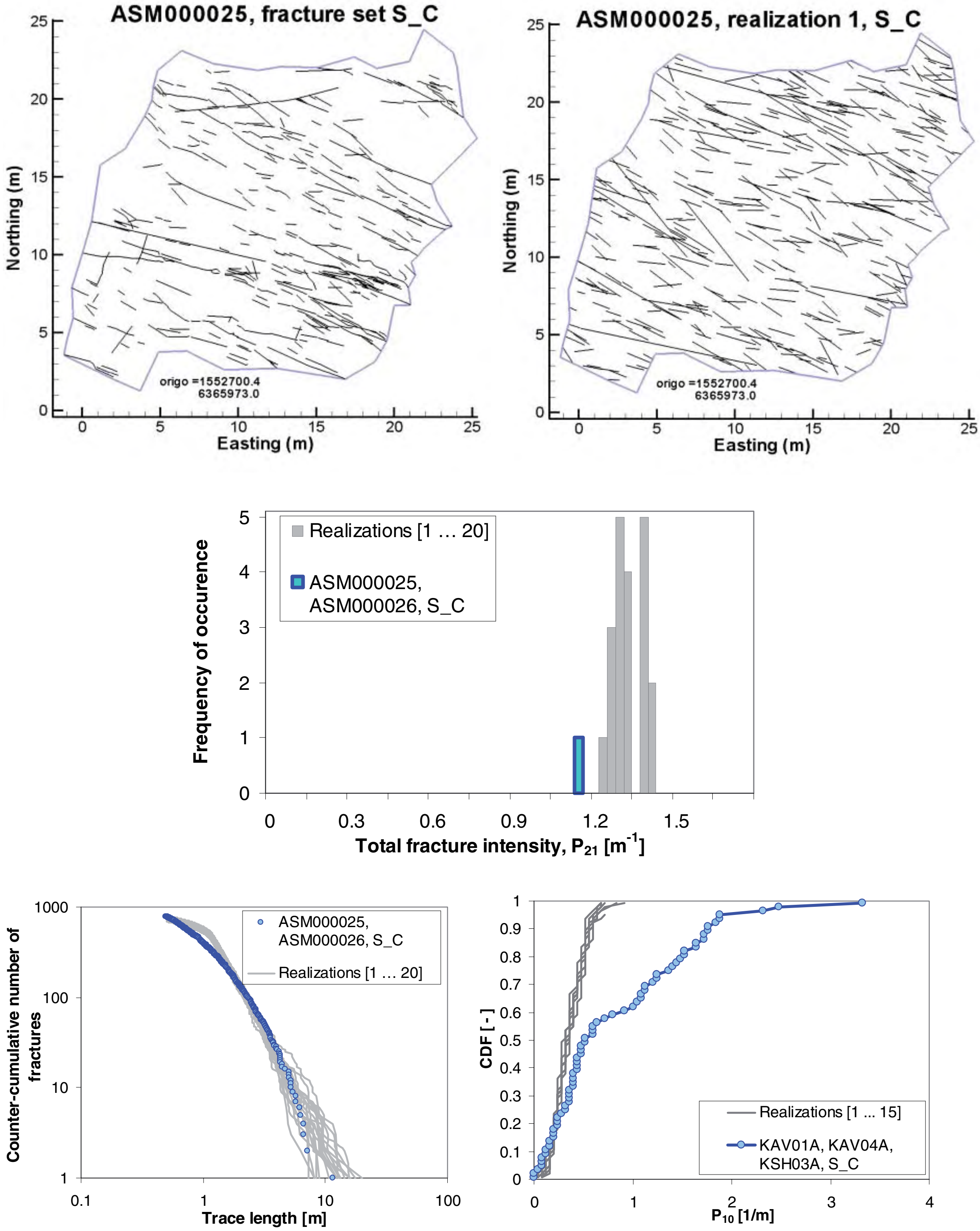

Figure D-33. *Evaluation of Simpevarp subarea, RSMA, fracture set S_C. Traces of outcrop ASM000025 compared to one realization. Simulated fracture properties (grey lines) are compared to field data (blue), in terms of: fracture intensity, P_{21}, fracture frequency, P_{10}, and trace length distribution.*

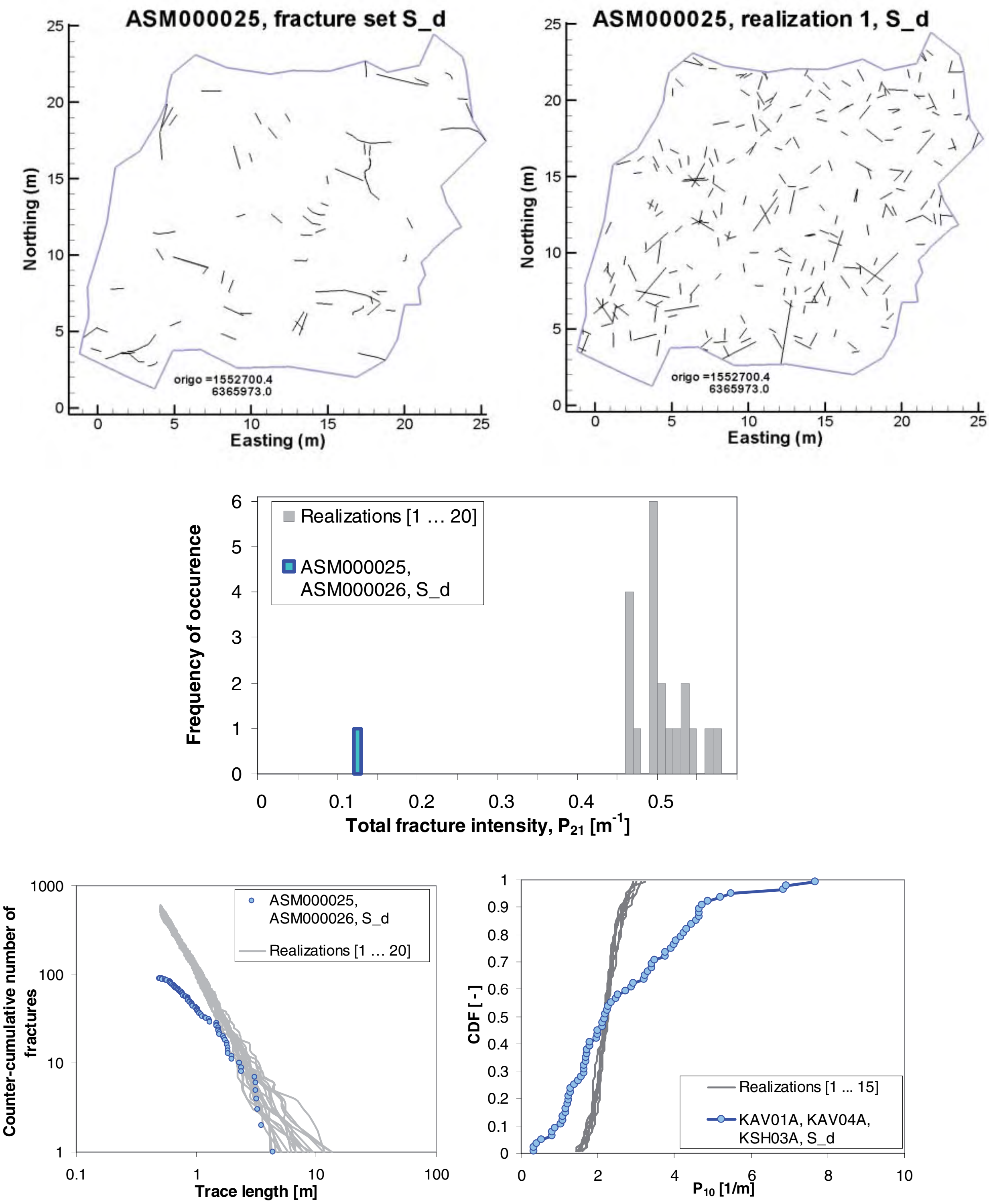

Figure D-34. *Evaluation of Simpevarp subarea, RSMA, fracture set S_d. Traces of outcrop ASM000025 compared to one realization. Simulated fracture properties (grey lines) are compared to field data (blue), in terms of: fracture intensity, P_{21}, fracture frequency, P_{10}, and trace length distribution.*

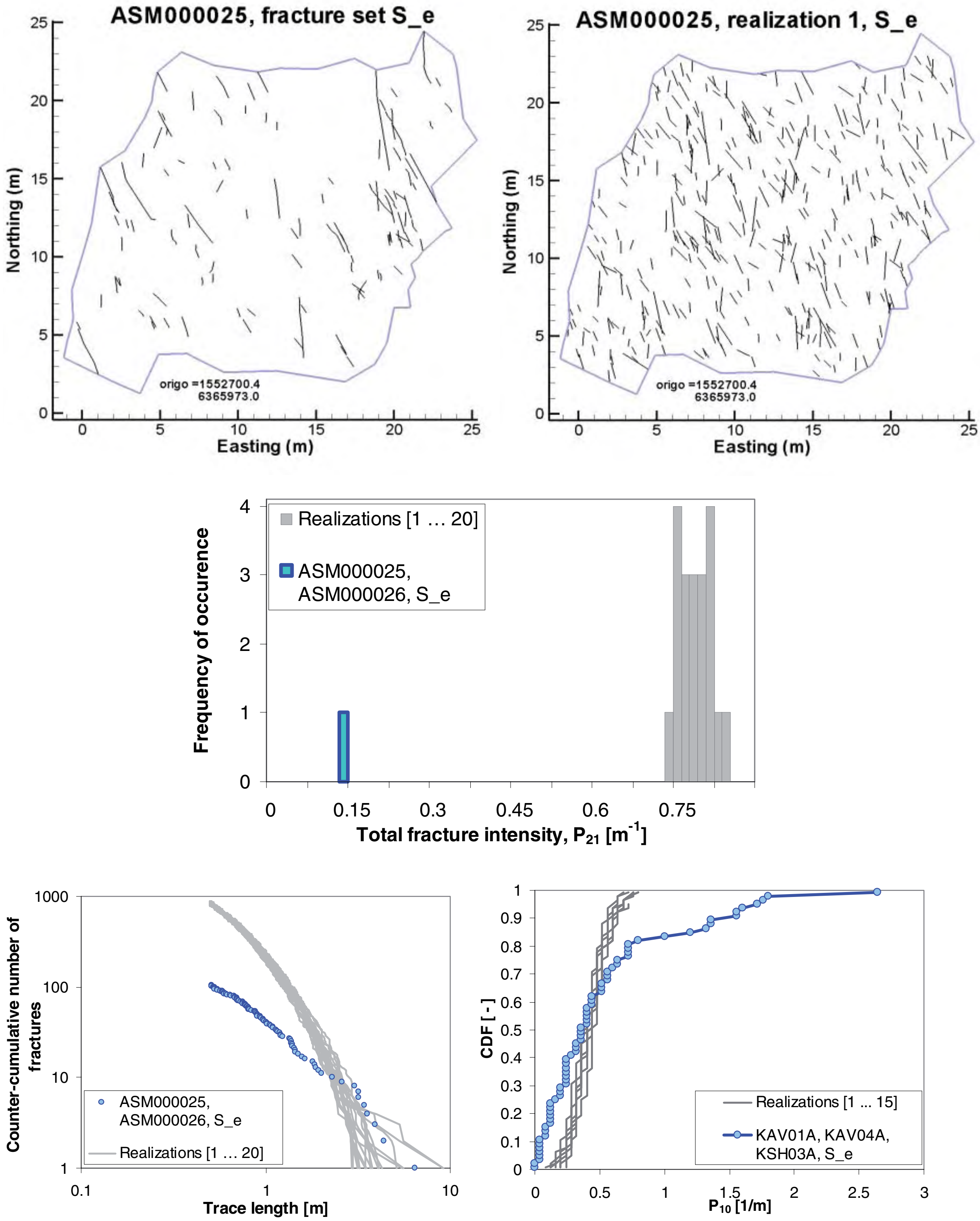

Figure D-35. *Evaluation of Simpevarp subarea, RSMA, fracture set S_e. Traces of outcrop ASM000025 compared to one realization. Simulated fracture properties (grey lines) are compared to field data (blue), in terms of: fracture intensity, P_{21}, fracture frequency, P_{10}, and trace length distribution.*

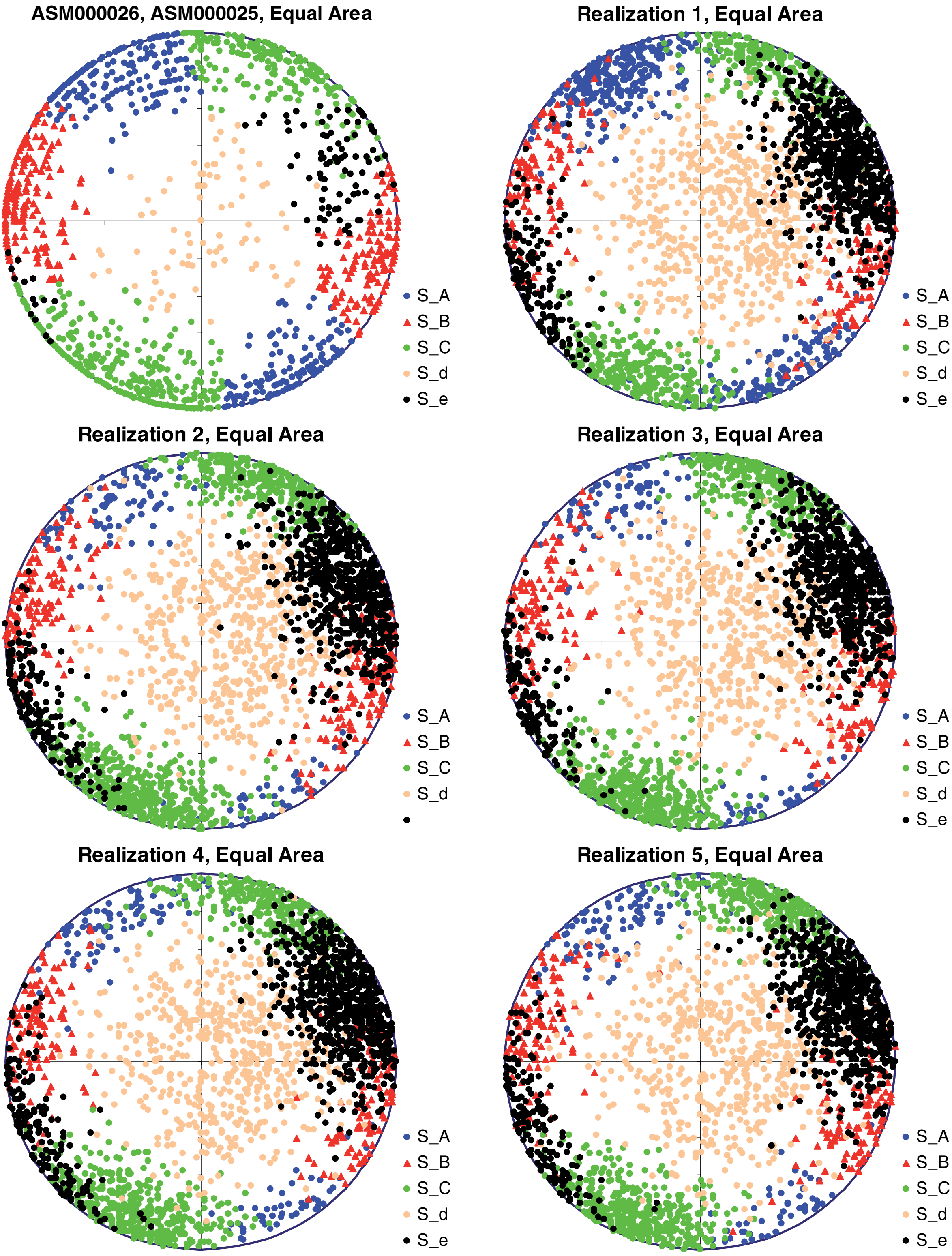

Figure D-36. *Stereoplots of simulated traces for the Laxemar subarea, RSMA: outcrop ASM000025 and ASM000026 data compared to five realizations.Simpevarp subarea, RSMB.*

Simpevarp subarea, RSMB

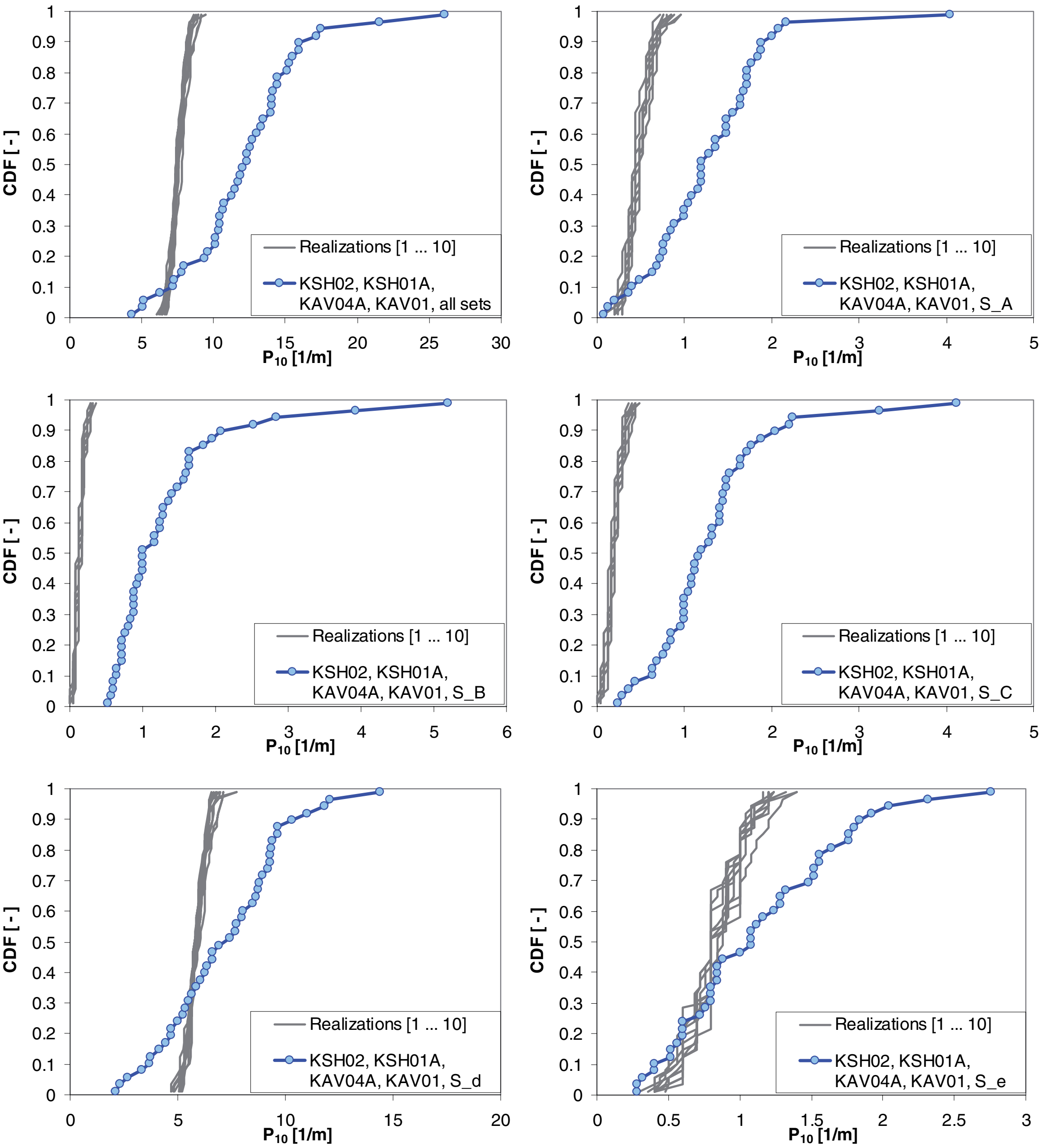

***Figure D-37.** Cumulative density graphs of P_{10} in 25 m-borehole sections of the Simpevarp subarea, RSMB: simulated data sets (grey) compared to field data (blue).*

Summary of observations made

General observations from the simulated exploration of the Laxemar SDM 1.2 DFN model are:

- The total simulated fracture intensity (P_{21}) in outcrops is overestimated.
- The total simulated fracture frequency in 25 m-borehole sections (P_{10}) is underestimated.
- The variability in simulated fracture frequency in 25 m-borehole sections (P_{10}) is underestimated.
- The simulated trace orientations match outcrop data poorly, both in terms of mean pole and in dispersion around their mean poles, at least for local sets (S_d, S_e, and S_f).

The total intensity (P_{21}) in outcrop is overestimated because the two local sets (S_d and S_f, or S_e) are based on borehole fracture frequency data whereas the global sets are based on outcrop intensity. Likewise, fracture frequency is underestimated for the same reasons. This emphasizes that there is a need for finding additional ways to constrain the local fracture set geometries. This is possible by either finding new subvertical outcrops for better sampling of subhorizontal fractures, or constraining the data better by using hydrotest and flowlog information.

The variability of fracture frequency is underestimated because P_{32} has been included as a constant in the model according to the summary tables in Section 7. However, if P_{32} variability from Tables 6-28 and 6-29 is included in the simulations, the necessary variability in observed data can be reproduced. The variability that is still visible in the simulations can be attributed to the variability in the orientation definitions (i.e. Fisher κ).

However, it is also evident that the global sets generally match outcrop data rather well, and the local sets match average fracture frequency in boreholes rather well. The main reason for this is that the global and local sets reflect different underlying types of data. Therefore, separate observations for global, respectively local, sets are summarized, below.

General observations for global fracture sets

The global fracture sets (S_A, S_B, and S_C) match outcrop data well in P_{21}, and rather well in trace length distributions and in orientations, but generally match poorly in borehole fracture frequency (P_{10}). This agrees with expectations as the global sets has been matched with fracture geometries at outcrop and with low intensity percentiles in the boreholes. For the Laxemar subarea, the global sets match fairly well to borehole data, although sets S_B and S_C fail to reproduce the peaks in P_{10} data. On comparison, for the Simpevarp subarea, the match to borehole data is much worse; P_{10} is clearly underestimated. The reason for this is that the P_{32} values used to match surface data (Section 6.2) correspond to exceptionally low percentiles of borehole data in the Simpevarp subarea, as compared to the Laxemar subarea (cf Tables 6-8, 6-20, 6-23). It was also noted that, generally, too few short fractures were simulated in outcrops. This is probably an effect of geometry, which occurs when the minimum fracture size is of similar magnitude to the sampling truncation limit (0.5 m).

General observations for local fracture sets

The local sets (S_d, S_e, and S_f) match the average P_{10} in borehole data rather well, although its variability is clearly underestimated. This agrees with expectations, as the average borehole data P_{32} values were used for the local sets (Tables D-1 to D-3).

The simulated local sets vastly overestimate the outcrop data P_{21} (the exception being S_e in outcrop ASM000205). The clearest example of this is the absence of set S_e in ASM000026 and ASM000205 outcrop data, and of set S_f in ASM000209 outcrop data, which, for obvious reasons cannot be reproduced by simulated exploration (as P_{32} is taken from borehole data where fracture frequency is high). The mismatch in fracture orientation between observed data and simulations, depend on the hard sector division of fracture sets (Section 4.8.1), which entails a step of redefining the set of belonging for many fractures (primarily local sets).

In summary, the verification process of demonstrating that the model reproduces data from the source outcrops and boreholes show results in line with expectations. The fracture intensity for the global sets shows matches similar to outcrop data and at stipulated intensity percentiles for borehole data. Fracture sizes for global sets show a reasonably good match with sampled data at outcrops. Local sets show a good match to borehole fracture frequency as well as a decent match to outcrop size distributions.

However, depending on the underlying data from boreholes, local sets overemphasize intensity at outcrop. Also, the variability in the sampled fracture intensity (P_{21} and P_{10}) is underestimated because the variability of P_{32} has not been included in the simulations.

The evaluation of model consistency with field data in the Laxemar and Simpevarp subareas shows similar results as presented above. The match point intensities for the global sets is consistent in the simulated data, but the real question is whether the low percentile match points give an adequate understanding of the fracture network behavior at the very small scale around the borehole. Local sets are clearly not fully understood in this model version and need further analysis. The subhorizontal fracture set potentially has major implications to the connectivity and flow behavior of the system and needs to better quantified with regards to both intensity and size.

Also, the variability in intensity and orientation (possibly also size) is large within the rock domains as stipulated by the rock domain model. To increase confidence in the DFN model it is necessary to analyse the Laxemar subarea in greater detail to examine possibilities to find better domains for the fracture network description. Rock type, alteration, closeness to deformation zones hydraulic properties as well as spatial trend of open fractures towards depth is necessary to evaluate in order to find if there is basis for other domains.